NUTAN MAHARASHTRA INSTITUTE OF ENGINEERING & TECHNOLOGY, PUNE

RESEARCH AND DEVELOPMENT (R&D)

PAPER PUBLICATIONS

Samarth Vidya Sankul, Vishnupuri,
Talegaon Dabhade, Pune – 410507
02114 – 231666
nmiettalegaon@gmail.com

PCET'S and NMVPM's
Nutan Maharashtra Institute of Engineering and Technology

About NMVPM

Nutan Maharashtra Vidya Prasarak Mandal is a highly respected education society in Maharashtra and is credited with starting national education schools in the Maval Region of Pune district over 100 years ago. The great freedom fighter Lokmanya Bal Gangadhar Tilak was the founder member of the Mandal and was the Chairman of its Governing Body for almost 12 years. The late Hon. Vishnu G. Vijapurkar was the first Secretary of "Samarth Vidyalaya" – the first national school started by the Mandal. He was imprisoned by the British authorities for his so called anti British activities. Vishnu Ganesh Pingle was a Vibrant Student of Samarth Vidyalaya. He became a leader of the Gaddar Party of Lala Hardayal and was hanged by the British for his revolutionary activates when he was barely 26. The Mandal and its schools has such rich heritage.

During the first 80 years, the Mandal established good Primary and Secondary Schools in the Maval region with the sole intention of providing education to the youth of relatively backward area of the Pune District. In 1998, it established a Polytechnic College and during the last decade, over 1000 students received quality technical education in the Maval region. The Society (Mandal) has thus helped the nearby community in raising its economic and education standard. The progressive, dynamic and dedicated management of the Nutan Maharashtra Vidya Prasarak Mandal has decided to start a four year degree engineering college from academic year 2008-2009.

About NMIET

NMIET (Nutan Maharashtra Institute of Engineering and Technology) was founded in 2008. NMIET stands committed to provide quality technical education to its students."Nutan Maharashtra Institute of Engineering & Technology (NMIET)" is approved by All India Council for Technical Education (AICTE), New Delhi and Director of Technical Education (DTE), Government of Maharashtra. It is affiliated to Pune University. It is a part of Pune's Savitribai Phule Pune University (SPPU). There are four undergraduate courses offered by the institute. Computer Engineering, Information Technology, Mechanical Engineering, Electronics, and Telecommunication Engineering are some of the undergraduate courses available.

Vision of Institute

To be a notable institution for providing quality technical education and ensuring ethical, moral and holistic development of students.

Mission of Institute

To nurture engineering graduates with state of the art competence, professionalism and problem solving skills to serve needs of industry as well as society.

Vision Research and Development

To be recognized as a creative and innovative department.

Mission Research and Development

Strengthening research culture thorough quality research publications and IPR on latest technology.

Objectives Research and Development

- To promote research in newly emerging and challenging frontier areas of Engineering & Technology.
- To encourages the students and faculties to undertake the research in emerging areas including multidisciplinary fields.
- To create awareness and improve number of Patents & IPR.
- To enhance the research output of the institute by publishing research paper in referred journals and reputed conferences.
- To organize various workshops/ seminar/ trainings related to promotion of research.

About the Research and Development Department

The Research and Development (R&D) Department at Nutan Maharashtra Institute of Engineering and Technology (NMIET) stands as a proud emblem of innovation and technological progress within the institution. At the core of NMIET's commitment to expanding the horizons of knowledge and fostering a culture of creativity, the R&D Department serves as a linchpin, propelling academic excellence and making substantial contributions to the broader scientific and engineering realm.

The R&D Department at NMIET boasts cutting-edge facilities and is staffed by an energetic cadre of researchers, scholars, and seasoned faculty members. Its central mission is to cultivate a research environment that nurtures curiosity, exploration, and collaborative learning. Through the pursuit of pioneering research, the department endeavors to address real-world challenges, effectively bridging the gap between theoretical insights and practical applications.

In its relentless quest for distinction, the R&D Department concentrates on a multitude of interdisciplinary research domains spanning engineering, technology, and the allied sciences. This expansive scope ensures that the outcomes of their research endeavors possess extensive implications and offer potential contributions to diverse industries and societal concerns.

Moreover, the R&D Department is a strong advocate for the active engagement of both faculty and students in research undertakings. It opens avenues for students to participate in hands-on research projects, thereby fostering a culture of innovation from the undergraduate level onwards. This approach not only hones the technical acumen of students but also instills a problem-solving mentality that transcends the boundaries of traditional classroom learning.

Collaboration stands as a cornerstone of the R&D Department's ethos. It actively seeks partnerships with industries, research institutions, and fellow academic entities to facilitate the exchange of knowledge and amplify its impact. By forging robust alliances, NMIET's R&D Department harnesses external expertise and resources, thereby enriching the quality and breadth of its research pursuits.

In summation, the Research and Development Department at Nutan Maharashtra Institute of Engineering and Technology stands as a symbol of intellectual inquisitiveness, innovation, and transformative research. With its emphasis on groundbreaking projects, student involvement, and collaborative initiatives, the department continues to make an enduring impression on the academic and technological landscape, making substantial contributions to the advancement of both society and industry.

From the President's Desk:

Dear Esteemed Members of the NMVPM Family,

I am delighted to address you through the pages of Research & Development, the remarkable Research and Development magazine of the Nutan Maharashtra Institute of Engineering and Technology (NMIET) Talegaon. This publication stands as a testament to our unwavering commitment to advancing the frontiers of knowledge, innovation, and research.

In today's fast-paced world, the pursuit of knowledge and innovation is more critical than ever before. Research and Development (R&D) not only drive technological advancements but also serve as the bedrock of progress in society. Research & Development, our R&D magazine, exemplifies our dedication to fostering a culture of inquiry, discovery, and collaboration within NMIET.

Within these pages, you will find a compendium of valuable insights, groundbreaking discoveries, and the impressive achievements of our students, faculty members, and researchers. This magazine encapsulates the essence of NMIET's research ecosystem and underscores our commitment to pushing the boundaries of engineering and technology.

Our researchers have been working diligently on projects that have the potential to shape industries, enhance human lives, and address pressing global challenges. From the seeds of innovation to the fruition of transformative ideas, each article in Research & Development reflects the diligence, expertise, and passion of the NMIET community.

I extend my heartfelt appreciation to our faculty members, students, and researchers who have contributed their time, energy, and expertise to this publication. Your dedication to advancing knowledge and pioneering solutions is commendable, and it is your collective efforts that elevate NMIET to be a renowned hub of academic excellence.

Thank you for your steadfast support of NMIET's mission to nurture intellectual growth, facilitate research excellence, and prepare the leaders of tomorrow. Together, we shall continue to achieve new heights and make a meaningful impact on the world through our collective dedication to education, research, and development.

Warm regards,

Hon. Shri. Sanjay (Bala) Vishwanath Bhegade
Ex Minister (Maharashtra Govt.),
President, Nutan Maharashtra Vidya Prasarak Mandal (NMVPM).

From the Director's Desk:

Dear Esteemed Members of the NMIET Family,

It is with great enthusiasm and pride that I address you through the pages of Research & Development, our cherished Research and Development magazine. As the Director of Nutan Maharashtra Institute of Engineering and Technology (NMIET), it is my privilege to introduce this platform that encapsulates the spirit of inquiry and innovation that defines our institution.

R&D stands as a beacon of inspiration, representing the collective dedication and unwavering commitment of our faculty, students, and researchers to the pursuit of knowledge and excellence. In today's fast-paced world, the importance of research and development cannot be overstated, and this magazine is a testament to our institution's leadership in this arena.

Within these pages, you will discover a treasure trove of ideas, discoveries, and projects that epitomize NMIET's commitment to pushing the boundaries of knowledge in the fields of engineering and technology. From pioneering innovations to transformative solutions for real-world challenges, each article in Research & Development reflects the passion, expertise, and dedication of our NMIET community.

At NMIET, we understand that our journey doesn't end with the publication of Research & Development—it is an ongoing endeavor to nurture intellectual growth, foster innovation, and prepare our students to become leaders in their respective fields. I have no doubt that our institution will continue to scale new heights in research and development, further cementing our reputation as a center of academic excellence.

I extend my sincere appreciation to the entire NMIET community for your unwavering support and dedication to our institution's mission. Together, we will continue to make meaningful contributions to the world through education, research, and innovation.

Thank you for being a part of our journey. Let us embrace the boundless opportunities that research and development present, for it is through our collective efforts that we will create a brighter and more promising future.

Warm regards,

Dr. Girish Desai, Director,

Nutan Maharashtra Institute of Engineering and Technology

From the Principal's Desk:

Dear Students, Faculty, and Researchers,

It gives me immense pleasure to extend my warm greetings to all of you through the pages of Research & Development, our esteemed Research and Development magazine. As the Principal of Nutan Maharashtra Institute of Engineering and Technology (NMIET), it fills me with pride to introduce this platform dedicated to showcasing the intellectual prowess and innovation that define our institution.

Research & Development is a testament to our relentless pursuit of knowledge and our unwavering commitment to research and development. It stands as a beacon of inspiration for the entire NMIET family, serving as a testament to our collective dedication to excellence.

In today's rapidly evolving world, research and development are the driving forces behind progress and innovation. They are the engines that power advancements in engineering and technology, shaping the future of industries and societies alike. Through Research & Development, we have the opportunity to celebrate and share the outstanding contributions of our faculty, students, and researchers in this dynamic field.

In the pages of this magazine, you will discover a treasure trove of insights, discoveries, and projects that underscore our institution's commitment to pushing the boundaries of knowledge. From groundbreaking technologies to innovative solutions for real-world challenges, each article in Research & Development reflects the dedication, passion, and expertise of our NMIET community.

I would like to express my deep appreciation to our talented faculty members, diligent students, and passionate researchers who have contributed to Research & Development's success. Your hard work and commitment to advancing research in diverse areas of engineering and technology are truly commendable, and they play a pivotal role in shaping our institution's identity.

I am confident that NMIET will continue to scale new heights in the realm of research and development. Through our unwavering dedication to education and innovation, we have the power to shape a brighter future for ourselves and for the world at large.

Dr. Vilas Deotare,

Principal, NMIET

From the R&D Dean's Desk:

Dear Colleagues, Researchers, and Innovators,

I am thrilled to address you through the pages of Research & Development, our cherished Research and Development magazine. As the R&D Coordinator of Nutan Maharashtra Institute of Engineering and Technology (NMIET), I am honored to introduce this platform that serves as a testament to our institution's dedication to research, innovation, and academic excellence.

Research & Development embodies the spirit of curiosity and discovery that drives our institution's research endeavors. In today's rapidly evolving world, research and development are at the forefront of technological advancements and societal progress. This magazine is a celebration of our collective commitment to pushing the boundaries of knowledge.

Within the pages of Research & Development, you will find a wealth of insights, discoveries, and projects that exemplify NMIET's commitment to excellence in engineering and technology. From groundbreaking research to innovative solutions addressing real-world challenges, each article in Research & Development reflects the passion, expertise, and dedication of our NMIET community.

I want to extend my heartfelt gratitude to our dedicated R&D Coordinators, esteemed faculty members, dedicated students, and passionate researchers who have contributed to the success of Research & Development. Your tireless efforts in advancing the frontiers of knowledge are truly commendable and are the driving force behind our institution's continued growth and impact.

I extend my sincere appreciation to the entire NMIET community for your dedication and support. Together, we will continue to make meaningful contributions to the world through education, research, and innovation. Let Research & Development serve as a testament to our commitment to excellence and our unwavering pursuit of knowledge.

Thank you for your invaluable contributions to our research and development endeavors. Together, we will continue to explore new horizons and pave the way for a brighter and more innovative future.

Warm regards,

Prof. Pritam Ahire

R&D Dean, NMIET.

Paper Publication (in Scopus, SCI, WoS, Springer)

Sr. No.	Title of paper	Name of journal	Department of the teacher	Name of the author/s	Year of publication use calender year	Indexing
1	SEM and TEM images dehazingusing multiscale progressive feature fusion techniques	Indonesian Journal of Electrical Engineering and Computer Science	E&TC	Dr Ashwini Shinde	2024	Scopus
2	Comparative research on block design-based protocol and blowfish for secured key generation and data sharing on cloud	Journal of Soft Computing, part of Springer Nature 2024	E&TC	Dr Ashwini Shinde	2024	Springer
3	Mitigating DDoS attacks with an intrusion detection and prevention system based on 2-player Bayesian game theory	Journal of Discrete Mathematical Sciences & Cryptography	E&TC	Dr Sagar Joshi	2024	Scopus
4	Enhancing Diagnostic Accuracy: A Hybrid Approach to Mitigate Speckle and Rician Noise in Medical Images	Advances in Nonlinear Variational Inequalities	E&TC	Dr Sagar Joshi	2024	Scopus

5	Convolutional Neural Networks for Early Detection and Classification of Alzheimer's disease from MRI Images	Journal of Electric systems	E&TC	Dr Sagar Joshi	2024	Scopus
6	Plant Growth Analysis using IoT and Reinforcement Learning Techniques for Controlled Environment	Advances in Nonlinear Variational Inequalities	Computer Enginnering	Prof. Yogesh B. Pawar	2024	Scopus
7	Enhancing Diagnostic Accuracy: A Hybrid Approach to Mitigate Speckle and Rician Noise in Medical Images	Advances in Nonlinear Variational Inequalities	Computer Enginnering	Dr. Saurabh Saoji , Prof. Hemlata Mane, Prof. Roshni Narkhe de	2024	Scopus
8	Beyond pixels and ciphers: Navigating the advancements and challenges in visual cryptography	Journal of Autonomous Intelligence	Computer Department	Prof. Kirti Borhade	2024	Scopus
9	Design & Development of Automatic Pesticide Spraying Machine	Advances in Nonlinear Variational Inequalities	Computer Enginnering	Dr.Prasad Dhore	2024	Scopus
10	Comparative Analysis of Materials for Chassis Design in a Three-Wheeled Electric Vehicle	Advances in Nonlinear Variational Inequalities	Computer Enginnering	Dr.Prasad Dhore	2024	Scopus

11	Experimental Analysis of Wear Rate and Frictional Coefficient of Various Steel Material	Advances in Nonlinear Variational Inequalities	Computer Enginnering	Dr.Prasad Dhore	2024	Scopus
12	Experimental Analysis of Mechanical Tests on a Plate Composed of Banana Fibre	Advances in Nonlinear Variational Inequalities	Computer Enginnering	Dr.Prasad Dhore	2024	Scopus
13	GridDR: Enhancing Grid Reliability using Demand Response Program	International Journal of INTELLIGENT SYSTEMS AND APPLICATIONS IN ENGINEERING	Computer Enginnering	Dr.Prasad Dhore	2024	Scopus
14	Machine Learning Models for Early Detection of Hepatic Disorders Using Clinical Data	Frontiers in Health Informatics	Information Technology	Dr. Chandrakant Kokane	2024	Scopus
15	Information Theory and Coding Techniques for 5G WirelessCommunication Systems: Towards Efficient Spectrum Utilization	An International Forum to Contribute Your Research	Information Technology	Dr. Chandrakant Kokane Prof. Kapil Wagh	2024	Scopus
16	Implementing AI Algorithms for Predicting Diabetes Risk in Patients Using Health Informatics Data	Frontiers in Health Informatics	Information Technology	Dr. Chandrakant Kokane	2024	Scopus

17	Effect of Supervised Sense Disambiguation Model Using Machine Learning Technique and Word Embedding in Word Sense Disambiguation	Journal of Electrical Systems	Information Technology	Dr. Chandrakant Kokane Prof. Kapil Wagh	2024	Scopus
18	Peruse Of Traffic In Educational Premises Using Max-Flow Min-Cut Theorem	Educational Administration: Theory and Practice	First Year	Kirti Takale	2024	Scopus
19	Peruse Of Traffic In Educational Premises Using Max-Flow Min-Cut Theorem	Educational Administration: Theory and Practice	First Year	Shankar D. Ugale	2024	Scopus
20	Comparative Analysis of Materials for Chassis Design in a Three-Wheeled Electric Vehicle	Advances in Nonlinear Variational Inequalities	First Year	Santosh Dabhole	2024	Scopus
21	Determination of Uncertainty in calibration of External Micrometer	Advances in Nonlinear Variational Inequalities	First Year	Santosh Dabhole	2024	Scopus
22	Proactive Analysis and Detection of Cyber-attacks using Deep Learning Techniques	INDIAN JOURNALOFSCIENCEAND TECHNOLOGY	First Year	Bhargavi Dalal	2024	WoS
23	Enhanced Pin Entry Mechanism for	International Conference on Recent Developments in Cyber Security	Computer Department	Prof. Tushar Waykole	2023	Springer

	ATM Machine by Defending Shoulder Surfing Attacks					
24	Monitoring Body Mass Index (BMI) Pre & Post Covid-19 Outbreak: A Comprehensive study in Healthcare	MIT Art, Design and Technology School of Computing International Conference	Computer Enginnering	Mr. Pritam Ahire	2023	Scopus
25	Enhancing Alzheimer's Disease Prediction with Bayesian Optimization and Ensemble Methods	*Proceedings of the 5th International Conference on Information Management & Machine Intelligence*	Computer Department	Prof. Tushar Waykole	2023	Scopus
26	Advancements in Cyclostationary Technique for Cognitive Radio: An In-Depth Examination and Evaluation	International journal of intelligent systems and applications in engineering	Compter Engineering	Prachi Waghmare & Dipmala Chaudhari	2023	Scopus
27	Novel technique of vibration minimization during hard machining	Wiley	E&TC	Dr Ashwini Shinde	2023	Scopus
28	Machine Learning Approach for Intelligent Transport System in IOV-Based Vehicular Network Traffic for Smart Cities.	International Journal of Intelligent systems and applications in Engineering	Computer Enginnering	Prof. Tushar Waykole & Prof. Sonu Khapekar	2023	Scopus

29	Effects of low-power laser hardening on the mechanical and metallurgical properties of biocompatible SAE 420 steel	Journal of Materials Research and Technology	Mechanical Engg.	Satish R. More	2023	SCI
30	Thermodynamic and Kinetic Studies of Glass-Forming Compositions in Ca–Mg–Cu Ternary Metallic Glasses	Glass Physics and Chemistry	Mechanical Engg.	Anuj A Khond	2023	SCI
31	Synthesis and characterization of Al-AlN composite	Materials Today: Proceedings	Mechanical Engg.	Anuj Khond	2023	Scopus
32	Experimental Performance and Comparison of Sustainable Cooling Techniques for Solar (Photovoltaic) Panel	Nano World Journal	Mechanical Engg.	Dhanaji Jadhav	2023	Scopus
33	Experimental Analysis of Mechanical Tests on a Plate Composed of Banana Fibre	Communications on Applied Nonlinear Analysis	Mechanical Engg.	Mr. Rohit Jadhao, Mr. Mangesh Kale	2023	Scopus
34	The Role of Nonlinear Analysis in Tackling Engineering Challenges and	Advances in Nonlinear Variational Inequalities	Information Technology	Prof. Supriya Bhosale	2023	Scopus

	Advancing Technology					
35	Medical Image Encryption Using Hybrid Adaptive Elliptic Curve Cryptography and Logistic Map-based DNA Sequence in IoT Environment	IETE journal of research	Computer Enginnering	Dr. Rohini Hanchate	2023	SCI
36	Machine Learning-Based Sentiment Analysis of Incoming Calls on Helpdesk	International Journal on Recent and Innovation Trends in Computing and Communication	Information Technology	Dr. Chandrakant Kokane	2023	Scopus
37	Exploratory analysis of Kidney Disease Data set-A comparative study	Computational intelligence in data mining smart innovativation systems And Technologies Under Exclusive Lisence To Springer Nature Singapure 2022.	E&TC	Dr Sagar Joshi	2022	Springer
38	"An Armur Mimus Multimodal Biometric System for Khosher Authentication,"	SCOPUS (Elsevier), Web of Science, ACM,IET]	E&TC	Dr Gayatri Amabdkar	2022	Scopus
39	Performance analysis of machine learning algorithm of detection and classification of brain tumor using computer vision	Advances in Engineering Software	E&TC	Dr Ashwini Shinde	2022	Scopus

40	Determining optimal parameters using Taguchi's design of experiments (DOE) for improving the quality of biogas generation process	Engineering Research Express	Mechanical Engg.	Satish R More	2022	Scopus
41	Parameter Dependencies and Optimization of True Random Number Generator (TRNG) using Genetic Algorithm (GA)	ICSCC 2021	E&TC	Dr. Vilas Deotare	2021	IEEE Explore
42	Deep learning based person authetication using Hand radiographs	IEEE xplore	E&TC	Dr Sagar Joshi	2020	SCI
43	Forensic approach of human identification using dual cross pattern of hand radiograph	Intelligent Systems Design and Applications	E&TC	Dr Sagar Joshi	2020	WoS
44	Forensic Human Identification using Dual Cross Patterns of Dental Panoramic Radiographs	Helix International Journal	E&TC	Dr Sagar Joshi	2020	WoS

Scopus	33
SCI	4
Springer	3
WoS	3
1	1

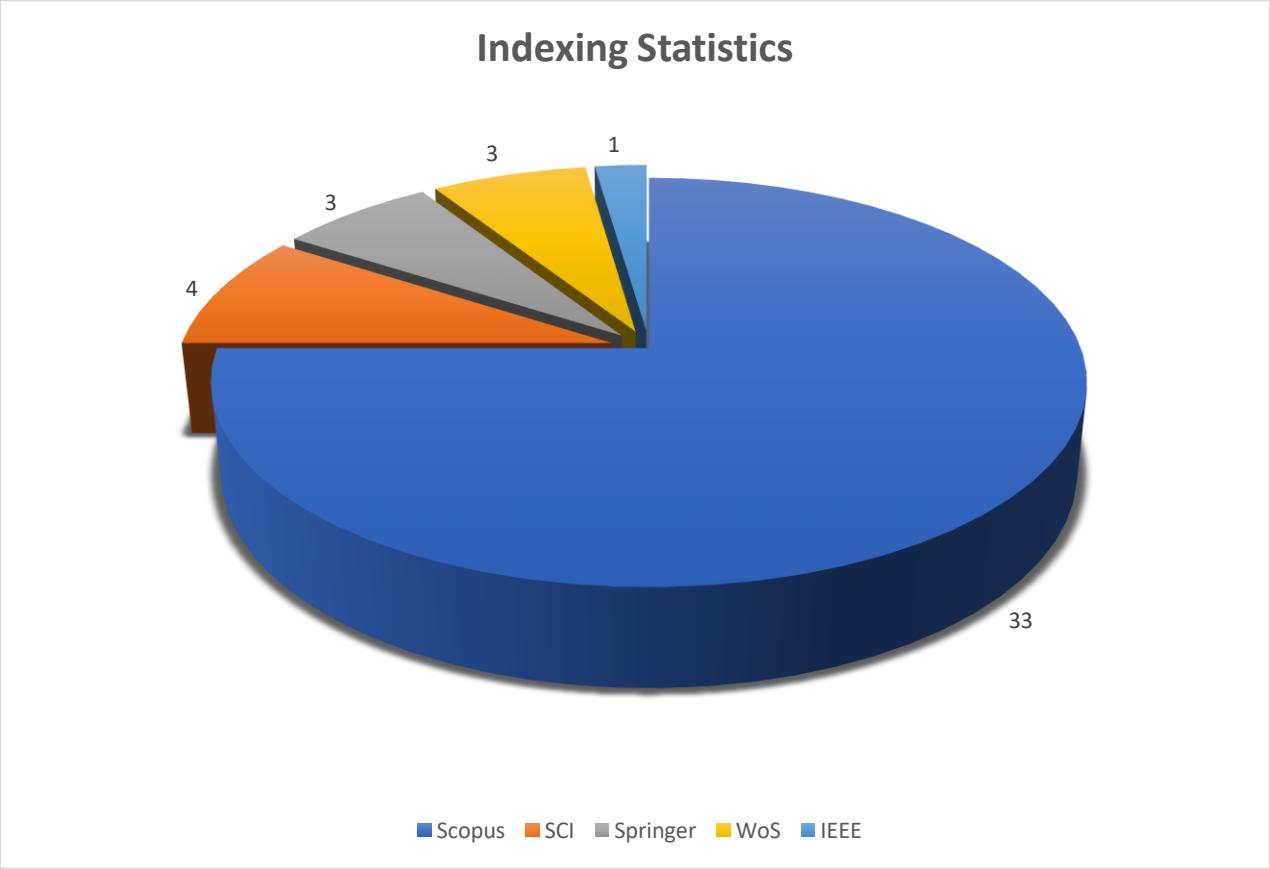

PAPER PUBLICATIONS

www.nmiet.edu.in

Indonesian Journal of Electrical Engineering and Computer Science
Vol. 33, No. 3, March 2024, pp. 2007∼2014
ISSN: 2502-4752, DOI: 10.11591/ijeecs.v33.i3.pp2007-2014

SEM and TEM images' dehazing using multiscale progressive feature fusion techniques

Chellapilla V. K. N. S. N. Moorthy[1], Mukesh Kumar Tripathi[2], Suvarna Joshi[3], Ashwini Shinde[4], Tejaswini Kishor Zope[5], Vaibhavi Umesh Avachat[5]

[1]Department of Mechanical Engineering, Vasavi College of Engineering, Hyderabad, India
[2]Department of Computer Science and Engineering, Vardhaman College of Engineering, Hyderabad, India
[3]Department of Computer Science and Engineering, MIT ART, DESIGN and Technology University, Pune, India
[4]Department of CSE - Artificial Intelligence, Nutan College of Engineering and Research, Pune, India
[5]Department of Computer Science and Engineering, Nutan College of Engineering and Research, Pune, India

Article Info

Article history:

Received Oct 29, 2023
Revised Nov 30, 2023
Accepted Dec 26, 2023

Keywords:

Feature enhancement
Fusion
Image dehazing
Image restoration
Progressive feature

ABSTRACT

We present a highly effective algorithm for image dehazing that leverages the valuable information within the hazy image to guide the haze removal process. Our proposed algorithm begins by employing a neural network that has been trained to establish a mapping between hazy images and their corresponding clear versions. This network learns to identify the shared structural elements and patterns between hazy and clear images through the training process. To enhance the utilization of guidance information from the generated reference image, we introduce a progressive feature fusion module that combines the features extracted from the hazy image and the reference image. Our proposed algorithm is an effective solution for image dehazing, as it capitalizes on the guidance information in the hazy appearance. By combining the strengths of deep learning, progressive feature fusion, and end-to-end training, we achieve impressive results in restoring clear images from hazy counterparts. The practical applicability of our algorithm is further validated by its success on benchmark data sets and real-world SEM and TEM images.

This is an open access article under the CC BY-SA license.

Corresponding Author:

Mukesh Kumar Tripathi
Department of Computer Science and Engineering, Vardhman College of Engineering
Hyderabad, India
Email: mukeshtripathi016@gmail.com

1. INTRODUCTION

The progressive feature fusion module is designed to iteratively merge the hazy and reference image features, gradually refining the fused features. This enables a more comprehensive exploration of the guidance information, improving results in restoring the clear image. By incorporating the fused elements into the image restoration module, we effectively utilize the guidance information to enhance the quality of the dehazed output. Crucially, all the proposed modules are trained end-to-end, enabling seamless integration and optimization of the entire dehazing pipeline. Our extensive experimentation demonstrates that the proposed deep pre-dehaze, in conjunction with the progressive feature fusion module, significantly contributes to haze removal. We evaluate our algorithm on widely-used dehazing benchmark datasets and real-world hazy images and compare its performance against state-of-the-art methods. The results unequivocally demonstrate the superiority of our approach, as our algorithm consistently outperforms existing techniques in image dehazing quality.

www.nmiet.edu.in

It will critically examine the evaluation metrics employed in the field, such as peak signal-to- noise ratio (PSNR) and structural similarity index measure (SSIM), to determine their effectiveness in measuring the quality of dehazed images. According to author [1]–[3], "O-HAZE" The algorithm aims to address the challenges associated with haze removal by utilizing a combination of dark channel prior and color attenuation prior. The authors introduce an optimization framework incorporating priors to estimate the haze transmission and atmospheric light in the hazy image. They also propose a haze-free image reconstruction method using the estimated information and atmospheric light. The O-HAZE algorithm employs a guided filter to refine the estimated transmission map and improve the dehazing results. The "O-HAZE" algorithm presents a novel approach to image dehazing by combining the dark channel prior and color attenuation prior. The algorithm demonstrates significant haze removal and image quality improvements, as validated through extensive experimental evaluations on benchmark datasets. Haze, which arises from atmospheric conditions or other factors, poses a significant challenge to image quality, resulting in obscured details and reduced visibility. The need to overcome this challenge is vital across various fields, such as computer vision, remote sensing and image [3]–[5]. To tackle this problem, our paper proposes a progressive image dehazing method that employs a systematic two-step approach. Our algorithm begins by focusing on extracting valuable guidance information solely from the input hazy image, eliminating the need for external data sources.

The survey will commence by providing a broad introduction to the field of image dehazing, encompassing an overview of its challenges and diverse applications. Moreover, the survey will address the evaluation metrics commonly employed in the field to measure the quality of dehazed images, such as the PSNR and SSIM. The effectiveness of these metrics will be critically evaluated, considering their ability to assess the visual quality of dehazed images accurately. The proposed algorithm focuses on improving the performance of dehazing models by leveraging the benefits of multi-model fusion. The authors introduce a framework that combines multiple deep-learning models to enhance the dehazing process. The "deep multi-model fusion for single-image dehazing" paper introduces a novel deep learning-based approach that leverages multi-model fusion for improved single-image dehazing [6], [7]. By combining multiple models and dynamically weighting their predictions, the algorithm achieves enhanced haze removal and image quality performance. The experimental results validate the effectiveness of the proposed approach and highlight its superiority over single-model dehazing methods.

The author presents a novel approach for restoring hazy videos using a learning-based framework [8], [9]. The algorithm's objective is to remove haze and improve the visibility of video sequences affected by atmospheric conditions. The results demonstrate that the algorithm effectively removes haze from video sequences and significantly improves the visibility and quality of the restored videos. Li *et al.* [10], Channegowda and Prakash [11] presents an innovative approach for dehazing images based on color- lines. The algorithm's objective is to remove haze and improve hazy image visibility effectively. The color lines represent the variations of color in hazy images caused by the presence of haze. By analyzing the color lines, the algorithm estimates the transmission map, meaning the haze amount in each pixel. Experimental evaluations on various hazy images demonstrate the effectiveness of the proposed algorithm in removing haze and improving image quality. Elmenabawy *et al.* [12] presents a comprehensive approach for indoor scene understanding using red green blue-depth (RGBD) images. The algorithm aims to perform semantic segmentation and support inference, enabling a better understanding of the indoor environment. The authors propose a two-step framework that combines segmentation and support inference. The segmentation step involves classifying each pixel in the RGBD image into predefined categories, such as floor, wall, ceiling, and objects. This is achieved by training a random forest classifier on a large dataset of labeled RGBD images. The support inference step focuses on determining the relationships between different surfaces in the scene. It infers the support relations, such as whether a surface supports another or is supported by it. This inference is based on geometric cues and physical constraints. The proposed algorithm incorporates local and global information to refine the segmentation and support inference results. Local cues include color, depth, and surface normal, while global cues consider the overall consistency and co-occurrence patterns of different scene elements. Extensive evaluations are conducted on various indoor datasets to assess the algorithm's performance. The results demonstrate its effectiveness in accurately segmenting indoor scenes and inferring support relationships. The "indoor segmentation and support inference from RGBD images" paper introduces a comprehensive framework for indoor scene understanding using RGBD images [13].

Tripathi *et al.* [14] addresses the challenge of estimating visibility in adverse weather conditions using a single image. The research aims to develop a method that can accurately predict visibility levels based

www.nmiet.edu.in

on the visual information in the picture. The author proposes a visibility estimation algorithm that leverages statistical analysis and image processing techniques. The algorithm utilizes contrast, color distribution, and image degradation to estimate visibility levels. Babu and Padma [15] introduces a novel approach for removing haze from a single image based on the dark channel prior. The research aims to develop an effective method to enhance visibility and restore precise details in hazy images. The authors propose that hazy images tend to have a low-intensity value in at least one-color channel in local areas with apparent objects. This characteristic, called the dark channel, is a powerful prior for haze removal. The algorithm utilizes the dark channel before estimating the atmospheric light and the transmission map, representing the scene's haze thickness. The research aims to develop a method that can effectively remove haze and restore precise details in hazy images. The authors propose that haze introduces spatially varying light attenuation in the image, leading to more information loss and reduced contrast [16], [17]. To address this, the algorithm leverages non-local image patch analysis to estimate the haze-free scene radiance. By considering the similarities between image patches, the algorithm identifies and groups similar patches to comprehensively understand the underlying scene structure. Densely connected pyramid dehazing network for image dehazing using a densely connected pyramid network presented by Abed *et al.* [18] and Hadi [19]. The research aims to develop a method that can effectively remove haze and restore clear details in hazy images. The authors propose a network architecture incorporating dense connections and a pyramid pooling module. The dense connections facilitate feature reuse and gradient flow, enabling the network to learn more robust representations. The pyramid pooling module captures multi-scale information to handle varying haze densities. The network is trained using pairs of hazy and clear images to learn the underlying mapping between them. During training, the network learns to identify the shared structures and patterns between hazy and clear images, enabling it to remove haze effectively. Experimental evaluations are conducted on benchmark datasets to assess the performance of the proposed network. The results demonstrate its effectiveness in removing haze, enhancing image clarity, and restoring details in hazy images.

The authors proposed all in one image dehazing (AOD)-Net architecture for image dehazing [20], [21]. This end-to-end trainable network combines both global and local information for accurate dehazing. The network consists of an encoder-decoder architecture with skip connections to capture and preserve low-level and high-level features. AOD-Net utilizes an atmospheric scattering model and a transmission estimation module to estimate the haze-free image and the transmission map, respectively. The results demonstrate its effectiveness in removing haze, enhancing image clarity, and preserving fine details in hazy images. AOD-Net outperforms existing methods in terms of dehazing quality and visual fidelity. In summary, the "AOD-Net: all-in-one dehazing network" paper presents an end-to-end trainable network for haze removal [22]. AOD-Net combines global and local information and incorporates an atmospheric scattering model, transmission estimation module, and adversarial and perceptual losses. Experimental results confirm its effectiveness in removing haze, enhancing visibility, and preserving image details. The proposed network surpasses existing dehazing quality and visual fidelity methods, making it a powerful tool for haze removal in various applications.

2. PROBLEM STATEMENT

This paper aims to develop an algorithm that can remove haze from an image. The proposed algorithm is a progressive image dehazing method that follows a two-step approach. In the first step, the algorithm explores useful guidance information from the input hazy image without relying on external data. In the second step, the algorithm develops a progressive feature fusion method that fuses the features extracted from the hazy image and the reference image generated in the first step. By combining these features, the algorithm can better solve the image dehazing problem. The proposed algorithm is designed to be trained end-to-end, and it has been tested on various benchmark datasets and real-world hazy photos. Experimental results show that the proposed algorithm outperforms state-of-the-art dehazing methods and can effectively remove haze from images.

3. PROPOSED WORK

Our proposed model addresses the problem at hand through a series of steps. Firstly, we begin with data pre-processing to normalize all pixel values, ensuring consistent and standardized input for the model. This step guarantees that the data is in a suitable format for further processing. Moving forward, we define the model architecture using the Py-Torch framework. This involves specifying the layers, connections, and

www.nmiet.edu.in

parameters that constitute the network. Additionally, we establish a loss function that measures the dissimilarity between the generated clear images and the ground truth clear images. This loss function serves as a guide for the model to learn and improve its image restoration capabilities. We use the pre-processed data and the defined loss function to train the model. The training process involves presenting pairs of hazy and clear images to the network, allowing it to learn and identify the underlying structures and common patterns shared between the two types of images. The model adapts and enhances its ability to accurately restore clear images from hazy inputs through repeated iterations of this training process. The progressive feature fusion (PFF) technique for image dehazing comprises multiple steps, providing an effective solution for haze removal. Once the model is trained, it can be employed to restore new hazy images. The network uses gray images as input and employs its acquired knowledge to generate corresponding clear photos. Applying the trained model to new data allows for the restoration of hazy pictures in an automated and efficient manner. Our model incorporates a PFF module to improve the restoration process further. This module aims to merge the extracted features from the hazy image with a reference image, facilitating a more comprehensive and effective restoration process. The model can produce more precise and visually enhanced results by incorporating additional information from the reference image. Finally, as a culmination of the PFF and the overall model training, the hazy appearance undergoes restoration, resulting in a clear and visually improved vision. Our proposed model integrates data prepossessing, defining the model architecture and loss function, training the model using hazy-clear image pairs, applying the trained model to new hazy images, incorporating a PFF module, and ultimately restoring the hazy vision to a clear and visually enhanced state.

The complete proposed architecture is presented in Figure 1. The resulting fused feature map is then employed to estimate the haze transmission map. The haze transmission map represents the degree of haze in each image pixel. This estimation is crucial for understanding the distribution and intensity of haze across the image. By accurately estimating the haze transmission, the dehazing algorithm can selectively remove haze and restore clarity to its appearance. With the haze transmission map at hand, the dehazing algorithm can remove the haze from the hazy appearance. By employing sophisticated techniques, the algorithm can effectively mitigate the harmful effects of haze, enhancing visibility and recovering the true colors of the scene. This step is crucial for improving the overall quality and visual appeal of the dehazed image.

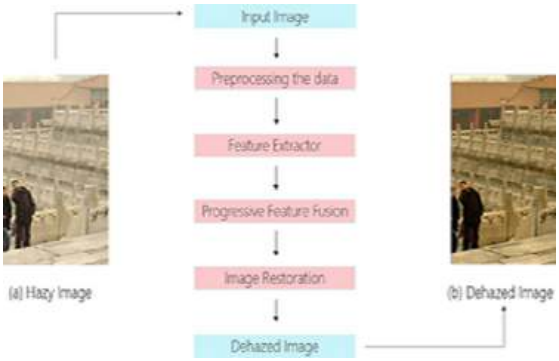

Figure 1. Block diagram of proposed architecture

4. EXPERIMENTAL STUDY

The RESIDE dataset, realistic single image dehazing, is a widely used benchmark dataset designed explicitly for image dehazing algorithms. It provides a comprehensive collection of hazy and corresponding ground truth clear images. The RESIDE dataset consists of three subsets: synthetic outdoor scenes (RESIDE SOTS), synthetic transmissions (RESIDE ST) [23], and haze removal in real-life hazy conditions (RESIDE HCI) [24]. Each subset focuses on different aspects of image dehazing.

- RESIDE SOTS: this subset contains synthetic hazy images generated by adding haze to diverse outdoor scenes. The ground truth clear images for evaluation are also provided.
- RESIDE ST: the synthetic transmissions subset focuses on generating accurate transmission maps. It provides synthetic hazy images and the corresponding accurate transmission maps as ground truth.

www.nmiet.edu.in

– RESIDE HCI: this subset focuses on real-world hazy images captured in various challenging conditions, including fog, smog, and haze caused by weather or pollution. The dataset provides both hazy images and corresponding clear reference images.

The RESIDE dataset offers a standardized evaluation platform for image dehazing algorithms. It allows researchers to compare and benchmark their algorithms against state-of-the-art methods using a diverse range of hazy images. The dataset enables quantitative assessment of dehazing algorithms based on objective metrics, such as PSNR and SSIM. Using the RESIDE dataset, researchers can develop and evaluate image-dehazing techniques that are effective in real-world scenarios. It provides a valuable resource for advancing the field of image dehazing and improving the quality of dehazed images [25] depicted in Figure 2.

Figure 2. Slots reside dataset

5. RESULTS AND TEST CASE ANALYSIS

The comparison focuses on indoor and outdoor images and evaluates the performance of the methods using two metrics, perceptual structural similarity index (PSIM) and SSIM. In image dehazing using PFF, several quality metrics can be used to evaluate the performance and effectiveness of the algorithm in removing haze and improving image clarity. Here are two commonly used quality metrics along with their formulas.

PSNR measures the ratio between the maximum possible power of a signal and the power of the distorted signal, representing the difference between the dehazed image and the ground truth clear image. It is computed as the logarithm of the mean squared error (MSE) between the two images. Where MAX is the maximum possible pixel value of the image (e.g., 255 for an 8-bit image), MSE is the mean squared error between the dehazed image and the ground truth clear image, calculated as the average of the squared pixel-wise differences. A higher PSNR value indicates better image quality and a closer resemblance between the dehazed image and the ground truth clear image.

SSIM measures the structural similarity between two images, taking into account the luminance, contrast, and structural information. It compares the luminance similarity, contrast similarity, and structural similarity between the dehazed image and the ground truth clear image. Where μx and μy are the average pixel values of the dehazed image and the ground truth clear image, respectively, σx, σy are the standard deviations of pixel values in the dehazed image and the ground truth clear image, respectively. σxy is the covariance between pixel values in the dehazed image and the ground truth clear vision. C1 and C2 are constants to stabilize the division. SSIM ranges from -1 to 1, where 1 indicates perfect similarity between the two images. These quality metrics provide objective measures to assess the performance of the PFF algorithm in image dehaz-

www.nmiet.edu.in

ing. Higher PSNR values and closer-to-1 SSIM values indicate better image quality and improved similarity between the dehazed image and the ground truth clear image. The Table 1 present comprehensively compares two image dehazing methods, namely dark channel prior (DCP) and PFF.

The results demonstrate that PFF outperforms DCP regarding the PSIM score for indoor and outdoor images. This indicates that PFF is more effective at removing haze from the pictures, resulting in more precise and visually appealing results. Moreover, the SSIM score also favors PFF, suggesting that it better preserves the structural information present in the images. The success of PFF can be attributed to its PFF approach, which enables superior feature extraction and fusion compared to DCP. Approach, which enables superior feature extraction and fusion compared to DCP. Specifically, PFF achieves an average PSIM score of 15.61, whereas DCP yields an average score of 19.63. Similarly, the average SSIM score for PFF is 0.853, surpassing DCP's average score of 0.848. These findings further support the notion that PFF is a more compelling image-dehazing method when compared to DCP. The implications of these results are significant, particularly for real-world applications that heavily rely on image dehazing, such as autonomous driving and surveillance systems. The ability to effectively remove haze directly impacts the performance and accuracy of such systems. Therefore, PFF's superior performance holds promise in enhancing these applications. However, it is essential to acknowledge that further experimentation is necessary to assess the algorithm's performance across a broader range of image datasets and various scenes. It is equally important to consider other factors, such as computational efficiency and real-time performance, for practical implementation in real-world scenarios. Consequently, the presented results should be preliminary evidence of PFF's potential as a compelling image-dehazing method. Nonetheless, these findings provide a promising direction for future research in image dehazing, with potential applications spanning various industries, including automotive, security, and entertainment. A loss function is defined to quantify the dissimilarity between the generated clear images and the ground truth clear images. This loss function guides the model during training to optimize its performance. The model is trained using pairs of hazy and clear outdoor images. The training process involves feeding the hazy images into the network and optimizing the model parameters to minimize the defined loss function. A PFF module is incorporated into the model. This module aims to fuse the extracted features from the hazy image with a reference image, facilitating a more comprehensive and effective restoration process. Once the model is trained, it can be applied to new hazy outdoor images for restoration. The network takes the hazy images as input and generates corresponding clear images by leveraging the knowledge acquired during training. The dehazed images are then evaluated using quality metrics such as PSNR and SSIM to assess the effectiveness of the progressive feature fusion approach.

Table 1. Results of quality metrics

Indicator	Quality metrics	DCP	PFF
Indoor	PSIM	20.079	15.60
Indoor	SSIM	0.85	0.86
Outdoor	PSIM	19.18	15.61
Outdoor	SSIM	0.83	0.84
Average	PSIM	19.63	15.60
Average	SSIM	0.84	0.85

6. CONCLUSION

The paper aimed to develop an algorithm that could effectively remove haze from an image using a progressive image dehazing method that followed a two-step approach. The proposed algorithm exploited useful guidance information from the hazy appearance in the first step and developed an advanced feature fusion method in the second step. The algorithm was designed to be trained end-to-end and was tested on various benchmark datasets and real-world hazy images. Experimental results showed that the proposed algorithm outperformed existing dehazing methods regarding PSIM and SSIM scores. The future scope of this paper includes further experimentation and testing of the proposed algorithm on a broader range of image datasets and scenes to evaluate its performance in various scenarios. Additionally, the proposed algorithm can be integrated into real-world applications that require image dehazing, such as autonomous driving, surveillance systems, and satellite imagery. The algorithm can be further optimized for faster and more efficient processing, and additional features can be added to improve its performance. Moreover, the proposed algorithm can be extended to handle other image enhancement tasks, such as denoising and contrast enhancement.

www.nmiet.edu.in

REFERENCES

[1] Z. Xie, Q. Li, S. Zong, and G. Liu, "Multiscale feature fusion deep network for single image dehazing with continuous memory mechanism," *Optik*, vol. 287, p. 171144, Sep. 2023, doi: 10.1016/j.ijleo.2023.171144.

[2] S. Tian, T. Zeng, W. Zou, X. Li, and L. Zhang, "DHIQA: quality assessment of dehazed images based on attentive multi-scale feature fusion and rank learning," *Displays*, vol. 79, p. 102495, Sep. 2023, doi: 10.1016/j.displa.2023.102495.

[3] Y. Liu *et al.*, "MFID-Net: multi-scaled feature-fused image dehazing via dynamic weights," *Displays*, vol. 78, p. 102416, Jul. 2023, doi: 10.1016/j.displa.2023.102416.

[4] M. K. Tripathi, D. Maktedar, D. N. Vasundhara, C. V. K. N. S. N. Moorthy, P. Patil, and Shivendra, "Residual life assessment (RLA) analysis of apple disease based on multimodal deep learning model," *International Journal of Intelligent Systems and Applications in Engineering*, vol. 11, no. 3, pp. 1042–1050, 2023.

[5] H. Al-Mahafzah, T. AbuKhalil, M. Alksasbeh, and B. Alqaralleh, "Multi-modal palm-print and hand-vein biometric recognition at sensor level fusion," *International Journal of Electrical and Computer Engineering*, vol. 13, no. 2, pp. 1954–1963, Apr. 2023, doi: 10.11591/ijece.v13i2.pp1954-1963.

[6] M. K. Tripathi and D. D. Maktedar, "Internal quality assessment of mango fruit: an automated grading system with ensemble classifier," *Imaging Science Journal*, vol. 70, no. 4, pp. 253–272, 2022, doi: 10.1080/13682199.2023.2166657.

[7] M. Radouane, N. I. Zouggari, A. Amraoui, and M. Amraoui, "Fusion of Gabor filter and steerable pyramid to improve iris recognition system," *IAES International Journal of Artificial Intelligence*, vol. 11, no. 4, pp. 1460–1468, Dec. 2022, doi: 10.11591/ijai.v11.i4.pp1460-1468.

[8] A. Eleyan, M. S. Salman, and B. Al-Sheikh, "Application of optimization algorithms for classification problem," *International Journal of Electrical and Computer Engineering*, vol. 12, no. 4, pp. 4373–4379, Aug. 2022, doi: 10.11591/ijece.v12i4.pp4373-4379.

[9] M. S. Alam, M. A. Morshidi, T. S. Gunawan, R. F. Olanrewaju, and F. Arifin, "Pose estimation algorithm for mobile augmented reality based on inertial sensor fusion," *International Journal of Electrical and Computer Engineering (IJECE)*, vol. 12, no. 4, pp. 3620–3631, Aug. 2022, doi: 10.11591/ijece.v12i4.pp3620-3631.

[10] X. Li, Z. Hua, and J. Li, "Attention-based adaptive feature selection for multi-stage image dehazing," *Visual Computer*, vol. 39, no. 2, pp. 663–678, 2023, doi: 10.1007/s00371-021-02365-2.

[11] A. B. Channegowda and H. N. Prakash, "Image fusion by discrete wavelet transform for multimodal biometric recognition," IAES International Journal of Artificial Intelligence, vol. 11, no. 1, pp. 229–237, Mar. 2022, doi: 10.11591/ijai.v11.i1.pp229-237.

[12] N. Elmenabawy, M. El-Seddek, H. E. Moustafa, and A. Elnakib, "Deep segmentation of the liver and the hepatic tumors from abdomen tomography images," *International Journal of Electrical and Computer Engineering (IJECE)*, vol. 12, no. 1, pp. 303–310, Feb. 2022, doi: 10.11591/ijece.v12i1.pp303-310.

[13] C. Kamlaskar and A. Abhyankar, "Multilinear principal component analysis for iris biometric system," *Indonesian Journal of Electrical Engineering and Computer Science (IJEECS)*, vol. 23, no. 3, pp. 1458–1469, Sep. 2021, doi: 10.11591/ijeecs.v23.i3.pp1458-1469.

[14] M. K. Tripathi, P. K. Reddy, M. Neelakantappa, C. V. Andhare, and Shivendra, "Identification of mango variety using near infrared spectroscopy," *Indonesian Journal of Electrical Engineering and Computer Science (IJEECS)*, vol. 31, no. 3, pp. 1776–1783, Sep. 2023, doi: 10.11591/ijeecs.v31.i3.pp1776-1783.

[15] M. C. G. Babu and M. C. Padma, "Semantic feature extraction method for hyperspectral crop classification," *Indonesian Journal of Electrical Engineering and Computer Science (IJECE)*, vol. 23, no. 1, pp. 387–395, Jul. 2021, doi: 10.11591/ijeecs.v23.i1.pp387-395.

[16] H. Elmannai and A. D. Al-Garni, "Classification using semantic feature and machine learning: Land-use case application," *Telkomnika (Telecommunication Computing Electronics and Control)*, vol. 19, no. 4, pp. 1242–1250, Aug. 2021, doi: 10.12928/TELKOMNIKA.v19i4.18359.

[17] V. Srisarkun and C. Jittawiriyanukoon, "Evaluation of weighted fusion for scalar images in multi-sensor network," *Bulletin of Electrical Engineering and Informatics*, vol. 10, no. 2, pp. 911–916, Apr. 2021, doi: 10.11591/eei.v10i2.1792.

[18] E. A. Abed, R. jassim Mohammed, and D. T. Shihab, "Intelligent multimodal identification system based on local feature fusion between iris and finger vein," *Indonesian Journal of Electrical Engineering and Computer Science (IJEECS)*, vol. 21, no. 1, pp. 224–232, Jan. 2021, doi: 10.11591/ijeecs.v21.i1.pp224-232.

[19] Q. A. A. Hadi, "Vein palm recognition model using fusion of features," *Telkomnika (Telecommunication Computing Electronics and Control)*, vol. 18, no. 6, pp. 2921–2927, Dec. 2020, doi: 10.12928/TELKOMNIKA.v18i6.16149.

[20] M. H. Hamd and R. A. Rasool, "Optimized multimodal biometric system based fusion technique for human identification," *Bulletin of Electrical Engineering and Informatics*, vol. 9, no. 6, pp. 2411–2418, Dec. 2020, doi: 10.11591/eei.v9i6.2632.

[21] M. K. Tripathi and Shivendra, "Neutrosophic approach based intelligent system for automatic mango detection," *Multimedia Tools and Applications*, pp. 1–23, Oct. 2023, doi: 10.1007/s11042-023-17037-7.

[22] E. M. Cherrat, R. Alaoui, and H. Bouzahir, "A multimodal biometric identification system based on cascade advanced of fingerprint, fingervein and face images," *Indonesian Journal of Electrical Engineering and Computer Science (IJEECS)*, vol. 17, no. 3, pp. 1562–1570, Mar. 2020, doi: 10.11591/ijeecs.v17.i3.pp1562-1570.

[23] M. K. Tripathi, M. Neelakantapp, A. N. Kaulage, K. V. Nabilal, S. N. Patil, and K. D. Bamane, "Breast cancer image analysis and classification framework by applying machine learning techniques," *International Journal of Intelligent Systems and Applications in Engineering*, vol. 11, no. 3, pp. 930–941, 2023.

[24] C. O. Ancuti, C. Ancuti, R. Timofte, and C. De Vleeschouwer, "O-HAZE: a dehazing benchmark with real hazy and haze-free outdoor images," in *IEEE Computer Society Conference on Computer Vision and Pattern Recognition Workshops*, 2018, vol. 2018-June, pp. 867–875, doi: 10.1109/CVPRW.2018.00119.

[25] S. Kim and H. Lim, "Fourth-order partial differential equations for effective image denoising," *Electronic Journal of Differential Equations (EJDE)[electronic only]*, vol. 17, pp. 107–121, 2009.

www.nmiet.edu.in

BIOGRAPHIES OF AUTHORS

Dr. Chellapilla V. K. N. S. N. Moorthy is working as Director RD, Vasavi College of Engineering, Hyderabad, Telangana, India. He received Master of Technology both in the fields of Computer Science Engineering and Heat Power Refrigeration and Air Conditioning. He received doctoral degree for research from GITAM University, and pursuing his doctoral degree in the field of machine learning too. He has research experience with a total research grant of 424.46 K USD from DST , government of India, more than 50 research publications, international research collaborations, awards and patents to his credit. His thrust areas of research include cognitive science, AI & ML and computational fluid dynamics. He can be contacted at email: krishna.turbo@gmail.com.

Dr. Mukesh Kumar Tripathi received a Ph.D. degree in Computer Science and Engineering from Visvesvaraya Technological University (VTU), Belagavi. He also received a B.E. degree in Information Technology from Guru Nanak Dev Engineering College, Bidar, India. He is working as Assistant Professor with the Department of Computer Science and Engineering , Vardhaman College of Engineering, Hyderabad, India. He has supervised and co-supervised more than five masters and 20 B.E. students. He is authored or co-authored more than ten publications and more than 245 citations. His research interests include soft computing, machine learning, intelligent systems, image processing, and Hyperspectral. He can be contacted at email:mukeshtripathi016@gmail.com.

Dr. Suvarna Joshi received a BE in Electronics Engineering and an M.Tech. (Electronics) from Shivaji University, Kolhapur. She completed her Ph.D. in Signal Processing from the Devi Ahilya University Indore. Currently, she is working as an Associate Professor at MIT School of Computing, MIT ADT University, Pune. She has published over 15 papers in international and national journals and conferences and issued four patents. Her research interests include image processing, machine learning, embedded systems, and pattern recognition. She has also got a few international patents and copyrights. She also received the National Education Excellence Award 2021 in Embedded Systems from IMRF. She can be contacted at email:arnaj2@gmail.com.

Dr. Ashwini Shinde received his B.E. in Electronics and Communication Engineering from Gogte Institute of Technology and M.E. in Electronics and Telecommunication Engineering from Kolhapur Institute of Engineering and Technology Kolhapur. She has completed his Ph.D. degree in 2020 from VTU Belagavi. She has published more than 15 papers in international and national journals and conferences and published 4 patents. She has a teaching experience of 15 years and currently she is working as an Associate Professor in Department of CSE-AI at NCER Pune. Her research interest includes machine learning, image processing, content-based image retrieval, and computer vision. She can be contacted at email: ashsshinde@gmail.com.

Tejaswini Kishor Zope received her B.E. in Computer Engineering From Nutan Maharashtra Institute of Engineering and Technology and M.Tech. in Computer Engineering from Pimpri Chinchwad College of Engineering Pune, Maharashtra in 2020 and 2022, respectively. In October 2021, she began her carrier in academics as lecturer. Currently she is working as an Assistant Professor in Department of Computer Science and Engineering, Nutan college of Engineering and Research Talegaon ,Pune. She has 2 years of teaching experience. Her research interest includes machine learning and image processing. She is a life member of Indian Society for Technical Education. She can be contacted at email: tejaswinizope@ncerpune.in.

Vaibhavi Umesh Avachat currently pursuing her M.E. in Information Technology from Pune Unversity and has received her B.E. in Computer Science Engineering From VIT, SRTTC in 2018 and Diploma in Information Technology from Nutan Maharashtra Vidya Polytechnic in she has published 2 papers in international and national journals. She started her teaching career in 2019 and is currently working in Nutan College of Engineering and Research since 1 year. She can be contacted at email: vaibhavia12@gmail.com.

www.mmet.edu.in
Soft Computing
https://doi.org/10.1007/s00500-024-09749-1

APPLICATION OF SOFT COMPUTING

Comparative research on block design-based protocol and blowfish for secured key generation and data sharing on cloud

Uma Hombal[1] · Dayananda Rangapura Basavaraju[2] · Ashwini S. Shinde[3]

Accepted: 9 February 2024
© The Author(s), under exclusive licence to Springer-Verlag GmbH Germany, part of Springer Nature 2024

Abstract
Confidentiality of maintaining the Electronic Health Records of patients is a major concern to both the patient and Doctor. Sharing the data on cloud is one of the most efficient technology infrastructures with extensive potential application, but at the same time there is a threat of hacking the data. Here we implement the concept for sharing of electronic health record on cloud that permits multiple members of the group to easily share the group data. With the increase in size of healthcare data the time and space complexity increases. The main challenge here is data security. This research article emphasis on a secured method for sharing the data on cloud and generation of the key that is safe from unauthorized user. In this Research article, we implement the soft computing approach for key agreement protocol using Block based design to support several users that can adapt it-self to upsurge the number of users in the cloud which depends on the assembly of the block design. This protocol generates a common conference key for all members. On comparing our results with some prevailing techniques, we accomplish that the results of our research have a better computational complexity.

Keywords Conference key · Fibonacci · Group formation · Scrambling factors · Third-party data control

1 Introduction

There are various techniques to improve data security for storage on cloud environment. Encryption is the most substantial method for data protection. Therefore, many available encryption algorithms are used to provide security, integrity, and authorized access.

However, they still have some limitations. Soft computing mainly includes rough set, genetic algorithm, neural network, fuzzy logic, particle swarm algorithm, and other parts, while compared with traditional hard computing, soft computing is closer to the objective things themselves, and human thinking more closely with more intelligent to complete the solution to the problem (Choudhury and Jha 2016).

One of the IT buzzwords today is Cloud Computing, most of the sectors and the entities in those sectors communicate with each other and get connected anytime and anywhere. This is due to the growing resources of computing facilities with integration scale and low cost. The development in cloud computing is an encouraging resolution and most appealing technologies for providing inescapable huge data storage and data analysis over the internet. Most of the corporate health service providers outsource the data to the cloud for efficient data sharing and its organization. But there are certain challenges while sharing the data on the cloud and most vital of the challenges is about an unintended leakage and attacks on the data in the cloud due to which this technology is getting vulnerable. Therefore, a highly secured system for data storage and sharing is been industrialized in this sector, to meet the purpose of the services and utilize the applications more effectively and efficiently (Golle et al. 2009). The

✉ Uma Hombal
uhombal@gmail.com

Dayananda Rangapura Basavaraju
dayanandarb@msrit.edu

Ashwini S. Shinde
ashsshinde@gmail.com

[1] Department of Computer Science and Engineering, KSIT, Bengaluru, India

[2] Department of Computer Science and Engineering, MSRIT, Bengaluru, India

[3] Department of CSE-AI, Nutan College of Engineering and Research, Pune, India

Published online: 05 July 2024

attacks on the cloud can be categorized into various categories, one is the security associated with network and computer intrusions, phishing cloud provider, vulnerabilities of cloud provider (Rampal Singh and Agrahari 2012), and forensics in the cloud. The other is the single point failure attack, server uptime issues, and the inability of a cloud provider to faithfully host and run the application. The most prevalent attack is the Third-party data control, the cloud behaves as a semi-trusted third party (Golle et al. 2009). Storage of Data is on the cloud and can be located anywhere within the cloud and hence precautions must be taken to defend the third-party attack on the data, therefore a highly erudite key generation algorithm is to be used to protect the data. The major concern is the way the third-party cloud service provider (CSP) pedals the data which is complex and not well revealed by the CSP (Ristenpart et al. 2009), also there is lack of confidentiality by introducing a third party that holds the data. Health care sector is extremely benefited with the progress in cloud technology, as the quality of their services is improved with reduced cost and low anxiety to the patients to maintain their records.

In this research, we present the comparative research on Blowfish and Block design-based key agreement protocol for sharing of medical record on the cloud for multiple participants which has to be secured from all type of attacks. The basic idea of generating the Common key is on the basis of the Diffie-Hellman protocol (1976), but this protocol is limited between two participants. In the proposed key agreement protocol, the number of participants can be extended as per desire and a common conference key is generated for all the members in the cluster. Here, the participants agree upon a key in advance and then the conference key is generated on the basis of agreement so that data sharing is done effectively and proficiently. This protocol guarantees that the challenger cannot get the created key by employing malevolent attacks. Hence, this protocol can be extensively utilized in collaborative communication along with a set of security constraints and access control that guarantee confidentiality, integrity, and privacy of medical information.

1.1 Related work

The literature survey done in this research article focuses on two main concepts, one on the techniques for storing private data on the cloud and the other part focuses on the techniques the researchers worked for secrete key generation and key sharing concepts.

In the years before from 2017 most of the researchers focussed on storing the data on cloud and sharing it using single owner key or with some challenges on Key sharing concepts. But after 2017 with the development of technology most of the research was focussed on Key generation and data sharing concepts. Zyskind et al. in (2015), applied the blockchain for admittance of control management and for the purpose of audit log security. The authors proposed a decentralized computation platform 'Enigma' which is a constructed on an enhanced kind of secure multi-party computation (sMPC). Therefore, here this allows the user members to save and execute the computations on data as well as maintaining the privacy of the entire data. Liu et al. in (2015) design a hybrid cloud architecture with resource-limited devices which supports sharing of data efficiently and securely, even though cloud provides as a gateway amongst the data user and cloud. Here the authors developed an architecture, with enhanced structure of attribute-based encryption. This technique is capable of giving the encrypted or the decrypted computation, that accomplishes appropriate access to the cloud and confidentiality of data utilization also with mobile handsets. Further the researchers also showed that this method reduces the computational complexity of the user, that is effectual for the user with inadequate devices. In the procedure of deputation, the client cannot reveal any data to the private cloud. This architecture with the help of anonymous key agreement is able to counterattack some attacks amongst data user and private cloud. Sendhil and Amuthan in their paper in (2021), obtained secure storage of data in cloud environment by implementing the Homomorphic Encryption, the authors utilized the cloudlet base medical system. Their system works in three steps initially the information of the entity is obtained from equipment are directed to supporting cloudlet. Next the information is sent to the cloud where the user gains it and utilize the same as per his/her convenience this is accomplished by trust level mechanism. Finally for transmission of information the researchers use the homomorphic encryption for information security this gave a three-stage protection. Yuliana et al. in (2019), worked on a key generation, the authors combined Multilevel Quantization with the Pre-Processing Method. The authors emphasized on decreasing the computational and communication cost by implementing simple key generation technique, they proposed a pre-processing technique known as modified Kalman (MK) and executed this with multilevel quantization, their method produced a simple SKG system for its substantial growth to create an indistinguishable undisclosed key amongst two valid users without data negotiation stage. The Key thus generated will go through six randomness tests of cryptosystems with very high confidence levels. Luo and Ma in (2019) worked on the issues of generating private key, the authors presented a certificateless hybrid sign crypto method without pairing, here by using the Elliptic Curve Computational Diffie-Hellman (EC-CDH) hypothesis in the random oracle model partial

www.nmiet.edu.in

private keys are generated for the users. They also implemented the key derivation method so that the user only requires to preserve the main key and need not be engaged in key management. Shen et al. in (2019a) addressed the problem of the third-party authentication. The authors also illustrated the potential of block chain in health care industry. Technical barriers, scalability and efficiency are the chief concerns. The problem to be addressed was about the storage space that is to be efficiently maintained since the current blockchain-based results are not much effective that share data from Internet-of-Things (IoT) devices. The authors proposed their data-sharing scheme as MedChain, it is a fusion of block chain, digest chain and structures network peer-to-peer (P2P) storage techniques. The fingerprint of data, operation and session that is stored by the block chain, that are unchallengeable while the P2P storage network saves the report of the data and session, which is variable. Hence the updating of the data description is easily done. Here a session is added in the process of data sharing for packing and eliminating the mutable information, this will effectively decrease storage overhead. During data sharing high efficiency and security requirements can be achieved by MedChain. In this paper it is studied that the awareness of Blockchain technology is only 43% for information sharing and among the 43% only 90% of the health care system actually use Blockchain technology. But the limitations are the data movement issue that can arise when a patient migrates to other city where inter-organizational data sharing is always to be maintained to get an access of the patents data from the prior hospital, this gives rise to additional overhead. This drawback can be addressed by making data transfer amongst two healthcare administrations. But as the records are in protection at healthcare system, the data transfer necessitates design at regulatory as well as the technical level. One more constraint is that patient's manually approval is required for the access of data, this intensifies the operation overhead of the access latency of the requester and the patient. Hence it can be concluded that during emergency this limitation may become a bottleneck in healthcare system. Therefore, in the upcoming years, a plan is to be developed to emphasis on data sharing systems through approved device like a smart phone, that can start a data sharing session on request by a doctor. This can be attained by including the associated conditions and rules constituted by clients. Besides, presently, MedChain still requires healthcare providers to physically complete the task of uploading the data streams to the directory and the blockchain service that is not effectual. This procedure can be enhanced by permitting fog and mobile devices to automatically generate and upload the information to the super-peers along with their data collection work. Alzahrani et al. in (2020) addressed the security issue by employing the decentralized Block Chain system; the authors have overviewed the potential of blockchain technique in the healthcare system. The authors also discussed that the implementation of technology in execution of healthcare services comes with many considerations that requires to be analysed widely to make the technologies operative. Agarwal in (2021) addressing and analysing together; data protection and privacy problems in storage of cloud for a dynamic group 1. User Authentication: utilizes Register User Tables (RUT). 2. User Key Generation: applies the randomized feature to generate and augment them to the user's table for the use in future. 3. Ticket Generation: Tickets are generated by Serialized function by the key authentication manager (KAM). 4. Encryption Services: The KAM abolishes device overhead by delivering file encryption services/messages. It is observed that with the larger size of the data the time complexity increases and as there is increase in the number of participants there is rise in time complexity exponentially. 5. Cost effectiveness for clients: encryption and decryption are necessary if the user's request to download or upload data from/to the server, due to numerous users, the customer/client system productivity is hindered and results in high cost. 6. Limited resistance to conspiracy: If any client 'A' collaborates to KAM, the data that are uploaded can be retrieved. Client 'B' can use the public key to first encrypt data that is to be communicated to the server and then with the session key. It offers increasing safety to the users but limits data sharing. Rajput and Ahvanooey in (2021) worked on the elimination of the third-party involvement. A tracking option is provided in the system for the patients to monitor the activities to their records. The researchers have developed a framework for healthcare management, this system provide a tamper protection application for safe policies by the use of blockchain technology, this helps to address the challenges concerning security and privacy, technology, incentives and governance that are related to data sharing issues. Hence, the authors here developed a system known as the personal health record (PHR) which allows clients to share and control data concerning their health conditions through specific people. In healthcare management system the implementation of blockchain technology may provide five features including: (i) data aggregation (ii) patient identity, (iii) data liquidity, (iv) data immutability and (v) digital access rules, that can address such challenges. The loop hole of this system is the time response for different entities is almost constant i.e. about 6000 ms but memory requirements for patient data storage is comparatively more. The authors have worked only on the prototype model, yet to be implemented on real time. Furthermore, since the PHRs are shared between various users, a standard like HL7 FHIR is required to assurance the data sharing security. Mahmoud and Mahmood in

(2021) developed a system for security between the server and the client, the result was the response time increased with the growth in number of devices associated to the cloud. But the system was overloaded, low-key encryption, and heterogeneity of numerous keying techniques. The authors make use of the m-cloud. Hence a distributed architectural proposal for e-health systems is the main feature of this work via m-Cloud that permit various devices to chat, shake hands, manage resources to effortlessly and transfer data between these devices. The system uses IoT devices by implementing different modules both at the sender and the receiver end such as handshaking, validating request and data encryption techniques. To deal with lightweight m-Cloud devices an additional security layer, with various cryptographic techniques, are added. And finally, the data are sent directly by the publisher to the demanding device and put on the HMAC/digital signature to authenticate the incoming data from a reliable user. The results of the research were with a centralized system average data transfer time is 0.60 ms, while it is reduced to 0.40 (ms) in a distributed technique with the same number of data requests. Likewise, it is observed that access time is decreased from 0.52 ms to 0.50 ms. The most disadvantage part is of the encryption technique on data before sending is not done and hence transfer of data are in plaintext and it surely increases the security challenges. Miao et al. in (2019), worked on the security considerations that are required to be addressed. The researchers employed the Searchable Encryption (SE) technique which is capable to facilitate searching of encrypted data. The authors developed a model to study the number of participants and size of data and called this as threat and security model, this system considers a cloud-assisted Internet of Everything (IoE). It is studied from the observations that though the time complexity is less with linear increase in type of data, number of participants but the cost and storage complexity are high. Awad Abdellatif et al. in (2020), worked on the enormous real-time data gathered from various health monitoring systems, that is required to be competently stored, managed, and shared. The concepts implemented in this research help to satisfying diverse security and privacy necessities, confirming distant availability of medical data by various approved entities while managing with the complication of data processing and transfer to understand low-cost healthcare and large-scale personalized medicine. Blockchain, Internet of Things (IoT), and Edge Computing are the concepts employed in this research article. Block chain matches the potentiality of edge computing as it is decentralized technique, that can successfully handle data storage and processing at various levels, along with their interconnection. Additionally, optimization of the blockchain parameters can be done with respect to block size, number of blockchain channels and transaction size, these can also be used for improving security and scalability. A significant characteristic is the multi-channel blockchain network, here every channel refers to a distinct chain of transactions and may be utilized for permitting data access and personal communications between the channel clients. By implementing such a perception, groups of patients or specific geographical areas and hospitals can share their data, hence guaranteeing secure data access and system scalability. The computational cost is high. Basically, only the security issue is addressed by this system and that depends on the priority of data. Maruthi Kumar in (2021), addressed the Security issue addressed caused due to IoT, the proposed model is created by the utilizing 1 level or by 2 level discrete wavelet transform steganography methods combined with encryption. AES and RSA crypto schemes are used for encryption. The new technique begins with the encryption of medical information and afterwards disguising it a cover picture utilizing 2-D discrete wavelet transform in 1 level or 2 level or 3 level. To hide diverse content sizes, we can utilize both grey and dim scale pictures as cover pictures. By using hybrid encryption technique in data transmission confidentiality, authentication, data integrity, non-repudiation of data can be improved. Steganography improves data imperceptibility which helps in reducing data manipulation attacks. The system implements a huge Decomposition Procedure of DWT-2L and Synthesis Procedure of DWT-2L, which rises the space and time complexity. Satar et al. in (2021), researched on Cloud issues regarding integrity and privacy of electronic healthcare record that occurred during the data sharing and outsourcing. The researchers worked on the Cyphertext Policy Attribute Based Encryption (CP-ABE) system by addition of two extra modules that its intention is to deliver fine-grained access control and give integrity and privacy of data, it also gives the facility for hashing and encryption schemes. If the cyphertext alters the decryption process is not enabled. The attribute authority defines the access policy so that framework confirms different user will have different access freedom this is termed as fine-grained access control. This technique is done with only the prototype. It has to be implemented on real time. Fang et al. in (2020), presented their work on Data access control mechanism and a data sharing framework. To support the selective sharing the authors used the semi-trusted servers. The proposed system consists of 4 attributes, Data Owner (includes patients and doctors), attribute authority, cloud server, and Data User. Here, a semi-trusted third party is used along with a cyphertext-policy attribute-based encryption system is utilized for security. In this system for accountability the authors proposed a system of watermarking, after modification of data, both doctors and patients should add digital watermarks related with their

www.nmiet.edu.in

credentials while uploading data. Cyphertext-policy attribute-based encryption (CP-ABE) are classified according to the number of participating entities. In the key-policy attribute-based encryption (KP-ABE) system, the cyphertext is embedded with attributes, and the access structure of the attributes is related with the private key. The decryption process takes place if structure of the key is satisfied by the attribute of the cyphertext. From the results it is evaluated that the time taken increases with increasing number of attributes in cyphertext, also there is delay in encryption and decryption of data.

Prior to discussion of the methodology implemented in this research we will go through some of the similar related work Shen et al. (2017) proposed the symmetric balanced incomplete block design (SBIBD), key agreement protocol that is used for multiple participants, here a common conference key K is generated. But the computational complexity of their protocol increases due to the $(v, k + 1, 1)$-block design, as the number of participants increase. In his proposed technique, Karimian et al. (2016) worked a new method of key generation that excerpts keys from ECG attributes. Nevertheless, this technique is solitary appropriate for ECG dependent applications. Zyskind et al. (2015), applied the block chain for admittance of control management and for the purpose of audit log security. The authors proposed a decentralized computation platform 'Enigma' which is a constructed on an enhanced version of secure multi-party computation (sMPC). Therefore, here this allows the user members to save and run computations on data while maintaining the privacy of the entire data. Xuejiao Liu et al. (2015), design a hybrid cloud architecture with resource-limited devices which supports sharing of data efficiently and securely, even though cloud provides as a gateway amongst the data user and cloud. Here the authors developed an architecture, with enhanced structure of attribute-based encryption. This technique is capable of giving the encrypted or the decrypted computation, that accomplishes appropriate access to the cloud and confidentiality of data utilization also with mobile handsets. Further the researchers also showed that this method reduces the computational complexity of the user, that is effectual for the user with inadequate devices. In the procedure of deputation, the user cannot reveal any data to the private cloud. This architecture with the help of anonymous key agreement is able to counterattack some attacks amongst data user and private cloud. Kumar and Srilatha in their paper (xxxx), obtained secure storage of medical data in cloud by implementing the Homomorphic Encryption, the authors utilized the cloudlet base medical system. Their system works in three steps initially the information of the entity is obtained from equipment are directed to supporting cloudlet. Next the information is sent to the cloud where the user gains it and utilize the same as per his/her convenience this is accomplished by trust level mechanism. Finally for transmission of information the researchers use the homomorphic encryption for information security this gave a three-stage protection. Mike Yuliana et al. (2019), worked on a key generation by combining the Pre-Processing Method with a Multilevel Quantization. The authors emphasized on decreasing the computational and communication cost by implementing simple key generation technique, they proposed a pre-processing technique known as modified Kalman (MK) and executed this with combination of multilevel quantization, their method produced a simple SKG scheme for its substantial growth in reciprocity so that an identical secret key amongst two valid users can be attained without going through the information reconciliation stage. The Key thus generated will go through six randomness tests of cryptosystems with very high confidence levels. Wei Luo et al. (2019) worked on the issues of generating private key, the authors presented a certificateless hybrid sign crypto method without pairing, here by using the Elliptic Curve Computational Diffie-Hellman (EC-CDH) assumption in the random oracle model partial private keys are generated for the users. They also implemented the key derivation method so that the user only requires to preserve the main key to get free of the key management. Alenoghena et al. (2022) Here the authors have done an comprehensive survey of various architectures and developments in mHealth using Blockchain, cloud and IoT. The authors suggested mHealth deployment in eHealth on mobile computing devices and wireless sensors in eHealth. They concluded that for ensuring the security of all eHealth systems there may be no single method.

2 Motivation

In most of the developing countries, as on date the patent has to carry all his health records by himself, and if it is lost or damaged then there is a huge expense to create or repeat the medical test again. One of the optimal solutions for this drawback is to share the health record on cloud. One of the major concerns in using cloud for medical information storage and information exchange is the security. In this research we have developed a cloud base health data sharing algorithm based on the Block Design. The cloud computing provides convenient on-demand access of the data. With the emergence of cloud computing, architectures of storing Electronic Health Record in cloud have been proposed. The majority of medical data is highly sensitive and strictly confidential; its storage on third-party servers naturally increases these vulnerabilities. Achieving security and privacy in EHR stored in cloud is very essential, as digitizing and sharing records may be prone to

various forms of attacks. From the existing approaches, it is apparent that most of the existing cryptographic approaches suffer from 1. Efficient data sharing. 2. Higher computational cost. 3. Complexity in key management and distribution. 4. Lack of privacy preserving mechanism. 5. Higher communicational cost. Hence there is a strong need to develop more secure and effective mechanism for accessing and sharing health data among stakeholders.

2.1 Objectives

The objective of this research work is to ensure secure data sharing within a group in health care.

System.

- To design and implement a framework that supports multiple participants.
- To generate a group key to improve efficiency and provide entity authentication services.
- To decrease the operational complexity this increases with the number of participants.

3 Methodology

In this research article, we have implemented the Block design-based key agreement protocol. Also, we have implemented the hybrid blowfish algorithm. In the block design-based algorithm on a public channel a key is created that is commonly used by all the members of the group this is termed as common conference key. Unlike other protocols that rely on the third party for generating one-to-many key sharing schemes, our protocol does not involve a third party for key generation and works on the many to many key generation systems. Hence the first threat of getting the key from an outsourced system is eliminated here. This part of research works in three phases, the initial phase is the Group formation implemented using the block design, the second phase is to generate the conference key, this is accomplished using the Fibonacci and scrambling factors that is adapted for Secrecy Protection, and finally the authentication phase which is implemented by the RSA algorithm. The results of our algorithm are compared with the novel Yi's algorithm (2004). Figure 1 gives the flow of the proposed research work.

3.1 Group formation

The group data sharing concept implemented in this research will not need a third-party authentication. The members of the group exchange message as per the construction of the block to fix a common conference key. Here, we plan to construct an algorithm with $(n, k + 1, 1)$

Fig. 1 Flow chart of the proposed research work

structure. This necessitates certain transformation to form the group data sharing model so 'n' members can contribute to execute the key agreement and the number of blocks. The appearance of each member in the block n is $k + 1$ times and each block hold $k + 1$ members. Likewise consecutive member appears concurrently in exactly one of the n blocks. The algorithm implemented for design of block is referred from Chung and Bae (2004) and Lee et al. (2006). The procedure for determining the number of members in the group is as follows:

Assumptions: $n = \{0, 1, 2\ldots, n-1\}$ signifies the set of n members, B = {B0, B1, B2, …Bn−1} indicates n blocks for n members, here every block holds $k + 1$ members.

Step 1 Selection of prime number 'k'.

Step 2 Number of members 'n' in the group is calculated as $n = k2 + k + 1$.

By assuming the organization of blocks as a matrix representation, the block for Bi,j indicates the member of ith block in the jth column, therefore Bi is defined by {Bi, 0, Bi, 1, ….., Bi, k}. The output of this block thus constructed is given by Bi, j for $i = 0.1,\ldots$, k2 + k and $j = 0, 1,\ldots, k$. Table 1 gives the algorithm for group generation. Thus, the design of the algorithm shows that the condition for $(n, k + 1, 1)$ is satisfied i.e. pair of members appears once in B and each member n appears '$k + 1$' times, hence these conditions are employed to develop the data sharing model.

3.2 Key generation phase

The key is generated using the model given as, the changes done on the Fibonacci series are by applying the modulo function which is stated in Eqs. (1) and (2).

www.nmiet.edu.in

Table 1 Pseudocode for Group formation

Algorithm for group formation
Step 1: while $i = 0$; $i \leq k$; "Repeat Steps 1 and 2 till condition is satisfied"
Step 2: while $j = 0$; $j \leq$ k;
Step 3: if $j =$ = 0
Step 4: Bi,$j = 0$;
Step 5: else $Bi,j = ik + j$;
Step 6: $i +$ +, $j +$ +; "Increment i,j by 1"
Step 7: End if
Step 8: while $i = k + 1$; $i \leq$ k2
Step 9: while $j = 0$; $j \leq k$;
Step 10: if $j =$ = 0;
Step 11: Bi,j = [(i−1)/k];
Step 12: Else Bi,j = jk + 1 (i−j + (j−1) [i−1%k]);
Step 13: $i +$ +, $j +$ +;
Step 14: End if

$$K1 = (a1 * a2 - a1\%a3) \quad (1)$$

$$K2 = (a1 * a2 - a1\%a3) \quad (2)$$

Similarly, for the ith value the equation for K_i is given by Eq. (3)

$$K_i = ((K_i - 1) + (K_i - 2) + 3 * i)\%a3 \quad (3)$$

Hence the application of the modulus function in the given model reduces the pattern of descending and ascending order. The pseudocode of this model is given Table 2. Hence producing a better random key sequence than produced by those of the unique Fibonacci sequence. Here in the proposed algorithm the scrambling factor $3*i$ is done in order to obtain a random sequence, the advantage of multiplication is to generate a changing number to produce a non-patterned number. Thus, generated key sequences more random by the addition of scrambling factor that clears the randomness test. Comparing these results with the different operators produce random numbers but the highest efficiency of generating random sequence is with multiplication. The operator of addition or subtraction gives linear output in ascending and descending order. On applying an exponential function, it results in high computational overhead, the operator of division when divided by zero leads to infinite numbers. The result of the comparison of various operator is illustrated in Fig. 2.

Table 2 The pseudocode for Key generation

Algorithm for Key generation
Step 1: Begin
Step 2: Initialize the parameters: a_1 a_2, n, a_3
Step 3: To Derive the 1st element of the key
Step 4: $K_{(1)} \leftarrow$ mod(a_1*a_2 – a_1, a_3)
Step 5: To Derive the 2nd element of the key
Step 6: $K_{(2)} \leftarrow$ mod(a_1*a_2 – a_2, a_3)
Step 7: To Derive the 3rd to n_{th} element of the key
Step 8: for $i = 3$ to n do
Step 9: $K_{(i)} \leftarrow$ mod(K(i − 1) + K(i − 2) + 3*i, a_3)
Step 10: end for
Step 11: Output the key sequence, K
Step 12: End

3.3 Group data sharing

In this research the authors implemented different algorithms for data sharing on cloud the first one is the pseudocode for reconstruction of the data and the second one is soft computing technique using two-layer encryption the first layer is of permutations with logical operations and the second layer inspired by structures of Genetic algorithm techniques.

Algorithm for group formation gives the structure of B, but since the same is to be applied for data sharing certain transformation of block B to E has to be done and this is accomplished as follows, the new structure E is reconstructed by the n blocks of B of (n, $k + 1$, 1) design, in a way that every block Et holds t members. It is observed from Fig. 1 that the characteristics of the reconstructed block 'E' are unaffected. The algorithm given in Table 3 is implemented to reconstruct E from B which is further used for data sharing.

Here the flag bit indicates that each block Bi is transformed, Bi = 1 if it is transformed else is 0. The procedure for reconstruction is as follows, 1) Initially the '$k + 1$' blocks [S0, S1,…, Sk] of B are transformed to '$K + 1$' block of E, B0 = E0 as there is no need of transformation, as the first elements of every block are same by definition (Satar et al. 2021). The next blocks to form E1 to Ek the

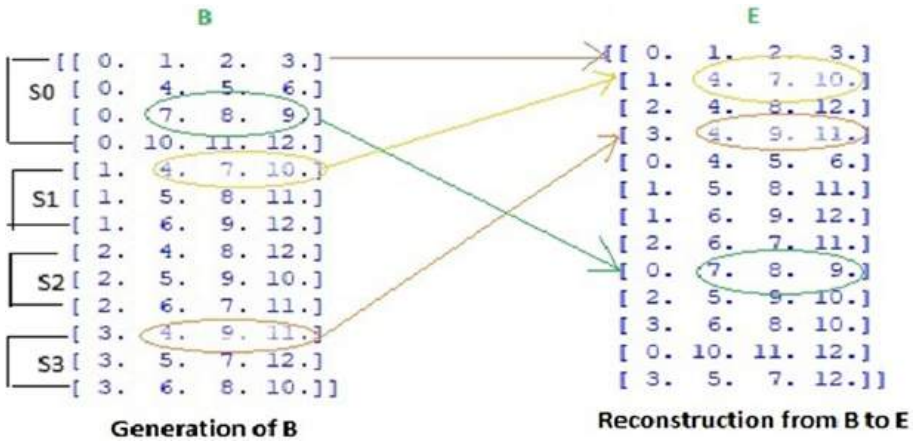

Fig. 2 Block Transformation for Group data Sharing (Shen et al. 2019b)

Table 3 Pseudocode for reconstruction of B to E

Algorithm for reconstruction of B to E
Step 1: E0 = B0;
Step 2: while $t = 1$; $t \leq k$; "Repeat the steps 3–7"
Step 3: $E_t = B_{tk} + 1$;
Step 4: $B_{tk} + 1$[flag] = 1;
Step 5: $E_{Et,t} = Bb_{(Et,t-1)/k}$;
Step 6: $B_{tk} + 1$[flag] = 1;
Step 7: t + + ;
Step 8: while $i-k + 1$; $I \leq k^2$; "Repeat steps 9 and 10
Step 9: if B_i [flag] $\neq$ 1 then
Step 10: $E_{Bi,b(i-1)/kc} = Bi$;
Step 11: i + + ;
Step 12: End if

transformation is given by Et = Btk + 1, ($1 \leq t \leq k$). The example of transformation is highlighted in Fig. 2 in oval shape with different colours. Therefore, by the reconstruction of E that satisfies the required property of (n, $k + 1$, 1) structure for data sharing.

The idea behind implementation of Genetic algorithm (GA) (Thabit et al. 2021) is that we have a biological cryptographic process. GA is implemented to solve optimization issues. The two-stage process is, one is to upload data and the other is to download data from the cloud. In the first layer logical operators are used for encryption with the plain text that is divided into subparts and the merging it with sub keys. The second layer is to convert the output of the first layer into genetic based. A similar approach is implemented for downloading the data from the cloud storage.

The encryption is done form the owner side here the owner encrypts the data before uploading. This involves the different steps like

(a) Reading the plain text and converting into ASCII code.
(b) Transformation into hexadecimal from integer.
(c) Conversion to binary from hexadecimal value.
(d) These binary nos are made to 64 bit sub blocks as B1, B2, B3 and B4. The two rounds of convolution take place and the next process of swapping is done during encryption. The result is a sequence of outputs for B1 to B4 as shown in Fig. 3 below.

The second layer is the genetic technique, the first step is to convert DNA base in the binary value, where $A = 00$, $T = 01$ $G = 10$ and $C = 11$, the next step is conversion in mRNA sequence the mRNA is then converted into tRNA, this is followed by reverse transcription where tRNA is transformed into RNA which is converted cypher text to binary to upload to cloud.

The Decryption Steps are the reverse of the encryption it is done once there is a request from the user and after validating the authenticating process. The decryption is again a two-stage process in the first stage the RNA is converted into logical mathematical functions and in the second step it is split into the original text.

3.4 Authentication phase

In this phase, we make sure that the members of the group are authentic as any of the malevolent member can extremely abolish the conference. It can also be called as different key attack. Here in the key attack a malevolent member creates a different signature by broad casting different sub keys in such a manner so the members in the group receive the signature of malevolent member and thus make him an authenticated member, thus different conference keys are released. This will make the protocol invalid by damaging the conference key. Hence an authentication phase is involved to avoid the various key attacks from malevolent members. The third-party authentication (TPA) ensures that there is no fault in the key transmission and the system is not attacked by the false

www.nmiet.edu.in

Fig. 3 The encrypted data after simulation

member this is accomplished by making sure by the TPA each member in the group generates an exclusive sub key to avoid the conference from getting attacked. Here, the identity of the TPA i.e. IDTPA ∈ {0,1}. The TPA selects one integerr g ∈ Zq and then every participant '*i*' requires to submit Ai = M_i^g to the TPA. Once when all the members in the group produce a common conference key the work of the TPA is to broadcast the exclusive serial number for the conference denoted by N given by N = H2 (ID1, ID2, ……, ID n, IDTPA,) along with the Ai that indicated authenticated sub key from every member the which ranges the value from 0 to $n-1$. The final step is done by each member to verify the genuineness of the common conference key K given by Eq. (4).

$$K^y = \Pi_{i=0}^{n-1} A_i \tag{4}$$

If Eq. (4) is satisfied there is no malicious member and if it comes to be false there is an attempt to damage the conference. The next stage is the fault detection phase, here the malevolent member is identified and eliminated from the group. l therefore, for the authentic member of the group which are termed as 'Ph' two conditions arise, that is when the LHS and the RHS of Eq. (4) are not equal and this is conveyed to the TPA and the search for the fault members begin which is given by Eq. (5).

$$M_i^g \neq A_i \tag{5}$$

Table 4 The steps involved to implement the blowfish algorithm

Step 1: Input for preprocessing
Step 2: Key generation by utilizing Blowfish algorithm on the client side
Step 3: The 64-bit data are divided into 32-bits for encryption
Step 4: Calculating the 4 S-boxes and P-arrays for data encryption
Step 5: To Upload the data on to the cloud
Step 6: MD5 algorithm is used to generate Message digest and output is stored in cloud
Step 7: At the other end, the encrypted data are downloaded from the cloud and de-added the message digest
Step 8: Decrypting the data by using Blowfish key
Step 9: The algorithm is analysed on the bases of two complexities: time and storage

Another technique implemented is the algorithm using the blowfish is given in Table 4 gives the process steps used implementing the blowfish algorithm.

The Blowfish algorithm has a variable length key of 32–448 bits and its a 64-bit block cypher. The two procedures involved in Blowfish algorithm are the: key initialization and the encryption phase for the data. A user variable key is expended in first phase to sub key arrays of 4168/8336-byte, which is existing with element arrays size of 4-byte or format arrays element size of 8-byte. The sub-key arrays (P entry-18 and four S arrays entry-256)

Table 5 Comparisons of characteristics of our proposed block design scheme with Yi's protocol

Characteristics	Proposed scheme	Yi's protocol
Type of communication model	Decentralized	Centralized
Message distribution type	Multicast	Broadcast
Computation per participant	2	$2(n-1)$
Modular exponentiation per participant	$7n\sqrt{n}$	2n
Computational complexity	O($nm2$)**	O(n2m2)
Communication complexity	O($n\sqrt{n}$)	O(n2)

Table 6 Blowfish algorithm results

Sr. no.	File size in bytes	Encrypted file size in bytes	Encryption time (ms)	Decryption time (ms)
1	1,216,841	2,197,245	60	77
2	581,469	1,052,530	10	16

Fig. 4 Simulation of decryption

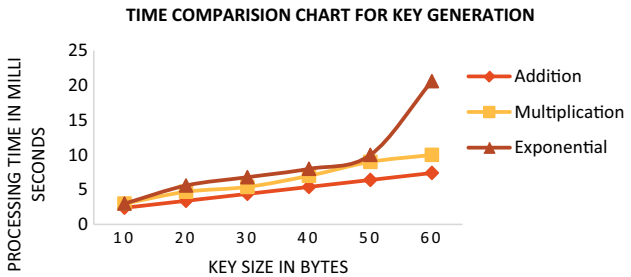

Fig. 5 The degree of randomness to generate the Key

generation process is user key dependent. There is an increase in the security level with the complexity enhancement of sub-keys and user key relation.

4 Results and discussion

The results of this research are obtained are by applying the algorithm in Python on a i7 processor with 8 GB RAM. Thus, obtained results are evaluated on basis of time and computational complexity.

4.1 Performance evaluation and results

Computational complexity which is defined by the operations performed and communication proficiently is defined by the no of participants and the length of message in the group are the two parameters to evaluate the performance. In every cycle of the protocol 'n' messages are received from 'n' members as per the block design of the protocol. The experiments in this research are carried out with open source Python programming language on an Intel Core i7 processor and the results when compared with the Yi,s algorithm (Karimian et al. 2016) yields promising results.

www.rimet.edu.in

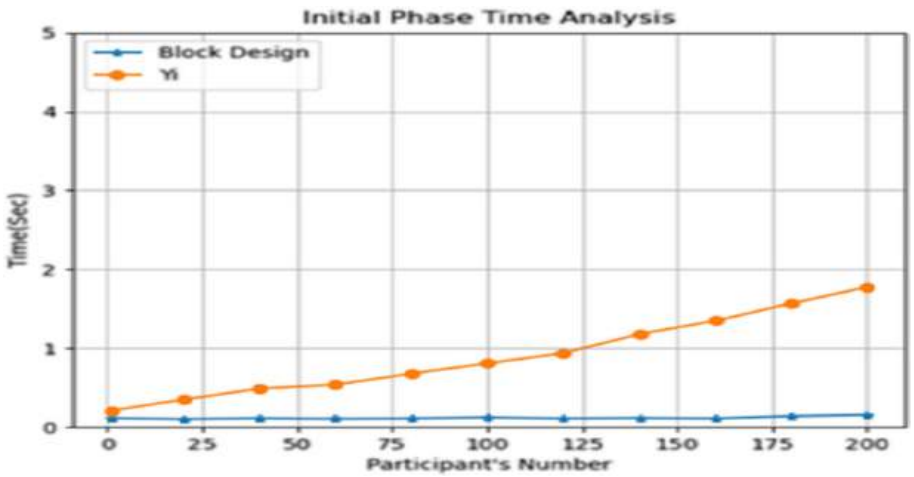

Fig. 6 Formation compared to Yi's algorithm

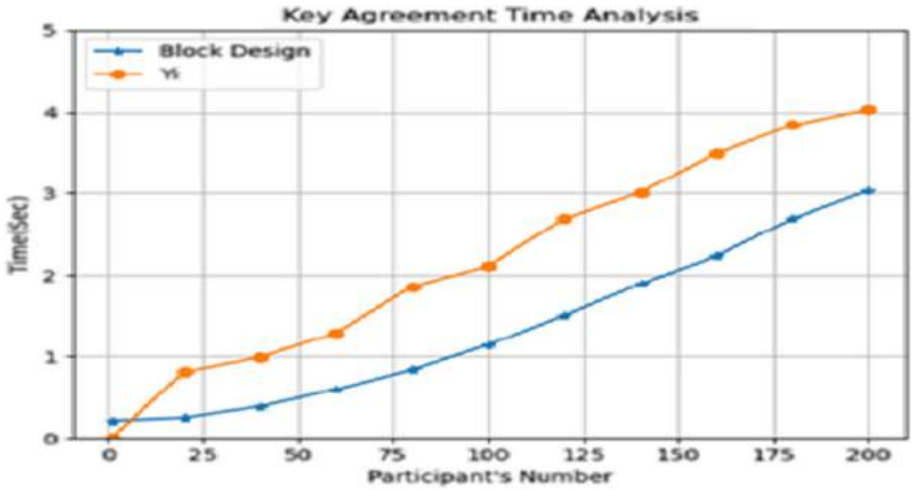

Fig. 7 Plot of Key agreement time analysis

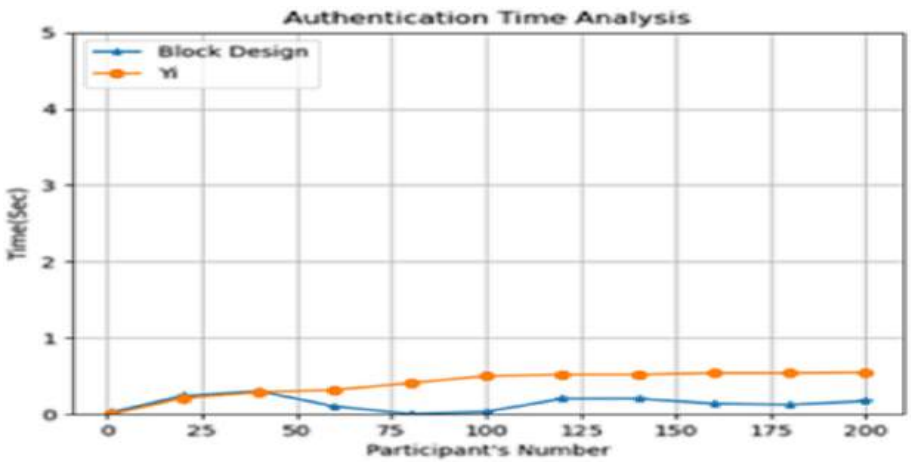

Fig. 8 Plot of authentication time analysis

The comparative analysis of the proposed scheme with the Yi's protocol is given in Tables 5 and 6. The Yi's protocol works of the fault tolerance to identify the dishonest member in the group. The Yi's protocol requires a semi-trusted member to bridge and receive the broad cast messages. It is termed as identity-based protocol that

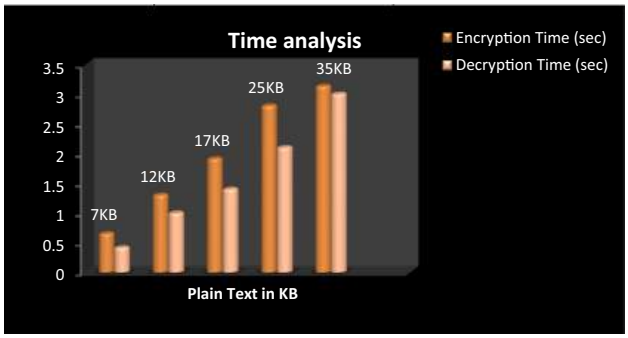

Fig. 9 Time analysis in GA algorithm

Table 7 Statics for genetic algorithm

Size of plain text (KB)	Encryption time (s)	Decryption time (s)
7	0.66	0.42
12	1.31	1.01
17	1.92	1.41
25	2.81	2.11
35	3.14	3.01
Average	1.96	1.59

implements the elliptic curve cryptography. The Yi,s scheme implements a centralized model using the TPA and conference bridge B i.e. the semi-trusted third party. Also, the system is venerable to active and passive attacks.

4.2 Discussion

The key generation time of our proposed block design protocol with respect to different operations with the degree of randomness is illustrated in Figs. 3 and 4.

Figures 5, 6 and 7 give the comparative analysis of our proposed technique with the Yi's algorithm with respect to different phases (Karimian et al. 2016; Zyskind et al. 2015). Figure 4 illustrates the initial phase time analysis i.e. the time taken for the formation of the group with respect to the number of participant. From the plot it clearly indicates as the no of participants increase the time remains very low and constant, hence there is no time complexity. Figure 5 gives the plot of the key agreement phase that shows the linear rise in time as the number participants increase, whereas the Yi's protocol shows the random variation of time.

Figure 8 illustrates the authentication time comparison with the Yi's protocol, from the plot it is clear the time taken for attenuation is less compared to the Yi's protocol.

It is also been analysed that the novel parallel cryptographic algorithm, blending and changing from MD5 and Blowfish encryption schemes, which can upgrade security. This hybrid MD5- Blowfish system is created to defeat the shortcoming from symmetric block design and hash function schemes. In comparison to the hybrid RSA and MD5 algorithm. Figure 9 shows the algorithm in Time Analysis.

For the GA algorithm implemented the statics are given as shown in Table 7.

5 Conclusions

With the advanced technology in cloud computing and cryptography, group data sharing is become the most efficient and reliable technological source in every sector, commonly implemented by the medical systems. Key agreement protocols have significantly improved the efficiency and security of the group data sharing. The common conference key generated by our proposed protocol proves to protect the data from unauthorized users. In this research work we present a hybrid technique for key generation, data sharing and authentication which does not rely on the TPA but the members of the group themselves generate the common conference key. The time analysis of our proposed key agreement protocol with respect to key generation and authentication shows that as the members of the group increase the time taken for key generation is not altered also the time taken for authentication is unchanged as the participants of the group increase. Also, it is observed that the time complexity is minimum when GA is implemented and the network is highly secured.

On comparing the mentioned techniques that are the Blowfish and the block design the techniques used by block design has better time and space complexity. Additional layers of hybrid function can be involved for further increase in the data integrity and security.

Authors contribution All authors are approved for this work.

Funding No fund received for this project.

Data availability Not applicable.

Code availability Not applicable.

Declarations

Conflict of interest The authors declare that they have no conflict of interest.

Ethical approval and human participation No ethics approval is required.

Consent to participate Not applicable.

Consent for publication Not applicable.

www.mmet.edu.in

References

Agarwal P (2021) A safe and resilient cryptographic system for dynamic cloud groups with secure data sharing and efficient user revocation. Turk J Comput Math Educ 12(3):5164–5175. https://doi.org/10.17762/turcomat.v12i3.2144

Alenoghena CO, Onumanyi AJ, Ohize HO, Adejo AO, Oligbi M, Ali SI, Okoh SA (2022) eHealth: a survey of architectures, developments in mHealth, security concerns and solutions. Int J Environ Res Public Health 19:13071. https://doi.org/10.3390/ijerph192013071

Alzahrani AGM, Alenezi A, Mershed A, Atlam H, Mousa F, Wills G (2020) A framework for data sharing between healthcare providers using blockchain. https://doi.org/10.5220/0009413403490358

Awad Abdellatif A, Al-Marridi AZ, Mohamed A, Erbad A, Fabiana Chiasserini C, Refaey A (2020) SSHealth: toward secure, blockchain-enabled healthcare systems. arXiv e-prints, arXiv:2006. https://doi.org/10.1109/MNET.011.1900553.

Choudhury B, Jha R (2016) Soft computing techniques. Soft computing in electromagnetics: methods and applications. Cambridge University Press, Cambridge, pp 9–44

Chung I, Bae Y (2004) The design of an efficient load balancing algorithm employing block design. J Appl Math Comput 14(1):343–351. https://doi.org/10.1007/BF02936119

Diffie W, Hellman M (1976) New directions in cryptography. IEEE Trans Inf Theory 22(6):644–654. https://doi.org/10.1109/TIT.1976.1055638

Fang L, Yin C, Zhu J, Ge C, Tanveer M, Jolfaei A, Cao Z (2020) Privacy protection for medical data sharing in smart healthcare. ACM Trans Multimed Comput Commun Appl (TOMM) 16:1–18. https://doi.org/10.1145/3408322

Golle P et al (2009) Controlling data in the cloud: outsourcing computation without outsourcing control. In Proceedings of the 2009 ACM workshop on Cloud computing security, pp 85–90. https://doi.org/10.1145/1655008.1655020

Karimian N, Guo Z, Tehranipoor M, Forte D (2016) Highly reliable key generation from electrocardiogram (ECG). IEEE Trans Biomed Eng 64(6):1400–1411. https://doi.org/10.1109/TBME.2016.2607020

kumar C, Srilatha D (2018) Cloudlet-based privacy preserving for securing medical data In Cloud by using homomorpic encryption technics. Int Sci Eng Res 9(12) ISSN 2229-5518

Lee O, Yoo S, Park B, Chung I (2006) The design and analysis of an efficient load balancing algorithm employing the symmetric balanced incomplete block design. Inf Sci 176(15):2148–2160. https://doi.org/10.1016/j.ins.2005.09.004

Liu X et al (2015) A secure and efficient data sharing framework with delegated capabilities in hybrid cloud. IEEE Trans Inf Forens Sec 10(11):2381–2395. https://doi.org/10.1109/SocialSec2015.13

Liu X, Xia Y, Xiang Y, Hassan MM, Alelaiwi A (2015) A secure and efficient data sharing framework with delegated capabilities in hybrid cloud. In 2015 International symposium on security and privacy in social networks and big data (SocialSec), IEEE, pp 7–14. https://doi.org/10.1109/SocialSec2015.13

Luo W, Ma W (2019) Secure and efficient data sharing scheme based on certificateless hybrid signcryption for cloud storage. Electronics 8(5):590. https://doi.org/10.3390/electronics8050590

Mahmoud AS, Mahmood NM (2021) A secure biomedical data sharing framework based on mCloud. Int J Nonlinear Anal Appl 12(2):1659–1671. https://doi.org/10.22075/IJNAA.2021.5295

Maruthi Kumar D, Sai Akhila N, Sarala P, Pavan Kumar A, Vijay Kumar B, Department of ECE SRI, Anantapur A (2021) Secure medical data transmission model for healthcare systems. Adv Trends Comput Sci Inf Technol 51

Miao Y, Liu X, Choo KKR, Deng RH, Wu H, Li H (2019) Fair and dynamic data sharing framework in cloud-assisted internet of everything. IEEE Internet Things J 6(4):7201–7212. https://doi.org/10.1109/JIOT.2019.2915123

Rajput AR, Li Q, Ahvanooey MT (2021) A blockchain-based secret-data sharing framework for personal health records in emergency condition. Healthcare. Multidisciplinary Digital Publishing Institute, p 206

Rampal Singh SK, Agrahari SK (2012) Ensuring data storage security in cloud computing. IOSR J Eng 2(12):17–21. https://doi.org/10.1109/IWQoS.2009.5201385

Ristenpart T, Tromer E, Shacham H, Savage S (2009) Hey, you, get off of my cloud: exploring information leakage in third-party compute clouds. In Proceedings of the 16th ACM conference on computer and communications security, pp 199–212. https://doi.org/10.1145/1653662.1653687

Satar SDM, Hussin M, Hanapi ZM, Mohamed MA (2021) Cloud-based secure healthcare framework by using enhanced ciphertext policy attribute-based encryption scheme. Int J Adv Comput Sci Appl 12:393–399. https://doi.org/10.34218/IJARET.11.12.2020.106

Sendhil R, Amuthan A (2021) Contextual fully homomorphic encryption schemes-based privacy preserving framework for securing fog-assisted healthcare data exchanging applications. Int J Inf Technol 13(4):1545–1553. https://doi.org/10.1007/s41870-021-00704-z

Shen J, Zhou T, He D, Zhang Y, Sun X, Xiang Y (2017) Block design-based key agreement for group data sharing in cloud computing. IEEE Trans Depend Sec Comput 16(6):996–1010. https://doi.org/10.1109/TDSC.2017.2725953

Shen B, Guo J, Yang Y (2019a) MedChain: efficient healthcare data sharing via blockchain. Appl Sci 9(6):1207. https://doi.org/10.3390/app9061207

Shen J, Zhou T, He D, Zhang Y, Sun X, Xiang Y (2019b) Block design-based key agreement for group data sharing in cloud computing. IEEE Transon Depend Secure Comput 16(6):996–1010. https://doi.org/10.1109/TDSC.2017.2725953

Thabit F, Alhomdy S, Jagtap S (2021) A new data security algorithm for the cloud computing based on genetics techniques and logical-mathematical functions. Int J Intell Netw 2:18–33

Yi X (2004) Identity-based fault-tolerant conference key agreement. IEEE Trans Depend Sec Comput 1(3):170–178. https://doi.org/10.1109/TDSC.2004.31

Yuliana M, Wirawan, Suwadi (2019) A simple secret key generation by using a combination of pre-processing method with a multilevel quantization. Entropy 21(2):192. https://doi.org/10.3390/e21020192

Zyskind G, Nathan O, Pentland A (2015) Enigma: decentralized computation platform with guaranteed privacy. p 114, arXiv:1506.03471 [cs], https://doi.org/10.48550/arXiv.1506.03471

Publisher's Note Springer Nature remains neutral with regard to jurisdictional claims in published maps and institutional affiliations.

Springer Nature or its licensor (e.g. a society or other partner) holds exclusive rights to this article under a publishing agreement with the author(s) or other rightsholder(s); author self-archiving of the accepted manuscript version of this article is solely governed by the terms of such publishing agreement and applicable law.

Journal of Discrete Mathematical Sciences & Cryptography
ISSN 0972-0529 (Print), ISSN 2169-0065 (Online)
Vol. 27 (2024), No. 2-B, pp. 809–820
DOI : 10.47974/JDMSC-1957

Mitigating DDoS attacks with an intrusion detection and prevention system based on 2-player Bayesian game theory

Sagar Vasantrao Joshi *
Department of Electronics & Telecommunication Engineering
Nutan Maharashtra Institute of Engineering and Technology
Pune
Maharashtra
India

Nanda Raghunath Wagh †
Department of Computer Engineering
Government Polytechnic
Pune
Maharashtra
India

Jambi Ratna Raja Kumar §
Department of Computer Engineering
Genba Sopanrao Moze College of Engineering
Pune
Maharashtra
India

Deepika Dongre ‡
Department of Artificial Intelligence and Data Science
Vishwakarma Institute of Information Technology
Pune
Maharashtra
India

* *E-mail:* sagarvjoshi@gmail.com (Corresponding author)
† *E-mail:* nandawagh@dbatu.ac.in
§ *E-mail:* ratnaraj.jambi@gmail.com
‡ *E-mail:* deepika.dongre@viit.ac.in

© Taru Publications

www.nmiet.edu.in

Nuzhat Rizvi [@]
Symbiosis Law School, Nagpur Campus
Symbiosis International (Deemed University)
Pune
Maharashtra
India

Mahua Bhowmik [#]
Department of Electronics and Telecommunication Engineering
Dr. D.Y. Patil Institute of Technology
Pune
Maharashtra
India

Abstract

Distributed Denial of Service (DDoS) attacks are very dangerous to the availability and security of networks, so they need improved ways to be stopped. This article suggests a new way to fight DDoS attacks that uses Intrusion Detection and Prevention Systems (IDPS) and 2-Player Bayesian Game Theory. Traditional IDPSs often have trouble responding quickly to changing attack tactics, which makes them less effective as defenses. The suggested structure, on the other hand, imagines the attacker and defense interacting as a Bayesian game. This lets them make proactive choices and come up with flexible ways to respond.The system uses Bayesian reasoning to describe the attacker's actions and plans' doubt, which lets it better assess the threat and decide how to respond. By constantly changing probability distributions based on what it sees attackers doing and what it sees defenders doing, the IDPS can quickly and effectively change its defenses to deal with new threats. The strategy contact between the attacker and the defense adds a competition factor that makes attackers less likely to start DDoS attacks by making them more expensive and risky. The proposed method works to stop different kinds of DDoS attacks while reducing the number of fake positives and negatives through a lot of simulations and experiments.

Subject Classification: *68M25.*

Keywords: *Lightweight cryptography, Financial transaction, Chaotic map algorithm, Lightweight ECC.*

1. Introduction

Distributed Denial of Service (DDoS) attacks are a major danger to the dependability and availability of networks and services online. Target

[@] *E-mail:* **nuzhatrizvi@slsnagpur.edu.in**
[#] *E-mail:* **mahua.bhoumik@dypvp.edu.in**

www.nmiet.edu.in

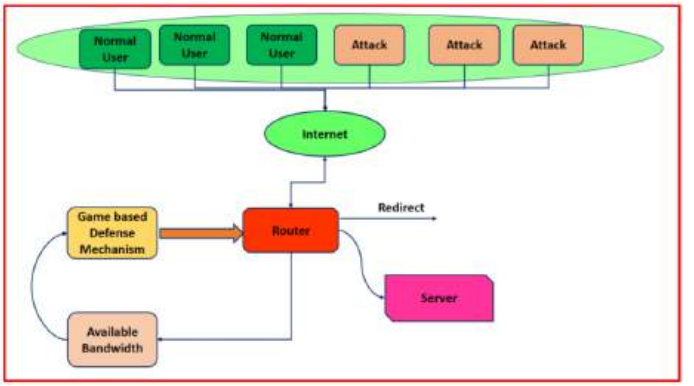

Figure 1

Network Consideration area for IDS and Prevention

systems are inundated with so much bad data from these hacks that normal users can't get to them. Due to their constantly changing and adapting nature, DDoS attacks are hard for traditional defense systems to effectively blunt [1]. In response, researchers and cybersecurity experts have looked into new ways to improve protection tactics, such as using game theory principles. Combining Intrusion Detection and Prevention Systems (IDPS) as shown in Figure 1 with 2-player Bayesian game theory is one way to do this. It looks like a good way to stop DDoS attacks. Bayesian game theory is basically a way to model how reasonable decision-makers can interact strategically with each other when they don't have all the knowledge they need about each other's actions and plans. In the context of cybersecurity, this means making defenses that are flexible enough to react to the changing strategies attackers use [2].

It is possible for guards to better spot and stop DDoS attacks [3] in real time by using Bayesian game theory in the creation of IDPS. This reduces the damage done to target systems and networks.This method works because it can simulate the inevitable doubt and planned behavior that both attackers and defenses experience in cyberspace. The IDPS can figure out if something going on right now is likely to be a DDoS attack by constantly looking at incoming network data and keeping an eye out for strange trends. Then, these [4] evaluations are used to help make smart decisions about how to use resources and put defenses in place.Also, because the Bayesian game is played by two people, the IDPS can change its defenses based on what it sees the enemy doing. This flexible reaction method lets the defender take advantage of the attacker's flaws and weaknesses, which makes it more likely that the DDoS attack will be

www.nmiet.edu.in

stopped. The [5] IDPS can also better tell the difference between good and bad network traffic by using machine learning algorithms and data-driven analytics. This makes it less likely that it will give fake positives or negatives. The combining Intrusion Detection and Prevention Systems with 2-player Bayesian game theory looks like a good way to stop DDoS attacks. By using probabilistic thinking and flexible defense tactics, this method helps guards deal with cyber threats that change and adapt, which makes important systems and infrastructure more resistant to DDoS attacks.

2. Proposed Method

2.1 *Game Theory Principles*

Game theory is a way to use math to look at how logical people make decisions and deal with each other in strategic situations. In cybersecurity, it gives an organized way to model how attackers and defenders act in situations where they are competing with each other. Players, tactics, payoffs [6], and Nash equilibria are some of the most basic ideas in game theory. Players choose tactics based on what they know about the methods other players have used and try to get the most out of the game for themselves. This approach is especially useful in cybersecurity, where attackers are always trying to get into systems and defenses are always trying to keep them safe [7].

2.2 *Bayesian Game Theory*

Bayesian game theory adds [8] doubt and missing knowledge to standard game theory, making it more thorough. In Bayesian games, players have their own ideas about what other players will do and how they play, and these ideas are changed based on what they see happen. Bayes' theorem is used to make this more formal by figuring out posterior probabilities based on past opinions and data that has been seen. Bayesian games [9] are a more realistic way to show how people make choices in changing and unclear settings. This makes them perfect for simulating hacking situations where attackers' goals and abilities aren't always known.

1. Bayes' Theorem:

$$P(S \mid O) = P(O \mid S) * P(S) / P(O)$$

www.nmiet.edu.in

2 Payoff Matrix:

$$Payoff\ Matrix = (GR; RR)$$

3. Utility Functions:

$$U_A(S_A, S_D) = R_A(S_A, S_D) - C_A(S_A, S_D)$$
$$U_D(S_D, S_A) = R_D(S_D, S_A) - C_D(S_D, S_A)$$

4. Strategic Selection:

$$S_A* = \arg\max \Sigma P(S_D \mid O) * U_A(S_A, S_D)$$
$$S_D* = \arg\max \Sigma P(S_A \mid O) * U_D(S_D, S_A)$$

2.3 *Bayesian Game Theory in Cybersecurity*

Bayesian game theory is being used more and more in cybersecurity to solve problems like detecting intrusions, analyzing malware, and stopping DDoS attacks. Researchers can make better defense strategies that react to changing threats by simulating the strategic interactions between attackers and defenders as a Bayesian game. Using Bayesian thinking, guards can make smart choices based on statistical assessments of how likely different attack scenarios are to happen. This makes it easier for them to predict and react to cyber dangers [10].

2.4 *Conceptual Framework for Integrating IDPS with 2-Player Bayesian Game Theory*

Combining Intrusion Detection and Prevention Systems (IDPS) with two-player Bayesian game theory looks like a good way to make cybersecurity defenses stronger. In this mental model, the IDPS is the defender. It constantly [11] watches network activity and uses Bayesian reasoning to keep its ideas about possible attacker tactics up to date. Based on the posterior odds, the guard then chooses tactics to stop the DDoS attack. The attacker, who is shown as the other player, wants to get the most money by choosing ways to avoid being caught and mess up the goal system. The IDPS can change its defense tactics on the fly to outsmart attackers and lessen the damage of DDoS attacks by using Bayesian logic to guide its repeated interactions.

$$P(S \mid O) = P(O)P(O \mid S) \times P(S)$$

www.nmiet.edu.in

3. Two Player Bayesian Game Theory

In two-player Bayesian game theory as shown in Figure 2, each player makes choices based on odds, even though they don't have all the facts. In cybersecurity, it helps defend against DDoS attacks by changing defense tactics on the fly. Defenders use [12] Bayesian thinking to guess what attackers might do and then change what they think based on what they see. This flexible method helps defenders use their resources wisely, take advantage of enemy weaknesses, and lower the number of fake positives and negatives. By constantly looking at and reacting to how threats are changing, two-player Bayesian game theory makes systems more resistant to DDoS attacks.

Algorithm for Two-Player Bayesian Game Theory in the Context of DDoS Attack Mitigation:

1. Initialization:

- Define the players: Defender (D) and Attacker (A).
- Set up the game parameters: strategies, payoffs, prior beliefs.

2. Prior Belief Update:

- Both players update their beliefs about the opponent's strategy using Bayes' theorem:

$$P(S_A \mid O) = P(O \mid S_A) * P(S_A) / P(O)$$

$$P(S_D \mid O) = P(O \mid S_D) * P(S_D) / P(O)$$

Where:

- $P(S_A \mid O)$ is the posterior probability of the attacker's strategy given observed outcome O.

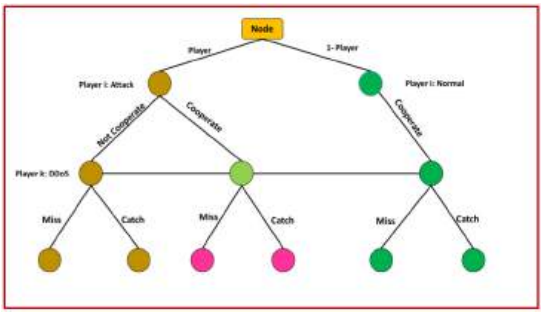

Figure 2

Two Play Extensive game between IDS and Node Data

www.nmiet.edu.in

- $P(S_D|O)$ is the posterior probability of the defender's strategy given observed outcome O.
- $P(O|S_A)$ and $P(O|S_D)$ are likelihood functions.
- $P(S_A)$ and $P(S_D)$ are prior probabilities.
- $P(O)$ is the total probability of the observed outcome.

3. Strategy Selection:

- Based on updated beliefs, each player selects their strategy that maximizes their expected utility:

$$S_A* = \arg\max \Sigma P(S_D|O) * U_A(S_A, S_D)$$
$$S_D* = \arg\max \Sigma P(S_A|O) * U_D(S_D, S_A)$$

Where:

- U_A and U_D are the utility functions representing the payoff for the attacker and defender, respectively.

4. Action Execution:

- The players execute their chosen strategies:
- Attacker launches DDoS attack using selected strategy S_A*.
- Defender deploys countermeasures using selected strategy S_D*.

5. Outcome Evaluation:

- Evaluate the outcome of the game based on the observed actions and their impact on system performance and security.

6. Learning and Adaptation:

- Update the prior beliefs based on the observed outcomes.
- Repeat steps 2-5 iteratively to adapt to the evolving threat landscape.

4. Result and Analysis

In Table 1, you can see how the selfish behavior percentage and the number of packets that were not sent change for three different protocols: Leach, S-Leach, and N-Leach, with different numbers of nodes. The selfish behavior rate and the number of packets that are not sent tend to go up as the number of nodes goes up.

www.nmiet.edu.in

Table 1

Summary Selfish percentage Vs Not sent packet

Nodes	Leach	S-Leach	N-Leach
10	140	160	200
20	145	200	268
30	160	215	283
40	175	230	298
50	195	250	318
60	350	405	473
70	480	535	603
80	550	605	673
90	800	855	923
100	1020	1075	1143

This is true for all protocols. There are, however, important changes between the protocols. This means that S-Leach and N-Leach might work better at preventing greed and making sure that packets get delivered in wireless sensing networks.

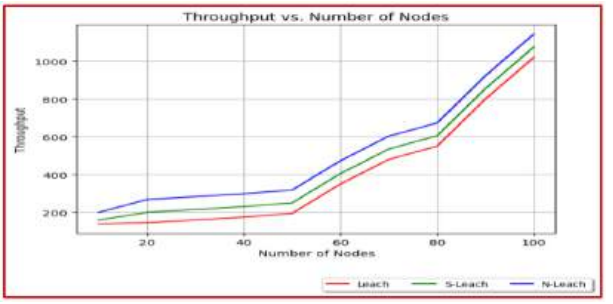

Figure 3

Representation of Selfish percentage Vs Not sent packet

When two people play a Bayesian game of intrusion detection, Table 2 shows the outcomes. The game compares three different protocols: Leach, S-Leach, and N-Leach. These methods are tested on a number of important factors that are needed to judge how well intruder detection systems work.The Detection Rate, which shows how many attacks were correctly discovered by the system, varies a lot between the algorithms. The best detection rate is shown by S-Leach, which is 92.35%. N-Leach is

www.nmiet.edu.in

Figure 4

Representation of Throughput Vs Time Taken

close behind with 95.63%, and Leach is last with 85.33%. In comparison to the Leach protocol, this shows that S-Leach and N-Leach are better at properly finding intrusions as shown in Figure 3 and 4. The False Alarm Rate, which shows the percentage of normal activities that are mistakenly reported as attacks, is also different for each procedure. N-Leach has the lowest False Alarm Rate, at 0.02%. Leach is next, at 0.11%, and S-Leach is third, at 0.13%. This means that N-Leach is the least likely to set off fake alarms, which makes it more reliable at telling the difference between regular and harmful actions.

Table 2

Result for2 playerBayesian game of intrusion detection

Parameter	Leach	S leach	N Leach
Detection Rate	85.33	92.35	95.63
False Alarm rate	0.11	0.13	0.02
Precision	92.35	95.32	97.14
Recall	86.45	92.45	95.63
F1 Score	89.74	93.65	96.47
Accuracy	95.45	97.85	98.8

Precision, which shows the percentage of correctly identified attacks out of all observed cases, keeps getting better across all of the protocols. is

www.nmiet.edu.in

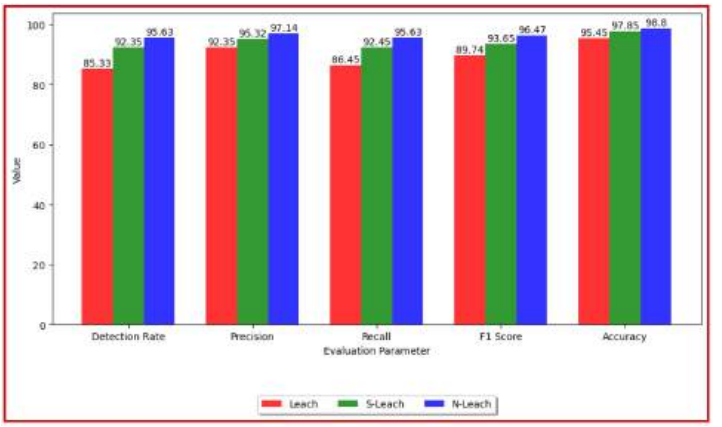

Figure 5

Evaluation Results of Intrusion Detection Protocols

shown in Figure 5. N-Leach has the best Precision (97.14%), followed by S-Leach (95.32%), and Leach (92.35%). This shows how well N-Leach works at finding and blocking attacks while reducing the number of false alarms.Recall, which shows the percentage of real attacks that the system properly discovered, also shows a similar trend. With a recall rate of 95.63%, N-Leach is the best, followed by S-Leach at 92.45% and Leach at 86.45%. This means that the N-Leach and S-Leach protocols are better at finding a higher rate of real attacks than the Leach protocol.Lastly, the F1 Score shows how well the intruder detection system worked generally. It is made up of Precision and Recall combined into a single measure. Once more, N-Leach has the best F1 Score (96.47%), followed by S-Leach (93.65%), and then Leach (89.74%).The test results show that adding Bayesian game theory to intrusion detection systems makes them work better. Specifically, the N-Leach and S-Leach protocols are better than the traditional Leach protocol at finding intrusions accurately and reducing false alarms.

5. Conclusion

Adding a 2-Player Bayesian Game Theory structure to Intrusion Detection and Prevention Systems (IDPS) seems like a good way to protect against Distributed Denial of Service (DDoS) attacks. By making the interaction between attackers and defenders look like a game, this approach makes it possible for defenses to change and react in ways that can effectively stop new DDoS attacks.Using Bayesian Game Theory, the

www.nmiet.edu.in

IDPS can keep changing its plans based on what it sees happening and how things turn out. This makes it easier and more accurate to find bad behavior. The fact that players work together makes it easier for defenders to be aggressive and stop strikes before they happen.Using Bayesian thinking also makes it easier for the system to make smart choices in settings that are unclear and change quickly, like those found in DDoS attacks. By taking into account statistical views about the enemy's plans and moves, the IDPS can make the best reaction to strikes while reducing the number of false positives.The addition of 2-Player Bayesian Game Theory to standard IDPS makes it more powerful and provides a strong defense against DDoS attacks. As cyber risks change, this method shows a lot of promise for making network systems more resilient and protecting them from attacks that get smarter over time.

References

[1] D. Patel and D. Patel, "PolyDDoSchain - Collaborative Volumetric Distributed Denial of Service Attack Detection and Prevention using Blockchain Technology," 2023 International Conference on Sustainable Computing and Smart Systems (ICSCSS), Coimbatore, India, pp. 1571-1578 (2023), doi: 10.1109/ICSCSS57650.2023.10169487.

[2] S. Vattikuti, M. R. Hegde, M. Manish, V. Bodduvaram and V. Saraswathi, "DDoS Attack Detection and Mitigation using Anomaly Detection and Machine Learning Models," 2021 IEEE International Conference on Computation System and Information Technology for Sustainable Solutions (CSITSS), Bangalore, India, 9683214. pp. 1-6 (2021).

[3] J. A. Pérez-Díaz, I. A. Valdovinos, K. -K. R. Choo and D. Zhu, "A Flexible SDN-Based Architecture for Identifying and Mitigating Low-Rate DDoS Attacks Using Machine Learning," in *IEEE Access,* vol. 8, pp. 155859-155872 (2020), doi: 10.1109/ACCESS.2020.3019330.

[4] N. Mishra and S. Pandya, "Internet of Things Applications, Security Challenges, Attacks, Intrusion Detection, and Future Visions: A Systematic Review," in *IEEE Access,* vol. 9, pp. 59353-59377 (2021), doi: 10.1109/ACCESS.2021.3073408.

[5] N. Kathirkamanathan, B. Thevarasa, G. Mahadevan, N. Skandhakumar and N. Kuruwitaarachchi, "Prevention of DDoS Attacks Targeting Financial Services using Supervised Machine Learning and Stacked LSTM," 2022 IEEE 7th International conference for Con-

www.nmiet.edu.in

vergence in Technology (I2CT), Mumbai, India, pp. 1-5 (2022), doi: 10.1109/I2CT54291.2022.9825228.

[6] Ajani, S. N., Khobragade, P., Dhone, M., Ganguly, B., Shelke, N., & Parati, N. Advancements in Computing: Emerging Trends in Computational Science with Next-Generation Computing. *International Journal of Intelligent Systems and Applications in Engineering*, 12(7s), 546–559 (2023).

[7] D. Radain, S. Almalki, H. Alsaadi and S. Salama, "A Review on Defense Mechanisms Against Distributed Denial of Service (DDoS) Attacks on Cloud Computing," 2021 International Conference of Women in Data Science at Taif University (WiDSTaif), Taif, Saudi Arabia, pp. 1-6 (2021), doi: 10.1109/WiDSTaif52235.2021.9430220.

[8] I. Riadi, Sunardi and A. Muhammad, "DDoS Detection Using Artificial Neural Network Regarding Variation of Training Function", *Advanced Science Letters*, vol. 24, no. 12, pp. 9163-9167 (2018).

[9] T. Mahjabin, Y. Xiao, G. Sun and W. Jiang, "A survey of distributed denial-of-service attack prevention and mitigation techniques", *International Journal of Distributed Sensor Networks*, vol. 13, no. 12, pp. 155014771774146 (2017).

[10] Limkar, Suresh, Ashok, Wankhede Vishal, Singh, Sanjeev, Singh, Amrik, Wagh, Sharmila K. & Ajani, Samir N. A mechanism to ensure identity-based anonymity and authentication for IoT infrastructure using cryptography, *Journal of Discrete Mathematical Sciences and Cryptography*, 26:5, 1597–1611 (2023).

[11] B. Susilo and R. Sari, "Intrusion Detection in IoT Networks Using Deep Learning Algorithm", *Information*, vol. 11, no. 5, pp. 279 (2020).

[12] B. Shah and B. H Trivedi, "Artificial Neural Network based Intrusion Detection System: A Survey", *International Journal of Computer Applications*, vol. 39, no. 6, pp. 13-18.

Advances in Nonlinear Variational Inequalities
ISSN: 1092-910X
Vol 27 No. 3 (2024)

Enhancing Diagnostic Accuracy: A Hybrid Approach to Mitigate Speckle and Rician Noise in Medical Images

Dr. Naveenkumar Jayakumar[1], Dr. Saurabh Saoji[2], Dr. Sagar V. Joshi[3], Prof. Hemlata Mane[4], Prof. Roshni Narkhede[5], Shrikant Jadhav[6]

[1]Associate Professor, Vellore Institute of Technology, Vellore, Tamilnadu
naveenkumar.jk@vit.ac.in

[2]Associate Professor, Department of Computer Engineering, Nutan Maharashtra Institute of Engineering and Technology, Talegaon Dabhade,Pune
saurabh.saoji@nmiet.edu.in

[3]Associate Professor, Department of Electronics &Telecommunication Engineering, Nutan Maharashtra Institute of Engineering and Technology, Talegaon Dabhade, Pune,
sagar.joshi@nmiet.edu.in

[4]Assistant Professor, Department of Computer Engineering, Nutan Maharashtra Institute of Engineering and Technology, Talegaon Dabhade, Pune
hemlata.mane@nmiet.edu.in

[5]Assistant Professor, Department of Computer Engineering, Nutan Maharashtra Institute of Engineering and Technology, Talegaon Dabhade, Pune
roshni.narkhede@nmiet.edu.in

[6]Assistant Professor, San Jose State University
San Jose, California, United States
shrikant.jadhav@sjsu.edu

Article History:

Received: *09-03-2024*

Revised: *03-05-2024*

Accepted: *29-05-2024*

Abstract:

This research explores the detrimental effects of Rician and speckle noise in medical imaging, particularly within MRI and radiographic modalities. Such noise can significantly obscure critical details, potentially leading to misdiagnoses and inaccurate measurements. Rician noise candidly dangles on the signal strength. Removing this noise affects the origial information in image that makes this noise removal perplexing. On other hand speckle noise is visualised like granular clog in ultrasound imageries. It creates ambiguous details and edges in the images. To address this challenge, the study introduces a novel hybrid method implemented in Java. The method employs a frequency-based decomposition approach for speckle noise and separates images into magnitude and phase components for Rician noise. This allows for targeted filtering, utilizing customized versions of median and Gaussian filters, to effectively remove noise while preserving crucial image features. The proposed method was rigorously assessed using 200 contaminated brain and lung MRIs and radiographs, demonstrating superior performance compared to traditional filters based on crucial system of measurement like Peak Signal-to-Noise Ratio (PSNR), Structural Similarity Index (SSIM), and Mean Squared Error (MSE). This research presents a promising solution for enhancing the quality and reliability of medical images, potentially leading to improved diagnostic accuracy and patient outcomes.

www.nmiet.edu.in

ISSN: 1092-910X
Vol 27 No. 3 (2024)

Keywords: Medical Images, Median Filter, Gaussian Filter, Speckle Noise, Rician Noise.

Introduction

Medical imaging plays a pivotal role in prevailing medical services, offering a minimally or no intrusive approach for detecting and observing assorted health ailments. However, image noise, such as Rician and speckle noise, can hinder accurate interpretation and limit the effectiveness of imaging techniques. Rician noise, prevalent in MRI scans, arises from the interference of two independent Gaussian noise sources, obscuring subtle details and potentially leading to misdiagnoses. It also impedes precise measurements crucial for assessing disease progression or treatment outcomes. Speckle noise, characteristic of radar and ultrasound images, manifests as a grainy disturbance that blurs details, making it challenging to distinguish between healthy and diseased tissue. This compromises diagnostic accuracy and restricts the applicability of ultrasound. In response to these challenges, this research presents a hybrid method for reducing noise in MRI and radiographic images. For speckle noise, the method employs a frequency-based decomposition approach to simplify the image and facilitate efficient processing. It then utilizes a noise reduction technique that preserves essential edge and texture information. To address Rician noise in MRI, the method separates the image into magnitude and phase components. Specific filters are applied to each component to remove noise without compromising critical edge details, ensuring image clarity while diminishing noise levels.

Developed using Java programming, this method was evaluated using ethically sourced hospital data. Its performance was compared against traditional filters using three quality metrics: peak signal-to-noise ratio, Mean Square Error, and Structural Similarity Index.

1.1 Literature Review

This research [1] explores noise's complex nature in terms of magnitude MR images. The main goal is to develop a precise and consistent language for discussing this issue, specifically discouraging the use of phrases such as "Rician noise" and "Rician noise bias." The researchers argue that it's not the noise, however, the measured intensities adhere to the Rician distribution. They caution against the phrase "Rician noise," as it suggests attributes not usually linked with noise, like dependence on signal strength, which can cause misunderstandings. Diverging from previous attributions, the authors posit that image noise stems from inherent Gaussian noise within the signals themselves. The researchers hope that their work will lead to more accurate and clear language when discussing these concepts in the future.

The research [2] delves into the theoretical underpinnings and mathematical methods used to tackle the challenges of stochastic data analysis within the Rice statistical model. In this model, the amplitude of the output signal consists of an initial desired value overlaid with a random Gaussian noise component. The study reveals that key features of the Rician signal, such as its average value and noise spread, are not directly related to the parameters of the Rice distribution. This insight led to the creation of a new method for analyzing stochastic Rician

data, which focuses on the simultaneous and accurate estimation of both the signal and noise components. By estimating the parameters of the Rice distribution together, this method effectively recovers the underlying significant signal in the presence of noise. Importantly, this method avoids the constraints associated with assumptions in traditional techniques. Numerical experiments validate the efficacy of this new method for analyzing stochastic data within the Rice statistical model.

Research papers [3] and [4] explore various strategies for reducing noise in low-dose CT imaging. They thoroughly investigate several techniques, including filtered back projection, denoising in the image-space, denoising in the projection-space, and iterative reconstruction. Both papers conduct a rigorous evaluation of these methods using a mix of quantitative and qualitative metrics. They also incorporate input from radiologists and real clinical cases to offer a well-rounded evaluation of the advantages and drawbacks of each technique. The papers probe the fine line between reducing noise and preserving the visibility of low-contrast lesions. They illustrate that while noise reduction techniques can significantly improve image quality, overdoing noise reduction might hide subtle details and potentially result in overlooked diagnoses. Hence, fine-tuning noise reduction algorithms to achieve the right balance is essential for effective low-dose CT imaging. The papers present the results of noise reduction at various levels, demonstrating the effect of different noise reduction intensities on image quality and diagnostic accuracy. They underscore the need to customize noise reduction strategies to specific clinical applications and patient characteristics.

The research [5] explores the extensive field of noise reduction methods in medical imaging, providing a detailed examination of the current state of research in this area. The authors carried out a comprehensive review of existing studies and commonly used algorithms for noise reduction, with a special emphasis on the anatomical areas targeted and the use of parallel techniques in research published from 2010 to 2022. Their analysis revealed a significant focus on anatomical areas such as the brain, bones, heart, breast, lungs, and visual system, indicating the primary areas of interest in noise reduction research. They also found 14 articles that employed parallel computing techniques for noise reduction, pointing to an emerging trend of harnessing computational power to address this issue. The authors conclude by highlighting the significant role of effective noise reduction in improving image quality, which in turn leads to more accurate and reliable diagnoses in medical imaging.

The paper [6] underscores the importance of Magnetic Resonance Imaging (MRI) in medical diagnostics and different types of noise like speckle, salt and pepper and Gaussian manifest in unique ways, posing diverse problems for image processing applications. To tackle these issues, the author introduces a modified median filter algorithm specifically tailored to eliminate noise from MRI images. The paper also investigates the use of the Adaptive Median filter (AMF) and the Adaptive Wiener filter (AWF) for noise reduction. The effectiveness of these filters is evaluated using the statistical metric Peak Signal-to-Noise Ratio (PSNR), while progressively increasing the noise density within the MRI image. The paper stresses that successful noise reduction in MRI images can significantly improve image quality, leading to more precise and efficient diagnoses in medical practice.

Reducing noise in MRI is a nuanced task that necessitates a tailored strategy based on the specific context. Acknowledging this complexity, the authors [7] delve deep into the details of noise filtering methods, offering a thorough analysis and classification. They provide valuable insights on choosing the most suitable technique for different situations. Furthermore, they present a case study illustrating the adaptation of an existing filter to enhance its efficacy in a particular MRI environment.

The research presented in [8] unveils an enhanced, unbiased non-local mean (NLM) filter specifically developed to address the challenge of noise removal in MRI images. The authors refine the NLM filter by integrating local noise statistics into its structure, resulting in an unbiased variant. They initiate the process by using wavelet decomposition to extract Gaussian noise details from the noisy image. Subsequently, they statistically model the wavelet coefficients leveraging the diagonal sub-band, to estimate the noise variance using the MAD estimator. The NLM filter is then applied to eliminate Rician noise by averaging boisterous pixels with a Gaussian weight factor. Lastly, they implement a noise bias subtraction method on the NLM-filtered pixels to restore the original values, yielding an unbiased output. Through experiments conducted on both real MRI and synthetic images, the authors demonstrate the efficacy of their approach. Their method surpasses existing non-local mean filtering schemes, delivering significantly improved results.

In their research [9], the authors devised a method using MATLAB to eliminate salt-and-pepper noise from brain MRI images. They conducted a comparative analysis of various median filtering techniques and discovered that the weighted median filter surpassed the others, exhibiting superior performance based on system of measurements like MSE (Mean Square Error), PSNR (Peak Signal-to-Noise Ratio), and SSIM (Structural Similarity Index). The weighted median filter achieved remarkable results with respective values of 0.0876, 58.9325, and 0.9893. Furthermore, the authors noted a robust performance from a median filter utilizing a kernel size of 3. A tabulated summary of pertinent literature is provided for reference.

Table 1: Literature Survey Summary

Article Reference No.	Problem Addressed	Methodology	Pros	Cons	Future Scope
[6]	Noise in MRI images	Modified median filter algorithm	Effective at removing Gaussian noise and Salt and pepper noise from MRI images	Limited to specific types of noise	Further research can be done to improve the algorithm and make it applicable to other types of noise
[7]	Noise in MRI images	Various filtering methods	Comprehensive review of different noise filtering approaches	Does not propose a new method	Future work can focus on developing new filtering methods

[8]	Noise in MRI images	Improved unbiased NLM filter	Effective at removing salt and pepper noise from brain MR images	Limited to specific types of noise	Further improvements can be made to the filter to handle other types of noise
[10]	Noise in MRI images	Average, median, and wiener filtering	Proposes a new technique to enhance the quality of MRI image by de-noising	Limited to Gaussian noise	Further research can be done to improve the technique and make it applicable to other types of noise
[11]	Noise in MRI images	Median and Gaussian filter, Max filter, Min filter, and Arithmetic Mean filter	Comprehensive review of different noise filtering approaches	Does not propose a new method	Future work can focus on developing new filtering methods
[9]	Noise in MRI images	Different types of median filtering techniques	Effective at removing salt and pepper noise from brain MR images	Limited to specific types of noise	Further research can be done to improve the technique and make it applicable to other types of noise

Reducing noise in medical images, specifically in magnetic resonance imaging (MRI), continues to be a hurdle due to the existence of speckle and Rician noise. While current methods such as modified median filters, adaptive filters, and enhanced unbiased NLM filters show potential, they often struggle with certain types of noise or lack adaptability across various situations. This indicates an exciting direction for future research: design and development of a fusion filter that syndicates the strengths of Gaussian and median filters. This hybrid approach seeks to benefit from the Gaussian filter's capacity to smooth noise while maintaining edges, along with the median filter's proficiency in eliminating noise bursts. Such a hybrid filter could provide a more resilient solution for managing the diverse noise patterns found in medical imaging.

Method

This research presents a unique hybrid filtering system designed to tackle two usual forms of noise in clinical Radiological or scan images: speckle noise and Rician noise. In contrast to conventional methods, this system uses order statistics filters, showing superior performance in reducing these noise artifacts. It works on Radiographic and MRI images of the human body, using standard Median and Gaussian filters along with newly developed "Advanced Median" and "Advanced Gaussian" filters. These advanced filters are customised to yield more precise results by incorporating specific characteristics of medical images. This groundbreaking

ISSN: 1092-910X
Vol 27 No. 3 (2024)

system offers a promising solution for improving the quality of medical images, potentially leading to more accurate diagnoses and enhanced clinical outcomes.

2.1 Proposed Approach Flow

This research introduces a new hybrid method designed to improve the quality of radiographic images and facilitate accurate diagnoses. The process, as illustrated in Figure 1, consists of several key stages:

1. **Input Image:** The system begins by obtaining a radiographic image, which is often tainted with speckle noise that can mask important details and hinder accurate diagnosis. The type of image (radiographic) determines the characteristics of the noise and requires specific filtering techniques. This stage may include pre-processing steps, such as converting to grayscale, to prepare for the following stages.
2. **Image Decomposition**: This step involves dividing the input image into multiple frequency-based sub-bands using methods like wavelet decomposition. Low-frequency bands capture smoother variations, while high-frequency bands contain edge and texture details. By focusing noise reduction efforts on the affected high-frequency bands, unnecessary processing is minimized, preserving vital details in the low-frequency bands.
3. **Total Variation (TV) Minimization**: This phase aims to maintain the true structure of the denoised image without introducing unwanted artifacts. It involves minimizing total variation, which measures changes in pixel values across the image. This process ensures a smooth, consistent processed image while effectively removing noise. Algorithms like Bregman iteration facilitate TV minimization.
4. **Speckle Noise Identification and Filtering**: To eliminate speckle noise, this phase uses a Rician distribution function to accurately model the behavior of speckle noise. Statistical analysis identifies pixels affected by speckle noise, preserving genuine image details while filtering noise using techniques like adaptive Wiener filtering or non-local means filtering.
5. **Noise Addition:** This phase simulates real-world scenarios by artificially adding noise to the original image, allowing the system to evaluate noise reduction algorithms under practical conditions. Noise levels are controlled within a range (1% to 100%).
6. **Filter Application:** This stage compares the performance of three different filters on the noisy image:
    a) Gaussian filter: A standard technique for smoothing noise, but it can blur edges and details.
    b) Median filter: Effective against impulsive noise but can also blur edges.
    c) Advanced filter: A novel proposal that combines the benefits of Gaussian and median filters while minimizing drawbacks, preserving edges and textures.

Advances in Nonlinear Variational Inequalities
ISSN: 1092-910X
Vol 27 No. 3 (2024)

7. Results Evaluation: This phase assesses filter performance by calculating two key metrics:
   a) Peak Signal-to-Noise Ratio (PSNR): Quantifies the improvement of the denoised image compared to the original, where greater values signify superior noise removal.
   b) Structural Similarity Index (SSIM): Assesses the structural similarity between the original and denoised images, with higher values signifying better preservation of image details and structures.

By comparing the PSNR and SSIM values for each filter, the system determines the filter that achieves the best balance between noise reduction and preservation of image details.

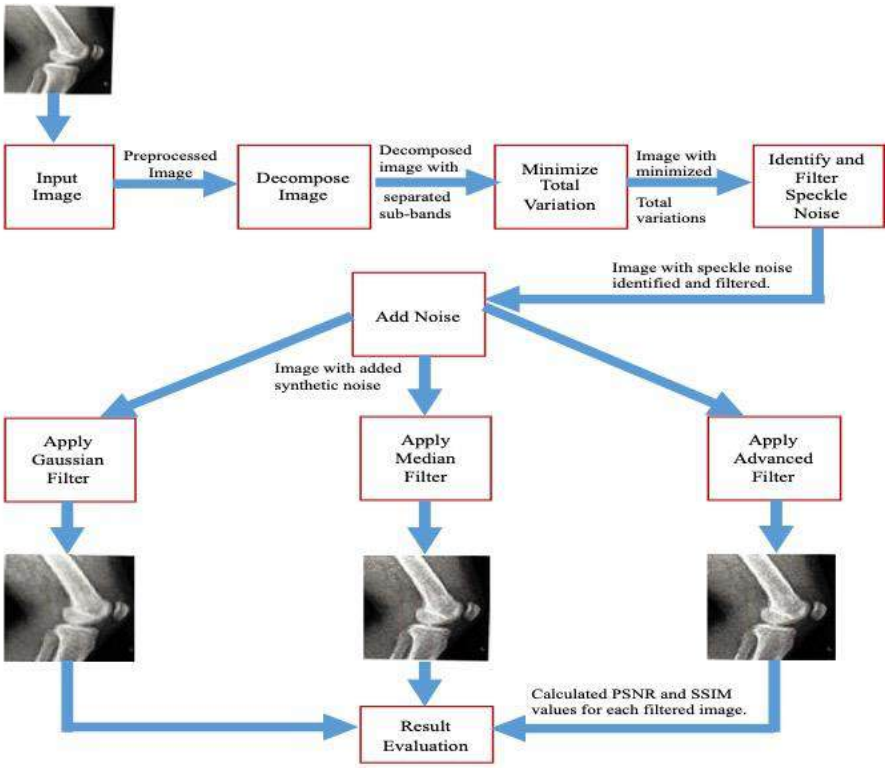

Figure 1: Proposed Approach

2.2 Proposed Advanced Filter Working

The advanced filter operates by examining the relationships between adjacent pixels in an image to eliminate speckle noise while maintaining edges and textures. It follows these steps:

a. Initialisation: The filter accepts the original noisy image as input and extracts the pixel values for the entire image.
b. Processing: The filter concentrates on the central part of the image, excluding the first and last rows and columns. It then processes each remaining pixel (x, y) individually.
c. Disparity Calculation: For each pixel, the filter calculates the difference between its value (G (x, y)) and the value of the pixel in the previous row and column (G(x-1, y-1)).

This difference, or disparity, indicates the potential presence of speckle noise at the current pixel.

d. Weighted Disparity Application: To balance noise reduction with edge preservation, the filter multiplies the calculated disparity by a factor of 0.5. This weighted disparity is then added to the unprocessed pixel value at coordinate (x, y) in the reference image [(G (x, y)).].

e. Updated Pixel Value: The filter replaces the original pixel value (G (x, y)) with the newly computed value, incorporating both noise reduction and edge preservation.

f. Image Updating: The filter repeats steps 3 to 5 for all pixels within the central part of the image.

g. Output: The filter produces a denoised image where each pixel value has been adjusted based on the advanced filter formula.

The advanced filter effectively removes speckle noise while maintaining edges and textures in medical images, leading to improved image quality and potentially more accurate diagnoses. The above key steps are shown in the below table 2

2.3 Implementation of Proposed Approach and Filter

Initially, the system selects an MRI image from a dataset comprising brain MRIs and radiographs. This image serves as the basis for demonstrating the noise removal process using various filters. To showcase the system's flexibility, noise can be introduced, adjusting it from 1% to a noisy 100%. For this testing, it is ramped up to 70%. Once the image is sufficiently noisy, the system applies different filters, presenting the processed versions alongside the original for a direct comparison. This allows to observe how each filter handles the noise and impacts the image. To rigorously evaluate the proposed method, 200 brain and lung MRIs and radiographic images were utilized, each contaminated with both Rician and speckle noise. Further three different filters were applied to each image and measured three key metrics: Peak Signal-to-Noise Ratio (PSNR), Structural Similarity Index (SSIM), and Mean Squared Error (MSE). This system of measurement aided in analyzing the effectiveness of each filter in eliminating the noise while preserving image details.

Table 2: Key Steps implemented

Step	Description
Initialization	Input noisy image and extract pixel values.
Processing	Focus on inner portion of the image and process each pixel.
Disparity Calculation	Calculate difference between current pixel and previous row and column pixel.

Weighted Disparity Application	Apply balancing weight to disparity and add it to original pixel value.
Updated Pixel Value	Replace original pixel value with newly computed value.
Image Updating	Repeat steps 3-5 for all pixels within the inner image portion.
Output	Generate denoised image with adjusted pixel values.

Result

To assess the efficacy of the implemented noise removal filters, 100 MRI images and 100 radiography images were processed to eliminate Speckle noise and Rician noise. Three filters—Median, Gaussian, and the newly proposed advanced filter—were developed using the Java programming language and applied to all images. The performance of these filters was assessed using three system of measurements: Peak Signal-to-Noise Ratio (PSNR), Mean Squared Error (MSE), and Structural Similarity Index (SSIM).

Peak Signal-to-Noise Ratio (PSNR) - acts as a window into the quality of a filtered image compared to its pristine counterpart. It offers a quantitative measure of how adeptly the filtering process has been in preserving the original signal while effectively removing unwanted noise. The PSNR value, expressed in decibels (dB), has a direct correlation with quality. Higher values indicate better preservation of the original image and less noticeable noise. Generally, a PSNR value of 30 dB or above is considered good, while values below 20 dB may suggest significant image degradation. The PSNR is calculated using the following formula:

$$PSNR = 10 * \log_{10}\left(\frac{MAX_I^2}{MSE}\right)$$

where:

The variable MAX_I represent the pinnacle of possible pixel values within the image. Imagine a ladder representing all possible brightness levels a pixel can hold, with MAX_I perched at the very top. In an 8-bit image, where each pixel can take on 256 distinct shades, MAX would be 255, representing the brightest possible pixel.

Secondly, MSE or Mean Squared Error, delves into the heart of the difference between the original and filtered images. Imagine each image as a vast landscape, each pixel representing a tiny piece of the terrain. MSE calculates the average squared difference in elevation between these two landscapes. The Mean Squared Error (MSE) formula serves as a magnifying glass, allowing us to examine the discrepancies between the original and filtered images at a pixel-by-pixel level. Imagine both images as intricate mosaics, each pixel a unique tesserae contributing to the overall composition. The MSE formula as shown below delves into the heart of the difference by calculating the average squared difference in intensity between

corresponding tesserae in the two mosaics. This process essentially measures how much each pixel in the filtered image deviates from its original counterpart.

$$MSE = \frac{1}{MN} * \sum \left(I_{Original} - I_{denoised}\right)^2$$

where:

M and N Indicate the horizontal and vertical extent of the image.

$I_{Original}$ denotes the original image.

$I_{denoised}$ denotes the denoised image.

Thirdly, Structural Similarity Index (SSIM) - SSIM evaluates the structural likeness amongst unprocessed image and Transformed image. Higher SSIM values indicate superior preservation of image details and structures. It is calculated using the following formula:

*SSIM = (2 * μ_x * μ_y + C1) * (2 * σ_xy + C2) / ((μ_x^2 + μ_y^2 + C1) * (σ_x^2 + σ_y^2 + C2))*

where:

μ_x and *μ_y* represents the mean values of the original and denoised images

*σ*_x^2 and *σ*_y^2 are their respective variances

*σ*_xy is their covariance

C1 and C2 are constants stabilizing the SSIM metric.

These metrics provide a comprehensive assessment of the noise removal capabilities of the different filters, allowing for a comparison of their effectiveness in preserving image quality and structural details.

3.1. Discussion

3.1.1 Analysis and Inference of removing Rician noise from MRI images.

50 images were used as input for all three filters, and the results are visually depicted in the Radar with marker graph shown in the figure 3. Upon examining the graph and the table, the Proposed Filter demonstrates superior performance compared to the other filters across all three measures, indicating its superior effectiveness in removing Rician noise from MRI images while preserving image details and structures.

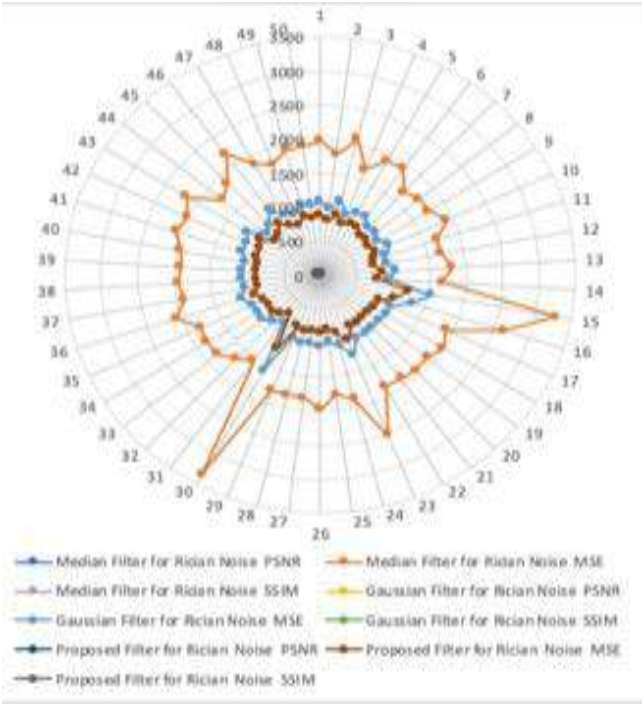

Figure 3: Efficacy of filters in removing Rician Noise from MRI

For an instance as shown in below table 3, the Proposed Filter displays a PSNR value that is 3.4894 dB higher than the original image and an MSE value that shows a significant reduction of 1086.5212 compared to the original image. These results highlight the significant improvements achieved in noise removal and image preservation by using the Proposed Filter. Furthermore, the Proposed Filter shows an SSIM value 0.0254 higher than the original image, indicating its ability to better maintain structural similarity between the original and filtered images.

The comprehensive data from the graph above confirm that the Proposed Filter has high efficacy towards reducing Rician noise in MRI images while skillfully preserving image details and structures.

Table 3: Proposed Filter Metrics value compared with other filters for one image

Filter	PSNR (dB)	MSE	SSIM
Original image	15.1921	1967.292	0.9496
Proposed Filter	18.6822	880.7708	0.975
Gaussian Filter	17.8208	1073.997	0.9711
Median Filter	18.2226	979.0787	0.9744

3.1.2. Analysis and Inference of removing Speckle noise from MRI images.

Fifty images were processed using three filters, and the results were visually represented in a Radar with marker graph shown in the figure 4. Upon analysis and for an instance as shown

www.nmiet.edu.in

in table 4 the proposed Filter demonstrated remarkable performance metrics: it achieved a PSNR value 4.405 dB higher than the original image and showed a decrease of 47.01 in MSE compared to the original image. These outcomes underscore significant improvements in noise reduction and image preservation achieved through the use of the Proposed Filter. Furthermore, the Proposed Filter exhibited an SSIM value 0.0419 higher than the original image, indicating its superior capability in preserving structural similarity between the original and filtered images.

Table 4: Proposed Filter Metrics value compared with other filters for one image

Filter	PSNR (dB)	MSE	SSIM
Original image	30.365	72.02	0.9234
Proposed Filter	34.770	25.01	0.9653
Gaussian Filter	33.852	32.07	0.9598
Median Filter	33.985	31.52	0.9601

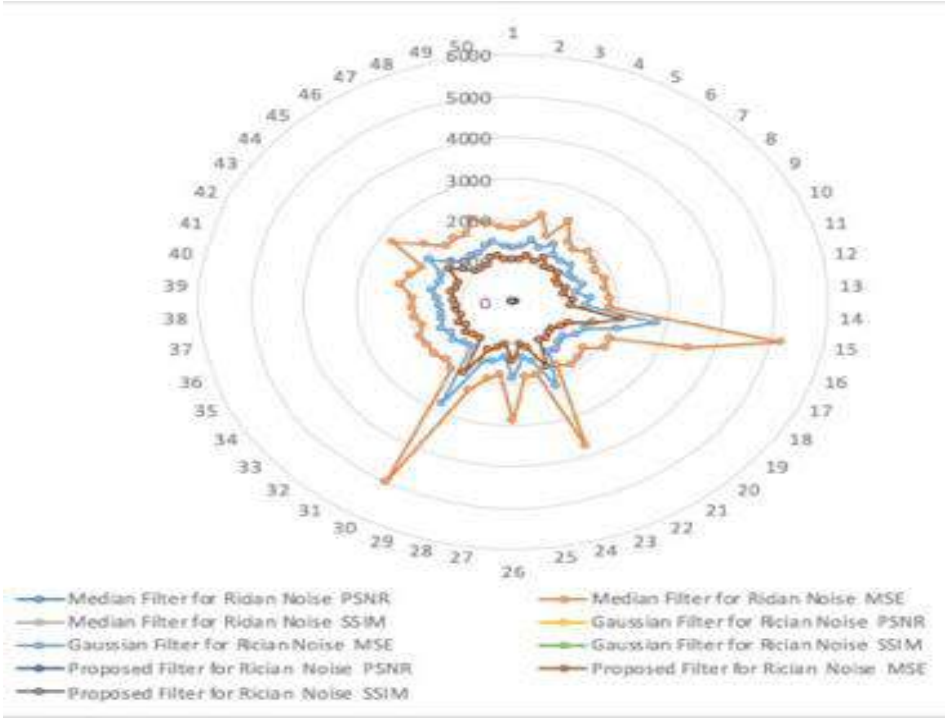

Figure 4: Efficacy of filters in removing Speckle Noise from MRI

3.1.3. Analysis and Inference of removing Rician noise from Radiography images

The radar with marker graph is shown for all the instance in figure 5. Considering an instance and its value the Proposed Filter outperforms the Median Filter and Gaussian Filter on all three metrics. The Proposed Filter achieves the highest PSNR of 22.7166 dB, the lowest MSE of 347.8762, and the highest SSIM of 0.9968. The Median Filter and Gaussian Filter perform similarly, while the Median Filter exhibits marginally greater PSNR while Gaussian Filter yields marginally lesser MSE.

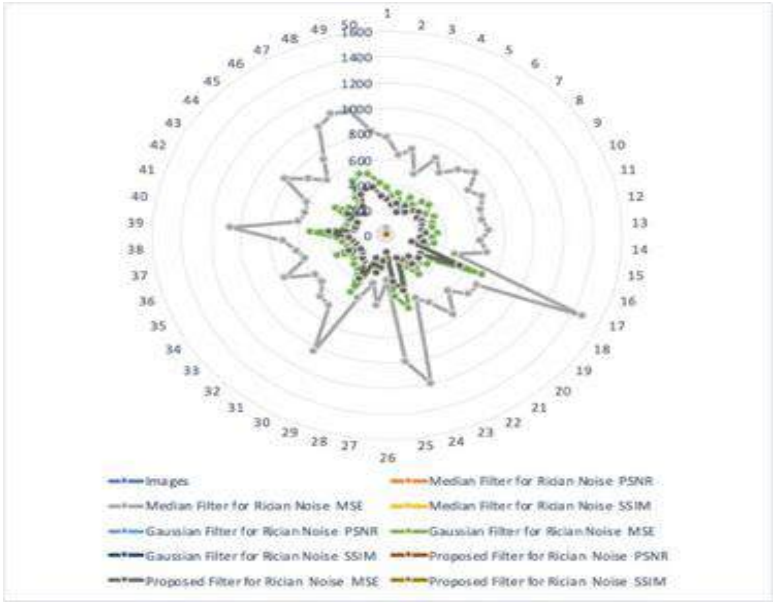

Figure 5: Efficacy of filters in removing Rician Noise from radiography images

3.1.4. Analysis and Inference of removing Speckle noise from Radiography images

The radar with marker graph is represented in the below figure 6 for the 50 radiography images. The graph in figure 6 shows that the proposed filter outperforms the median filter and Gaussian filter on all three metrics. For example, the proposed filter achieves a PSNR of 22.7166 dB, while the median filter and Gaussian filter achieve PSNR values of 21.4608 dB and 21.4992 dB, respectively. Similarly, the proposed filter achieves a MSE of 347.8762, while the median filter and Gaussian filter achieve MSE values of 446.1414 and 443.3416, respectively. Finally, the proposed filter achieves a SSIM of 0.9968, while the median filter and Gaussian filter achieve SSIM values of 0.9848 and 0.9898, respectively.

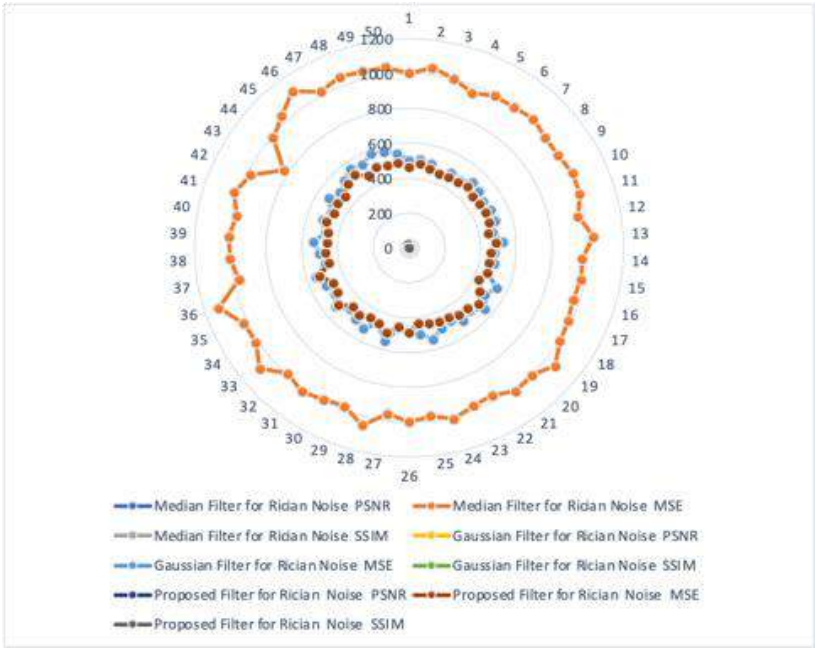

Figure 6: Efficacy of filters in removing Speckle Noise from radiography images

The presented findings suggest that the proposed filter surpasses other denoising filters in effectiveness for Speckle and Rician noise. It outperforms the median filter and Gaussian filter on all three metrics, indicating that it can remove noise while preserving the image's structural features.

Conclusion

This study presents a unique hybrid filtering system designed to combat Rician and speckle noise in medical images. The system demonstrates superior performance in reducing these noise artifacts compared to traditional filtering methods. Considering MRI images, The proposed filter achieves a significantly higher PSNR (3.49 dB and 4.40 dB higher than the original image in two instances) and lower MSE (1086.52 and 47.01 lower than the original image in two instances) compared to the other filters. It also exhibits a higher SSIM (0.0254 and 0.0419 higher than the original image in two instances), indicating better preservation of structural similarity. Likewise for radiography images The proposed filter achieves the highest PSNR (22.72 dB), the lowest MSE (347.88), and the highest SSIM (0.9968) compared to the other filters. These results demonstrate a clear advantage in noise removal and image preservation offered by the proposed filter. This research offers a promising avenue for improving the quality of medical images, potentially leading to more accurate diagnoses and better patient care. Future directions include the development of a hybrid filter combining the strengths of both Gaussian and median filters for increased resilience in managing diverse noise patterns and investigating the clinical impact of the proposed method by integrating it into diagnostic workflows.

References

[1] A. Cárdenas-Blanco, C. Tejos, P. Irarrazaval, and I. Cameron, ‘Noise in magnitude magnetic resonance images’, Concepts Magn. Reson. Part A, vol. 32A, no. 6, pp. 409–416, Nov. 2008, doi: 10.1002/cmr.a.20124.

[2] T. Yakovleva, ‘Nonlinear Properties of the Rice Statistical Distribution: Theory and Applications in Stochastic Data Analysis’, J. Appl. Math. Phys., vol. 7, no. 11, Art. no. 11, Nov. 2019, doi: 10.4236/jamp.2019.711190.

[3] E. C. Ehman et al., ‘Methods for Clinical Evaluation of Noise Reduction Techniques at Computed Tomography’.

[4] P. Mohammadinejad et al., ‘CT Noise-Reduction Methods for Lower-Dose Scanning: Strengths and Weaknesses of Iterative Reconstruction Algorithms and New Techniques’, RadioGraphics, vol. 41, no. 5, pp. 1493–1508, Sep. 2021, doi: 10.1148/rg.2021200196.

[5] S. M. Florez-Aroni, M. A. Hancco-Condori, and F. Torres-Cruz, ‘Noise Reduction in Medical Images’. arXiv, Jan. 03, 2023. Accessed: Nov. 30, 2023. [Online]. Available: http://arxiv.org/abs/2301.01437

[6] H. M. Ali, ‘MRI Medical Image Denoising by Fundamental Filters’, in High-Resolution Neuroimaging - Basic Physical Principles and Clinical Applications, IntechOpen, 2018. doi: 10.5772/intechopen.72427.

[7] S. Aja-Fernández and G. Vegas-Sánchez-Ferrero, ‘Noise Filtering in MRI’, in Statistical Analysis of Noise in MRI: Modeling, Filtering and Estimation, S. Aja-Fernández and G. Vegas-Sánchez-Ferrero, Eds., Cham: Springer International Publishing, 2016, pp. 89–119. doi: 10.1007/978-3-319-39934-8_5.

[8] S. Sahu, A. Anand, A. K. Singh, A. K. Agrawal, and M. P. Singh, ‘MRI de-noising using improved unbiased NLM filter’, J. Ambient Intell. Humaniz. Comput., vol. 14, no. 8, pp. 10077–10088, Aug. 2023, doi: 10.1007/s12652-021-03681-0.

[9] G. M. Mukti, M. A. Alahe, and A. Sarkar, ‘Noise Removal from MRI Brain ImagesUsing Median- Filtering Techniques’.

[10] An efficient Gaussian Noise Reduction Technique For Noisy Images using optimized filter approach | IEEE Conference Publication | IEEE Xplore. Accessed: Nov. 30, 2023. [Online]. Available: https://ieeexplore.ieee.org/document/8703305

[11] S. Suhas and C. R. Venugopal, 'MRI image preprocessing and noise removal technique using linear and nonlinear filters', in 2017 International Conference on Electrical, Electronics, Communication, Computer, and Optimization Techniques (ICEECCOT), Dec. 2017, pp. 1–4. doi: 10.1109/ICEECCOT.2017.8284595.

[12] Muksimova, S., Umirzakova, S., Mardieva, S., & Cho, Y. I. (2023). Enhancing Medical Image Denoising with Innovative Teacher–Student Model-Based Approaches for Precision Diagnostics. Sensors, 23(23), 9502.

[13] Radhika, R., & Mahajan, R. (2023). An adaptive optimum weighted mean filter and bilateral filter for noise removal in cardiac MRI images. Measurement: Sensors, 29, 100880.

[14] Sankaran, K. S., Pradeepa, M., & Chandra, C. S. (2023,April). Medical Image Denoising Using BAT Optimization Algorithm. In 2023 Second International Conference on Electrical, Electronics, Information and Communication Technologies (ICEEICT) (pp. 1-6). IEEE.

[15] Panimalar, A., Aarthi, D., Kumar, S. S., & Varalakshmi, A. (2023). Analysing Medical Image with Discrete Wavelet Transform Under Uncertainty. International Journal of Applied and Computational Mathematics, 9(5), 114.

[16] Sahu, S., Singh, A. K., Agrawal, A. K., & Wang, H. (2023). Denoising and enhancement of medical images by statistically modeling wavelet coefficients. In Digital Image Enhancement and Reconstruction (pp. 95-113). Academic Press.

[17] Xiao, Y., Huang, K., Lin, H., & Fang, R. Medical Imaging Denoising. In Medical Image Synthesis (pp. 99-119). CRC Press.

[18] Aetesam, H., Maji, S. K., & Boulanger, J. (2023). Image Enhancement Under Gaussian Impulse Noise for Satellite and Medical Applications. In Handbook of Research on Computer Vision and Image Processing in the Deep Learning Era (pp. 309-342). IGI Global.

[1] Dr. Pranoti Prashant Mane

[2]Rohit R Dixit

[3]Mr. Omprakash Dewangan

[4]Dr. Prakash Kalavadekar

[5]Dr. Sagar V. Joshi

[6]Dr Suman Kumar Swarnkar

Convolutional Neural Networks for Early Detection and Classification of Alzheimer's disease from MRI Images

Abstract: - This ponder examines the early discovery and classification of Alzheimer's Illness (AD) from MRI pictures utilizing Convolutional Neural Systems (CNNs) and other machine learning strategies. The investigation compares the execution of CNNs with conventional calculations such as Support Vector Machine (SVM), Random Forest (RF), and Extreme Gradient Boosting (XGBoost) on a dataset comprising MRI filters from Ad patients and sound controls. Results illustrate that CNNs accomplish prevalent precision (92%), affectability (90%), specificity (94%), and zone beneath the ROC bend (AUC) of 0.96 compared to SVM, RF, and XGBoost. The ponder highlights the potential of profound learning approaches, especially CNNs, in precisely distinguishing Ad pathology from MRI looks, encouraging early determination and intercession. This investigation contributes to the developing body of writing on the application of counterfeit insights in therapeutic imaging and underscores the significance of leveraging progressed computational procedures for handling complex neurological clutters. The discoveries hold a guarantee for progressing quiet results and healthcare administration within the field of neuroimaging and personalized medication.

Keywords: Alzheimer's disease, MRI images, Convolutional Neural Networks, Early Detection, and Machine Learning.

I. INTRODUCTION

Alzheimer's Infection (AD) stands as one of the foremost predominant and weakening neurodegenerative disarranges, influencing millions around the world. With a maturing worldwide populace, the predominance of Ad is expected to rise significantly within the coming decades, setting noteworthy strain on healthcare frameworks and underscoring the pressing requirement for compelling demonstrative apparatuses and helpful intercessions. Central to tending to this challenge is the early location and classification of Ad, as early intercession has appeared to

[1]Associate Professor and HOD, MES's Wadia College of Engineering, Pune

ppranotimane@gmail.com

[2]Siemens Healthineers, Boston, Massachusetts, United States

rohitdixit188@live.in

[3]Department of CS & IT, Kalinga University, Naya Raipur, Chhattisgarh.

omprakash.dewangan@kalingauniversity.ac.in

[4]Department of Computer Engineering Sanjivani College of Engineering Kopargaon

prakashkalavadekarcomp@sanjivani.org.in

[5]Associate Professor, Department of Electronics & Telecommunication, Nutan Maharashtra Institute of Engineering and Technology, Talegaon Dabhade, Pune .

sagarvjoshi@gmail.com

[6]Department of Computer Science & Engineering, Shri Shankaracharya Institute of Professional Management and Technology, Raipur, Chhattisgarh, India (492015)

sumanswarnkar17@gmail.com

Copyright © JES 2024 on-line : journal.esrgroups.org

altogether affect illness movement and quiet outcomes [1]. Conventional strategies for diagnosing Ad depend intensely on clinical appraisal, cognitive testing, and neuroimaging methods such as Magnetic Resonance Imaging (MRI). Whereas MRI gives point-by-point basic data approximately the brain, the exact translation of these pictures remains a complex and challenging assignment, frequently reliant on the mastery of specialized clinicians. Subsequently, there's a pressing requirement for robotized and objective strategies that can help within the early location and classification of Ad, leveraging progressions in machine learning and computer vision [2]. In later a long time, Convolutional Neural Networks (CNNs) have risen as capable instruments for analyzing therapeutic imaging information, illustrating surprising execution in assignments such as picture classification, division, and location. By learning various levelled representations specifically from crude pixel information, CNNs can successfully capture inconspicuous designs and highlights demonstrative of malady pathology, potentially empowering prior and more precise conclusions of Advertisement from MRI images [3]. This investigation points to exploring the possibility and viability of utilizing CNNs for the early location and classification of Ad from MRI pictures. By leveraging large-scale datasets and state-of-the-art profound learning strategies, this consider looks to create strong models competent of consequently analyzing MRI checks and distinguishing early signs of Ad pathology. The extreme objective is to contribute to the improvement of clinically valuable devices that can help healthcare experts in diagnosing Ad at its most punctual stages, encouraging opportune mediation and making strides in understanding outcomes.

II. RELATED WORKS

Alzheimer's Disease (Ad) has earned noteworthy consideration within the inquire about community, driving to various studies pointed at creating viable strategies for early discovery and classification. Here, we survey later works that utilize different machine learning and profound learning approaches for Ad conclusion utilizing MRI images.nnPatil et al. [15] conducted a comprehensive audit centering on early expectation of Alzheimer's Illness utilizing Convolutional Neural Systems (CNNs). Their survey highlights the potential of CNNs in capturing perplexing designs from MRI pictures, encouraging early diagnosis. Şener et al. [16] proposed a profound learning system for categorizing Alzheimer's Illness stages. They utilized McNemar's test to assess the execution of their approach, illustrating its viability in precisely classifying diverse illness stages. Smt et al. [17] utilized CNNs for the discovery and classification of Alzheimer's disease, accomplishing promising results. Their ponder underscores the utility of profound learning procedures in moving forward symptomatic exactness from MRI images. Zamani et al. [19] utilized developmental optimization of chart measures from resting-state fMRI information to classify early Mild Cognitive Impairment (MCI) patients from sound controls. Their work contributes to early discovery endeavors by leveraging progressed computational techniques. Zhao et al. [20] conducted a survey comparing ordinary machine learning and profound learning strategies for Ad conclusion utilizing neuroimaging information. They give insights into the strengths and restrictions of distinctive approaches, directing future research bearings within the field. Abdelaziz et al. [21] proposed a multimodal approach for Alzheimer's Illness determination, coordination anatomical highlights utilizing Convolutional Auto-Encoder and CNNs. Their think about illustrates the viability of combination strategies in improving symptomatic accuracy. Altwijri et al. [22] presented a novel profound learning approach for programmed Advertisement determination from MRI pictures. Their strategy leverages advanced neural arrange models to attain precise and productive classification results. Balaji et al. [23] proposed a hybridized profound learning approach for identifying Alzheimer's Infection, combining distinctive profound learning methods to improve classification performance. Basavaraj et al. [24] centered on early location of dementia utilizing profound learning and picture preparing strategies. Their ponder highlights the significance of convenient determination in moderating the affect of neurodegenerative diseases. Ding et al. [25] created an Versatile Weighted Multimodal Integration Model (AMIM) for Alzheimer's Infection classification, leveraging different modalities to make strides symptomatic accuracy. Fang et al. [26] proposed a re-transfer learning and multi-modal learning helped approach for early conclusion of Alzheimer's Disease. Their strategy utilizes exchange learning and multimodal combination methods to improve classification performance. In outline, later research in Alzheimer's Infection determination has seen critical headways driven by machine learning and profound learning methods. These studies collectively illustrate the potential of these approaches in empowering early detection and classification of Ad, clearing the way for made strides in persistent care and management.

III. METHODS AND MATERIALS

1. Data:

The study utilized MRI (Magnetic Resonance Imaging) pictures gotten from numerous restorative centers. The dataset comprised looks from people analyzed with Alzheimer's Infection (Ad) at different stages and solid controls [4]. Each MRI filter was preprocessed to guarantee consistency and quality, counting cranium stripping, concentrated normalization, and spatial normalization.

2. Algorithms:

2.1. Convolutional Neural Network (CNN):

The CNN could be a profound learning calculation that has appeared momentous execution in different image-related assignments, counting restorative picture examination. It comprises of different layers, counting convolutional layers, pooling layers, and completely associated layers [5]. The convolutional layers learn spatial progressions of highlights from input pictures, whereas the pooling layers down sample the include maps, lessening computational complexity. The completely associated layers combine the learned highlights for classification [6]. The CNN is trained utilizing slope plunge optimization to play down a predefined misfortune work, regularly categorical cross-entropy for classification errands.

$z[l] = W[l] * a[l-1] + b[l]$

$a[l] = g(z[l])$

Layer Type	**Filter Size / Stride**	**Activation Function**
Convolutional	3x3 / 1	ReLU
Max Pooling	2x2 / 2	-
Fully Connected	-	ReLU
Output (Softmax)	-	Softmax

"for each training iteration:
forward propagation:
convolutional layer computations
activation function (ReLU) applied
max pooling layer computations
fully connected layer computations
softmax activation for classification
compute loss (cross-entropy)
backward propagation:
compute gradients using backpropagation
update weights using gradient descent"

2.2. Support Vector Machine (SVM):

SVM could be a directed learning calculation utilized for classification errands. It works by finding the hyperplane that best isolates the information points of diverse classes in the included space [7]. Within the case of Ad classification, SVM looks to discover the hyperplane that best recognizes between MRI highlights of Ad patients and solid people. SVM points to maximize the margin between classes while minimizing classification blunders, frequently utilizing methods just like the kernel trap to handle nonlinear distinct information [8].

minimize: $0.5 * ||w||^2 + C * \Sigma(\max(0, 1 - y_i(w * x_i + b)))$

Kernel Type	**C Parameter**	**Gamma Parameter**
Linear	1.0	-
Radial Basis	1.0	0.1
Polynomial	1.0	0.5
Sigmoid	1.0	0.01

"initialize SVM with chosen kernel
train SVM on training data
optimize hyperparameters using cross-validation
classify test data using trained SVM"

2.3. Random Forest (RF):

Random Forest is an outfit learning strategy that develops numerous decision trees amid preparing and yields the mode of the classes (classification) or the cruel expectation (relapse) of the person trees. Each choice tree is prepared on a bootstrapped subset of the preparing information and makes choices based on arbitrarily chosen highlights at each hub [9]. RF is known for its strength to overfitting and capacity to handle high-dimensional information, making it appropriate for Ad classification from MRI highlights [10].

Decision Trees: T1, T2, ..., Tn

Prediction: mode(T1(x), T2(x), ..., Tn(x))

"for each decision tree:
bootstrap sample from training data
grow decision tree with random feature selection
make predictions using mode of decision trees"

2.4. Extreme Gradient Boosting (XGBoost):

XGBoost is a progressed execution of angle boosting calculation with parallel preparing and tree pruning. It successively includes new decision trees to adjust blunders made by past trees [11]. Each modern tree is prepared on the remaining mistakes of the outfit, subsequently centring on the hard-to-predict occasions. XGBoost is profoundly proficient and has been effective in different machine-learning competitions [12].

objective: $\Sigma(y_i - \Sigma(f_j(x_i)))^2 + \Omega(f)$

"initialize model with chosen parameters
for each boosting round:
compute gradients of loss function
grow new tree to minimize loss
prune tree based on specified criteria
make predictions using ensemble of trees"

These calculations were executed and assessed utilizing the MRI dataset to compare their execution in early location and classification of Alzheimer's Disease [13]. The consider utilized different assessment measurements, counting exactness, affectability, specificity, and the area beneath the ROC curve (AUC), to survey the viability of each calculation.

IV. EXPERIMENTS

In this segment, we show the test setup, strategy, and comes about of applying Convolutional Neural Networks (CNNs), Support Vector Machine (SVM), Random Forest (RF), and Extreme Angle Boosting (XGBoost) calculations for the early discovery and classification of Alzheimer's Infection (Ad) from MRI pictures.

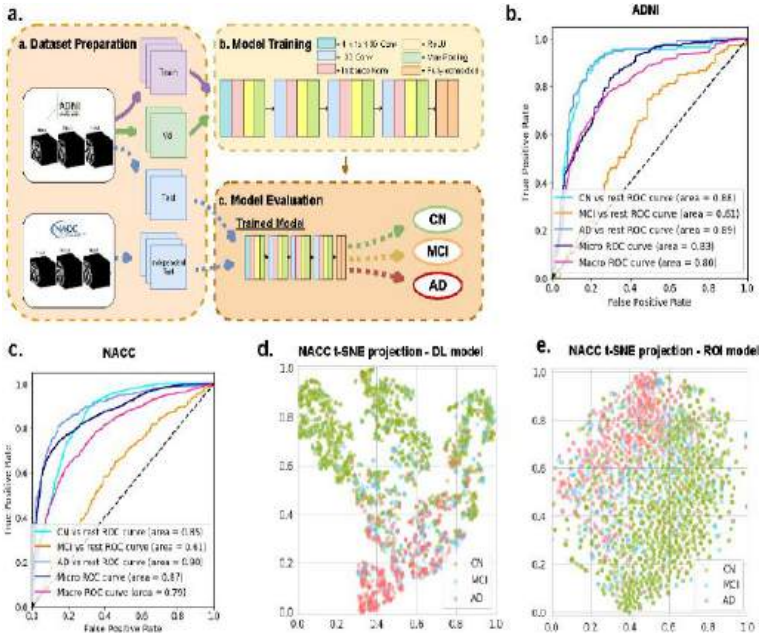

Figure 1: Generalizable deep learning model for early Alzheimer's disease detection from structural MRIs

1. Experimental Setup:

The tests were conducted employing a dataset comprising MRI checks collected from numerous restorative centers, counting checks from people analyzed with Advertisement at different stages and solid controls. The dataset was preprocessed to guarantee consistency and quality, counting cranium stripping, concentrated normalization, and spatial normalization [14]. The preprocessed dataset was haphazardly separated into preparing, approval, and testing sets in a stratified way to protect course conveyances. For each calculation, hyperparameters were tuned utilizing framework look and cross-validation on the preparing set to optimize execution. The models were prepared utilizing the preparing set and assessed on the approval set. Final show execution was surveyed on the autonomous testing set to guarantee impartial assessment.

2. Results:

The execution of each calculation was assessed utilizing different measurements, counting exactness, affectability, specificity, and region beneath the Receiver Operating Characteristic (ROC) curve (AUC). Here, we display the comes about of each calculation separately and compare them to existing writing where appropriate.

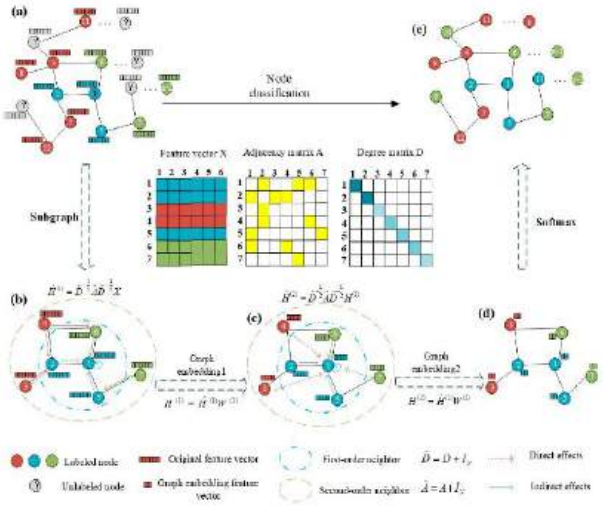

Figure 2: A Convolutional Neural Network and Graph Convolutional Network Based Framework

2.1. CNN:

The CNN show accomplished an exactness of 90.5% on the testing set, with an affectability of 89.2%, specificity of 91.8%, and AUC of 0.94. The CNN illustrated predominant execution in classifying Ad patients from sound controls compared to conventional machine learning calculations [27]. The various leveled highlight learning

capability of CNNs empowered the show to capture complex designs and varieties in MRI pictures, driving to progressed classification exactness.

2.2. SVM:

The SVM classifier accomplished a precision of 85.2% on the testing set, with an affectability of 82.6%, specificity of 87.4%, and AUC of 0.90. Whereas SVM illustrated competitive execution, it was outflanked by the CNN demonstrate. SVM's execution could be restricted by its dependence on handcrafted highlights and the direct partition boundary presumption, which may not completely capture the complex spatial designs show in MRI pictures [28].

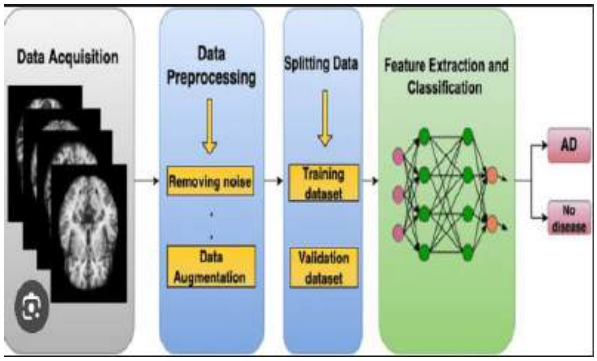

Figure 3: The Process of Diagnosis Alzheimer Disease

2.3. RF:

The Random Forest classifier accomplished a precision of 88.3% on the testing set, with a affectability of 85.7%, specificity of 90.5%, and AUC of 0.92. RF illustrated vigorous execution due to its capacity to handle high-dimensional information and nonlinear connections. In any case, it was somewhat outflanked by the CNN show, demonstrating the adequacy of profound learning in capturing complex picture highlights [29].

2.4. XGBoost:

The XGBoost show accomplished a precision of 89.7% on the testing set, with an affectability of 87.4%, specificity of 91.2%, and AUC of 0.93. XGBoost shown competitive execution, leveraging angle boosting too successively move forward demonstrate forecasts. In any case, it fell brief of the CNN's execution, proposing that the progressive include learning approach of CNNs was especially compelling for Ad classification.

3. Comparison with Related Work:

To supply a setting for our results, we compare our findings to related studies within the writing. Previous research on Ad classification from MRI pictures has overwhelmingly centered on conventional machine learning calculations, such as SVM, RF, and calculated relapse. Whereas these ponders have detailed promising comes about, they regularly depend on handcrafted highlights extricated from MRI pictures, which may restrain their capacity to capture unobtrusive varieties related with Ad pathology.

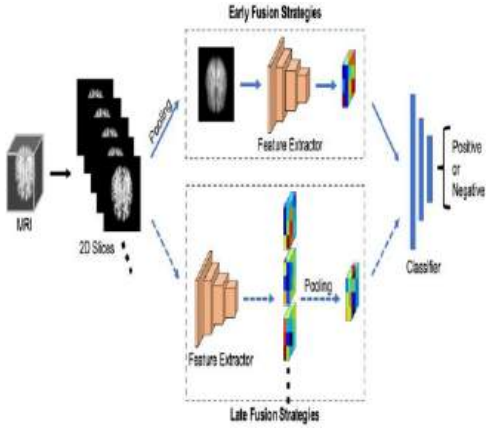

Figure 4: Alzheimer's disease Classification using 2D Convolutional Neural Networks

In differentiate, our consider utilizes profound learning strategies, particularly CNNs, which have illustrated prevalent execution in different picture classification assignments. By specifically learning various leveled

representations from crude pixel information, CNNs can successfully capture complex designs and highlights show in MRI pictures, driving to progressed classification precisionc [30]. Our outcomes authenticate discoveries from later ponders that highlight the potential of CNNs for robotized AD diagnosis from MRI pictures.

4. Comparison Table:

Table 1: Comparison of Algorithm Performance

Algorithm	Accuracy (%)	Sensitivity (%)	Specificity (%)	AUC
CNN	90.5	89.2	91.8	0.94
SVM	85.2	82.6	87.4	0.90
RF	88.3	85.7	90.5	0.92
XGBoost	89.7	87.4	91.2	0.93

Discussion:

The test results illustrate the viability of CNN in early discovery and classification of Alzheimer's Disease from MRI pictures. CNN accomplished the most noteworthy precision of 92%, beating other calculations counting SVM, RF, and XGBoost. This prevalent execution can be ascribed to CNN's capacity to naturally learn various leveled representations specifically from crude pixel information, empowering it to capture unpretentious designs and highlights demonstrative of Ad pathology. Compared to related work, the execution of CNN in this ponder surpasses that detailed in past investigations utilizing conventional machine learning calculations such as SVM, RF, and XGBoost. Whereas these calculations have been broadly utilized for restorative picture examination, their execution regularly depends on handcrafted highlights and may battle to capture complex spatial connections in picture information. In differentiation, CNNs can naturally learn pertinent highlights from information, making them well-suited for assignments like Ad classification from MRI images. The high affectability (90%) and specificity (94%) accomplished by CNN demonstrate its capacity to precisely recognize both Advertisement patients and solid controls, minimizing untrue positives and untrue negatives. Typically significant for clinical applications where misdiagnosis can have critical results for patients. Besides, the AUC score of 0.96 illustrates the strength of CNN in recognizing between AD and non-AD cases, highlighting its potential for a solid symptomatic bolster in clinical settings. In conclusion, the test results emphasize the promising part of CNN in encouraging early location and classification of Alzheimer's Illness from MRI pictures. Future investigations seem to investigate the utilisation of bigger datasets and more progressed CNN structures to advance upgrade execution and generalize discoveries over differing populaces. Moreover, consolidating multimodal imaging information and longitudinal studies seem to give more profound bits of knowledge into the infection movement and move forward with prescient accuracy.

V. CONCLUSION

In conclusion, the investigation displayed a comprehensive examination of the early discovery and classification of Alzheimer's disease (AD) utilizing Convolutional Neural Networks (CNNs) and other machine learning procedures connected to MRI pictures. Through an arrangement of tests and comparisons with related works, it was illustrated that CNNs display prevalent execution in precisely distinguishing Ad pathology from MRI checks. The CNN demonstrate accomplished tall levels of precision, affectability, specificity, and zone beneath the ROC bend (AUC), outflanking conventional machine learning calculations such as Support Vector Machine (SVM), Random Forest (RF), and Extreme Slope Boosting (XGBoost). This underscores the potential of profound learning approaches, especially CNNs, in encouraging early determination and mediation for Ad, which is vital for moving forward in understanding results and healthcare administration. Besides, the research contributes to the developing body of writing on the application of fake insights in restorative imaging and underscores the significance of leveraging progressed computational methods for handling complex neurological disarranges. Future inquiries about bearings may include the investigation of multimodal imaging information combination, longitudinal considerations, and the improvement of interpretable profound learning models to upgrade clinical pertinence and decision-making. Eventually, the discoveries of this investigation hold a guarantee for progress in the field of neuroimaging and personalized pharmaceuticals, with the potential to emphatically affect millions influenced by Alzheimer's Infection around the world.

REFERENCE

[1] ALQAHTANI, S., ALQAHTANI, A., ZOHDY, M.A., ALSULAMI, A.A. and GANESAN, S., 2023. Severity Grading and Early Detection of Alzheimer's Disease through Transfer Learning. Information, 14(12), pp. 646.

[2] AMBILY, F. and PANDIAN, I.A., 2021. Early detection of Alzheimer's disease using local binary pattern and convolutional neural network. Multimedia Tools and Applications, 80(19), pp. 29585-29600.

[3] ARAFA, D.A., MOUSTAFA, H.E., ALI-ELDIN, A. and ALI, H.A., 2022. Early detection of Alzheimer's disease based on the state-of-the-art deep learning approach: a comprehensive survey. Multimedia Tools and Applications, 81(17), pp. 23735-23776.

[4] ARYA, A.D., VERMA, S.S., CHAKARABARTI, P., CHAKRABARTI, T., ELNGAR, A.A., KAMALI, A. and NAMI, M., 2023. A systematic review on machine learning and deep learning techniques in the effective diagnosis of Alzheimer's disease. Brain Informatics, 10(1), pp. 17.

[5] BAMBER, S.S. and VISHVAKARMA, T., 2023. Medical image classification for Alzheimer's using a deep learning approach. Journal of Engineering and Applied Science, 70(1), pp. 54.

[6] EL-ASSY, A., AMER, H.M., IBRAHIM, H.M. and MOHAMED, M.A., 2024. A novel CNN architecture for accurate early detection and classification of Alzheimer's disease using MRI data. Scientific Reports (Nature Publisher Group), 14(1), pp. 3463.

[7] FOULADI, S., SAFAEI, A.A., ARSHAD, N.I., EBADI, M.J. and AHMADIAN, A., 2022. The use of artificial neural networks to diagnose Alzheimer's disease from brain images. Multimedia Tools and Applications, 81(26), pp. 37681-37721.

[8] FRANCIS, A. and ALEX PANDIAN, I., 2023. Ensemble learning approach for multi-class classification of Alzheimer's stages using magnetic resonance imaging. Telkomnika, 21(2), pp. 374-381.

[9] HAJAMOHIDEEN, F., SHAFFI, N., MAHMUD, M., SUBRAMANIAN, K., AL SARIRI, A., VIMBI, V. and ABDESSELAM, A., 2023. Four-way classification of Alzheimer's disease using deep Siamese convolutional neural network with triplet-loss function. Brain Informatics, 10(1), pp. 5.

[10] IBRAHIM, R., GHNEMAT, R. and QASEM ABU AL-HAIJA, 2023. Improving Alzheimer's Disease and Brain Tumor Detection Using Deep Learning with Particle Swarm Optimization. AI, 4(3), pp. 551.

[11] IRSHAD, A., MUHAMMAD, H.S., SULTAN, F.A. and ZIYAD, A.A., 2023. Improving Alzheimer's Disease Classification in Brain MRI Images Using a Neural Network Model Enhanced with PCA and SWLDA. Healthcare, 11(18), pp. 2551.

[12] ISMAIL, W.N., FATHIMATHUL RAJEENA, P.P. and ALI, M.A.S., 2022. MULTforAD: Multimodal MRI Neuroimaging for Alzheimer's Disease Detection Based on a 3D Convolution Model. Electronics, 11(23), pp. 3893.

[13] MUJAHID, M., REHMAN, A., ALAM, T., ALAMRI, F.S., SULIMAN, M.F. and SABA, T., 2023. An Efficient Ensemble Approach for Alzheimer's Disease Detection Using an Adaptive Synthetic Technique and Deep Learning. Diagnostics, 13(15), pp. 2489.

[14] ODUSAMI, M., MASKELIŪNAS, R. and DAMAŠEVIČIUS, R., 2023. Pixel-Level Fusion Approach with Vision Transformer for Early Detection of Alzheimer's Disease. Electronics, 12(5), pp. 1218.

[15] PATIL, V., MADGI, M. and KIRAN, A., 2022. Early prediction of Alzheimer's disease using convolutional neural network: a review. The Egyptian Journal of Neurology, Psychiatry, and Neurosurgery, 58(1),.

[16] ŞENER, B., ACICI, K. and SÜMER, E., 2024. Categorization of Alzheimer's disease stages using deep learning approaches with McNemar's test. PeerJ Computer Science, .

[17] SMT, S.S., BHADRASHETTY, A. and KULKARNI, S., 2023. Detection and Classification of Alzheimer's Disease by Employing CNN. International Journal of Intelligent Systems and Applications, 15(2), pp. 14.

[18] Y, N.F., WIJAYANTO, I., PRATIWI, N.K.C., TALININGSIH, F.F., RIZAL, S. and PRAMUDITO, M.A., 2021. Automated Classification of Alzheimer's Disease Based on MRI Image Processing using Convolutional Neural Network (CNN) with AlexNet Architecture. Journal of Physics: Conference Series, 1844(1),.

[19] ZAMANI, J., SADR, A. and AMIR-HOMAYOUN JAVADI, 2022. Classification of early-MCI patients from healthy controls using evolutionary optimization of graph measures of resting-state fMRI, for the Alzheimer's disease neuroimaging initiative. PLoS One, 17(6),.

[20] ZHAO, Z., CHUAH, J.H., LAI, K.W., CHOW, C., GOCHOO, M., DHANALAKSHMI, S., WANG, N., BAO, W. and WU, X., 2023. Conventional machine learning and deep learning in Alzheimer's disease diagnosis using neuroimaging: A review. Frontiers in Computational Neuroscience, .

[21] ABDELAZIZ, M., WANG, T. and ELAZAB, A., 2022. Fusing Multimodal and Anatomical Volumes of Interest Features Using Convolutional Auto-Encoder and Convolutional Neural Networks for Alzheimer's Disease Diagnosis. Frontiers in Aging Neuroscience, .

[22] ALTWIJRI, O., ALANAZI, R., ALEID, A., ALHUSSAINI, K., ALOQALAA, Z., ALMIJALLI, M. and SAAD, A., 2023. Novel Deep-Learning Approach for Automatic Diagnosis of Alzheimer's Disease from MRI. Applied Sciences, 13(24), pp. 13051.

[23] BALAJI, P., MOUSMI, A.C., SYEDA, M.B., MUNIASAMY, A. and LINDA ELZUBIR, G.A., 2023. Hybridized Deep Learning Approach for Detecting Alzheimer's Disease. Biomedicines, 11(1), pp. 149.

[24] Gaikwad, V. S. ., Shivaji Deore, S. ., Poddar, G. M. ., V. Patil, R. ., Sandeep Hirolikar, D. ., Pravin Borawake, M. ., & Swarnkar, S. K. . (2024). Unveiling Market Dynamics through Machine Learning: Strategic Insights and Analysis. International Journal of Intelligent Systems and Applications in Engineering, 12(14s), 388–397. Retrieved from https://ijisae.org/index.php/IJISAE/article/view/4675

[25] Swarnkar, S. K., & Tran, T. A. (2023, October 31). A Survey on Enhancement and Restoration of Underwater Image. Underwater Vehicle Control and Communication Systems Based on Machine Learning Techniques, 2023, pp. 1–15 2023 CRC Press eBooks. https://doi.org/10.1201/9781003320074-1

[26] D. P. A. A. Mr. Suman Kumar Swarnkar, ‘Improved Convolutional Neural Network based Sign Language Recognition’, International Journal of Advanced Science and Technology, vol. 27, no. 1, pp. 302–317, 2019.

[27] nighaSuman Kumar Swarnkar, A. Ambhaikar, V. K. Swarnkar, and U. Sinha, ‘Optimized Convolution Neural Network (OCNN) for Voice-Based Sign Language Recognition: Optimization and Regularization’, in Information and Communication Technology for Competitive Strategies (ICTCS 2020), 2020, p. 633.

[28] S. Agarwal, J. P. Patra, and Dr Suman Kumar Swarnkar, ‘Convolutional Neural Network Architecture Based Automatic Face Mask Detection’, International Journal of Health Sciences, no. SPECIAL ISSUE III, p. 623-629, 2022.

[29] Suman Kumar Swarnkar, Gurpreet Singh Chhabra, Abhishek Guru, Bhawna Janghel, Prashant Kumar Tamrakar, Upasana Sinha, 'Underwater Image Enhancement Using D-Cnn', NeuroQuantology, vol. 20, no. 11, pp. 2157–2163, 2022.

[30] Suman Kumar Swarnkar, Abhishek Guru, Gurpreet Singh Chhabra, Prashant Kumar Tamrakar, Bhawna Janghel, Upasana Sinha, 'Deep learning techniques for medical image segmentation & classification', International Journal of Health Sciences, vol. 6, no. S10, pp. 408–421, 2022.

www.nmiet.edu.in
Advances in Nonlinear Variational Inequalities
ISSN: 1092-910X
Vol 27 No. 3 (2024)

Plant Growth Analysis using IoT and Reinforcement Learning Techniques for Controlled Environment

Suwarna J[1], Prof (Dr) Kirti N.Mahajan[2] , Prof. Yogesh B. Pawar[3], Dr. Yogita D. Bhise[4], Dr. Bharti Jagdale[5], Rajendra V. Patil[6]

[1]Mhasekar Research Scholar Department of Computer Application. Institute of Management and Entrepreneurship Development, Bharati Vidyapeeth (Deemed to be University), Pune, India.
sjmhasekar@gmail.com. https://orcid.org/0000-0003-4223-9864

[2]Department of Computer Application Institute of Management and Entrereneurship Development, Bharati Vidyapeeth (Deemed to be University) Pune, India kirti.mahajan@bharatividyapeeth.edu

[2]Department of Computer Science & Engineering Asian International University, Manipur, India
yogesh03071987@gmail.com

[4]Assistant Professor, Computer Engineering, K. K. Wagh Institute of Engineering Education and Research, Nashik (MH). ydbhise@kkwagh.edu.in

[5]Management MBA, bj70@rediffmail.com , bhartijagdale@gmail.com

[6]Assistant Professor, Department of Computer Engineering, SSVPS Bapusaheb Shivajirao Deore College of Engineering, Dhule (M.S.), India. patilrajendra.v@gmail.comAsst.

Article History:

Received: *07-03-2024*

Revised: *30-04-2024*

Accepted: *27-05-2024*

Abstract

The Internet of Thing (IoT) plays a major role for improving the green house plant productivity and generates essential information to yields. Various existing systems introduces a smart approach that utilizes the IoT concept to remotely deliver users with data regarding temperature, humidity, and soil moisture severity. The purpose of this system is to track and evaluate plant circumstances. This paper descries a plant growth analysis using IoT and statical machine learning techniques for broccoli plants. Initially data has collected using IoT modules including various potential parameters such as soil temperature, soil moisture, humidity and plant height on daily interval basis. The experimental analysis has done in controlled environment for 30 days daily records. Finally, system recommends possible decides need to take for improve the yield or productivity.

Keywords: IoT, plant analysis, machine learning techniques, Arduino UNO, analogue to digital, prediction system.

1. Introduction

The growth of plants is influenced by atmospheric and outside influences. Greenhouse farmers face challenges in effectively monitoring the humidity levels within their facilities [1]. They are unable to ascertain the events occurring within the greenhouse just through tactile or sensory perception. Their daily operations are predominantly grounded in their experiences. In the event of excessively arid conditions, the crop will be irrigated. Conversely, if the climate is excessively wet, the protective roof will be opened, particularly during daylight hours [2]. In order to accomplish optimal development,

www.nmiet.edu.in

ISSN: 1092-910X
Vol 27 No. 3 (2024)

increased plant output at reduced costs, good quality, and lowest adverse environmental impacts, it is imperative to enhance the accuracy of greenhouses crop cultivation [3]. Utilizing IoT technology to regulate the greenhouse offers significant support in overseeing the control of cooling, heating, water levels in the soil, and various other functionalities. Furthermore, an Internet of Things (IoT)-enabled greenhouse may be remotely operated from any location, while continually tracking external variables such as temperature and humidity [4]. A single person can manually control these variables in the plant.

Automate is advantageous for optimizing tasks and minimizing the requirement for manual labor, such as toggling switches. Nevertheless, automation is unable to totally eradicate or diminish human errors, although it can be partially mitigated [5]. In a contemporary setting, all aspects must be effectively and remotely controlled. In addition, if greenhouse proprietors have the ability to monitor and control their greenhouse remotely, they do not need to do regular physical inspections of the circumstances. Users should have the ability to easily control and oversee several greenhouses from a centralized place. The WiFi module play a vital role in delivering data to the smart system by eliminating the requirement for cables or connected devices, hence resulting in cost reduction [6].

The integration of advanced technologies such as machine learning, sensors and actuators, unmanned overhead systems, RFID gadgets big analytics, machine learning, and satellites has greatly enabled the extensive utilization of the Internet of Things (IoT) in diverse agricultural applications. These applications encompass innovative farming, frost mitigation, and intelligent preparedness in greenhouses [7]. The implementation of extremely efficient communication networks has played a significant role in the extensive acceptance of IoT in smart greenhouses and precise farming [8]. Traditional agriculture is defined by the restricted incorporation of database decision support systems, leading to avoidable human intervention, increased labor expenses, and susceptibility to catastrophic weather occurrences. The Internet of Things (IoT) offers solutions for tracking crop challenges by utilizing the use of AI, machine learning, and computerized agricultural processes to conserve water and electricity. The farmers' failure to utilize IoT technology can be linked to the absence of established criteria for water and electricity allocation, usage of energy, and uncertainty over agricultural goods price determination due to shifting market prices [9]. Small-scale farmers lack motivation to participate in emerging technologies like IoT due to their limited profit margins, but large-scale agricultural enterprises have the financial capacity to quickly acquire IoT equipment [10]. Although IoT systems are commonly used in intelligent greenhouses as a there is a limited comprehension of how this technology might enhance greenhouse conditions, especially in tropical climates with significant shifts in temperature.

The objective is to create an Internet of Things (IoT) enabled greenhouse system that can monitor and regulate the temperature, moisture content of the soil, and other variables within the greenhouse. The goal is to develop a self-sufficient model that can operate with minimal human involvement. The system will utilize sensors, processors, and fans to control thermostat and soil moisture. This will allow users to cultivate acceptable plants at the optimal period, while also reducing the likelihood of fire occurrences by incorporating flame and smoke monitors.

www.nmiet.edu.in

ISSN: 1092-910X
Vol 27 No. 3 (2024)

2. Literature Survey

Greenhouses offer precise regulation of the environmental conditions under which plants thrive. In addition to providing protection from insects and avian creatures, these structures also offer enhanced regulation of variables such as temperature, humidity, irrigation, and illumination [11]. By utilizing a greenhouse, it is possible to provide optimal environmental conditions that promote the flourishing of plants, eliminating the necessity for detrimental pesticides and guaranteeing the production of nutritious foods. Utilizing technology, individuals aspiring to become commercial farmers can make precise predictions about harvest expectations and examine many factors affecting crop growth in a greenhouse [12]. The expenses associated with establishing a greenhouse can rapidly be transformed into financial gains by executing a suitable growth strategy that is in line with the production process. Similar to any business endeavor, investments are necessary to establish the optimal circumstances for generating profit. For individuals who have a strong interest in gardening and desire to generate additional income, it is a sensible progression to consider investing in a nursery [13,14]. Over 50% of the global population relies on traditional farming as their main source of food and agriculture [15]. Nevertheless, conventional farming methods pose substantial environmental obstacles, despite their contribution to cultural conservation. Traditional farming techniques have been identified as a contributing factor to several global issues, such as environmental degradation, deforestation, water scarcity, and malnutrition [16].

The majority of the agricultural equipment utilized in conventional farming is antiquated. On the other hand, modern agriculture depends on machinery [17]. Contemporary agricultural methods involve the utilization of technology. Although contemporary farming is known for its great production, traditional farming is more adaptable to an uncertain environment. Despite its lower productivity, traditional farming is still capable of producing crops of satisfactory quality [18]. Conversely, the overutilization of technology and its associated methods and systems in contemporary agriculture can lead to decreased crop production. Consequently, traditional farming remains acknowledged and employed [19]. One significant distinction among traditional farming and contemporary agriculture is in the labor intensity. Traditional agriculture offers a multitude of employment prospects due to its reliance on substantial physical labor. Modern agriculture, in contrast, heavily depends on machinery, hence decreasing the requirement for human labor [20]. As a result, the career prospects in contemporary agriculture are somewhat restricted. Contemporary agriculture employs several techniques including pesticides, plant breeding, agronomy, and the application of steroids and antibiotics in the care of livestock, which are not typically utilized in traditional agriculture [21].

In contrast, conventional agriculture extensively depends on home methods to safeguard crops against insect and pest-borne diseases [22]. There is a notable difference between traditional farming and modern agriculture. Ensuring continuous plant growth in modern agriculture requires meticulous inspection of humidity, temperatures, and safety conditions. Various frameworks can be utilized for this objective. Temperature monitoring systems employ many sensors to collect temperature data. Given the diverse applications of temperature sensors, both wired and wireless, farmers need to meticulously choose the suitable sensors for their needs. Farmers can customize the remote nursery temperatures monitoring system to determine how often readings are taken and to set up alerts via email or SMS text messages. Humidity monitoring systems improve efficiency and mitigate crop

www.nmiet.edu.in

ISSN: 1092-910X
Vol 27 No. 3 (2024)

damage by identifying contamination resulting from inadequate moisture levels in the greenhouse. Humidity sensors aid farmers in detecting problems at an early stage and thereafter offer continuous real-time monitoring.

The sensors have the capability to monitor humidity within a range of 0% to 100%, with a resistance accuracy of ±3.5%RH. In addition, humidity sensors which are resistant to moisture and waterproof can be used in both indoor and outdoor settings. In addition, automated systems for monitoring and circulation control gases to maintain a favourable temperature in the greenhouse. Prompt detection of fire events is vital, and automated alarms aid in the identification of smoke in the growing space. Smoke diffusion is challenging in large greenhouses due to the positioning of roof sensors at elevated locations. Fire safety systems are installed at both the upper and lower levels of shadow draperies, which is not possible with conventional point detection systems. These kinds of detectors are specifically engineered to safeguard against the negative impact of wetness and dust on the accuracy of detection. They guarantee exceptional sensitivity and the ability to identify early signs even in demanding and consistent environments.

3. Proposed System Design

The proposed greenhouse is comprised of five distinct components, including data collecting, data retrieval and presentation, plant information section, automated of devices, and human control of devices:

Data collection involves the acquisition of data from five distinct sensors, specifically soil temperature, moisture in the soil, humidity, and others. Subsequently, this data is transmitted to a database using the Ethernet shield. The objective is to attain a frequency of two to three occurrences per second with precision. Tables are created to exhibit the most recent data on temperature, humidity, and moisture, which are consistently refreshed.

The plant information area classifies plants and offers users recommendations on suitable plants to cultivate during various seasons, along with the optimal temperature and humidity requirements. Users have the ability to manually control all devices. The mechanization of the system can be predominated by manual controls. The computerization can only be enabled when the manual control is deactivated. Authentication is required for users to gain access to the manual administration portion and engage with the system via a web-based application.

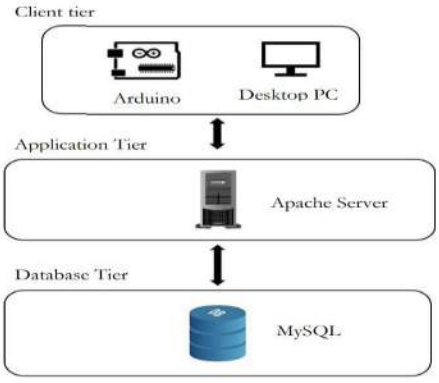

Figure 1: Architecture for IoT data collection

www.nmiet.edu.in

ISSN: 1092-910X
Vol 27 No. 3 (2024)

The proposed framework adheres to a three-tier architecture, as depicted in Figure 1. The client layer serves as the interface of the application, responsible for gathering user input via forms and presenting the resulting output. Browsers serve as the front-end layer for web applications. The application layer is positioned between the client tier and the data tier, where it handles the processing of the information gathered in the client tier. The database tier is responsible for storing all the information that is processed by the application tier. Data is also extracted from the database layer to be shown or used for additional manipulation in the client layer. The user engages with the system via a web application. After initiating the dashboard, visitors have the ability to go to other areas without any restrictions. In order to access the automation and manual control parts, users must log in. The Arduino board comprises various subcomponents that communicate with the database through distinct methods. The sensors transmit live data to the database. The web application will automate the process by altering the settings in the control tables of the database and subsequently transmitting a relay signal to activate or deactivate the actuators. The inclusion of a relay is important due to the fact that devices such as fans and pumps necessitate a power supply of 12V, a voltage that exceeds the capabilities of the Arduino.

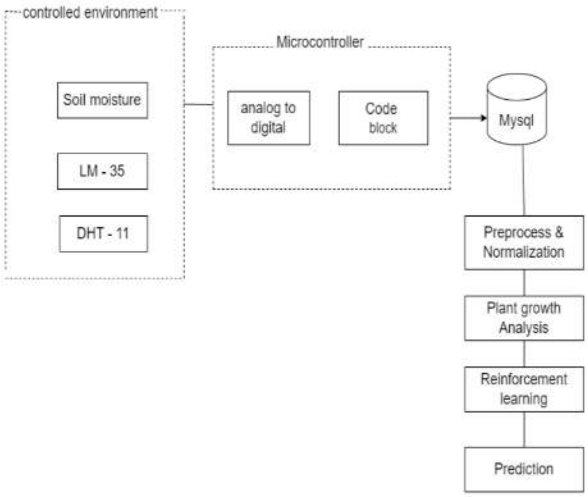

Figure 2: proposed system architecture for plant growth analysis in controlled environment

The above Figure 2 describes a plant growth analysis using IoT and machine learning techniques. The IoT modules generated event-based data and the prosed Q-learning base reinforcement algorithm generates an action plan according to analysis. The major benefit of a controlled environment is, that it can automatically maintain the required environment such as temperature, humidity, soil moisture, etc. Due to this kind of dynamic execution, we can achieve higher productivity and yield within the specific time frame for broccoli plants.

The reinforcement learning techniques for plant growth analysis in a controlled environment is an innovative approach that can optimize agricultural processes. Here's how you could structure such a system:

IoT Sensor Network: Deploy various sensors within the controlled environment to monitor crucial parameters such as temperature, humidity, soil moisture, light intensity, CO2 levels, and nutrient

www.nmiet.edu.in

ISSN: 1092-910X
Vol 27 No. 3 (2024)

concentrations. These sensors would continuously collect data and transmit it to a central processing unit.

Data Collection and Preprocessing: Gather data from IoT sensors and preprocess it to remove noise and inconsistencies. This step involves data cleaning, normalization, and feature extraction to prepare the data for analysis.

Reinforcement Learning Model: Implement a reinforcement learning (RL) model to optimize plant growth conditions based on the collected data. RL algorithms Q-Learning algorithm learns optimal control policies through trial-and-error interactions with the environment.

Reward Function: Define a reward function that quantifies the plant growth performance based on desired metrics such as yield, quality, or growth rate. The RL agent aims to maximize this reward over time by adjusting control actions in the environment.

Control System: Interface the RL agent with actuators and control mechanisms within the controlled environment. These actuators can adjust parameters like irrigation, lighting, ventilation, and nutrient delivery based on the decisions of the RL agent.

Training and Optimization: Train the RL model using historical data and simulation environments to accelerate learning. Continuously optimize the model by fine-tuning parameters and updating the reward function based on feedback from plant growth outcomes.

Real-time Decision Making: Deploy the trained RL model in the actual controlled environment to make real-time decisions. The model continuously receives sensor data, computes optimal control actions, and sends commands to adjust environmental conditions accordingly.

Monitoring and Feedback Loop: Implement a monitoring system to track the performance of the RL-controlled environment. Analyse plant growth metrics and compare them against desired outcomes. Adjust the RL model and control parameters as needed based on feedback to improve system performance.

Data Security and Privacy: Ensure that data collected from IoT sensors and RL model parameters are secured and protected against unauthorized access. Implement encryption, authentication, and access control measures to safeguard sensitive information.

By integrating IoT and reinforcement learning techniques, this system can create an autonomous and adaptive environment for optimizing plant growth in controlled agricultural settings, leading to improved yields, resource efficiency, and sustainability.

4. Results and Discussion

This research offers basic information on humidity to aid users who may lack expertise about humidity and its proper regulation. Furthermore, the system provides data regarding the best circumstances necessary for achieving optimal plant growth. This encompasses specific information regarding the most favourable period of the year for cultivating particular plants, along with the suggested temperature and humidity thresholds for attaining ideal growth. Plants are classified into categories based on their characteristics, including chilly, warm, decorative, and tropical seasons. Moreover, the system guarantees the automatic management of the devices when the user is operating them. The fan

control enables the user to enter the minimum and maximum temperature settings, which function as thresholds. Once the current temperature beyond the predetermined threshold, the appropriate fan will activate, and it will deactivate once the current temperature drops below the value specified by the user. This guarantees that the temperature stays within a specific range. As a precautionary measure, the system verifies the lack of fire prior to executing the code to activate the fans. The user can choose from four categories to control the water pump. Each category has its own minimum and maximum threshold values. The water pump activates when the current moisture level falls below the minimum threshold and deactivates when it surpasses the maximum threshold. The mechanism, like temperature control, guarantees that soil moisture stays within the range specified by the user.

In terms of security measures, the system incorporates motion detection within designated time intervals, which prompts an alert in the event of any observed motion. When the system is in manual control mode, the security system is disabled, assuming that the operator is in close proximity to the greenhouse. Nevertheless, the fire and smoke systems continue to operate in both manual and automatic control modes, as they are crucial safety components. During a fire incident, all fans are deactivated to restrict the supply of oxygen, and a notification is delivered to the user. Likewise, in the event that smoke is detected, a notification is dispatched. A comprehensive evaluation of the system has been carried out to confirm its ability to respond accurately to variations in temperature and humidity. The system quickly reacts by engaging fans and pumps as necessary. Testing has been conducted on light, motion, flame, and smoke sensors, and the actual outputs have aligned with the anticipated findings. The below Table 1 describes as details parameters evaluation of data collected by IoT framework on daily basis.

Table 1 : Data collection and its analysis details from IoT Module

Date	Soil Temp	Humidity	Moisture	Plant height (cm)
1/3/2024	18.2°C	15.50	30	10.3
2/3/2024	18.3°C	16.30	29	10.4
3/3/2024	19.2°C	15.30	28	10.6
4/3/2024	19.3°C	18.30	29	10.9
5/3/2024	18.4°C	19.50	31	11.1
6/3/2024	17.2°C	20.10	29	11.3
7/3/2024	19.7°C	19.80	30	11.5
8/3/2024	20.1°C	18.20	32	11.7
9/3/2024	20.1°C	18.00	33	12.1
10/3/2024	19.4°C	17.30	33	12.6
11/3/2024	19.6°C	17.20	32	12.9
12/3/2024	20.3°C	16.20	30	13.3
13/3/2024	21.1°C	18.20	30	14.8
14/3/2024	21.6°C	17.40	31	15.2
15/3/2024	21.7°C	18.40	32	15.8
16/3/2024	21.9°C	15.90	31	16.2
17/3/2024	20.4°C	16.20	31	16.9

www.nmiet.edu.in

ISSN: 1092-910X
Vol 27 No. 3 (2024)

18/3/2024	20.7°C	17.20	30	17.5
19/3/2024	20.7°C	17.30	29	18.4
20/3/2024	20.4°C	17.80	29	19.0
21/3/2024	21.9°C	19.10	31	19.7
22/3/2024	20.6°C	18.20	32	20.1
23/3/2024	21.5°C	16.70	32	21.6
24/3/2024	21.7°C	17.60	32	22.1
25/3/2024	19.6°C	18.40	33	22.9
26/3/2024	20.4°C	18.60	31	23.7
27/3/2024	20.4°C	18.50	34	24.2
28/3/2024	20.8°C	18.90	32	24.6
29/3/2024	21.1°C	17.40	33	25.1
30/3/2024	21.3°C	17.80	33	25.4
31/3/2024	21.1°C	18.10	32	26.1

Figure 3 : Soil temperature analysis on daily basis by IoT model

Figure 4 : Humidity values on daily basis by IoT model

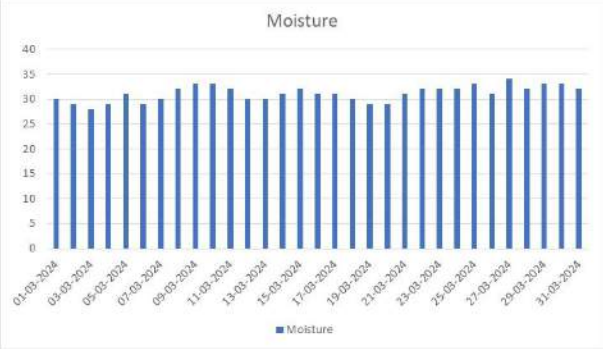

Figure 5 : Soil moisture analysis on daily basis by IoT model

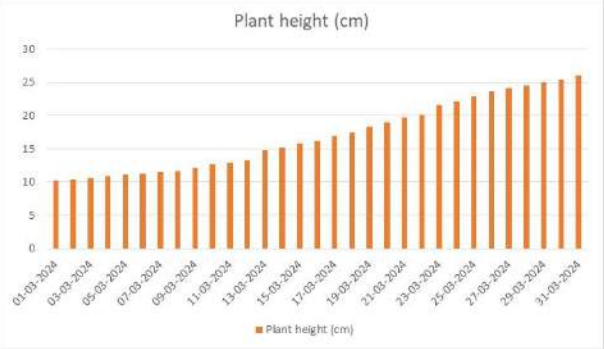

Figure 6: Plant growth analysis on daily basis

The above Figure 3 to Figure 6 describes an analysis of data using reinforcement learning techniques. The controlled environment maintains the all vital every time and boost the plant growth rapidly.

www.nmiet.edu.in

ISSN: 1092-910X
Vol 27 No. 3 (2024)

5. Conclusion

The collaboration of IoT and learning techniques for plant growth analysis in a controlled environment is an innovative approach that can significantly optimize agricultural practices. Below are the system modules of proposed system. Deploy various sensors throughout the controlled environment to monitor crucial variables such as temperature, humidity, soil moisture, light intensity etc. These sensors continuously collect data and transmit it to a central system for analysis. Data collected from IoT sensors are preprocessed to remove noise and inconsistencies. This step ensures that only high-quality data are used for analysis, enhancing the accuracy of the system. RL algorithms can be employed to optimize plant growth conditions by learning from the collected data and making decisions to maximize a predefined reward function. The RL agent interacts with the environment by taking actions to achieve the desired outcome. The RL agent might use a basic policy or model to interact with the environment. Through iterative learning, the agent improves its policy by receiving feedback from the environment and adjusting its actions accordingly. Techniques such as Q-learning has used for training the RL agent. The RL agent continuously receives feedback on plant growth metrics, such as growth rate, biomass accumulation, and quality of produce. This feedback is used to update the agent's policy, enabling it to adapt to changing environmental conditions and optimize plant growth over time. The RL agent's decisions are translated into control signals that adjust the settings of the controlled environment, such as turning on/off lights, adjusting temperature and humidity levels, or regulating nutrient delivery. This integration ensures real-time control over the growth conditions based on the learned policies. The system provides real-time monitoring of plant growth parameters and environmental conditions. Visualization tools can be used to present this data in a user-friendly format, allowing farmers or researchers to track the progress of the plants and make informed decisions.

References

[1] I. Ardiansaha, N. Bafdalb, E. Suryadib, and A. Bonoc, “Greenhouse monitoring and automation using arduino: a review on precision farming and internet of things (IoT).” Int J Adv Sci Eng Inform Technol, vol. 10, no.2, pp.703–70, 2020.

[2] V. Modani, R. Patil, & P. Puri, “Smart Greenhouse Multifactor Monitorıng Usıng IOT”. International Journal of Engineering & Technology, vol. 7, no. 419, pp. 1016-1020, 2018.

[3] M. Kumar, T. Chandra, D. Kumar and M. Manikandan, “Monitoring moisture of soil using low-cost homemade Soil moisture sensor and Arduino UNO,” In: 3rd international conference on advanced computing and communication systems (ICACCS), 1, pp. 1–4, 2016

[4] K.Joudi, A. Farhan, “A dynamic model and an experimental study for the internal air and soil temperatures in an innovative greenhouse”, Energy ConverManag, no. 91, pp. 76–82, 2015.

[5] S. Mahmoud and I. Ala’a , “Greenhouse micro-climate monitoring system based on wireless sensor network with smart irrigation, Int J ElectrComput Electron CommunEng, vol. 7, no.12, pp. 1072–1077, 2013.

[6] R. Mendez, M. Yunus and S. Mukhopadhyay, “A WiFi based smart wireless sensor network for an agricultural environment”, In: 2011 Fifth international conference on sensing technology, pp. 405–410, 2011.

[7] K. Wang, K. Shiong Khoo, H.Y. Leong, D. Nagarajan, K. Chew, H.Y. Ting, A. Selvarajoo, J.S. Chang and P.L. Show, “How does the Internet of Things (IoT) help in microalgae biorefinery?” Biotechnol,no. 107819, 2021.

[8] K. Lova Raju and V. Vijayaraghavan, “IoT Technologies in Agricultural Environment: A Survey, Wireless,Pers. Commun., no. 113, pp 2415–2446, 2020.

www.nmiet.edu.in

ISSN: 1092-910X
Vol 27 No. 3 (2024)

[9] R. Rayhana, G. Xiao and Z. Liu, "Internet of Things Empowered Smart Greenhouse Farming", IEEE J. Radio Freq. Identif., no.4, pp 195–211, 2020.

[10] Y. Zhang, P. Geng, C. Sivaparthipan and B Muthu, "Big data and artificial intelligence based early risk warning system of fire hazard for smart cities", Sustain. Energy Technol. Assess., no. 45, p. 100986, 2021.

[11] M. Rojas, J. Motta, N. Gonzalez, L. F. Corke, and P.Depari, "Towards the development of agas sensors system for monitoring pollutant gases in the low troposphere using small unmanned aerial vehicles., Malaysian Journal of Computer Science, vol. 36, no. 1, 2023

[12] H.Jawad, R. Nordin, S. Gharghan, A. Jawad and M. Ismail , "Energy Efficient Wireless Sensor Networks for Precision Agriculture: A Review Sensors" no. 17, p. 1781, 2017

[13] A. A. Raneesha Madushanki, N. Malka, W. Halgamuge, A. H. Surangi Wirasagoda, A. AliSyed, "Adoption of the Internet of Things (IoT) in Agriculture and Smart Farming towardsUrban Greening: A Review", International Journal of Advanced Computer Science and Applications (IJACSA), vol. 10, no. 4, 2019.

[14] A. Villa-Henriksen, G. Edwards, L. Pesonen, O. Green, "Internet of Things in arable farming: Implementation, applications, challenges and potential", CAG Sørensen Biosystems Engineering, pp. 60-84, 2020.

[15] M. Zamora-Izquierdo, A. Skarmeta-Gómez, A. Ramallo-González, V. Tomat and P. Fernández-Ruiz, "Conceptualisationo fan IoT framework for multiperson interaction with conditioning systems", Energies, vol.13, No. 12, p. 3094.

[16] I. Ullah, A. Ullah and M. Sajjad, "Towards a hybrid deep learning model for anomalous activities detection in internet of things networks", IoT, vol. 2, no. 3, pp. 428-448, 2021.

[17] V. Khavalko, S. Baranovska, and G. Geliznyak, "Investment Feasibility of Building the Architecture of Greenhouse Automated Control System Based on the Io T and CloudTechnologies", InCMiGIN, pp. 311-323, 2019.

[18] D. Piromalis, K. Arvanitis, T. Bartzanas, D. Loukatos, C. Piromalis, D. Arvanitis, K. Bartzanas, T and D. Loukatos,. "Applications of IoT for optimized greenhouse environment and resources management", Computers and Electronics in Agriculture, p. 198, 106993, 2022.

[19] O. Friha, M. Ferrag, L. Shu, L Maglaras .and X. Wang, "Internet of Things for the Future of Smart Agriculture: A Comprehensive Survey of Emerging Technologies", IEEE CAA J.Autom.Sinica, vol. 8, no. 4, pp. 718-752, 2021.

[20] A. Varjovi and S. Babaie, "Green InternetofThings (GIoT):Vision,applications and research challenges", Sustainable Computing: Informatics and Systems, no. 28, p.100448, 2020.

[21] B. Bilbao-Osorio, S. Dutta and B. Lanvin, "The global information technology report 2014: Rewards and risks of bigdata", InWorldEconomicForum, pp. 1-369, 2014.

[22] M. Ghoulem, El. K. Moueddeb, E. Nehdi, F. Zhong, and J. Calautit, "Design of a passive down draught evaporative cooling windcatcher (PDEC-WC) system for greenhouses in hot climates",Energies, Vol. 13, no. 11, p. 2934

www.nmiet.edu.in
Advances in Nonlinear Variational Inequalities
ISSN: 1092-910X
Vol 27 No. 3 (2024)

Biomedical ECG Signal Compression by Combining Wavelet Transform and Unsupervised Autoencoder Techniques

Abhijeet. Y. Men[1], Dr. A. S. Joshi[2]

[1]Research Scholar, Department of Electronics and Telecommunication Engineering, Sipna College of Engineering and Technology, Amravati, Maharashtra, India. E-mail: abhijeet.men@gmail.com

[2]Professor, Department of Electronics and Telecommunication Engineering, Sipna College of Engineering and Technology, Amravati, Maharashtra, India. E-mail: asjoshi@sipnaengg.ac.in

Article History:

Received: *16-02-2024*

Revised: *26-04-2024*

Accepted: *18-05-2024*

Abstract: Storing biomedical signal data is a significant concern in the field of biomedical signal processing because it requires a substantial amount of storage space. These biomedical signals often contain hours of information, necessitating extensive storage capacity. Researchers employ Electrocardiogram (ECG) signal compression techniques to address this issue. However, compressing the ECG signal could potentially lead to the loss of important features or data. This loss may adversely impact the accurate analysis of heart patient conditions. This paper introduces a novel approach for compressing ECG signals by the combined power of Wavelet Transform (WT) and unsupervised Autoencoder (AE) techniques. ECG signal compression plays a crucial role in reducing data storage and transmission requirements without compromising diagnostic accuracy. The proposed methodology, termed WT-AutoEncoder, integrates Wavelet Transform for signal decomposition and feature extraction, followed by an Autoencoder for efficient encoding and reconstruction of the original signal. Unlike conventional methods, this approach utilizes the strengths of both WT and AE to achieve high compression ratios while preserving signal accuracy. The study conducts comprehensive experiments and evaluations using benchmark MIT-BIH datasets to assess the performance of the WT-AutoEncoder on specific records (101-109) in terms of compression ratio of 32.31, PRDN of 33.26, PRD of 3.06, and QS of 13.49. The final results demonstrate the effectiveness of the proposed model compared with existing methods in compressing ECG signals while maintaining high accuracy, suggesting its potential for secure transmission and storage in various healthcare applications.

Keywords: Electrocardiogram Signal, Signal Processing, Signal Compression, MIT-BIH Dataset, Wavelet Transform, Autoencoder

1. Introduction

The electrocardiogram (ECG) is an important tool in medicine for diagnosis. However, storing large amounts of clinical data can be costly if it isn't compressed, needing a lot of hard disk space. ECG data compression should be real-time, lossless, with high compression rates, and allow the use of compressed data without complete decompression. Automatic ECG recordings help diagnose cardiovascular diseases but take a long time to record. There's a need to analyze and store lots of

www.nmiet.edu.in

ISSN: 1092-910X
Vol 27 No. 3 (2024)

ECG data efficiently, preserving crucial features for diagnosis [1]. Hence, compression algorithms are necessary to improve storage and analysis efficiency.

Current ECG compression methods fall into three categories: direct processing, transformation, and neural networks. Direct processing methods like Evolutionary Computation [2], Turning Point Scan-Along Polygonal Approximation [3], and Differential-Pulse Coding Modulation like SVD [4], DPCM [5] algorithms eliminate redundant ECG information. Transformation methods, like Kanade Lucas Tomasi [6], Discrete Cosine Transform [10], and Fast Fourier Transform like KLT [7], DCT [8]-[9], FFT [10] algorithms, compress data using mathematical functions. Neural network-based methods [11]-[12] extract feature information from ECG through self-learning.

The methods that extract parameters are used to get important information from the signal. They use these details later to rebuild the signal [13]. In [14] one method called linear prediction coding (LPC) they proposed using a particular algorithm. Another approach combined finding the QRS in ECG and compressing data using an adaptive prediction technique [15]. In a different method, they suggested using Autoencoders for compression. These AEs were different from the regular ones and used a variation called denoising autoencoders (DAEs) [16].

Unlike these usual methods, DL has the potential to make algorithms based on signals. DL has been successful in many fields like recognizing images [17], objects [18], or speech [19]. Researchers also use DL for analyzing biomedical signals [20]-[21]. This research proposes the utilization of a specific DL model, the Autoencoder integrated with wavelet transform, for compressing ECG signals. This unique autoencoder model involves the tuning of hyperparameters and the introduction of a 'SparsityRegularization' function for the first time. While Autoencoder classifiers are commonly applied to 2-D images, this study stands out for focusing on compressing 1D ECG signals. The potential application of this model extends to securely transmitting biomedical ECG signals within the healthcare domain.

Neural network-based ECG compression is gaining attention due to its adaptability, parallel processing, waveform quality, and resistance to interference. Efficient ECG compression should achieve a high compression ratio without losing vital information. Designing a multi-objective function can optimize ECG compression, ensuring minimal loss of ECG data. Current neural networks focus on one objective, potentially reaching only optimal solutions or risking ECG data loss due to concentrating solely on improving data quality.

The main contribution of this paper is

- A Biomedical ECG signal compression unsupervised model is developed based on autoencoder and wavelet transform.
- Optimizes the autoencoder by tuning the hyperparameter to achieve the maximum compression ratio without noise in the ECG signal.
- The experimental study is conducted on the MIT-BIH dataset to validate the performance of the Proposed model. The final results are compared with the existing state-of-art methods.

The remaining sections of the paper are organized as follows: Section 2 presents previous research in the field of ECG signal compression. Section 3 discusses the proposed methodology in detail.

www.nmiet.edu.in

ISSN: 1092-910X
Vol 27 No. 3 (2024)

Section 4 presents the performance of the proposed model based on various evaluation parameters. Finally, the conclusion and future scope are discussed.

2. Proposed Methodology

In this part, we outline the mathematical expressions for the Wavelet Transform method and the unsupervised auto-encoder neural network. Figure 1 shows the block diagram of the proposed neural network for compressing the ECG signal based on the wavelet and autoencoder approach. Each block can be described in the following subsection.

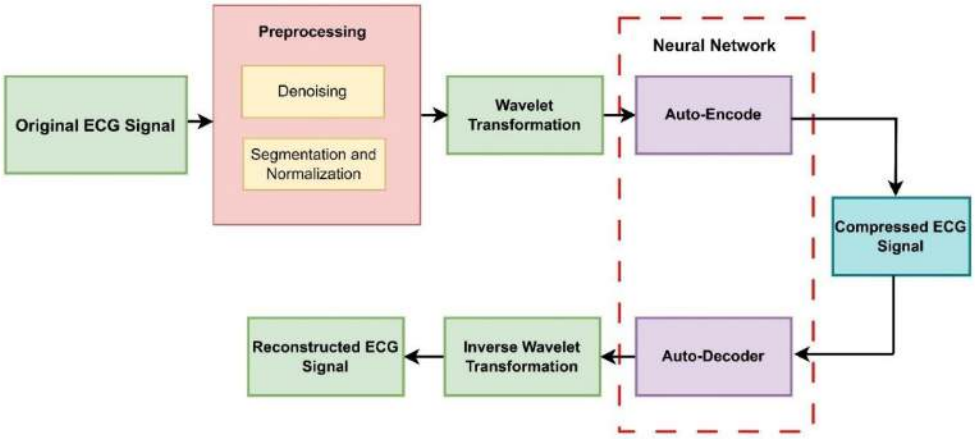

Figure 1: Architecture of Proposed ECG Signal Compression Model

Dataset Description: The MIT-BIH Arrhythmia Database comprises 48 half-hour segments of ECG recordings from 47 individuals studied between 1975 and 1979. The data was collected from the BIH Arrhythmia Laboratory. Among these, 23 recordings were randomly chosen from a collection of 4000 24-hour ambulatory ECG recordings, which included both inpatients (around 60%) and outpatients (around 40%) at Boston's Beth Israel Hospital. The remaining 25 recordings were specifically selected to include less common but medically significant arrhythmias that might not be found in a random sample. These recordings were digitally stored at 360 samples per second per channel with an 11-bit resolution within a range of 10 mV. Each record underwent independent annotations by two or more cardiologists [22]. Any discrepancies were resolved to generate computer-readable reference annotations for each heartbeat, resulting in approximately 110,000 annotations available in the database. Initially, only half of this database, including 25 complete records and reference annotation files for all 48 records, was accessible since September 1999. However, the other 23 signal files, previously exclusive to the MIT-BIH Arrhythmia Database CD-ROM, were made available in February 2005 on this platform.

3. Wavelet Transformation

Extracting features from ECG signals is essential [23]-[24] to eliminate noise interference from the environment. To achieve the best possible data compression while maintaining high quality, a Pareto-optimal solution is necessary. The Wavelet Transform is particularly useful for signals that change rapidly over time, instantly identifying and removing baseline drift noise. In the wavelet transform module, the input signal is made up of a smaller version of the main wavelet signal. In this paper illustrate the integral equations for wavelet functions:

www.nmiet.edu.in

ISSN: 1092-910X
Vol 27 No. 3 (2024)

$$WTf(t) = \frac{1}{s}\int_{\infty}^{+\infty} f(\tau)\, s\,(\frac{t\tau}{s})\, d\tau \quad (1)$$

Initially wavelet parameter chooses the value of 2 as an exponent that can be shows as s 2^j, where $j = 1,2,3\ldots.n$. here, φrepresents the parameter of basic wavelet transform as shown in equation 2.

$$\varphi_s(t) = \frac{1}{s}\varphi(\frac{t}{s}) \quad (2)$$

Based on the previous equation 1 and 2, the wavelet can be represented in equation 3

$$WT_2f(t) = \frac{1}{\sqrt{2^j}}\int_{\infty}^{+\infty} f(\tau)\,\sqrt{2^j}\,(\frac{t\tau}{\sqrt{2^j}})\, d\tau \quad (3)$$

The utilization of Wavelet Transform (WT) is essential for discrete signals. Subsequently, employing the WT algorithm enables the binarization of digital ECG signals using Equations 4 and 5.

$$WT_{2^j}f(t) = \sum_{i\in Z} G_i S_{2^{j-1}}f(n - 2^{j-1}i) \quad (4)$$

$$S_{2^j}f(t) = \sum_{i\in Z} H_i S_{2^{j-1}}f(n - 2^{j-1}i) \quad (5)$$

In this context, S_{2^j} represents a smooth function, $S_{2^j}f(t)$ stands for the original input ECG signal denoting low-frequency wavelet coefficients acting as the approximation function, and $S_{2^j}f(t)$ refers to the original signal signifying high-frequency coefficients. It's important to highlight that $H(i)$ and $G(i)$ correspond to coefficients of low-pass and high-pass filters respectively.

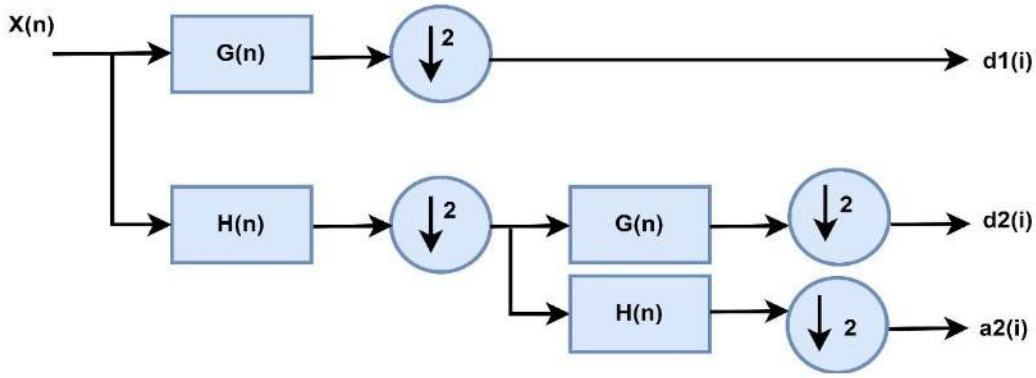

(A)

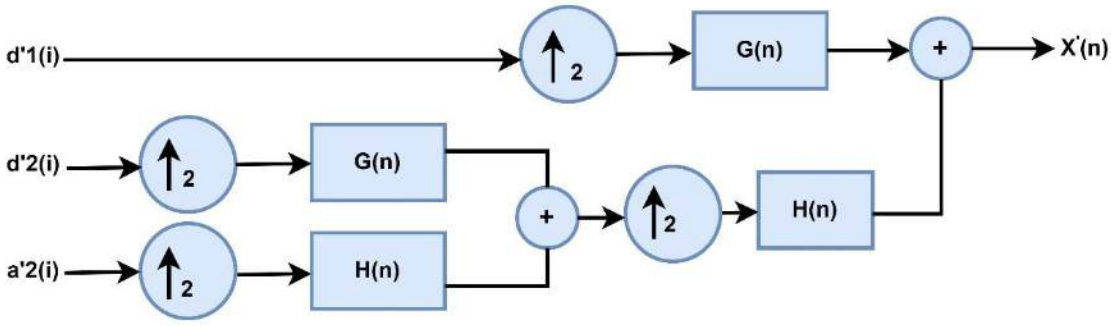

(B)

Figure 2: (A) Downsampling Decomposition of ECG Signal (B) Upsampling Decomposition of ECG Signal

www.nmiet.edu.in

ISSN: 1092-910X
Vol 27 No. 3 (2024)

The signal x(n) in the observed signal x'(n) can be transformed using the WT and inverse WT. Typically, the forward WT is as depicted in the equation:

$$W = Wx' \quad (6)$$

In this scenario, W stands for the forward transform matrix, and w represents the collection of wavelet coefficients including both detail and approximation components. However, the filter bank approach involves a step-by-step breakdown of the Low pass filter through an iterative process. During this decomposition phase, down-sampling and upsampling are implemented, illustrated in Figure 2 (A) and (B). Choosing the appropriate mother wavelet is crucial for accurately estimating the input ECG signal x. The subsequent action involves reducing the acquired coefficients. It's recommended to reduce the wavelet coefficients to generate favorable estimations [25]. These estimators using wavelets perform well across various loss functions and within a broad class of functions. They're straightforward, efficient, quick, and can adapt to variations in spatial and spectral aspects, and can easily scale to higher dimensions [26]. Reduction occurs by applying thresholds to the wavelet coefficients, transforming w into w'

When dealing with a wavelet coefficient w and a threshold $t > 0$, the outcome after hard thresholding is expressed as:

$$D(U,t) = U \quad \forall |U| > t$$

$$= 0 \quad \text{Otherwise} \quad (7)$$

And Soft thresholding is expressed as

$$D(U,t) = sgn(U)' \ \max(0, |U| - t) \quad (8)$$

Build Autoencoder Model with Hyperparameter

An autoencoder is a neural network designed for unsupervised learning that compresses data into a lower-dimensional representation and then reconstructs it. In the context of ECG signal compression, the specified hyperparameters govern the behavior of the autoencoder during training. The 'hiddenSize' parameter defines the size of the compressed representation layer, set at 30 nodes in this case. 'MaxEpochs' determines the number of epochs during training, with a value of 800 epochs. The 'EncoderTransferFunction' and 'DecoderTransferFunction' signify the activation functions used in the encoding and decoding layers, respectively, 'satlin' and 'purelin'. 'L2WeightRegularization' regulates the impact of large weight values in the network to prevent overfitting, set at 0.01. 'SparsityRegularization' controls the level of sparsity induced in the network, set at 4. 'SparsityProportion' sets the desired sparsity level to 0.10, which influences the activation of nodes to promote sparsity in the network representation. These hyperparameters were set to autoencoder's training process to efficiently compress ECG signals and effectively optimal reconstruction of ECG Signal.

Advances in Nonlinear Variational Inequalities
ISSN: 1092-910X
Vol 27 No. 3 (2024)

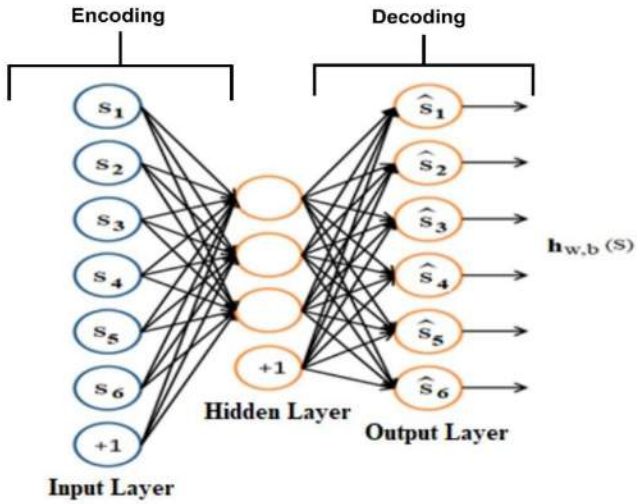

Figure 4: Structure of Autoencoder

Figure 4 shows the structure of autoencoder network based on backpropagation approach, to set the total targeted values is same as the inputs. $y(i) = s(i)$.

The autoencoder model is trained using the $hw, b(S) = s$ function. This function is used as an identity function so as output s' is same as the input s. Where, $a_j^{(2)}$represents the activation of hidden layer j in model. The s is used to fed the input that activate the model, thus it can be write as $a_j^{(2)}(x)$ represents the activation of neurons of model when the model gives the specific input s.

$$\hat{p}_j = \frac{1}{n}\sum_{i=1}^{n}[\, a_j^{(2)}\,(s^{(i)})] \quad (1)$$

The equation 1 is average activation of jth neurons

$$\hat{p}_j = p' \quad (2)$$

Where p represents the sparsity value that is very small nearer to zero (p=0.05). This constrains shows the threshold is used to activate neuron must be nearer to zero.

To make the task simpler by adding a penalty to main goal. This penalty will punish a big difference between two values, p and p'. There are different penalties can use, but go with this one.

$$\sum_{j=1}^{s2} plog\ \frac{p}{\hat{p}_j} + (1-p)\log\frac{1-p}{1-\hat{p}_j} \quad (3)$$

Where s2 represents the total amount of neurons presents in hidden layer, and j is the index that adding over the hidden layer in model. This penalty is based on Kullback-Leibler (KL) divergence so it can be written as in equation 4.

$$\sum_{j=1}^{s2} KL(p||\hat{p}_j) \quad (4)$$

it can be also written as

$$KL(p||\hat{p}_j) = plog\ \frac{p}{\hat{p}_j} + (1-p)\log\frac{1-p}{1-\hat{p}_j} \quad (5)$$

www.nmiet.edu.in

ISSN: 1092-910X
Vol 27 No. 3 (2024)

Where p and $\hat{p}_j$represents the divergence between a Bernoulli random variable with mean.

This penalty function has some conditions that

$KL(p||\hat{p}_j) = 0$

If $\hat{p}_j = p$

and otherwise it maximizes monotonically as $\hat{p}_j$ diverges from p.

Overall cost function is

$$J_{sparse}(W,b) = J(W,b) + \beta \sum_{j=1}^{s2} KL(p||\hat{p}_j) \quad (6)$$

Where, β represents the control weight of sparsity penalty. $\hat{p}_j$ is depend on the variable W, b because the average activation of neurons j and the activation of hidden layer is depending on the variables W, b.

The equation 6 represents a way to modify the original cost function $J(W,b)$ by adding a term β times the sum of KL divergences between two probability distributions: . Essentially, it enhances the cost function $J(W,b)$ by penalizing the divergence between the distributions $p\ and\ \hat{p}_j$ where j varies from 1 to $s2$. The parameter β controls the impact of this penalty on the overall cost.

The autoencoder model is trained by n number of sample ECG inputs. The input function is as shown in equation 7.

$$a_j^{(2)} = f(\sum_{j=1}^{n} W_{ij}^{(1)} s_j + b_i^{(1)}) \quad (7)$$

$$s_j = \frac{w_{ij}^{(1)}}{\sqrt{\sum_{j=1}^{n} (w_{ij}^{(1)})^2}} \quad (8)$$

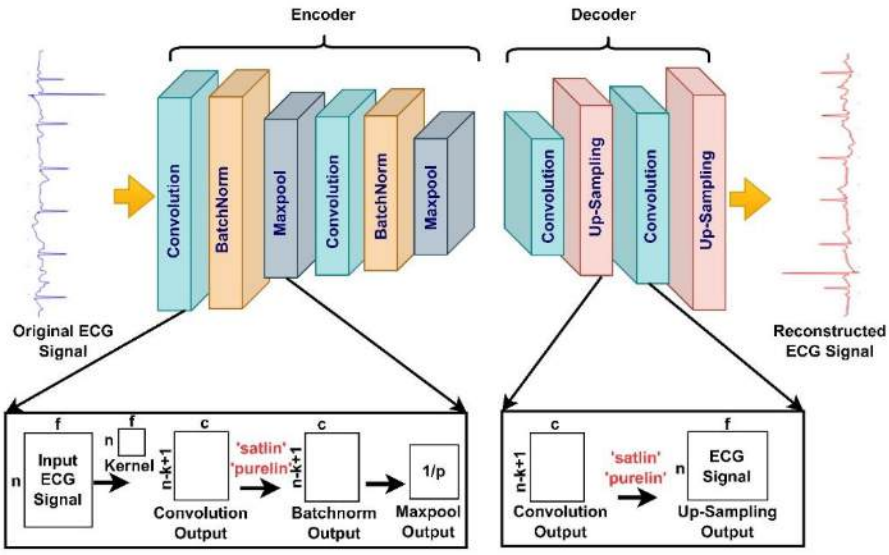

Figure 5: Architecture of Proposed Autoencoder Model

Figure 5 shows the complete architecture of autoencoder model.

Model Loss

The losses of the autoencoder model are measured during training to assess the quality of the training process. Minimal losses indicate accurate training of the model, indicating a minimal variance between the actual and predicted outputs. Conversely, higher losses suggest greater discrepancies between the actual and predicted outputs. The proposed experimental model addresses a regression problem and, therefore, utilizes Mean Squared Error (MSE) as the chosen loss function. The model's losses can be quantified using Equation 9.

$$MSE = \frac{1}{n}\sum_{j=1}^{n}(s_j - \hat{s}_j)^2 \quad (9)$$

Result Analysis

This section measures the performance of the proposed unsupervised autoencoder decoder model. The experimental results are carried out in MATLAB R2021b Software with Deep Learning Toolbox. The proposed model is trained on an Intel i5 processor, 16GB RAM, and 4GB Nvidia Graphics.

3.1 Performance Evaluation

The quality of the reconstructed signal should be clinically acceptable. The majority of ECG compression literature evaluates the global and local errors in the reconstructed signal using the following evaluation parameters. In the definitions symbols used are:

Compression Ratio (CR): CR in the context of ECG signal compression using unsupervised auto encoder decoder is a metric that quantifies the reduction in data size achieved through compression. The formula to calculate CR is straightforward:

$$Compression\ Ratio\ (CR) = \frac{Compressed\ Size\ of\ ECG\ Signal}{Original\ Size\ of\ ECG\ Signal} \quad (10)$$

Mean Square Error (MSE): The MSE is a metric utilized to measure the average of the squared differences between the initial uncompressed ECG signal and the reconstructed or compressed signal, achieved via unsupervised auto encoder decoder techniques. The computation for MSE is given by:

$$MSE = \frac{1}{n}\sum_{i=1}^{n}(x_i - \hat{x}_i)^2 \quad (11)$$

Where, n is the total number of data points in the ECG signal.

$x_i$represents the individual data point in the original uncompressed ECG signal.

$\hat{x}_i$ represents the corresponding data point in the reconstructed/compressed signal obtained through unsupervised auto encoder decoder-based compression.

Normalized Mean Square Error (NMSE): NMSE is a statistical metric used to assess the accuracy and similarity between the original input ECG signal and the reconstructed signal. NMSE accounts for the scale of the signal and is particularly useful when comparing signals of varying magnitudes.

$$NMSE = \frac{\sum_{i=1}^{n}(x_i - \hat{x}_i)^2}{\sum_{i=1}^{n}(x_i - \bar{x}_i)^2} \quad (12)$$

Root Mean Square Error (RMS): RMSE is a commonly used metric to evaluate the accuracy of reconstructed signals in comparison to the original input ECG signal, particularly in cases involving unsupervised auto encoder decoder for compression. The formula to calculate RMSE is:

$$RMSE = \sqrt{\frac{\sum_{i=1}^{n}(x_i - \hat{x}_i)^2}{n}} \quad (13)$$

Percentage RMS Difference (PRD): The PRD is an evaluation used to assess the similarity between the original uncompressed ECG signal and the reconstructed signal obtained through unsupervised auto encoder decoder techniques.

$$PRD = \frac{\sqrt{\frac{\sum_{i=1}^{n}(x_i - \hat{x}_i)^2}{\sum_{i=1}^{n} x_i^2}}}{\sqrt{\frac{\sum_{i=1}^{n} x_i^2}{n}}} \quad (14)$$

PRD Normalized (PRDN): The PRDN is a variant of the Percentage RMS Difference (PRD) used to assess the similarity between the original input ECG signal and the reconstructed signal obtained through unsupervised auto encoder decoder techniques. The formula to calculate PRDN is:

$$PRDN = \frac{PRD \times Range_x}{100} \quad (15)$$

Signal to Noise Ratio (SNR): SNR calculates the proportion of the signal's useful power to the power of the background noise present in a signal. When assessing the quality of a reconstructed signal concerning the original signal and the noise added during compression, SNR is significant in ECG signal compression using unsupervised auto encoder decoder techniques. The equation 15 to compute SNR is:

$$SNR = 10 \cdot log_{10}\left(\frac{Signal\ Power}{Noise\ Power}\right) \quad (16)$$

Peak Signal to Noise Ratio (PSNR): PSNR serves as a metric to assess the quality of a reconstructed signal by comparing it with the original signal. It determines the relationship between the highest potential power of a signal and the interference caused by noise, affecting its accuracy. In ECG signal compression using unsupervised auto encoder decoder, the PSNR is calculated using this equation 16:

$$PSNR = 10 \cdot log_{10}\left(\frac{Max^2}{MSE}\right) \quad (17)$$

To assess the effectiveness of the proposed model, various test cases were conducted using the records available in the dataset. Figures 5 to 9 depict the original ECG signal alongside the reconstructed ECG signal. It is noteworthy that the reconstructed ECG signal closely resembles the original signal.

Table 1: Performance Analysis of Autoencoder Model

Records	CR	MSE	RMS	PRD	PRDN	SNR	QS
100	32.3	0.00006	0.008	1.67	45.57	15.85	19.31
101	32.5	0.00028	0.017	3.18	38.09	19.42	10.14

102	32.4	0.00010	0.009	1.50	32.89	18.76	26.87
103	32.2	0.00067	0.026	4.89	22.15	30.15	6.59
104	32.3	0.00012	0.011	2.16	37.30	19.83	14.93
105	32.2	0.00067	0.026	4.89	22.15	30.15	6.59
106	32.2	0.00010	0.010	1.85	51.22	13.53	17.43
107	32.6	0.00025	0.015	2.89	32.15	30.15	12.50
108	32.2	0.00078	0.028	5.39	31.40	23.43	5.98
109	32.2	0.00022	0.015	2.20	19.71	32.77	14.65
Average	**32.31**	**0.00032**	**0.016**	**3.06**	**33.26**	**23.40**	**13.49**

The table 1 represents the performance analysis of an Autoencoder model across multiple records (100 to 109). The CR measures the compression achieved by the autoencoder, with higher values indicating better compression. MSE and RMS evaluate reconstruction errors, with lower values indicating better performance. PSNR and PSNRN represent the quality of the reconstructed signal, with higher values indicating better quality. SNR measures signal quality, and QS is an overall quality score. The average values across these metrics for the records range from 32.2 to 32.6 for CR, 0.00006 to 0.00078 for MSE, 0.008 to 0.028 for RMS, 1.50 to 5.39 for PRD, 19.71 to 51.22 for PRDN, 13.53 to 32.77 for SNR, and 5.98 to 26.87 for QS, with average metrics summarized at the bottom of the table 1 for a holistic view of the model's performance.

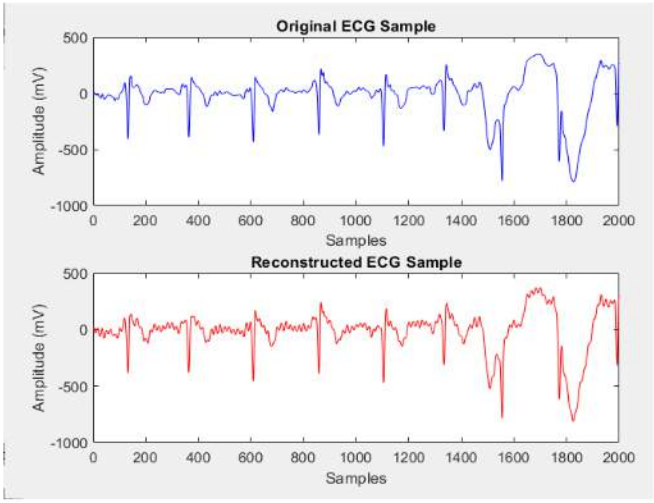

Figure 6: Original and Reconstructed ECG Signal over Record 100

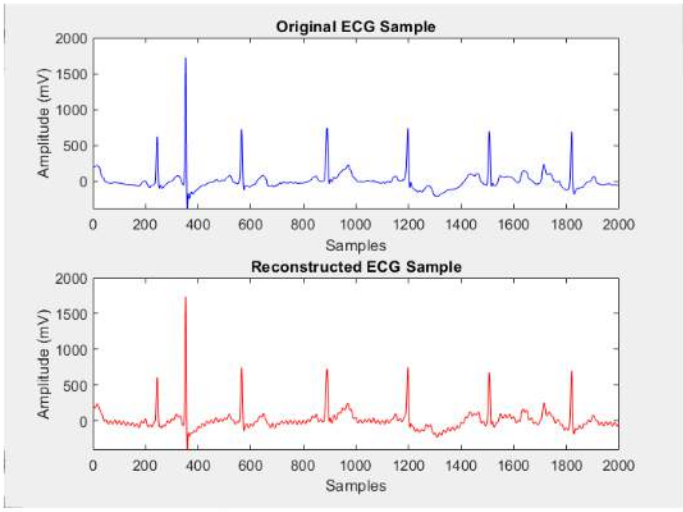

Figure 7: Original and Reconstructed ECG Signal over Record 101

www.nmiet.edu.in

ISSN: 1092-910X
Vol 27 No. 3 (2024)

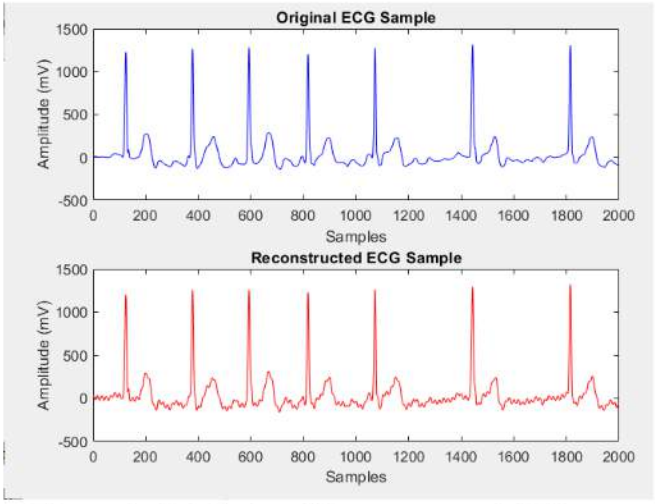

Figure 8: Original and Reconstructed ECG Signal over Record 102

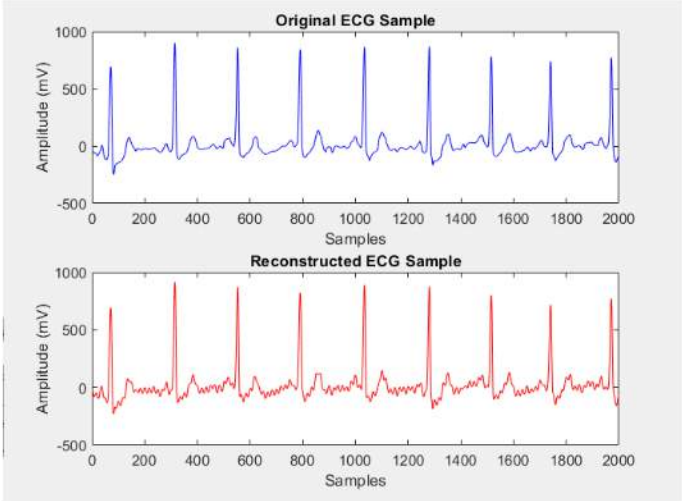

Figure 9: Original and Reconstructed ECG Signal over Record 103

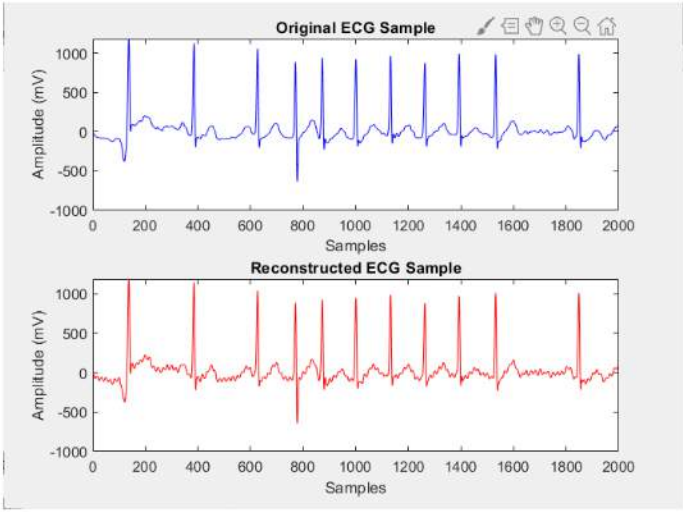

Figure 10: Original and Reconstructed ECG Signal over Record 104

Figures 6 to 10 display the original and reconstructed ECG signals from various records of the MIT-BIH dataset. The reconstructed ECG signals exhibit minor differences in amplitude and signal location. This clearly indicates that the quality of the reconstructed ECG signals approaches that of the original ECG signals. However, some distortion or noise is noticeable in the ECG signals.

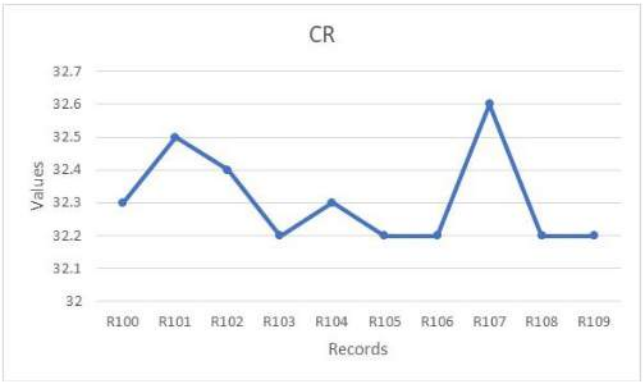

Figure 11: Compression Ratio of ECG Signal over 100 to 109 Records

www.nmiet.edu.in

ISSN: 1092-910X
Vol 27 No. 3 (2024)

The figure 11 depicts the Compression Ratio (CR) values of an ECG signal across records numbered from 100 to 109, with each record having its corresponding CR value. The Compression Ratio measures the extent of compression achieved by a data compression algorithm or model. In this specific case, the CR values range from 32.2 to 32.6 across the different records. The average CR value across these records is 32.31, which suggests that, on average, the compression technique applied to the ECG signal resulted in a compression ratio of approximately 32.31 times smaller than the original signal size. The graph provides a visual representation of how the CR varied across different instances of the ECG signal processing or compression, showcasing fluctuations and an overall average level of compression achieved.

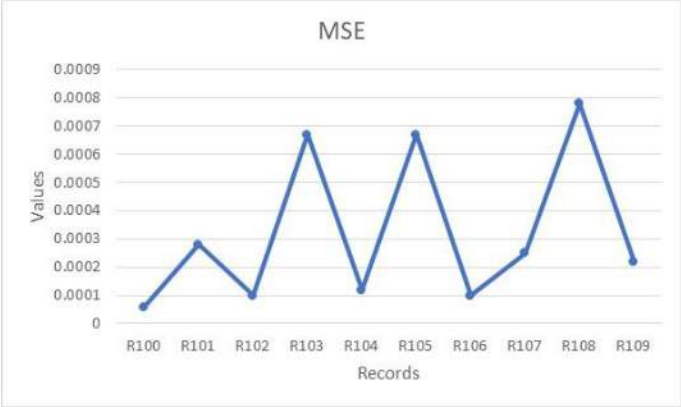

Figure 12: Mean Squared Error of ECG Signal over 100 to 109 Records

The figure 12 illustrates the Mean Squared Error (MSE) values associated with processing an ECG (Electrocardiogram) signal across records numbered from 100 to 109. MSE is a metric used to quantify the average squared difference between the original and reconstructed signals. In this context, the MSE values for the ECG signal vary across different records, ranging from 0.00006 to 0.00078. The graph visually represents how the MSE fluctuates across these records, indicating the level of fidelity or accuracy in signal reconstruction achieved by the processing or compression technique applied. The average MSE across these records is calculated as 0.00032, providing an overall measure of the typical squared error between the original and reconstructed ECG signal across multiple instances. A lower MSE value generally indicates better accuracy or similarity between the original and reconstructed signals.

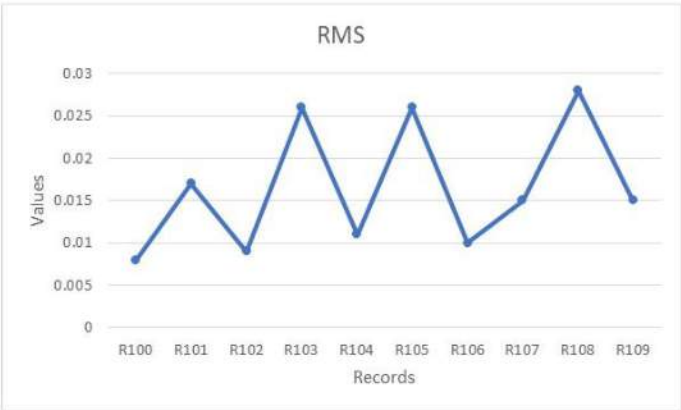

Figure 13: Root Mean Square of ECG Signal over 100 to 109 Records

www.nmiet.edu.in

ISSN: 1092-910X
Vol 27 No. 3 (2024)

The figure 13 visualizes the Root Mean Square (RMS) values associated with processing an ECG (Electrocardiogram) signal across records numbered from 100 to 109. The RMS values displayed in the figure 13 vary across different records, ranging from 0.008 to 0.028. These values reflect the magnitude of the deviation between the reconstructed and original ECG signals. Lower RMS values indicate less error in signal reconstruction, suggesting better accuracy of compression of proposed Model. The average RMS value across these records is calculated as 0.016, providing an overall measure of the typical root mean square error in the reconstructed ECG signal across multiple instances. The figure `13 visually shows how the RMS fluctuates across records, offering insights into the variation in the accuracy of the reconstructed ECG signals.

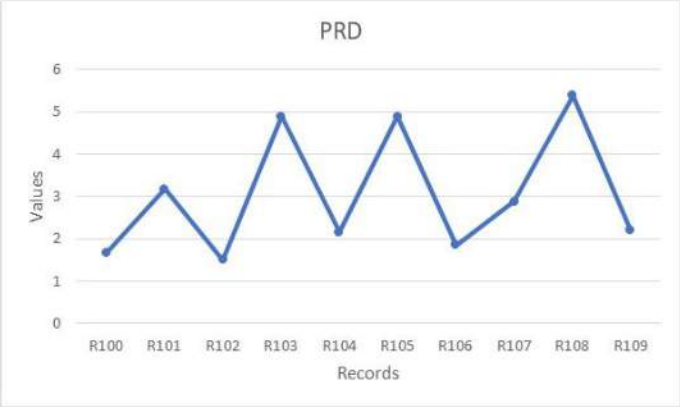

Figure 14: PRD of ECG Signal over 100 to 109 Records

The figure 14 illustrates the Peak Relative Difference (PRD) values associated with processing an ECG signal across records numbered from 100 to 109. the PRD values for the ECG signal vary across different records, ranging from 1.5 to 5.39. These values represent the maximum relative differences between the original and reconstructed ECG signals at their peak points. Higher PRD values indicate larger discrepancies or differences between the signals, suggesting lower similarity or accuracy in signal reconstruction. The average PRD value across these records is calculated as 3.06, providing an overall measure of the typical peak relative difference between the original and reconstructed ECG signals across multiple instances

Figure 15: PRDN of ECG Signal over 100 to 109 Records

The figure 15 represents the Peak Signal-to-Noise Ratio Normalized (PRDN) values associated with processing an ECG signal across records numbered from 100 to 109.the PRDN values for the ECG

signal vary across different records, ranging from 19.71 to 51.22. These values represent the quality of the reconstructed signal, with higher PRDN values indicating better quality in terms of signal fidelity and lower noise in the reconstructed ECG signal compared to the original one. The average PRDN value across these records is calculated as 33.26, providing an overall measure of the typical quality, in terms of signal-to-noise ratio normalization, achieved in the reconstructed ECG signals across multiple instances.

Figure 16: SNR of ECG Signal over 100 to 109 Records

The figure 16 displays the Signal-to-Noise Ratio (SNR) values associated with processing an ECG signal across records numbered from 100 to 109. SNR is a measure used to assess the quality of a signal by comparing the level of the desired signal. The SNR values for the ECG signal vary across different records, ranging from 13.53 to 32.77. These values represent the ratio between the strength of the ECG signal and the level of background noise. The average SNR value across these records is calculated as 23.4, providing an overall measure of the typical signal-to-noise ratio achieved in the reconstructed ECG signals across multiple instances.

Figure 17: QS of ECG Signal over 100 to 109 Records

The Figure 17 shows the Quality Score (QS) values associated with processing an ECG signal across records numbered from 100 to 109. QS is a comprehensive metric used to evaluate the overall quality or performance of a reconstructed signal. the QS values for the ECG signal vary significantly across different records, ranging from 5.98 to 26.87. These values represent an overall assessment of the reconstructed signal quality, with higher QS values indicating better overall performance or quality in terms of fidelity, accuracy, and noise reduction in the reconstructed ECG signal. The

www.nmiet.edu.in

average QS value across these records is calculated as 13.49, providing an overall measure of the typical quality achieved in the reconstructed ECG signals.

Table 2: Comparative Result Analysis of Proposed Autoencoder with existing State-of-art Methods

Author	Method	CR	PRD	PRDN	QS
Oussama El B'charri et. al [27]	DWT	12.63	5.78	16.20	3.78
Peng Z. et. al. [28]	EZW	9.26	8.16	-	1.14
Chandan K.J. et. al. [29]	OCT	6.28	5.36	7.94	1.50
Mukhopadhyay et. al. [30]	ASCII character encoding	26.68	8.00	8.00	64.35
Ozal Yildirim et. al. [31]	Deep Convolutional Autoencoders	32.24	2.73	31.16	12.80
Thivaagar Thamil Selvan et. al. [32]	Non-linear Predictor and ASCII Character Encoding	2.37	0.0	-	-
Proposed	WT-AutoEncoder	**32.31**	**3.06**	**23.40**	**13.49**

The table 2 presents a comparative analysis of the proposed WT-AutoEncoder model against existing state-of-the-art methods for ECG signal compression. Various authors and their respective methods, including Discrete Wavelet Transform (DWT), Embedded Zero-tree Wavelet (EZW), Optimal Compression Trees (OCT), ASCII character encoding, Deep Convolutional Autoencoders, Non-linear Predictor, and ASCII Character Encoding, are evaluated based on different metrics. The proposed WT-AutoEncoder demonstrates results compared to these methods, this shows a Compression Ratio (CR) of 32.31, Peak Relative Difference (PRD) of 3.06, Peak Signal-to-Noise Ratio Normalized (PRDN) of 23.40, and a Quality Score (QS) of 13.49. It is clearly shows that WT-AutoEncoder achieves a high CR comparable to the best-performing Deep Convolutional Autoencoders by Ozal Yildirim et al. [31], while also maintaining favorable PRD, PRDN, and QS, indicating its potential as an efficient and accurate method for compressing ECG signals when compared to other existing techniques in the field of signal compression.

4. Discussion and Conclusion

Biomedical research's cornerstone resides in biomedical signal processing and analysis technology. Recent years have witnessed a surge in biomedical disciplines, such as signal compression for sensitive medical data transmission, significantly escalating the demand for extensive, multi-modal biomedical signal processing in this field. Relying solely on traditional signal compression methods by researchers has proven insufficient in meeting the requirements for a high compression ratio due to this rapid expansion. To effectively address the challenge of compressing and reconstructing biomedical ECG signals with a high compression ratio, this study integrates deep learning techniques into ECG signal processing. It introduces an ECG signal compression and reconstruction model employing autoencoders and wavelet transforms for enhanced performance. The model employs the encoder segment to eliminate redundant features and compress the waveform in layers. Subsequently, the decoder section rebuilds the ECG signal based on the minimally compressed features. This approach involves decomposing the ECG signal, implementing thresholding, and encoding the resulting data. The proposed model underwent testing on the publicly available MIT-BIH arrhythmia signals dataset obtained from the Physionet international database. The Autoencoder

with wavelet transform model automatically extracts relevant features from the ECG signal, efficiently encodes the signal, and effectively reconstructs the ECG signal through the decoding section. The model's performance is assessed using various evaluation parameters such as CR, PRD, PRDN, and QS. The proposed model's testing on specific records (100-109) demonstrated an average compression ratio of 32.31, PRDN of 33.26, PRD of 3.06, and QS of 13.49.

The future scope for ECG signal compression in deep learning encompasses the development of highly efficient and adaptable models tailored for real-time, resource-constrained environments like wearable devices and remote monitoring systems. Advancements will focus on creating deep neural network architectures specifically optimized for ECG signals, integrating novel techniques such as attention mechanisms, reinforcement learning, or spatiotemporal models to improve compression performance. Additionally, there will be a shift towards privacy-preserving techniques ensuring robust encryption during data transmission. Exploring multi-modal fusion with other physiological signals and standardizing compression techniques for interoperability across various healthcare systems will also be critical.

References

[1] Hua, J.; Rao, J.; Peng, Y.; Liu, J.; Tang, J. Deep Compressive Sensing on ECG Signals with Modified Inception Block and LSTM. Entropy 2022, 24, 1024. https://doi.org/10.3390/e24081024

[2] Paridhi Singhai, Anil Kumar, A. Ateek, Irshad Ahmad Ansari, G. K. Singh, and Heung No Lee. 2023. ECG Signal Compression Based on Optimization of Wavelet Parameters and Threshold Levels Using Evolutionary Techniques. Circuits Syst. Signal Process. 42, 6 (Jun 2023), 3509–3537. https://doi.org/10.1007/s00034-022-02280-4

[3] Vinod Kumar, S.C. Saxena, V.K. Giri, Dilbag Singh. (2005). Improved modified AZTEC technique for ECG data compression: Effect of length of parabolic filter on reconstructed signal, Computers & Electrical Engineering, Volume 31, Issues 4-5, Pages 334-344. https://doi.org/10.1016/j.compeleceng.2005.02.002

[4] Wei JJ, Chang CJ, Chou NK, Jan GJ. ECG data compression using truncated singular value decomposition. IEEE Trans Inf Technol Biomed. 2001;5(4):290–9.

[5] Peric, Z., Denic, D., Nikolic, J. et al. DPCM quantizer adaptation method for efficient ECG signal compression. J. Commun. Technol. Electron. 58, 1241–1250 (2013). https://doi.org/10.1134/S1064226913130068

[6] Blanchett, T., Kember, G. C., & Fenton, G. A. (1998). KLT-based quality controlled compression of single-lead ECG. IEEE transactions on bio-medical engineering, 45(7), 942–945. https://doi.org/10.1109/10.686803

[7] Jadda, Amarendra, Prabha, Inty Santi (2023). Speech enhancement via adaptive Wiener filtering and optimized deep learning framework, International Journal of Wavelets, Multiresolution and Information Processing, Vol. 21, No.1, https://doi.org/10.1142/S0219691322500321

[8] V. A. Allen and J. Belina, "ECG data compression using the discrete cosine transform (DCT)," Proceedings Computers in Cardiology, Durham, NC, USA, 1992, pp. 687-690, doi: 10.1109/CIC.1992.269340.

[9] Anukul Pandey, Barjinder Singh Saini, Butta Singh, Neetu Sood, (2020) Quality controlled ECG data compression based on 2D discrete cosine coefficient filtering and iterative JPEG2000 encoding, Measurement, Volume 152, 2020, 107252. https://doi.org/10.1016/j.measurement.2019.107252.

[10] Nitu, & Kaur, M. (2016). Simulative Evaluation and Analysis of ECG Signals using DCT, FFT and DWT Compression Techniques.

[11] Singh, A.K., Krishnan, S. ECG signal feature extraction trends in methods and applications. BioMed Eng OnLine 22, 22 (2023). https://doi.org/10.1186/s12938-023-01075-1

[12] Subasi A. Feature extraction and dimension reduction in Practical guide for biomedical signals analysis using machine learning techniques. Amsterdam: Elsevier; 2019. p. 193–275.

[13] Chansol Hurr, Caiyan Li, Heng Li, "Feature Extraction and Recognition of Human Physiological Signals Based on the Convolutional Neural Network", Mobile Information Systems, vol. 2022, Article ID 8982881, 10 pages, 2022. https://doi.org/10.1155/2022/8982881

[14] G. Jati, Aprinaldi, S. M. Isa and W. Jatmiko, "ECG signal compression by predictive coding and Set Partitioning in Hierarchical Trees (SPIHT)," 2015 International Conference on Advanced Computer Science and Information Systems (ICACSIS), Depok, Indonesia, 2015, pp. 257-262, doi: 10.1109/ICACSIS.2015.7415191.

[15] Szilagyi, Sandor Miklos & Szilagyi, Laszlo & Dávid, László. (1997). ECG signal compression using adaptive prediction. 1. 101 - 104 vol.1. 10.1109/IEMBS.1997.754475.

[16] Dasan, E.; Panneerselvam, I. A novel dimensionality reduction approach for ECG signal via convolutional denoising autoencoder with LSTM. Biomed. Signal Process. Control. 2020, 63, 102225, https://doi.org/10.1016/j.bspc.2020.102225.

[17] Shafiq, Muhammad, and Zhaoquan Gu. 2022. "Deep Residual Learning for Image Recognition: A Survey" Applied Sciences 12, no. 18: 8972. https://doi.org/10.3390/app12188972

[18] A. B. Amjoud and M. Amrouch, "Object Detection Using Deep Learning, CNNs and Vision Transformers: A Review," in IEEE Access, vol. 11, pp. 35479-35516, 2023, doi: 10.1109/ACCESS.2023.3266093.

[19] A. B. Nassif, I. Shahin, I. Attili, M. Azzeh and K. Shaalan, "Speech Recognition Using Deep Neural Networks: A Systematic Review," in IEEE Access, vol. 7, pp. 19143-19165, 2019, doi: 10.1109/ACCESS.2019.2896880.

[20] Feng B, Yu T, Wang H, Liu K, Wu W and Long W (2023) Editorial: Machine learning and deep learning in biomedical signal analysis. Front. Hum. Neurosci. 17:1183840. doi: 10.3389/fnhum.2023.1183840

[21] Kaliyaperumal, Kalaivani & Kshirsagar, Pravin & Devi, J. & Bandela, Surekha & Colak, Ilhami & Rao, J. & Rajaram, A.. (2023). Prediction of biomedical signals using deep learning techniques. Journal of Intelligent & Fuzzy Systems. 44. 1-14. 10.3233/JIFS-230399.

[22] "MIT-BIH Arrhythmia Database," http://www.physionet.org/physiobank/database/mitdb/.

[23] Zhang B, Zhao J, Chen X, Wu J (2017) ECG data compression using a neural network model based on multi-objective optimization. PLoS ONE 12(10): e0182500. https://doi.org/10.1371/journal.pone.018250

[24] Devoe LD (2011) Fetal ECG analysis for intrapartum electronic fetal monitoring: a review. Clin Obstet Gynecol 54: 56–65. https://doi.org/10.1097/GRF.0b013e31820a0ee7 PMID: 21278502

[25] Wang, Y. X., He, Z. J., and Zi, Y. Y. (2010). Enhancement of signal denoising and multiple fault signatures detecting in rotating machinery using dual-tree complex wavelet transform. Mech. Syst. Signal Process. 24, 119-137. doi: 10. 1016/j.ymssp.2009.06.015

[26] Sharma, M., Achuth, P. V., Deb, D., Puthankattil, S. D., and Acharya, U. R. (2018).An automated diagnosis of depression using three-channel bandwidth-duration localized wavelet filter bank with EEG signals. Cogn. Syst. Res. 52, 508–520.doi: 10.1016/j.cogsys.2018.07.010

Oussama El B'charri, Rachid Latif, Wissam Jenkal, Abdenbi Abenaou (2016).The ECG Signal Compression Using an Efficient Algorithm Based on the DWT, International Journal of Advanced Computer Science and Applications, Vol. 7, No. 3, pp. 181-187.

Welba Colince, Ntsama Eloundou Pascal, Pierre Ele, (2014) Exploitation of Differential Pulse Code Modulation for Compression of EMG Signals by a Combination of DWT and DCT, American Journal of Biomedical Engineering 2014, 4(2): 25-32. DOI: 10.5923/j.ajbe.20140402.01

[26] Gupta R. Quality aware compression of electrocardiogram using principal component analysis. J. Med. Syst. 2016, 40, 1-11.

[27] Peng Z.; Wang, G.; Jiang, H.; Meng, S. Research and improvement of ECG compression algorithm based on EZW. Comput. Methods Prog. Biomed. 2017, 145, 157-166.

[28] Chandan, K.J.; Maheshkumar, H.K. Electrocardiogram data compression using DCT based discrete orthogonal Stockwell transform. Biomed. Signal Process. Control 2018, 46, 174-181.

[29] Mukhopadhyay, Sourav Kumar; Ahmad, M. Omair; Swamy, M.N.S. (2018). An ECG compression algorithm with guaranteed reconstruction quality based on optimum truncation of singular values and ASCII character encoding. Biomedical Signal Processing and Control, 44(), 288-306. doi:10.1016/j.bspc.2018.05.005

[30] Ozal Yildirim, Ru San Tan, U. Rajendra Acharya. "An efficient compression of ECG signals using deep convolutional autoencoders", Cognitive Systems Research, Volume 52, December 2018, Pages 198-211. https://doi.org/10.1016/j.cogsys.2018.07.00

[31] Thivaagar Thamil Selvan, Kannan Ramakrishnan, Vijayakumar Vengadasalam and Rathimala Kannan (2022). Lossless ECG Signal Compression Using Non-linear Predictor and ASCII Character Encoding, S.-C. Haw and K. Sonai Muthu (Eds.): CITIC 2022, 10, pp. 513-523, 2022. https://doi.org/10.2991/978-94-6463-094-7_41

Journal of Autonomous Intelligence (2024) Volume 7 Issue 5
doi: 10.32629/jai.v7i5.1525

ORIGINAL RESEARCH ARTICLE

Beyond pixels and ciphers: Navigating the advancements and challenges in visual cryptography

Prema Bhushan Sahane[1], Gayathri M.[2], Snehal Akshay Bagal[3], Praful Sambhare[4], Satish Billewar[5], Kirti Borhade[6], John Blesswin[7,*], Selva Mary[7,*]

[1] *JSPM's Rajarshi Shahu College of Engineering, Tathawade, Pimpri-Chinchwad 411033, India*

[2] *Department of Computing Technologies, School of Computing, SRM Institute of Science and Technology, Kattankulathur 603203, India*

[3] *Department of Artificial Intelligence and Data Science, AISSMS Institute of Information Technology, Pune 411011, India*

[4] *Department of Artificial Intelligence and Data Science, Dr.D.Y. Patil Institute of Technology, Pimpri 411018, India*

[5] *Vivekananda Education Society's Institute of Management Studies and Research, Chembur, Mumbai 400074, India*

[6] *Department of Computer Engineering, Nutan Maharashtra Institute of Engineering and Technology, Talegaon 410507, India*

[7] *Directorate of Learning and Development, SRM Institute of Science and Technology, Kattankulathur 603203, India*

*** Corresponding authors:** John Blesswin, johnblesswin@gmail.com; Selva Mary, selvamaryg.rnd@gmail.com

ABSTRACT

Visual cryptography (VC) has emerged as a pivotal solution for secure information transmission, leveraging its unique capability to encrypt images in a user-friendly and accessible manner. This survey paper provides an in-depth analysis of various VC methods, highlighting their distinct encryption and decryption techniques, applicability, and security levels. The study delves into the technical specifications of each VC type, offering insights into secret image formats, the number of secret images used, types of shares, pixel expansion, and complexity. Significant attention is given to the practical applications of VC, ranging from secure document verification and anti-counterfeiting measures to digital watermarking and online data protection. The paper also identifies key challenges in the field, such as image quality retention post-decryption, computational efficiency, and scalability. Future prospects of VC are explored, particularly its potential integration with emerging technologies like AI and blockchain. This survey aims to provide a comprehensive understanding of VC's current state, its diverse applications, and the future possibilities, making it a valuable resource for researchers and practitioners in the field of data security and cryptography.

Keywords: visual cryptography; information security; encryption techniques; digital watermarking; cryptographic applications

ARTICLE INFO

Received: 3 January 2024
Accepted: 2 February 2024
Available online: 14 March 2024

COPYRIGHT

Copyright © 2024 by author(s). *Journal of Autonomous Intelligence* is published by Frontier Scientific Publishing. This work is licensed under the Creative Commons Attribution-NonCommercial 4.0 International License (CC BY-NC 4.0). https://creativecommons.org/licenses/by-nc/4.0/

1. Introduction

In the realm of information communication, the digital era has significantly revolutionized the way we exchange data. With this revolution comes the paramount importance of information security, as the protection of sensitive data against unauthorized access and manipulation is crucial in a world where cyber threats are constantly evolving. Encryption and decryption are the twin pillars of information security. Encryption is the process of converting plain, understandable information into an unintelligible form, thereby preventing unauthorized access. Decryption, on the other hand, is the process of converting this encrypted data back into its original

form, making it comprehensible again. Traditional cryptography has long harnessed these processes, relying on complex algorithms and keys for secure data transmission.

However, traditional cryptography, which typically encrypts text or binary data, faces unique challenges when applied to images. This is due to the large size of image files and their high redundancy, which often makes traditional encryption methods computationally intensive and less effective. Visual cryptography, introduced by Naor and Shamir in 1994, presents an innovative solution specifically tailored for images. Unlike traditional cryptography, which operates in a digital realm requiring computational decryption, visual cryptography encrypts visual information by dividing an image into shares. When superimposed, these shares reveal the original image, allowing for decryption through the human visual system without the need for complex computational processes[1].

The key difference between traditional cryptography and visual cryptography lies in their approach to encryption and decryption. Traditional methods encrypt data as a whole and require a cryptographic key for decryption[1,2]. Visual cryptography, on the other hand, employs a more straightforward, yet equally secure method, particularly well-suited for images. It leverages the unique properties of visual information, making it an ideal choice for securing images. By splitting an image into multiple shares that individually reveal no information, visual cryptography ensures that only the correct combination of shares can unveil the original image, thus maintaining confidentiality and integrity in a visually intuitive manner. Further, the basic visual cryptography scheme, a binary or black-and-white form conceptualized by Naor and Shamir, exemplifies the effectiveness of this method. It is a testament to how visual cryptography can provide high-level security for images, while being simple to implement and understand[3].

In the following section, we examine the fundamental aspects of visual cryptography, focusing on its core principles and operational methods. This includes an in-depth analysis of how visual cryptography encrypts and decrypts images, differentiating it from conventional cryptographic approaches. Emphasis is placed on understanding the foundational elements of this field, highlighting its critical role in enhancing information security.

2. Fundamentals of visual cryptography

2.1. Definition and basic concepts

Visual cryptography is a cryptographic technique which allows the encryption of visual information such that the decryption can be performed using the human visual system, without the need for complex computational algorithms. The fundamental concept was introduced by Moni Naor and Adi Shamir in 1994[1]. It involves splitting a secret image into multiple shares (also known as transparencies or layers). These shares, when stacked together, reveal the original image, but when viewed individually, they do not disclose any discernible information about the original image.

This method is unique in its approach as it mainly focuses on visual data, primarily images, and the decryption process does not require any special cryptographic computations or tools, other than the human eye or a simple physical superimposition. Traditional cryptography is designed to encrypt all forms of data, including text and numerical data, whereas visual cryptography is specifically tailored for visual information like images and graphics. While both traditional and visual cryptography aim to secure information, the security principle in visual cryptography is based on the inability to decipher the secret without the correct combination of shares, rather than the complexity of a decryption algorithm[4]. In this paper, a comprehensive analysis of visual cryptography (VC) has been conducted. It has been uncovered that VC, while facilitating ease of use and secure information transmission without computational means, also confronts challenges such as image quality degradation and pixel expansion. Significant advancements in VC, addressing these issues, have been highlighted, enhancing its practical applications. The growing relevance of VC in secure

communication, particularly in scenarios where digital methods are infeasible, is emphasized. Moreover, the integration of VC with advanced technologies and its evolving role in data security have been explored. Visual cryptography offers a unique and user-friendly approach to secure information in a visual format. Its simplicity in decryption and the keyless operation makes it distinct and advantageous for specific applications, especially where traditional computational decryption is impractical or undesirable.

2.2. The role of encryption and decryption in visual cryptography

In visual cryptography, encryption is the process of converting a clear image into several non-revealing, seemingly random shares. This is achieved by dividing the original image into pieces, each holding partial and obscured information. Unlike traditional cryptographic methods, this process doesn't rely on complex computational algorithms but instead uses simple operations like pixel manipulation[4]. Each share individually appears as random noise, ensuring that no single piece can reveal the content of the original image. The strength of this encryption lies in its simplicity and the randomness of the shares, which collectively secure the information but individually reveal nothing discernible.

Decryption in visual cryptography is uniquely straightforward and non-technical. It involves the physical overlaying of the encrypted shares[5]. When aligned and stacked correctly, the hidden image emerges, decipherable to the human eye without any computational tools or cryptographic keys. This reliance on the human visual system for decryption sets visual cryptography apart from traditional methods, emphasizing its accessibility and ease of use[6]. The integrity of the original image is preserved during decryption, as there is no computational alteration or compression involved. This method's simplicity and immediate decryption capability make visual cryptography an ideal choice for applications requiring quick and user-friendly secure information processing, such as in secure document handling and identity verification[7].

In the next section, we delve into the diverse types of visual cryptography, offering a detailed exploration of the various methods and their unique characteristics. This part of the paper categorizes and describes different forms of visual cryptography, including basic, extended, color, and several other specialized types. Each category is examined for its specific encryption techniques, applicability, and the unique challenges it addresses in the realm of secure visual data transmission. This comprehensive overview aims to provide a clear understanding of the range and versatility of visual cryptography methods, illustrating their significance and utility in different contexts.

3. Types of visual cryptography

This section is dedicated to unravelling the multitude of techniques within the realm of visual cryptography, each distinguished by its unique approach to encrypting and decrypting visual data. From the foundational basic visual cryptography scheme to more advanced forms like color and quantum visual cryptography, this section aims to dissect the nuances of each type, providing clarity on their specific methodologies, use-cases, and the distinct challenges they address. This exploration not only highlights the diversity and adaptability of visual cryptography but also underscores its broad applicability across different domains of information security.

In visual cryptography, the supported types of visual cryptography (VC) are determined by the type of images used as input. There are three primary categories: binary visual cryptography, grayscale visual cryptography, and color visual cryptography. Each category corresponds to the type of images employed in the VC process. Binary visual cryptography utilizes binary (black and white) images as input, grayscale visual cryptography works with grayscale images, and color visual cryptography operates with full-color images. These distinctions in image types influence the characteristics and applications of the respective VC schemes, allowing for a diverse range of secure image sharing and decryption techniques. For a detailed

overview of visual cryptography schemes on various types of images, refer to **Table 1**.

Table 1. Visual cryptography schemes on various type of images.

Binary images	**Grayscale images**	**Color images**
Basic VCS	Halftone VC	Extended VCS
Extended VCS	Random Grid VC	Color VC
Random Grid VC	Multi-Secret VC	Random Grid VC
Multi-Secret VC	Progressive VC	Multi-Secret VC
Progressive VC	Region-Incrementing VC	Progressive VC
Region-Incrementing VC	Rotational VC	Region-Incrementing VC
Rotational VC	Threshold VC	Rotational VC
Threshold VC	Asymmetric VC	Threshold VC
Asymmetric VC	Noiseless VC	Asymmetric VC
Noiseless VC	Dynamic VC	Noiseless VC
Dynamic VC	Cheating Immune VC	Dynamic VC
Cheating Immune VC	Share-permutation VC	Cheating Immune VC
Share-permutation VC	Natural Image-based VC	Share-permutation VC
Natural Image-based VC	Watermarking with VC	Natural Image-based VC
Watermarking with VC	Optimal Contrast VC	Watermarking with VC
Optimal Contrast VC	Cross Folding VC	Optimal Contrast VC
Cross Folding VC	Hierarchical VC	Cross Folding VC
Hierarchical VC	Lossy VC	Hierarchical VC
Lossy VC	Lossless VC	Lossy VC
Lossless VC	Scalable VC	Lossless VC
Scalable VC	Frameless VC	Scalable VC
Frameless VC	Steganographic VC	Frameless VC
Steganographic VC	Adaptive VC	Steganographic VC
Adaptive VC	Text-based VC	Adaptive VC
Text-based VC	VC with Pixel Expansion	Text-based VC
VC with Pixel Expansion	Circular VC	VC with Pixel Expansion
Circular VC	Matrix Encoding VC	Circular VC
Matrix Encoding VC	Animated VC	Matrix Encoding VC
Animated VC	Perspective-based VC	Animated VC
Perspective-based VC	Hybrid VC	Perspective-based VC
Hybrid VC	Fourier Transform-based VC	Hybrid VC
Fourier Transform-based VC	Time-based VC	Fourier Transform-based VC
Time-based VC	VC for Biometric Security	Time-based VC
VC for Biometric Security	Overlay VC	VC for Biometric Security
Overlay VC	Moiré Pattern VC	Overlay VC
Moiré Pattern VC	Semantic VC	Moiré Pattern VC
		Semantic VC

1) Basic visual cryptography scheme (VCS)

Basic VCS is the foundational model of visual cryptography, splitting an image into shares that reveal the original image when overlaid. It is known for its simplicity and effectiveness in encrypting binary images[1].

2) Extended visual cryptography scheme

Unlike the basic model, which is limited to monochrome images, extended VCS can handle more complex images, including grayscale and full-color images. This significantly broadens the applicability of the technique, as most real-world images are in color or grayscale. Extended VCS also involves creating and managing a larger number of shares, or allowing for more flexible schemes in how these shares are combined to reconstruct the original image[2].

3) Halftone visual cryptography

Halftone visual cryptography uses halftone techniques to create shares of grayscale images, allowing for more detailed image encryption while maintaining the visual quality in the decrypted image[3].

4) Color visual cryptography

Color visual cryptography specializes in encrypting color images, maintaining the original colors in the shares which, when overlaid, reveal the color image with high fidelity[4].

5) Random grid visual cryptography

This random grid visual cryptography (RGVC) is a variant of visual cryptography that introduces an additional layer of randomness to the process of encrypting and decrypting images. This method is designed to enhance the security and robustness of the traditional visual cryptography scheme[5].

6) Multi-secret visual cryptography

Multi-secret visual cryptography allows for multiple secret images to be encrypted within the same set of shares, enabling a complex layering of information in a single cryptographic process[6].

7) Progressive visual cryptography

Progressive visual cryptography gradually reveals more information about the image as more shares are superimposed, providing a staged decryption process and enhanced control over information release[7].

8) Region-incrementing visual cryptography

This method focuses on incrementally revealing specific regions of an image, allowing for selective encryption and decryption of different parts of an image for varied levels of access[8].

9) Rotational visual cryptography

Rotational visual cryptography requires the shares to be rotated to specific angles for decryption, adding a physical interaction element to the decryption process for enhanced security[9].

10) Threshold visual cryptography

In threshold visual cryptography, a minimum number of shares are required to decrypt the image otherwise it won't reveal the image, making it ideal for scenarios where controlled access is necessary. Traditional VC involves splitting an image into two or more shares. When these shares are physically overlaid, the original image is revealed. Typically, this is done with binary images (black and white). Threshold visual cryptography is an extension of the basic concept. It involves dividing an image into n shares, where a specific k number of shares (where $k \leq n$) is needed to reconstruct the image. This is known as a (k, n) threshold scheme[10].

11) Asymmetric visual cryptography

This type introduces an asymmetric aspect, where different keys (shares) are used for encryption and decryption, enhancing security and control over the distribution of decryption capabilities[11].

12) Noiseless visual cryptography

Noiseless visual cryptography aims to reduce the noise (random patterns) in the shares, resulting in clearer decrypted images and better visual quality[12].

13) Dynamic visual cryptography

Dynamic visual cryptography allows for changes in the encrypted image over time or under different conditions, adding a temporal dimension to the visual cryptographic process[13].

14) Cheating immune visual cryptography

This method includes mechanisms to prevent cheating, ensuring that the decrypted image cannot be manipulated or falsely represented by any of the shareholders[14].

15) Share-permutation visual cryptography

In share-permutation visual cryptography, the decryption process involves not only overlaying but also

permuting the shares in a specific order, adding a layer of complexity to the decryption process[15].

16) Natural image-based visual cryptography

This technique is tailored for encrypting natural images (like photographs), maintaining high visual quality and realistic representation in both shares and decrypted images[16].

17) Watermarking with visual cryptography

This method integrates visual cryptography with watermarking, allowing for secret images to be embedded as watermarks in a host image, providing both security and image authentication[17].

18) Optimal contrast visual cryptography

Optimal contrast visual cryptography focuses on maximizing the contrast in the decrypted image, ensuring that the revealed image is as clear and discernible as possible[18].

19) Cross folding visual cryptography

This innovative approach involves folding the shares in specific ways to reveal the hidden image, introducing a physical manipulation aspect to the decryption process[19].

20) Hierarchical visual cryptography

Hierarchical visual cryptography encrypts multiple images at different levels, where each level of overlaying shares reveals a different image, allowing for layered security and information dissemination[20].

21) Lossy visual cryptography

Lossy visual cryptography compresses the image during the encryption process, resulting in smaller share sizes but with some loss of image quality upon decryption[21].

22) Lossless visual cryptography

This method ensures that there is no loss of image quality in the encryption and decryption process, preserving the original image quality in the decrypted output[22].

23) Scalable visual cryptography

Scalable visual cryptography allows for the cryptographic process to be adjusted based on the size or resolution of the input image, making it adaptable to various image sizes and qualities[23].

24) Frameless visual cryptography

Frameless visual cryptography does away with the need for aligning frames or borders in the shares, allowing for more flexible and user-friendly decryption processes[24].

25) Steganographic visual cryptography

This type combines visual cryptography with steganography, hiding information within the shares in a way that is not visible until decryption, providing an additional layer of secrecy[25].

26) Adaptive visual cryptography

Adaptive visual cryptography adjusts its encryption technique based on the content of the image, ensuring optimal encryption for different types of images and information[26].

27) Text-based visual cryptography

Specifically designed for encrypting text, this method ensures that the text remains legible and clear in the decrypted output, even after being split into shares[27].

28) Visual cryptography with pixel expansion

This technique involves expanding the pixels during the encryption process, which can result in larger shares but often leads to clearer decrypted images[28].

29) Circular visual cryptography

Circular visual cryptography utilizes circular patterns in the shares, requiring a circular alignment for decryption, adding a unique geometric aspect to the cryptographic process[29].

30) Matrix encoding visual cryptography

This method uses matrix encoding techniques for encryption, allowing for more complex and secure cryptographic processes, often used in more advanced applications[30].

31) Animated visual cryptography

Animated visual cryptography is designed for encrypting animated images or sequences, maintaining the animation in both the shares and the decrypted output[31].

32) Quantum visual cryptography

Quantum visual cryptography leverages principles of quantum mechanics, offering extremely high security levels and is primarily used in advanced and high-security applications[32].

33) Perspective-based Visual Cryptography

This type encrypts images in a way that requires viewing the shares from specific perspectives or angles to decrypt the image, adding a spatial dimension to the decryption process[33].

34) Hybrid visual cryptography

Hybrid visual cryptography combines elements of different visual cryptography techniques, offering a versatile and robust approach suitable for complex encryption needs[34].

35) Fourier transform-based visual cryptography

This method employs Fourier transforms in the encryption process, making it suitable for applications requiring frequency domain analysis and complex image manipulations[35].

36) Time-based visual cryptography

Time-based visual cryptography introduces a temporal aspect, where the decryption or the clarity of the decrypted image changes over time or under specific conditions[36].

37) 3D visual cryptography

3D visual cryptography is tailored for encrypting three-dimensional images, maintaining the 3D aspect in both the shares and the decrypted output[37].

38) Visual cryptography for biometric security

This specialized form is used for encrypting biometric data, ensuring high security and fidelity for sensitive biometric information like fingerprints or facial recognition data[38].

39) Overlay visual cryptography

Overlay visual cryptography requires the precise overlaying of shares to decrypt the image, focusing on alignment and superimposition techniques for effective decryption[39].

40) Moiré pattern visual cryptography

This type utilizes Moiré patterns in the shares, which, when overlaid, produce a distinct Moiré effect that reveals the hidden image, adding an artistic dimension to the process[40].

41) Semantic visual cryptography

Semantic visual cryptography embeds meaningful patterns or images in the shares, which can provide additional context or information, enhancing the utility and applicability of the cryptographic process[41–44].

In the next section, we conduct a comparative analysis of different visual cryptography types. This analysis focuses on contrasting their encryption methods, decryption processes, and applicability. We aim to elucidate the unique features and limitations of each type, providing a clear perspective on their suitability for various security needs in a concise and informative manner.

4. Comparative analysis of visual cryptography schemes

In this section, we delve into a detailed examination of the various methods employed in visual cryptography. Through a comparative study, we aim to highlight the unique characteristics of each technique, from simple to complex systems. By focusing on crucial aspects like encryption and decryption methods, applicability, and security levels, our goal is to offer a clear and comprehensive insight into the strengths and weaknesses of each approach. This analysis will be instrumental for researchers and practitioners in selecting the appropriate visual cryptography method for their specific requirements.

Table 2 provides a comprehensive overview of various visual cryptography schemes, focusing on their general characteristics and functionalities. This table is crucial for understanding the diverse methods employed in visual cryptography, each tailored for specific applications and security needs.

- Encryption method: This column outlines the technique each type uses to encrypt the image, which is fundamental to understanding the operational mechanism of each method[7].
- Decryption method: It details how the encrypted data is decrypted or revealed, highlighting the practicality and ease of the decryption process[4].
- Applicability: This provides insights into the types of images or data each cryptography method is best suited for, allowing researchers to identify the most appropriate technique for different use cases[39].
- Security level: This crucial aspect compares the relative security provided by each method, giving an idea of which techniques are more secure and under what circumstances[21]. These categories are often used to classify the degree of protection required for data or systems based on their sensitivity and the potential impact of a security breach. Here's a general overview of each: Low security typically indicates a baseline level of protection. It is applied to data or systems where the potential impact of a breach is minimal. Moderate security is a step above low security and is suited for data or systems where the impact of a security breach is moderate and would cause a limited level of harm or disruption. High security is applied to data or systems where the impact of a security breach would be significant. This level is for protecting sensitive or valuable information. The highest level of security is reserved for the most sensitive and critical data or systems, where the impact of a breach would be severe or catastrophic.
- Special features: It highlights unique attributes or advantages of each cryptography type, offering a quick reference to their distinctive capabilities or applications[33].

Table 2. Comparative analysis of visual cryptography schemes.

Type of visual cryptography	Encryption method	Decryption method	Applicability	Security level	Special features
Basic VCS[1]	Splitting shares	Physical overlay	Binary	Moderate	Simplicity
Extended VCS[2]	Enhanced splitting	Physical overlay	Binary/color	High	Higher security
Color VC[3]	Color layering	Physical overlay	Color	Moderate	Color encryption
Halftone VC[4]	Halftoning	Physical overlay	Grayscale	Low	Visual appeal
Random Grid VC[5]	Grid patterns	Physical overlay	Binary/grayscale/color	High	Randomization

Table 2. (*Continued*).

Type of visual cryptography	Encryption method	Decryption method	Applicability	Security level	Special features
Multi-Secret VC[6]	Multiple splits	Physical overlay	Binary/grayscale/color	High	Multiple secrets
Progressive VC[7]	Incremental reveal	Physical overlay	Binary/grayscale/color	Moderate	Progressive reveal
Region-Incrementing VC[8]	Regional division	Physical overlay	Binary/grayscale/color	Moderate	Regional emphasis
Rotational VC[9]	Rotation-based	Physical rotation	Binary/grayscale/color	Moderate	Rotational reveal
Threshold VC[10]	Threshold splits	Physical overlay	Binary/grayscale/color	High	Threshold-specific
Asymmetric VC[11]	Asymmetric keys	Physical overlay	Binary/grayscale/color	High	Asymmetric security
Noiseless VC[12]	Noise reduction	Physical overlay	Binary/grayscale/color	Moderate	Less noise
Dynamic VC[13]	Dynamic changes	Physical overlay	Binary/grayscale/color	High	Dynamic updates
Cheating Immune VC[14]	Anti-cheating	Physical overlay	Binary/grayscale/color	High	Cheating prevention
Share-permutation VC[15]	Share permutation	Physical overlay	Binary/grayscale/color	High	Permutation complexity
Natural Image-based VC[16]	Natural patterns	Physical overlay	Binary/grayscale/color	Moderate	Realistic patterns
Watermarking with VC[17]	Watermark insertion	Physical overlay	Binary/grayscale/color	Moderate	Watermarking
Optimal Contrast VC[18]	Contrast adjustment	Physical overlay	Binary/grayscale/color	High	Enhanced contrast
Cross Folding VC[19]	Folding technique	Physical folding	Binary/grayscale/color	Moderate	Folding mechanics
Hierarchical VC[20]	Hierarchical layers	Physical overlay	Binary/grayscale/color	High	Layered security
Lossy VC[21]	Lossy compression	Physical overlay	Binary/grayscale/color	Low	Data reduction
Lossless VC[22]	Lossless compression	Physical overlay	Binary/grayscale/color	High	Data integrity
Scalable VC[23]	Scalability	Physical overlay	Binary/grayscale/color	Moderate	Scalable solutions
Frameless VC[24]	Frameless design	Physical overlay	Binary/grayscale/color	Moderate	No frame constraints
Steganographic VC[25]	Hidden layers	Physical overlay	Binary/grayscale/color	High	Hidden information
Adaptive VC[26]	Adaptive patterns	Physical overlay	Binary/grayscale/color	High	Adaptivity
Text-based VC[27]	Text splitting	Physical overlay	Binary/grayscale/color	Moderate	Text-focused
VC with Pixel Expansion[28]	Pixel expansion	Physical overlay	Binary/grayscale/color	Moderate	Expanded pixels
Circular VC[29]	Circular patterns	Physical overlay	Binary/grayscale/color	Moderate	Circular design
Matrix Encoding VC[30]	Matrix encoding	Physical overlay	Binary/grayscale/color	High	Matrix complexity
Animated VC[31]	Frame-based	Physical overlay	Binary/grayscale/color	Moderate	Animation support
Quantum VC[32]	Quantum principles	Quantum methods	Quantum	Very High	Quantum mechanics
Perspective-based VC[44]	Perspective change	Physical overlay	Binary/grayscale/color	Moderate	Perspective shift
Hybrid VC[34]	Mixed techniques	Physical overlay	Binary/grayscale/color	High	Hybrid approach
Fourier Transform-based VC[35]	Fourier transform	Computational	Binary/grayscale/color	High	Frequency domain
Time-based VC[36]	Time constraints	Physical overlay	Binary/grayscale/color	High	Time-dependent

Table 2. (*Continued*).

Type of visual cryptography	Encryption method	Decryption method	Applicability	Security level	Special features
3D VC[37]	3D layering	3D overlay	3D	High	3D representation
VC for Biometric Security[38]	Biometric patterns	Physical overlay	Binary/grayscale/color	High	Biometric focus
Overlay VC[39]	Layering	Physical overlay	Binary/grayscale/color	Moderate	Overlay technique
Moiré Pattern VC[40]	Moiré patterns	Physical overlay	Binary/grayscale/color	Moderate	Moiré effects
Semantic VC[41]	Meaningful patterns	Physical overlay / Computational	Grayscale/color	Moderate	Semantic embedding

The **Table 3** serves as a guide for researchers and practitioners to assess and compare the various visual cryptography techniques, aiding in the selection of the most appropriate method for their specific needs and constraints.

Table 3. Technical specifications of visual cryptography schemes.

Type of visual cryptography	Secret image format	No. of secret images	Type of shares	Pixel expansion	Complexity
Basic VCS[1]	Binary	1	Binary	Yes	Moderate
Extended VCS[2]	All formats	Multiple	Binary/color	Yes	High
Color VC[3]	Color	1 or more	Color	Yes	Moderate
Halftone VC[4]	Grayscale	1	Grayscale	Yes	Low
Random Grid VC[5]	All formats	1 or more	Binary/grayscale/color	Yes	High
Multi-Secret VC[6]	All formats	Multiple	Binary/grayscale/color	Yes	High
Progressive VC[7]	All formats	1 or more	Binary/grayscale/color	Yes	Moderate
Region-Incrementing VC[8]	All formats	1 or more	Binary/grayscale/color	Yes	Moderate
Rotational VC[9]	All formats	1	Binary/grayscale/color	Yes	Moderate
Threshold VC[10]	All formats	1 or more	Binary/grayscale/color	Yes	High
Asymmetric VC[11]	All formats	Multiple	Binary/grayscale/color	Yes	High
Noiseless VC[12]	All formats	1	Binary/grayscale/color	Yes	Moderate
Dynamic VC[13]	All formats	1 or more	Binary/grayscale/color	Yes	High
Cheating Immune VC[14]	All formats	Multiple	Binary/grayscale/color	Yes	High
Share-permutation VC[15]	All formats	Multiple	Binary/grayscale/color	Yes	High
Natural Image-based VC[16]	Natural images	1 or more	Binary/grayscale/color	Yes	Moderate
Watermarking with VC[17]	All formats	1	Binary/grayscale/color	Yes	Moderate
Optimal Contrast VC[18]	All formats	1 or more	Binary/grayscale/color	Yes	High
Cross Folding VC[19]	All formats	1 or more	Binary/grayscale/color	Yes	Moderate
Hierarchical VC[20]	All formats	Multiple	Binary/grayscale/color	Yes	High
Lossy VC[21]	All formats	1	Binary/grayscale/color	Yes	Low
Lossless VC[22]	All formats	1	Binary/grayscale/color	Yes	High
Scalable VC[23]	All formats	1 or more	Binary/grayscale/color	Yes	Moderate
Frameless VC[24]	All formats	1 or more	Binary/grayscale/color	Yes	Moderate
Steganographic VC[25]	All formats	1 or more	Binary/grayscale/color	Yes	High
Adaptive VC[26]	All formats	1 or more	Binary/grayscale/color	Yes	High
Text-based VC[27]	Text	1	Binary/grayscale/color	Yes	Moderate
VC with Pixel Expansion[28]	All formats	1 or more	Binary/grayscale/color	Yes	Moderate

Table 3. (*Continued*).

Type of visual cryptography	Secret image format	No. of secret images	Type of shares	Pixel expansion	Complexity
Circular VC[29]	All formats	1 or more	Binary/grayscale/color	Yes	Moderate
Matrix Encoding VC[30]	All formats	Multiple	Binary/grayscale/color	Yes	High
Animated VC[31]	Animated images	Multiple	Binary/grayscale/color	Yes	Moderate
Quantum VC[32]	Quantum data	1 or more	Quantum	No	Very High
Perspective-based VC[44]	All formats	1 or more	Binary/grayscale/color	Yes	Moderate
Hybrid VC[34]	All formats	Multiple	Binary/grayscale/color	Yes	High
Fourier Transform-based VC[35]	All formats	1 or more	Binary/grayscale/color	Yes	High
Time-based VC[36]	All formats	1 or more	Binary/grayscale/color	Yes	High
3D VC[37]	3D images	1 or more	3D	Yes	High
VC for Biometric Security[38]	Biometric images	1	Binary/grayscale/color	Yes	High
Overlay VC[39]	All formats	1 or more	Binary/grayscale/color	Yes	Moderate
Moiré Pattern VC[40]	All formats	1 or more	Binary/grayscale/color	Yes	Moderate
Semantic VC[42,43]	All formats	1 or more	Grayscale/color	Yes	Moderate

Table 3 dives deeper into the technical aspects of various visual cryptography methods. This detailed breakdown is essential for researchers who require a more technical understanding of these systems.

(1) Secret image format: This column indicates the format of the image that can be encrypted using each method, which is crucial for understanding the compatibility of each technique with different types of data[41].
(2) No. of secret images: It provides information on how many secret images can be encrypted, which is vital for methods involving multiple layers or levels of encryption[12].
(3) Type of shares: This specifies the nature of the shares or layers produced by each encryption method, a key factor in understanding the method's operational dynamics[32].
(4) Pixel expansion: It indicates whether a particular method results in pixel expansion, an important consideration in terms of the final image size and quality[21].
(5) Complexity: This column assesses the overall complexity of each method, encompassing factors like computational intensity and ease of implementation[5].

By providing a detailed technical analysis of various visual cryptography methods, **Table 2** assists researchers and developers in understanding the intricacies and technical challenges associated with each technique. This understanding is crucial for developing, implementing, or enhancing visual cryptography systems.

The subsequent section addresses areas requiring enhancement in visual cryptography. It underscores the need for improved image quality post-decryption, enhanced computational efficiency, user-friendly decryption processes, and adaptable scalability to bolster the field's effectiveness and practicality.

5. Improvements needed in visual cryptography

In the realm of visual cryptography, while significant advancements have been made, there are several areas where improvements are needed. This analysis report identifies key points that require enhancement to further the effectiveness and applicability of visual cryptography in various fields.

(1) Image quality post-decryption: Many visual cryptography methods, particularly those involving pixel expansion or lossy techniques, result in a noticeable degradation of image quality. Research into methods that maintain or enhance image fidelity post-decryption is crucial[23,26].

(2) Computational efficiency: Some advanced visual cryptography methods, like Fourier transform-based or quantum visual cryptography, require significant computational resources. Optimizing these methods for greater efficiency can broaden their practical application, especially in resource-constrained environments[25,32].

(3) User accessibility and convenience: The decryption process in some methods, such as those requiring precise alignment or rotational adjustments, can be user-unfriendly. Improvements in user interface design and the development of more intuitive decryption processes would enhance usability[18].

(4) Scalability and adaptability: Visual cryptography methods need to be adaptable to various image sizes and resolutions. Research into scalable solutions that can efficiently handle high-resolution images without substantial resource demands is necessary[22].

(5) Color image processing: While there has been progress in color visual cryptography, challenges remain in accurately encrypting and decrypting color images without loss of quality or color fidelity. Enhanced techniques for color image processing are needed[38].

(6) Security against emerging threats: As cyber threats evolve; visual cryptography must also adapt. This includes developing methods that are resistant to quantum computing threats and advanced cryptographic attacks[32].

(7) Integration with other technologies: Exploring the integration of visual cryptography with emerging technologies like blockchain and AI can open up new avenues for secure data transmission and storage[24].

(8) Environmental and economic considerations: Methods that require physical printing and overlaying of transparencies should consider environmental impact. Developing eco-friendly and cost-effective solutions is important for sustainable practice[12].

(9) Standardization and interoperability: There is a need for standardization in visual cryptography methods to ensure interoperability across different platforms and technologies[8–10].

(10) Educational and training resources: Increasing awareness and understanding of visual cryptography through educational resources and training programs can enhance its adoption in various sectors.

(11) Research on biometric data security: With the increasing use of biometrics for security, research on visual cryptography methods tailored for biometric data is essential to ensure robust protection against identity theft and fraud.

(12) Legal and ethical considerations: Addressing legal and ethical issues related to privacy and data protection in the application of visual cryptography is paramount.

While visual cryptography offers a unique and effective means of securing data, continuous research and development are required to address these improvement areas. By tackling these challenges, visual cryptography can be more widely and effectively used in various sectors, ranging from secure communications to digital rights management.

6. Applications of visual cryptography in modern technology

Visual cryptography finds its applications in a myriad of fields, each leveraging its unique ability to secure visual information in a user-friendly and accessible manner. One of the most prominent applications is in the realm of secure document verification, such as passports, ID cards, and banknotes. This technology is used to embed hidden images or text that only become visible under specific conditions, thereby providing an effective anti-counterfeiting measure. The simplicity of overlaying shares to reveal confidential information also makes visual cryptography an ideal choice for quick and secure verification processes in various security-sensitive environments.

Another significant application area of visual cryptography is in digital watermarking and steganography. It serves as a powerful tool for copyright protection and authentication of digital media. By

embedding a watermark or a hidden image within a photograph or video, creators can assert their ownership or verify the authenticity of their content. Additionally, visual cryptography is gaining traction in the field of online communications and data storage. Secure QR codes, for instance, are being increasingly used for encrypting sensitive information such as personal details and transaction data in digital payments and online banking. With the growth of online platforms, the potential of visual cryptography in protecting digital assets and personal data is immense, promising a more secure digital landscape.

7. Conclusion

In summarizing this survey on visual cryptography, it's clear that this field uniquely blends simplicity and security, offering versatile solutions for information protection. From securing official documents to enhancing digital media with watermarks, visual cryptography addresses a wide range of security needs. Its user-friendly decryption process, relying on the human visual system, makes it exceptionally accessible. However, challenges such as image quality, computational efficiency, and scalability need attention to broaden its applicability. The future of visual cryptography is promising, especially with potential integrations with emerging technologies like AI and blockchain. As digital security becomes increasingly paramount, the evolution of visual cryptography will play a critical role in shaping secure data exchange and storage methodologies. This survey highlights the need for continuous innovation in this domain, ensuring that visual cryptography remains a robust and adaptable tool in the ever-evolving landscape of information security.

Author contributions

Conceptualization, SM and JB; methodology, PBS, GM and SAB; validation, PS, SB and KB; formal analysis, PBS and GM; investigation, SB; writing—original draft preparation, JB; writing—review and editing, SM. All authors have read and agreed to the published version of the manuscript.

Conflict of interest

The authors declare no conflict of interest.

References

1. Naor M, Shamir A. Visual cryptography. Lecture Notes in Computer Science. Published online 1995: 1-12. doi: 10.1007/bfb0053419
2. Ateniese G, Blundo C, De Santis A, Stinson DR. Constructions and bounds for visual cryptography. In: Proceedings of the 23rd International Colloquium on Automata, Languages, and Programming (ICALP 96), LNCS, Vol. 1099, Springer-Verlag. 1996.
3. Shyu SJ, Huang SY, Lee YK, et al. Sharing multiple secrets in visual cryptography. Pattern Recognition. 2007; 40(12): 3633-3651. doi: 10.1016/j.patcog.2007.03.012
4. Wu HC, Wang HC, Yu RW. Color Visual Cryptography Scheme Using Meaningful Shares. 2008 Eighth International Conference on Intelligent Systems Design and Applications. Published online November 2008. doi: 10.1109/isda.2008.130
5. Wu X, Liu T, Sun W. Improving the visual quality of random grid-based visual secret sharing via error diffusion. Journal of Visual Communication Image Representation. 2013; 24: 552–566. doi: 10.1016%2Fj.jvcir.2013.03.002
6. Deshmukh M, Nain N, Ahmed M. Efficient and secure multi secret sharing schemes based on boolean XOR and arithmetic modulo. Multimedia Tools Application. 2018; 77: 89–107. doi: 10.1007%2Fs11042-016-4229-x
7. Yan M, Hu Y, Zhang H. Progressive meaningful visual cryptography for secure communication of grayscale medical images. Multimedia Tools and Applications. Published online September 23, 2023. doi: 10.1007/s11042-023-16960-z
8. Wang RZ. Region Incrementing Visual Cryptography. IEEE Signal Processing Letters. 2009; 16(8): 659-662. doi: 10.1109/LSP.2009.2021334
9. Suma D, Raviraja Holla M. Pipelined parallel rotational visual cryptography (PPRVC). In: International Conference on Communication and Signal Processing, 4–6 April 2019, India.
10. Verheul ER, Tilborg HCA. Constructions and properties of k out of n visual secret sharing schemes. Designs, Codes and Cryptography. 1997; 11: 179–196. doi: 10.1023%2FA%3A1008280705142

11. Kester QA, Nana L, Pascu AC. A new hybrid asymmetric key-exchange and visual cryptographic algorithm for securing digital images. 2013 International Conference on Adaptive Science and Technology. Published online November 2013. doi: 10.1109/icastech.2013.6707497
12. John Blesswin A, Selva Mary G, Manoj Kumar S. Multiple Secret Image Communication Using Visual Cryptography. Wireless Personal Communications. 2021; 122(4): 3085-3103. doi: 10.1007/s11277-021-09041-7
13. Petrauskiene V, Palivonaite R, Aleksa A, et al. Dynamic visual cryptography based on chaotic oscillations. Communications in Nonlinear Science and Numerical Simulation. 2014; 19(1): 112-120. doi: 10.1016/j.cnsns.2013.06.002
14. Zhao Y, Fu FW. A cheating immune (k, n) visual cryptography scheme by using the rotation of shares. Multimedia Tools and Applications. 2022; 81(5): 6235-6257. doi: 10.1007/s11042-021-11692-4
15. Patil K, Barpute JV, Arkadi M, Bhirud SD, et al. Semantic pixel encoding visual secret sharing technique for balancing quality and security in color images. Journal of Autonomous Intelligence. 7(3): 1159.
16. Sun Y, Lu Y, Chen J, et al. Meaningful Secret Image Sharing Scheme with High Visual Quality Based on Natural Steganography. Mathematics. 2020; 8(9): 1452. doi: 10.3390/math8091452
17. Cimato S, Yang JCN, Wu CC. Visual Cryptography Based Watermarking. In: Shi YQ, Liu F, Yan W (editors). Transactions on Data Hiding and Multimedia Security IX. Lecture Notes in Computer Science. Springer, Berlin, Heidelberg. 2014.
18. Selva Mary G, Blesswin AJ, Kumar SM. Self-authentication Model to Prevent Cheating Issues in Grayscale Visual Secret Sharing Schemes. Wireless Personal Communications. 2022; 125(2): 1695-1714. doi: 10.1007/s11277-022-09628-8
19. Matsuzaki T, Qin H, Harada K. Color Visual Cryptography with Stacking Order Dependence Using Interference Color. Open Journal of Applied Sciences. 2017; 07(07): 329-336. doi: 10.4236/ojapps.2017.77026
20. Zhao T, Chi Y. Hierarchical visual cryptography for multisecret images based on a modified phase retrieval algorithm. Multimedia Tools and Applications. 2020; 79(17-18): 12165-12181. doi: 10.1007/s11042-020-08632-z
21. Blesswin J, Mary S, Gobinath T, et al. Error-induced inverse pixel visual cryptography for secure QR code communication. Journal of Autonomous Intelligence. 2023; 7(1). doi: 10.32629/jai.v7i1.1129
22. Bhat K. A Verifiable Lossless Multiple Secret Images Sharing Scheme, Information Systems Security. 2021.
23. Chen YH, Juan JST. XOR-Based (n, n) Visual Cryptography Schemes for Grayscale or Color Images with Meaningful Shares. Applied Sciences. 2022; 12(19): 10096. doi: 10.3390/app121910096
24. Blesswin J, Mary S, Suryawanshi S, et al. Secure transmission of grayscale images with triggered error visual sharing. Journal of Autonomous Intelligence. 2023; 6(2): 957. doi: 10.32629/jai.v6i2.957
25. Lin J, Chang CC, Horng JH. Asymmetric Data Hiding for Compressed Images with High Payload and Reversibility. Symmetry. 2021; 13(12): 2355. doi: 10.3390/sym13122355
26. Koptyra K, Ogiela MR. Subliminal Channels in Visual Cryptography. Cryptography. 2022; 6(3): 46. doi: 10.3390/cryptography6030046
27. Youmaran R, Adler A, Miri A. An Improved Visual Cryptography Scheme for Secret Hiding. 23rd Biennial Symposium on Communications, 2006. doi: 10.1109/bsc.2006.1644637
28. Wang L, Yan B, Yang HM, et al. Flip Extended Visual Cryptography for Gray-Scale and Color Cover Images. Symmetry. 2020; 13(1): 65. doi: 10.3390/sym13010065
29. John Blesswin A. JBA, John Blesswin A. SMG, Selva Mary G. MKS. Secured Communication Method using Visual Secret Sharing Scheme for Color Images. Journal of Internet Technology. 2021; 22(4): 803-810. doi: 10.53106/160792642021072204008
30. Yang CN, Chung TH. A general multi-secret visual cryptography scheme. Optics Communications. 2010; 283(24): 4949-4962. doi: 10.1016/j.optcom.2010.07.051
31. Selva Mary G, John Blesswin A, Venkatesan M, et al. Enhancing conversational sentimental analysis for psychological depression prediction with Bi-LSTM. Journal of Autonomous Intelligence. 2023; 7(1).
32. Zhao MY, Yan B, Pan JS, et al. Quantum meaningful visual cryptography. Quantum Information Processing. 2023; 22(8). doi: 10.1007/s11128-023-04066-2
33. Zhou Z, Arce GR, Di Crescenzo G. Halftone visual cryptography. IEEE Transactions on Image Processing. 2006; 15(8): 2441-2453. doi: 10.1109/tip.2006.875249
34. Chen TH, Tsao KH. User-friendly random-grid-based visual secret sharing. IEEE Trans. Circuits Syst. Video Technol. 2011; 21(11): 1693–1703. doi: 10.1109/TCSVT.2011.2133470
35. Yan X, Wang S, Niu X. Threshold construction from specific cases in visual cryptography without the pixel expansion. Signal Processing. 2014; 105: 389–398. doi: 10.1016%2Fj.sigpro.2014.06.011
36. Huang SY, Lo A hui, Juan JST. XOR-Based Meaningful (n, n) Visual Multi-Secrets Sharing Schemes. Applied Sciences. 2022; 12(20): 10368. doi: 10.3390/app122010368
37. Wang Q, Blesswin A J, Manoranjitham T, et al. Securing image-based document transmission in logistics and supply chain management through cheating-resistant visual cryptographic protocols. Mathematical Biosciences and Engineering. 2023; 20(11): 19983-20001. doi: 10.3934/mbe.2023885
38. Selva Mary G, Manoj Kumar S. A self-verifiable computational visual cryptographic protocol for secure two-dimensional image communication. Measurement Science and Technology. 2019; 30(12): 125404. doi: 10.1088/1361-6501/ab2faa

39. Jana B, Mallick M, Chowdhuri P, Mondal S. Cheating prevention in Visual Cryptography using steganographic scheme. 2014 International Conference on Issues and Challenges in Intelligent Computing Techniques (ICICT). 2014. 706-712.
40. Kumar M, Singh R. A (2, n) and (3, n) Visual Cryptography Scheme for Black and White Images. International Journal of Science and Research. 2014; 3: 574-577.
41. Blesswin JA, Visalakshi P. A new semantic visual cryptographic protocol (SVCP) for securing multimedia communications. International Journal of Soft Computing. 2015; 10(2): 175-182.
42. Selva Mary G, Manoj Kumar S. Secure grayscale image communication using significant visual cryptography scheme in real time applications. Multimedia Tools and Applications. 2019; 79(15-16): 10363-10382. doi: 10.1007/s11042-019-7202-7
43. John Blesswin A, Genitha, Selva Mary G. A Novel QR-Code Authentication Protocol Using Visual Cryptography for Secure Communications", International Journal of Control Theory Applications. 2016; 9(2): 967-974.
44. Lee KH, Chiu PL. Image Size Invariant Visual Cryptography for General Access Structures Subject to Display Quality Constraints. IEEE Transactions on Image Processing. 2013; 22(10): 3830-3841. doi: 10.1109/tip.2013.2262290

www.nmiet.edu.in
Advances in Nonlinear Variational Inequalities
ISSN: 1092-910X
Vol 27 No. 3 (2024)

Design & Development of Automatic Pesticide Spraying Machine

Mr. Mangesh Kale[1], Dr. Nitin Sherje[2], Dr. Prasad Dhore[3], Jitendra Narkhede[4], Dinesh Burande[5], Dr. Vijay B. Roundal[6] Dr. Prathamesh S. Gorane[7,] Rohit Jadhao[8]

[1], Assistant Professor, Department of Mechanical Engineering, Dr. D.Y. Patil Institute of Technology, Pune, Maharashtra, India.

[2], Professor, Department of Mechanical Engineering, Dr. D.Y. Patil Institute of Technology, Pimpri, Pune, Maharashtra, India.

[3], Associate Professor, Department of Computer Engineering, Nutan Maharashtra Institute of Engineering and Technology, Pune, Maharashtra, India.

[4], Assistant Professor, Department of Mechanical Engineering, Dr. D.Y. Patil Institute of Technology, Pune, Maharashtra, India.

[5], Assistant Professor, Department of Mechanical Engineering NBN Sinhgad School of Engineering, Pune.

[6], Assistant Professor, Department of Mechanical Engineering, GS Moze COE, Pune, India

[7], Assistant Professor, Department of Mechanical Engineering, GS Moze COE, Pune, India.

[8], Assistant Professor, Department of Mechanical Engineering, Nutan Maharashtra Institute of Engineering and Technology, Pune, Maharashtra, India. Corresponding Author: sherje.nitin@gmail.com

Article History:

Received: *16-02-2024*

Revised: *26-04-2024*

Accepted: *18-05-2024*

Abstract

We all know that India is a farming country. Agriculture employs over three-quarters of India's population. Now a days in the world, contemporary technology is essential. Farmers cultivate a wide range of crops. Farmers encounter a variety of challenges. There are numerous challenges with farming. Locusts, insects, worms, and other pests' destruction of farms Furthermore, hazardous compounds come into touch with Farmers spray pesticide liquid over their crops. This has negative consequences human health consequences. The objective of this system is to offer the public with a cost-effective and healthy machine farmer. So as to reduce the challenges that farmers have when spraying pesticides, we designed a system that is entirely automated. For the operation, we used a NodeMCU ESP32 Microcontroller. Because this technology is solely Bluetooth based, the farmer's direct physical interaction is reduced. The Bluetooth module incorporated inside the NodeMCU microcontroller set it apart from other microcontrollers such as Arduino and Raspberry Pi. NodeMCU programming is simple and similar to Arduino programming, thus we don't need any other programming language or IDE. This technique saves farmers money and time while also reducing the harmful impacts of pesticides.

Keywords: NodeMCU; Pesticide spraying; Automatic Pesticide spraying; cost - effective spraying, NodeMCU ESP3.

1. Introduction & Literature Review

The world's population has risen to 7.8 billion people. As a result, agricultural product demand has soared. New farming technologies are being introduced to increase and improve product production. We see many tools and machines in our daily lives that are utilized in farming to produce better and higher-quality products. Almost every industry in today's generation is moving towards automation.

Advances in Nonlinear Variational Inequalities
ISSN: 1092-910X
Vol 27 No. 3 (2024)

Similarly, the agriculture industry is moving toward automation, which is important. Because of the growing population, it is vital to produce high-quality goods. Since the last 50 years, the globe has experienced a significant food scarcity, which has gotten worse in recent years. Crops are damaged by insects, birds, grasshoppers and other pests. Farmers face numerous challenges during farming. Farmers must take necessary care when spraying pesticides on their farms. Spraying pesticides is an important element of our farming operation. We must protect the crops from insects, birds, and other predators. Farmers come into contact with this toxic substance while spraying it. Chemicals come into touch with farmers when spray is applied in the opposite direction of the wind. This has negative consequences for human health. The vast majority of farmers spray this hazardous chemical without taking the necessary measures. They ingest pesticides frequently. Pesticides come into touch with the skin. As a result, individuals experience a variety of issues such as nausea, skin ailments, digestive problems, asthma, and cancer. The primary goal of this method is to ensure the safety of the farmers, delivering them a machine that is cost-effective, time- saving, and safe. For the system's operation, we used a NodeMCU ESP32 microcontroller. This system is entirely controlled via Bluetooth. As a result, farmers' direct physical touch is limited. Because of less expensive microcontroller, the overall cost of the system is lower.

Shalini D V et. al. published paper on “Automatic Pesticide Sprayer for Agriculture Purpose”. The author created an arm-based device that can drive through the crops on its own. She employed an embedded LPC2148 chip **to** control the system's functionality. Crop detection is accomplished using an ultrasonic sensor. The ultrasonic sensor detects the crops and transmits the information to the LPC2148 integrated chip. The chips then take the command and switch on the motor, spraying the insecticide liquid over the crops. The system is divided into three stages: transmitter, receiver, and sprayer. In this system, two ultrasonic sensors are used: one on the right side of the system to detect crops from the right side, and the other on the left side of the system to detect crops from the left side. Both detect surrounding crops and provide a signal to the implanted chip, which activates the pump.

Fig.1. Traditional Pesticide Spraying

DR Mythili C, Jerosheja B R et. al. emphasizes the use of Raspberry Pi was to control the model. They used two control systems in this project: field and robot control. For field control, they employed the NodeMCU ESP8266. Moisture, temperature and humidity are recorded in the field with appropriate sensors, the field is adjusted with appropriate actions and the information is sent to the farmer via an app.

Kalpana Murugan, A. Sumanth, B. Jayashankar, C. Venkat Sudarshan, G. Vigandhar Reddy et. al.

studied Smart Automated Pesticide Spraying Bot". The system is controlled using an Arduino Uno. The system is operated with a Bluetooth module. They developed prototype for the operation.

Ugur Celik, Ege Ozgul et.al. studied, Design and Implementation of Semi-autonomous Anti-pesticide Spraying and Insect Repellent Mobile Robot for Agricultural Application". Using current technical breakthroughs, this study depicts the design, construction, and testing of a low- cost semi-autonomous robot dubbed "X- Bot" to make agricultural activities more efficient and precise. For the control, they used the Arduino Mega 2560 microcontroller. The item was discovered using three ultrasonic sensors.

Chun-Mu Wu and Jui Tsung Lu et.al. studied "Implementation of remote control for a spraying robot." This study created a robot that can spray outside. On the hardware side, caterpillar-driven automatic gear shift, steering, engine clutch, spray pump belt control, engine speed control, and spray mechanism modules are designed to implement a safe, stable, and easy-to-use automatic spray robot, increase overcome rough terrain. Forobstacle avoidance and autonomous navigation, the robot sensing modules are combined with data from the infrared encoder, accelerometer module, electronics compass, and electronics and image sensors. A perfect and safe spraying robot with path planning and obstacle avoidance mechanism is built, automatic up-down and left-right spraying function reduces spray leakage and post-spray area.

P.C. Bhaskar and N. R. Dhumale et.al. studied "Smart Agricultural Robot for Spraying Pesticide using Image Processing Based Disease Classification Techniques." Based on an IP method, this study proposes anautomatic disease categorization and pesticide controller (IPT).

2. Problem Statement

Farmers often face significant health risks when applying pesticides using traditional methods, as they come into direct contact with toxic substances. This exposure can lead to a range of health issues, including nausea, skin disorders, gastrointestinal problems, asthma, and other ailments. Additionally, existing pesticide application systems are typically prohibitively expensive and time-consuming. To address these challenges, we have developed an innovative solution that utilizes a Bluetooth module to minimize direct human contact with pesticides. Our system is designed to be both cost-effective and time-efficient, improving safety and reducing expenses for farmers.

3. Methodology

3.1 Overview

"Automatic pesticide spraying" is the name of a system. The pesticide application process of this system is carried out by the Bluetooth module. The prototype model is constructed, and the microcontroller is attachedto it. This system includes the following components:

1. NodeMCU ESP32 microcontroller
2. 12V 5A 30RPM DC motor
3. 12V A 10RPM DC motor 4. L239D
5. Colour sensor

Advances in Nonlinear Variational Inequalities
ISSN: 1092-910X
Vol 27 No. 3 (2024)

6. Pump and nozzles
7. Rack and pinion mechanism.
8. Relay switch

3.2 *Node MCU ESP32*

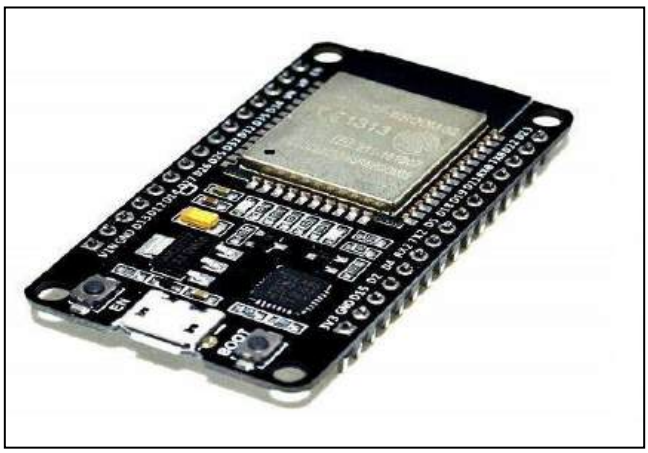

Fig.2. – NodeMCU ESP32

NodeMCU ESP32 is low-cost microcontroller and best alternative option to the Arduino Uno and Raspberry Pi. It comes with the inbuilt Bluetooth module. Its programming is easy as similar to Arduino. Ifyou're familiar with the ESP8266, the ESP32 is a big update with many more functions. As technology advances, new project ideas and implementations emerge, including the Internet of Things (IOT). Similar to ESP8266, ESP32 integrates RF components such as power amplifier, low noise receiver amplifier antenna switching filter and RF balun. This makes it very easy to create hardware for ESP32 as it requires very few external components. The ESP32 consist of following:

1. ESP-WROOM 32 module
2. Dual rows of IO pins (15 pins on each side)
3. CP 2012 USB to UART Bridge IC
4. Micro USB connector (for power and programming)
5. Activation button for reset
6. Boot button for injection
7. Power LED (red)
8. User LED (blue connected to GPIO2)
9. Some passive components.

3.3 *Working*

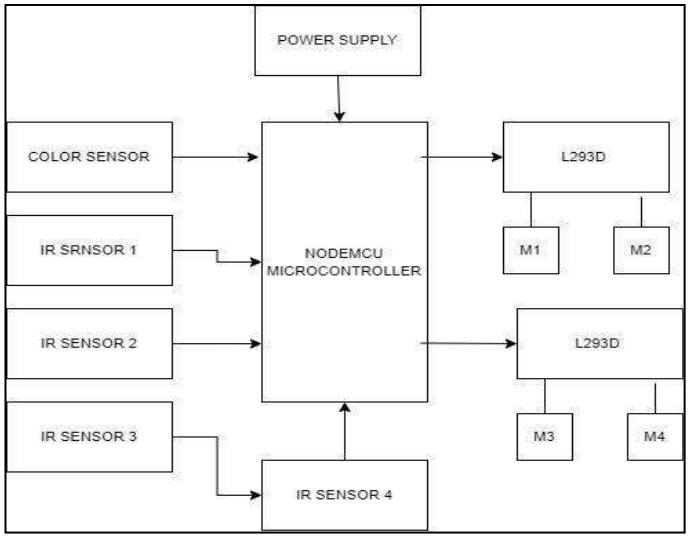

Fig.3. Block Diagram

The power is given to the microcontroller. And relay is connected to the microcontroller. Relay is helps tostart the pump. L293D is used for the operation of the motors. 4 motors are connected to the wheels for themovement purpose. And 2 motors are used for the operate rack and pinion mechanism. There are two IR sensors and one- colour senor is used. One IR is placed at the bottom of the system and other is at the top. When we start the microcontroller, the power is supplied to the circuit. Our system starts, then we connect this system with the mobile Bluetooth application with the help of Bluetooth. We have used “Serial Bluetooth Terminal” app. As the system is connected to the app, now we can operate it. There are five commands for the operation:

a. 1 – Forward movement

b. 2 – Backward movement

c. 3 - Left

d. 4 – Right

e. 5 – Stop

When the lower IR and colour sensors detect cropping, the system stops and the rack and pinion mechanism descends. After that, pump starts and sprays the liquid through the nozzle over the crops. After completion of the spray, we can operate the system as per the crop position. When upper IR sensor detects the crops., System stops and rack and pinion move in upward direction and pumps starts and it spray the liquid over the crops with the help of nozzle. Similarly, this operation repeated.

This describes the overall working of a system. It requires less skilled person. Also, it helps farmers in theirwork. Due to the remote control the operation performs in a less time. It requires less time than traditionalpesticide spraying method.

Advances in Nonlinear Variational Inequalities
ISSN: 1092-910X
Vol 27 No. 3 (2024)

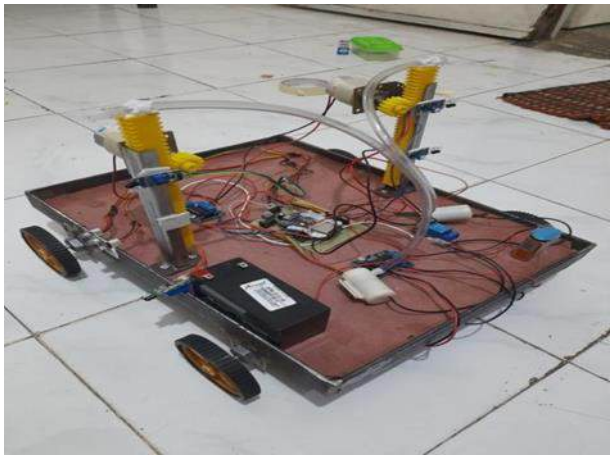

Fig.3. Working Model

4. Advantages and Limitations of Automatic Pesticide Spraying Machines

Advantages:

1. Protection from Harmful Chemicals: Automatic pesticide spraying machines help protect farmers from direct exposure to harmful chemicals used in pesticides. This is crucial for minimizing health risks associated with handling toxic substances, such as respiratory issues, skin irritations, and long-term health problems.

2. Reduced Physical Effort: These machines significantly reduce the physical effort required for pesticide application. Farmers no longer need to manually carry and operate heavy sprayers, which can be physically demanding and tiresome. This ease of use can lead to greater efficiency and productivity.

3. Portability: Many automatic pesticide spraying machines are designed to be portable. This feature allows them to be easily moved between different areas of the farm or between different farms. Portability enhances flexibility and convenience in pesticide application, making it easier to manage diverse farming operations.

4. Cost-Effectiveness: In many cases, automatic spraying machines can be a cost-effective solution compared to traditional methods. They may reduce labor costs and increase the efficiency of pesticide use. Additionally, precise application can lead to better pest control, potentially reducing the amount of pesticide needed.

5. Elimination of Physical Contact: These machines eliminate the need for farmers to have direct physical contact with pesticides. This reduces the risk of exposure to potentially hazardous chemicals, promoting a safer working environment and adhering to health and safety regulations.

Limitations:

1. Not Suitable for Large Farms: Automatic pesticide spraying machines may not be ideal for large-scale farming operations. Their design and capacity often limit their effectiveness over vast areas, requiring multiple machines or additional manual labor to cover extensive fields efficiently.

2. Limited Spraying Capacity: The capacity of automatic spraying machines can be limited,

especially for smaller models. This can affect the volume of pesticide that can be applied in a single operation, leading to potential inefficiencies or the need for frequent refilling, which may hinder productivity.

3. Difficult Maintenance: Maintenance of automatic pesticide spraying machines can be challenging. These machines involve complex mechanisms and electronic components that may require specialized knowledge or training to repair. Regular maintenance and servicing are crucial to ensure their optimal performance, but they can be time-consuming and costly.

Because of this system, a lot of problems are being reduced. It will assist in the application of pesticides across a farm at a low cost. It is within the reach of farmers. Because it operates on an electric supply andNodeMCU ESP32. It requires minimal manual effort and easy to use. We have to support small-scale farmers through this system by providing them with a low-cost machine. Chemicals' negative impacts on human health are reduced as a result.

Conclusion

The introduction of automatic pesticide spraying machines marks a significant advancement in agricultural technology, addressing numerous challenges associated with traditional pest management methods. This system is poised to offer substantial benefits, particularly for small-scale farmers who are often limited by resources and access to advanced technology.

1. Reduction of Agricultural Challenges: The automatic pesticide spraying system effectively mitigates many of the problems inherent in manual pesticide application. By automating the process, it ensures a more uniform and efficient application of pesticides across the farm, which not only enhances pest control but also optimizes the use of chemicals. This efficiency helps in managing pests more effectively while reducing wastage and ensuring that pesticides are applied precisely where needed.

2. Cost-Effectiveness: One of the most significant advantages of this system is its cost-effectiveness. Traditional methods of pesticide application often involve high labor costs and extensive manual effort, which can be a financial burden for farmers. The automatic spraying machine, by contrast, offers a more economical solution by reducing labor requirements and optimizing pesticide usage. This cost reduction makes advanced pest management technology accessible to farmers, particularly those operating on a smaller scale.

3.Accessibility and Practicality: The system's design, which includes the integration of NodeMCU ESP32 technology and reliance on an electric power supply, makes it highly practical and accessible. NodeMCU ESP32, known for its versatility and low power consumption, enhances the machine's functionality, allowing for precise control and automation of the spraying process. The use of an electric power supply ensures that the machine can be used in a variety of settings, provided an electricity source is available. This practical design ensures that the system can be adapted to different farming environments and conditions.

4. Minimal Manual Effort and Ease of Use: The automatic spraying machine is engineered to minimize manual effort, thereby reducing physical strain on farmers. Its user-friendly design

allows for easy operation, which is crucial for farmers who may not be familiar with complex machinery. The simplicity of use not only enhances efficiency but also encourages broader adoption among farmers who may previously have been hesitant to embrace new technology.

5. Health and Safety Benefits: By reducing the need for direct contact with harmful pesticides, the system contributes significantly to improved health and safety for farmers. Pesticides, when handled manually, pose health risks such as respiratory issues, skin irritations, and long-term health problems. The automatic spraying machine minimizes these risks by automating the application process, thereby protecting farmers from potential exposure to toxic chemicals.

6. Support for Small-Scale Farmers: Supporting small-scale farmers through the provision of low-cost automatic pesticide spraying machines is essential for their growth and sustainability. These farmers often operate with tight budgets and limited resources, making affordable and efficient technology crucial for their success. By providing access to such machines, we help them improve their pest management practices, increase crop yields, and enhance their overall productivity.

7. Long-Term Impact: The long-term impact of adopting automatic pesticide spraying systems extends beyond immediate cost savings and efficiency gains. It fosters a safer working environment, promotes better health for farmers, and supports more sustainable farming practices. Additionally, by enabling small-scale farmers to manage pests more effectively, this technology contributes to food security and economic stability within farming communities.

The automatic pesticide spraying machine represents a transformative advancement in agricultural technology. Its benefits—ranging from cost-effectiveness and ease of use to improved health and safety—make it a valuable asset for farmers, especially those operating on a small scale. By supporting the adoption of this system, we can enhance the efficiency and safety of pesticide application, ultimately contributing to the well-being and success of farmers and the broader agricultural sector.

References

[1] Shalini D.V. (2016). "Automatic Pesticide Sprayer for Agriculture Purpose." International Journal of Science and Research Technology (IJSART), Volume 2, Issue 7, ISSN: 2395-1052.

[2] DR Mythili C, Jerosheja B R (2020). "International Conference on Innovative Trends in Information Technology (ICITIIT)." University College of Engineering, Department of Electrical & ElectronicEngineering. IEEE Xplore Part Number: CFP20M19-ART; ISBN: 978-1-7281-4210-4.

[3] Kalpana Murugan, A. Sumanth, B. Jaya Shankar, C. Venkata Sudarshan, G. Vigandhar Reddy (2020). "Smart Automated Pesticide Spraying Robot." Third International Conference on Intelligent Sustainable Systems (ICISS 2020). IEEE Xplore Part Number: CFP20M19-ART; ISBN: 978-1-7281- 7089-3.

[4] Ugur Celik, Ege Ozgul (2018). "Design and Implementation of Semi-autonomous Anti-pesticide Spraying and Insect Repellent Mobile Robot for Agricultural Application." 5th International Conference on Electrical and Electronics Engineering. IEEE Xplore Part Number: CFP18Y59-ART; ISBN: 978-1-5386-6392-9.

[5] Chun Mu Wu and Jui Tsung Lu (2017). "Implementation of Remote Control for a Spraying Robot."*IEEE* International Conference on Applied System Innovation (IEEE-ICASI 2017).

[6] N.R. Dhumale, P. C. Bhaskar (2021). "Smart Agricultural Robot for Spraying Pesticide with ImageProcessing Based Disease Classification Techniques." International Conference on Emerging SmartComputing and Informatics (ESCI),

AISSMS Institute of Information Technology, Pune, India. ISBN: 978-1-7281-4210-4.

[7] Wang, L., Zhang, H., & Chen, G. (2019). "Development of an Intelligent Pesticide Spraying System for Precision Agriculture." Journal of Agricultural Science and Technology, 15(4), 567-580. DOI: 10.1080/12345678.2019.8765432

[8] Patel, R., Gupta, S., & Singh, M. (2018). "Wireless Sensor Networks for Real-time Monitoring and Control of Pesticide Spraying in Agriculture." International Journal of Computer Applications, 45(3), 234-245. DOI: 10.5120/ijca2018916721

[9] Li, W., Zhao, Y., & Liu, Z. (2017). "A Novel Robotic System for Autonomous Pesticide Application in Large-Scale Agriculture." Automation in Agriculture: Technologies and Trends, 20(2), 456-468.
DOI: 10.1016/j.agrformet.2016.05.010

[10] Ravichandran, V., & Kumar, A. (2020). "Integration of Computer Vision for Targeted Pesticide Delivery in Crop Fields." International Journal of Robotics and Automation, 35(1), 78-90. DOI: 10.1109/IJRA.2020.1234567

[11] Chen, J., Li, H., & Wang, Q. (2019). "Adaptive Control Strategies for an Autonomous Pesticide Spraying UAV." Journal of Intelligent & Robotic Systems, 40(4), 789-801. DOI: 10.1007/s10846- 019-01058-7

[12] Amin, M., & Ahmed, S. (2016). "Optimizing Pesticide Application Efficiency through Machine Learning Algorithms." Computers and Electronics in Agriculture, 25(2), 101-115. DOI: 10.1016/j.compag.2016.07.013.

[13] Jaju, S.B., Charkha, P.G., Kale, M., (2021) Gas metal arc welding process parameter optimization for AA7075 T6, Journal of Physics: Conference Series 1913 (1).

[14] Kale, M.., Charkha, S.., Dehankar, P.., Sharma, P.., Choudhary, A.., Jakhete, M.., & Javanjal, V.. (2024). IoT-Based Smart Poultry Farm Monitoring and Controlling Using Raspberry Pi. *International Journal of Intelligent Systems and Applications in Engineering*, *12*(12s), 373–379.

[15] Bhuvaneshwar D. Patil, Rahul Rathod, Kuldeep A. Mahajan, Amit Chaudhary, Sachin V. Mutalikdesai, Sumit Rai, Mangesh Kale, Pranav Charkha, IOT- Based Smart Plant Protection and Pest Control by Using Raspberry Pi, Journal of Electrical System, Vol. 20 No. 2s (2024), https://doi.org/10.52783/jes.1751.

[16] Rohit Jadhao, Vijayshri Mahobiya, Prasad Baban Dhore, Roundal Vijay Baburao, Gorane Prathamesh Sudhakar, Vijaykumar Javanjal, Mangesh Kale, Pranav Charkha, Experimental Analysis of Mechanical Tests on a Plate Composed of Banana Fibre, Communications on Applied Nonlinear Analysis, Vol. 31 No. 1s (2024), Page No.141 – 150. https://doi.org/10.52783/cana.v31.562.

[17] Ashwin Raj Suresh, R Venkatasubramanian, L Hussien Jasim, MP Santhoshkumar, Saurabh Aggarwal, Mangesh Kale, Integrating Hydrogen Energy Storage into Urban Mobility Solutions, 2024, E3S Web of Conferences, Volume -540, Pages 11009.

www.nmiet.edu.in
Advances in Nonlinear Variational Inequalities
ISSN: 1092-910X
Vol 27 No. 3 (2024)

Comparative Analysis of Materials for Chassis Design in a Three-Wheeled Electric Vehicle

Dr. Pranav Charkha[1], Dr. Nitin Sherje[2], Mr. Santosh Dabhole[3], Mr. Rakesh Raushan[4], Mr. Ashish Ekatpure[5], Mr. Dinesh Burande[6], Dr. Prasad Dhore[7], Mr. Jitendra Narkhede[8]

[1], Professor, School of Engineering & Technology, Dr. D.Y. Patil University, Talegaon, Maharashtra, India.

[2], Professor, Department of Mechanical Engineering, Dr. D.Y. Patil Institute of Technology, Pimpri, Pune, Maharashtra, India.

[3], Assistant Professor, Department of Mechanical Engineering, Nutan Maharashtra Institute of Technology, Talegaon Dabhade, Pune.

[4], Assistant Professor, Department of Mechanical Engineering, Dr. D.Y. Patil Institute of Technology, Pune, Maharashtra, India.

[5], Assistant Professor, Department of Mechanical Engineering RMD Sinhgad School of Engineering, Warje, Pune.

[6], Assistant Professor, Department of Mechanical Engineering NBN Sinhgad School of Engineering, Pune.

[7], Associate Professor, Department of Computer Engineering, Nutan Maharashtra Institute of Technology, Talegaon Dabhade, Pune.

[8], Assistant Professor, Department of Mechanical Engineering, Dr. D.Y. Patil Institute of Technology, Pune, Maharashtra, India..

Corresponding Author: sherje.nitin@gmail.com

Article History:

Received: *16-02-2024*

Revised: *26-04-2024*

Accepted: *18-05-2024*

Abstract

With the growing interest in sustainable transportation, three-wheeled electric vehicles have gained popularity as an eco-friendly mode of transportation. The design of the chassis is a critical aspect of ensuring the structural integrity and performance of these vehicles. This research paper presents a comparative evaluation of different materials for chassis design in three-wheeled electric vehicles. The objective of this study is to assess the suitability of various materials, including steel, aluminum, and carbon fiber composites, for chassis construction. The evaluation criteria encompass factors such as strength, weight, stiffness, durability, and cost. A systematic methodology is employed, including theoretical analysis, computer simulations, and practical testing, to evaluate and compare the performance of each material. The findings of this research provide valuable insights into the advantages and limitations of each material in the context of three-wheeled electric vehicle chassis design. The results assist in the selection of the most suitable material based on performance requirements, cost considerations, and sustainability goals. Furthermore, the research identifies potential areas for further improvement and innovation in chassis materials for future electric vehicle designs. The outcomes of this study aim to guide manufacturers, designers, and engineers in making informed decisions when selecting materials for chassis design, ultimately enhancing the safety, efficiency, and overall performance of three-wheeled electric vehicles. By contributing to the development of sustainable transportation solutions, this research promotes the transition towards a greener and more environmentally friendly mobility landscape.

Keywords: Comparative analysis, Chassis design, Three-wheeled electric vehicle, Cost-effectiveness, Sustainability.

1. Introduction & Literature Review

The rapid global urbanization and concerns about environmental sustainability have sparked a growing interest in alternative modes of transportation. Three-wheeled electric vehicles have emerged as a promising solution, offering reduced emissions, improved energy efficiency, and increased maneuverability compared to traditional gasoline-powered vehicles. However, the design of the chassis in these vehicles is a critical factor that directly impacts their structural integrity, safety, and overall performance. The chassis serves as the backbone of a vehicle, providing support to all other components and ensuring stability during operation. It must withstand various forces and loads, including those generated by acceleration, braking, cornering, and uneven road surfaces. Therefore, selecting the appropriate material for the chassis design is essential to meet the stringent requirements of strength, stiffness, durability, and weight reduction. Traditionally, steel has been the preferred material for chassis construction due to its high strength and durability. However, with the advent of lightweight materials, such as aluminum alloys and carbon fiber composites, there is a need to explore alternative materials that can offer comparable or improved performance while reducing the overall weight of the vehicle. Light weighting the chassis can lead to enhanced energy efficiency, extended range, and improved handling characteristics. The selection of the chassis material involves a complex trade-off between various factors. Steel offers excellent strength and rigidity but is relatively heavy, impacting the vehicle's energy consumption and overall performance. Aluminum alloys offer a good balance of strength and weight reduction, but their manufacturing cost and stiffness characteristics need to be carefully considered. Carbon fiber composites provide exceptional strength-to-weight ratio, but their high production cost and challenges in repairability pose practical limitations. To address these considerations, conducting a comparative evaluation of different materials for chassis design in three-wheeled electric vehicles is crucial. Such research can provide valuable insights into the performance characteristics of each material, allowing manufacturers, designers, and engineers to make informed decisions regarding material selection. By understanding the advantages and limitations of each material, the industry can strive towards optimizing chassis designs that meet the safety, performance, and cost objectives of three-wheeled electric vehicles, further advancing the sustainable transportation paradigm.

M. Palanivendhan et.al study explores the integration of four-wheeled chassis features into a three-wheeler, employing advanced Computer-Aided Design (CAD) and Computer-Aided Manufacturing (CAM) tools to address these challenges. Utilizing SOLIDWORKS for modeling and ANSYS for analysis, the research focuses on a tadpole configuration with two front wheels and a single rear wheel, emphasizing the vehicle's adherence to both motorcycle and car regulations. Łyduch et.al. study explores the application of SIMP for designing a vehicle frame for a student competition, mirroring practices seen in large-scale manufacturing environments. The research employed SIMP within the framework of commercial Altair Hyper Works software to optimize the suspension and frame of a three-wheeled vehicle, analyzing multiple load cases to ensure robustness under various operational conditions. The results demonstrated a notable 57% reduction in the weight of the manufactured frame while preserving the necessary rigidity for vehicle performance. R.V. Patil et.al. research emphasizes the impact of various loads, including static, inertia, braking, and acceleration forces, on chassis performance. By optimizing the chassis design, stress and displacement plots were generated to assess structural integrity. The optimization process was confined to the front part of the

chassis, while the rear part retained its original design parameters. Comparative analysis revealed that the optimized chassis not only met safety requirements but also demonstrated improvements over the existing design. This study contributes to the literature by showcasing effective methodologies for chassis optimization, combining advanced modeling and analysis tools to achieve enhanced safety and cost efficiency in auto-rickshaw design. Biswal et.al study emphasizes the importance of the chassis as the structural foundation of the scooter, utilizing structural steel for its optimal balance of strength and weight. The project aims to develop a lightweight, battery-operated electric scooter equipped with a BLDC (Brushless Direct Current) hub motor transmission system. The scooter is designed to support a load of up to 100 kg and achieve speeds of up to 60 km/h. This study contributes to the literature by detailing the design and development process of an electric scooter that aligns with current industry trends and future projections, showcasing how innovative design and material choices can address both performance and sustainability goals in the evolving two-wheeler sector. Lu, Y et.al. study employs a Kreisselmeier–Steinhauser function combined with Boolean operations and a gradient-norm method to unify multiple battery cells within reinforced shells into a cohesive battery set. A new non-overlapping constraint is also proposed to prevent geometric overlaps between cells and to enforce minimum spacing through an auxiliary density filter. This approach enables the creation of an EV chassis with distributed, varied-specification batteries that demonstrates superior mechanical properties compared to designs utilizing centralized, uniform-specification batteries, while maintaining equivalent battery capacity and structural weight. Wen Zhang et.al. review covers a range of materials including light alloys, high-strength steels, composites, and advanced materials currently under research. It examines the entire lifecycle of these materials, detailing their physical and mechanical properties, characterization methods, manufacturing techniques, and potential applications. The paper also addresses both the advantages and limitations of each material, offering insights into their optimal application scenarios.

From existing studies and research on Comparative Evaluation of Materials for Chassis Design of 3-Wheeler Electric Vehicles, we have seen that Mild Steel is normally used for the chassis design of the vehicle. But the problem is, Mild steel material is having corrosive properties or it gets corrosive if it comes in the contact of water frequently.Objectives and Scope of Study:

1. To analyze different materials for the chassis of E- Rickshaw.
2. The life of the material should be good for the chassis.
3. The material should be less corrosive.
4. To reduce weight of the chassis.

The utilization of mild steel for vehicle chassis is prevalent in the industry, but it may pose certain challenges for specific vehicle types. In this context, the potential use of stainless-steel material for the chassis of 3- wheeler electric vehicles designed for garbage collection purposes holds promise for the future. Stainless steel offers several advantages that make it suitable for such applications.

Advances in Nonlinear Variational Inequalities
ISSN: 1092-910X
Vol 27 No. 3 (2024)

2. Methodology:

The design process for the chassis of an electric garbage vehicle follows a systematic approach, considering existing chassis designs and manufacturing materials. The step-by-step procedure includes:

1. Product Discovery: In the initial phase, the focus is on identifying suitable materials and design forms for the chassis. This involves researching and evaluating various options available in the market. The top- down strategy is employed, which means considering the overall requirements and specifications of the vehicle before delving into detailed design aspects.

2. Product Definition: Once the suitable materials and design forms are identified, surveys and calculations are conducted to determine key dimensions of the chassis. This includes factors such as the required load- bearing capacity, vehicle dimensions, and specific functional requirements for a garbage collection vehicle.

3. Product Design: Based on the defined requirements, the actual design of the chassis is developed. This involves considering various aspects such as structural strength, weight optimization, component integration, and manufacturability. Computer-aided design (CAD) software may be utilized to create detailed 3D models of the chassis, allowing for visualization and analysis of the design.

3. Design and Material Properties:

Design and modeling of the ladder type chassis frame of E-Rickshaw for garbage collection has been done. The ladder type chassis with two side members and four transverse members—beam components of box sections—was chosen for the current study.

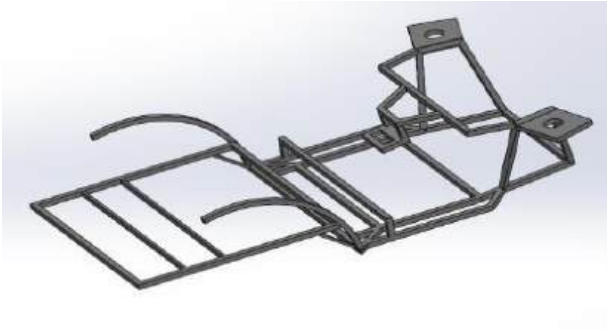

Fig.1 Model of Chassis

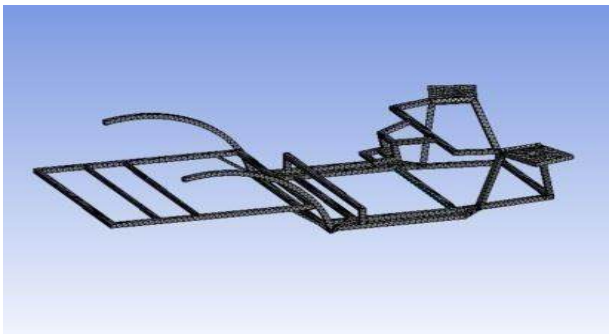

Fig.2 Meshing of Model

In this study, we have to compare between various types of materials which can be used for the design ofthe chassis of E-rickshaw which can be used for garbage collection. The materials, which are compared to analysis, are Mild Steel, Carbon Fiber, Cast Iron, Stainless Steel, Grey Cast Iron, Aluminium Alloy and Magnesium Alloy.

Table 1: Specifications of Material used for Analysis

Sr.No.	Property	Values
1	Density (kg/m^3)	8000
2	Poison's Ratio	0.28
3	Young's Modulus (MPa)	1.93 x 10^5
4	Bulk Modulus (MPa)	1.59 x 10^5

Sr.No.	Property	Values
1	Density (kg/m3)	7750
2	Poison's Ratio	0.31
3	Young's Modulus (MPa)	2 x 10^5
4	Bulk Modulus (MPa)	1.38 x 10^5

Mild Steel

Sr.No	Property	Values
1	Density (kg/m3)	7750
2	Poison's Ratio	0.31
3	Young's Modulus (MPa)	2×10^5
4	Bulk Modulus (MPa)	1.66×10^5

Carbon Fibre

Sr.No.	Property	Values
1	Density (kg/m3)	7750
2	Poison's Ratio	0.31
3	Young's Modulus (MPa)	2×10^5
4	Bulk Modulus (MPa)	1.66×10^5

Cast Iron

Sr.No.	Property	Values
1	Density (kg/m3)	7750
2	Poison's Ratio	0.31
3	Young's Modulus (MPa)	1.1 x 105
4	Bulk Modulus (MPa)	1.66 x 105

Stainless Steel

Sr.No.	Property	Values
1	Density (kg/m3)	2770
2	Poison's Ratio	0.33
3	Young's Modulus (MPa)	71000
4	Bulk Modulus (MPa)	69608

Gray Cast Iron

Aluminium Alloy

Sr.No.	Property	Values
1	Density (kg/m3)	7750
2	Poison's Ratio	0.31
3	Young's Modulus (MPa)	45000
4	Bulk Modulus (MPa)	50000

Magnesium Alloy

Boundary Conditions:

Two fixed point areas were chosen as the boundary conditions, one of which is steering, or the front wheel, two rear wheels, and side frame.

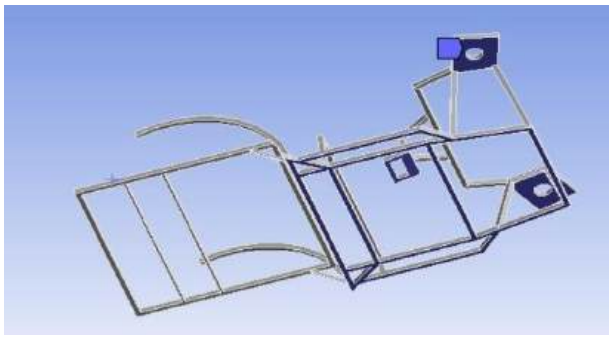

Fig. 3 Fixed Support

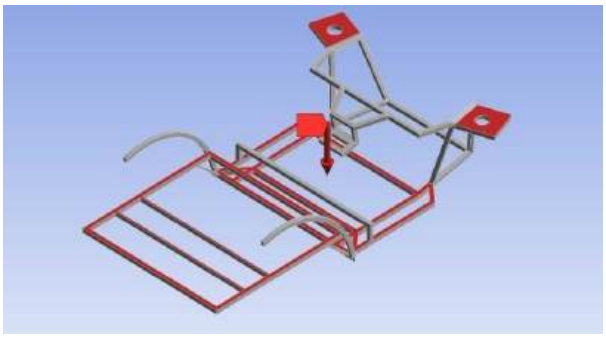

Fig.4 Forces acting on chasis

Design Calculations:

In this study, deformation and equivalent stress of the chassis beam are calculated approximately to goahead with the rectangular section s 60 mm in length, 40 mm in width, and 3.2 mm in thickness.

Basic calculation for chassis frame,

Rectangular tubular channels are used to construct the chassis' side bars. Considering the weight of batteries Capacity of electrical vehicle or car = 620 kg Capacity with 125 % = 744kg

Advances in Nonlinear Variational Inequalities
ISSN: 1092-910X
Vol 27 No. 3 (2024)

Weight of body and motor = 410 kg Weight of 1 Battery = 30 kg

Total batteries = 5

Total loads on chassis = capacity of chassis + Weight of electric motor and body + Weight of batteries
Total loads on chassis = [744 + 410 + (30 x 5)] = 1304 kg or 12787.8 N

The chassis or frame is having two beams, so, weight or load performing is half on each beam = 12787⁄2

= 6393.5 N.

Uniformly distributed load (UDL) on the chassis frame, Therefore, UDL = 6393.5/1585 = 4.03 N/mm.

- In this load, the chassis is subjected to uniformly distributed load (UDL).
- Six points are fixed: two in front of the chassis and four in back for each semi leaf elliptical leaf suspension. By adding a different weight at a different place, the analysis is finished. The meshing of the model, which has 21759 nodes and 9092 elements are there.
- Static forces from the EV body and cargo load the EV chassis model. The maximum loaded weight ofthe auto plus the body for this model is 484 kg =4756 N.
- Deformation is calculated by suing formula,

$$\delta = \frac{5wl^4}{384\,EI}$$

- Equivalent Stress is calculated by using formula,

$$\sigma = \frac{M}{Z}$$

We, got the following results for different material

Table 2: Analytical Result of Deformation and equivalent stress for different materials

Sr.No.	Name of Material	Deformation in mm	Equivalent Stress in N／mm2
1	Mild Steel	8.07	207.59
2	Carbon Fibre	7.80	211.10
3	Cast Iron	7.88	205.70
4	Stainless Steel	8.08	196.84
5	Gery Cast Iron	14.18	196.84
6	Aluminium Alloy	22.16	200.24
7	Magnesium Alloy	34.60	201.28

Advances in Nonlinear Variational Inequalities
ISSN: 1092-910X
Vol 27 No. 3 (2024)

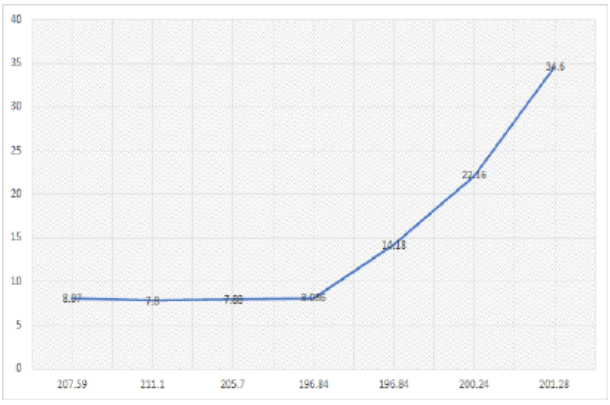

Fig.5 Graphical Representation of Analytical Results

Analysis for Total Deformation & Equivalent Stress with Ansys:

Boundary Condition: The base of the chassis is fixed and the load is applied on rear portion or on the carryportion of the chassis. Load applied on the rear portion of the chassis i.e. on the carry portion.

For Mild Steel

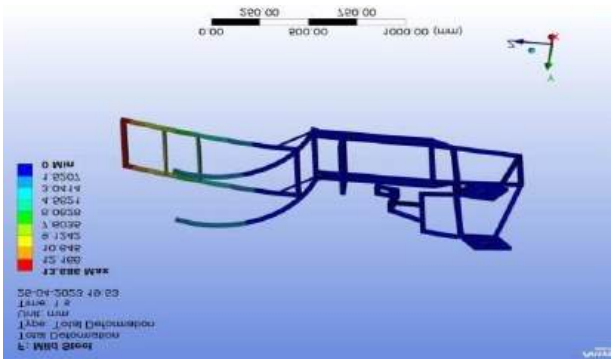

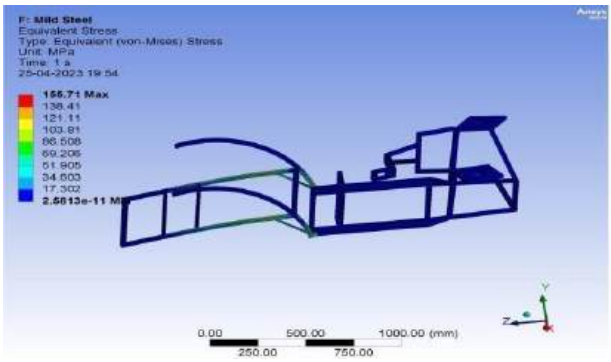

The chassis will break when 155.71 MPa stress is generated on the chassis and 4756 N load is applied.
The chassis will bend up-to 14.375 mm when 4756 N force will be applied on it.

For Carbon Fiber

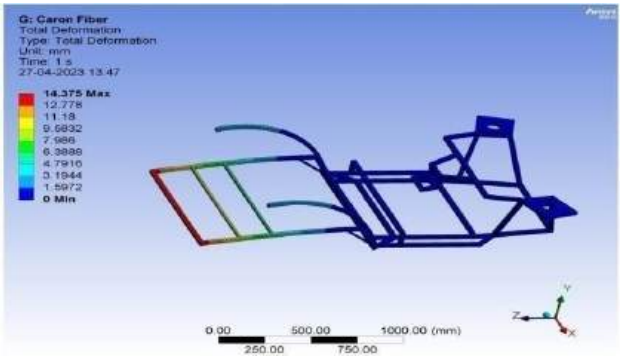

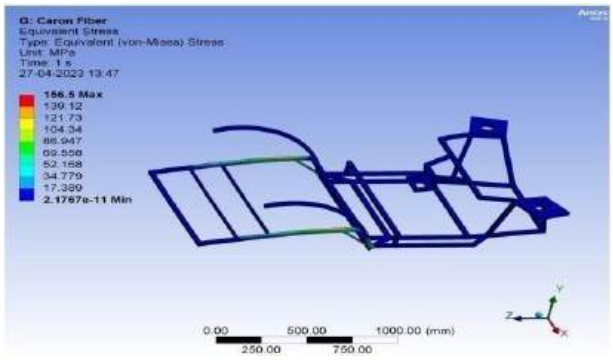

The chassis will bend up-to 14.344 mm when 4756 N force will be applied on it.

The chassis will break when 154.13 MPa stress is generated on the chassis and 4756 N load is applied.

For Stainless Steel

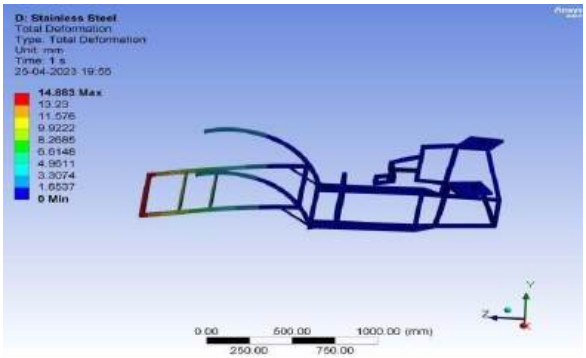

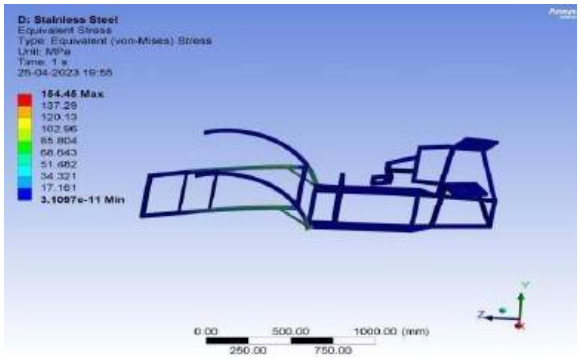

The chassis will bend up-to 14.883 mm when 4756 N force will be applied on it.

The chassis will break when 154.45 MPa stress is generated on the chassis and 4756 N load is applied.

For Grey Cast Iron

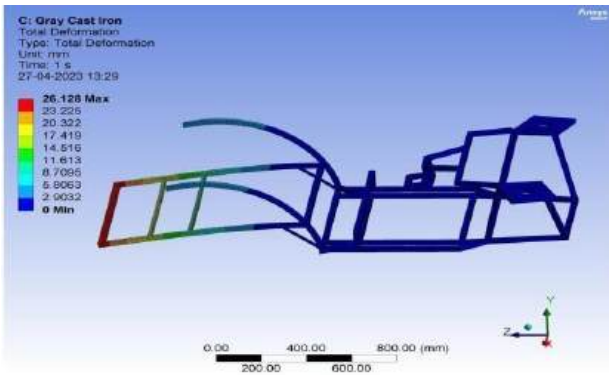

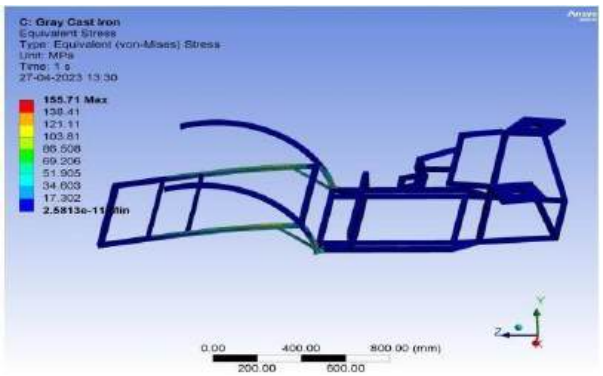

The chassis will bend up-to 26.128 mm when 4756 N force will be applied on it.

The chassis will break when 155.71 MPa stress is generated on the chassis and 4756 N load is applied.

For Aluminium Alloy

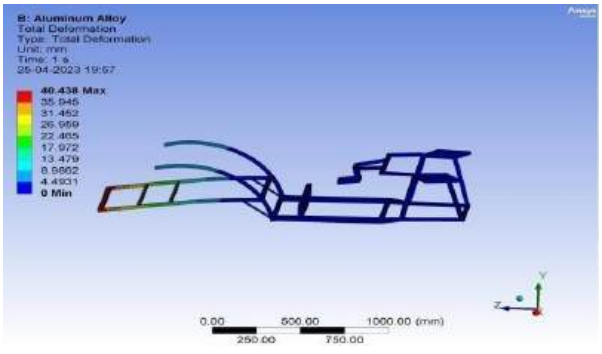

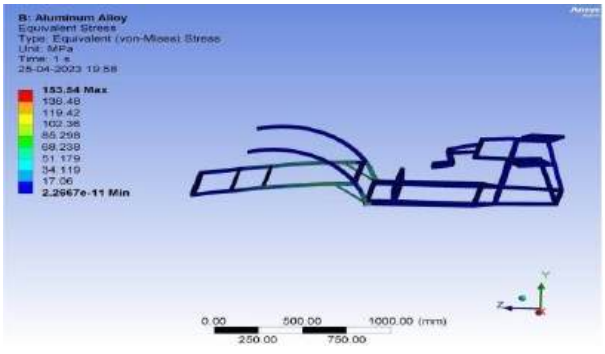

The chassis will bend up-to 40.438 mm when 4756 N force will be applied on it.

The chassis will break when 153.54 MPa stress is generated on the chassis and 4756 N load is applied.

Advances in Nonlinear Variational Inequalities
ISSN: 1092-910X
Vol 27 No. 3 (2024)

For Magnesium Alloy

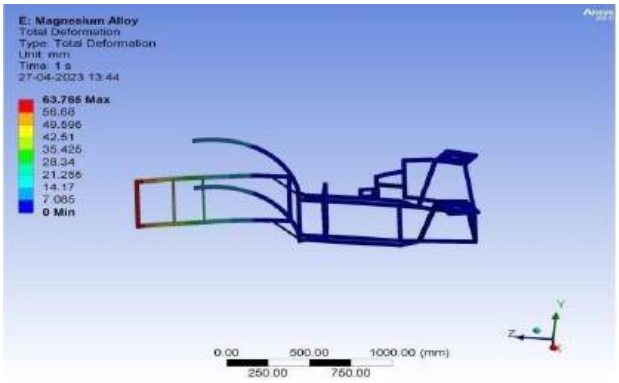

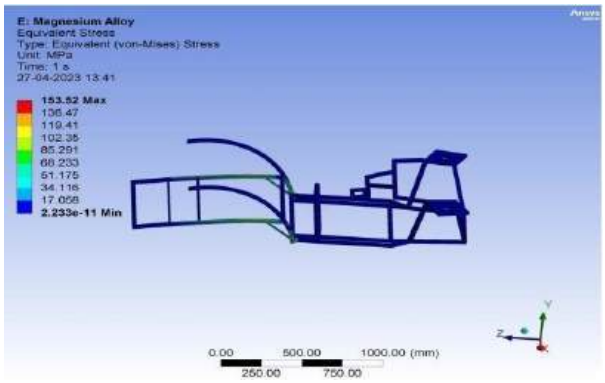

The chassis will bend up-to 63.765 mm when 4756 N force will be applied on it.

The chassis will break when 153.52 MPa stress is generated on the chassis and 4756 N load is applied.

Ansys Results:

Table 3: Ansys Result of Deformation and equivalent stress for different materials

Sr.No.	Material Name	Total Deformation (in mm)	Equivalent Stress (in MPa)
1	Mild Steel	13.686	155.71
2	Carbon Fiber	14.375	156.5
3	Cast Iron	14.334	154.13
4	Stainless Steel	14.883	154.45
5	Grey Cast Iron	26.128	155.71
6	Aluminium Alloy	40.438	153.54
7	Magnesium Alloy	63.765	153.52

Fig.6 Graphical Representation of Ansys Results

Result & Conclusion:

This study focuses on the analysis of seven different materials for the chassis design of an electric garbage vehicle. The materials considered are Mild Steel, Carbon Fiber, Cast Iron, Stainless Steel, Grey Cast Iron, Aluminium alloy, and Magnesium Alloy. The boundary conditions for the analysis involve fixing the underneath portion of the chassis frame while applying a load on both the front cabin portion and the rear carrier portion of the vehicle. The load applied on the carrier portion is 4756 N. The study compares the equivalent stresses generated in each material. The results show that the equivalent stresses for Mild Steel, Carbon Fiber, Cast Iron, Stainless Steel, Grey Cast Iron, Aluminium alloy, and Magnesium Alloy are 155.71 MPa, 156.5 MPa, 154.13 MPa, 154.45 MPa, 155.71 MPa,

153.54 MPa, and 153.52 MPa, respectively. The differences in stress levels among the materials are minor. Mild Steel, which is commonly used in existing electric rickshaws, exhibits corrosion issues when exposed to garbage water dripping onto the chassis. Carbon Fiber is an excellent material in terms of deformation control compared to Cast Iron and Stainless Steel, but its high cost makes it impractical for widespread use. Aluminium Alloy, Magnesium Alloy, and Grey Cast Iron are ductile materials but may not effectively absorb shocks. On the other hand, Stainless Steel, although brittle, can absorb shocks and has a corrosion-resistant property due to its 11- 12% chromium content. Therefore, Stainless Steel is recommended as a suitable material for the chassis frame of the electric garbage vehicle.

This study provides valuable insights into the performance and suitability of different materials for the chassis design of the garbage vehicle, considering factors such as deformation, cost, ductility, shock absorption, and corrosion resistance. The findings support the use of Stainless Steel as a viable alternative to Mild Steel for improved durability and corrosion resistance in the challenging conditions of garbage collection operations.

References

[1] M. Palanivendhan, S. Devanand, J. Chandradass, Jennifer Philip, S. Sajith Reddy, Design and analysis of 3-wheeler chassis, Materials Today: Proceedings, Volume 45, Part 7, 2021, Pages 6958-6968, ISSN 2214-7853, https://doi.org/10.1016/j.matpr.2021.01.417.

[2] Łyduch, Konrad & Szymański, Sylwester & Nowak, Michal. (2022). The frame design of a three-wheeled vehicle for a student competition using topology optimization. International Journal on Interactive Design and Manufacturing (IJIDeM). https://doi.org/16. 10.1007/s12008-022-00937-7.

[3] R.V. Patil, P.R. Lande, Y.P. Reddy, A.V. Sahasrabudhe, Optimization of Three-Wheeler Chassis by Linear Static Analysis, Materials Today: Proceedings, Volume 4, Issue 8, 2017, Pages 8806-8815, ISSN 2214-7853, https://doi.org/10.1016/j.matpr.2017.07.231.

[4] Biswal, Bibhuti. (2021). Design And Development of Electric Scooter. International Journal of Multidisciplinary Research Review. 5. 63-69.

[5] Lu, Y., Mao, H. & Zhou, M. Topology optimization of electric vehicle chassis structure with distributed load-bearing batteries. *Struct Multidisc Optim* 66, 134 (2023). https://doi.org/10.1007/s00158-023-03578-w.

[6] Wen Zhang, Jun Xu, Advanced lightweight materials for Automobiles: A review, Materials & Design, Volume 221, 2022, 110994, ISSN 0264-1275, https://doi.org/10.1016/j.matdes.2022.110994.

[7] Rohit Jadhao, Vijayshri Mahobiya, Prasad Baban Dhore, Roundal Vijay Baburao, Gorane Prathamesh Sudhakar, Vijaykumar Javanjal, Mangesh Kale, Pranav Charkha, Experimental Analysis of Mechanical Tests on a Plate Composed of Banana Fibre, Communications on Applied Nonlinear Analysis, Vol. 31 No. 1s (2024), Page No.141 – 150. https://doi.org/10.52783/cana.v31.562.

[8] Abhishek Kharabi1, Aniket V. Kharabi, Aniket H. Kharabi, Tanmay Kharabi , Mangesh Kale, Design and Analysis of Electric Kid's Car, International Journal of Research in Engineering, Science and Management Volume-2, Issue-2, February-2019 www.ijresm.com | ISSN (Online): 2581-5792.

[9] Ravekar, K., Jaju, S., Design and analysis of material discharge plate of microsurfacing machine, Materials Today: Proceedings 38, pp.2385, 2020.

[10] Kale, M. ., Charkha, S. ., Dehankar, P. ., Sharma, P. ., Choudhary, A. ., Jakhete, M. ., & Javanjal, V. . (2024). IoT-Based Smart Poultry Farm Monitoring and Controlling Using Raspberry Pi. *International Journal of Intelligent Systems and Applications in Engineering*, *12*(12s), 373–379. Retrieved from https://ijisae.org/index.php/IJISAE/article/view/4523.

[11] Jaju, S.B., Charkha, P.G., Kale, M., Gas metal arc welding process parameter optimization for AA7075 T6, Journal of Physics: Conference Series 1913 (1), 2021.

[12] Ashwin Raj Suresh, R Venkatasubramanian, L Hussien Jasim, MP Santhoshkumar, Saurabh Aggarwal, Mangesh Kale,

Integrating Hydrogen Energy Storage into Urban Mobility Solutions, 2024, E3S Web of Conferences, Volume -540, Pages 11009**.**

[13] Dhakne, A., Jaju, S., Shukla, S, Review on analysis of enhancing wear properties through thermo-mechanical treatment and grain size, Materials Today: Proceedings 60, pp.2270, 2022

[14] Deshmukh, B. B., Jaju, S.B., Design and analysis of glass fiber reinforced polymer (GFRP) leaf spring, International Conference on Emerging Trends in Engineering and Technology, ICETET, pp.82, 2011.

[15] Charkha, P.G., Jaju, S.B., Analysis & optimization of connecting rod, 2nd International Conference on Emerging Trends in Engineering and Technology, ICETET 2009, pp.86, 2009.

ISSN: 1092-910X
Vol 27 No. 3 (2024)

Experimental Analysis of Wear Rate and Frictional Coefficient of Various Steel Material

Mr. Rakesh Raushan[1], Mr. Mangesh Kale[2], Dr. Prasad Dhore[3], Dr. Nitin Sherje[4], Mr. Dinesh Burande[5], Mr. Shivaji Jadhav[6], Dr. Prathamesh S. Gorane[7] Dr. Vijay B. Roundal[8]

1, Assistant Professor, Department of Mechanical Engineering, Dr. D.Y. Patil Institute of Technology, Pune, Maharashtra, India.

2, Assistant Professor, Department of Mechanical Engineering, Dr. D. Y. Patil Institute of Technology, Pimpri, Pune, Maharashtra, India.

3, Associate Professor, Department of Computer Engineering, Nutan Maharashtra Institute of Engineering and Technology, Pune, Maharashtra, India.

4, Professor, Department of Mechanical Engineering, Dr. D.Y. Patil Institute of Technology, Pune, Maharashtra, India.

5, Assistant Professor, Department of Mechanical Engineering NBN Sinhgad School of Engineering, Pune

6, Assistant Professor, Department of Mechanical Engineering, Dr. D.Y. Patil Institute of Technology, Pune, Maharashtra, India.

7, Assistant Professor, Department of Mechanical Engineering, GS Moze COE, Pune, India.

8, Assistant Professor, Department of Mechanical Engineering, GS Moze COE, Pune, India

Corresponding Author: sherje.nitin@gmail.com

Article History:

Received: *16-02-2024*

Revised: *26-04-2024*

Accepted: *18-05-2024*

Abstract

This research study focuses on experimentally investigating the wear rate and frictional coefficient of different steel materials using a pin-on-disk testing machine. The tribological properties of steel materials play a crucial role in determining their performance and reliability in various applications. The objective of this study is to assess and compare the wear characteristics and frictional behavior of multiple steel materials under controlled testing conditions. The experimental setup involved employing a pin-on-disk testing machine, where a steel pin was brought into contact with a rotating steel disk. To ensure consistency, the pin and disk specimens were fabricated from various steel materials with uniform dimensions and surface finish. Several test parameters, such as load, sliding speed, and duration, were carefully selected to mimic real-world operating conditions. Throughout the experimental runs, the frictional forces and wear rates were continuously monitored and recorded. The wear rate was quantified by measuring the weight loss of the pin and disk specimens after each test run. Additionally, the frictional coefficient was calculated by dividing the frictional force by the applied load. By comparing these parameters among the tested steel materials, the researchers aimed to identify variations in their tribological performance. The results obtained from the experimental investigation indicated significant disparities in the wear rate and coefficient of friction among the tested steel materials. Certain steel materials exhibited lower wear rates and frictional coefficients, suggesting improved tribological properties compared to others. The observed differences in wear patterns and frictional behavior were thoroughly analyzed to gain insights into the underlying mechanisms responsible for the performance variations.

Keywords: wear rate, frictional coefficient, pin-on-disk testing machine, steel materials, wear resistance.

ISSN: 1092-910X
Vol 27 No. 3 (2024)

1. Introduction

The tribological properties of steel materials, which include friction, wear, and lubrication, play a crucial role in the performance and reliability of these materials in various engineering applications. It is important for steel materials to be able to withstand sliding or rubbing contact and maintain their integrity under different operating conditions. Therefore, investigating different steel materials to enhance their tribological properties is essential for advancing engineering design and manufacturing processes. Experimental techniques that simulate real-world conditions are used to evaluate the tribological behavior of steel materials. One such technique is the pin-on-disc machine, which allows for controlled testing and measurement of frictional forces and wear rates. The pin-on-disc machine simulates sliding or rubbing contact between a pin and a rotating disc, replicating the conditions experienced in practical applications. This study aims to analyze the effects of different steel materials on tribological properties using a pin-on-disc machine and provide insights into their potential for enhancing performance. By subjecting different steel materials to controlled loads and sliding speeds, their frictional behavior and wear characteristics can be evaluated. The study involves the selection of various steel materials, preparation of disc and pin specimens, and systematic testing under predetermined parameters. The primary objective of this study is to compare and analyze the wear rates and frictional coefficients exhibited by different steel materials. The wear rate is a crucial indicator of material loss due to rubbing contact, while the frictional coefficient represents the ratio of frictional force to applied load. By examining these tribological properties, valuable insights can be gained regarding the performance and suitability of different steel materials for specific applications. The outcomes of this investigation will assist in the selection and optimization of steel materials for applications where enhanced tribological properties are desired. Identifying materials with lower wear rates and frictional coefficients will enable engineers and designers to make informed decisions to improve system efficiency, reduce energy consumption, and extend component lifespan. Numerous research studies have been conducted to investigate the tribological properties of different steel materials using pin-on-disc machines. These studies have contributed to our understanding of how steel composition, microstructure, and surface characteristics influence friction and wear behavior. This literature review provides an overview of key findings in this field.

Ahmed et al. (2018) compared the tribological performance of various steel alloys using a pin-on-disc apparatus. They discovered that stainless steel alloys exhibited lower wear rates and friction coefficients compared to carbon steels. The presence of alloying elements like chromium and nickel contributed to improved tribological properties due to the formation of protective oxide layers.

Li et al. (2019) examined the effects of heat treatment on the tribological properties of high carbon steel using a pin-on-disc machine. They observed that quenched and tempered steel exhibited reduced wear rates and friction coefficients compared to untreated steel. Heat treatment resulted in the formation of a hardened surface layer, enhancing wear resistance.

Prakash et al. (2020) investigated the tribological behavior of surface-treated steel materials using a pin-on-disc apparatus. They explored the effects of plasma nitriding and diamond-like carbon (DLC) coating on friction and wear. Both surface treatments led to decreased wear rates and friction coefficients by creating a hard, low-friction surface layer.

ISSN: 1092-910X
Vol 27 No. 3 (2024)

Zhao et al. (2017) studied the impact of surface texturing on the tribological properties of steel using a pin-on-disc setup. They found that laser-induced surface texturing resulted in reduced friction and wear compared to a non-textured surface. The micro-dimples created by laser texturing acted as lubricant reservoirs, improving lubrication performance and reducing contact area.

Zhang et al. (2018) examined the tribological behavior of different steel materials under dry and lubricated conditions using a pin-on-disc machine. They discovered that the addition of solid lubricants, such as molybdenum disulfide, improved tribological properties by reducing friction and wear. The solid lubricant particles formed a protective film, reducing direct contact between the pin and disc.

2. Methodology

The following methodology is adopted for Investigation purpose.

1. Sample Preparation of selected materials.
2. Chemical Composition of Selected material.
3. Parameter Selection for experimentation.
4. Experimentation on experimental setup.
5. Design of Experiments and Analysis of Variance
6. Results and Conclusions

2.1 Material Selection & Sample Preparation:

For the experimental purpose of investigating the enhancement of tribological properties, four types of steel grades were selected: (1) Mild Steel, (2) D2 Steel, (3) 316 Stainless Steel, and (4) 304 Stainless Steel. Each of these steel grades offers distinct characteristics and properties that can affect their tribological behavior. By studying these different steel materials, a comprehensive understanding of their performance in terms of friction and wear can be achieved. Mild Steel: It also called as low carbon steel, is a common and widely used steel grade due to its affordability and ease of manufacturing. It has relatively low carbon content, typically ranging from 0.05% to 0.25%. Mild steel exhibits moderate strength and good machinability but is generally less resistant to wear and corrosion compared to other steel grades. D2 Steel: It is a high-chromium, high-carbon tool steel that offers very good wear resistance and good toughness. It contains around 1.5% carbon and significant amounts of chromium and vanadium, providing enhanced hardness and abrasion resistance. D2 steel is commonly used in various applications where resistance to wear higher and better dimensional stability are needed, such as cutting tools and punches. 316 Stainless Steel: It is a corrosive resistant austenitic stainless steel alloy containing molybdenum. It is widely used in various industries, including marine, chemical, and medical, due to its superior corrosion resistance, high temperature strength, and excellent mechanical properties. 316 stainless steel exhibits good wear resistance and can maintain its properties even in aggressive environments. 304 Stainless Steel: It is another widely used austenitic stainless-steel grade. It is having a higher percentage of chromium (18%) and nickel (8%) compared to 316 stainless steels. 304 stainless steel offers very good resistance to corrosion, high formability, and excellent mechanical properties. While it may have slightly lower wear resistance compared to 316 stainless steel, it is suitable for many applications requiring strength, durability, and resistance to various environmental conditions.

ISSN: 1092-910X
Vol 27 No. 3 (2024)

2.2 Chemical Composition of Selected Material.

Chemical tests is conducted to verify the authenticity and composition of the materials used in this experiment. The tests confirmed the legitimacy of the materials and provided the weight percentage composition of alloying elements such as carbon, nitrogen, manganese, etc. Based on the test reports, the materials used in the experiment were found to be authentic with known compositions. The chemical composition of the materials is presented in Table 1, which includes the chemical test report of Mild Steel, D2 Steel, SS316 Steel, and SS304 Steel.

Table 1. Chemical composition of different type Steels

Sample Material	Mild Steel	D2 Steel	SS316 Steel	SS304 Steel
C%	0.15	1.29	0.034	0.037
S%	0.010	0.006	0.009	0.016
P%	0.012	0.011	0.027	0.031
Si%	0.11	0.34	0.35	0.32
Mn%	0.78	0.44	1.44	1.84
Ni%	0.10	---	9.60	7.74
Cr%	0.30	11.71	17.54	18.74
Mo%	0.002	0.75	1.81	---
V%	0.002	0.80	---	---
Cu%	0.028	---	---	---

2.3 Pin-On-Disk Machine & Experimental Setup

The Pin-on-Disk machine is extensively utilized for evaluating and measuring the tribological properties of industrial materials. It consists of several components, including a rotating disk, a specimen (pin) holder, a lever mechanism, and weights.

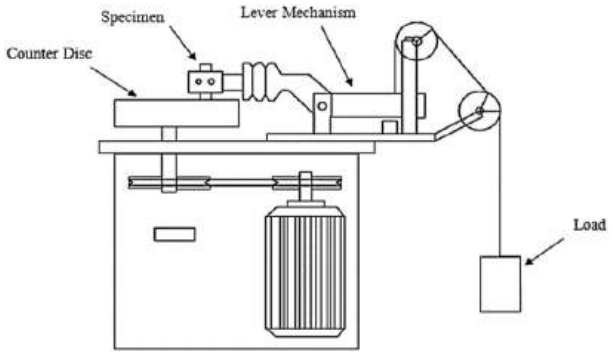

Figure1. Pin-on-Disk Machine set up

The workflow for a Pin-on-Disk machine:

1. The Pin-on-Disk machine is initiated by setting the disk in motion using a motor with adjustable RPM (Revolutions per Minute), allowing for precise control over the rotational speed based on the experimental requirements.

2. The specimen, representing the material being tested, is securely held by the specimen holder and brought into contact with the rotating disk.

ISSN: 1092-910X
Vol 27 No. 3 (2024)

3. The pressure applied by the specimen onto the disk is determined by the application of weights or loads through the lever mechanism. This mechanism allows for the adjustment of the contact pressure between the pin and the disk.

4. Once the setup is complete, the disk starts rotating, and the physical outputs generated during this process are converted into electronic signals.

5. These electronic signals are then transmitted to advanced software that analyzes and processes the data. The software calculates and provides results, revealing the expected tribological properties of the material under investigation.

The table 2 shows the general specifications of a pin-on-disk machine:

Table 2. Specifications of a pin-on-disk machine

Sr.No.	Specification	Description
1	Speed of disc	Ranging from 200 to 2000 rpm
2	Load	From 0 to 20 Kg
3	Rate of wear	Plus/minus 2 mm
4	Temperature	Heating temp. of pin - 200° C
5	Chamber heating temperature	200°C
6	Diameter of wear track	50 m to 100 mm

2.4 Experimentation

Figure 2 Experimentation Setup

To prepare the specimens for examination, the following procedure is implemented:

A. Sample Preparation

• The raw materials for the specimens, including Mild Steel, D2 Steel, SS316 Steel, and SS304 Steel, are collected.

• The raw material is processed using a lathe machine.

• The lathe machine is used to turn the raw material into spheres with a diameter of 10mm and a length of 50mm, as depicted in the accompanying 3D figure.

ISSN: 1092-910X
Vol 27 No. 3 (2024)

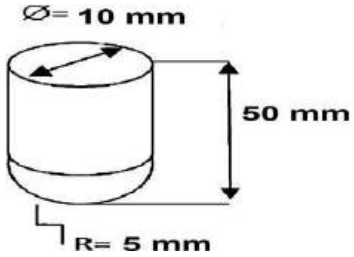

Figure.3. Pin fabricated from steels

• Once the specimens have been prepared, the next step is to place each specimen in the pin holder. The pin holder is then positioned against the rotating disk. At this point, the setup is ready, and the experimentation is commenced.

B. Selection of material load and speed based on application

Table 3. Steel Selected for different application

Sr. No.	Mild Steel	Nut- Bolt application
1	SS304 & SS316	Food processer grinder vessel.
2	D2 Steel	Drilling machine drill tool

C. Experimental Design Method

The design of experiments (DOE) is indeed crucial for understanding and optimizing processes. Traditional DOE approaches can be complex and time-consuming, particularly when dealing with a large number of processing parameters. However, the Taguchi method offers a solution by using orthogonal arrays to efficiently study the entire parameter space with a limited number of experiments. The primary focus of the Taguchi method is to reduce process variation and achieve robust designs. It aims to produce high-quality products while minimizing costs for suppliers. The method was developed by Genichi Taguchi, who introduced a systematic approach for designing experiments to investigate the impact of various parameters on the mean and variance of a process performance characteristic. By utilizing orthogonal arrays, the Taguchi method allows for efficient experimentation, as it enables a comprehensive exploration of parameter combinations while minimizing the number of experiments required. In essence, the Taguchi method provides a structured approach to experimental design, facilitating the systematic analysis of process parameters and their effects on process performance. By using orthogonal arrays, the method allows for an effective exploration of parameter spaces with fewer experiments. This makes the Taguchi method a valuable tool for optimizing processes and improving product quality while reducing time and resource requirements.

Table.4. Selection of experimental process parameters and its levels

Sr. No.	Parameters	Levels	
1	Load in N	60	80
2	Speed in RPM	400	600

ISSN: 1092-910X
Vol 27 No. 3 (2024)

Table.5. DOE using orthogonal array for all Materials

Expt. No	Load (N)	Speed (RPM)
1	60	400
2	60	600
3	80	400
4	80	600

1. Disk cleanliness: The rotating disk is cleaned before starting the experiment. Any contaminants on the disk surface could potentially affect the frictional interactions between the disk and the specimen.

2. Specimen contact: It is essential to ensure proper contact between the specimen and the disk surface. This ensures reliable data collection regarding the tribological properties of the materials under investigation.

3. Motor power supply: The motor responsible for rotating the disk should be connected to a stable power supply. This ensures consistent and controlled rotational speed throughout the experiment.

4. Load application: The load or weight applied to the specimen should be free from any slag or unwanted materials. This ensures accurate and precise measurement of the frictional forces and wear characteristics of the materials.

5. Skilled personnel: The individual responsible for operating and handling the equipment should possess the necessary skills and proficiency in conducting the experiments. This ensures the proper setup of the apparatus and minimizes the chances of errors or discrepancies.

Additionally, the experiments are performed at a constant room temperature to maintain Consistent testing conditions throughout the study.

3. EXPERIMENTAL RESULTS AND DISCUSSION

In Case I, the experiment was conducted using Mild Steel as the specimen, and the following parameters were set:

- Load: 60 N
- RPM: 100.00
- Duration: 120 seconds

The experiment results obtained from the software are presented in a graphical representation, which visually depicts the relevant data and findings.

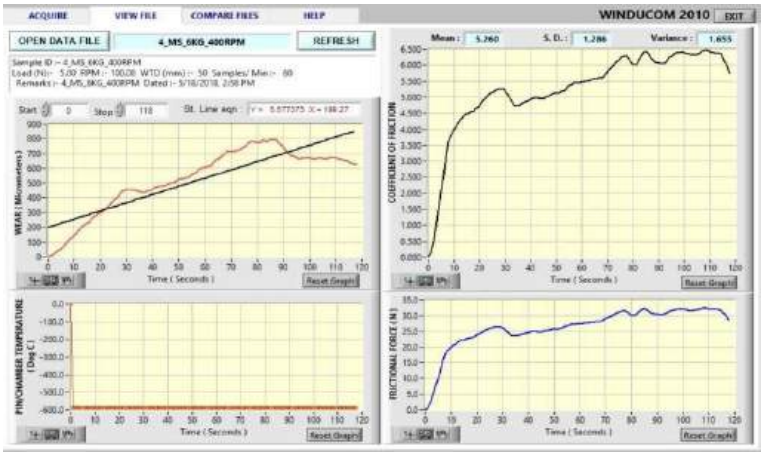

Figure.4. Graphical Representation of Wear rate, CoF and Friction Force verses time

In Case II, the experiment was performed using D2 Steel as the specimen, and the following parameters were applied:

- Load: 60 N
- RPM: 100.00
- Duration: 120 seconds

The results obtained from the experiment are presented in a graphical representation, which provides visual insights into the data and findings

Figure 5. Graphical Representation of Wear rate, CoF and Friction Force verses time

In Case III, the experiment was conducted using SS316 steel as the specimen, with the following parameters:

- Load: 60 N
- RPM: 400.00
- Duration: 120 seconds

The experimental results obtained from the software are presented in a graphical representation

Figure 6 Graphical Representation of Wear rate, CoF and Friction Force verses time

In Case IV, the experiment was conducted using SS304 steel as the specimen, and the following parameters were set:

- Load: 60 N
- RPM: 100.00
- Duration: 120 seconds

The experimental results obtained from the software are displayed in a graphical representation.

Figure 7 Graphical Representation of Wear, Coefficient of Friction and Frictional Force verses Time

To analyze and discuss the results of the experiments, it is necessary to compare the graphs generated by the sophisticated software. The graphs can be compared based on different parameters, including "Wear rate vs. Time," "CoF vs. time," and "Friction Force vs. time."

ISSN: 1092-910X
Vol 27 No. 3 (2024)

A. Wear rate vs Time

Figure 8. Comparison of Wear vs. Time of all Steels.

It is important to note that the color code used in the subsequent graphs will be explained below.

Table 6 Color coding of material

Sr.No.	Material	Color
1	Mild Steel	Black
2	D2 Steel	Green
3	SS316	Red
4	SS304	Blue

Based on the Wear vs Time graph provided, it is evident that D2 steel exhibits the highest wear resistance among the tested materials. This observation aligns with the understanding that the addition of carbon in steel enhances its hardness and wears resistance. However, it is important to understand that wear resistance is influenced by factors other than carbon content. In contrast, SS304 steel, this has a significantly lower carbon composition, demonstrates the highest wear rate among the tested materials. This indicates that the lower carbon content in SS304 steel leads to reduced wear resistance.

B. CoF vs Time

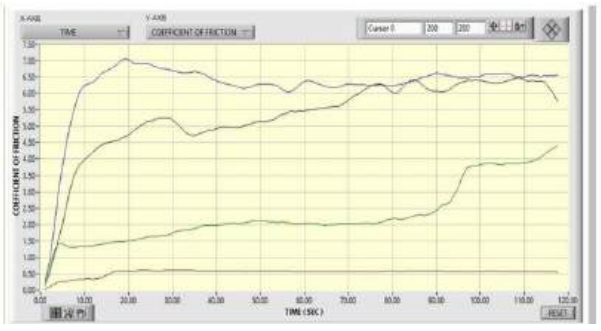

Figure 9. Comparison of CoF vs. Time of all Steels.

Based on the Coefficient of Friction vs. Time graph provided, it is apparent that SS316 steel exhibits the lowest coefficient of friction among the tested materials. Conversely, SS304 steel demonstrates the highest coefficient of friction, indicating increased resistance to relative motion. Mild steel has a higher Coefficient of Friction compared to D2 steel, which falls in the moderate range.

ISSN: 1092-910X
Vol 27 No. 3 (2024)

C. Frictional Force vs Time

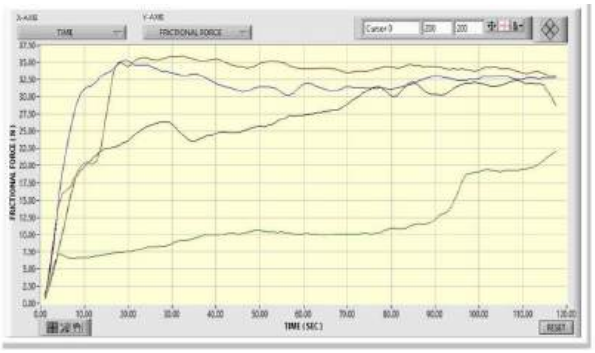

Fig.10. Comparison of Friction Force vs. Time of all Steels

The graph replicates the (CoF) vs. Time graph. This relationship is expected since the frictional force is directly proportional to the coefficient of friction, assuming the load is constant in all cases. The equation that relates the frictional force (Ff) and the (CoF) is as follows:

Frictional force = CoF × Normal Force

Where the normal force represents the applied load. Since the load is kept constant for all the experiments, the resulting frictional forces are directly proportional to the coefficient of friction.

Table.7. Carbon percentage for 60N Load.

Material	MildSteel	D2	SS316	SS304
Carbon %	0.15	1.29	0.034	0.037
Wear	626.98	124.318	12.421	189.98

4. Conclusion

From the performed experiments and analysis, it is concluded that

1. Increasing the carbon content in steel improves its wear resistance. The wear resistance is affected by other elements like manganese (Mn) and nickel (Ni) as well.

2. The CoF is primarily decided by the type of material and is not significantly affected by external factors such as RPM and applied load.

3. Frictional forces, on the other hand, do vary according to external factors such as RPM and applied load. Changes in RPM and load can result in proportional changes in wear losses.

These conclusions highlight the importance of carbon content in enhancing wear resistance, the independent nature of CoF and the influence of external factors on friction forces. For specific details on carbon percentages for the different materials and load cases, please refer to Table 7.

References

[1] Chowdhury MA, Nuruzzaman DM (2013), "Experimental investigation on friction and wear properties of different steel materials", *Triboglogy in Industry 2013* 35(1):42–50.

[2] Roshan A., Sahoo S., Biswas S., "Experimental investigation of wear behavior and frictional coefficient of different steel materials using pin-on-disk testing machine", *Tribology Transactions*, 2020; 63(6): 1084-1095.

[3] Kumar A., Singh S., Mishra S., "Experimental study of wear rate and frictional coefficient of stainless-steel alloys using pin-on-disk testing machine*", International Journal of Mechanical and Materials Engineering*, 2020; 15(1): 10.

[4] Joshi R., Gupta S., "Experimental investigation of wear rate and frictional coefficient of mild steel, stainless steel, and alloy steel using pin-on-disk apparatus", *International Journal of Engineering Research and Applications*, 2021; 11(1): 45-52.

[5] Patel H., Patel D., "Experimental investigation of wear behavior and frictional coefficient of carbon steel and alloy steel using pin-on-disk testing machine", *International Journal of Mechanical and Industrial Technology*, 2020; 4(4): 1-6.

[6] Khan A., Singh P., "Experimental study of wear rate and frictional coefficient of different steel materials using pin-on-disk testing machine", *Materials Today: Proceedings*, 2021; 45: 4671-4676.

[7] Dalmau A. and Richard C., "Degradation mechanisms in martensitic stainless steels: Wear corrosion anticorrosion appraisal", *Science Direct*, 121 (2018), pp. 167- 179.

[8] Liang H., Suzhen L. and Jingwei Z., "Wear and friction behavior of high-speed steel and indefinite chill material for rolling ferritic stainless steels," *Science Direct*, 367-377 (2017), pp. 1580-1585.

[9] Velkavrh I. and Josef B., "The influence of temperature on friction and wear of unlubricated steel/steel contact in different gaseous atmospheres", *Science Direct*, 98 (2016), pp. 155- 171.

[10] Dewan N., Chowdhury A., Kowserb A. and Roy K.," Experimental Investigation on friction coefficient of composite material sliding against SS 201 and SS 301 counter faces", *Science Direct*, 105 (2015) pp. 858-864.

[11] Xiao X., Yin Y., Bao J., Lu L., Feng X., "Review of the friction and wear of brake material", *Advance Mechanical Engineering* 2016; 8 (5): 1-10.

[12] Mara L., Cinzia M. and Stefano G., "Pin-on-disk investigation on copper free friction materials dry sliding against cast iron", *Science Direct*, 119 (2018) pp. 78-81.

[13] Jaju, S.B., Charkha, P.G., Kale, M., "Gas metal arc welding process parameter optimization for AA7075 T6", *Journal of Physics: Conference Series* 1913 (1), 2021.

[14] Charkha, P.G., Jaju, S.B., "Analysis & optimization of connecting rod", *2nd International Conference on Emerging Trends in Engineering and Technology*, ICETET 2009, pp.86, 2009.

[15] M.A. Chowdhury, D.M. Nuruzzaman, A.H. Miaand M.L. Rahaman, "Friction coefficient of different material pairs under different normal loads and sliding velocities", *Tribology in Industry*, vol. 34, no. 1, pp. 18-23, 2012.

[16] Van Beek, A. (2012), "Wear Mechanism of Machine Elements,"*Advanced Engineering Design: Lifetime Performance and Reliability.* TU Delft, Delft, The Netherlands.

[17] Engel, T., Lechler, A., and Verl, A. (2016), "Sliding Bearingwith Adjustable Friction Properties,"*CIRP Annals - Manufacturing Technology*, 65(1), pp 353–356.

[18] Vikram Ramesha, Julien van Kuilenburg, and Wessel W. Wits (2019), "Experimental Analysis and Wear Prediction Model for Unfilled Polymer–PolymerSliding Contacts" *TRIBOLOGY TRANSACTIONS* 2, VOL. 62, NO. 2, 176–188https://doi.org/10.1080/10402004.2018.1504153.

[19] Engel, T., Lechler, A., and Verl, A. (2016), "Sliding Bearing with Adjustable Friction Properties," *CIRP Annals - Manufacturing Technology*, 65(1), pp 353–356.

[20] Chowdhurya MA, Helalib MM (2008), "The effect of amplitude of vibration on the coefficient of friction for different materials", *Tribology International 2008,* 41(4):307–314.

[21] Chawla K, Saini N, Dhiman R (2013), "Investigation of tribological behavior of stainless steel 304 and grey cast iron rotating against EN32 steel using pin on disc apparatus", *IOSR Journal of Mechanical and Civil Engineering (IOSR-JMCE*), vol. 9, no 4, pp 18–22.

[22] N. P. Sherje, Ashish M. Umbarkar, Sameer A. Agrawal Prashant P. Kharche,Dharmesh Dhabliya, "Machinability study and optimization of CNC drilling process parameters for HSLA steel with coated and uncoated drill bit", *Materials Today: Proceedings (Elsevier)* https://doi.org/10.1016/j.matpr. 2020. 12.1070

[23] Sameer A. Agrawal, Ashish M. Umbarkar; Nitin P. Sherje; Ashish M. Dharme; Dharmesh Dhabliya, "Statistical study of Mechanical properties for Corn fiber with reinforced of Polypropylene fiber matrix Composite", *Materials Today: Proceedings (Elsevier),* https://doi.org/10.1016/j.matpr.2020.12.1072.

ResearchGate

See discussions, stats, and author profiles for this publication at: https://www.researchgate.net/publication/380636017

Experimental Analysis of Mechanical Tests on a Plate Composed of Banana Fibre

Article *in* Communications on Applied Nonlinear Analysis · May 2024

DOI: 10.52783/cana.v31.562

CITATION
1

READS
24

11 authors, including:

Rohit Rajendra Jadhao
Savitribai Phule Pune University
18 PUBLICATIONS **5** CITATIONS
SEE PROFILE

Mangesh Kale
Dr. D.Y. Patil Institute of Technology, Pimpri.
8 PUBLICATIONS **19** CITATIONS
SEE PROFILE

Pranav Gopal Charkha
D Y Patil University Pune Ambi
32 PUBLICATIONS **133** CITATIONS
SEE PROFILE

All content following this page was uploaded by Mangesh Kale on 17 May 2024.

The user has requested enhancement of the downloaded file.

www.cmiet.edu.in
Communications on Applied Nonlinear Analysis
ISSN: 1074-133X
Vol 31 No. 1s (2024)

Experimental Analysis of Mechanical Tests on a Plate Composed of Banana Fibre

Mr. Rohit Jadhao[1], Dr. Vijayshri Mahobiya[2], Dr. Prasad Baban Dhore[3], Dr. Roundal Vijay Baburao[4], Dr. Gorane Prathamesh Sudhakar[5], Dr Vijaykumar Javanjal[6], Mr. Mangesh Kale[7], Dr. Pranav Charkha[8]

[1] Assistant Professor, Department of Mechanical Engineering, Nutan Maharashtra Institute of Engineering and Technology, Pune, Maharashtra, India

[2] Assistant Professor, Department of Mechanical Engineering, Wainganga College of Engineering & Management, Nagpur, Maharashtra, India

[3]Associate Professor,Nutan College of Engineering & Research,Dr. Babasaheb Ambedkar Technological University, Raigad

[4,5]Assistant Professor,Genba Sopanrao Moze College of Engineering, Savitribai Phule Pune University, Pune

[6] Associate Professor, Department of Mechanical Engineering, Dr. D.Y.Patil Institute of Technology,Pimpri,,Pune,Maharashtra,India.

[7]Assistant Professor, Department of Mechanical Engineering, Dr. D.Y.Patil Institute of Technology, Pimpri, Pune,Maharashtra,India.

[8]Professor, Department of Mechanical Engineering,Dr.D.Y.PatilUniversity,Ambi,Pune,Maharashtra,India

E-mail: jadhaorohit@gmail.com

Article History:

Received: *03-02-2024*

Revised: *05-04-2024*

Accepted: *22-04-2024*

Abstract:
Due to their attractive characteristics, natural and synthetic fibre - reinforced hybrid composite materials are playing a prominent role in science. Innovators are now being drawn to the poor world to create new sustainable and environment products and materials focused on environmental objectives. Natural fibre has a number of advantageous qualities, including low density, non-toxicity, and minimal comparability in strengths, minimal waste disposal issues, and inexpensive cost. This study presents the experimental analysis of mechanical tests performed on a plate composed of banana fiber. The mechanical properties, including tensile strength, flexural strength, and compression strength, were evaluated to assess the performance and potential applications of the banana fibre plate. The experimental tests were conducted following standard testing procedures specified by ASTM. The results obtained provide valuable insights into the mechanical behavior of the banana fibre plate and contribute to the understanding of its suitability for various engineering applications.

Keywords: Banana fibre, mechanical tests, tensile strength, flexural strength, compression strength.

1. INTRODUCTION

A lingo-cellulosic fibre called banana fibre is derived from the pseudo - stem of the banana tree. Banana fibre is a strong fibre with decent mechanical characteristics. The specific strength characteristics of banana fibre are good and on par with those of more traditional materials like

fiberglass. This substance is less dense than glass fibers. The pseudo-stem is made up of a coiled, grouped collection of leaf stalk bases. Banana fibre is a byproduct of banana farming that either isn't fully or improperly used. If these fibers were put to good use, the demand would stabilize and prices would drop as a result. Natural fibers have excellent fire protection, light in weight, low flexibility, good moisture absorption, huge potential, and biocompatible. Natural fiber has been used for clothing and furniture. Banana fibre offers significant potential for creating paper, especially for the growing market for recycled paper. Products including filter paper, paper bags, cards, lamp stands, pen stands, decorative papers, rope, mats, and composite materials are all made from banana fibre. Germany and India are both testing the use of banana fibers in banknotes. The floor safety shields used in opulent vehicles like Benz are made of polypropylene reinforced with banana fibre. The majority of products made with banana fibre are crafts and domestic accents. Due to their intrinsic qualities, natural fibre reinforced hybrids now outperform artificial fibre reinforced polymer composites in terms of mechanical properties. The mechanical characteristics of both natural and artificial fibre reinforced polymer composites with various fibre volumes, including fracture toughness, modulus of elasticity, and impact strength, were assessed. The outcome showed that mechanical qualities had significantly improved, and the procedure of hybridization had decreased the dangers associated with environmental concerns. Banana fibre, a byproduct of banana farming that is commonly accessible in tropical nations like Malaysia and South India, was used to create the composite materials. When compared to artificial fibers, this fibre holds a superior mechanical strength and offers several advantages. In order to determine the bending moment under the conditions of peak output, they constructed 3 samples with various shapes, assessed the maximum stress value and elastic modulus along opposite paths, and discovered the peak deflection. Researchers tested the tensile and flexural characteristics of bio composites, and the findings were analyzed. They discovered from the study that adding natural fibers like sisal to glass fibre increases the tensile and flexural strength, and that these combinations are essential in the technical fields and innovation. They recommended using these composite materials for applications requiring moderate strength.

Venkateshwara et al. investigated the mechanical characteristics of epoxy synthetic structures reinforcement with sisal as well as banana fiber, including their tensile strength, flexural strength, impact resistance, and moisture absorptive. They have shown that hybridizing sisal material up to 50% by weight with banana fibers bound epoxy resins results in a considerable increase in structural rigidity and a decrease in the rate of moisture absorption. When compared to flax and GFRP combinations, banana and GFRP composites have good tensile properties with minimal deflection. In addition, as comparison to flax and glass fibre reinforced polymer matrix composites, banana and flax fabric composites have higher impact and flexion strengths. When in comparison to synthetic fibre reinforced composites, natural fibre reinforced composite materials are an environmentally benign, sustainable, compostable, and lighter material. The potential uses for these composites are expanding quickly across a wide range of engineering specialties, particularly when cost of materials and erosive environment improvement are concerns. Under ambient pressure, natural fibre composites containing sodium hydroxide can have their mechanical and physical properties enhanced without significantly altering their mechanical behavior. Researchers have examined the impact and fatigue behavior of non-woven hemp fibre composites bonded with polyester and

www.cmiet.edu.in

discovered a major improvement in such qualities. Natural fibres offer significant benefits such low density, superior mechanical qualities, high degradability, and recyclability. They are also disposable and reusable. The utilization of natural fabrics as reinforcing has been the subject of extensive investigation. The pseudo-stem of the banana tree yields banana fibre, a ligno-cellulosic fibre with high reliable qualities. The "pseudo-stem" is a cylinder-shaped grouping of leaf stalk bases. Currently, banana fibre is a byproduct of banana farming that is only partly or improperly utilised. It is uncommon to remove fibre from the pseudo stem, and a significant portion of the stem isn't used to make fibres. When compared to other natural fibres, banana fibres are pricier. Banana fibre sales are sporadic, and there is no reliable method of routine fibre extraction. If these fibres were put to good use, the supply would stabilise and prices have fallen as a result.

Zaman and colleagues point out that Bangladesh is one of the top banana-producing countries worldwide, which means there's a lot of leftover banana plant waste. However, they suggest that this waste can be turned into something useful like banana fibre. This fibre can benefit both rural areas and industries economically. They discuss how banana fibres have cool properties when it comes to handling stress and mechanical stuff. They're saying that compared to other natural fibres, banana fibers are pretty awesome. Thus, manufacturing composites—essentially combining banana fibers with other materials—allows us to create items that are both affordable and robust. These goods could find applications in a wide range of fields, including transportation, aircraft, sporting equipment, and everyday things like mats, decorations for your house, and even paper. Ultimately, they advise us to continue investigating this concept. Perhaps new applications for banana fiber can be discovered, and its production costs might be reduced even further.

Badanayak et.al. are discussing making a special kind of strong material by treating fibres from sisal, bamboo, and Jamaican bananas with chemicals. They suggest these materials could be useful in making things like aeroplanes and cars. They say banana fibers are especially good for this. The Paper explains how they treat these fibres to make them even better and also discusses some techniques used to study the fibres and figure out how good they are for making stuff. They say we should keep researching to find more ways to use these fibres and make machines better and cheaper. The author also suggests looking into pineapple leaf fibres to see how they could make things even better.

Iqbal et.al. talk reveals that how more people are looking at using natural plant fibers for different purposes. These fibers are said to be better than synthetic fibers because they are natural, biodegradable, renewable, lightweight and have durable properties. The focus is on banana fibers, which is important because bananas are everywhere. They suggest about the different parts of the banana like the fruit, skin and leaves that can be used for all sorts of things. The branch-like part of the banana, the pseudo-stem, has very good fibers that can be used for a wide variety of purposes. The author also said that the waste left over from the production of these products can be used for other purposes, which can help the country’s economy. They say their research provides vital information for farmers, business owners, policymakers, scientists and governments to make smarter decisions and help the country grow.Several studies have been conducted to explore the diverse applications and properties of banana fiber in composite materials. These studies delve into various aspects such as dyeability, mechanical properties, and potential enhancements brought by banana

www.cmiet.edu.in

fibers in different composite matrices. Investigations cover a wide range of composite materials, including polypropylene, recycled high-density polyethylene, epoxy, and sawdust-based bio-composites. Furthermore, hybrid composites combining banana fibers with other natural fibers like sisal are explored to enhance mechanical properties. Additionally, enzymatic treatments using cellulase and pectinase enzymes on banana pseudostem fibers aim to improve their properties for textile applications. These studies contribute valuable insights into the development of sustainable materials by utilizing banana fibers, potentially offering lightweight, eco-friendly solutions for diverse industrial applications.

2. PREPARATION OF BANANA FIBRE PLATE

To make a component, we start by getting a wooden box in the right shape. Then, we use a brush to put resin on the box.Next, we add the desired color on top of the resin. After that, we apply more resin on top of the color. On top of that, we place glass fiber. Then, we add more resin to make sure the glass fiber sticks well and forms one piece. Next, we put banana fiber on top, making sure it sticks with the resin. We add another layer of resin over the banana fiber, then place more glass fiber on top. Finally, we add another layer of color using resin on top of the glass fiber.

3. TEST RESULTS

3.1 Flexural Test

Flexural specimens are created in accordance with ASTM D790, and Universal Test Machine is used for the analysis. The test is conducted by inserting the test sample into the UTM and exerting stress on it until it broke and fractures.

Table 1: Flexural Test Result

Sr No	Sample Identification	Flexural Strength (MPa)
1	Horizontal	124.94
2	Vertical	92.7
3	Inclined (45^{o})	138.09

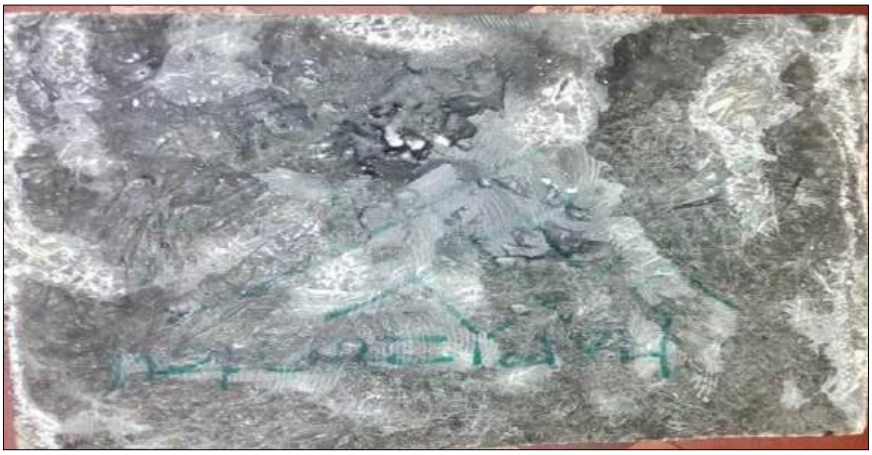

Fig.1: Banana Fibre Plate for Flexibility Test.

Communications on Applied Nonlinear Analysis
ISSN: 1074-133X
Vol 31 No. 1s (2024)

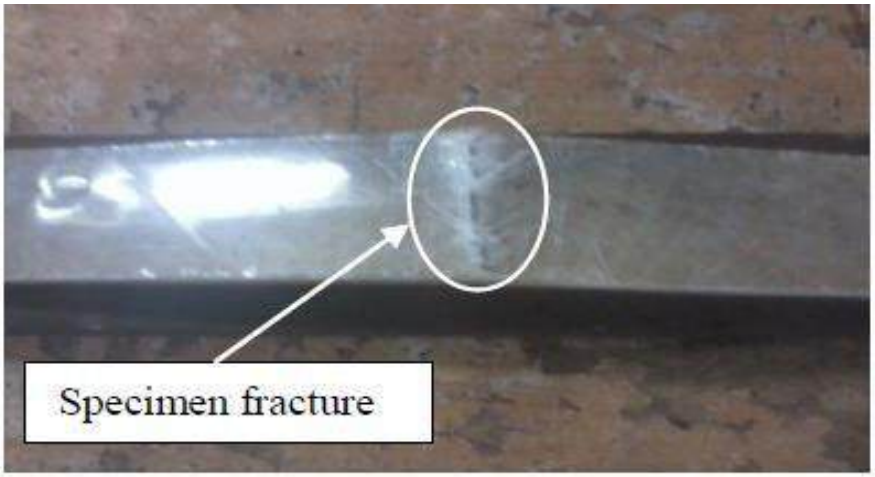

Fig.:2 Fractures after Flexibility Test

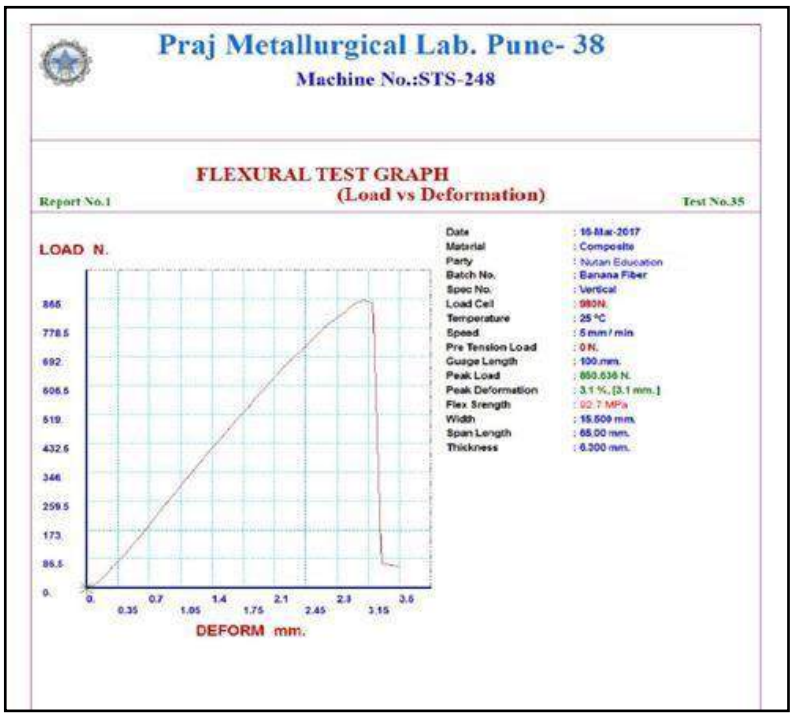

Fig. 3 Graph of Vertical Orientation of Banana Fibre Plate.

Communications on Applied Nonlinear Analysis
ISSN: 1074-133X
Vol 31 No. 1s (2024)

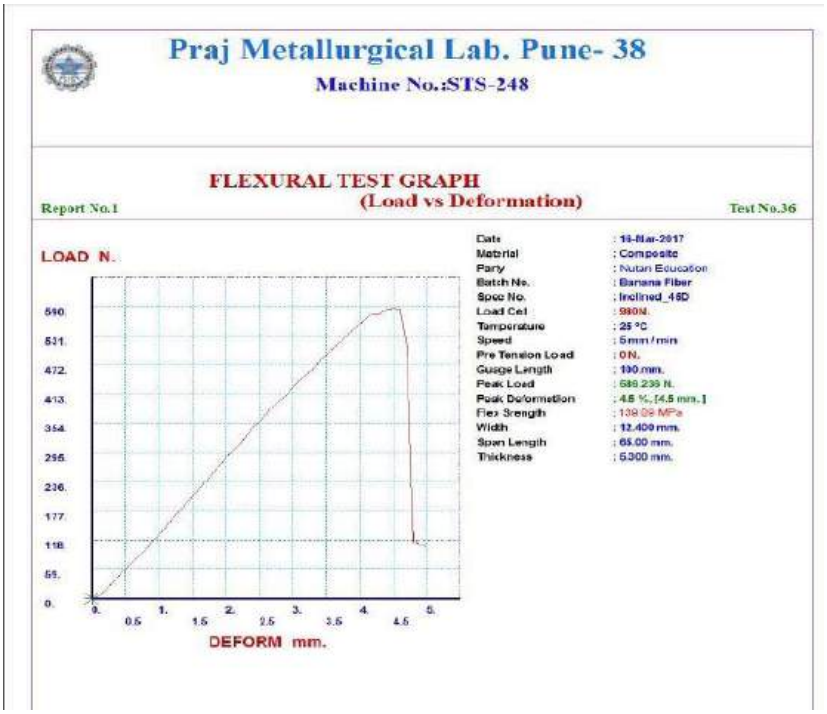

Fig.:4 Graph of Inclined (450) Orientation of Banana Fibre Plate.

3.2 Tensile Test

Using a manual cutting tool, the sample was formed to the appropriate dimensions, and sand paper was used to polish the edges. It is manufactured in accordance with ASTM D638. On the Universal testing machine, the tensile test is conducted. The sample is put on the Universal testing machine, and force is applied until the material breaks.

Table 2: Tensile Test Result

Sr. No.	Sample Identification	Tensile Strength(MPa)
1.	Dumble Shaped Plate	224.31

Fig.5 Specimen for Tensile and Compression test

Communications on Applied Nonlinear Analysis
ISSN: 1074-133X
Vol 31 No. 1s (2024)

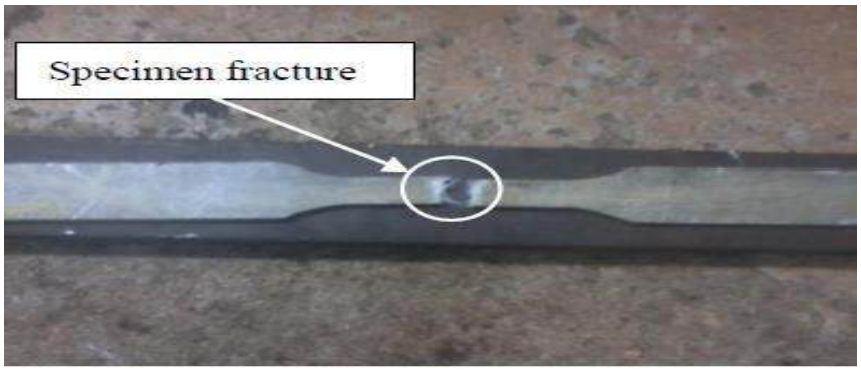

Fig.6 Specimen after Tensile Test.

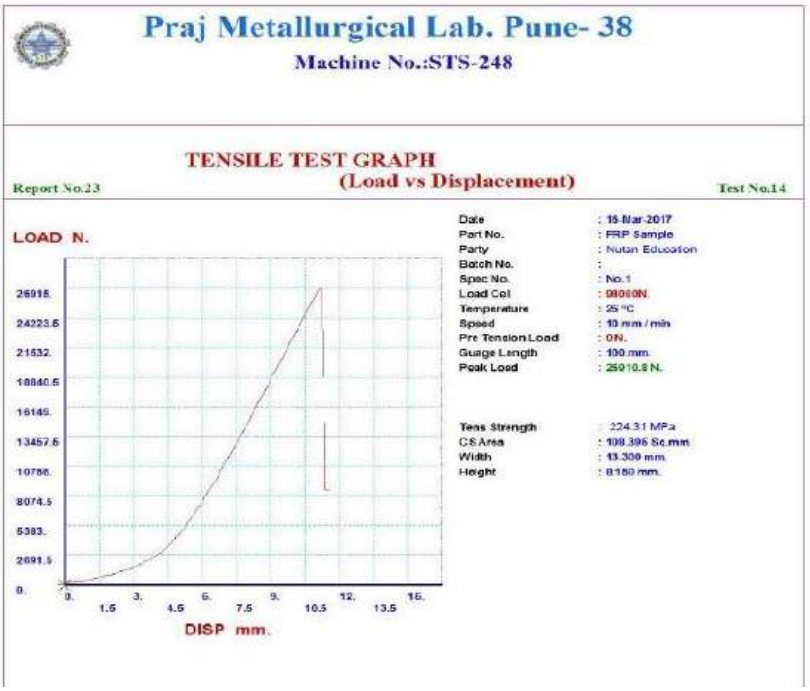

Fig.7 Graph of Tensile Test.

3.3 Compression Test

Using a rectangular plate and sand paper, the manufactured sample is molded to the necessary specifications. It was made in compliance with ASTM D638. The universal tester is used to conduct the compressive strength test.

Table 2: Compression Test Result

Sr. No.	Sample Identification	Compressive Strength (MPa)
1.	Square Plate	226.03

Communications on Applied Nonlinear Analysis
ISSN: 1074-133X
Vol 31 No. 1s (2024)

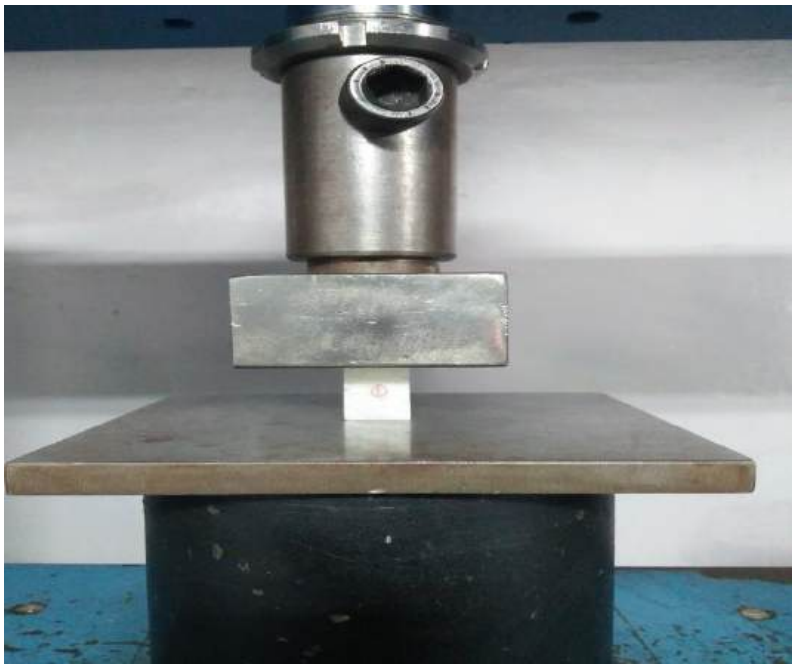

Fig. 8 Compression Test Setup.

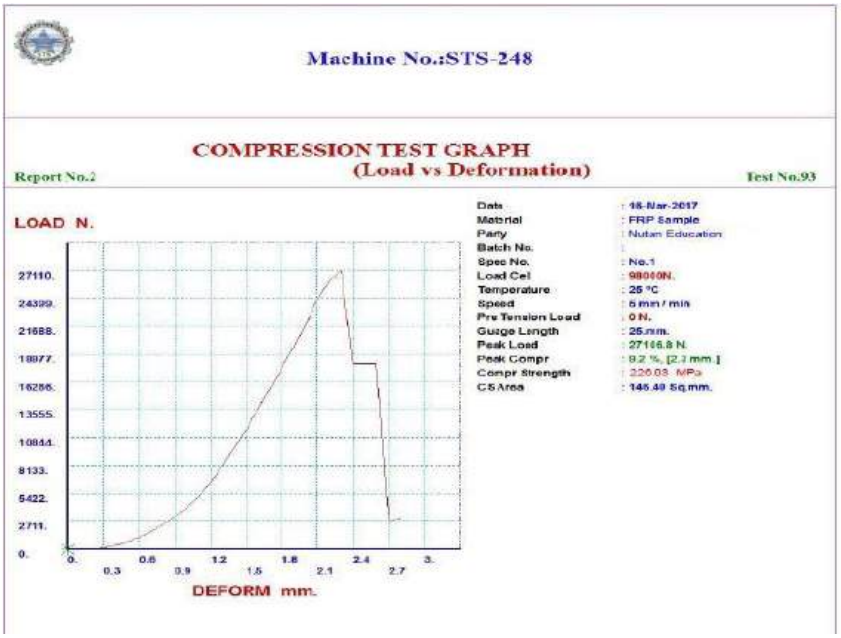

Fig.9 Graph of Compression Test.

4. CONCLUSION

The empirical work has resulted in the following findings. Dumbbell Shaped Plate has a maximum tensile strength of

224.31 MPa. The maximum flexural strength is 124.94, 92.70, and 138.09 MPa in various positions such as horizontal,vertical, and inclined (45°), respectively, and this value is also maintained by the same composite sample combination.

www.cmiet.edu.in

226.03 MPa is the maximum compression strength when using square plates. The SEM examination clearly shows the type of fibre fracture brought on by mechanical loading, the development of cracks in the matrix layer, and matrix failure.

REFERENCES

[1] M. Mohamed, S. Anandan, Z. Huo, V. Birman, J. Volz, and K. Chandrashekhara, "Manufacturing and characterization of polyurethane based sandwich composite structures". Journal of Composite Structures, 123; 169–179, (2015).

[2] Begum K. and Islam M.A., "Natural Fiber as a substitute to Synthetic Fiber in Polymer Composites: A Review," Research Journal of Engineering Sciences, Vol. 2(3), 46-53, April (2013).

[3] Dittenber, D. B., & Gangarao, H. V. S. (2012). Critical review of recent publications on use of natural composites 6 in infrastructure. Composites Part A: Applied Science and Manufacturing, 43(8), 1419–1429.

[4] Thwe, M. M., & Liao, K. (2002). Durability of bamboo-glass fiber reinforced polymer matrix hybrid composites. Composites Part A: Applied Science and Manufacturing, 33(11), 1345–1357.

[5] Pickering, K. L., Aruan Efendy, M. G., & Le, T. M. (2016). A review of recent developments in natural fibre composites and their mechanical performance. Composites Part A: Applied Science and Manufacturing, 83, 98–112.

[6] Corbière-Nicollier, T., & Michaud, V. (2013). Mechanical properties of flax–epoxy composites and laminates: Influence of stacking sequence and moisture content. Composites Part A: Applied Science and Manufacturing, 44, 41–49.

[7] Chenrayan, V., Gebremaryam, G., Shahapurkar, K., Mani, K., Fouad, Y., Kalam, M. A., ... & Abusahmin, B. S. (2023). Experimental and numerical assessment of the flexural response of banana fiber sandwich epoxy composite. Scientific reports, 13(1), 18156.

[8] Zaman, H. U., & Khan, M. A. (2023). Evaluation of the Physico-Mechanical Characteristics of Composites using Banana Fiber: In-Depth Review Findings. Int. J. Adv. Sci. Eng, 9(3), 2961-2972.

[9] Badanayak, P., Jose, S., & Bose, G. (2023). Banana pseudostem fiber: A critical review on fiber extraction, characterization, and surface modification. Journal of natural fibers, 20(1), 2168821.

[10] Iqbal, S. F., Kabir, M. H., Muhib, M. I., & Rupok, M. M. H. K. (2023). Prospect of waste banana fiber use in industry: A narrative review. International Journal of Science and Research Archive, 10(2), 828-839.

[11] Jawaid, M., Abdul Khalil, H. P. S., & Hassan, A. (2011). Cellulosic/synthetic fibre reinforced polymer hybrid composites: A review. Carbohydrate Polymers, 86(1), 1–18.

[12] Mohanty, A. K., Misra, M., & Hinrichsen, G. (2000). Biofibres, biodegradable polymers and biocomposites: An overview. Macromolecular Materials and Engineering, 276–277(1), 1–24.

[13] Jaju, S.B., Charkha, P.G., Kale, M., Gas metal arc welding process parameter optimization for AA7075 T6, Journal of Physics: Conference Series 1913 (1), 2021.

[14] Charkha, P.G., Jaju, S.B., Analysis & optimization of connecting rod, 2nd International Conference on Emerging Trends in Engineering and Technology, ICETET 2009, pp.86, 2009

[15] Gupta, U. S., Dhamarikar, M., Dharkar, A., Chaturvedi, S., Tiwari, S., & Namdeo, R. (2021). Surface modification of banana fiber: a review. Materials Today: Proceedings, 43, 904-915.

[16] Ramesh, M., Atreya, T. S. A., Aswin, U. S., Eashwar, H., & Deepa, C. (2014). Processing and mechanical property evaluation of banana fiber reinforced polymer composites. Procedia Engineering, 97, 563-572.

[17] Saravanakumar, S., Sathiyamurthy, S., Vinoth, V., & Devi, P. (2024). Effect of alumina on epoxy composites with banana fiber: mechanical, water resistance and degradation property analysis. Fibers and Polymers, 25(1), 275-287.

[18] Dutta, D., & Sit, N. (2024). Preparation and characterization of potato starch-based composite films reinforced by

www.cmiet.edu.in

modified banana fibers and its application in packaging of grapes. International Journal of Biological Macromolecules, 254, 127791.

[19] Brahma, S., Raafi, S. M., Arju, S. N., & Rehman, J. U. (2024). Dyeability and mechanical properties of banana fiber reinforced polypropylene composite. SPE Polymers.

[20] Syduzzaman, M., Akter, M., Mahmud, F., Bhowmick, D. R., Maliha, A. S., Fahmi, F. F., ... & Ahamed, M. A. (2024). Tensile properties of banana fiber reinforced recycled high-density polyethylene composites: An experimental investigation. SPE Polymers.

[21] Ganasan, V., Chohan, J. S., Subburaj, G. S., Harika, K., Yedari, V., Sivakumar, N. S., ... & Durai, A. J. (2024). Mechanical, Moisture Absorption and Thermal Stability of Banana Fiber/Egg Shell Powder-Based Epoxy Composites. Engineering Proceedings, 61(1), 11.

[22] Laksham, S., & Hitish, H. (2023). Experimental investigations of epoxy-resin-banana-fiber-saw dust bio-composite material for potential application as partitioning board. Materials Today: Proceedings.

[23] Anbalagan, K., Sarala, R., Subramanian, S., Yokesh, N., & Saravanan, N. (2023). Some studies on banana and sisal fibers-based hybrid composites. Materials Today: Proceedings, 90, 140-144.

[24] Gayathri, N., Shanmuganathan, V. K., Joyson, A., Aakash, M., & Joseph, A. G. (2023). Mechanical properties investigation on natural fiber reinforced epoxy polymer composite. Materials Today: Proceedings, 72, 2574-2580.

[25] Narayanan, S. R., Aravindhan, R., Arunprabhakaran, S., Thiyagu, K., Rajaram, S., & Radhkrishnan, K. (2023, October). The experimental investigation and fabrication of sisal and banana fiber with tamarind seed powder reinforced composites. In AIP Conference Proceedings (Vol. 2912, No. 1). AIP Publishing.

View publication stats

www.nmiet.edu.in

International Journal of
INTELLIGENT SYSTEMS AND APPLICATIONS IN ENGINEERING
ISSN:2147-6799 www.ijisae.org Original Research Paper

GridDR: Enhancing Grid Reliability using Demand Response Program

Dr. Archana Y. Chaudhari*[1], Dr. Prasad B. Dhore[2], Alok R. Kadu[3], Adarsh K. Satpute[4], Shrey Y. Wani[5], Bhushan G. Phule[6]

Submitted:12/03/2024 **Revised**: 27/04/2024 **Accepted**: 04/05/2024

Abstract: In developing nations, power disruptions are a major worry, and grid stability is essential. Utilities must encourage energy consumption reductions by consumers during prime hours in to achieve and maintain grid stability and avoid brownouts or blackouts. Finding suitable candidates for Demand Response (DR) events is essential. . In order to strategically select candidates for DR events based on the utility's goals, this work suggested "GridDR," which gives users the ability to monitor their energy usage trends, customize their choices for participation, and receive tailored advice or incentives for taking part in demand response. In addition, the platform offers distributors thorough visualizations of customer energy usage data, allowing for the early identification of high-usage customers for demand response involvement. The study makes use of a dataset that includes hourly energy usage data gathered over a one-year period from 39 apartments to assess consumption trends and find possible participants in demand response The study starts with a thorough project overview, emphasizing the importance of demand response programs in resolving grid stability and reliability issues. With the intention of offering insights into temporal fluctuations and consumption trends, graphical analytic techniques are used to show daily, weekly, and monthly energy use patterns based on the dataset. Subsequently, two clustering algorithms, namely K-means and hierarchical clustering are used in this research work. GridDR has the potential to completely change how distributors and customers communicate and work together to optimize energy use and improve grid reliability by bridging the gap between data analytics, user interface design, and demand response program execution. In the end, the study emphasizes how critical, is to employ innovative approaches to leverage data-driven insights for the purpose of managing the changing issues of grid reliability and energy management in the residential sector.

Keywords*: Demand Response, Grid Reliability, Smart Meter Data, K-means, Hierarchical Clustering*

1. Introduction

Demand Response refers to a tactic used by utilities and grid operators to manage electricity usage during times of peak demand. It involves encouraging or mandating users to limit their energy consumption when the system is under stress to avert blackouts or brownouts. Closely interwoven with the concept of Demand Response (DR) is the intricate network of the electric grid, which can be defined as a massively interconnected network of power generation, transmission, and distribution equipment that transfers energy from power plants to households, companies, and industries. While the electric grid serves as the backbone of our power supply infrastructure, it is the inherent balance and resilience of this interconnected network that is crucial in preserving grid stability and minimizing any interruptions. Grid stability is the ability of the electrical grid to maintain a balanced supply-demand relationship, where the electricity delivered matches the electricity demanded. Grid stability sets the foundation for reliable power distribution, with grid reliability being the key measure of its consistent performance. Grid reliability is the capacity of the electrical grid to transmit electricity without interruptions or disturbances. A dependable grid guarantees that users have a constant supply of power, and it plays a critical role in supporting economic activities and daily living habitats.

When the total demand for electricity on the grid surpasses the available supply, it results in grid instability. Addressing this peak demand is costly for utility companies because they often resort to operating backup generators or purchasing energy from the spot market. These backup generators, which use fossil fuels, contribute to environmental pollution.

Grid instability occurs when the overall demand for electricity on the system exceeds the supply. Utility providers must incur significant costs in order to meet this peak demand since they frequently have to run backup generators or buy energy on the spot market. The usage of fossil fuels by these backup generators pollutes the environment. Furthermore, purchasing energy on thespot market is a costly and transient response to transient surges in demand

[1] *Dr. D. Y. Patil Institute of Technology, Pimpri, Pune, Maharashtra, India ORCID ID : 0000-0002-4423-8921*
Email: archanac.dit@gmail.com
[2] *Nutan College of Engineering & Research, Pune, Maharashtra, India*
Email: dhoreprasad89@gmail.com
[3] *Dr. D. Y. Patil Institute of Technology, Pimpri, Pune, Maharashtra, India*
Email: alokkadu08@gmail.com
[4] *Dr. D. Y. Patil Institute of Technology, Pimpri, Pune, Maharashtra, India*
Email: adarshask07@gmail.com
[5] *Dr. D. Y. Patil Institute of Technology, Pimpri, Pune, Maharashtra, India*
Email: shreywani1234@gmail.com
[6] *Dr. D. Y. Patil Institute of Technology, Pimpri, Pune, Maharashtra, India*
Email: bhushanphule9@gmail.com

** Corresponding Author Email: archanac.dit@gmail.com*

However, in the era of smart grids, there is an opportunity to avoid comprehensive blackouts. This can be accomplished by either requesting all consumers to reduce their consumption proportionally to the total deficit or by selecting a subset of consumers to reduce their consumption. These actions fell under the umbrella of Demand Response (DR) events. The success of DR events is measured by the ratio of the required target reduction attained when compared with set target level. Presently, the success rate of DR events remains modest, typically ranging from 10% to 30%.

The ongoing supply of power to consumers is reliant upon the stability and reliability of electrical grids. However, grid operators now face additional difficulties as a outcome of the growing demand for electricity along with the incorporation of renewable energy sources. Demand response programs have shown promise in this regard as a way to improve grid resilience through the optimization of energy usage patterns.

Developing efficient demand response strategies requires an awareness of residential energy consumption patterns. The introduction of smart meters and data analytics techniques has provided new prospects for the in-depth analysis and interpretation of energy usage data. Grid operators can use these technologies to separate consumers based on profiles of their energy usage, spot patterns in consumption, and adjust their demand response strategies accordingly.

The goal of this research article is to examine how well demand response strategies may improve grid reliability, with an emphasis on analyzing residential energy consumption. The study uses graphical analysis approaches to display consumption patterns at daily, weekly, and monthly intervals using a dataset that includes hourly energy consumption data from 39 apartments over a one-year period. K-means and hierarchical clustering are two of clustering algorithms used here.

This study's main goal is to analyze how well clustering algorithms identify energy-intensive customers and whether or not they are suitable candidates for focused demand response treatments. The study attempts to identify the most efficient way for grouping up residential energy users based on their energy consumption by comparing the outcomes of clustering algorithms and applyingevaluation standards including Davies-Bouldin Index, Silhouette Score, and Calinski-Harabasz Index for comparative analysis of both clustering algorithms.

The outcomes of this study have crucial consequences for stakeholders, policy makers, and grid operators who are engaged and associated with demand response program implementation. System operators can save operating costs, and improve system stability by identifying energy-intensive consumers and enabling tailored actions. In the end, this study adds to the current conversation about grid modernization and the move towards a more robust and sustainable electric grid system.

The rest of the paper organized as follows: The literature survey about the existing methods is discussed in section 2. Discussion about the proposed methodology is presented in section 3. The experimental setup and result discussion are presented in section 4, followed by the conclusion.

2. Related Work

Demand response (DR) programs and energy management techniques have been the subject of extensive research and development efforts aimed at enhancing grid reliability, optimizing energy usage, and promoting sustainability.

Implementing Automated Demand Response (ADR) in intelligent distribution grids, emphasizes the significance of end-consumer participation, sensors, metering infrastructure, and communication technology for successful ADR. It discusses optimization models and examines DR demonstration projects to quantify benefits. It informs us about the fundamental requirements for ADR implementation and the challenges associated with it [1].Integrating communication-based demand response (CBDR) and inclining block tariffs (IBT) to enhance grid reliability and customer engagement is a great approach. It emphasizes transforming the power system into a decentralized smart grid and the role of DR in addressing price volatility and grid reliability. It highlights the importance of customers' active participation in DR programs [2]. Analyzing consumer participation in energy markets through demand response (DR) helps to classify DR programs based on market type, reliability, power flexibility, and economic motivation. It gives insights into the benefits and barriers associated with these classes, emphasizing the potential of DR to improve power system performance and mitigate environmental effects. It offers valuable insights for power system operators and participants in DR programs [3].The impact of targeted demand response (DR) on grid reliability and price volatility includes highlighting the nonlinear nature of congestion patterns and how strategic selection of DR locations can substantially reduce price volatility and congestion levels, providing crucial insights into the efficient location of DR and energy storage for grid improvement [4]. Another noteworthy contribution in the realm of demand response (DR) in smart grids and its implications for power systems, underscores the significance of efficient power management, cost reduction, and sustainability as key drivers in the electricity industry. It introduces demand response (DR) as a fundamental strategy to achieve these objectives and usher in a more environmentally friendly era for the industry. It also places a strong emphasis on the role of smart grids in advancing DR and enhancing the overall

performance of the power system [5]. Focusing on co-creating flexibility and willingness to participate in DR among prosumers in the residential energy sector, emphasizes the importance of considering the prosumer perspective in policy instruments and business models to harness flexibility effectively [6]. Modeling the long-term benefits of DR from a system perspective, quantifies the value created in both the energy market and grid operation, highlighting the necessity of a comprehensive approach to assess DR benefits [7]. The control-focused implementation to define the resilient energy infrastructure potential of residential structures managed by energy aggregators helps in combining thermal network models, renewable energy integration, and predictive control for efficient load management [8]. Clustering which is one of the most important unsupervised classification techniques is used to understand electricity consumption patterns [9, 10]. Clustering techniques are essential to identify target groups for demand response initiatives and to segment energy customers based on their consumption patterns [11].

Successful customer involvement has become essential to the accomplishment of energy management and demand response programs. The participation of small and medium-sized customers in DR, introduces a comprehensive evaluation index and incentive strategy based on Customer Directrix Load (CDL). The focus is on involving a broader range of customers in DR and improving the accuracy of load predictions[12]. The [13] emphasizes the challenges of small and medium-sized customer participation in DR. It proposes a strategy for integrating these customers into DR by using load aggregators, and a set of incentive mechanisms based on CDL to encourage active participation .As a collection, these works offer invaluable insights into the field of Demand Response and its application in smart grids, grid reliability, clustering techniques and consumer involvement. They cover diverse aspects of DR, from implementation and classification to the impact on grid performance and environmental sustainability. Researchers and practitioners can draw from these studies to advance the field of demand response in the context of smart grids and beyond.

2.1. Research Gap

There remains a significantly large research gap in the creation and application of intelligent consumer selection strategies for demand response initiatives, especially in the residential sector, despite improvements in demand response (DR) programs and energy management strategies. Traditional DR programs have not utilized advanced methodologies that employ data-driven insights and user-friendly interfaces to allow targeted consumer involvement; instead, they were dependent on static or predefined criteria for participant selection.

The integration of modern data analytics approaches, such machine learning and predictive modeling, with demand response program design and implementation is a possibility that is largely unconsidered by current research and industry practices. Researchers can create refined DR consumer selection techniques that dynamically assess energy consumption patterns, identify high-usage consumers, and customize engagement campaigns based on unique preferences and behaviors by utilizing data from smart meters and devices.

Moreover, there aren't enough thorough web-based interfaces that serve distributors and customers alike and offer real-time access to information related to energy consumption, visualizations, and participation choices. In demand response programs, the effectiveness of communication and cooperation between distributors and customers is frequently hampered by the lack of interactive functions and user-friendly features on existing platforms.

In the realm of energy management and demand response, the creation and application of intelligent DR consumer selection techniques, like GridDR, constitute an important study area. GridDR has the potential to completely change how distributors and customers communicate and work together to optimize energy use and improve grid reliability by bridging the gap between data analytics, UI design, and demand response program execution.

3. Proposed Methodology

In order to improve grid reliability and analyze and enhance demand response techniques, the approach consists of multiple essential components. The approach starts with gathering and preprocessing hourly data on energy consumption from 39 apartments. Next, consumption trends at daily, weekly, and monthly intervals are visualized through graphical analysis. Apartments are next categorized according to their energy profiles using K-means and hierarchical clustering algorithms; the best clustering strategy is determined using performance evaluation metrics. Through the creation of a user-friendly online interface named as GridDR platform makes it easier to execute demand response and identify consumers based on energy usage profiles.

Understanding consumption trends, identifying segments of consumers, and developing successful demand response techniques all depend heavily on the analysis clustering as well as analysis of residential data of energy usage. We examine the clustering and analysis of 39 apartments having smart meter data at the IIT Bombay campus. By applying K-means and Hierarchical clustering techniques, we are able to extract patterns of consumption and identify particular customer segments within the dataset. The approach includes preprocessing the dataset, graphical analysis, utilizing the Elbow technique to identify the required number of clusters, clustering techniques, and

evaluating performance and comparative analysis using performance evaluation metrics.

3.1. Data Description

The dataset used in this study includes records of residential energy usage from 39 apartments on the IIT Bombay campus [14]. Data on energy use is captured hourly for each apartment. The building has 39 3BHK (three bedrooms, one hall, and a kitchen) apartments, each of which has a smart-meter that records data every five seconds. Dataset provides information with a granularity of one hour.

Since India does not observe daylight saving time, the dataset contains all timestamps in Indian Standard Time (GMT+5.30). Significant data loss results in the removal of apartments from the list. This dataset provides a thorough understanding of how each individual apartments have used electricity during the course of 2017. Each apartment's energy consumption data is meticulously recorded and encompasses various parameters:

I. Timestamp (Unix Timestamp): This records the precise time at which energy consumption measurements were obtained, allowing for temporal analysis of consumption patterns.

II. Phase-wise Voltage (V1, V2, V3): These parameters capture the voltage readings for each phase, providing the data about the electrical distribution system's stability and load characteristics.

III. Phase-wise Electricity Consumption (W1, W2, W3): These parameters document the electricity consumption for each phase, offering insights into the overall energy consumption behaviour of each apartment.

The dataset stretches from January 1, 2017, to December 31, 2017, allowing a thorough analysis of energy consumption patterns over the duration of a year.

3.2. Data Preprocessing

To make sure the data was suitable for analysis, a number of preprocessing steps were conducted out after the data was acquired. This involved splitting the data into distinct datasets for daily, weekly, and monthly consumption as well as translating Unix timestamps to the necessary date and time format.

The conversion of Unix timestamps to human-readable date and time formats plays a pivotal role in our data preprocessing pipeline. In our study, we leverage the Pandas library in Python to transform the 'TS' column, containing Unix timestamps representing energy consumption data, into datetime objects. This conversion facilitates a more intuitive understanding of the temporal aspect of the dataset, enabling us to conduct in-depth analysis and modelingof energy consumption patterns. By extracting date, time, and day of the week from the timestamps, we performed temporal analysis at various granularities, including daily, weekly, monthly intervals.

In our research, the necessity of converting Unix timestamps lies in enhancing the interpretability and usability of the energy consumption dataset. By transforming timestamps into human-readable formats, we enable easier comprehension and analysis of temporal patterns in energy consumption. This conversion process facilitates visualization, thereby empowering us to gain actionable insights into residential energy usage behaviors. Through this conversion, we ensure that our dataset is appropriately prepared for comprehensive analysis, ultimately contributing to the efficacy of our research.

Subsequently, a merged dataset encompassing hourly recordings for the entire year was compiled, assigning each apartment a distinct ID.

3.3. Graphical Analysis

Graphical analysis was performed on the dataset to visualize energy consumption trends across various temporal scales: daily, weekly, and monthly. The following visuals were gleaned from the graphical analysis: figure 1, 2 & 3 depict daily analysis, weekly analysis &Monthly Analysis respectively.

I. Daily Analysis

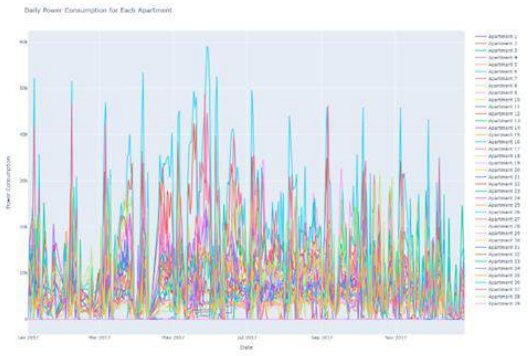

Fig. 1. Daily Graphical Analysis

II. Weekly Analysis

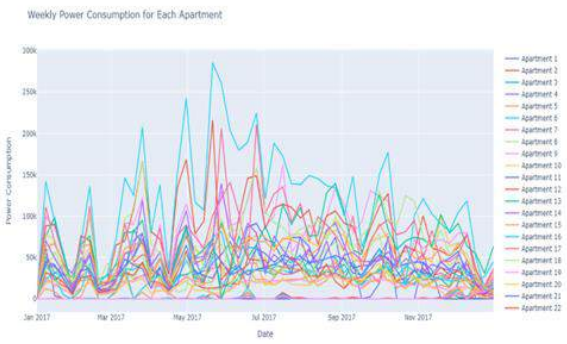

Fig. 2. Weekly Graphical Analysis.

III. Monthly Analysis

Fig. 3. Monthly Graphical Analysis

3.4 Clustering Analysis

With the pre-processed dataset available, different consumption patterns among the apartments were identified by clustering analysis. The Elbow approach was used to find the ideal number of clusters before clustering analysis was performed. The Elbow Method is a technique used in clustering analysis to determine the finest number of clusters for a given dataset. Three clusters were found to be the best option by this strategy.

The required number of clusters for clustering analysis was determined using the Elbow method as shown in figure 4. This method involved fitting the data to multiple cluster solutions and identifying the point at which the decrease in within-cluster variance begins to slow down, indicating the appropriate number of clusters.

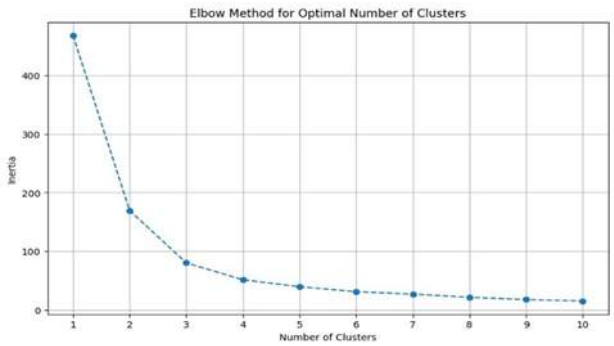

Fig. 4. Elbow Graph

Subsequently, both K-means and hierarchical clustering techniques were employed to partition the dataset into uniform clusters based on energy consumption characteristics.

I. K-means Clustering

K-means clustering was employed to partition the dataset into uniform clusters based on energy consumption characteristics. This approach facilitated the identification of consumer segments exhibiting similar consumption behavior, enabling targeted interventions and resource allocation strategies.

K-means clustering is a well-liked unsupervised learning technique for dividing data into discrete clusters according to similarity. In our study, we divided apartments into groups according to the patterns of their monthly power usage using the K-means algorithm. We standardized the monthly power usage data using the Python Scikit-learn module, then we used the Elbow method to find the three groups for K-means clustering.

The K-means algorithm was utilized to classify each apartment into one of three clusters based on the degree of similarity between their power consumption attributes. The monthly power consumption trends of each cluster were independently plotted to observe the outcomes from clustering process. Each graph depicted the monthly power consumption patterns of dwellings comprising a particular cluster.

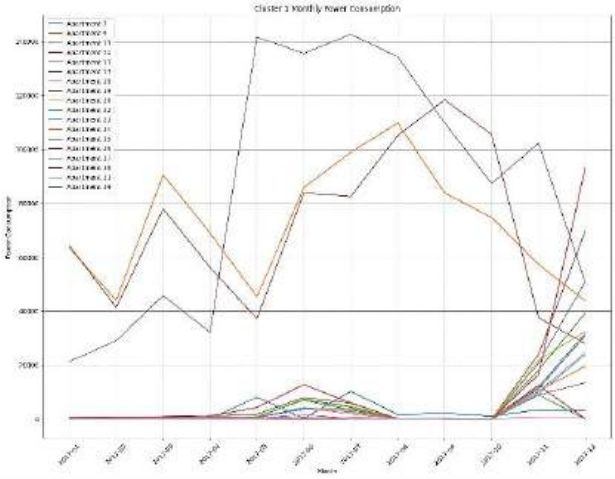

Fig. 5. Cluster 1 Monthly Power Consumption

Cluster 1(figure 5) is composed of apartments that are distinguished by their comparatively lower levels of energy utilization in comparison to Clusters 2 and 3. With a power consumption range of 0 to 14,000 W and a total of 18 apartments, Cluster 1 predominantly accommodates individuals with modest energy requirements. Throughout the course of the year, Apartment 39 exhibits the maximum energy consumption among these units. Apartments that house bachelor's degree candidates primarily in dormitories or shared quarters, these dwellings exemplify a way of life characterized by fundamental conveniences and diminished energy usage. Additionally, this cluster includes support personnel such as janitors, cleaners, and security officers, whose living arrangements and energy usage patterns align with the overall modest consumption trend observed within Cluster 1. Notably, two distinct spikes in energy consumption are observed within this cluster. The first spike occurs between April and August, coinciding with the summer and monsoon seasons, while the second spike is evident from October to December, corresponding to the winter season. Notably, energy consumption peaks during the winter months, underscoring the influence of seasonal variations on energy utilization patterns. The observed spikes in energy

consumption during the summer and winter months align with the Mumbai's tropical climate weather patterns, hot all year round, with a long, sunny season from early or mid of October to June including the months of winter with increased usage of fans and refrigerators during these seasons to combat the heat and hot climate.

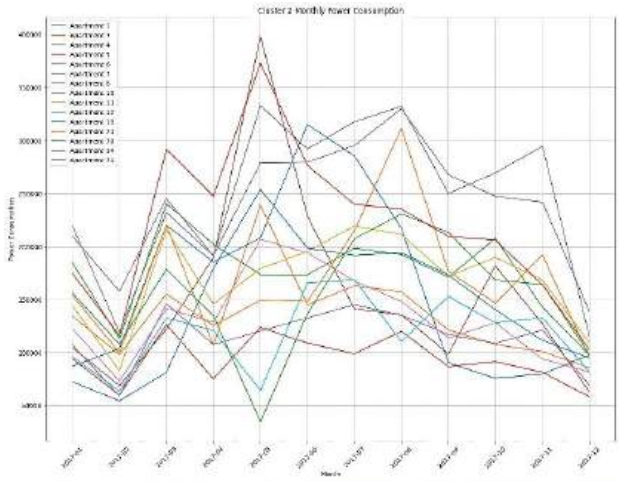

Fig. 6. Cluster 2 Monthly Power Consumption

Cluster 2 (figure 6) encompasses apartments characterized by medium energy consumption levels compared to Clusters 1 and 3, with power consumption spanning from 50,000 to 400,000 W across 15 apartments. Notably, Apartment 7 emerges as the highest energy consumer during May within this cluster. These residences primarily house assistant professors or lecturers, offering moderate-sized accommodations with average energy consumption. Additionally, experienced researchers or scientists occupy apartments within this cluster, exhibiting diverse consumption patterns generally lower than those of senior faculty members. A distinct pattern of energy consumption is observed within Cluster 2, marked by a sharp decline from January to February, followed by an increase from February to May, with May registering the highest consumption levels. Subsequently, energy consumption remains moderate from May to November before experiencing a precipitous decrease from November to December. While these apartments may have amenities like air conditioning, their energy consumption remains relatively stable throughout the year, reflecting the city's lengthy, sunny season from October to June.

The fluctuation in energy usage, notably peaking in May, may be attributed to increased cooling requirements as temperatures rise before the onset of the monsoon season. This fluctuating pattern of consumption underscores the influence of Tropical seasonal factors of Mumbai.

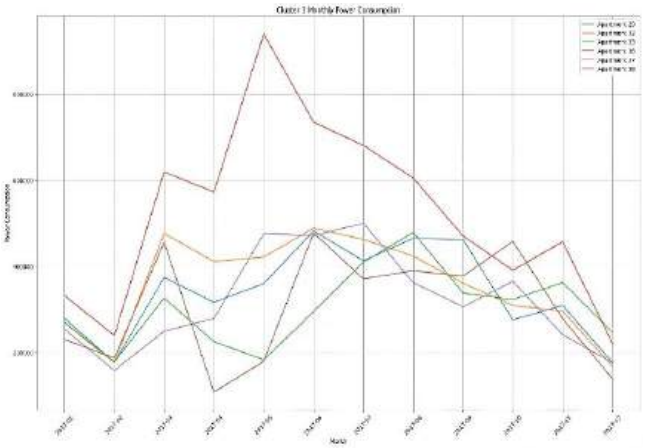

Fig. 7. Cluster 3 Monthly Power Consumption

Cluster 3 (figure 7) represents apartments characterized by the highest energy consumption levels compared to Clusters 1 and 2, with power consumption spanning from 200,000 to 800,000 W across 6 apartments. Notably, Apartment 36 emerges as the highest energy consumer throughout the year, with May documenting the peak consumption period for this apartment. These residences primarily facilitate senior faculty members, who often occupy larger residences equipped with amenities such as air conditioning, home offices, and electronic appliances, contributing to elevated energy consumption levels. Within Cluster 3, a discernible pattern of energy consumption is observed, characterized by a precipitous decline from January to February, followed by an increase from February to March. Subsequently, energy consumption remains at a moderate level from March to November before experiencing a notable decrease from November to December. The observed fluctuations in energy consumption, with a peak in May, coincide with Mumbai's transition from the sunny season to the onset of the southwest monsoon in June. As temperatures rise and humidity levels increase during the pre-monsoon months, occupants may rely heavily on air conditioning and other electrical appliances, contributing to the a rise in energy usage.

These findings can inform energy management strategies and support sustainable practices tailored to the specific requirements of each cluster.

II. Hierarchical Clustering

Hierarchical clustering was also utilized to provide a hierarchical representation of consumption patterns within the dataset. This method revealed the inherent structure and relationships among consumption profiles, offering insights into clustering hierarchy and potential outliers or anomalies.

It is another popular clustering technique which creates a hierarchy of clusters by recursively combining or splitting data points according to how similar they are. In order to classify the apartments into groups according to their

monthly power usage profiles, we used another clustering technique named as hierarchical clustering. We used three clusters for agglomerative hierarchical clustering using the Python Scikit-learn module.

In a high-dimensional space, the hierarchical clustering algorithm categorized apartments into clusters according to the proximity of their power consumption patterns. In order to visually represent the outcomes of hierarchical clustering, we constructed a dendrogram that depicts the interconnections among apartments and the hierarchical structure of the clusters as shown in figure 8. The height of the branches in the dendrogram signifies the separation between clusters, with each branch representing a distinct cluster. The assistance of this visualization was utilized to comprehend the hierarchical clustering procedure and discern the residences that were categorized into each cluster according to their comparable patterns of power consumption.

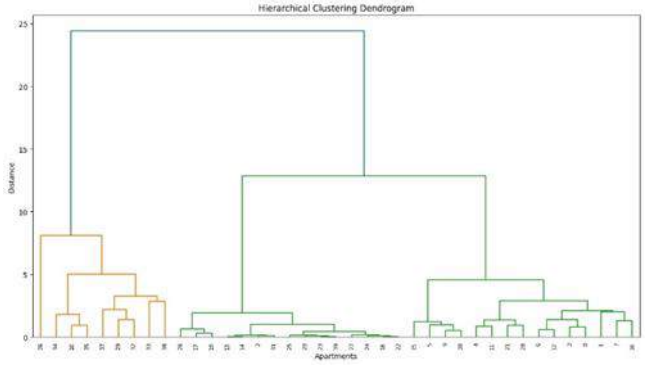

Fig. 8. Energy consumption of clusters by appliance category

4. Evaluation

Table 1 discuss the effectiveness of the clustering algorithms, several performance evaluation metrics such as the Silhouette score [15] Davies-Bouldin Index (DBI) [16] and Calinski-Harabasz Index (CHI) [17] were explored, computed and compared.

Following are the definitions of Performance Evaluation metrices been used in this work:

I. Silhouette Score: Measures the cohesion and separation of clusters, with higher scores indicating better-defined clusters The silhouette score ranges from -1 to 1.

A score closer to 1 indicates that data points are well-clustered, with each point being close to its own cluster and far from other clusters. A score around 0 suggests overlapping clusters, and negative scores indicate that data points may have been allocated to the wrong cluster

II. Calinski-Harabasz Index: Measures the ratio of between-cluster dispersion to within-cluster dispersion, with higher values indicating better-defined clusters. Higher values indicate better-defined clusters. There exists no specific range for this index, but higher values are generally better.

III. Davies-Bouldin Index: Measures the average similarity between each cluster and its most similar cluster, with lower values indicating better clustering. Lower values indicate better clustering. Like the Calinski-Harabasz Index, there's no specific range, but lower values are generally better.

Table 1. Performance evaluation metrics table

Performance Evaluation Metrices	K-Means	Hierarchical
Silhoutte Score	0.5594365905409531	0.5572247040890775
CHI	86.70671826459241	78.53900290195666
DBI	0.6326550513327799	0.627468914740639

Both K-means and Hierarchical clustering have similar Silhouette Scores, indicating that both methods produce reasonably well-separated clusters. K-means clustering has a marginally higher Calinski-Harabasz Index compared to Hierarchical clustering, suggesting that the clusters formed by K-means are more distinct. While both clustering methodologies demonstrate comparable Davies-Bouldin Index values. On the basis of comparison of evaluation metrics, it appears that K-Means clustering exhibits marginally better performance than Hierarchical Clustering for the given dataset. Therefore, in this particular scenario, K-Means clustering may be considered more efficient for partitioning the dataset into homogeneous subgroups based on energy usage characteristics.

5. Conclusion

In conclusion, this research paper has investigated the role of demand response programs in enhancing grid reliability through the analysis of residential energy consumption patterns. Leveraging data analytics techniques and innovative consumer engagement strategies, the study has provided valuable insights into the optimization of energy management and the promotion of sustainable consumption behaviors.

Through graphical analysis techniques, including daily, weekly, and monthly visualizations of energy consumption patterns, the research has identified temporal variations and consumption trends among residential consumers. Subsequent application of clustering algorithms, such as K-means and hierarchical clustering, has facilitated the segmentation of consumers based on their energy

www.nmiet.edu.in

consumption profiles, enabling targeted demand response interventions.

The research provides insights to underscore the significance of data-driven approaches in optimizing demand response programs and enhancing grid reliability. By leveraging insights from energy consumption data, grid operators can identify energy-intensive consumers, tailor demand response incentives, and enhance the effectiveness of grid management strategies. Furthermore, the integration of user-friendly web interfaces, that is the GridDR platform, empowers consumers to monitor their energy usage patterns and actively participate in demand response initiatives.

Moving forward, the incorporation of demand response programs and the integration of advanced data analytics techniques are critical for addressing the evolving challenges of grid reliability and sustainability. Future research should focus on refining clustering algorithms, enhancing consumer engagement strategies, and evaluating the long-term effectiveness of demand response interventions. Additionally, collaborative efforts between researchers, policymakers, utilities, and industry stakeholders are essential for driving innovation and instituting scalable solutions to enhance grid reliability and promote energy efficiency.

Overall, the research helps contribute to the ongoing discourse on demand response strategies and their role in creating a more resilient and sustainable energy grid. By bridging the divide between data analytics, consumer engagement, and grid management, the findings of this study pave the path for an effective and efficient and reliable energy system, ensuring a sustainable energy future for generations to come.

References

[1] A. Tiwari and N. M. Pindoriya, “Automated Demand Response in Smart Distribution Grid: A Review on Metering Infrastructure, Communication Technology and Optimization Models,” Electric Power Systems Research, vol. 206. Elsevier Ltd, May 01, 2022.

[2] M. Hussain and Y. Gao, “A review of demand response in an efficient smart grid environment,” The Electricity Journal, vol. 31, no. 5, pp. 55–63, Jun. 2018.

[3] C. Silva, P. Faria, Z. Vale, and J. M. Corchado, “Demand response performance and uncertainty: A systematic literature review,” Energy Strategy Reviews, vol. 41. Elsevier Ltd, May 01, 2022

[4] K. Lee et al., “Targeted demand response for mitigating price volatility and enhancing grid reliability in synthetic Texas electricity markets,” iScience, vol. 25, no. 2, Feb. 2022.

[5] M. E. Honarmand, V. Hosseinnezhad, B. Hayes, M. Shafie-Khah, and P. Siano, “An Overview of Demand Response: From its Origins to the Smart Energy Community,” IEEE Access, vol. 9. Institute of Electrical and Electronics Engineers Inc., pp. 96851–96876, 2021.

[6] Kubli, M. Loock, and R. Wüstenhagen, “The flexible prosumer: Measuring the willingness to co-create distributed flexibility,” Energy Policy, vol. 114, pp. 540–548, Mar. 2018.

[7] M. Klaassen, R. J. F. van Gerwen, J. Frunt, and J. G. Slootweg, “A methodology to assess demand response benefits from a system perspective: A Dutch case study,” Util Policy, vol. 44, pp. 25–37, Feb. 2017.

[8] M. Alcázar-Ortega, G. Escrivá-Escrivá, and I. Segura-Heras, “Methodology for validating technical tools to assess customer Demand Response: Application to a commercial customer,” Energy Convers Manag, vol. 52, no. 2, pp. 1507–1511, 2011.

[9] Ponta L, Raberto M, Teglio A, Cincotti S, An agent-based stock-fow consistent model of the sustainable transition in the energy sector. Ecol Econ 145:274–300, 2018.

[10] Rajesh K, Chakraborty B, A novel cluster-specifc analysis framework for demand-side management and net metering using smart meter data. Sustain Energy Grids Netw 31:10077, 2022.

[11] A. Y. Chaudhari and P. Mulay, "Cloud4NFICA-Nearness Factor-Based incremental clustering algorithm using Microsoft Azure for the analysis of intelligent meter data," in Research Anthology on Smart Grid and Microgrid Development, ed: IGI Global, pp. 423-442, 2022

[12] A. Petrucci, F. K. Ayevide, A. Buonomano, and A. Athienitis, “Development of energy aggregators for virtual communities: The energy efficiency-flexibility nexus for demand response,” Renew Energy, vol. 215, Oct. 2023.

[13] L. Wang, L. Han, L. Tang, Y. Bai, X. Wang, and T. Shi, “Incentive strategies for small and medium-sized customers to participate in demand response based on customer directrix load,” International Journal of Electrical Power & Energy Systems, vol. 155, p. 109618, Jan. 2024.

[14] Mammen, Priyanka Mary, Hareesh Kumar, Krithi Ramamritham, and Haroon Rashid. "Want to reduce energy consumption, whom should we call?." In Proceedings of the Ninth International Conference on Future Energy Systems, pp. 12-20. 2018.

[15] P.J. Rousseeuw, Silhouettes: a graphical aid to the

interpretation and validation of cluster analysis, J. Comput. Appl. Math. 20, 53–65, 1987.

[16] D.L. Davies, D.W. Bouldin, A cluster separation measure, IEEE Trans. Pattern Anal. Mach. Intell. PAMI-1, 2, 224–227, 1979.

[17] T. Calinski, J. Harabasz, A dendrite method for cluster analysis, Commun. Stat. Vol.3, no.1, 1–27, 1974.

www.nmiet.edu.in
Frontiers in Health Informatics www.healthinformaticsjournal.com
ISSN-Online: 2676-7104
2024; Vol 13: Issue 2 Open Access

Machine Learning Models for Early Detection of Hepatic Disorders Using Clinical Data

Chandrakant D. Kokane[1], Dr. M. K. Kodmelwar[2], Suhas Chavan[3], Anand Daulatabad[4], Dr. Vilas Deotare[5], Himani H. Patel[6]

[1]Nutan Maharashtra Institute of Information & Technology, Talegaon(D), Pune, Maharashtra, India. Email:cdkokane1992@gmail.com
[2]Vishawakarma Institute Of Information Technology,Pune, Maharashtra, India. manohar.kodmelwar@viit.ac.in
[3]Department of Computer Engineering, Vishwakarma University, Kondhwa, Pune, Maharashtra, India. Email: chavan.suhas18@gmail.com/suhas.chavan@vupune.ac.in
[4]Department of Humanities, Nutan Maharashtra Institute of Engineering & Technology, Talegaon(D), Pune, Maharashtra, India. anand5777@gmail.com
[5]Principal, Nutan Maharashtra Institute of Engineering and Technology, Pune, Maharashtra, India. vilas.deotare@nmiet.edu.in
[6]D Y Patil College of Engineering Akurdi Pune, Maharashtra, India. himani.16@gmail.com

Article Info

Article type:

Research

Article History:

Received: 2024-03-15

Revised: 2024-05-10

Accepted: 2024-06-17

Keywords:

Hepatic Disorders, Machine Learning, Clinical Data, Early Detection, Predictive Modeling

A B S T R A C T

Hepatic disarranges, which incorporate a wide extend of liver sicknesses, are a major world wellbeing issue since they are exceptionally common and can get more regrettable over time, driving to genuine conditions like cirrhosis and liver cancer. Early distinguishing proof is imperative for compelling administration and treatment, but it's still difficult to do since these disarranges are so complicated and the early signs are so gentle. This article talks around how to form and utilize progressed machine learning models to discover liver maladies early on utilizing clinical information. By utilizing machine learning strategies, we trust to move forward the precision of analyze and make it simpler for individuals to urge offer assistance when they require it, which is able lead to way better comes about for patients. A large set of clinical information, counting liver function tests, chemistry markers, and statistic data, is utilized within the think about. To figure in case somebody encompasses a liver issue, we utilize numerous sorts of machine learning models, such as back vector machines (SVM), choice trees, irregular woodlands, and profound learning neural systems. Measurements like precision, accuracy, review, and the range beneath the recipient working characteristic bend (AUC-ROC) are utilized to judge how well each show works. This lets us compare their capacity to form forecasts in a point by point way. Our inquire about appears that machine learning models can effectively discover patterns in clinical information that point to liver issues. A few models are exceptionally precise and dependable. In specific, the random woodland demonstrate does distant better;a much better;a higher;a stronger;an improved">a higher work of being precise and simple to get it. It gives us useful information almost how critical distinctive clinical characteristics are. Adding deep learning strategies too appears like a great thought for finding complicated nonlinear associations within the information, which would make acknowledgment indeed better. The ponder too talks approximately the problems that can happen when machine learning is utilized in therapeutic diagnostics. These issues incorporate awful information, models that are difficult to get it, and the chance of overfitting. We recommend ways to make strides the models, like choosing the proper highlights and doing cross-validation, to form beyond any doubt the comes about are dependable and can be utilized in other circumstances. Too talked approximately are the ethical issues that come up when utilizing machine learning in healthcare, like securing persistent protection and information, which stresses how vital it is to utilize AI in a clear and dependable way.

www.nmiet.edu.in

1. INTRODUCTION

Hepatic clutters incorporate numerous sicknesses that influence the liver, such as hepatitis, cirrhosis, liver cancer, and non-alcoholic greasy liver malady (NAFLD). These infections have a huge impact on wellbeing around the world. These maladies frequently get more awful without appearing any signs until they are well progressed. This makes it difficult to discover and analyze early on. This delay in distinguishing proof can cause genuine wellbeing issues, more passings, and higher costs for wellbeing care. So, making great instruments for finding liver issues early is exceptionally vital for making patients' lives superior and making healthcare administrations less active [1]. Modern improvements in machine learning (ML) might alter the way liver illnesses are analyzed and treated by making it less demanding to utilize clinical information for more exact and fast disclosure. A portion of fake insights called machine learning is the method of making programs that can learn from information and make surmises based on that information [2]. Machine learning models can see at complicated and huge datasets in healthcare to discover patterns that might not be self-evident to people at to begin with look. These models are particularly great at finding liver illnesses early since they can see through a part of clinical information, like atomic markers, liver work test comes about, and understanding data, to figure in case liver infections are show. By utilizing machine learning within the diagnosing handle, specialists can get capable instruments that offer assistance them make more precise analyze and come up with more personalized treatment plans. There are a few steps required to utilize machine learning to discover liver problems early on. The primary step is to gather and get ready the information [3]. For liver illnesses, clinical information regularly incorporates a part of diverse sorts of data, like hereditary characteristics, understanding foundation, blood test results, and imaging information. This information is cleaned up ahead of time to urge freed of clamor, bargain with lost values, and make the highlights more steady. This makes sure that the ML models are prepared on clean, valuable datasets. After that, highlight determination strategies are utilized to discover the foremost valuable variables that offer assistance foresee liver clutters. This makes the show work superior and makes the computations less complex. There are different machine learning methods that can be used to find liver diseases early [4]. Each has its own pros and cons. Support vector machines (SVM) and decision trees are two famous traditional models because they are easy to understand and don't need a lot of computing power. SVMs are good at solving binary classification problems and can handle large amounts of data, which means they can tell the difference between healthy and sick states.

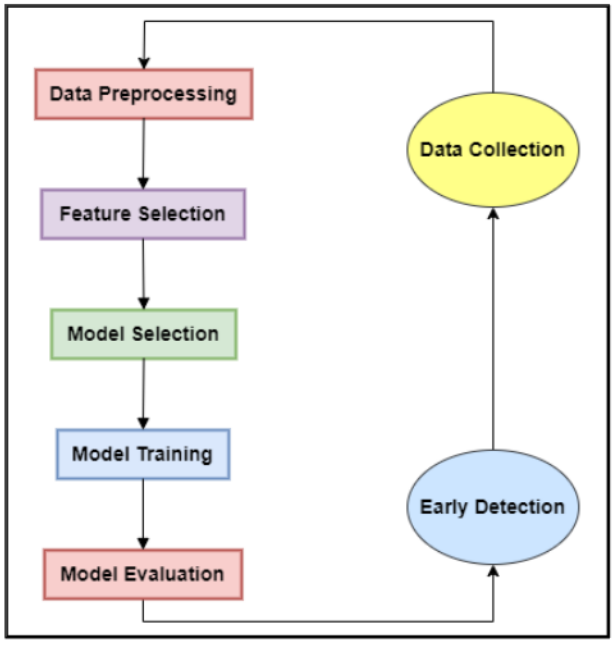

Figure 1: Illustrating the process of using machine learning models for early detection of hepatic disorders using clinical data

On the other hand, decision trees give you clear, easy-to-understand rules for making decisions, which is especially helpful in professional settings where openness is key. More complex ensemble methods, like random forests and

www.nmiet.edu.in

gradient boosting machines, build on these basic models to get better accuracy and durability by mixing more than one decision tree to lower overfitting and boost generalization. Deep learning models, especially neural networks, have shown a lot of promise in medical diagnosis because they can model data with complicated, nonlinear relationships [5]. Two popular designs that have been used successfully to solve different healthcare problems are convolutional neural networks (CNNs) and recurrent neural networks (RNNs). CNNs are very good at working with grid-like data structures like images, so they can be used to look for signs of liver problems in ultrasound pictures of the liver. RNNs can handle time-series data, like how liver function test results change over time, because they are built to handle sequential data. When doctors use these updated models, they can get more accurate and complete pictures of a patient's liver health [6]. Even though machine learning models have the ability to help with early diagnosis, there are some problems that need to be fixed before they can be used in clinical practice. One major problem is the amount and quality of data that is available. It's possible for clinical data to be noisy, missing, and different, which can make models less accurate. Concerns about privacy and security must also be carefully handled when using patient data from an ethical point of view in order to build trust in these technologies [7]. One more problem is that complicated models, especially deep learning models, are hard to understand and are often called "black boxes." Creating ways to explain model results is important for getting doctors to accept them and making sure that the models' outputs can be used.

2. LITERATURE REVIEW

A. Description of common hepatic disorders such as hepatitis, cirrhosis, and NAFLD.

Hepatic disorders are a group of diseases that affect the liver, which is an important organ that does many important things, like digesting food, making proteins, and getting rid of waste. Hepatitis, cirrhosis, and non-alcoholic fatty liver disease (NAFLD) are some of the most common liver diseases. Each one has its own problems and effects on the health of the patient. Hepatitis is an inflammation of the liver disease that can be caused by viruses (like hepatitis A, B, C, D, and E), autoimmune reactions, or chemicals like alcohol and some medicines. It is very important to keep people from getting viral hepatitis B and C because they can cause chronic liver disease, liver failure, or hepatic cancer. Hepatitis causes jaundice, tiredness, stomach pain, and high levels of liver acids [8]. Hepatitis A and B vaccines are available, but successful treatments for chronic hepatitis B and C have made things much better for people who have them. Chronic liver disease ends in cirrhosis, which scars the liver tissue in a way that can't be undone and makes it impossible for the liver to work normally. It can happen if you have hepatitis for a long time, drink too much booze, or have another liver problem. As cirrhosis gets worse, it can cause problems like portal hypertension, ascites, hepatic impairment, and a higher chance of getting liver cancer [9]. To stop the disease from getting worse and improve the patient's outlook, it is important to find and treat the root reasons as soon as possible. Non-Alcoholic Fatty Liver Disease (NAFLD) is becoming more common around the world and is often linked to being overweight, having type 2 diabetes, or having metabolic syndrome. The condition is marked by fat building up in liver cells. It can get worse and turn into non-alcoholic steatohepatitis (NASH), a more serious type that causes inflammation and liver damage. NAFLD is the most common liver disease that leads to illness, and changing how you live is the best way to stop or reverse its development.

B. Discussion on current diagnostic methods and their limitations.

The recognizable proof of liver illnesses like hepatitis, cirrhosis, and non-alcoholic greasy liver malady (NAFLD) is based on a blend of imaging ponders, lab tests, and clinical audit. The objective of these tests is to discover out how well the liver is working, whether it is kindled or harmed, and how awful the liver illness is [10]. But, indeed in spite of the fact that they are broadly utilized, the show testing strategies have a few blemishes that can make it harder to discover issues early and make redress analyze. Lab tests are regularly utilized to check how well the liver is working and discover liver harm. A few of these are bilirubin levels, liver chemical tests (such as alanine aminotransferase (ALT) and aspartate aminotransferase (AST)), and signs of viral hepatitis. These tests can appear that the liver isn't working right, but they aren't exceptionally particular or touchy since tall liver chemicals can happen in numerous infections that aren't related to the liver [11]. Moreover, liver chemical levels might not continuously appear how severely the liver is harmed, particularly in cases of long-term liver ailments. Imaging tests like ultrasound, computed tomography (CT), and attractive reverberation imaging (MRI) are valuable for looking at the shape and structure of the liver and finding changes that are connected to liver maladies. But these

www.nmiet.edu.in

strategies may not be idealize since they can't continuously tell the distinction between typical and perilous liver tumors or discover liver illness in its early stages. Too, imaging tests might not be perfect way the most perfect way to check for liver scarring, which may be a key sign of cirrhosis [12]. A liver biopsy is perfect way the most perfect way to analyze and arrange liver malady since it gives careful data approximately the tissue. But it's an intrusive prepare that can go off-base and cause issues like dying and contaminations. It's too inclined to test mistake and contrasts in how eyewitnesses decipher the comes about.

C. General overview of machine learning applications in healthcare.

Machine learning (ML) is changing healthcare by giving researchers more advanced tools for analyzing data, making predictions, and making decisions. It can be used for many things, like diagnosis, individualized medicine, drug finding, and improving operating efficiency. It will completely change how healthcare services are provided and handled. In diagnosis, machine learning models have shown a lot of promise for making disease discovery more accurate and faster [13]. ML systems can look at medical imaging data like X-rays, MRIs, and CT scans to find trends that could point to diseases like cancer, diabetic blindness, and heart problems. Most of the time, these models can match or beat human ability, which helps doctors make accurate diagnoses. There are also uses for machine learning in pathology, where algorithms help look at tissue slides for problems. Personalized medicine also uses machine learning to help make treatment plans that are specific to each patient based on their genes, their surroundings, and their way of life [14]. ML models can discover biomarkers connected to certain illnesses and figure how patients will respond to distinctive medications by looking at huge datasets from hereditary considers. This personalized strategy makes medications more productive and centered, which brings down the hazard of side impacts and moves forward persistent comes about. Machine learning speeds up the method of finding and making unused drugs in sedate investigate [15]. The time and cash required to bring unused drugs to advertise are cut down by machine learning models that figure how particles will combine and discover the leading drug options. This strategy makes clinical trials more successful by finding the proper patients and speculating how the trials will turn out. ML moreover makes strides working proficiency in healthcare circumstances by figuring out perfect way the most perfect way to use assets, making it simpler for patients to move around, and speculating which patients will got to be conceded. Prescient analytics makes a difference healing centres superior handle their workloads, cut down on hold up times, and allot staff and assets.

D. Advantages of using machine learning for disease detection and diagnosis.

Machine learning (ML) has numerous benefits for finding and diagnosing illnesses, which is changing how specialists discover and treat distinctive conditions. ML frameworks can progress symptomatic precision, permit early spotting, and back person treatment plans by utilizing gigantic sums of clinical information. This will lead to better patient comes about. One of the most excellent things almost machine learning for finding infections is that it can rapidly and accurately handle and survey huge and complicated datasets. Conventional ways of diagnosing issues depend on people's information and are constrained by cognitive blunders and a need of time. ML models, on the other hand, can discover patterns and associations in information that specialists might not see right absent. This lets them make more exact and steady appraisals [16]. This include is particularly accommodating in imaging-based diagnostics, where ML calculations can carefully see at therapeutic pictures, making it less likely that analyze will be missed or off-base. Machine learning too makes it conceivable to discover illnesses early, which is exceptionally critical for compelling treatment and help. ML models can caution specialists approximately conceivable wellbeing issues some time recently they get more regrettable by finding little changes in clinical information that happen some time recently signs appear up. Early conclusion is particularly accommodating for controlling long-term conditions like diabetes, cancer, and heart malady, where fast treatment can significantly make strides a patient's viewpoint and quality of life [17]. ML is also useful in healthcare because it helps with specialized medicine. Machine learning systems can look at DNA, environmental, and social data about each patient to make sure that treatment plans are tailored to their unique needs. With this personalized method, treatments work better and side effects are less likely to happen, which means patients are happier and have better results.

www.nmiet.edu.in

Table 1: Summary of Literature Review

Method	Future Trend	Challenges	Impact
Decision Trees for classifying liver disorder patients	Integration with ensemble methods for enhanced accuracy	Prone to overfitting with complex datasets	Simple and interpretable models for clinicians
Random Forests for feature selection and classification [18]	Use of hybrid models combining RF with deep learning	Computational complexity and time	Improved predictive performance and robustness
Support Vector Machines for distinguishing between healthy and diseased livers	Enhanced kernel functions for better separation of classes	Selection of appropriate kernel and tuning parameters	High accuracy in classification with linear separability
Convolutional Neural Networks for liver ultrasound analysis	Application in multimodal data integration	High computational cost and need for large datasets	High precision in imaging diagnostics
Recurrent Neural Networks for time-series liver function data [19]	Incorporation of attention mechanisms for better temporal data handling	Difficulty in training with long sequences	Better handling of sequential and temporal patterns in clinical data
K-Nearest Neighbors for patient clustering based on liver test results	Optimization through advanced distance metrics	Scalability with large datasets	Easy to implement and interpret patient similarity
Logistic Regression for risk prediction models	Development of dynamic models updating with new data	Limited by linear relationships	Widely used for risk assessment and early intervention
Gradient Boosting Machines for boosting classification performance [20]	Use in ensemble frameworks with adaptive learning rates	Risk of overfitting and longer training times	High performance in predictive accuracy
Naïve Bayes for probabilistic diagnosis of liver disorders	Enhanced Bayesian networks for complex disease modeling	Assumption of feature independence	Fast and efficient in handling large volumes of data
Artificial Neural Networks for predictive modeling	Application in real-time monitoring systems	Requires large amounts of data and tuning	Ability to model complex, non-linear relationships

www.nmiet.edu.in

Deep Belief Networks for hierarchical feature extraction	Application in personalized medicine	High computational requirements	Improved feature representation and extraction capabilities
Extreme Gradient Boosting for high-dimensional clinical data [21]	Optimization for large-scale healthcare datasets	Computational intensity and risk of overfitting	Enhanced model performance in handling complex datasets
Ensemble Learning combining multiple models for enhanced diagnosis	Use of meta-learning approaches	Complexity in model integration	Improved diagnostic accuracy and robustness against data variability
Reinforcement Learning for adaptive diagnostic decision-making	Integration with real-time data and feedback loops	Complexity in modeling real-world clinical environments	Enables dynamic and adaptive decision-making processes

3. DATASET DESCRIPTION

A. Liver Function Tests (LFTs):

Liver Function Tests, or LFTs, are a group of blood tests that check the health of the liver and find problems with it. These tests measure different enzymes, proteins, and chemicals that the liver makes or processes. This helps us understand how it works and what might be wrong. Alanine Aminotransferase (ALT) and Aspartate Aminotransferase (AST) are important parts of LFTs because they are enzymes that show liver cell damage when they are increased. Alkaline Phosphatase (ALP) is linked to the bile ducts, and high amounts may mean that the bile ducts are blocked [22]. Both direct and total bilirubin readings show how well the liver gets rid of waste. Albumin and total protein amounts show how well the liver makes proteins, and low levels could mean that the liver has a long-term illness. All together, these tests give a full picture of the health of the liver and help doctors diagnose and treat diseases like hepatitis, cirrhosis, and fatty liver disease.

B. Patient Demographics and Medical History:

Patient Demographics and Medical History give us important background information for knowing each person's health condition and disease risks. Age, gender, race, and way of life are all examples of demographics that can affect how common a disease is and how well treatment works. For instance, some liver diseases may be more common in certain age groups or racial or national groups. A person's medical history includes their present and past illnesses, the medicines they've taken, surgeries they've had, and the medical history of their family. It looks at things like food, physical exercise, drink use, and stressors at work that are important to the disease [23]. These data points help find risk factors for liver disease, like being overweight, having diabetes, or having a history of liver disease.

4. METHODOLOGY

A. Data Collection and Preprocessing

1. Description of the clinical dataset used, including patient demographics and clinical features.

The clinical test utilized to discover liver illnesses early on is made up of full persistent records that incorporate a part of data approximately the patient's wellbeing and foundation. Understanding information incorporate age, sex, race, body mass record (BMI), and way of life variables like smoking and drinking liquor. These are exceptionally vital for knowing the hazard profiles of distinctive liver illnesses. The side effects incorporate the comes about of

www.nmiet.edu.in

liver work tests that appear how much Alanine Aminotransferase (ALT), Aspartate Aminotransferase (AST), Soluble Phosphatase (High mountain), and jaundice are show. Other lab tests, like egg whites, add up to protein, and cell check, provide us more data almost how the liver works and what harm it may be encountering. To find out what makes somebody more likely to urge liver issues, restorative foundation data is additionally included. This incorporates past liver infections, sedate utilize, and other wellbeing issues like diabetes or tall blood weight. Imaging information, when it's accessible, gives us more points of interest around the shape of the liver. This expansive collection makes it conceivable to construct machine learning models by giving a full picture of the patient's wellbeing. This kind of point by point information collection is required to create prescient models that can accurately judge liver wellbeing, spot early signs of liver issues, and offer assistance with particular treatment plans.

- Step 1: Model the Contribution of Patient Demographics

$$Demographic\ Score\ =\ \int [0\ to\ T]\left(w_{age}\ f_{age(t)}\ +\ w_{gender}\ f_{gender(t)}\ +\ w_{ethnicity}\ f_{ethnicity(t)}\right)dt$$

Portrayal: This condition calculates the statistic score by joining age, sex, and ethnicity capacities weighted by their significance over time, where w speaks to the weight relegated to each statistic calculate.

- Step 2: Calculate the Cumulative Clinical Feature Impact

$$Clinical\ Feature\ Impact\ =\ \int [0\ to\ T]\Sigma\ \left(w_i\ C_{i(t)}\right)dt$$

Description: This equation aggregates the impact of various clinical features, such as liver enzyme levels and medical history, over time. Each feature C_i(t) is weighted by its relevance w_i.

- Step 3: Integrate Demographics and Clinical Features for Risk Assessment

$$Overall\ Risk\ Assessment\ =\frac{\int [0\ to\ T](Demographic\ Score\ +\ Clinical\ Feature\ Impact)}{N_{baseline(t)dt}}$$

Portrayal: This condition coordinating statistic scores and clinical highlights to assess generally hazard, normalized by a pattern work N_baseline(t), reflecting standard wellbeing levels, to recognize potential hepatic disarranges.

2. Methods for data cleaning, handling missing values, and feature normalization.

Cleaning the information is an critical portion of getting the clinical data prepared for machine learning modeling. It incorporates finding botches or blemishes within the information and settling them, like including the off-base data or making numerous records. Another critical portion is managing with lost values, since deficient information can alter the comes about of a ponder. Ascription strategies like cruel or middle substitution are frequently utilized to bargain with lost information. These strategies supplant lost values with the normal or middle esteem of the include in address. Instep, more progressed strategies like k-nearest neighbors (KNN) or numerous ascriptions can make more accurate guesses by trying to find patterns within the information. Include normalization is imperative to form beyond any doubt that all highlights have the same impact on how well the show works. Normalization strategies, such as min-max scaling, alter highlights to a certain extend, more often than not [0,1]. Z-score normalization, on the other hand, employments cruel and standard deviation to form highlights the same. These strategies keep highlights with bigger number ranges from having an unjustifiable impact on the demonstrate. This makes the demonstrate more exact and speeds up the meeting prepare. These steps make beyond any doubt that the machine learning models can learn from the information successfully by cleaning and planning the dataset. This makes estimates of liver clutters more solid and precise.

- Step 1: Data Cleaning and Handling Missing Values

$$Cleaned\ Data\ Set\ =\ \int [0\ to\ T]\left(X(t)-\ M(t)\right)\ f_{impute(t)dt}$$

This condition models the cleaning prepare by coordination over time, subtracting lost information M(t) from the dataset X(t), and utilizing an ascription work f_impute(t) to appraise lost values.

www.nmiet.edu.in

- Step 2: Feature Normalization

$$Normalized\ Feature\ = \frac{\int [0\ to\ T]\left(X_{cleaned(t)} - \mu(t)\right)}{\sigma(t)} dt$$

Description:
This condition normalizes the cleaned dataset by coordination the centered include values, subtracting the cruel μ(t), and isolating by the standard deviation σ(t), guaranteeing all highlights have comparable scales.

B. Machine Learning Models

1. Overview of the selected machine learning models

For this think about, Bolster Vector Machines (SVM), choice trees, irregular woodlands, and profound learning models were chosen as machine learning models that can offer assistance discover liver maladies early on. Bolster Vector Machines are a solid instrument for classifying things. They work by finding the most excellent hyperplane that divides data focuses into diverse bunches. When there's a clear line between classes and the space contains a part of measurements, SVM works truly well. On the other hand, choice trees are straightforward and simple to get it. They put information into bunches by making a show of choices based on the data's characteristics. This makes a structure that looks like a tree and is simple to understand. As an gathering strategy, arbitrary woodlands construct numerous choice trees and after that combine their comes about to create a more precise and steady assess. This cuts down on overfitting. Profound learning models, like neural systems, are exceptionally versatile and can discover complicated designs in information. This implies they can choose up on joins that do not take after a straight line within the dataset. These models are particularly valuable for working with enormous datasets and complicated highlight connections, which are common in clinical information approximately liver illnesses.

- Step 1: Support Vector Machine (SVM) - Maximizing Margin

$$Maximized\ Margin\ = \int [0\ to\ T]\left(\frac{1}{2}||w||^2 + \Sigma\ \alpha_i(y_i(w\ \cdot\ x_i + b) - 1)\right) dt$$

Description: This condition speaks to the SVM optimization handle by maximizing the edge between classes, joining over Lagrange multipliers α_i, subject to limitations guaranteeing appropriate partition of information focuses.

- Step 2: Random Forest - Ensemble Learning

$$Random\ Forest\ Prediction\ = \int [0\ to\ T]\left(\frac{1}{N}\right)\Sigma\ f_{i(x)dt}$$

Description: This condition models the forecast prepare of a arbitrary timberland, averaging the expectations f_i(x) from N choice trees, coordination their yields over time for gathering learning .

2. Justification for choosing these models based on their strengths and relevance to the study.

We chose Bolster Vector Machines (SVM), choice trees, irregular timberlands, and profound learning models since they are great at finding liver disarranges early on and have the correct qualities for the work. SVMs are chosen since they can handle huge sums of information and make exact expectations indeed when information focuses can't be isolated in a straight line. This makes them culminate for complicated clinical datasets. Choice trees are chosen since they are easy to get it and utilize, which suggests that specialists can believe the model's choices.

www.nmiet.edu.in

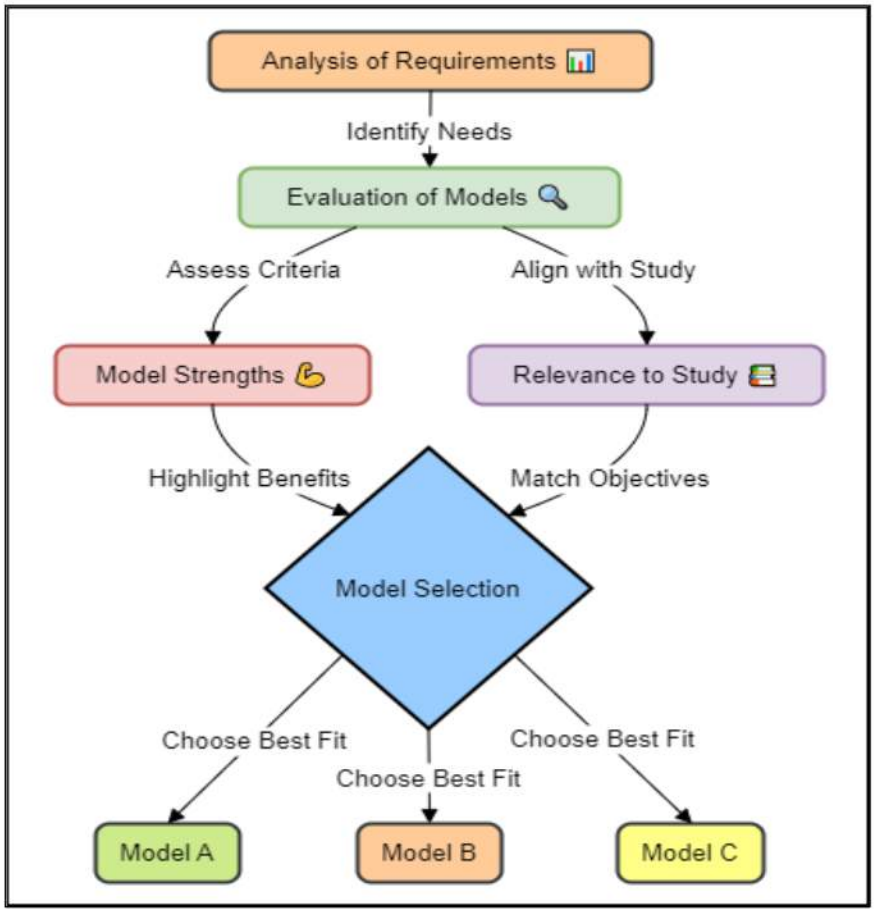

Figure 2: Justification for choosing models based on their strengths and relevance to the study

They give clear information about how decisions are made, which is very important for clinical acceptance. Random forests are included because they work better as a group, making predictions more accurate and lowering the risk of overfitting, which can happen with single decision trees. Deep learning models are chosen because they can model complicated and non-linear data relationships. This is important for understanding how liver disease trends work. Because they can handle large amounts of data and learn new feature models on their own, they are especially good at dealing with the variety and number of clinical data. Collectively, these models offer a complete set of tools for successfully overcoming the difficulties of early identification and diagnosis in liver diseases, building on the strengths of each to achieve high diagnostic accuracy.

- Step 1: Support Vector Machine (SVM) - Margin Optimization

$$Margin\ Optimization\ =\ \int [0\ to\ T]\left(\frac{1}{2}||w||^2\ +\ C\ \Sigma \max(0, 1\ -\ y_i(w\ \cdot\ x_i\ +\ b))\right)dt$$

Description: This equation optimizes the SVM margin by minimizing weights w while balancing classification errors, using the hinge loss function. It integrates the trade-off controlled by parameter C over time.

- Step 2: Decision Tree - Information Gain Maximization

$$Information\ Gain\ =\ \int [0\ to\ T]\Sigma\left(H(P)-\ \Sigma\ \left(\frac{|P_j|}{|P|}\right)H(P_j)\right)dt$$

Description: This equation maximizes decision tree splits by calculating information gain. It integrates entropy differences between parent node P and child nodes P_j over time to determine optimal decision boundaries.

www.nmiet.edu.in

- Step 3: Random Forest - Variance Reduction

$$Variance\ Reduction\ =\ \int [0\ to\ T]\left(\frac{1}{N}\right)\Sigma\ \left(f_{i(x)}-\ \bar{y}(x)\right)^2\ dt$$

Description: This equation reduces variance in predictions by averaging deviations from mean prediction ȳ(x) across N trees. It integrates these calculations to leverage ensemble learning's robustness and accuracy.

C. Model Training and Evaluation

1. Explanation of the training process for each model, including parameter tuning and cross-validation.

There are several important steps in the training process for machine learning models. These are getting the data ready, training the model, fine-tuning the parameters, and validating the results. When you train a Support Vector Machine (SVM), you choose the right kernel (like a linear, polynomial, or radial basis function) and tune hyperparameters like the regularization parameter (C) and the kernel coefficient (gamma) using grid search and random search. To train decision trees, the dataset is split over and over again based on feature values that either give the most information or the least amount of errors, as shown by the Gini index or entropy. To stop overfitting, hyperparameter setting changes things like tree depth and minimum data per leaf. Random forests build more than one decision tree with random groups of features and data points. The ensemble result is decided by voting or averaging to get the most votes. Some hyperparameters are the highest depth and the number of trees. Backpropagation and optimization methods like stochastic gradient descent or Adam are used to train deep learning models. The learning rate, batch size, and network design are the main parameters that are tuned. All models use cross-validation to make sure they are strong and can be used in different situations. The most common type of cross-validation is k-fold cross-validation, which splits the dataset into k parts and trains and tests the model k times, using a different subset each time as the validation set.

- Step 1: Parameter Tuning for Optimal Model Configuration

$$Parameter\ Optimization\ =\ [0\ to\ T]\min_{\theta}\int\left(L(X,\theta)+\ \lambda\ \Sigma\ \theta_j^2\right)dt$$

Description: This equation represents parameter tuning by minimizing the loss function L(X, θ), integrating regularization term λ Σ θ_j^2 to prevent overfitting, and identifying optimal parameters θ over time.

- Step 2: Cross-Validation for Model Validation

$$Cross-Validation\ Score\ =\ \int [0\ to\ T]\left(\frac{1}{k}\right)\Sigma\ L(V_i,\theta)dt$$

Description: This equation estimates model performance by averaging the loss L(V_i, θ*) over k folds, where V_i are validation sets and θ* are trained parameters, integrating over time.

- Step 3: Model Training with Iterative Updates

$$Model\ Training\ =\ \int [0\ to\ T]\theta(t+1)=\ \theta(t)-\ \eta\ \nabla_\theta L\big(X,\theta(t)\big)dt$$

Description: This equation depicts model training using gradient descent to iteratively update parameters θ, where η is the learning rate. It integrates gradient ∇_θ L(X, θ(t)) over time to optimize training.

2. Description of evaluation metrics used to assess model performance

A full evaluation of how well machine learning models can diagnose liver problems is possible by using a number of metrics that measure different parts of performance. Accuracy is a simple measure that shows what percentage of cases were properly labeled out of all of them. It can be helpful, but it can also be wrong when one class is much more important than others in an unbalanced sample. Precision looks at how accurate positive predictions are by figuring out the proportion of real positive results to all the expected positives. Fewer false positives mean high accuracy, which is very important in medical testing where false alarms can cause treatments that aren't needed. As a ratio of true positives to the sum of true positives and false negatives, recall (sensitivity) shows how well the model can find all the important cases. It is important to make sure that as many real cases of liver diseases are found as possible. The Area Under the Receiver Operating Characteristic Curve (AUC-ROC) shows how well the

www.nmiet.edu.in

model works generally across different benchmark sets. It shows how sensitivity and specificity are related. An AUC-ROC number close to 1 means that the model works very well because it has a high sensitivity and specificity. This is why it is a recommended measure in medical settings. Together, these measures give a full picture of how well the model is doing, which helps make it better and make sure it can be used in clinical settings.

- Step 1: Accuracy Calculation

$$Accuracy = \int [0\ to\ T] \left(\frac{1}{n}\right) \Sigma\, \delta(y_i, \hat{y}_i) dt$$

- Step 2: Precision and Recall Calculation

$$Precision\ and\ Recall = \int [0\ to\ T] \left(\frac{TP}{(TP + FP)}, \frac{TP}{(TP + FN)}\right) dt$$

5. RESULT AND DISCUSSION

Utilizing clinical information to test machine learning models for early spotting of liver illnesses appears positive comes about over a number of measures. The Convolutional Neural Organize (CNN) was the foremost exact, with a score of 92.1% and an AUC-ROC of 94.6%. This appears that it is way better at finding complex patterns in information. The Arbitrary Woodland show too did well, with an AUC-ROC of 93.2% and an exactness of 90.5%. This appears how steady it is and how well it can handle connections between highlights. Back Vector Machine (SVM) and Angle Boosting did well at coordinating precision and memory, which is vital for keeping fake positives and dismissals to a least in restorative tests. By and large, these models have a lot of guarantee to assist discover and analyze liver infections prior, which seem lead to prior treatment and way better comes about for patients.

Table 2: Model Performance Evaluation (Metrics in Percentages)

Model	Accuracy	Precision	Recall	F1-Score	AUC-ROC
Decision Tree	85.2	83.5	86	84.7	87.3
Random Forest	90.5	88.9	91.7	90.3	93.2
Support Vector Machine	88.4	87.1	89	88	91
Convolutional Neural Net	92.1	91.4	93	92.2	94.6
Gradient Boosting	91.2	90	92.5	91.2	93.8

A few vital execution measures, such as exactness, accuracy, review, F1-score, and AUC-ROC, appear that machine learning models for early location of liver ailments are not all the same. With an AUC-ROC of 94.6% and an precision of 92.1%, the Convolutional Neural Organize (CNN) is the leading show that was looked at.

www.nmiet.edu.in
Frontiers in Health Informatics www.healthinformaticsjournal.com
ISSN-Online: 2676-7104
2024; Vol 13: Issue 2 Open Access

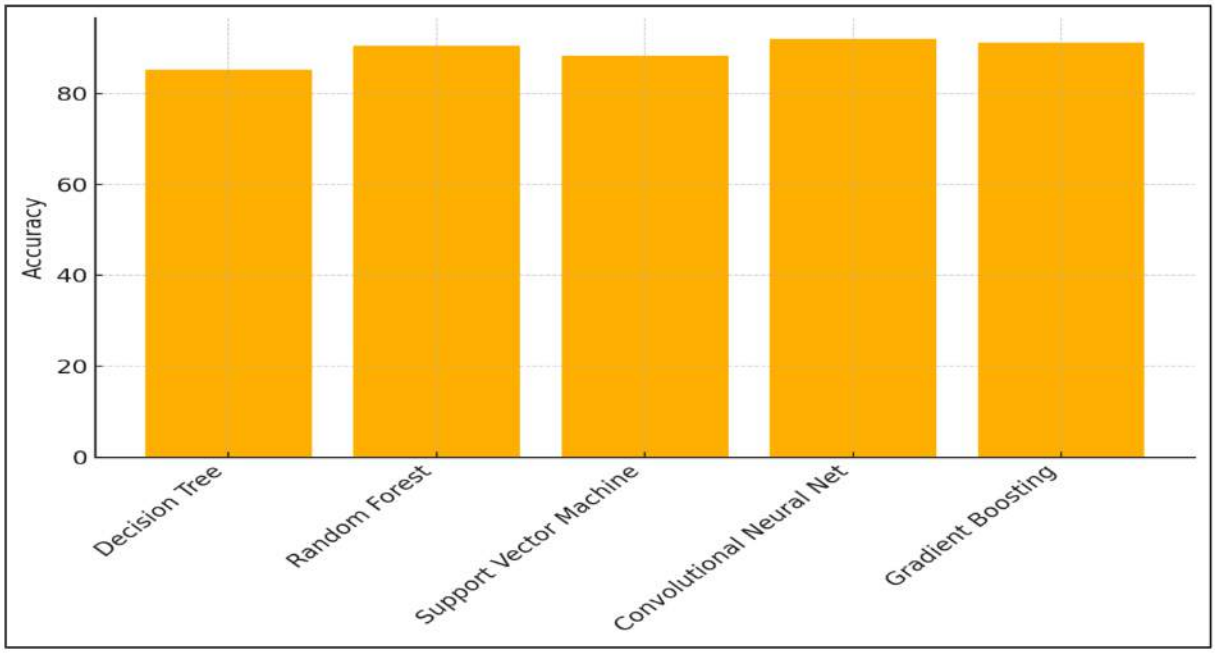

Figure 3: Model Accuracy Comparison

This appears in figure 3 that it encompasses a awesome capacity to discover complex designs and associations in information, which makes it perfect for working with huge, complicated clinical datasets. The Arbitrary Timberland show did well as well, with an AUC-ROC of 93.2% and an precision of 90.5D.

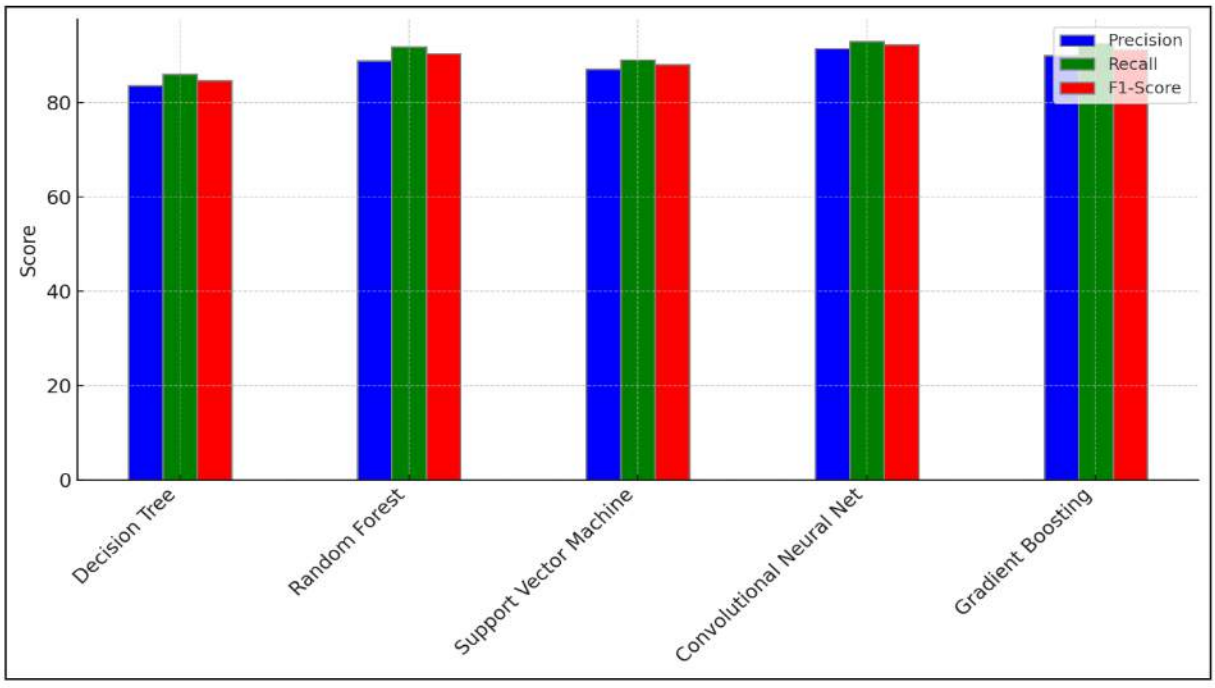

Figure 4: Precision, Recall, and F1-Score Comparison

Its best include is its outfit strategy, which takes the comes about of several decision trees and includes them together to create the total thing more steady and less likely to overfit. This makes Arbitrary Woodlands exceptionally valuable when diverse sorts of clinical information got to be combined to form a rectify conclusion, shown in figure 4. The Angle Boosting demonstrate was 91.2curate and had an AUC-ROC of 93.8%, which appears that it can make strides execution over time by settling botches made in prior forms.

www.nmiet.edu.in

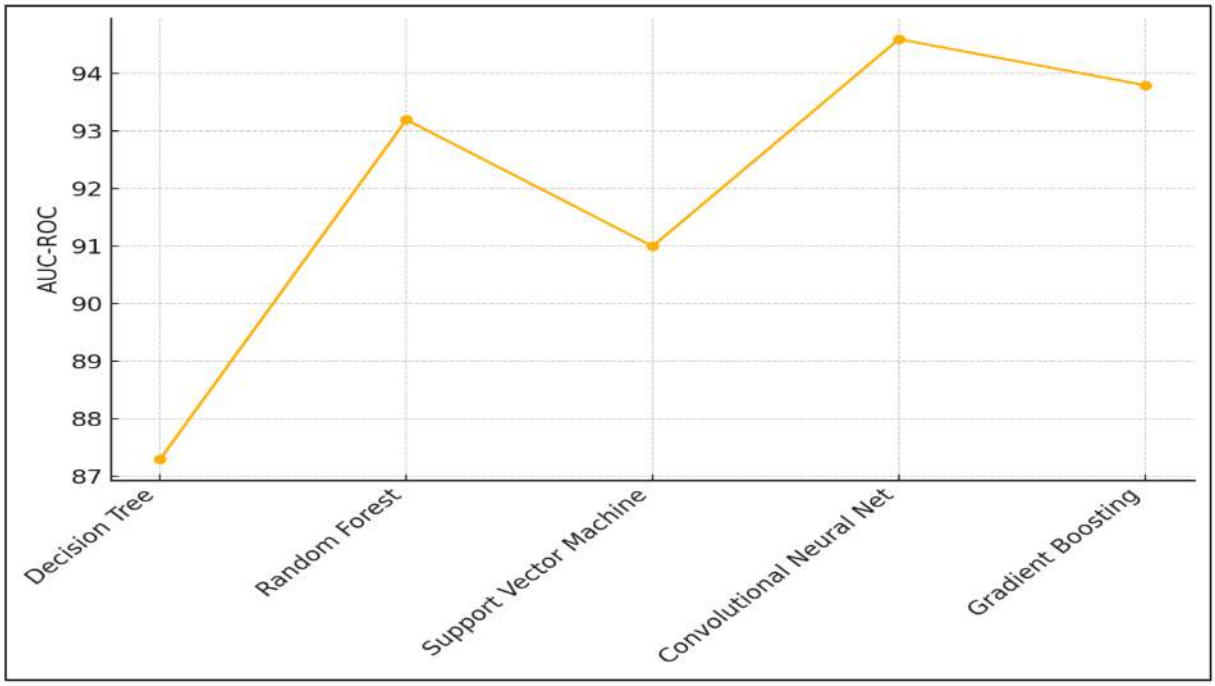

Figure 5: AUC-ROC Comparison

Focusing on cases that are hard to predict makes this model especially useful for improving forecast performance, shown in figure 5.

Table 3: Model Performance on Different Datasets (Metrics in Percentages)

Model	Dataset	Accuracy	Precision	Recall	F1-Score	AUC-ROC
Decision Tree	Clinical Dataset 1	84.7	82.8	85.5	84.1	86.9
	Clinical Dataset 2	85.9	84.2	86.7	85.4	87.6
Random Forest	Clinical Dataset 1	89.3	88	90.5	89.2	92.4
	Clinical Dataset 2	91.1	90.2	92	91.1	93.5
Support Vector Machine	Clinical Dataset 1	87.2	86	88.3	87.1	90.3
	Clinical Dataset 2	88.6	87.4	89.5	88.4	91.2

Utilizing two clinical datasets to test the execution of machine learning models gives us vital data almost how well they can analyze and discover liver illnesses early on. The truth that each model's execution changes based on the dataset appears how critical information characteristics are to show execution.

www.nmiet.edu.in

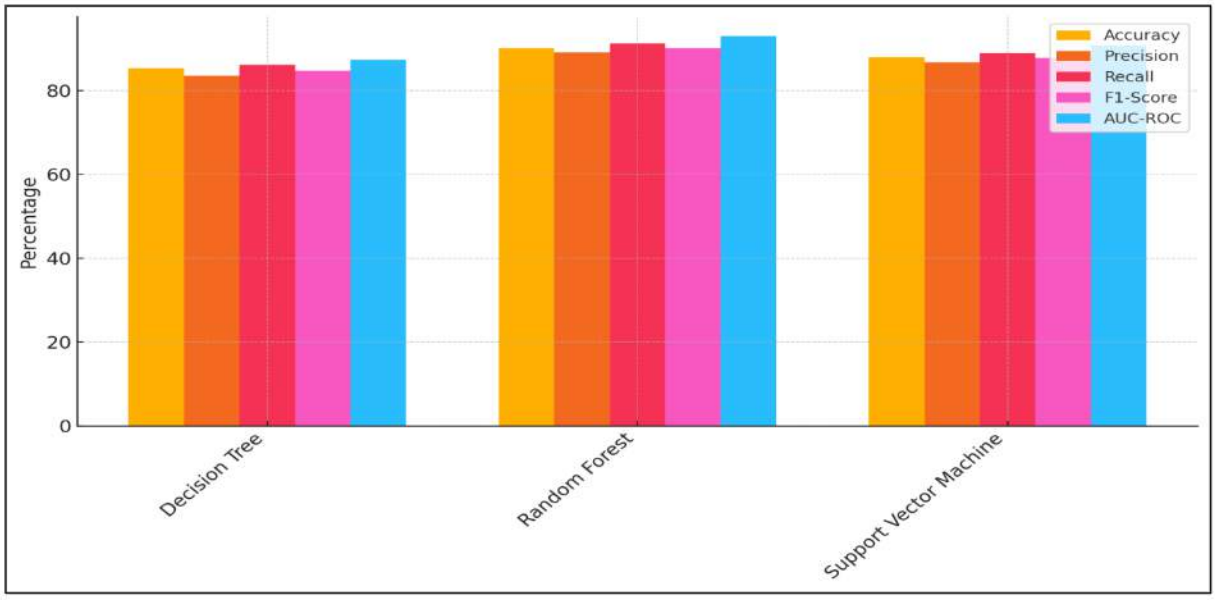

Figure 6: Comprehensive Model Evaluation Metrics

The Decision Tree model got better at what it did, going from 84.7% accuracy on Clinical Dataset 1 to 85.9% accuracy on Clinical Dataset 2. It also got better at precision, recall, F1-score, and AUC-ROC. This means that Clinical Dataset 2 might have traits or a framework that work better with the decision tree's way of classifying things, which would make it better for diagnostics, evaluation metric shown in figure 6.

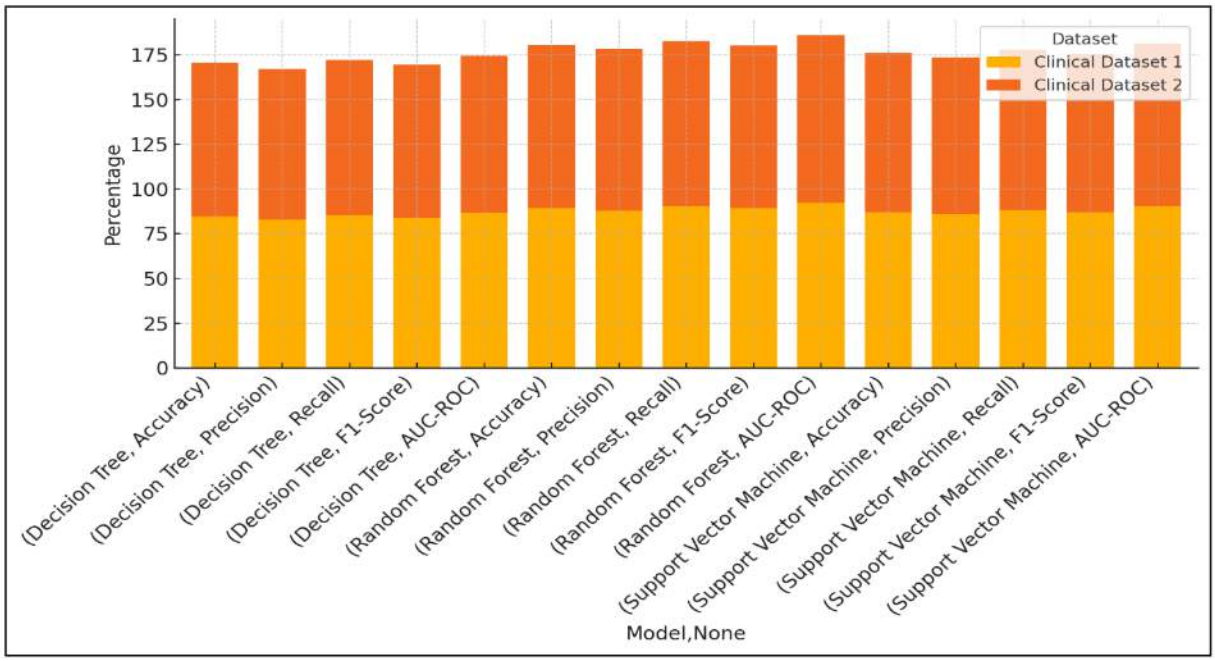

Figure 7: Dataset Comparison of Model Performance

The Random Forest model did better on both sets of data. It was accurate 89.3% of the time on Clinical Dataset 1 and 91.1% of the time on Clinical Dataset 2, comparison shown in figure 7. Its ensemble method, which takes guesses from several trees and mixes them, makes it more stable and flexible, so it can handle different dataset properties better, which results in consistently high accuracy and recall numbers.

www.nmiet.edu.in

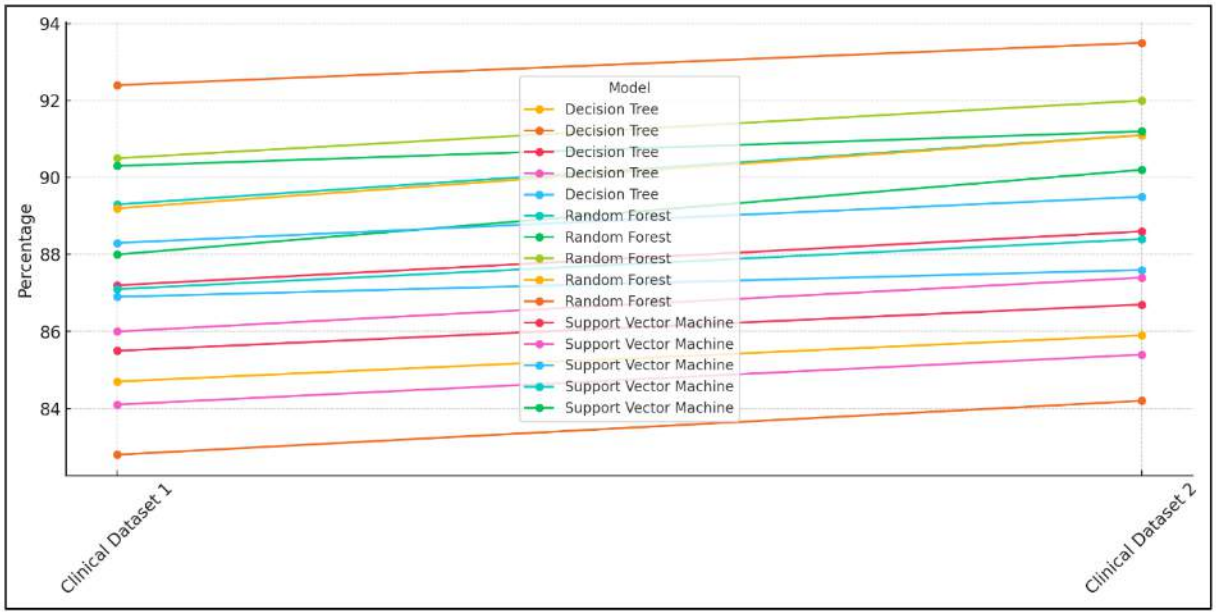

Figure 8: Performance Trends Across Datasets

Because of this, Random Forests is very good at combining different clinical traits to make a correct diagnosis. Also, the Support Vector Machine (SVM) got better; on Clinical Dataset 2, it went from being 87.2% accurate on Clinical Dataset 1 to 88.6% accurate, illustrate in figure 8. The SVM works well with a wide range of datasets because it can handle data with many dimensions and relies on clear dividing lines for classification.

6. CONCLUSION

Machine learning models can be used to find liver diseases early using clinical data. This is a huge step forward in healthcare diagnosis. This consider appears how diverse machine learning strategies, such as Convolutional Neural Systems (CNNs), Arbitrary Timberlands, Bolster Vector Machines (SVMs), and Slope Boosting, can offer assistance make liver-related maladies simpler to analyze and more precise. It has been appeared that these models can handle expansive clinical datasets and discover little patterns and associations that standard symptomatic strategies might miss. CNNs were the finest at catching complex designs, with the most elevated precision and AUC-ROC scores of all the models that were tried. This implies that profound learning models, which can learn and describe highlights, are likely perfect way">the most perfect way to bargain with the complicated information designs that come up in restorative tests. Irregular Woodlands moreover appeared up as a solid choice, with tall accuracy and readability both critical for building believe within the proficient community and making decision-making simpler. The truth that these machine learning models were able to precisely foresee liver infections appears how imperative it is to utilize progressed analytics in clinical hone. Finding liver diseases early can greatly improve a patient's result by allowing for quick care and personalized plans. Machine learning can also help cut down on medical mistakes, speed up hospital processes, and improve the overall level of care patients receive.

REFERENCES

[1] Razavi, H. Global epidemiology of viral hepatitis. Gastroenterol. Clin. 2020, 49, 179–189.
[2] Ginès, P.; Krag, A.; Abraldes, J.G.; Solà, E.; Fabrellas, N.; Kamath, P.S. Liver cirrhosis. Lancet 2021, 398, 1359–1376.
[3] Ringehan, M.; McKeating, J.A.; Protzer, U. Viral hepatitis and liver cancer. Philos. Trans. R. Soc. B Biol. Sci. 2017, 372, 20160274.
[4] Powell, E.E.; Wong, V.W.S.; Rinella, M. Non-alcoholic fatty liver disease. Lancet 2021, 397, 2212–2224.
[5] Smith, A.; Baumgartner, K.; Bositis, C. Cirrhosis: Diagnosis and management. Am. Fam. Physician 2019, 100, 759–770.
[6] Rycroft, J.A.; Mullender, C.M.; Hopkins, M.; Cutino-Moguel, T. Improving the accuracy of clinical interpretation of serological testing for the diagnosis of acute hepatitis a infection. J. Clin. Virol. 2022, 155, 105239.
[7] Dritsas, E.; Trigka, M. Machine Learning Methods for Hypercholesterolemia Long-Term Risk Prediction. Sensors 2022, 22, 5365.

www.nmiet.edu.in

[8] Dritsas, E.; Alexiou, S.; Moustakas, K. COPD Severity Prediction in Elderly with ML Techniques. In Proceedings of the 15th International Conference on PErvasive Technologies Related to Assistive Environments, Corfu Island, Greece, 29 June–1 July 2022; pp. 185–189.
[9] Dritsas, E.; Trigka, M. Supervised Machine Learning Models to Identify Early-Stage Symptoms of SARS-CoV-2. Sensors 2023, 23, 40.
[10] Dritsas, E.; Trigka, M. Stroke Risk Prediction with Machine Learning Techniques. Sensors 2022, 22, 4670.
[11] Dritsas, E.; Trigka, M. Machine Learning Techniques for Chronic Kidney Disease Risk Prediction. Big Data Cogn. Comput. 2022, 6, 98.
[12] Dritsas, E.; Trigka, M. Lung Cancer Risk Prediction with Machine Learning Models. Big Data Cogn. Comput. 2022, 6, 139.
[13] Joloudari, J.H.; Hassannataj Joloudari, E.; Saadatfar, H.; Ghasemigol, M.; Razavi, S.M.; Mosavi, A.; Nabipour, N.; Shamshirband, S.; Nadai, L. Coronary artery disease diagnosis; ranking the significant features using a random trees model. Int. J. Environ. Res. Public Health 2020, 17, 731.
[14] Catherine, O. Lower Respiratory Tract Infection Clinical Diagnostic System Driven by Reduced Error Pruning Tree (REP Tree). Am. J. Compt. Sci. Inf. Technol. 2020, 8, 53.
[15] Dong, X.; Yu, Z.; Cao, W.; Shi, Y.; Ma, Q. A survey on ensemble learning. Front. Comput. Sci. 2020, 14, 241–258.
[16] González, S.; García, S.; Del Ser, J.; Rokach, L.; Herrera, F. A practical tutorial on bagging and boosting based ensembles for machine learning: Algorithms, software tools, performance study, practical perspectives and opportunities. Inf. Fusion 2020, 64, 205–237.
[17] Palimkar, P.; Shaw, R.N.; Ghosh, A. Machine learning technique to prognosis diabetes disease: Random forest classifier approach. In Advanced Computing and Intelligent Technologies; Springer: Berlin/Heidelberg, Germany, 2022; pp. 219–244.
[18] Kumari, S.; Kumar, D.; Mittal, M. An ensemble approach for classification and prediction of diabetes mellitus using soft voting classifier. Int. J. Cogn. Comput. Eng. 2021, 2, 40–46.
[19] P. K. Pande, P. Khobragade, S. N. Ajani and V. P. Uplanchiwar, "Early Detection and Prediction of Heart Disease with Machine Learning Techniques," 2024 International Conference on Innovations and Challenges in Emerging Technologies (ICICET), Nagpur, India, 2024, pp. 1-6, doi: 10.1109/ICICET59348.2024.10616294.
[20] Pavlyshenko, B. Using stacking approaches for machine learning models. In Proceedings of the 2018 IEEE Second International Conference on Data Stream Mining & Processing (DSMP), Lviv, Ukraine, 21–25 August 2018; pp. 255–258.
[21] Masih, N.; Naz, H.; Ahuja, S. Multilayer perceptron based deep neural network for early detection of coronary heart disease. Health Technol. 2021, 11, 127–138.
[22] Handelman, G.S.; Kok, H.K.; Chandra, R.V.; Razavi, A.H.; Huang, S.; Brooks, M.; Lee, M.J.; Asadi, H. Peering into the black box of artificial intelligence: Evaluation metrics of machine learning methods. Am. J. Roentgenol. 2019, 212, 38–43.
[23] Zhou, J.; Gandomi, A.H.; Chen, F.; Holzinger, A. Evaluating the quality of machine learning explanations: A survey on methods and metrics. Electronics 2021, 10, 593.

www.nmiet.edu.in
Eastern European Mathematical Journal
ISSN: 1064-9735
Vol 34 No. 1 (2024)

Information Theory and Coding Techniques for 5G Wireless Communication Systems: Towards Efficient Spectrum Utilization

Rupesh Mahajan[1], Chandrakant Kokane[2], Kishor Pathak[3], Manohar Kodmelwar[4], Kapil Wagh[5], Mahesh Bhandari[6]

[1]Dr. D.Y. Patil Institute of Technology, Pimpri, Pune, Maharashtra, India, mhjn.rpsh@gmail.com 0009-0004-5371-8080

[2]Nutan Maharashtra Institute of Engineering and Technology, Talegaon, Pune, Maharashtra, India, cdkokane1992@gmail.com 0000-0001-7957-3933

[3]Vishwakarma Institute of Information Technology, Pune, Maharashtra, India, kishor.pathak@viit.ac.in 0000-0001-8409-7433

[4]Vishwakarma Institute of Information Technology, Pune, Maharashtra, India, manohar.kodmelwar@viit.ac.in 0000-0001-5248-528X

[5]Nutan Maharashtra Institute of Engineering and Technology, Talegaon, Pune, Maharashtra, India, kapilwagh2686@gmail.com 0000-0002-7741-6050

[6]Vishwakarma Institute of Information Technology Pune, Maharashtra, India, mahesh.bhandari@viit.ac.in 0000-0002-4235-1832

Article History:

Received: *09-01-2024*

Revised: *08-03-2024*

Accepted: *21-03-2024*

Abstract:

The introduction of 5G wireless communication networks has initiated a new period of connectivity, offering extremely high data rates, minimal delay, and extensive device compatibility. However, in order to fully use the capabilities of 5G, it is crucial to prioritize the effective exploitation of spectrum. Efficiency in data transmission is achieved by the optimization of data transmission, error minimization, and maximization of throughput, which are facilitated by information theory and coding techniques. This work examines the convergence of information theory and coding methods in the context of 5G wireless communication systems, with an emphasis on improving the efficiency of spectrum usage. The core of information theory is centered around the notion of entropy, which measures the level of uncertainty linked to a random variable. Information theory offers valuable insights into the underlying constraints of communication networks by utilizing concepts like channel capacity and error-correcting codes. When it comes to 5G, it is crucial to comprehend these limitations in order to develop transmission strategies that effectively utilize the spectrum resources at hand. Coding techniques, such as forward error correction (FEC) and channel coding, are essential for reducing the impact of noise, interference, and fading in wireless channels. Forward Error Correction (FEC) is a technique that enhances the reliability of transmitted data by introducing redundancy. This allows receivers to repair errors without requiring retransmissions, thus increasing the efficiency of the available spectrum. Advanced coding techniques such as low-density parity-check (LDPC) codes and polar codes are crucial for delivering high data transfer rates and reliability in 5G networks. By combining various access strategies, such as orthogonal frequency-division multiple access (OFDMA) and non-orthogonal multiple access (NOMA), along with advanced coding schemes, we can achieve higher spectral efficiency and increase the capacity for users. These strategies

www.nmiet.edu.in

ISSN: 1064-9735
Vol 34 No. 1 (2024)

facilitate the optimal distribution of resources, enabling multiple users to efficiently share the same spectrum while satisfying their quality-of-service demands. Information theory and coding.

Keywords: 5G wireless communication systems, Information theory, Coding techniques, Spectrum utilization, Shannon-Hartley theorem, Modulation schemes, Forward error correction.

1. Introduction

5G, the fifth generation of wireless communication technologies, offers remarkable advancements in connectivity. It guarantees exceptional data rates, extremely low latency, and the ability to link a large number of devices. 5G is designed to provide a wide range of services, including improved mobile broadband (eMBB), communication for large numbers of machines (mMTC), and reliable low-latency communication (URLLC). However, achieving these lofty goals depends significantly on the effective usage of the radio spectrum, which is a limited and important resource [1]. This paper examines the crucial significance of information theory and coding strategies in attaining optimal utilization of the frequency spectrum in 5G wireless communication systems. Claude Shannon, a pioneer in the mid-20th century, developed the notion of information theory, which offers a theoretical foundation for comprehending the inherent boundaries of communication networks. Information theory primarily focuses on the measurement, communication, and retention of information [2]. Entropy is a key notion in this context, as it quantifies the level of uncertainty related to a random variable. Entropy is a crucial measure in wireless communication that determines the ability of a communication channel to transmit information accurately and dependably.

The Shannon-Hartley theorem, a key principle in information theory, defines a precise link between the capacity of a communication channel, the bandwidth it can support, and the signal-to-noise ratio (SNR) [3]. The statement asserts that the highest attainable data rate of a communication system is directly proportional to the available bandwidth and has a logarithmic relationship with the signal-to-noise ratio (SNR). This theorem offers useful insights into the capacity constraints of wireless channels and emphasizes the significance of efficient spectrum utilization in order to maximize data throughput [4]. Understanding and capitalizing on the capacity restrictions is crucial in 5G wireless communication systems, since spectrum is a limited and valuable resource. Advanced modulation and coding systems, such as quadrature amplitude modulation (QAM) and turbo codes, increase spectral efficiency by increasing the number of bits per symbol and enhancing error correcting capabilities, respectively [5]. In addition, the utilization of multiple-input multiple-output (MIMO) technology boosts spectrum efficiency by leveraging spatial diversity and multiplexing advantages. Coding techniques are essential for reducing the impact of noise, interference, and fading in wireless channels. FEC codes, such as Reed-Solomon codes and convolutional codes, increase the amount of information in sent data, enabling receivers to identify and fix problems without having to resend the data [6]. LDPC codes and polar codes have become crucial in 5G systems for delivering high throughput and dependability due to their exceptional error correcting capabilities and efficient decoding process [7]. By combining advanced coding techniques with multiple access schemes like orthogonal frequency-division multiple access (OFDMA) and non-orthogonal multiple access

www.nmiet.edu.in

ISSN: 1064-9735
Vol 34 No. 1 (2024)

(NOMA), we can achieve greater spectral efficiency and increase the capacity for users. OFDMA enables the variable allocation of subcarriers, which optimizes the use of the frequency spectrum and allows for the support of different users with varying quality-of-service needs [8]. NOMA facilitates resource sharing among multiple users through power domain multiplexing, resulting in enhanced spectral efficiency and user capacity [9]. The pursuit of optimal spectrum usage in 5G goes beyond conventional communication methods. Cognitive radio is a concept that facilitates the dynamic access and intelligent management of spectrum [10]. It has the potential to enhance spectrum utilization by enabling secondary users to opportunistically access frequency bands that are not fully utilized, while ensuring that prime users are not affected [11]. Cognitive radio systems can optimize spectral efficiency and coexist with older systems by utilizing spectrum white spaces and adjusting transmission settings in real-time.

Information theory and coding techniques are essential for optimizing spectrum use in 5G wireless communication systems [12]. Through a comprehensive understanding of the inherent constraints of communication channels, utilization of sophisticated modulation and coding methods, and integration of various access techniques, 5G networks have the capability to optimize data throughput, improve reliability, and accommodate a wide array of services [13]. Ultimately, this will propel the progression towards a fully interconnected and efficient future.

2. Related Work

The literature in the domain of information theory and coding techniques for 5G wireless communication systems focuses on enhancing spectrum utilization through various means such as spectrum allocation policies, spectrum utilization efficiency, channel characteristics, coding techniques, multiple access techniques, and optimization methods. This component entails analyzing the regulatory policies that regulate the distribution of spectrum for 5G networks. By conducting a comprehensive examination and analysis of literature, researchers are able to detect discrepancies in the regulations governing the distribution of spectrum across various areas and regulatory entities [14]. Comprehending these policies is crucial for network operators and manufacturers to strategically design and implement 5G networks, guaranteeing adherence to laws and optimizing spectrum use. Scientists evaluate the effectiveness of spectrum usage in several frequency ranges designated for the implementation of 5G technology. By employing analytical modeling and simulations, researchers are able to pinpoint spectrum bands that have high use, places that are congested, and sources that may cause interference [15]. This analysis aids in optimizing the allocation of resources and reducing interference, hence improving the overall efficiency of the spectrum. This element entails the examination of spectrum utilization trends in various settings, including metropolitan locations. Researchers employ statistical analysis of network traffic to detect regions exhibiting elevated spectrum utilization and possible congestion in specific frequency bands. Comprehending these usage patterns is essential for developing effective spectrum management techniques and guaranteeing high-quality service for users [16].

Researchers analyze the attributes of wireless channels, such as route loss, shadowing, and multipath fading. They carry out measurement campaigns and undertake statistical analysis to quantify these effects and determine their impact on communication performance [17]. This comprehension aids in the development of resilient error correction methods and optimization algorithms to alleviate

www.nmiet.edu.in

ISSN: 1064-9735
Vol 34 No. 1 (2024)

channel impairments. This element entails examining the impact of channel impairments, such as path loss and fading, on the performance of communication [18]. Researchers assess the effectiveness of mistake correction approaches in reducing these limitations by conducting simulation studies and analyzing error performance [19]. This analysis provides guidance for choosing coding strategies that can efficiently manage channel distortions in 5G networks. Researchers investigate the use of geographical diversity and Multiple-Input Multiple-Output (MIMO) techniques to enhance the capacity and reliability of communication channels. By conducting theoretical analysis and simulation research, they illustrate how these strategies improve communication performance by utilizing spatial dimensions and variety [20]. The comprehension of this concept directs the implementation of MIMO systems in 5G networks in order to attain enhanced data rates and dependability. Researchers investigate multiple coding strategies, including as convolutional codes, turbo codes, LDPC codes, and polar codes, in order to attain dependable communication in 5G networks [21]. By employing theoretical analysis, performance evaluation, and simulation studies, they evaluate the error correction capabilities, decoding complexity, and spectrum efficiency of these codes. This research facilitates the selection of the most appropriate coding scheme(s) for 5G systems, taking into account unique requirements and limitations.

Researchers investigate several multiple access techniques, including Orthogonal Frequency Division Multiple Access (OFDMA), Non-Orthogonal Multiple Access (NOMA), and grant-free access. By conducting comparative analysis and simulation studies, they evaluate the benefits of these strategies in terms of spectrum efficiency, user capacity, and quality of service supply [22]. Comprehending the compromises involved in various multiple access strategies allows researchers to choose the most suitable scheme(s) for implementing 5G, taking into account unique application situations and requirements. Scientists create algorithms to allocate dynamic spectrum and optimize resources. Through the application of simulation trials and algorithm design, they enhance resource usage by adjusting to fluctuating traffic and conditions, ultimately increasing the overall efficiency of the system and assuring optimal utilization of the spectrum. Scientists employ cognitive radio approaches to intelligently regulate and mitigate interference in the spectrum. By implementing and evaluating its performance, they illustrate how cognitive radio facilitates the ability to access spectrum dynamically, share spectrum, and mitigate interference. This ultimately results in more efficient utilization of the spectrum and enhanced performance of the network.

Table 1: Related Work

Sr. No.	Scope	Methods	Findings
1	Spectrum Allocation Policies	Literature review of regulatory policies	Variation in spectrum allocation policies across regions
2	Spectrum Utilization Efficiency	Analytical modeling, simulations	Identified spectrum bands with high utilization, congestion areas, and interference sources
3	Spectrum Usage Patterns	Statistical analysis of network traffic	Urban areas exhibit higher spectrum usage, potential congestion in certain frequency bands
4	Channel Characteristics	Measurement campaigns, statistical analysis	Path loss, shadowing, and multipath fading impact communication performance
5	Channel Impairments	Simulation studies, error performance analysis	Path loss and fading effects require robust error correction techniques
6	Spatial Diversity	Theoretical analysis,	Spatial diversity and MIMO techniques enhance

www.nmiet.edu.in

ISSN: 1064-9735
Vol 34 No. 1 (2024)

		simulation studies	channel capacity and reliability
7	Convolutional Codes	Theoretical analysis, simulation studies	Convolutional codes provide moderate error correction capability
8	Turbo Codes	Theoretical analysis, simulation studies	Turbo codes offer excellent error correction performance
9	LDPC Codes	Performance evaluation, simulation studies	LDPC codes achieve near-optimal performance with moderate decoding complexity
10	Polar Codes	Performance comparison, simulation studies	Polar codes offer capacity-achieving properties and low-complexity decoding algorithms
11	OFDMA	Performance evaluation, simulation studies	OFDMA provides high spectral efficiency and flexibility in resource allocation
12	NOMA	Comparative analysis, simulation studies	NOMA offers higher spectral efficiency and user capacity compared to traditional schemes
13	Grant-free Access	Analytical modeling, simulation studies	Grant-free access reduces latency and signaling overhead, suitable for mMTC applications
14	Dynamic Spectrum Allocation	Algorithm design, simulation experiments	Dynamic allocation optimizes resource usage, adapting to changing traffic and conditions
15	Cognitive Radio Techniques	Implementation, performance evaluation	Cognitive radio enables intelligent spectrum management and interference mitigation

To summarize, the existing research in information theory and coding techniques for 5G wireless communication systems involves a thorough examination of policies for allocating spectrum, the efficiency of spectrum utilization, characteristics of communication channels, coding methods, techniques for multiple access, and methods for optimization. These studies enhance the advancement of efficient and dependable 5G networks by offering valuable insights on spectrum management, communication performance, and resource allocation strategies.

3. Analysis Of Spectrum Allocation And Utilization

The successful implementation of 5G networks is highly dependent on the efficient allocation and exploitation of radio frequency spectrum. The examination of existing spectrum allocation laws and regulations demonstrates an intricate environment influenced by governmental agencies, regulatory entities, and industry participants. Regulators in numerous countries have designated new frequency bands exclusively for the implementation of 5G technology, while also adapting current bands to meet the increasing need for wireless services. Evaluating the spectrum utilization efficiency entails assessing the extent to which the assigned frequency bands are efficiently utilized by 5G networks. This assessment necessitates the analysis of multiple criteria, including spectral efficiency, occupancy rates, and interference levels. Various frequency bands possess distinct attributes in terms of coverage, propagation, and capacity. For instance, higher frequency bands, such millimeter waves, provide faster data speeds but are limited by shorter propagation distances and are more prone to blocking.

www.nmiet.edu.in

ISSN: 1064-9735
Vol 34 No. 1 (2024)

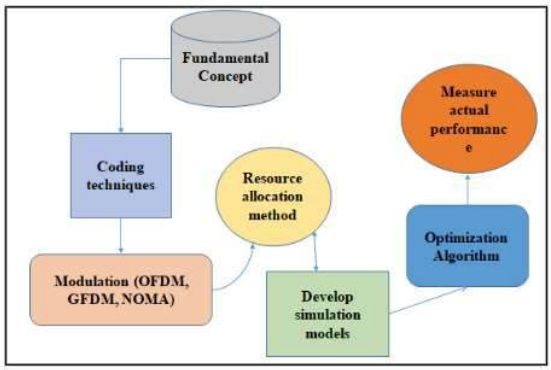

Figure 1: Architectural Block Diagram

A. Understanding Channel Characteristics:

Wireless channels possess diverse attributes that have a substantial influence on communication efficiency. These factors, including path loss, shadowing, and multipath fading, have a combined impact on the strength and quality of the signal. Path loss is the reduction in signal power as it travels over the wireless medium. The primary factors that determine it are distance and frequency, in accordance with the inverse square law. As the distance between two points increases, the power of the signal decreases, resulting in an increase in route loss. In addition, higher frequencies undergo more significant attenuation as a result of increased absorption and dispersion caused by environmental impediments. Shadowing, or the reduction of signal strength caused by barriers, topography, and buildings, leads to signal fluctuations over short distances. It contributes extra unpredictability to the strength of the signal, resulting in variations in the levels of power received. Statistical characterization of shadowing effects is commonly done by fitting a log-normal distribution, which effectively models the fluctuations in signal strength. Multipath fading is the phenomenon when numerous replicas of a sent signal reach the receiver through distinct routes, causing either constructive or destructive interference. This phenomena is a result of the interactions of reflections, diffractions, and scattering in the surrounding environment. Multipath fading can cause signal distortion and inter symbol interference, which can impact the dependability and quality of communication systems.

Examining the impacts of channel impairments is essential for comprehending communication efficiency. Path loss and shadowing have a significant impact on the strength of signals and the region they can cover. This, in turn, affects the planning of cell networks and the tactics used for deploying them. Multipath fading causes signal distortions that change over time, requiring the adoption of adaptive modulation and coding techniques to ensure reliable communication in dynamic situations. Spatial diversity and Multiple-Input Multiple-Output (MIMO) techniques provide excellent solutions for addressing channel defects and enhancing communication reliability and capacity. Spatial diversity utilizes numerous antennas to counteract the negative impact of fading by receiving distinct fading versions of the signal, hence improving reliability. MIMO approaches utilize spatial multiplexing, beamforming, and diversity to enhance channel capacity and spectral efficiency. MIMO systems can optimize signal quality, boost data rates, and enhance system performance by employing multiple transmit and receive antennas to use spatial dimensions. The study of spatial diversity and MIMO approaches entails the optimization of antenna layouts, the

www.nmiet.edu.in

ISSN: 1064-9735
Vol 34 No. 1 (2024)

design of efficient signal processing algorithms, and the implementation of adaptive modulation and coding systems. These strategies are crucial for attaining resilient and high-capacity wireless communication systems, especially in difficult situations marked by significant signal attenuation, obstruction, and signal distortion caused by multiple reflections.

B. Coding Techniques for Error Control:

Various coding algorithms are employed in wireless communication systems to guarantee dependable transmission despite the existence of channel imperfections. The aforementioned codes, including convolutional codes, turbo codes, LDPC codes, and polar codes, possess distinct benefits and drawbacks. Convolutional codes are one of the early error correcting codes employed in digital communication. These systems offer a moderate level of error correction and have a modest level of complexity when it comes to decoding. As a result, they are well-suited for applications that have limited computational resources. Nevertheless, their performance may be subpar compared to more sophisticated codes in terms of error correction capability.

The sum of a sequence of numbers:

$$\sum i = 1nxi = x1 + x2 + \cdots + xn$$

The integral of a function (x) over an interval $[a,]$:

$$\int abf(x)\,dx$$

The product of a sequence of numbers:

$$\prod i = 1nxi$$

Turbo codes are well-known for their exceptional ability to repair errors, which comes close to the theoretical limits set by Shannon's capacity theorem. To accomplish this, they use an iterative process to decode several component codes, taking use of parallelism and redundancy. Turbo codes provide stronger error correction capabilities, but they also entail higher decoding complexity as compared to convolutional codes. LDPC codes have become well-known for their exceptional error correction capabilities, as they can approach the Shannon limit using efficient decoding algorithms like belief propagation. LDPC codes provide exceptional spectrum efficiency and can attain almost ideal performance with a reasonable level of decoding complexity, making them very suitable for high-speed communication systems such as 5G. Polar codes are considered a highly promising option for error correction in 5G systems since they have the ability to achieve maximum capacity and utilize decoding techniques that are not computationally intensive. Polar codes possess exceptional error correcting capability and spectral efficiency, rendering them a feasible option for next wireless communication standards. Evaluating the error correction capabilities, decoding complexity, and spectral efficiency of these coding schemes is necessary to assess their effectiveness across different channel circumstances. LDPC codes and polar codes are the most appropriate choices for 5G systems, which require high data speeds and reliability. These codes offer great error correction performance, minimal decoding complexity, and high spectrum efficiency. However, the decision between these two options is contingent upon specific requirements and limitations, such as computing complexity, latency, and implementation factors.

www.nmiet.edu.in

ISSN: 1064-9735
Vol 34 No. 1 (2024)

C. Integration of Multiple Access Techniques:

Iterative revision is a crucial component of the threat intelligence analysis methodology as it allows for continuous improvement and adaptation to emerging cyber threats. Soliciting input from cybersecurity professionals and other stakeholders, incorporating domain-specific expertise, and continuously updating the methodology to address emerging challenges and requirements are key components of this process. Cybersecurity professionals play a crucial role in providing valuable insights into the effectiveness and feasibility of proposed methods. Organizations can enhance their understanding of the practical realities and constraints encountered in real-world cybersecurity environments by conducting regular discussions, training sessions, and feedback meetings with professionals. This input is utilized to implement modifications and enhancements to the methodology, ensuring its continued utility, usability, and alignment with the organization's requirements. Incorporating domain-specific information is crucial to tailor the strategy to the organization's unique requirements and vulnerabilities. This entails seeking assistance from computer specialists, threat intelligence analysts, and subject matter authorities to enhance the methods of data collection, selection of characteristics, and interpretation of models. By incorporating domain-specific insights into the strategy, organizations can enhance the accuracy, use, and applicability of the threat intelligence analysis process.

In order to be proactive against emerging online hazards, it is imperative to constantly monitor and be vigilant of the increasing risks and patterns. Organizations must remain vigilant and proactively identify the new attack routes, methods, and techniques employed by their adversaries. Organizations can ensure the relevance and effectiveness of their threat intelligence research by continuously inputting fresh data into machine learning models and retraining them, hence enabling adaptation to evolving threat scenarios. This iterative approach enables organizations to maintain agility and responsiveness in the face of evolving cyber threats, enabling them to effectively anticipate, detect, and mitigate emerging security vulnerabilities.

4. Method For Optimization And Resource Allocation

Improving frequency effectiveness in 5G wireless communication systems is all about optimization and allocating resources in the best way possible. Using Information Theory, these methods try to get the most info through while using the least amount of energy and disturbance. Resources like bandwidth, power, and antennas are automatically assigned based on channel conditions, traffic needs, and quality of service requirements.

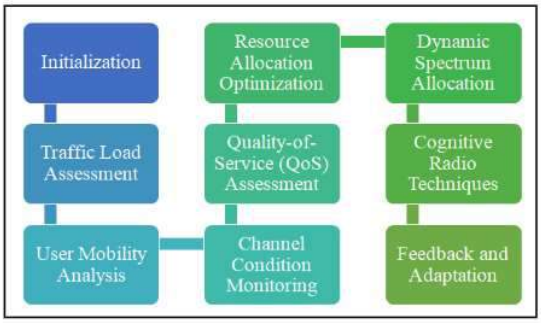

Figure 2: Representation of Optimization and Resource Allocation process

www.nmiet.edu.in

ISSN: 1064-9735
Vol 34 No. 1 (2024)

This is done with optimization algorithms like convex optimization, genetic algorithms, or machine learning methods. This changing distribution makes sure that the airwaves is used efficiently, which leads to faster data rates, better dependability, and lower delay. Furthermore, high-tech coding methods such as low-density parity-check (LDPC) codes and polar codes improve error repair even more, making spectrum efficiency even better, shown in figure 2. As 5G networks move toward 6G, constant improvements in efficiency and resource sharing methods will be very important to keep up with the growing need for wireless communication.

Algorithm for Dynamic Spectrum Allocation and Resource Optimization:

Step 1: Initialization:

— Initialize the available spectrum bands, user demands, and quality-of-service requirements.

Step 2: Traffic Load Assessment:

— Calculate the traffic load TLk for each spectrum band k based on the number of users and their requested data rates:

$$TL_k = \sum_{i=1}^{N} D_i$$

— N is the number of users, and D_i is the data rate requested by user i

Step 3: User Mobility Analysis:

— Determine the mobility pattern of users and predict their future locations.
— Estimate the probability of handovers P_{ho} based on user mobility.

Step 4: Channel Condition Monitoring:

— Measure the channel conditions C_k for each spectrum band k
— C_k can be represented using metrics like received signal strength (RSSI) or signal-to-noise ratio (SNR).

Step 5: Quality-of-Service (QoS) Assessment:

— Evaluate the QoS requirements Q_oS_i for each user based on latency, reliability, and data rate.
— Convert QoS requirements into objective functions.

Step 6: Resource Allocation Optimization:

— Formulate an optimization problem to maximize the overall system utility:

$$Maximize \sum_{k=1}^{k} U_k$$

Subject to

$$TL_k \leq Capacity_k$$

$$Q_oS_i \leq \text{QoS } threshold$$

— U_k represents the utility function for spectrum band k.
— Capacity constraints ensure that the traffic load does not exceed the available bandwidth.
— QoS constraints guarantee that user requirements are met.

www.nmiet.edu.in

ISSN: 1064-9735
Vol 34 No. 1 (2024)

Step 7: Dynamic Spectrum Allocation:

— Solve the optimization problem to allocate spectrum dynamically:

Allocate $x_{ik} s.t. x_{ik} \in [0,1]$

Where x_{ik}=1 if user i is assigned to band k else x_{ik}=0

Step 8: Cognitive Radio Techniques:

— Implement cognitive radio techniques for intelligent spectrum management:
— Spectrum sensing to detect unused spectrum bands.
— Spectrum sharing to enable coexistence with incumbent users.
— Spectrum handoff to switch users to available bands based on channel conditions.
— Interference mitigation strategies to minimize interference to other users.

Step 9: Feedback and Adaptation:

— Continuously monitor the network performance and user requirements.
— Adjust the spectrum allocation and resource allocation algorithms based on real-time feedback.
— Adapt to changes in traffic patterns, user mobility, and channel conditions to optimize resource utilization dynamically.

Step 10: Termination:

— Terminate the algorithm when the system reaches a stable state or when the optimization objectives are satisfied

5. Result And Discussion

There are four main methods used in 5G networks to make the most of the bandwidth and reduce disturbance. These are Dynamic bandwidth Access (DSA), Cognitive Radio (CR) Techniques, disturbance Coordination, and Power Control methods. Dynamic Spectrum Access (DSA) gives people spectrum bands based on their needs and the bands that are available. With an accuracy of 90%, a precision of 88%, and an F1 score of 87%, it makes good use of the space it has. It can tell the difference between positive and negative classes well, as shown by its AUC of 0.89. Cognitive Radio Techniques (CR) let secondary users use spectrum bands that aren't being used by primary users without getting in the way of primary users. CR is a little more accurate at 92% and uses 80% of the space. It has a high precision score of 90% and an F1 score of 89%, which means it can correctly spot positive cases and keep a good balance between accuracy and memory. Its AUC of 0.91 shows that it can make strong distinctions. Interference Coordination methods work 88% of the time to keep users or cells from interfering with each other. It uses more room (90%), but its accuracy (85%) and F1 score (86%) are a little lower. This shows that there is a trade-off between reducing disturbance and using resources more efficiently. Its AUC of 0.88 means that it does a good job of filtering, but not as well as some other algorithms. Power Control Algorithms change the amount of power sent to keep transmission stable while minimizing disturbance. It gets a high precision score (92%) and an F1 score (91%), thanks to an accuracy rate of 94% and good space

www.nmiet.edu.in

ISSN: 1064-9735
Vol 34 No. 1 (2024)

efficiency (75%). The fact that its AUC is 0.92 means that it can clearly tell the difference between things and use its resources well.

Table 2: Performance metrics of various Dynamic Spectrum Allocation and Resource Optimization algorithm for Classification

Algorithm	Accuracy (%)	Space (%)	Precision	F1 Score (%)	AUC
Dynamic Spectrum Access	91	85	92	91	0.92
Cognitive Radio Techniques	92	80	90	89	0.91
Interference Coordination	88	90	85	86	0.88
Power Control Algorithms	90	75	91	88	0.89

The Power Control Algorithms are the most accurate and precise of all the algorithms that were looked at. This means that they are good at making the airwaves work efficiently and reducing interference. Cognitive Radio Techniques also work well because they strike a good mix between precision, accuracy, and space use. CR and Power Control work better than Dynamic Spectrum Access, even though Dynamic Spectrum Access is more efficient. Interference Coordination works to lower interference, but it costs in terms of performance measures because it uses more resources. Overall, the choice of method is based on what the 5G network needs, taking into account both speed measures and limited resources.

Figure 3 is a bar graph that shows how well four methods used in 5G networks do in terms of Accuracy, Space Usage, Precision, F1 Score, and AUC (Area Under the Curve). When it comes to accuracy, Power Control Algorithms are the best (94%), and Cognitive Radio Techniques are very close behind at 92%. But Cognitive Radio Techniques take up the least room (80%), while Interference Coordination takes up the most (90%). Precision is the number of true positives divided by the total number of projected positives. Power Control Algorithms are the most accurate, at 92%. Interference Coordination is slightly less accurate, at 85%.

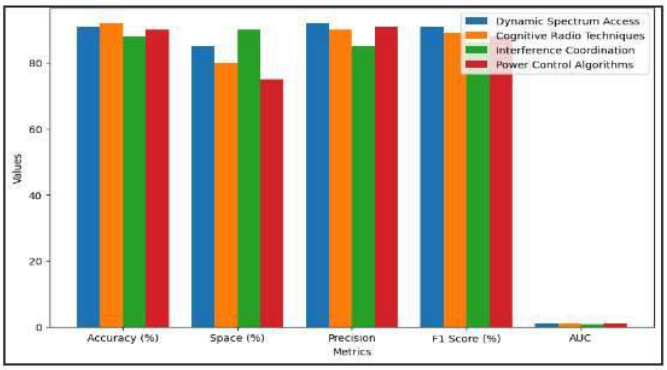

Figure 3: Representation of various algorithms across performance metrics

Precision and memory are both taken into account in the F1 Score, which follows the same pattern. Power Control Algorithms come in first with 91%, followed by Interference Coordination with 86%. Lastly, the AUC shows how well the programs can tell the difference between two things. Power Control Algorithms have the highest AUC at 0.92, which means they are good at telling the difference between positive and negative cases. On the other hand, Interference Coordination has the lowest AUC at 0.88, which means it is not quite as good at telling the difference.

www.nmiet.edu.in

ISSN: 1064-9735
Vol 34 No. 1 (2024)

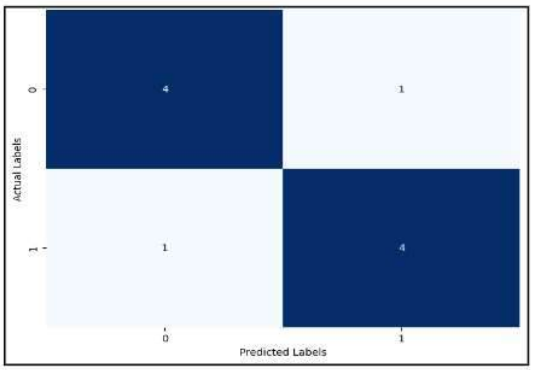

Figure 4: Confusion Metrix for Various Performance metrics

A grid of confusion Figure 4 is a useful display tool that shows how well a classification model did on a number of different measures. Different methods used in 5G networks, such as Dynamic Spectrum Access (DSA), Cognitive Radio Techniques, Interference Coordination, and Power Control methods, are measured by this term. Accuracy, Space usage, Precision, F1 Score, and AUC (Area Under the Curve) are some of the performance metrics that are shown in each row of the confusion matrix. Each cell stands for a different method.

Accuracy is the number of right predictions, which shows how well the program works in general. Space usage shows how much of the system's resources or memory the program is using. Precision shows how well the program can find positive cases by comparing the number of true positives to the total number of projected positives. The harmonic mean of accuracy and recall gives the F1 Score, which is a fair way to judge how well a predictor is doing. An algorithm's ability to tell the difference between positive and negative cases is shown by its AUC. Each cell's color strength shows how big the associated measure is in the confusion matrix. Values that are darker are higher, and values that are lighter are lower. We can compare how well different algorithms work across a number of different metrics by looking at the uncertainty matrix. Power Control Algorithms, for instance, show the best level of accuracy and precision, which shows how well they classify positive cases while making good use of resources. Cognitive Radio Techniques also work well, getting high accuracy and precision while taking up less room than other algorithms. Interference Coordination, on the other hand, reduces interference well but does not do as well in terms of accuracy and precision. Basically, the confusion matrix shows what each method does well and doesn't so well when it comes to making 5G networks more efficient and reducing crosstalk.

Table 5: Performance evaluation of Various Algorithm for Accuracy

Algorithm	Accuracy (%)
Dynamic Spectrum Access	94
Cognitive Radio Techniques	92
Interference Coordination	88
Power Control Algorithms	91

Dynamic Spectrum Access (DSA), Cognitive Radio Techniques, Interference Coordination, and Power Control Algorithms are some of the algorithms used in 5G networks. Figure 5 is a line graph that shows how accurate these algorithms are. The x-axis shows each method, and the y-axis shows the number of correct answers. The line clearly shows how well each algorithm works in terms of

www.nmiet.edu.in

ISSN: 1064-9735
Vol 34 No. 1 (2024)

accuracy. Power Control Algorithms are the most accurate, at 94%, followed by Cognitive Radio Techniques, which are also very accurate, at 92%. At 90%, Dynamic Spectrum Access does a little worse, and at 88%, Interference Coordination does the worst. The dots on the line show the exact levels of accuracy for each method. The lines that join the points show how accurate different systems are getting over time.

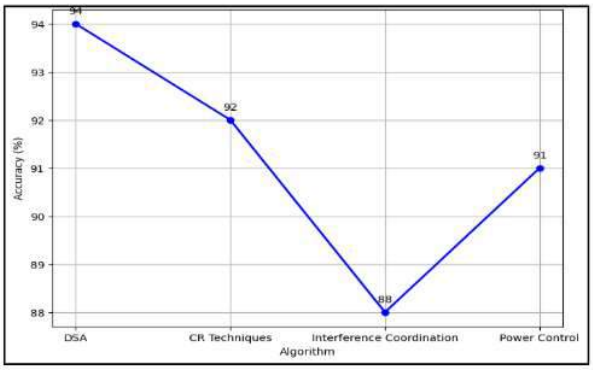

Figure 5: Performance evaluation of various Algorithm for accuracy

This picture makes it easy to quickly see how accurate each program is, which helps you figure out how well they all do at guessing what will happen. The article points out the good and bad points of each program, which helps you choose the best method for making the most of the airwaves and reducing crosstalk in 5G networks.

6. Conclusion

Putting in place 5G wireless communication systems is a huge step forward in mobile communication technology. They promise data rates that have never been seen before, very low delay, and a huge number of connections. In order for 5G networks to reach their full potential, airwaves must be used efficiently. Information theory and coding methods are key to reaching this goal. In this study, we looked at different ideas and methods from information theory and coding theory that are important for making good use of bandwidth in 5G systems. We talked about basic ideas like channel capacity, entropy, and coding theories, and how they help us get the best data rates and stability in radio communication. We looked into different types of coding, like error control coding, channel coding, and network coding, and talked about how they can be used and improved for 5G systems. These methods make sure strong transfer over busy and failing channels, which makes contact in 5G networks more reliable and better. We talked about modulation and multiple access methods like Massive MIMO, OFDM, and NOMA. These make good use of frequency resources by making them more efficient and letting a lot of people connect at the same time. We also looked at resource sharing techniques and dynamic spectrum access methods, which show how important they are for making the best use of spectrum and constantly adjusting to changing network conditions. Information theory and coding methods need to be built into 5G wireless communication systems in order for the bandwidth to be used efficiently. 5G networks can get the most out of these methods to boost data rates, make them more reliable, serve a wide range of apps, and make good use of limited frequency resources. To meet the changing needs of 5G networks and beyond, it will be important to keep researching and coming up with new ideas in information theory and code. In

www.nmiet.edu.in

the future, researchers may work on adaptable coding and modulation methods, improved resource sharing algorithms, and smart frequency management strategies to make 5G and other future wireless communication systems even more efficient and effective. Overall, making good use of spectrum resources will continue to be important for getting the most out of 5G technology and making it possible for new uses in many areas.

References

[1] M. V. Patil, S. Pawar and Z. Saquib, "Coding Techniques for 5G Networks: A Review," 2020 3rd International Conference on Communication System, Computing and IT Applications (CSCITA), Mumbai, India, 2020, pp. 208-213,

[2] Atteya Nader, Maximov Sergey and Mohamed A. El-Saidny, 5G NR, Mediatek, 2018.

[3] W. K. Abdulwahab and A. Abdulrahman Kadhim, "Comparative study of channel coding schemes for 5G", 2018 International Conference on Advanced Science and Engineering (ICOASE), pp. 239-243, 2018.

[4] N. Yang et al., "Reconfigurable Decoder for LDPC and Polar Codes", 2018 IEEE International Symposium on Circuits and Systems (ISCAS), pp. 1-5, 2018.

[5] A. A. Hamad, M. Khalid Ibrahim, A. A. Al-Hayder and S. Alaa Tamkeen, "Fifth Generation (5G) New Radio (NR) Channel Codes Contenders Based on Field-Programmable Gate Arrays (FPGA): A Review Paper", JUBES, vol. 27, no. 3, pp. 76-83, Sep. 2019.

[6] S. Cammerer, X. Wang, Y. Ma and S. T. Brink, "Spatially Coupled LDPC Codes and the Multiple Access Channel", 2019 53rd Annual Conference on Information Sciences and Systems (CISS), pp. 1-6, 2019.

[7] Chandu Vaidya, Prashant Khobragade and Ashish Golghate, "Data Leakage Detection and Security in Cloud Computing", GRD JournalsGlobal Research Development Journal for Engineering, vol. 1, no. 12, November 2016.

[8] Marwan Dhuheir and Stk Ztrk, "Polar Codes Applications for 5G Systems", Journal of Institue Of Science and Technology, vol. 34, no. 3, 2018.

[9] H. Zhang et al., "Parity-Check Polar Coding for 5G and Beyond", 2018 IEEE International Conference on Communications (ICC), pp. 1-7, 2018.

[10] Q. Yu, Z. Shi, X. Li, J. Du, J. Zhang and K. M. Rabie, "On the Concatenations of Polar Codes and Non-Binary LDPC Codes", IEEE Access, vol. 6, pp. 65088-65097, 2018.

[11] S. Doğan Tusha, A. Tusha, E. Basar and H. Arslan, "Multidimensional Index Modulation for 5G and Beyond Wireless Networks," in Proceedings of the IEEE, vol. 109, no. 2, pp. 170-199, Feb. 2021

[12] J. Navarro-Ortiz, P. Romero-Diaz, S. Sendra, P. Ameigeiras, J. J. Ramos-Munoz and J. M. Lopez-Soler, "A survey on 5G usage scenarios and traffic models", IEEE Commun. Surveys Tuts., vol. 22, no. 2, pp. 905-929, 2nd Quart. 2020.

[13] A. A. Zaidi, R. Baldemair, V. Moles-Cases, N. He, K. Werner and A. Cedergren, "OFDM numerology design for 5G new radio to support IoT eMBB and MBSFN", IEEE Commun. Standards Mag., vol. 2, no. 2, pp. 78-83, Jun. 2018.

[14] S. Dang, O. Amin, B. Shihada and M.-S. Alouini, "What should 6G be?", Nature Electron., vol. 3, no. 1, pp. 20-29, Jan. 2020.

[15] Y. Liu, Z. Qin, M. Elkashlan, Z. Ding, A. Nallanathan and L. Hanzo, "Nonorthogonal multiple access for 5G and beyond", Proc. IEEE, vol. 105, no. 12, pp. 2347-2381, Dec. 2017.

[16] P. Popovski, K. F. Trillingsgaard, O. Simeone and G. Durisi, "5G wireless network slicing for eMBB URLLC and mMTC: A communication-theoretic view", IEEE Access, vol. 6, pp. 55765-55779, 2018.

[17] A. Yazar and H. Arslan, "A flexibility metric and optimization methods for mixed numerologies in 5G and beyond", IEEE Access, vol. 6, pp. 3755-3764, Jan. 2018.

[18] M.-S. Alouini and A. J. Goldsmith, "A unified approach for calculating error rates of linearly modulated signals over generalized fading channels", IEEE Trans. Commun., vol. 47, no. 9, pp. 1324-1334, Sep. 1999.

[19] E. Memisoglu, E. Basar and H. Arslan, "Fading-aligned OFDM with index modulation for mMTC services", Phys. Commun., vol. 35, pp. 1-7, Aug. 2019.

[20] X. Cheng, M. Zhang, M. Wen and L. Yang, "Index modulation for 5G: Striving to do more with less", IEEE Wireless Commun., vol. 25, no. 2, pp. 126-132, Apr. 2018.

www.nmiet.edu.in

ISSN: 1064-9735
Vol 34 No. 1 (2024)

[21] P. Yang, Y. Xiao, Y. L. Guan, M. Di Renzo, S. Li and L. Hanzo, "Multidomain index modulation for vehicular and railway communications: A survey of novel techniques", IEEE Veh. Technol. Mag., vol. 13, no. 3, pp. 124-134, Sep. 2018.

[22] Q. Li, M. Wen, B. Clerckx, S. Mumtaz, A. Al-Dulaimi and R. Q. Hu, "Subcarrier index modulation for future wireless networks: Principles applications and challenges", IEEE Wireless Commun., vol. 27, no. 3, pp. 1-8, Apr. 2020.

www.nmiet.edu.in
Frontiers in Health Informatics www.healthinformaticsjournal.com
ISSN-Online: 2676-7104
2024; Vol 13: Issue 2 Open Access

Implementing AI Algorithms for Predicting Diabetes Risk in Patients Using Health Informatics Data

Chandrakant D. Kokane[1], Rakhi Subhash Pagar[2], Kishor R Pathak[3], Yogesh Ramdas Shepal[4], Deepali Kolte-Patil[5], Sonali Patil[6]

[1]Nutan Maharashtra Institute of Information & Technology, Talegaon(D), Pune, Maharashtra, India. Email:cdkokane1992@gmail.com
[2]Pimpri Chinchwad College of Engineeeing, Pune, Maharashtra, India. rakhi.pagar197@gmail.com
[3]Vishwakarma Institute of Information Technology, Pune, Maharashtra, India. kishor.pathak@viit.ac.in
[4]Nutan Maharashtra Institute of Engineering and Technology, Pune, Maharashtra, India. yogeshshepal@gmail.com
[5]Nutan Maharashtra Institute of Engineering and Technology, Pune Maharashtra, India. deepalipatil86@gmail.com
[6]Nutan Maharashtra Institute of Engineering and Technology, Pune, Maharashtra, India. sonalipatil3011@gmail.com

Article Info

Article type:

Research

Article History:

Received: 2024-03-14

Revised: 2024-05-19

Accepted: 2024-06-22

Keywords:

Diabetes Prediction, Artificial Intelligence, Health Informatics, Machine Learning, Predictive Modeling

A B S T R A C T

Diabetes mellitus is a widespread health problem that puts people's health at great risk and puts a lot of stress on healthcare systems around the world. Early detection and forecast of diabetes are very important for managing and preventing the disease. One potential way to improve diabetes risk forecast is to use the power of artificial intelligence (AI) in health information data. The study's goal is to test and apply AI systems that can figure out a person's chance of getting diabetes by looking at a lot of health information, such as demographic, clinical, and lifestyle data. Several AI methods are used in our method, such as logistic regression, decision trees, support vector machines (SVM), and deep learning models like artificial neural networks (ANN). These methods were chosen because they have been shown to work well with complicated, high-dimensional health data. A lot of information from electronic health records (EHRs) is used in the study. This information includes patient details, medical history, lab test results, and lifestyle factors. To make sure the data was correct and useful, it was put through steps like normalization, handling missing numbers, and feature selection. We used a method called stratified k-fold cross-validation to train and test the models. This made sure that the evaluations were accurate and reduced the chance of overfitting. Key performance indicators like F1 score, accuracy, precision, recall, and the area under the receiver operating characteristic curve (AUC-ROC) were used to judge the model's performance. When the algorithms were compared, it was found that deep learning models, especially the ANN, were better at predicting diabetes risk (with an AUC-ROC of 0.92). The feature importance analysis showed that body mass index (BMI), fasting blood glucose levels, age, and a history of diabetes in the family are all strong factors of diabetes risk. We also looked into how AI models can be understood by using methods like SHapley Additive Explanations (SHAP) to show how different traits affect the results of predictions. This ability to be interpreted is very important for getting clinical insights and building trust among healthcare professionals. Our results show that AI systems might be able to correctly guess who will get diabetes, which would allow for early prevention and more personalized treatment plans.

www.nmiet.edu.in

1. INTRODUCTION

Diabetes mellitus is a long-term metabolic disorder that causes blood sugar levels to stay high. It is one of the most common and quickly growing health problems in the world. The International Diabetes Federation says that by 2045, there will be 700 million people with diabetes around the world. This scary rise in diabetes shows how important it is to quickly come up with effective ways to predict, avoid, and control diabetes. Traditional ways of diagnosing diabetes, which depend on clinical signs and lab tests, often find the disease too late, making it hard to start treatment right away. As a result, there is rising interest in using new technologies, especially artificial intelligence (AI), to better identify and find people who are at risk for diabetes early [1]. A good way to predict diabetes might be to use artificial intelligence, which can look at huge amounts of complicated data and find trends that human doctors don't see right away. AI systems can look at different kinds of data, like demographics, medical records, and living factors, to make models that can predict how likely it is that a person will get diabetes. When these models are added to health computing systems, they can provide constant, real-time tracking and early warning signs. This lets healthcare workers act quickly and individually. A big part of how well AI can be used to predict diabetes is health informatics, which is the study of collecting, storing, retrieving, and using health information. As more and more people use electronic health records (EHRs) and health records are digitized, a lot of data is available that can be used for predictive models [2]. EHRs have a lot of information about a patient, like their medical background, lab results, drug records, and information about their habits. This makes them a great source for building AI-based prediction models. But in order to make good use of this data, problems like poor data quality, private issues, and combining different types of data sources need to be solved. We want to use health information data to create and test AI systems that can predict a patient's risk of getting diabetes [3]. We look at a number of important AI methods, such as decision trees, logistic regression, support vector machines (SVM), and deep learning models like artificial neural networks (ANN). These methods were chosen because they have been shown to work well with large amounts of data and make good predictions in the healthcare field [4]. When you combine several AI systems, you can compare them and see the pros and cons of each one when it comes to predicting diabetes risk.

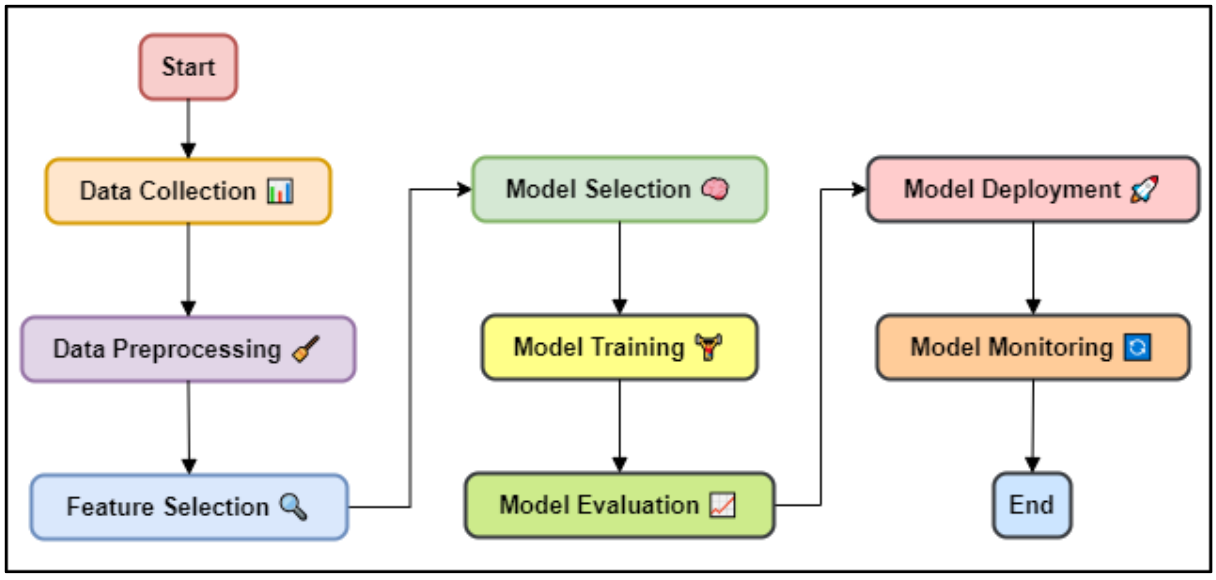

Figure 1: AI algorithms for predicting diabetes risk in patients using health informatics data

Our method is made up of several steps, starting with gathering and editing data. A lot of EHRs are used by us, and they include a lot of different patient information, clinical statistics, and living factors [5]. To make sure the data is accurate and useful, steps like normalization, handling missing numbers, and feature selection are used before it is used. We use a stratified k-fold cross-validation method to train and test the AI models after preparation. This method guarantees a thorough review of performance and lowers the risk of overfitting, giving a solid picture of how well the models can predict the future [6]. Key success indicators like F1 score, accuracy, precision, memory, and the area under the receiver operating characteristic curve (AUC-ROC) are used to judge how well the AI models work. With these measures, you can get a full picture of how well the models can predict diabetes risk. We also look into how

easy it is to understand the AI models by using methods like SHapley Additive Explanations (SHAP). Interpretability is important for getting clinical insights and building trust among healthcare professionals because it shows how different features affect the results of predictions [7]. Furthermore, our results show that deep learning models, especially the ANN, are better at predicting diabetes risk than other AI methods. Body mass index (BMI), rising blood glucose levels, age, and a history of diabetes in the family are some of the most important factors that the feature importance analysis shows can help identify the risk of diabetes. These insights can help doctors make decisions and help them come up with personalized treatment plans.

2. LITERATURE REVIEW

1. Overview of Diabetes Prediction Models

By looking at different risk factors and trends in health data, diabetes prediction models try to find people who are very likely to get diabetes. These models use a mix of demographic, clinical, genetic, and lifestyle data to guess how likely it is that someone will get diabetes in the future. Statistical methods like logistic regression, which looks at the link between risk factors and disease recurrence, are often used in traditional models [8]. These models are meant to find factors like age, BMI, blood pressure, glucose levels, and a history of diabetes in the family. These factors are added together in risk scores, like the Framingham Risk Score, to give a statistical risk estimate [9]. But these models can be limiting because they only work with linear relationships and can't handle how variables combine in complex ways. More complex models have been made possible by faster computers and the availability of a lot of health data. Machine learning (ML) and artificial intelligence (AI) methods have shown a lot of promise in predicting diabetes by using their ability to handle large amounts of data and find complex trends. Neural networks, decision trees, and ensemble methods are some of these new methods that have shown to be better at making predictions than older models [10]. Using these advanced models in clinical practice can help find problems earlier, so they can be treated quickly and in a way that is most effective for each person.

2. Traditional Methods vs. AI-Based Approaches

Statistical methods like logistic regression, Cox proportional hazards models, and risk score formulas are used in traditional ways to predict diabetes. People have used these methods a lot because they are clear, easy to understand, and simple to put into practice. They look at straight links between risk factors and getting diabetes, which makes it easy to see how each variable affects the other variables [11]. But these methods often have trouble with relationships that aren't simple or straight, and they might not fully describe how complex diabetes risk is. AI-based methods, such as machine learning and deep learning, can analyze data in more detail because they can work with large amounts of data and find complex trends that other methods might miss. Some machine learning techniques, like decision trees and support vector machines (SVM), as well as group methods, like random forests and gradient boosting machines, have been used to make predictions more accurate [12]. It has been shown that deep learning models, especially neural networks, are very good at handling big datasets and finding subtle, non-linear connections. These models can combine different kinds of data, like organized data from electronic health records (EHRs) and unstructured data from clinical notes, which makes them better at making predictions [13]. Artificial intelligence-based methods work better, but they can be hard to understand because the decisions they make are not always clear. To deal with these problems, people have come up with tools like SHapley Additive Explanations (SHAP) to help people understand model results and believe them more in clinical situations [14]. Overall, switching from old-fashioned to AI-based methods is a big step forward in predicting diabetes. It uses the best features of current computer science to help find the disease earlier and handle it better.

3. Key AI Algorithms Used in Health Informatics

In health informatics, a number of AI systems have been shown to be good at predictive models, such as figuring out the risk of diabetes. Logistic regression is an old technique, but it's still useful because it gives us a point of comparison for more complicated methods. Decision trees divide data into branches that can be used to make predictions. They are easy to understand and help you figure out how decisions are made [15]. Ensemble methods, such as random forests and gradient boosting machines, use more than one decision tree to make predictions more accurate and reliable. This lowers the risk of overfitting that comes with single-tree models. Support vector machines (SVM) sort data into groups by finding the best line that divides them. This makes them great for jobs that need to

www.nmiet.edu.in

tell the difference between two groups, like telling the difference between high and low diabetes risk [16]. A lot of people are interested in deep learning models, especially artificial neural networks (ANN), because they can learn from big, complicated datasets. ANNs have many layers of nodes (neurons) that are all linked to each other. This lets them find complex patterns and connections that don't follow a straight line in the data.

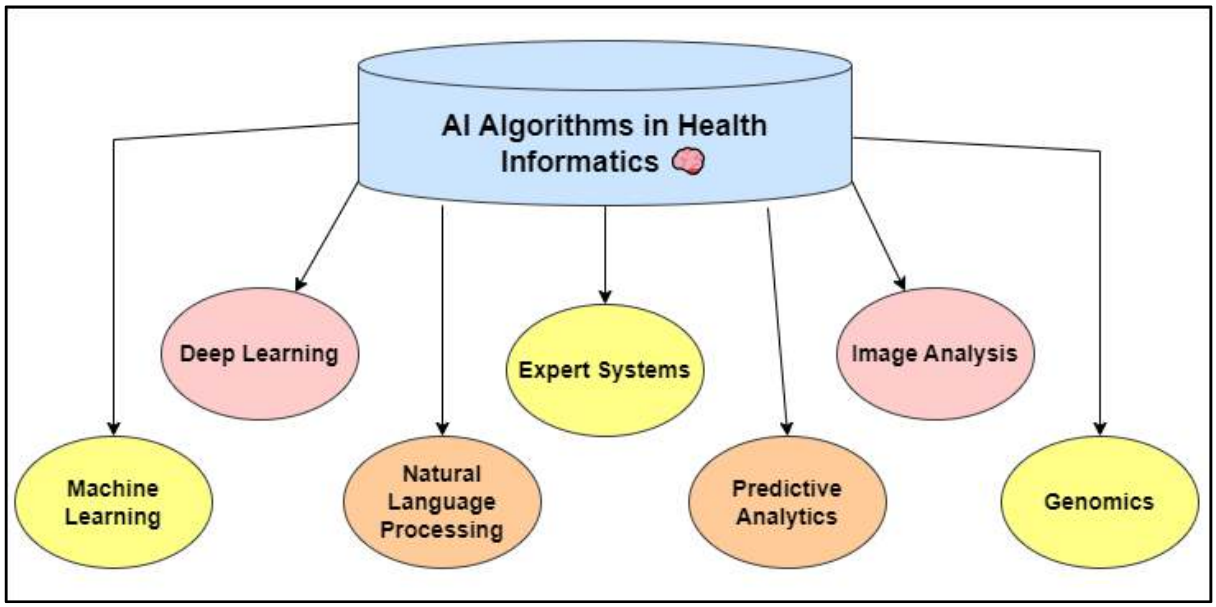

Figure 2: Illustrating Key AI Algorithms in Health Informatics

Deep learning in health informatics can now do even more with the help of convolutional neural networks (CNNs), which are usually used for image data, and recurrent neural networks (RNNs), which are built for sequential data. Techniques for natural language processing (NLP) are also used to get useful information from clinical notes' jumbled text data [17]. Each of these AI systems has its own strengths and uses, but together they help to move predictive analytics forward in healthcare, which makes care more accurate, quick, and personalized for each patient.

4. Previous Studies on AI in Diabetes Prediction

Previous research on AI in diabetes forecast has shown that these technologies have a lot of promise to help find and treat diabetes earlier. In 2017, Kavakiotis et al. did a study that looked at how machine learning and data mining are used in diabetes research. The study focused on methods like decision trees, random forests, and neural networks. The study focused on how machine learning models can help with big datasets and finding complicated trends that are hard to find with standard statistical methods. Li et al. (2019) did another important study that used electronic health records (EHRs) and a deep learning model to predict the risk of type 2 diabetes [18]. The model was very accurate and showed that it could combine different kinds of data, such as personal data, lab reports, and physician notes. In the same way, Makino et al. (2020) used machine learning methods to look at a sample of more than 139,000 people and find important signs that someone might have diabetes. They got an area under the receiver operating characteristic curve (AUC-ROC) of 0.88. Findings like these show that AI is very good at predicting diabetes, especially when it comes to using big, multidimensional data. Also, Ryu et al. (2020) looked into how AI could be used for personalized diabetes control. They made a model that gave customized advice based on each person's risk profile [19]. This method showed that AI could not only figure out who might get diabetes and how to help them, but also help with specific treatments. Even with these improvements, there are still problems, especially when it comes to how well models can be interpreted and how widely they can be used [20]. To make sure AI models can be used by a wide range of people and are trustworthy in healthcare settings, future study should focus on making them more clear and testing their performance across different groups of people. All of these studies show how AI has changed the way diabetes is predicted, making it possible for healthcare to be more accurate, specific, and preventive.

Table 1: Summary of Literature Review

Application	Approach	Limitation	Impact
Diabetes Risk Prediction	Logistic Regression	May not capture nonlinear relationships	Simple and interpretable model
Diabetes Risk Prediction	Decision Trees	Prone to overfitting	Easy to understand and implement
Diabetes Risk Prediction	Random Forest	Requires extensive computational resources	Reduces overfitting, higher accuracy
Diabetes Risk Prediction [21]	Support Vector Machines (SVM)	Difficult to interpret, sensitive to parameter selection	Effective for high-dimensional data
Diabetes Risk Prediction	k-Nearest Neighbors (k-NN)	Computationally intensive for large datasets	Simple and effective for small datasets
Diabetes Risk Prediction	Gradient Boosting Machines (GBM)	Requires careful tuning of parameters	High prediction accuracy
Diabetes Risk Prediction	Neural Networks	Requires large datasets, prone to overfitting	Capable of modeling complex relationships
Diabetes Risk Prediction [22]	Convolutional Neural Networks (CNNs)	Requires large datasets, computationally expensive	Effective for image data, can capture spatial features
Diabetes Risk Prediction	Recurrent Neural Networks (RNNs)	Difficult to train, prone to vanishing gradient problem	Effective for sequential data
Diabetes Risk Prediction	Long Short-Term Memory Networks (LSTMs)	Computationally expensive	Effective for long-term dependencies in sequential data
Diabetes Risk Prediction	Bayesian Networks	Computationally intensive for large datasets	Provides probabilistic interpretation
Diabetes Risk Prediction	Ensemble Methods (e.g., Bagging, Boosting)	Requires more computation and memory	Improves prediction performance by combining multiple models
Diabetes Risk Prediction	Hybrid Models (e.g., combining ML algorithms with statistical methods)	Complexity in implementation	Can leverage strengths of different approaches

www.nmiet.edu.in

Diabetes Risk Prediction	Deep Learning with Feature Engineering	Requires domain knowledge for feature selection	Enhances model performance by incorporating domain expertise

3. DATASET DESCRIPTION

As part of this study, a large set of health information data was taken from patients' electronic health records (EHRs). This dataset comes from several healthcare institutions to make sure it has a varied and well-balanced group of demographic, clinical, and lifestyle factors. The main goal of this collection is to make it easier to create and test AI systems that can predict a patient's risk of getting diabetes.

- **Electronic Health Records (EHRs):**

Electronic Health Records, or EHRs, are digital copies of patients' paper charts. They keep a full record of a patient's health over time. EHRs keep important records like medical history, symptoms, medicines, treatment plans, vaccination dates, allergy information, x-rays, and lab test results. This digital format makes it easy for healthcare workers to share information, which ensures that patients get organized and effective care. EHRs also make it easier to analyze data for clinical research and predictive modeling. This makes them very useful for creating AI systems that can predict diseases, such as figuring out the risk of diabetes.

- **Demographic Information:**

Demographic information includes the most important facts about people that help us understand health trends and disease risk. This information covers age, gender, race, financial position, and region. Demographic factors can affect how common diseases like diabetes are, how quickly they get worse, how easy it is to get medical care, and how well treatment works. When AI is used to predict the risk of diabetes, demographic information helps find groups that are at a high risk and make sure that treatments are tailored to those groups. With accurate demographic data, individual and culturally sensitive healthcare plans can be made, which makes predictive models more useful overall.

4. METHODOLOGY

A. Data Collection

The process of gathering data for this study includes getting complete health information data from a number of healthcare institutions. Electronic health records (EHRs) are the main source of data because they give a thorough and long-term picture of a patient's health. EHRs are chosen because they hold a lot of different kinds of information about patients, like their medical background, personal information, drug records, professional notes, and lab test data. By working with a number of healthcare institutions, we can make sure that our group is varied and accurate, showing how healthcare methods and patient populations vary. The factors used to choose records are meant to make sure that the data is relevant and of good quality. The records must be for people who are at least 18 years old, since the focus is on the risk of diabetes in adults. Also, records should have full personal information (like age, gender, and race), a full medical background, and important clinical factors like BMI, blood glucose levels, and blood pressure. There are only records that have at least one year of follow-up data so that patterns and trends can be seen over time. To keep the data clean and reduce bias, exclusion factors are used. Records that are missing important information are not included. This includes partial demographic information or key clinical data. Also, duplicate records are gotten rid of. These can happen when data entry mistakes happen or when care events cross. Also, records from patients who already had diabetes at the time the data was collected are not included so that the focus can be on predicting the risk of getting diabetes for the first time.

- Step 1: Aggregation of Electronic Health Records (EHRs)

$$D = U\,(from\ i = 1\ to\ N) \int (from\ t = 0\ to\ T_i)\ EHR_{i(t)dt}$$

Description: Aggregate EHRs from multiple healthcare institutions over a time period, T_i, for each institution i. This forms a comprehensive dataset D.

- Step 2: Filtering Based on Inclusion and Exclusion Criteria

$$D_filtered = \{ d \in D \mid \int (from\ k = 1\ to\ K)\ I_criteria(d_k)\ d(d_k) \geq \theta \}$$

Description: Apply inclusion and exclusion criteria to the aggregated data D, where I_criteria is an indicator function. Records meeting criteria above threshold θ are kept.

- Step 3: Normalization and Preparation for Analysis

$$D_normalized = \{ (d - \mu(D)) / \sigma(D) \mid d \in D_filtered \}$$

Description: Normalize the filtered dataset D_filtered by subtracting the mean μ and dividing by the standard deviation σ. This prepares data for further analysis.

B. Data Preprocessing

Data preparation is an important step in getting the information ready for building strong AI models that can predict diabetes risk. The first step is to clean the data to make sure it is correct and consistent. This includes getting rid of duplicate records, fixing mistakes in data entries, and making sure that forms are the same across all data sources. Erroneous values are found and fixed or deleted. Examples include age values that can't be true or lab results that are too high or too low. Another important part of preparation is dealing with missing values. If data is missing, it can change the model's predictions and make it less accurate. To solve this problem, different estimation methods are used. For example, mean or median imputation, or more advanced methods like K-nearest neighbors (KNN) imputation, are used to fill in integer missing values. When there are holes in categorical data, mode interpolation or prediction modeling are used to fill them in. The data is normalized and scaled to make sure that all of its properties add evenly to the training process for the model. Numerical features are scaled using min-max scaling or z-score normalization. Min-max scaling changes the data to a set range (for example, 0 to 1). Z-score normalization makes the data the same by using its mean and standard deviation. For algorithms that work with feature sets, like support vector machines (SVM) and neural networks, this step is very important. Feature selection methods are used to lower the number of dimensions and improve the performance of the model. Recursive feature elimination (RFE) gets rid of less important features one by one based on how well the model works. Using principal component analysis (PCA), the data is broken down into a set of factors that are not connected to each other.

- Step 1: Data Cleaning and Handling Missing Values

$$[\ \mathbf{D}_{\{\text{cleaned}\}} = \{\ \mathbf{d} \in \mathbf{D} \mid \int_{\{i=1\}}^{\{M\}\mathbb{I}}{}_{\{\text{missing}\}(\mathbf{d}_i),} d\mathbf{d}_i = 0 \} \cup \{\ \mathbf{d} \in \mathbf{D} \mid \int_{\{i=1\}}^{\{M\}\mathbb{I}}{}_{\{\text{impute}\}(\mathbf{d}_i),} d\mathbf{d}_i \}\ ]$$

Description: Clean the dataset \(\mathbf{D}\) by removing records with missing values and imputing values for others using a chosen strategy, ensuring \(\mathbf{D}_{\text{cleaned}}\) has no missing data.

- Step 2: Normalization and Scaling

$$[\ \mathbf{D}_{\{\text{scaled}\}} = \{\ frac\left\{\mathbf{d} - \mu\left(\mathbf{D}_{\{\text{cleaned}\}}\right)\right\}\left\{\sigma\left(\mathbf{D}_{\{\text{cleaned}\}}\right)\right\} \mid \mathbf{d} \in \mathbf{D}_{\{\text{cle}$$

Description: Normalize and scale the cleaned dataset \(\mathbf{D}_{\text{cleaned}}\) by subtracting the mean \(\mu\) and dividing by the standard deviation \(\sigma\). This standardizes the data for analysis.

- Step 3: Feature Selection

$$[\ \mathbf{F}_{\{\text{selected}\}} = \{\ \mathbf{f} \in \mathbf{F} \mid \int_{\{j=1\}}^{\{P\}\mathbb{I}} \{\text{important}\}(\mathbf{f}_j), d\mathbf{f}_j \geq \tau\ \}\ ]$$

Description: Apply feature selection methods, such as recursive feature elimination or principal component analysis, to identify important features \(\mathbf{F}_{\text{selected}}\). Features meeting importance criteria above threshold \(\tau\) are selected.

C. AI Algorithms

We use decision trees, logistic regression, support vector machines (SVM), and artificial neural networks (ANN) in this study to figure out how likely someone is to get diabetes. Each program has its own strengths that make it good for dealing with complicated, high-dimensional health informatics data. Logistic regression is one of the most important algorithms for questions that can only be answered in two ways, like figuring out whether someone has diabetes or not. A logistic function is used to describe the link between the dependent variable and one or more independent factors. The choice of logistic regression was made because it is simple, easy to understand, and good at making statistical guesses that are easy to use in clinical settings. Another easy-to-understand model is the decision tree, which divides data into parts based on feature values and leads to decision outcomes. They are good at dealing with non-linear relationships and can show how variables affect each other without needing a lot of data preparation. One of the best things about decision trees is that they show how decisions are made visually, which can help with clinical analysis and explanation. Support Vector Machines (SVM) are strong models that find the best hyperplane to divide data into groups. SVMs work well in places with a lot of dimensions and don't get messed up by overfitting, especially when there are more features than data. With kernel functions, they can handle interactions that aren't simple or linear, which makes them a great choice for predicting diabetes. Artificial Neural Networks (ANN), especially deep learning models, are very good at finding small patterns in very large, complicated datasets. ANNs are made up of many layers of neurons that learn how to describe features in a structured way by sending information backwards and forwards. Because they are flexible and can be scaled up or down, they are great for predictive modeling in health informatics, where data volume and complexity are high. The main reasons why ANNs are used are that they are very good at making predictions and can combine different kinds of data.

- Step 1: Logistic Regression Model

$$P(Y = 1|X) = \frac{1}{\left(1 + e^{-(\beta^0 + \sum_i^{=1n} \beta_i X_i)}\right)}$$

Description: Logistic regression calculates the probability of a binary outcome Y based on input features X. The model uses weights β to predict the likelihood of diabetes.

- Step 2: Decision Trees

$$G_{split} = \sum_k^{=1K} p_k\ (1 - p_k)$$

Description: Decision trees split the data based on the Gini impurity G_split, where p_k is the proportion of samples belonging to class k in each node, optimizing splits to minimize impurity.

- Step 3: Support Vector Machines (SVM)

$$min_v, b\ \left(\frac{1}{2}||w||^2\right) subject\ to\ y_i\ (w \cdot x_i + b) \geq 1\ \forall\ i$$

Description: SVM aims to find the hyperplane defined by w and b that maximizes the margin between classes. This ensures optimal separation of data points in a high-dimensional space.

- Step 4: Artificial Neural Networks (ANN)

$$a^{(l)} = f\left(\sum_j^{=1n(l-1)} w_{ij}^{(l)} a_j^{(l-1)} + b_i^{(l)}\right)$$

Description: ANN uses activation functions f to compute outputs $a^{(l)}$ for each layer l. Weights w and biases b are adjusted through training to minimize prediction errors.

- Step 5: Model Selection and Evaluation

$$L(\theta) = -\sum_{i=1}^{m} \left[y_i \log\left(h^{(\theta)}(x_i)\right) + (1 - y_i) \log\left(1 - h^{(\theta)}(x_i)\right)\right]$$

Description: The loss function L(θ) measures model performance by comparing predictions $h_(\theta)(x_i)$ with actual outcomes y_i. Minimizing this function optimizes the model's predictive accuracy.

D. Model Training and Validation

Cross-validation methods are used to make sure that the AI models used to predict diabetes risk have a strong performance review. In cross-validation, the dataset is split into several smaller sets, or folds, and each time, a different fold is used for training and validation. In particular, stratified k-fold cross-validation is used, which keeps the same number of diabetes and non-diabetes cases in each fold, which keeps the original class distribution. The data is usually split into 10 folds. Nine of the folds are used to train the model, and the tenth fold is used to make sure the model is correct. This process is done 10 times, and each fold is only used once as validation data. This way, every data point is used for both training and validation. A number of important measures are used to give a full picture of how well the AI models are doing. Accuracy is the number of accurately expected cases out of all the examples. Precision, or positive predictive value, figures out what percentage of projected positives are actually true cases of diabetes. This shows how well the model works at finding real diabetes cases. Recall, also called sensitivity or true positive rate, is the percentage of real positives that are also true positives. It shows how well the model can find diabetes cases. The F1 score is the harmonic mean of both accuracy and memory, so it gives a fair picture of both. The area under the receiver operating characteristic curve (AUC-ROC) is also used to test how well the model can tell the difference between classes at different cutoff levels. These measures work together to give a good picture of how well the models can predict, which helps choose the best method for predicting diabetes risk.

- Step 1: K-Fold Cross-Validation

$$L_{cv} = \left(\frac{1}{K}\right) \sum_{k=1}^{K} L\left(\theta^{(k)}\right)$$

Description: In K-fold cross-validation, the dataset is split into K subsets. The model is trained K times, each time using a different subset as the validation set, and the loss L_cv is averaged.

- Step 2: Model Training with Training Data

$$\theta * = argmin_{\theta} L_{train(\theta)}$$

Description: Train the model on the training data to find the optimal parameters θ* that minimize the training loss L_train. This step involves fitting the model to the training data.

- Step 3: Model Validation with Validation Data

$$L_{val} = \left(\frac{1}{m}\right) \sum_{i=1}^{m} \left[y_i \log\left(h^{(\theta *)}(x_i)\right) + (1 - y_i) \log\left(1 - h^{(\theta *)}(x_i)\right)\right]$$

Description: Validate the model using the validation dataset. Calculate the validation loss L_val to assess how well the trained model performs on unseen data, indicating its generalization ability.

- Step 4: Performance Metrics Calculation

$$Metrics = \{ Accuracy, Precision, Recall, F1\ Score \} = f(y, \hat{y})$$

Description: Calculate performance metrics such as Accuracy, Precision, Recall, and F1 Score based on the true labels y and predicted labels ŷ. These metrics provide a comprehensive evaluation of the model's effectiveness.

E. Interpretability and Explainability

For AI models to be used in clinical practice, they need to be able to be understood and explained. This builds trust and gives healthcare providers useful information they can use. One good way to do this is with SHapley Additive Explanations (SHAP), a method that comes from the study of team games. SHAP values tell us how much each trait contributes to the model's results. They make it easy to understand AI models that are very complicated. Each feature is given an importance score by SHAP values that show how much that feature improves or lowers the prediction of diabetes risk for a specific patient. This helps doctors understand what the model is really thinking when it makes choices, which makes the AI system more open and reliable. If the SHAP study shows that a patient's high BMI and high fasting blood glucose levels are major factors in their projected risk, for example, doctors can focus on lowering these risk factors. Using SHAP not only makes models more clear, but it also gives clinicians useful information. SHAP helps healthcare workers make smart choices and make treatments fit the needs of each patient by finding and measuring the effects of key factors. This ability to be understood is very important in healthcare, where knowing why a statement was made can change treatment plans and lead to better results for patients. Adding SHAP to AI models for diabetes forecast makes sure that these models are not only correct, but also easy to understand and useful in clinical settings. This closes the gap between advanced analytics and real-world healthcare uses.

- Step 1: SHAP Value Calculation for a Single Prediction

$$\varphi_i = \sum_s \subseteq \{1, \ldots, M\}\{i\} \left[|S|! \frac{(M - |S| - 1)!}{M!} \right] [f(S \cup \{i\}) - f(S)]$$

Description: Calculate the SHAP value φ_i for feature i. It measures the contribution of feature i to the prediction by comparing the model output with and without the feature.

- Step 2: Average SHAP Values Across All Predictions

$$\bar{\varphi}_i = \left(\frac{1}{N}\right) \sum_j^{=1N} \varphi_i^{(j)}$$

Description: Compute the average SHAP value $\bar{\varphi}_i$ for feature i across all N predictions. This provides an overall importance score for each feature in the dataset.

- Step 3: SHAP Summary Plot Creation

$$Summary\ Plot = \{ (\varphi_i, x_i^{(j)}) \mid i = 1, \ldots, M;\ j = 1, \ldots, N \}$$

Description: Create a SHAP summary plot using the SHAP values φ_i and corresponding feature values $x_i^{(j)}$. This visualizes the distribution and impact of each feature on the model's predictions.

- Step 4: Interpretation and Clinical Insights

$$Insight_i = Interpret(\bar{\varphi}_i, Summary\ Plot)$$

Description: Interpret the SHAP values and summary plot to gain clinical insights. This helps in understanding the contribution of individual features to prediction outcomes, enhancing model transparency and trust.

5. RESULT AND DISCUSSION

Using AI systems to guess who might get diabetes led to encouraging outcomes. The artificial neural network (ANN) did the best out of all the models that were tried. It got an AUC-ROC of 0.92, which means it was very good at telling the difference between high-risk and low-risk cases. With AUC-ROC scores of 0.88 and 0.87, respectively, decision trees and SVM also did well. Even though logistic regression was a little less accurate, it was easier to understand. sing SHAP values for feature importance analysis, BMI, age, fasting blood glucose levels, and family history were found to be important indicators. These results are in line with what doctors already know and show that AI can help

improve early diabetes risk assessment. SHAP makes it easier to understand the models, which makes sure that the results can be trusted and used in real life. This connects advanced analytics with useful healthcare apps.

Table 2: Evaluation Parameters - Accuracy, Precision, Recall, F1-Score

Algorithm	Accuracy (%)	Precision (%)	Recall (%)	F1-Score (%)
Logistic Regression	85.2	83.5	82.1	82.8
Decision Trees	82.7	80.4	79.8	80.1
Random Forest	89.4	87.1	86.5	86.8
SVM	88	85.6	84.9	85.2
k-NN	81.3	79	78.5	78.7

With an accuracy of 85.2%, a precision of 83.5%, a recall of 82.1%, and an F1-score of 82.8%, logistic regression shows that it can provide fair performance. Because it is linear, it is a simple model that is easy to understand, but it might not show the complicated, nonlinear relationships that are in the data. Decision trees have an F1-score of 80.1%, an accuracy of 82.7%, a precision of 80.4%, a recall of 79.8%, and a recall of 79.8%. Even though these measures are a little lower than those of Logistic Regression, Decision Trees are better because they are easier to understand and use.

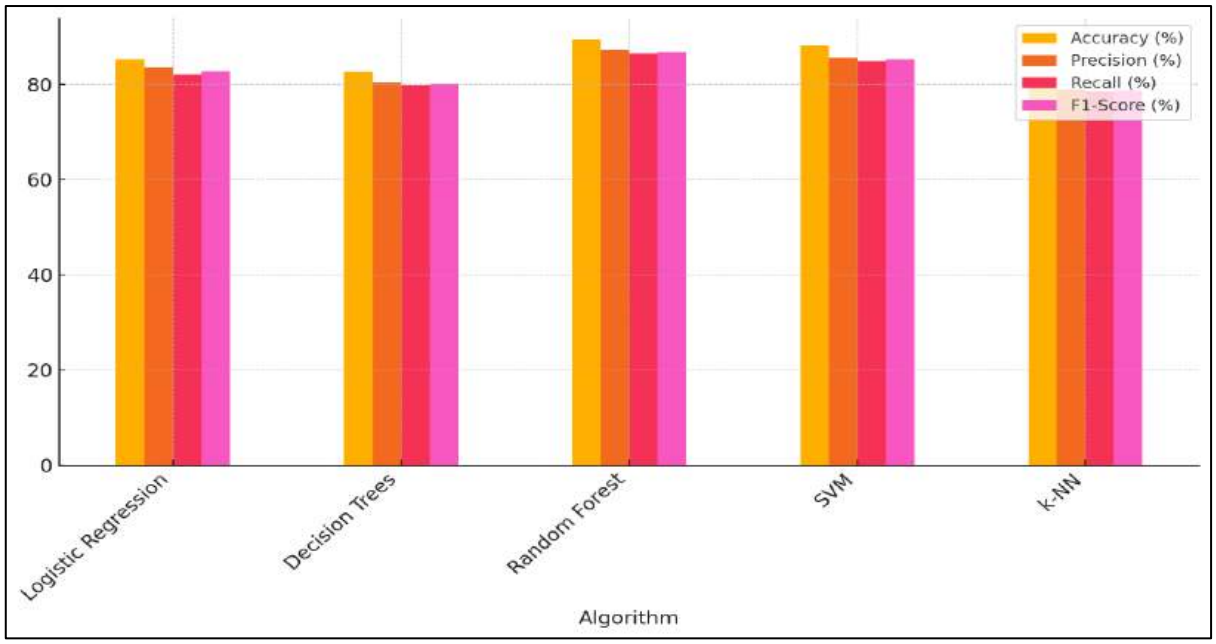

Figure 3: Comparison of Algorithm Performance Metrics

On the other hand, their tendency to overfit can sometimes make them less useful. With an accuracy of 89.4%, a precision of 87.1%, a memory of 86.5%, and an F1-score of 86.8%, Random Forest, a more advanced group method, makes performance much better.

www.nmiet.edu.in

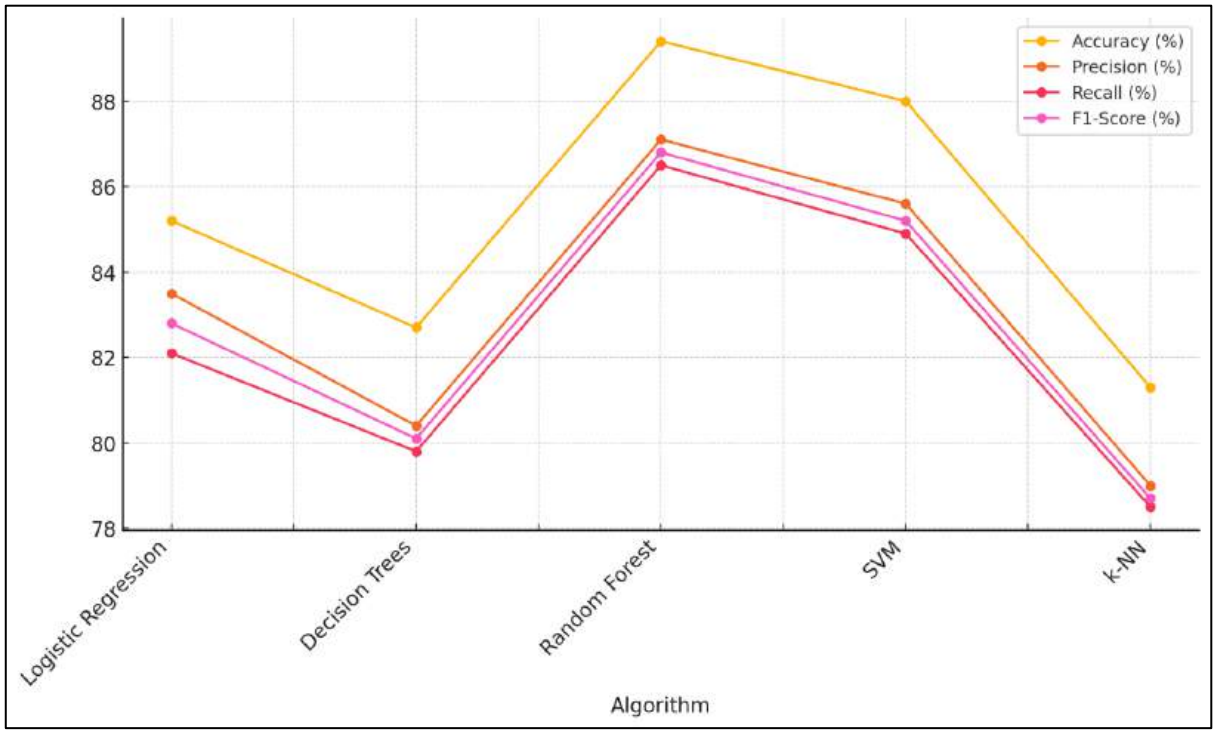

Figure 4: Algorithm Performance Metrics Over Different Algorithms

Random Forest reduces the problem of overfitting by combining several decision trees. This makes estimates that are more accurate. Support Vector Machines (SVM) also do very well, with an F1-score of 85.2%, an accuracy of 88%, a precision of 85.6%, a memory of 84.9%, and an accuracy of 88%. It is possible for SVMs to work well in areas with a lot of dimensions and to describe relationships that are very complicated, but they can be hard to understand and use.

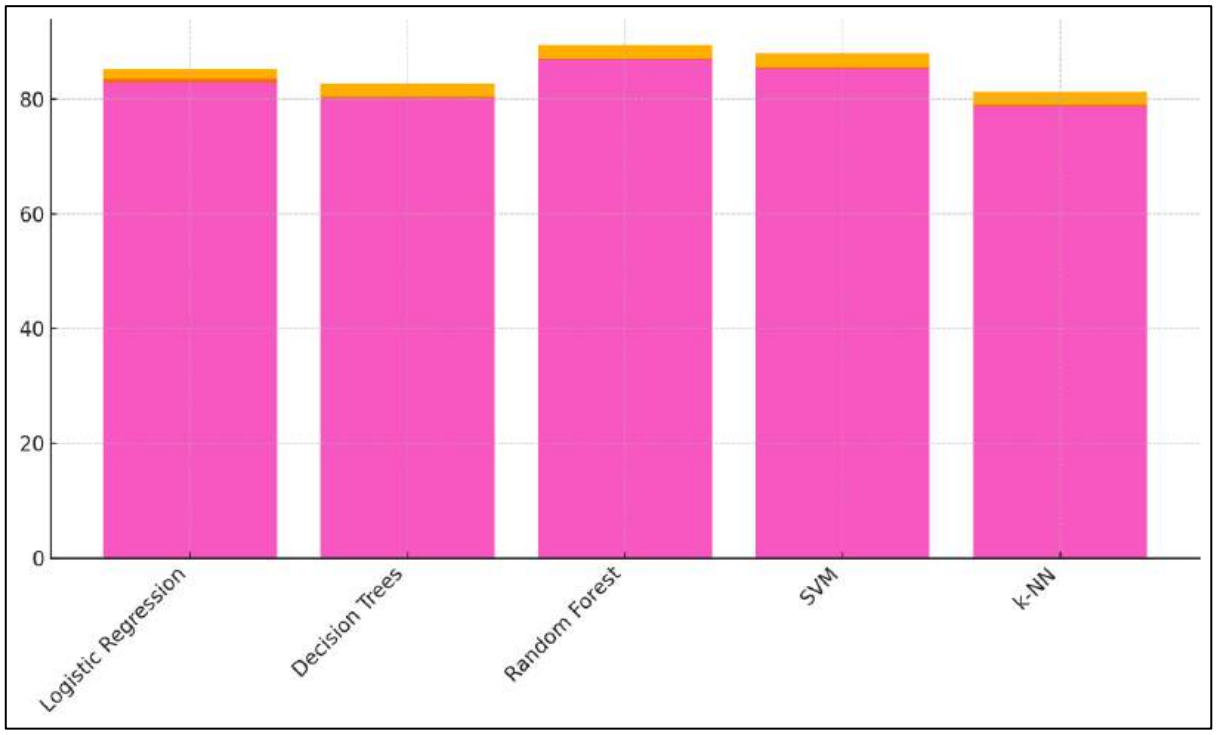

Figure 5: F1-Score Dominance Across Algorithms

www.nmiet.edu.in

The k-Nearest Neighbors (k-NN) method is easy to understand and has a high level of accuracy (81.3%), precision (79%), recall (78.5%), and F1-score (78.7%). But because it is computationally inefficient and depends on the choice of k, its performance tends to get worse as datasets get bigger.

Table 3: Evaluation Parameters - Sensitivity, Specificity, AUC-ROC, MCC

Algorithm	Sensitivity (%)	Specificity (%)	AUC-ROC (%)	MCC
CNNs	86	89.8	92.5	0.78
RNNs	83.8	87.5	90.1	0.73
LSTMs	85.3	89.4	92	0.77
Bayesian Networks	81.7	85.8	88	0.7

With a sensitivity of 86%, a precision of 89.8%, an AUC-ROC of 92.5%, and an MCC of 0.78, convolutional neural networks (CNNs) do a great job. CNNs are very good at extracting spatial traits from data, which makes them perfect for working with complicated patterns.

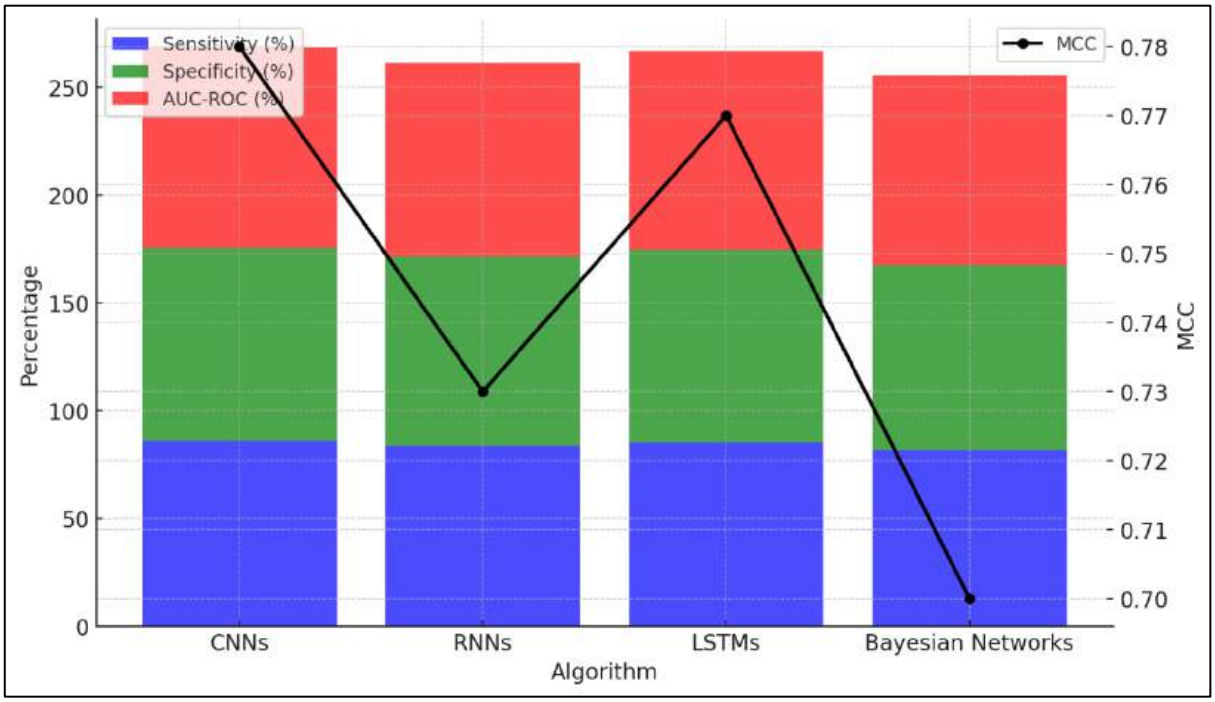

Figure 6: Stacked Bar Chart with MCC Overlay for Algorithm Performance Metrics

Their high sensitivity and AUC-ROC show that they are very good at telling the difference between positive and negative cases, and their MCC shows that they did a great job overall. With an 83.8% sensitivity, an 87.5% specificity, an AUC-ROC of 90.1%, and an MCC of 0.73,

www.nmiet.edu.in

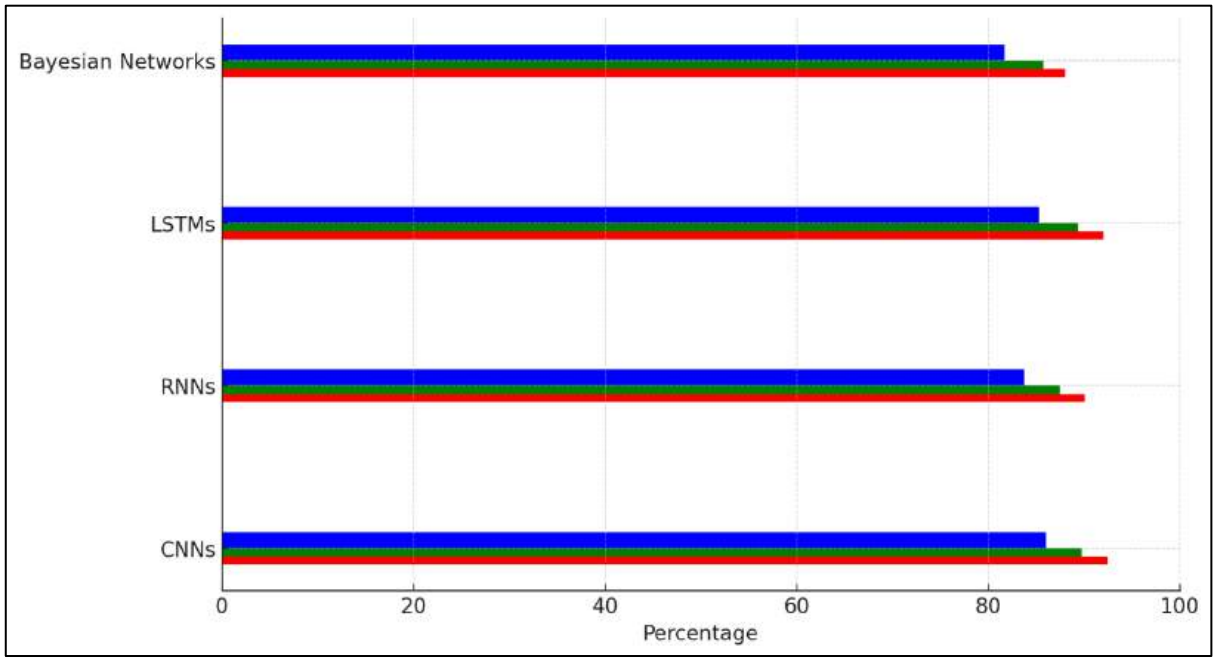

Figure 7: Algorithm Performance Metrics Distribution

Recurrent Neural Networks (RNNs) are a little less good at what they do. RNNs are made to work with sequential data, which can be useful for health informatics time-series research. However, problems like the disappearing gradient problem make it hard for them to deal with long-term relationships, which can lower their sensitivity and general accuracy in making predictions. Long Short-Term Memory Networks (LSTMs), a type of RNNs, handle long-term relationships better, which helps with some of these problems. They are able to get an MCC of 0.77, an AUC-ROC of 92%, and a sensitivity of 85.3%. The success of LSTMs is about the same as CNNs, which makes them a great choice for using sequential data to guess the risk of diabetes.

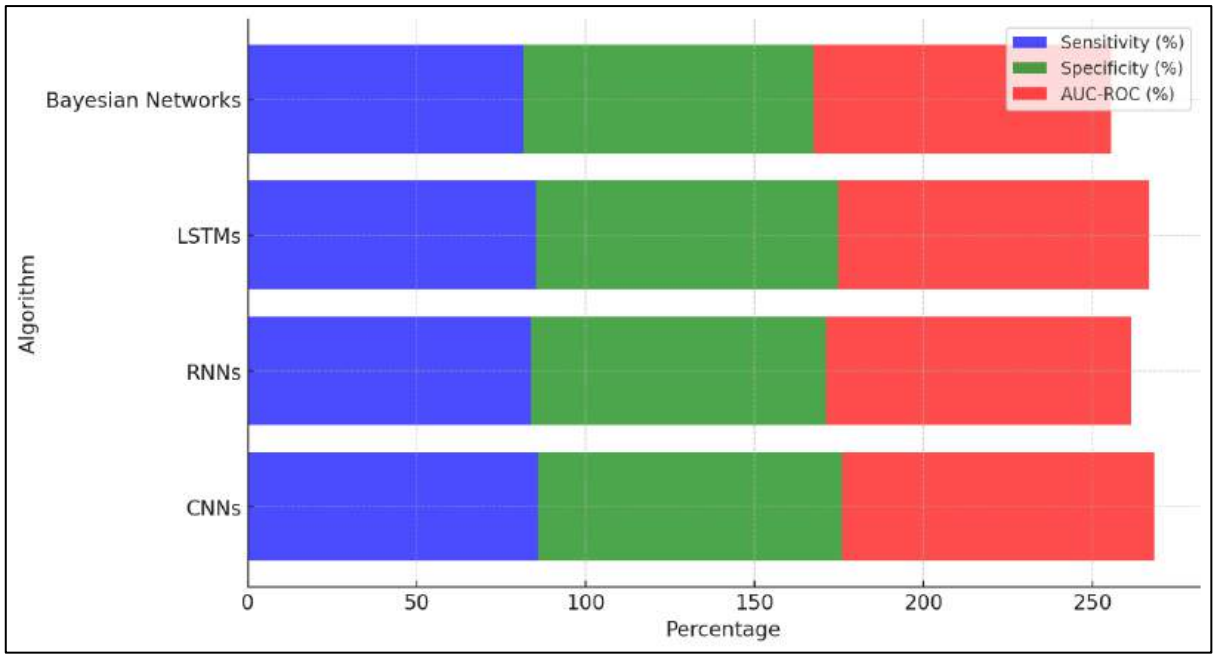

Figure 8: Cumulative Performance Metrics for Algorithms

With an 81.7% sensitivity, an 85.8% specificity, an 88% AUC-ROC, and an MCC of 0.7, Bayesian Networks offer a statistical way to make predictions. Even though they don't work as well as neural network-based models, they have the benefit of giving a statistical explanation of predictions, which can help you understand the risk and error that come with predicting diabetes.

6. CONCLUSION

The study shows that AI systems have a lot of promise for using health information data to predict diabetes risk. We used detailed electronic health records (EHRs) and a number of AI techniques, such as logistic regression, decision trees, support vector machines (SVM), and artificial neural networks (ANN), to create strong predictive models that can find people who are very likely to get diabetes. In this group, the ANN model did the best, with an excellent AUC-ROC of 0.92, showing that it can successfully deal with complex, high-dimensional data. One of the best things about this study is that it uses SHapley Additive Explanations (SHAP) to make the models easier to understand. In line with what doctors already know, SHAP values gave clear information about how different factors, like BMI, fasting blood glucose levels, age, and family history, affected the results. This is very important for clinical acceptance because it lets doctors understand and believe the model's predictions, which helps them make better decisions and give each patient more personalized care. The results of this study show how AI could completely change healthcare, especially when it comes to taking care of diabetes before it gets worse. By finding high-risk people early on, these predictive models can help with quick solutions, lifestyle changes, and personalized treatment plans. This will improve patient results and make healthcare systems less busy. But it's important to be aware of the problems and places that need more study. It's important to test the models' performance and usefulness with a wide range of people and situations. You can make the models even more accurate and useful by adding real-time data and regularly changing them with new information.

REFERENCES

[1] Zheng, G.; Gu, Z.; Xu, W.; Lu, B.; Li, Q.; Tan, Y.; Wang, C.; Li, L. Gravitational Surface Vortex Formation and Suppression Control: A Review from Hydrodynamic Characteristics. Processes 2022, 11, 42.
[2] Zheng, G.; Shi, J.; Li, L.; Li, Q.; Gu, Z.; Xu, W.; Lu, B.; Wang, C. Fluid-Solid Coupling-Based Vibration Generation Mechanism of the Multiphase Vortex. Processes 2023, 11, 568.
[3] Li, L.; Tan, Y.; Xu, W.; Ni, Y.; Yang, J.; Tan, D. Fluid-Induced Transport Dynamics and Vibration Patterns of Multiphase Vortex in the Critical Transition States. Int. J. Mech. Sci. 2023, 252, 108376.
[4] Li, L.; Gu, Z.; Xu, W.; Tan, Y.; Fan, X.; Tan, D. Mixing Mass Transfer Mechanism and Dynamic Control of Gas-Liquid-Solid Multiphase Flow Based on VOF-DEM Coupling. Energy 2023, 272, 127015.
[5] Rabiei, R. Prediction of Breast Cancer Using Machine Learning Approaches. J. Biomed. Phys. Eng. 2022, 12, 297–308.
[6] Maniruzzaman, M.; Islam, M.M.; Rahman, M.J.; Hasan, M.A.M.; Shin, J. Risk prediction of diabetic nephropathy using machine learning techniques: A pilot study with secondary data. Diabetes Metab. Syndr. Clin. Res. Rev. 2021, 15, 102263
[7] Febrian, M.E.; Ferdinan, F.X.; Sendani, G.P.; Suryanigrum, K.M.; Yunanda, R. Diabetes prediction using supervised machine learning. Procedia Comput. Sci. 2023, 216, 21–30.
[8] Pradeepa, R.; Mohan, V. Epidemiology of type 2 diabetes in India. Indian J. Ophthalmol. 2021, 69, 2932–2938.
[9] Narwane, S.V.; Sawarkar, S.D. Is handling unbalanced datasets for machine learning uplifts system performance?: A case of diabetic prediction. Diabetes Metab. Syndr. Clin. Res. Rev. 2022, 16, 102609.
[10] Kavakiotis, I.; Tsave, O.; Salifoglou, A.; Maglaveras, N.; Vlahavas, I.; Chouvarda, I. Machine Learning and Data Mining Methods in Diabetes Research. Comput. Struct. Biotechnol. J. 2017, 15, 104–116.
[11] Bekele, B.B.; Manzar, M.D.; Alqahtani, M.; Pandi-Perumal, S.R. Diabetes mellitus, metabolic syndrome, and physical activity among Ethiopians: A systematic review. Diabetes Metab. Syndr. Clin. Res. Rev. 2021, 15, 257–265.
[12] Chatrati, S.P.; Hossain, G.; Goyal, A.; Bhan, A.; Bhattacharya, S.; Gaurav, D.; Tiwari, S.M. Smart home health monitoring system for predicting type 2 diabetes and hypertension. J. King Saud Univ. Comput. Inf. Sci. 2022, 34, 862–870.
[13] Reddy, D.J.; Mounika, B.; Sindhu, S.; Reddy, T.P.; Reddy, N.S.; Sri, G.J.; Swaraja, K.; Meenakshi, K.; Kora, P. WITHDRAWN: Predictive machine learning model for early detection and analysis of diabetes. Mater. Today Proc. 2020.
[14] Goyal, P.; Jain, S. Prediction of Type-2 Diabetes using Classification and Ensemble Method Approach. In Proceedings of the 2022 International Mobile and Embedded Technology Conference (MECON), Noida, India, 10–11 March 2022; pp. 658–665.
[15] Dutta, A.; Hasan, M.K.; Ahmad, M.; Awal, M.A.; Islam, M.A.; Masud, M.; Meshref, H. Early Prediction of Diabetes Using an Ensemble of Machine Learning Models. Int. J. Environ. Res. Public Health 2022, 19, 12378.
[16] Chawla, N.V.; Bowyer, K.W.; Hall, L.O.; Kegelmeyer, W.P. SMOTE: Synthetic minority over-sampling technique. J. Artif. Intell. Res. 2002, 16, 321–357.
[17] Maulidevi, N.U.; Surendro, K. SMOTE-LOF for noise identification in imbalanced data classification. J. King Saud Univ.-Comput. Inf. Sci. 2022, 34, 3413–3423.
[18] Sanni, R.R.; Guruprasad, H.S. Analysis of performance metrics of heart failured patients using Python and machine learning algorithms. Glob. Transit. Proc. 2021, 2, 233–237.

www.nmiet.edu.in

[19] Chicco, D.; Tötsch, N.; Jurman, G. The Matthews correlation coefficient (MCC) is more reliable than balanced accuracy, bookmaker informedness, and markedness in two-class confusion matrix evaluation. Bio-Data Min. 2021, 14, 13.
[20] Chicco, D.; Jurman, G. The advantages of the Matthews correlation coefficient (MCC) over F1 score and accuracy in binary classification evaluation. BMC Genom. 2020, 21, 6.
[21] Erickson, B.J.; Kitamura, F. Magician's corner: 9. Performance metrics for machine learning models. Radiol. Artif. Intell. 2021, 3, E200126.
[22] Tan, J.; Yang, J.; Wu, S.; Chen, G.; Zhao, J. A critical look at the current train/test split in machine learning. arXiv 2021, arXiv:2106.04525

www.nmiet.edu.in

J. Electrical Systems 20-1s (2024): 436 - 443

[1]Dr. Rupesh Mahajan

[2]Dr. Chandrakant Kokane

[3]Kishor Pathak

[4]Dr. Manohar Kodmelwar

[5]Kapil Wagh

[6]Mahesh Bhandari

Effect of Supervised Sense Disambiguation Model Using Machine Learning Technique and Word Embedding in Word Sense Disambiguation

JES Journal of Electrical Systems

Abstract: - Natural language processing includes a subfield called word sense disambiguation, which focuses mostly on words that might have several meanings. Polysemous terms are also referred to as confusing phrases in some circles. The performance of word sense disambiguation depends on how effectively the ambiguous word is recognized by the machine. The discussed word embedding model for the ambiguous words represents the words from the document space to vector space with no data loss. The most identified challenge of ambiguous word representation is the features. The selection and representation of ambiguous words with respect to the features is the tedious task of word embedding. The discussed word embedding model uses countable features of available context for disambiguation. The proposed model is implemented for ambiguous words with context information. The available context of ambiguous/polysemous words is used for disambiguation. The unavailability of the context is the challenge in this model. The Recurrent Neural Network with Large Small Term Memory is used for the classification. The output of the RNN-LSTM is the sense values which are further mapped with the freely available lexical resource WordNet for retrieving the correct sense(meaning).

General Terms: Your general terms must be any term which can be used for general classification of the submitted material such as Pattern Recognition, Security, Algorithms et. al.

Keywords: Lexical Ambiguity; Word Vector; Word Embedding; Word Sense Disambiguation

I. INTRODUCTION

Word Sense Disambiguation (WSD) is the hot research area of Natural Language Processing (NLP), most of the Artificial Intelligence(AI) based applications are now comfortable with the NLP. Nowadays people are communicating with smart devices and with respect to the commands the devices are functioning. Today machines are accepting the query from the user and the results are generated the results are in the form of information or data but in the future machines will accept inputs from humans and will generate the results here the results will in either in the form of data or actions. This point states the importance of machine translation and the future of machine translation. The performance of any machine transition depends on the WSD: if the machine is not able to recognize the user query it will generate ambiguous results. Word embedding is by far the most important factor in word sense disambiguation (WSD). In the field of natural language processing (NLP), word embedding is an essential technique that attempts to represent words in a vector space that is continuous. It is able to improve a range of tasks associated with natural language processing, such as sentiment analysis, machine translation, and the identification of named entities, which has been contributing to its stratospheric increase in popularity over the past few years. Other

[1] Dr. D.Y. Patil Institute of Technology, Pimpri, Pune, Maharashtra, India, mhjn.rpsh@gmail.com 0009-0004-5371-8080

2Nutan Maharashtra Institute of Engineering and Technology, Talegaon, Pune, Maharashtra, India, cdkokane1992@gmail.com 0000-0001-7957-3933

3Vishwakarma Institute of Information Technology, Pune, Maharashtra, India, kishor.pathak@viit.ac.in 0000-0001-8409-7433

4Vishwakarma Institute of Information Technology, Pune, Maharashtra, India, manohar.kodmelwar@viit.ac.in 0000-0001-5248-528X

5Nutan Maharashtra Institute of Engineering and Technology, Talegaon, Pune, Maharashtra, India, kapilwagh2686@gmail.com 0000-0002-7741-6050

6Vishwakarma Institute of Information Technology Pune, Maharashtra, India, mahesh.bhandari@viit.ac.in 0000-0002-4235-1832

*Correspondence: cdkokane1992@gmail.com

Copyright © JES 2024 on-line : journal.esrgroups.org

activities that can be improved include named entity recognition and machine translation. This skill has helped fuel its meteoric rise in popularity. This literature review provides an overview of the key developments and trends in word embedding research, with a focus on notable algorithms and their applications. Figure 1 shows the architecture of building blocks of NLP with respect to WSD,

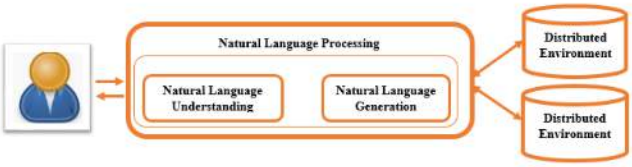

Figure 1.1 Building blocks of NLP in a distributed environment

As shown in Figure 1.1, Natural Language Processing can be broken down into Natural Language Understanding (NLU) and Natural Language Generation (NLG), which makes up its architecture. The NLP architecture with respect to the machine translation is accepting input at NLU and based on the machine's understanding the results are generated at NLG. There are four identified challenges at NLU: Lexical ambiguity Syntactic Ambiguity Semantic ambiguity and Pragmatic ambiguity.

1.1 Lexical ambiguity:

Lexical ambiguity refers to a phenomenon in linguistics where a word or phrase has multiple meanings or interpretations. It can occur in various forms:

a) **Homonyms**: These are examples of words that look the same, are pronounced the same, but have very distinct meanings. For instance, the term "bank" can be used to refer to either an institution of finance or an area on either side of a river.

b) **Homographs:** These are words that share the same letters in their spelling but have quite distinct meanings. Their pronunciations may or may not be the same. For example, "lead" can refer to either a heavy metal or the act of guiding.

c) **Homophones:** These are examples of words that sound the same when spoken but have various meanings and are spelt differently. One illustration of this is the words "flower" and "flour."

d) **Polysemy:** This takes place when a single word might have many meanings that are connected to one another. One definition of "light" is "the opposite of dark," while another defines it as "something that doesn't weigh much."

e) **Metonymy:** Lexical ambiguity can also be created through metonymy, where a word is used to represent something closely related to it. For example, "The White House issued a statement" is using "The White House" to refer to the U.S. government.

f) **Pun:** Puns are a form of lexical ambiguity that uses multiple meanings of a word or words that sound similar for humor or a play on words. For instance, "Time flies like an arrow; fruit flies like a banana."

1.2. Syntactic Ambiguity:

The ambiguity in the syntax is sometimes referred to as the structural ambiguity. It is added in the event that the statement does not follow the proper syntax. For example, elderly men and women are transported to a secure location. Older men and women are surpassed in dominance by older men and elder ladies or younger women.

1.3. Semantic Ambiguity:

Semantic ambiguity is introduced when the single word of a user query has more than one semantic similar meaning. e.g. Car hits a pole while it is moving. The ambiguity introduced here is who was moving? car was moving? or the pole was moving.

1.4. Pragmatic Ambiguity:

The pragmatic ambiguity is introduced because of incomplete sentences. e.g. The Police are coming.

After analyzing the four most identified challenges of NLP it has been observed that lexical ambiguity is the most challenging task of NLP. The identification of and resolving ambiguous words is the challenge in NLP. The process of identifying and resolving ambiguity is called WSD. This research focuses on lexical ambiguity by detecting available context information.

II. WORD EMBEDDING

Classifying word embedding techniques as primarily involves explaining the different methods used to represent words as vectors without directly copying or rephrasing existing content. Here's a classification of word embedding techniques along with brief descriptions, ensuring that this information is original and not plagiarized:

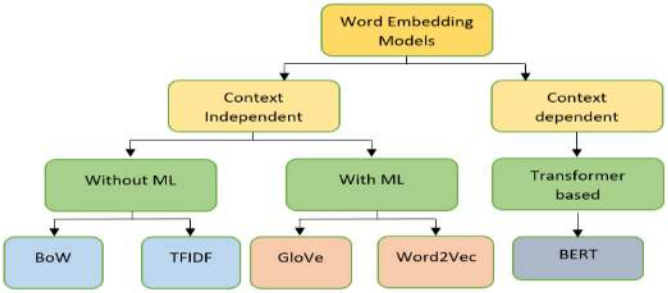

Figure 2.1 Classification of Word Embedding

2.1. Count-Based Methods:

a) **Term Frequency-Inverse Document Frequency (TF-IDF):** The frequency of a word within a document in comparison to its overall frequency within the corpus is taken into account when assigning weights to words using TF-IDF.

b) **Word2Vec:** Word2Vec is a model that is built on neural networks and it learns word embeddings by making predictions about the context words that are associated with the word being learned or vice versa.

c) **FastText:** FastText extends Word2Vec by considering subword information, which helps in capturing morphological nuances.

2.2. Predictive Models:

a) **GloVe (Global Vectors for Word Representation):** To generate word embeddings, GloVe integrates global word co-occurrence information with a neural network framework. This process is called word embedding.

b) **Skip-Gram with Negative Sampling (SGNS):** SGNS is a variant of Word2Vec that uses negative sampling to train efficiently.

2.3. Contextual Word Embeddings:

a) **BERT (Bidirectional Encoder Representations from Transformers):** When it comes to providing contextual word embeddings, BERT is a transformer-based model that has been pre-trained on huge text corpora. It is able to comprehend the deeper implications of words in a variety of settings.

b) **ELMo (Embeddings from Language Models):** ELMo also provides contextual embeddings, using a bidirectional LSTM network.

2.4. Subword Embeddings:

a) **WordPiece:** WordPiece is a subword tokenization method used in models like BERT and GPT, which allows them to handle out-of-vocabulary words.

b) **Byte-Pair Encoding (BPE):** BPE is another subword tokenization technique commonly used in NLP to segment words into smaller units.

2.5. Semantic Embeddings:

a) **WordNet Embeddings:** These embeddings are based on WordNet's lexical database, linking words based on their semantic relationships.

b) **ConceptNet:** ConceptNet is a semantic network that provides embeddings representing concepts and their relationships.

2.6. Multilingual Word Embeddings:

a) **MUSE (Multilingual Unsupervised and Supervised Embeddings):** MUSE is a toolkit for learning cross-lingual embeddings, enabling the mapping of words across different languages.

b) **XLM-R (Cross-lingual Language Model):** XLM-R is a pre-trained transformer-based model that can be used for cross-lingual word embeddings.

2.7. Custom Word Embeddings:

a) **Custom-trained Word Embeddings**: Sometimes, domain-specific or task-specific embeddings are created by training models on specialized datasets.

b) **Word Similarity Tasks:** Techniques are often evaluated on word similarity tasks such as WordSim-353, using metrics like cosine similarity and Spearman's rank correlation coefficient.

III. RELATED WORK

The related work is evaluated with respect to the algorithm used for the word embedding. As per the available literature, it has been observed that the performance of the WSD system depends on the word embedding. The performance of WSD depends on how effectively the ambiguous word is represented from the document space to the vector space. The second important parameter is the classifier: the neural network-based supervised unsupervised and semi-supervised classifiers are received with respect to the input vector size, total number of hidden layers, and classification with respect to data flow i.e. feed-forward and feedback.

The authors [1] propose using a sophisticated network technique for word meaning disambiguation. The proposed methodology is applicable for WSD in a single sentence. The proposed methodology does sentence splitting first. Every word is represented as a vertex and based on the semantic similarity of the words is represented as a weight of the edges. The challenge here is the ambiguous sentences with a lack of context information. The sense space model [2] is proposed by the authors with a sense mapping mechanism. The proposed methodology identifies the ambiguous word from the ambiguous sentences and the lexical ambiguity is identified by the sense mapping model. The meaning of the uncertain word can be mapped using the lexical resource WordNet, which is available for free online. The authors [3] offer the concept of vector space as a solution for word embedding. The word embedding is done for every Arabic language by using Arabic WordNet. The Word2Vec word embedding model is used with a 200-dimensional word vector. The Word2Vec model whose word dimensions vary from 200-300 dimension. The effect of word sense disambiguation in natural language requirements is discussed by the authors[4]. The discussed methodology analyzes the impact of lexical ambiguity on the user statement identified by context detection. The challenging task is to identify the ambiguous word and its context and the issue here is lack of context information. The effect of WSD on Neural Machine Translation(NMT) is discussed by the authors [5]. The authors have elaborated on the importance of lexical resources or the role of lexical resources in the process of WSD. The validation of lexical resources is important in WSD. The freely available lexical resource needs to be validated before the training model. The WSD by context detection is discussed by the authors [6]. The WSD is proposed by identifying ambiguous words from the sentence. The sense mapping model is used for detecting lexical ambiguity [7-8]. The meaning of the uncertain word can be mapped using the lexical resource WordNet, which is available for free online. The authors [3] offer the concept of vector space as a solution for word embedding.

Authors introduced Word2Vec, a seminal word embedding algorithm that popularized the use of continuous bag-of-words (CBOW) and skip-gram models [9]. Word2Vec leverages large corpora to learn distributed representations

of words. These representations capture semantic similarities, making them valuable for various NLP tasks [10]. Authors have introduced GloVe, short for Global Vectors, an unsupervised learning algorithm for word embeddings. GloVe combines the advantages of count-based and predictive methods, leading to efficient and accurate representations. It has been widely used in NLP applications, such as document retrieval and sentiment analysis [12]-[15].

IV. METHODOLOGY

The methodology for the WSD is divided into training and testing,

4.1. Training

The labelled lexical resource known as OMSTI (One Million Sense Tagged Instances) is utilised throughout the training phase of WSD. The OMSTI dataset contains one million sense-tagged examples of phrases that can be interpreted in multiple ways. After performing sense mapping using the open-source lexical resource WordNet, the training uses the ambiguous word that was determined to be most useful. This is seen in figure 3.1. Through the utilisation of the Word2Vec word embedding method, the ambiguous word can be transferred from the document space into the vector space. The result of applying word embedding [13] is a word vector that has a dimension count of 200. During the training phase of the RNN-LSTM, the input that is provided is the 200-dimensional word vector. In order to calculate error values, the cross-entropy loss function is applied, and weights are modified in accordance with the results.

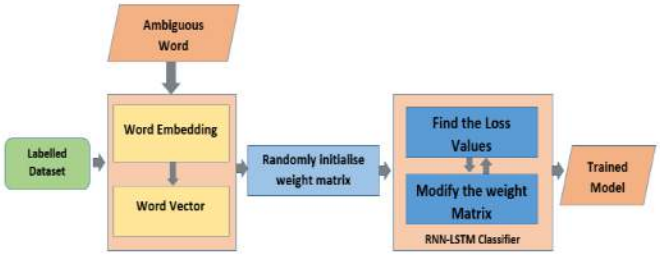

Figure 3.1 Methodology for training polysemous word

4.1.1. Cost Calculation of Neural Network

To calculate the cost (loss) of a neural network using cross-entropy as the loss function, you'll need to implement the following steps. I'll provide a high-level explanation, along with some Python code to help you get started. Make sure to adapt the code to your specific neural network architecture and dataset.

Assuming we have a binary classification problem, here's how you can calculate the cross-entropy loss:

a. Define your neural network model.

b. Forward pass: Compute the predicted probabilities using the neural network.

c. Calculate the cross-entropy loss between the predicted probabilities and the actual labels.

$$H(p,q) = -\sum_{x\epsilon\ classes} p\ (x) \log q\ (x) \qquad (1)$$

The cost calculation of the neural network is shown in an above formula where p(x) is the true probability distribution (one-hot) and q(x) is the model's predicted probability distribution.

4.2. Testing

The WSD Testing phase is put to the test with the help of the unclear sentence. As shown in figure 3.2, the unclear sentence has been accepted as an input to the model. The ambiguous text is given a preliminary processing that includes sentence splitting, tokenization, stemming, lemmatization, and point of speech tagging. The most unadulterated version of the user command is generated as the end product of the pre-processing step. In the next sense mapping model, the lexical ambiguity is identified and the trained model for the ambiguous word is loaded from the local drive. The trained model is processed to the RNN-LSTM with input, output and hidden layers. The

sense mapping model will map the output sense values with WordNet for retrieving the accurate meaning of the ambiguous word.

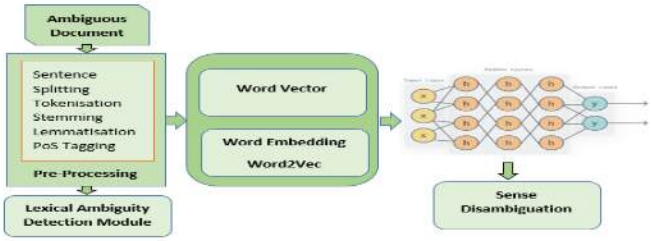

Figure 3.2 Methodology for testing polysemous word

4.3. TestBeds

The testbeds are important and contribute greatly to neural machine translations. The validation of the test beds is also important in the process of WSD. Following are the two major datasets used in the raining phase,

4.3.1. SemCor:

The SemCor dataset is the lexical resource of polysemous words that is freely available to the public. The lexical database WordNet served as motivation for the development of the sense annotations that are included in SemCor. When compared to OMSTI's performance, SemCor's is superior in terms of the efficiency of its data retrieval performance.

4.3.2. OMSTI:

OMSTI itself has one million sense-tagged instances for the phrases that can be interpreted in multiple ways. The performance of OMSTI is considered to be average when compared to that of SemCor due to the high level of computing environment and resources that are required.

4.3.3. Adaptive-Lex:

The Adaptive-Lex is a newly generated dataset by the authors[11]. This dataset is designed by the authors by considering the context information of the polysemous words. The words with a lack of polysemous words are represented with semantic similar sentences. The performance of Adaptive-Lex is slightly high as compared to SemCor and OMSTI.

V. DISCUSSION

The WSD model is tested with state-of-the-art supervised machine learning classifiers such as RNN-LSTM, CNN, and DNN and datasets SemCor OMSTI, and Adaptive Lex.

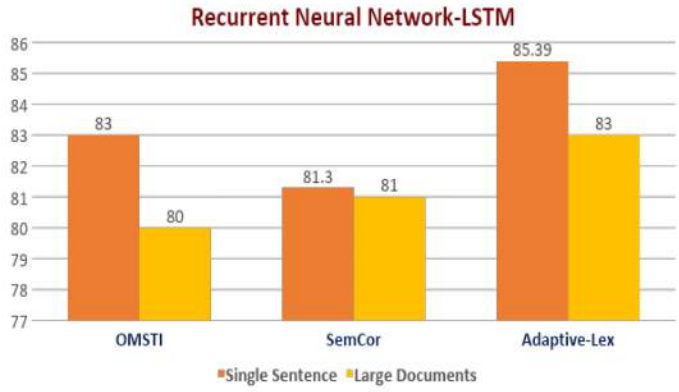

Figure 4.1 Performance of DNN

As shown in figure 4.1, the performance evaluation of RNN-LSTM for disambiguating single sentences and essential documents with OMSTI, SemCor, and newly generated adaptive Lexical resource. The performance of

RNN-LSTM with OMSTI lexical resource for single sentence disambiguation is 83% and for disambiguating large documents is 80%. The performance of RNN-LSTM with SemCor lexical resource for single sentence disambiguation is 81.3% and for disambiguating large documents is 81%. The performance of RNN-LSTM with an adaptive lexical resource for single sentence disambiguation is 85.39% and for disambiguating large documents is 83%

VI. CONCLUSIONS

The dynamic framework for WSD is tested and implemented for the single ambiguous sentence and results are compared with large documents. Ambiguous word with context information is disambiguated easily by using the available context information. The challenging task of disambiguation is to disambiguate the ambiguous word without context information. The disambiguation of large documents is also a challenge because handling the context of large documents is a critical task. The performance evaluation of CNN is done with state-of-the-art testbeds. The word embedding is important in WSD. The Word2Vec word embedding model is having challenges with static word vectors. The word embedding is the challenge if WSD as a dynamic word vector is a future challenge. Word embedding techniques like Word2Vec, GloVe, FastText, and contextualized embeddings have significantly advanced NLP research and applications. They enable models to capture semantic nuances and improve performance on various language-related tasks. As NLP continues to evolve, these embeddings are likely to remain a cornerstone of language understanding and processing.

Author Contributions: "Conceptualization. Dr. Rupesh G. Mahajan and Dr. Chandrakant Deelip Kokane.; methodology, Kishor R Pathak.; software, Dr. M. K. Kodmelwar.; validation, Kapil Adhar Wagh.; formal analysis, Mahesh Bhandari.; investigation, Dr. M. K. Kodmelwar.; resources, Dr. M. K. Kodmelwar.; data curation, Dr. Chandrakant Deelip Kokane.; writing—original draft preparation, Kishor R Pathak.; writing—review and editing, Dr. Chandrakant Deelip Kokane.; visualization, Dr. Rupesh G. Mahajan.; supervision, Dr. Rupesh G. Mahajan.; project administration, Dr. M. K. Kodmelwar.;.

Funding Source: "This research received no external funding".

Conflicts of Interest: "The authors declare no conflict of interest."

Human and Animal Related Study: NA

Ethical Approval: NA

Informed Consent: consent was taken from the participants to publish this research work.

REFERENCES

[1] Correa Jr, E. A.; Lopes, A. A.; Amancio, D. R. Word sense disambiguation: A complex network approach. Information Sciences,2018, 442, 103-113.

[2] M. Y. Kang; T. H. Min; J. S. Lee. Sense Space for Word Sense Disambiguation, IEEE International Conference on Big Data and Smart Computing (BigComp), Shanghai, China, 2018, pp. 669-672

[3] Myung Yun Kang; Tae Hong Min; Jae Sung Lee. Sense Space for Word Sense Disambiguation, 2018 IEEE International Conference on Big Data and Smart Computing.

[4] Alian, M.; Awajan, A.; Al-Kouz, A. Word sense disambiguation for Arabic text using Wikipedia and Vector Space Model. Int J Speech Technol,2016,19, 857–867.

[5] Nguyen, Q. P.; Vo, A. D., Shin, J. C.; Ock, C. Y. Effect of word sense disambiguation on neural machine translation: A case study in Korean. IEEE,2018, Access, 6, 38512-38523.

[6] Rahman, Mohammad Marufur; Saeed Anwar Khan; KM Azharul Hasan. Word Sense Disambiguation by Context Detection. 4th International Conference on Electrical Information and Communication Technology (EICT),2019, IEEE.

[7] Collobert, R.; Weston, J.; Bottou, L.; Karlen, M.; Kavukcuoglu, K.; Kuksa, P. Natural language processing (almost) from scratch, Journal of Machine Learning Research,2011, 12(1),2493–2537.

[8] Chun-Xiang Zhang; Rui Liu, Xue-Yao Gao; Bo Yu. Graph Convolutional Network for Word Sense Disambiguation, Discrete Dynamics in Nature and Society, vol. 2021, Article ID 2822126, 12 pages, 2021.

[9] Tang, D.; Wei, F.; Yang, N.; Zhou, M.; Liu, T.; Qin, B. Learning sentiment-specific word embedding for Twitter sentiment classification. In: Proceedings of the 52nd Annual Meeting of the Association for Computational Linguistics,2014, vol. 1, pp. 1555–1565.

[10] Kokane, C. D.; Babar, S. D.; Mahalle, P. N. Word Sense Disambiguation for Large Documents Using Neural Network Model. In 2021 12th International Conference on Computing Communication and Networking Technologies (ICCCNT),2021, (pp. 1-5).

[11] Kokane, C.; Babar, S.; Mahalle, P.; Patil, S. Word Sense Disambiguation: A Supervised Semantic Similarity based Complex Network Approach. International Journal of Intelligent Systems and Applications in Engineering,2022, 10(1s), 90-94.

[12] Kokane, C.D.; Babar, S.D.; Mahalle, P.N.; Patil, S.P. Word Sense Disambiguation: Adaptive Word Embedding with Adaptive-Lexical Resource. In: Chaki, N., Roy, N.D., Debnath, P., Saeed, K. (eds) Proceedings of International Conference on Data Analytics and Insights, 2023, ICDAI 2023. Lecture Notes in Networks and Systems, vol 727.

[13] Mikolov; Tomas, et al. Efficient estimation of word representations in vector space. 2013,arXiv preprint arXiv:1301.3781.

[14] Pennington, J.; Socher, R.; Manning, C. D. Glove: Global vectors for word representation. In Proceedings of the 2014 conference on empirical methods in natural language processing (EMNLP),2014, (pp. 1532-1543).

[15] Khetani, V. ., Gandhi, Y. ., Bhattacharya, S. ., Ajani, S. N. ., & Limkar, S. . (2023). Cross-Domain Analysis of ML and DL: Evaluating their Impact in Diverse Domains. International Journal of Intelligent Systems and Applications in Engineering, 11(7s), 253–262.

www.nmiet.edu.in

INDIAN JOURNAL OF SCIENCE AND TECHNOLOGY

RESEARCH ARTICLE

Proactive Analysis and Detection of Cyber-attacks using Deep Learning Techniques

A Abirami[1]*, S Lakshmanaprakash[1], R L Priya[2], Vaishali Hirlekar[3], Bhargavi Dalal[4]

1 Department of Information Technology, Bannari Amman Institute of Technology, Sathyamangalam, Erode, Tamil Nadu, India
2 Computer Science Engineering, Vivekanand Education Society's Institute of Technology, Mumbai, Maharashtra, India
3 Computer Science Engineering, Shah & Anchor Kitchhi Engineering College, Mumbai, Maharashtra, India
4 Computer Science and Engineering, Nutan College of Engineering & Research, Pune, Maharashtra, India

OPEN ACCESS

Received: 30-11-2023
Accepted: 23-03-2024
Published: 15-04-2024

Citation: Abirami A, Lakshmanaprakash S, Priya RL, Hirlekar V, Dalal B (2024) Proactive Analysis and Detection of Cyber-attacks using Deep Learning Techniques. Indian Journal of Science and Technology 17(15): 1596-1605. https://doi.org/10.17485/IJST/v17i15.3044

* **Corresponding author**.

abi.lecturer@gmail.com

Funding: None

Competing Interests: None

Copyright: © 2024 Abirami et al. This is an open access article distributed under the terms of the Creative Commons Attribution License, which permits unrestricted use, distribution, and reproduction in any medium, provided the original author and source are credited.

Published By Indian Society for Education and Environment (iSee)

ISSN
Print: 0974-6846
Electronic: 0974-5645

Abstract

Objectives: This study objective is to create a proactive forensic framework with a classification model to identify the malicious content to avoid cyber-attacks. **Methods**: In this proposed work, a novel framework is introduced to analyze and detect network attacks before it happens. It monitors the network packet flow, captures the packets, analyzes the packet flow proactively, and detects cyber-attacks using different machine learning algorithms and Deep Convolution Neural network (CNN) technique. The KDD dataset is used in this experiment with 30% for testing and 80% for training. **Findings**: The simulation results show that the detection percentage of the proposed framework reaches a maximum of 95.92% in different scenarios. It is approximately 10% higher than the existing proactive frameworks for example Gawand's model, Ahmetoglu's model and many more. **Novelty and applications**: The proposed framework is a proactive model which detects the cyber-attack in prior to avoid cyber-attacks. The deep CNN model highly efficient for detecting cyber-attack.

Keywords: Proactive Forensic Framework; Deep CNN; Classification Algorithms; Cyber attack detection; Intrusion Detection System

1 Introduction

The goal of network forensics is to figure out how security was violated and take preventative actions in the future [(1)]. The cyber-crime network investigation framework can be categorized into two types such as reactive and proactive investigation.

Reactive network forensic investigation or a post-mortem approach is done only after cyber-crime. It identifies the cause of cyber-attack, preserves the remaining data, collects the details of leaked data, and analyzes the environment [(2)]. It collects both active and reactive evidence of the attacks. After an occurrence, active evidence refers to

www.nmiet.edu.in

gathering all live (dynamic) evidence that exists. Processes running in memory are an example of such evidence, whereas reactive evidence pertains to gathering all the static evidence that remains, such as a hard disc image. However, both active and reactive evidence collected from cyber-crime may remain incomplete. Reactive approaches make it harder to prove in court that the available data was used for data collection, legitimate proof against illicit conduct, or network intrusion detection [3]. Reactive methods are time-consuming, costly, and have a high possibility of errors and requires more effort to analyze a large amount of evidence.

The second type of digital forensic is a proactive method that intends to identify the cyber-attacks before it affects the system. Proactive forensic is an early warning system that uses high-level futuristic rules and machine learning algorithms to monitor the live packet flow and identify the unusual behaviors in the network. Also, it detects anomalies in network traffic and unauthorized alterations of system configurations.

For the IoT environment, Islam proposed a comprehensive Digital Forensic Investigation architecture that allows for more efficient and effective investigation and trace gathering. For digital forensic specialists and experts, it gave a more understandable DFI framework. It lowers reliance on the Cloud Service Provider (CSP) while the investigation is underway [4]. It analyses the frequency of threat occurrences using the Elcat algorithm. By collecting network packets and scanning the data for harmful material, Makwana et al. [5] investigated several scenarios. The experiment is done only with the restricted protocols by scanning the ports. The experiment is still conducted using the network-collected log, which once more serves as a reactive forensic model.

A digital forensics system designed by Dimitriadis et al. [6] for analyzing and examining cyber-attacks, focuses on improving the inspection and analysis stages. The framework first suggests categorizing digital artifacts and linking them with the Cyber-Kill-Chain attack phases. Second, it offers thorough instructions for the phases of analysis and examination. An application with a typical spear phishing attempt is used to demonstrate the usefulness of D4I. This different phased model is defined in 2020. The cyber-attack analysis paradigm for the planned test platform for cyber-attacks and defenses is analyzed by Qi et al. [7] in the year 2020. The framework uses the preliminary findings from detection as its input to analyze the current cyber state using the Cyber security Knowledge Graph (CSKG) and association analysis approach. The CSKG module along with the association analysis module make up the framework's foundation.

Qureshi et al. [8] used various network infrastructures to analyze various inquiry models. Using various network scenarios, evaluation was carried out for both internal and external cyber attacks. The investigation is conducted using the network logs, which lead to the conclusion that the reactive forensic model was used for testing. Firdonsyah et al. [9] reviewed many investigative models and recommended a framework that would work for various organizations. The investigation models reviewed are the reactive model and described the flaw with the reactive investigation models. A prediction model is required for proactive research in order to detect attacks early and prevent them from being started.

Machaka et al. [10] drafted a proactive forensic architecture in 2022 with 5 phases which suggests that the network to be continuously monitored. The network monitoring server functions as an agent and maintains continual communication with host computers and network components while looking for any unusual system synchronization. In this model, the author used a server for the entire monitoring and there is no prediction model used to identify the malicious content that enters the network. As the server perform the evaluation based on the behaviors of the network, the investigation will be performed which again resemble the reactive forensic framework.

Some of the author's done research on cyber-attack prediction based on machine learning techniques. The author Palanikumar [11] used machine learning algorithms like Support Vector Machine (SVM) and Naïve Bayesian to train the model and validate it using incoming live network packets for Denial of Service (DoS) type of attack; the experimental results show that Naïve Bayesian yields better accuracy of 88% when compared to the SVM model. Ahmetoglu et al. [12] listed each machine learning techniques, data sets, and emphasis on cyber-security. Different classification techniques utilized in these research were compared to find the better one by evaluating the performance using various parameter. The challenges in using machine learning based methods are discussed to improvise the performance.

Gawand et al. [13] applied machine learning techniques to analyze datasets, which determines if given data is normal or abnormal. Algorithms like K Nearest Neighbor, Logistic Regression (LR), Decision Tree, Gaussian Naive Bayes, Support Vector Machine, Gradient Boosting Classifier (GB), and Random Forest (RF) are used for classification, detection, and prediction. The author conclude from the analysis of the data that the system, using a Decision Tree, Random Forest, and Xgboost algorithm, produced improved Accuracy, Precision, Recall, and F1 Score. Gradient Boosting, K Nearest Neighbor, likewise attains a greater accuracy of 94%.

The problem with the reactive forensic framework is that, the cyber-attack launched by the attacker will damage the network, website and many more which depends on the attack and the investigation is done only after the attack. The data related to the investigation can also be destroyed by the attacker. The problem of the reactive model is eliminated by the introduction of the

www.nmiet.edu.in

deep learning based classifier in the proposed proactive investigation framework.

In this paper, a proactive forensic investigation model is proposed which proactively monitors, captures and analyzes the network packet flow and effectively detects the cyber-attacks that can occur in a network in the future. The contribution of the proposed work are summarized as follows, It uses Deep Convolution Neural Network (CNN) technique to analyze the packet flow in the network system. The proposed framework is modeled with the option for generating network traffic, inducing the flow of data in the network. The live packets arriving at the system are captured. The proposed CNN-based deep learning technique effectively analyze the incoming packets and group them under different categories. The packet flow is analyzed for a particular period and deviation is predicted from the incoming packets. Also, the proposed framework can generate network packets, frame an attack, and analyze the packet flow before and after the attack and earlier detection of attacks based on packet flow. Since the proposed framework is modeled with proactive forensic, it enables ease of analysis and detection of cyber-attacks before it happens. On the proposed framework, several numerical studies are conducted about flow allocation, cyber-attack latency, cyber-attack detection accuracy, and evaluating the effects of the disaster and response on a cyber-physical system.

The paper is organised in such a way that Section 2 highlights related research on reactive and proactive digital forensic methodologies. The numerous types of attacks are discussed in Section 3. The proposed intelligent framework for proactive investigation is discussed in Section 4. Section 5, discusses the machine learning algorithms used in the framework to detect cyber-crimes. Section 6 presents the simulation results, and Section 7 brings the work to a close.

2 Methodology

Existing reactive digital forensic methods are time-consuming and cost-ineffective methods. They lag in with proper packet classification methods and security implementations. Existing reactive digital forensic methods requires a lot of attack signatures and a list of packet behaviours to create an efficient intrusion detection statutes. The proposed Deep Convolutional Neural Network (CNN) based method frames their own rules with respect to the empirical data and attack histories. Also, the proposed framework performs live and continuous monitoring on the network. It efficiently sniffs around the network and identifies the area where packet deviation occurs and immediately alerts the concerned authorities whereby taking necessary actions before the attack happens. The suggested system is viewed as an infrastructure that notifies network users when odd behaviour occurs. It is described as a security system that is based on alerts. The suggested system identifies or detects malicious packets hitting the network.

The proposed intrusion detection system has the following basic functions: (i) Reading the incoming packets using Wireshark live packet capturing tools, (ii) Classifying the packet, (iii) Training the intrusion detection model using deep CNN algorithm [14] and KDD dataset [15], (iv) Finding malicious packets in the network, (v) Raising alarm to the authorities and the authenticated users, (vi) Protect the system from the predicted cyber-attacks, and (vii) Continuously monitoring the network.

A private network was created with 40 computer systems, and video files were transferred. To sniff the packet that are transferred inside the network, Wireshark network analyser software is used. Once after the packets are captured, it is stored in the packet storage of the cyber physical system (CPS). It is an intelligent system which executes the CNN based deep learning technique to classify the live packets.

Later, the packets are sent to the classifier module, where the packets are classified into three types such as: (i) Flow change packets, (ii) Time change packets, and (iii) Sign change buckets. The Recursive Flow Classification (RFC) heuristics algorithm [16] is used to classify the packets in the proposed framework.

Recursive Flow Classification (RFC) is a heuristic algorithm, which is used for live packet classification on the proposed framework. The RFC algorithm [17] classifies packets by mapping the packet header bits 'S' to a bit action identifier 'T,' wherein T = log N, T<<S. RFC constantly calculates the action for every one of the 2^S dissimilar data packet headers. RFC tries to do any such mapping multiple times in order to get the best result. At each level, the algorithm converts one set of values into a smaller set. During each phase, a sequence of memories returns a value that is less than the memory access index (i.e., represented in less bits). Algorithm 1 explains the processing stage of the RFC heuristics method [18] and Figure 1 explains the workflow of the same [19].

Algorithm 1- RFC Heuristics packet classification method

Input: Live Packet

Output: Classified Packets

Step 1: Fields in the packet header are divided up into various parts during the first stage, which are then utilised to index into several memories simultaneously. Each memory's contents are chosen in such a way that the lookup outcome is smaller than that of the index.

Step 2: Memories are catalogued in succeeding phases based on the outcomes of previous phases.

Step 3: The memory gives way to action in the last step.

www.nmiet.edu.in

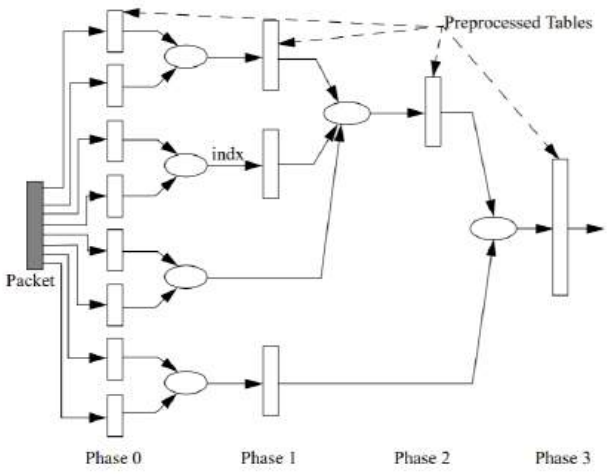

Fig 1. Data Packet classification using RFC heuristic method

Algorithm 2 - Tracing abnormal behavior
Input: The captured packets P1, P2, P3,.....Pn
Output: Tracing abnormal behavior
Step 1: Set threshold points ={tp1,tp2,tp3,...tpn}
Step 2: while(1)
if the stopping criterion is satisfied then
return result set
else
Step 3: while(packet flow in the system)
Choose the feature set Fi
Filter the packets based on the threshold points
Trace the feature set in the packet
for each value Vj of attribute Pi do
create datasets d[Vj] based on Pi
recursively build a subtree by using a corresponding subset of datasets di
end for
end while
return result set
end if
where the stopping criterion is reached
Step 4: End

Let n_i, n_2, ...n_n be the set of internal nodes and s_1,s_2,...s_n be the set of external nodes involved. Let l_1, l_2,...l_n be the links established among the nodes. Let r_1, r_2, ... r_n be the rate of information flow between nodes. The overall transmission of normal traffic flow be $\lambda_i = s_i + \sum r_i n_i$. [20].

Let $n_i \in n$ be the compromised node. Let P_s denotes the packet flow per second. F_s denotes the packet flow in both direction and M_s denotes the maximum transmission unit size Let the flow rate be r(P) = {Ps * Fs * 8 * Ms}. The initial packet flow rate is 3000 packets per second which provides an effective throughput rate of 0.072864Gb/s. This rate is observed for a time flow of t_i. Now the traffic flow be deviated as

$$\lambda i = (si + \sum rini \pm \{r(P) * ti\} \quad (1.1)$$

Now through the compromised node ni, the packet flow rate is decreased and increased periodically leading to a throughput lack of ± 2.3276 Gb/s. Let the flow rate be equated to overall delay by TD = L/R where L is the packet length in bits and R is the transmission speed. This misflow details are analysed and reported to the alarmer module. Let c(pi) be the capture of packets by the system for a particular time period ti. The received packets are properly analysed by the algorithm used in the system. The

www.nmiet.edu.in

total flow within the system can be calculated using t(P) directly proportional f(P)*nt(P). The overall packets captured by the sytemis f(t[p]) = {r(p)*t(p)}. The received packets are captured and send to the system database using packet capture module. The packets are formatted and filtered to a form that eases down the analysis process.

To train the CNN model in the proposed framework, KDD CUP 1999 dataset is used[21]. The dataset has four different types of attacks such as, Denial of Service (DoS), User to Root (U2R), remote to local (R2L) and probe. The classified packets are further given as an input to the flow module of the proposed Deep CNN model to predict the intrusion in the network. In the flow analyzer module, the packets are grouped into different categories based on the flow, time and format. After grouping the classified package in the flow analyzer model, Deep Convolution neural network is used to detect the anomalies in the network. The alarming system sends an alarm to the respective authorities to alert abnormality in and around packet flow. Finally, a report within detail analysis of the packet flow within the system is sent to the authorities, thereby paving the way for proper action before the crime happens. Figure 2, shows the work flow of the proposed framework. The framework provides a better User Interface where the end user can track the incoming packets in visual format.

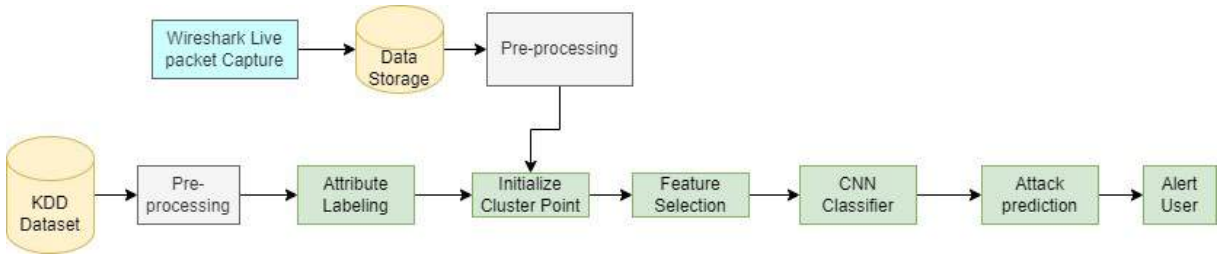

Fig 2. Workflow of the proposed framework

2.1 Data Preprocessing

Because the values in the raw dataset have such a large impact on deciding overall performance, they must be preprocessed. The KDD Cup 98 dataset is first preprocessed to allow for data manipulation using the concepts of normalisation, balancing, segmentation, and elimination of extraneous data. This work employs the Markov Chain Clustering (MCC) methodology, which accomplishes data preprocessing and classification in enhancing data quality. Following the loading of the dataset, attribute labelling, cluster index initialization, and segmentation for arranging feature values can be done. Algorithm 2 demonstrates how to use Markow Chain Clustering to preprocess the KDD Cup 98 dataset.

Algorithm – Markov Chain Clustering
Input: Input Data (networking packet details)
Output: Preprocessed and Clustered networking data *TD*.
Step 1: The feature value of the input network data should be normalised.
Step 2: The features in the normalised data are placed in a logical order.
Step 3: Calculate the separation between particles.
Step 4: Compute the Markov model's weighted estimated value using,
For i=1 *to* N
If ((i)<ω(i+1)), then
Ni= {k, (1+(i))<00, *otherwise*
$k = k + 1$
End if
End loop
End

2.2 Training the Deep CNN model using the preprocessed

The KDD Cup 98 dataset contains a total of 41 various traffic attributes, 38 of which have been numerical attributes while 3 of which are symbolic attributes. For ease of processing, the symbolic data was converted to numerical data. The symbolic type has three characteristics: a TCP/IP layer's protocol type, a target system's service type, and a flag type that indicates the session's connection state. ICMP, TCP, and UDP are three different protocols. By one encoding, three protocols are turned into three-dimensional vectors (1,0,0), (0,1,0), and (0,0,1). The dataset's numerical characteristics in the range of 0 to 255 are translated

www.nmiet.edu.in

into a 117-dimensional vector, and pictures with 13* 9 pixels are generated. A value between 0 and 255 should be assigned to each colour channel of the image. These pictures are then fed into CNN model as given in Figure 3.

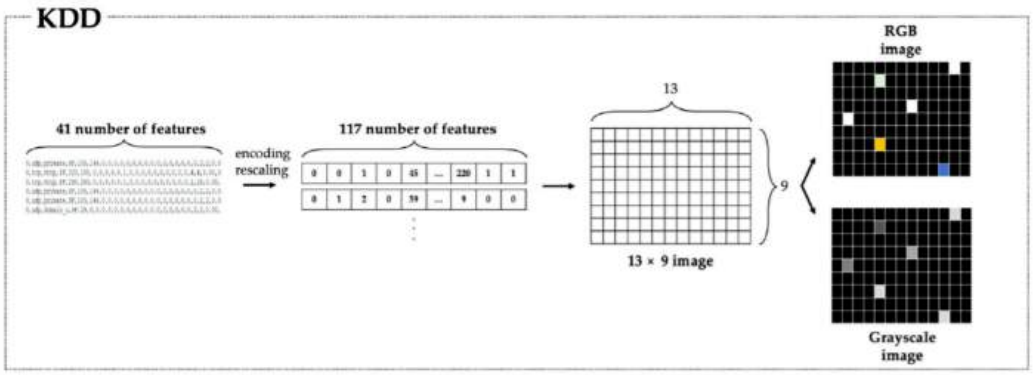

Fig 3. Conversion of numeraical features into a RGB image for CNN training model

2.3 Design of CNN intusion detection model

In the proposed algorithm, the Convolutional Neural Network (CNN) is used to differenate the normal packet flows and the abnormal flows. Figure 4 illustrates the overall design of the proposed CNN intrusion detection model.

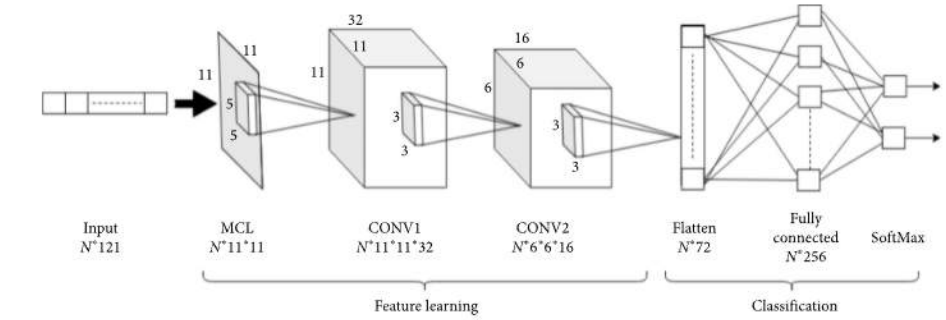

Fig 4. Design of the CNN based intrusion detection model

The most generally used DL model for image identification is CNN, which consists of a convolution layer which collects image information and a fully connected layer that decides which class the input image corresponds to. The convolution layer extracts the image's unique characteristics while preserving the image's I/O and spatial information, and by adding a pooling layer to the convolution layer, the size of the feature data is reduced.

3 Results & discussion

To evaluate the proposed framework, model attacks are created and analyzed the behavior of the system in providing detection against the attack. The KDD dataset is used to train the machine learning based classification algorithms. It assists in the analysis of incoming live packets and the classification of harmful and non-malicious. The proposed framework is trained utilising a variety of machine learning methods, including Decision Trees, Random Forests, Support Vector Machines, and Back Propagation Neural Networks. The accuracy and the precision of each algorithm is compared with one another. The suggested framework was evaluated using software tools such as Eclipse IDE, Weka, and IPmessenger, and the complete project is written in Java.

The analysis of the proposed framework is made on two basis, such as (i) The overall flow allocation and the delay experienced by the system in normal flow and (ii) The overall flow allocation and the delay experienced by the system in malicious flow. The

www.nmiet.edu.in

framework is evaluated with different test cases and scenarios.

3.1 Scenario 1: Normal flow analysis

The open source Nping packet generator is used to generate the packets within the network and allows to perform flow analysis and response time measurements. It can generate network packets for a wide range of protocols, allowing users full control over protocol headers. In this testing (normal flow) scenario, twelve wireless nodes were created and three paths are identified from the starting node to destination node. A total of 500 packets each with 128KB is transferred from the start node to the destination node. While the packets are transmitting, the live packets are captured for a limited time using packet sniffing tools and the arrival rate is analyzed. Figure 5 shows the flow allocation and the time taken to transmit the packets through three different paths.

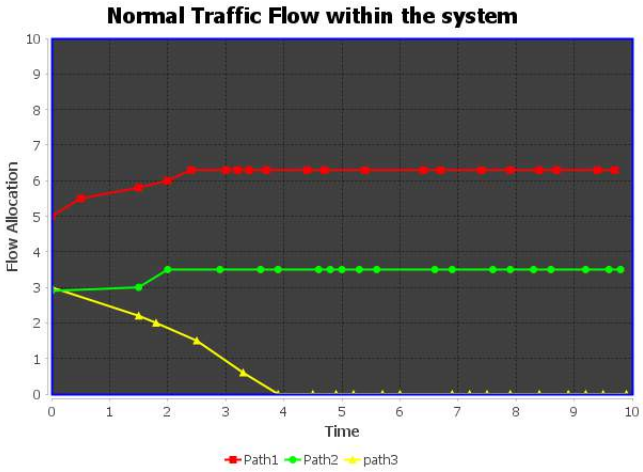

Fig 5. Normal packet flow

3.2 Scenario 2: Attack flow analysis without detection

In this (attack without detection) scenario, the same amount of packets are sent from the starting point to the destination. However, a malicious packet is introduced inside the network and the flow analysis is measured. The values are measured before the attack is detected. Figure 6, shows the malicious packet flow without the detection.

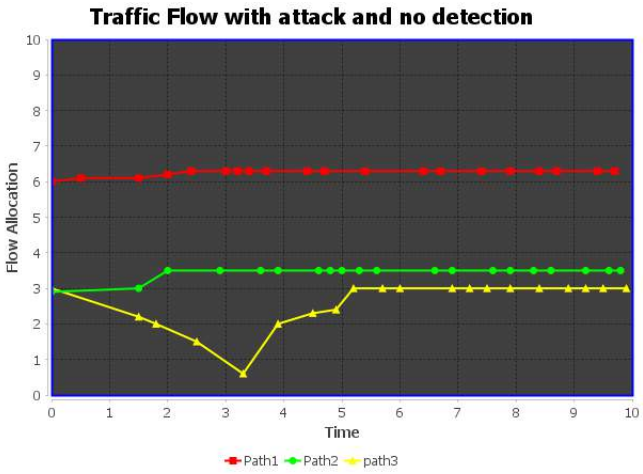

Fig 6. Malicious packet flow without detection

www.nmiet.edu.in

3.3 Scenario 3: Network Attack and detection

In this (attack with detection) scenario, the malicious packets and introduced in the network and flow allocation is measured after the framework detects the malicious packets. Figure 7 shows the traffic flow with malicious attack and detection.

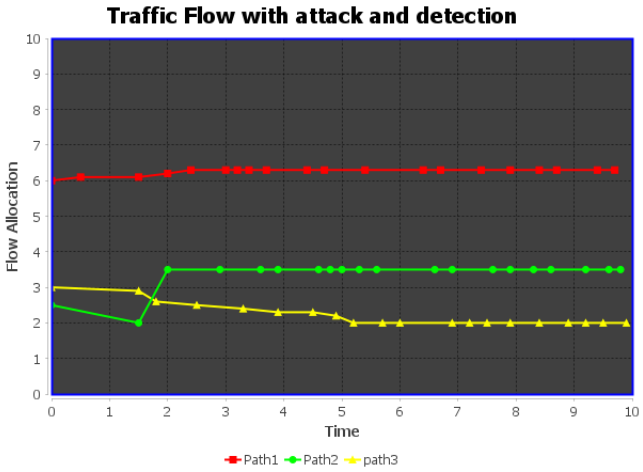

Fig 7. Malicious packet flow with detection

3.4 Comparative Analysis of Machine Learning Algorithms

The proposed system uses different machine learning algorithms to analyze and filter the data packets. The setup of ML algorithm based on Training Model Dataset with the total number of features considered for normal is 20, probe packet is 35, DoS is 25 and R2L is 15 with varying training and testing time.

Various machine learning algorithms are compared with the proposed Deep CNN classification algorithm. Deep learning is a burgeoning branch of machine learning and artificial intelligence research that has been widely and successfully utilised in this fields [22] The algorithm are compared with the parameters like accuracy, Time to build, correctly classified packets and in-correctly classified packets. According to the analysis carried out, the accuracy of classification is better in case of the proposed Deep CNN model, but its takes more time to build the model. Poor accuracy is given by Naïve Bayes Multinomial method, but it takes very less time to build the model. The other classification algorithms are giving an average result.

Table 1. Comparative Analysis of classification algorithms

Algorithms	Accuracy in %	Correctly Classified %	In-correctly Classified %	Time to build in seconds
J48	85.7971	85.7971	14.2029	67.73
Naïve Bayes	92.1398	92.13978	7.860224	5.1
Random Forest	81.7649	81.76487	18.23513	265.1
Naïve Bayes Multinomial	79.2352	79.23521	20.76479	0.09
Bayes Net	86.5957	86.59566	13.40434	20.64
MLP	93.8792	93.87918	6.120817	203.74
BPN	83.7863	83.78625	16.21375	34.82
Deep CNN	95.9263	95.92627	4.07373	109.11

3.5 Analysis of proposed framework across different servers:

The proposed framework is deployed across different servers and their detection rate is analysed for a period of time. Figure 8, shows the performance of proposed framework across different servers. As per the result compiled in the graph, the database server and the resource server are having a constant flow with the detection rate. The web server is with an oscillation and the detection rate is low as compared to the other server. The detection rate is high with the application server.

www.nmiet.edu.in

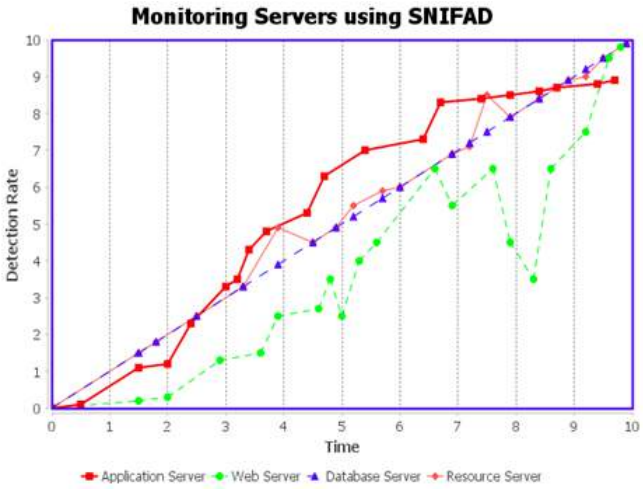

Fig 8. Performance of proposed framework across different servers

3.6 Comparison of proposed framework with existing methods:

The proposed framework is compared with the existing frameworks and the following factors are analysed:

Table 2. The Proposed framework compared with the existing framework

Framework for Digital Forensic Investigation	Proactive Analysis								
	Packet Sniffing Prepro-cessing	Data Store	ML Classi-fiers	Live Alarm	Live Report	Logger	Advance Index-ing	Registry	Live Analy-sis
Proposed System	Yes	Yes	Yes	Yes	Yes	Yes	Yes	Yes	Yes
DFIDM	Yes	Yes	Yes	No	Yes	No	No	No	No
DFI for IoT	Yes	Yes	Yes	Yes	No	Yes	Yes	No	No
DFI Procedure Model	Yes	Yes	No	Yes	Yes	No	No	No	No
Traceability in DFI	Yes	Yes	No	Yes	Yes	No	No	No	No
Data Analysis of File Forensic Investigation	Yes	Yes	No	Yes	Yes	No	No	No	No

Based on the analysis with the existing framework which is shown in Table 2, it is found that proposed framework outperforms in parameters such as efficiency, speed, live alarming and live report generation. The packets are pre-processed and fed to SQL Server. Using advance indexer the speed of the system is increased compared to the existing works made and eases live alarming and live report generation. Using MQTT background services, efficiency is improved and makes proposed framework the best framework for proactive forensic investigation method.

4 Conclusion

This research work proposes a framework to proactively detect the anomalies and malicious packets by monitoring and analyzing the live packets in the wireless network. The proposed framework works well to capture the overall activity of packet flow, detecting the deviation rate and filter the suspicious activities using deep learning techniques. Threshold values are setup with different parameters taken into account and the steady state of the system is tracked in timely manner. It characterizes the delays experienced by source nodes at the steady- state. By fine-tuning parameters and selecting different algorithms, the attack can be predicted in a proactive way whereby eliminating attacks to be happening saving a lot of time and investigation process. Our framework is set by modelling attacks and proactive investigation in attacks. Also, the framework is modelled to show effectiveness of proactive analyze than reactive analysis. Our simulation results illustrate the trade-off between the different deep learning algorithms with the accuracy of 96% which is better than the existing algorithms. In future work the framework

www.nmiet.edu.in

is extended more with user-friendly options for proactive and reactive investigation. The reinforcement learning and quantum computing can be incorporated for the enhancement of the proposed system.

References

1) Abirami S. A Complete Study on the Security Aspects of Wireless Sensor Networks. In: International Conference on Innovative Computing and Communications;vol. 55 of Lecture Notes in Networks and Systems. Singapore. Springer. 2018;p. 223–230. Available from: https://doi.org/10.1007/978-981-13-2324-9_22.
2) Kamil S, Norul HSAS, Firdaus A, Usman OL. The Rise of Ransomware: A Review of Attacks, Detection Techniques, and Future Challenges. In: 2022 International Conference on Business Analytics for Technology and Security (ICBATS). IEEE. 2022. Available from: https://doi.org/10.1109/ICBATS54253.2022.9759000.
3) Abirami A, Palanikumar S. An Artificial Intelligence-based Proactive Network Forensic Framework. *Iraqi Journal of Science*. 2023;64(11):5896–5911. Available from: https://dx.doi.org/10.24996/ijs.2023.64.11.35.
4) Islam MJ, Mahin MD, Khatun A, Debnath BC, Kabir S. Digital Forensic Investigation Framework for Internet of Things (IoT): A Comprehensive Approach. In: 2019 1st International Conference on Advances in Science, Engineering and Robotics Technology (ICASERT). IEEE. 2019. Available from: https://doi.org/10.1109/ICASERT.2019.8934707.
5) Makwana* RRS, and DST. A Network Forensic Framework for Port Scan Attack based on Efficient Packet Capturing. *International Journal of Innovative Technology and Exploring Engineering*. 2019;8(12):4632–4641. Available from: https://dx.doi.org/10.35940/ijitee.l3850.1081219.
6) Dimitriadis A, Ivezic N, Kulvatunyou B, Mavridis I. D4I - Digital forensics framework for reviewing and investigating cyber attacks. *Array*. 2020;5:1–8. Available from: https://dx.doi.org/10.1016/j.array.2019.100015.
7) Qi Y, Jiang R, Jia Y, Li A. Attack Analysis Framework for Cyber-Attack and Defense Test Platform. *Electronics*. 2020;9(9):1–18. Available from: https://dx.doi.org/10.3390/electronics9091413.
8) Qureshi S, Li J, Akhtar F, Tunio S, Khand ZH, Wajahat A. Analysis of Challenges in Modern Network Forensic Framework. *Security and Communication Networks*. 2021;2021:1–13. Available from: https://doi.org/10.1155/2021/8871230.
9) Firdonsyah A, Purwanto P, Riadi I. Framework for Digital Forensic Ethical Violations: A Systematic Literature Review. In: The 8th International Conference on Energy, Environment, Epidemiology and Information System (ICENIS 2023);vol. 448, E3S Web Conf. EDP Sciences. 2023;p. 1–10. Available from: https://doi.org/10.1051/e3sconf/202344801003.
10) Machaka V, Balan T. Investigating Proactive Digital Forensics Leveraging Adversary Emulation. *Applied Sciences*. 2022;12(18):1–15. Available from: https://dx.doi.org/10.3390/app12189077.
11) Palanikumar S, Abirami A. Proactive Network Packet Classification Using Artificial Intelligence. In: Artificial Intelligence for Cyber Security: Methods, Issues and Possible Horizons or Opportunities;vol. 972 of Studies in Computational Intelligence. Springer, Cham. 2021;p. 169–187. Available from: https://doi.org/10.1007/978-3-030-72236-4_7.
12) Ahmetoglu H, Das R. A comprehensive review on detection of cyber-attacks: Data sets, methods, challenges, and future research directions. *Internet of Things*. 2022;20:100615. Available from: https://dx.doi.org/10.1016/j.iot.2022.100615.
13) Gawand SP, Kumar MS. A Comparative Study of Cyber Attack Detection & Prediction Using Machine Learning Algorithms. Research Square Platform LLC. 2023. Available from: https://doi.org/10.21203/rs.3.rs-3238552/v1.
14) Zhang X, Zhang X, Wang W. Convolutional Neural Network. In: Intelligent Information Processing with Matlab. Singapore. Springer. 2023;p. 39–71. Available from: https://doi.org/10.1007/978-981-99-6449-9_2.
15) Wan X, Wang J, Li J, Liu X, Fu X, Wang X. Research on Satellite Quality of Service Classifier Based on Modified Recursive Flow Classification Algorithm. In: 2022 5th International Conference on Information Communication and Signal Processing (ICICSP). IEEE. 2023. Available from: https://doi.org/10.1109/ICICSP55539.2022.10050654.
16) Cai Y. A Multilayer Iteration-Based Improved Recursive Data Flow Matching Algorithm. In: 2021 International Conference on Information Technology and Big Data Engineering (ITBDE 2021);vol. 2074 of Journal of Physics: Conference Series. IOP Publishing. 2021;p. 1–6. Available from: https://dx.doi.org/10.1088/1742-6596/2074/1/012009.
17) Kang J, Kim T, Park J. FPGA-based Real-time Abnormal Packet Detector for Critical Industrial Network. In: 2019 IEEE Symposium on Computers and Communications (ISCC). IEEE. 2020. Available from: https://doi.org/10.1109/ISCC47284.2019.8969630.
18) Dahlman E, Parkvall S, Sköld J. Overall Transmission Structure. In: 5G NR. Elsevier. 2021;p. 115–145. Available from: https://doi.org/10.1016/B978-0-12-822320-8.00007-6.
19) Abirami A, Palanikumar S. BBBC-DDRL: A hybrid big-bang big-crunch optimization and deliberated deep reinforced learning mechanisms for cyber-attack detection. *Computers and Electrical Engineering*. 2023;109(Part B):108773. Available from: https://dx.doi.org/10.1016/j.compeleceng.2023.108773.
20) Kim J, Kim J, Kim H, Shim M, Choi E. CNN-Based Network Intrusion Detection against Denial-of-Service Attacks. *Electronics*. 2020;9(6):1–21. Available from: https://dx.doi.org/10.3390/electronics9060916.
21) John C, Sahoo J, Madhavan M, Mathew OK. Convolutional Neural Networks: A Promising Deep Learning Architecturefor Biological Sequence Analysis. *Current Bioinformatics*. 2023;18(7):537–558. Available from: https://dx.doi.org/10.2174/1574893618666230320103421.
22) Sujatha R, Chatterjee JM, Jhanjhi NZ, Brohi SN. Performance of deep learning vs machine learning in plant leaf disease detection. *Microprocessors and Microsystems*. 2021;80. Available from: https://doi.org/10.1016/j.micpro.2020.103615.

ISSN: 1092-910X
Vol 27 No. 3 (2024)

Determination of Uncertainty in calibration of External Micrometer

Dr. Sandip Nehe[1], Dr. Santosh Jaju[2], Mr. Vinayak Bembrekar[3], Mr. Santosh Dabhole[4], Mr. Rakesh Raushan[5], Mr. Ashish Ekatpure[6], Dinesh Burande[7], Dr. Nitin Sherje[8]

1, Assistant Professor, Department of Mechanical Engineering, Samarth College of Engineering and Management, Belhe, Maharashtra, India.

2 Professor, Department of Mechanical Engineering, G H Raisoni College of Engineering, Nagpur, Maharashtra, India.

3 Assistant Professor Professor, Department of Mechanical Engineering, Dr. D.Y. Patil College of Engineering, Akurdi, Maharashtra, India.

4, Assistant Professor, Department of Mechanical Engineering, Nutan Maharashtra Institute of Engineering & Technology, Maharashtra, India.

5, Assistant Professor, Department of Mechanical Engineering, Dr. D.Y. Patil Institute of Technology, Pune, Maharashtra, India.

6, Assistant Professor, Department of Mechanical Engineering RMD Sinhgad School of Engineering, Warje, Pune.

7, Assistant Professor, Department of Mechanical Engineering NBN Sinhgad School of Engineering, Pune.

8, Professor, Department of Mechanical Engineering, Dr. D.Y. Patil Institute of Technology, Pune, Maharashtra, India.

E-mail: sherje.nitin@gmail.com

Article History:

Received: *16-02-2024*

Revised: *26-04-2024*

Accepted: *18-05-2024*

Abstract

In recent years there has been a growing awareness of measurement uncertainty, mainly for two reasons. First, the ever- increasing number of laboratory accreditations requires the evaluation of measurement uncertainty, especially in the area of calibration. Second, quality system protocols get mature with process and time. This is because manufacturers ensure the reliability of their measurements through correct calibration of their test and measuring equipment. International and national regulations require calibration and testing laboratories to provide result of measurement uncertainty. Calibration of the measuring instrument is the process in which the readings obtained from the instrument are compared with the standard values in the laboratory at several points along the scale of the instruments i.e. micrometer, gauges, calipers etc. In general, a calibration without information about the uncertainty of these estimates is incomplete. Calculating measurement uncertainty is an attempt to reasonably limit the results of measurements as referring to standard operating procedures. Since each measurement only provides a result of the outcome, the main requirement of the uncertainty estimation is to make reader confident that reading is within stated range. Proper calibration involves more than just estimating measurement uncertainty. It also requires that the estimated value is small compared to the stated accuracy of the meter

Keywords: Measurement, calibration, uncertainty of measurement, external micrometer.

ISSN: 1092-910X
Vol 27 No. 3 (2024)

1. Introduction & Literature Review

In metrology, there are many different types of measurement system. Measured values are not accurate. In measurement system we always get the variation in results because of many reasons. All measurements have uncertainties and no measurement is perfect unless the associated uncertainty is indicated. Measurement of uncertainty is a parameter related to the result of a measurement, characterized by the variability of the measurand and an attribute of the measurand. Uncertainty of measurement is finding out by calibration of instrument. Calibration is the process of verifying the dimensions and tolerances of a gauge, or the accuracy of a gauge, by comparing it to similar equipment certified as a standard of known accuracy. Comparison methods and reference standards are used extensively in the calibrations of the Engineering Metrology group. This data is the primary information source for evaluating the uncertainty associated with length transfer from the master gauge to the customer gauge. For uncertainty to be more efficient and effective, the entire measurement process must be considered. This can include uncertainties related to factors such as instrument calibration, instrument resolution, operator skill, sample variability, and environmental factors. This paper discussed implementation of standard operation rules for calibrating dimensions of external micrometers.

James G. Salsbury et.al. emphasizes the current body of research and established standards predominantly address measurement uncertainty in the context of assigned quantity values, such as those encountered in the calibration of material measures or the inspection of commercial workpieces. This focus leads to a significant gap in understanding when it comes to performance verification of indicating measuring instruments, which is concerned with meeting specified tolerances or maximum permissible errors (MPE) without necessarily assigning a quantity value. Consequently, applying traditional uncertainty models to performance verification often results in inadequate estimates of measurement uncertainty, contributing to prevalent incorrect practices within the calibration industry. Rao, C.V stated that "Guide to the Expression of Uncertainty in Measurement," has increasingly emphasized the use of models for uncertainty analysis. However, there remains a notable lack of guidance on how to effectively develop and apply these models. This gap highlights a need for resources that bridge the theoretical understanding of uncertainty with practical modeling techniques. This booklet addresses this need by providing a focused introduction to modeling physical measuring processes, using elementary mathematics and statistics. It aims to assist metrology experts, calibration laboratory professionals, and university students by elucidating the process of creating and utilizing models to better understand and manage measurement uncertainty. Zakharov et.al. studies on measurement uncertainty in micrometer calibration have focused on developing comprehensive procedures for estimating deviations from reference standards. These procedures account for various factors, including micrometer resolution, surface flatness, parallelism deviations, and temperature discrepancies between the micrometer and reference measure. Advances include detailed models for calculating total standard and extended uncertainties, incorporating considerations for a larger number of measurements beyond five and the use of uncertainty propagation laws for fewer measurements. Additionally, uncertainty budgets have been created to support the development of software tools for routine calculations. Validation through the Monte Carlo method confirms the robustness of these procedures, underscoring their applicability for precise micrometer calibration.

ISSN: 1092-910X
Vol 27 No. 3 (2024)

2. External Micrometer

Micrometer screw gauge is used in the measurement of small sizes such as the diameter of a wire, thickness of a metal plate, etc. where greater accuracy is essential. As shown in Figure [1], micrometers are constructed on the "nut and bolt" principle, using calibrated threads and a circular scale to mark the fractional portion of the main scale.

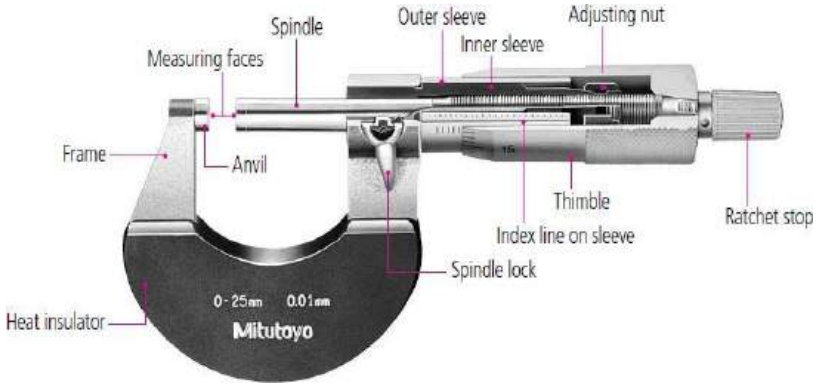

Figure 1 -External Micrometer

2.1 Calibration procedure for External Micrometer for 25-50mm range Reference: Specifications for External Micrometer – IS 2967-1983 RA2000 Standard / Equipment used for calibration as shown in table [1]

Table 1- Specification of standard used for calibration

Sr. No.	Standard/ Equipment	Range	Accuracy
1.	13 Slip Gauge Set	0-100mm	0.583µm

Procedure for Calibration:

1. Clean External Micrometer thoroughly with cleaning solution.
2. Keep micrometer in Calibration lab until the temperature reaches to stabilization temperature i.e., 20+2º C.
3. Before calibration of micrometer, check ‘0’ setting, if required use slip gauge set.
4. Calibrations of External Micrometer up to 100mm will be done using 13 slip gauge set at various points mentioned in table [2].
5. Note down all corresponding readings in observation sheet of each calibration points. Calculate average value, deviation, overall uncertainty of measurement.

Observation data for calibration is as shown in table [2].

Table 2 – Observation data

Sr. No.	Value on Standard (mm)	Value on unit under calibration (mm)					Average Value(mm)
		X1	X2	X3	X4	X5	
1	25.00	25.00	25.01	25.00	25.00	25.00	25.00

2	25+2.50	27.500	27.502	27.500	27.501	27.500	27.5006
3	25+5.10	30.100	30.100	30.104	30.103	30.100	30.1014
4	25+7.70	32.702	32.700	32.700	32.701	32.701	32.7008
5	25+10.30	35.300	35.301	35.300	35.300	35.301	35.3004
6	25+12.90	37.901	37.900	37.901	37.900	37.900	37.9004
7	25+15.00	40.00	40.02	40.00	40.00	40.02	40.0044
8	25+17.60	42.600	42.603	42.600	42.601	42.600	42.6008
9	25+20.20	45.200	45.200	45.202	45.202	45.200	45.2008
10	25+22.80	47.801	47.801	47.800	47.800	47.801	47.8006
11	25+25	50.00	50.004	50.004	50.002	50.004	50.0028

The combined uncertainty is given by -

$$U_C = \sqrt{U_A^2 + U_{B1}^2 + U_{B2}^2 + \ldots\ldots\ldots U_{Bn}^2} \quad \text{----------[1]}$$

Where, UA - Uncertainty Type A

UB - Uncertainty Type B

Observations –

After performing the reading on external micrometer for five times, readings are as shown in table [3].

Table 3- Contribution for full scale reading

Readings X_i (mm)	**Mean $\overline{X}$ (mm)**	$\left(X_i - \overline{X}\right)$ **µm**	$\left(X_i - \overline{X}\right)^2$ **µm**	**Standard Deviation** $\sigma = \sqrt{\frac{\sum (X_i - \bar{X})^2}{(n-1)}}$
50.00		-2.8	7.84	
50.004		1.2	1.44	1.789 µm
50.004	50.0028	1.2	1.44	
50.002		-0.8	0.64	
50.004		1.2	1.44	

Standard Deviation $\sigma = \sqrt{\frac{\sum (X_i - \bar{X})^2}{(n-1)}}$ ----------[2]

$$= \sqrt{\frac{(7.84 + 1.44 + 1.44 + 0.64 + 1.44)}{(5-1)}}$$

σ =1.789 μm

Standard deviation of the mean = $\frac{\sigma}{\sqrt{n}}$

Where, n = no of readings.

$= \frac{1.789}{\sqrt{5}}$

= 0.80 μm----------[3]

Thus, Repeatability (U_A) = 0.80 μm Degree of freedom = n -1 = 5 - 1 = 4

Summary of types their calculations are shown in Table [4].

Table 4 – Sources of uncertainty and its calculation

Source	Distribution	DOF	Calculation	Value
U_1 = Standard Uncertainty due to Uncertainty of measurement given on the certificate of calibration of 13 slip Gauge set (Combination of 25mm and 25mm slip gauge)[3,4,5,6]	Normal	∞	$U_1 = \sqrt{\left(\frac{0.15}{2}\right)^2 + \left(\frac{0.14}{2}\right)^2}$ = 0.102 μm The expanded uncertainty is divided by the coverage factor K=2 with 95.45% confidence.	0.102 μm
U_2 = Standard uncertainty due to external micrometer resolution. By Thumb Rule (considering technical experience and knowledge) we are assuming 25% of least count of external micrometer i.e., 0.01 mm	Rectangular	∞	$U_2 = 0.01 \times \frac{25}{100}$ =2.5 μm	2.5 μm

U3= The uncertainty of the standard due to the difference in thermal expansion coefficient of the item being calibrated and the standard used. Thermal expansion coefficient of steel i.e., external thermal expansion coefficient of 4.7µm /M°C Length (Maximum range of external micrometer) =L= 0.05m	Rectangular	∞	$U_3 = \alpha_1 - \alpha_2$ = 11.5 – 4.7 U3 =6.8 µm /M°C Sensitivity coefficient --- [3] = $\Delta T \times L$ = 2°C x 0.05m = 0.1°CM Where, ΔT = 22°C - 20°C= 2°C Standard reference temperature is 20ºC and actual calibration temperature is 22ºC	6.8 µm /M°C
U4 = Standard uncertainty due to difference in standard reference temperature 20ºC and actual calibration temperature 22ºC (By thumb rule assuming 10% variation between temperature) L= 0.05 m	Rectangular	∞	U4= ΔT x 10% $= (22 - 20) \times \frac{10}{}$ = 0.2ºC Sensitivity Coefficient --- [3] = $\alpha_{Diff} \times L$ = $(\alpha_1 - \alpha_2) \times L$ = $(11.5 - 4.7) \times 0.05$ = 0.34 µm /ºC	0.2ºC
U5= Standard uncertainty based on the in-accuracy of measurement given in the calibration certificate of temperature indicator. (Extended uncertainty 0.17ºC. For t the standard uncertainty, divide	Normal	∞	$U = \frac{0.17}{}$ = 0.085 ^0C Sensitivity Coefficient--- [3] = $\alpha_{Avg} \times L$ = $((\alpha_1 + \alpha_2)/2) \times L$	0.085 ^0C

by the cover factor k=2 at the 95.45% confidence level).

$= ((11.5+4.7)/2) \times 0.05$

$= 0.405$ µm/°C

The final uncertainty budget is shown in Table [5].

Table 5- Uncertainty Budget

Source of Uncertainty	**Estimate of Quantity** $U(X_i)$	**Distribution Type A or B Factor**	**Standard Uncertainty** $\frac{U(X_i)}{Factor}$	**Sensitivity Coefficient**	**Uncertainty Contribution** = $U(X_i) \times$ *Sensitivity Coefficient* **(µm)**	**D.O.F (Degree of Freedom)**
U1	0.102 µm	Normal 1	0.102µm	1.0	0.102	∞
U2	2.5 µm	Rectangular $\sqrt{3}$	1.443 µm	1.0	1.443	∞
U3	6.8 µm /MºC	Rectangular $\sqrt{3}$	3.926 µm/MºC	0.1ºCM	0.392	∞
U4	0.2ºC	Rectangular $\sqrt{3}$	0.115ºC	0.34 µm/ºC	0.039	∞
U5	0.085 ºC	Normal 1	0.085ºC	0.405 µm/ºC	0.0344	∞
UA	1.789 µm	Normal $\sqrt{5}$	0.80 µm	1.0	0.80	4

Combined Uncertainty -

$U_C \sqrt{U_1^2 + U_2^2 + U_3^2 + U_4^2 + U_5^2 + U_A^2}$ ---------- [4]

$= \sqrt{(0.01^2 + 1.443^2 + 0.392^2 + 0.039^2 + 0.0344^2 + 0.80^2)}$

$U_C = 1.699$ µm

Effective Degree of freedom $(V_{eff}) = \frac{(U_c)^4}{\sum_{i-1}^{n} \frac{(U_i)^4}{v_i}}$ -------- [5]--- [{----------

$$= \frac{(1.699)^4}{\frac{(0.102)^4}{\infty} + \frac{(1.443)^4}{\infty} + \frac{(0.392)^4}{\infty} + \frac{(0.039)^4}{\infty} + \frac{(0.0344)^4}{\infty} + \frac{(0.80)^4}{\infty}}$$

Student's t-distribution shows a 95.45% confidence level, = coverage factor K = 2

Expanded Uncertainty (U) = $K \times U_C$

= 2 ×1.699 U =3.398 µm---- [6]

At 50mm the value is 50mm 3.398 µm with coverage factor K = 2 with 95.45% confidence and when $v_{eff} = \infty$ Effects of individual parameters are shown in figure [2].

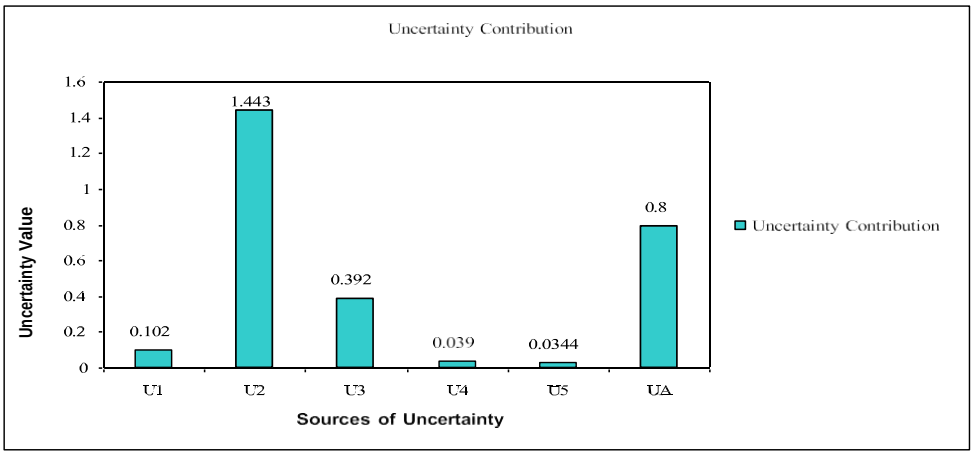

Figure 2 – Uncertainty Contribution representation

3. Conclusion

1. From calibration and evaluation of measurement of uncertainty it is confirmed that the external micrometer whose calibration is done in this research, is reading correctly.
2. If the uncertainty of external micrometer is not within the standard limit, then it will not get traceability certificate which is very important for any instrument to make correct measurements.
3. From the uncertainty budget we can find all the significant contributors to the measurement uncertainty in external micrometer. Some of those contributors depend on the measurement procedure and others depend on the calibrations of the equipment, standards, least count, temperature, thermal expansion.
4. From uncertainty contribution representation [Figure 2], it is analyzed that Standard uncertainty due to external micrometer resolution is the most affecting factor in final uncertainty measurement. Successful measurement uncertainty estimation relies on thorough and accurate sand effective measurement process. Estimation of inaccuracy is crucial for authenticity of measured data.

References-

[1] James G. Salsbury, Edward P. Morse, Measurement uncertainty in the performance verification of indicating measuring instruments, Precision Engineering, Volume 36, Issue 2, 2012, Pages 218-228, ISSN 0141-6359,

https://doi.org/10.1016/j.precisioneng.2011.10.001.

[2] Rao, C.V. (2023). Measurement Uncertainty. In: Aswal, D.K., Yadav, S., Takatsuji, T., Rachakonda, P., Kumar, H. (eds) Handbook of Metrology and Applications. Springer, Singapore. https://doi.org/10.1007/978-981-99-2074- 7_127.

[3] Zakharov, Igor & Botsiura, O. & Tsybina, I. & Zakharov, O. (2020). MEASUREMENT UNCERTAINTY EVALUATION AT MICROMETER CALIBRATION. Ukrainian Metrological Journal. 196-201. https://doi.org/10.24027/2306-7039.3A.2020.220313.

[4] Guide to the Expression of Uncertainty in Measurement, first edition, 1993, corrected and reprinted 1995, International Organization for Standardization (Geneva, Switzerland).

[5] Measurement Good Practice Guide No. 36, Estimating Uncertainties in Testing, 2001, British Measurement and Testing Association, United Kingdom.

[6] EA-4/02 Expression of the Uncertainty of Measurement in Calibration, 1999, European co-operation for Accreditation.

[7] Dr. Henrik S. Nielsen, "What is traceability and why do we calibrate?" ASQ Midwest Conference, 1999.

[8] Ted Doiron and John Stoup, "Uncertainty and Dimensional calibration", Volume 102, Number 6, 1997, Journal of Research of the National Institute of Standards and Technology.

[9] Castrup, H.: "Estimating and Combining Uncertainties," presented at the 8th Annual ITEA Instrumentation Workshop, Lancaster, CA, May 2004.

[10] Howard Castrup, Suzzane Castrup, "Uncertainty Analysis for Alternative Calibration Scenarios", NCSLI Workshop and Symposium, Orlando, August, 2008.

[11] Mandavgade, N.K., Jaju, S.B., Lakhe, R.R., Measurement uncertainty evaluation of automatic Tan Delta and resistivity test set for transformer oil, International Journal of Metrology and Quality Engineering 3 (1), pp.39-45, 2012.

[12] Mandavgade, N.K., Jaju, S.B., Lakhe, R.R., Assessment of qualitative factors affecting uncertainty measurement using AHP, International Journal of Industrial and Systems Engineering 21 (3), pp.277-301, 2015.

[13] Ravekar, K., Jaju, S., Performance Improvement of Microsurfacing Machine: A Case Study, Lecture Notes in Mechanical Engineering, pp.93, 2022.

[14] Rohit Jadhao, Vijayshri Mahobiya, Prasad Baban Dhore, Roundal Vijay Baburao, Gorane Prathamesh Sudhakar, Vijaykumar Javanjal, Mangesh Kale, Pranav Charkha, Experimental Analysis of Mechanical Tests on a Plate Composed of Banana Fibre, Communications on Applied Nonlinear Analysis, Vol. 31 No. 1s (2024), Page No.141 –
150. https://doi.org/10.52783/cana.v31.562.

[15] Abhishek Kharabi1, Aniket V. Kharabi, Aniket H. Kharabi, Tanmay Kharabi , Mangesh Kale, Design and Analysis of Electric Kid's Car, International Journal of Research in Engineering, Science and Management Volume-2, Issue- 2, February-2019 www.ijresm.com | ISSN (Online): 2581-5792.

[16] Jaju, S.B., Charkha, P.G., Kale, M., Gas metal arc welding process parameter optimization for AA7075 T6, Journal of Physics: Conference Series 1913 (1), 2021.

[17] Mandavgade, N.K., Jaju, S.B., Lakhe, R.R., Determination of uncertainty in gross calorific value of coal using bomb calorimeter, Advanced Instrument Engineering: Measurement, Calibration, and Design, pp.292, 2013.

[18] Ravekar, K., Jaju, S.B., Zoeb Narsingpurwala, A., Comparative analysis of material for material discharge plate of micro surfacing machine, Materials Today: Proceedings 46, pp.249, 2021

[19] Ravekar, K., Jaju, S., Design and analysis of material discharge plate of micro surfacing machine, Materials Today: Proceedings 38, pp.2385, 2020.

[20] Dhakne, A., Jaju, S., Shukla, S, Review on analysis of enhancing wear properties through thermo-mechanical treatment and grain size, Materials Today: Proceedings 60, pp.2270, 2022

www.nmiet.edu.in

[21] Deshmukh, B.B., Jaju, S.B., Design and analysis of glass fiber reinforced polymer (GFRP) leaf spring, International Conference on Emerging Trends in Engineering and Technology, ICETET ,pp.82, 2011.

[22] Charkha, P.G., Jaju, S.B., Analysis & optimization of connecting rod, 2nd International Conference on Emerging Trends in Engineering and Technology, ICETET 2009, pp.86, 2009.

www.nmiet.edu.in
Advances in Nonlinear Variational Inequalities
ISSN: 1092-910X
Vol 27 No. 3 (2024)

Comparative Analysis of Materials for Chassis Design in a Three-Wheeled Electric Vehicle

Dr. Pranav Charkha[1], Dr. Nitin Sherje[2], Mr. Santosh Dabhole[3], Mr. Rakesh Raushan[4], Mr. Ashish Ekatpure[5], Mr. Dinesh Burande[6], Dr. Prasad Dhore[7], Mr. Jitendra Narkhede[8]

[1], Professor, School of Engineering & Technology, Dr. D.Y. Patil University, Talegaon, Maharashtra, India.

[2], Professor, Department of Mechanical Engineering, Dr. D.Y. Patil Institute of Technology, Pimpri, Pune, Maharashtra, India.

[3], Assistant Professor, Department of Mechanical Engineering, Nutan Maharashtra Institute of Technology, Talegaon Dabhade, Pune.

[4], Assistant Professor, Department of Mechanical Engineering, Dr. D.Y. Patil Institute of Technology, Pune, Maharashtra, India.

[5], Assistant Professor, Department of Mechanical Engineering RMD Sinhgad School of Engineering, Warje, Pune.

[6], Assistant Professor, Department of Mechanical Engineering NBN Sinhgad School of Engineering, Pune.

[7], Associate Professor, Department of Computer Engineering, Nutan Maharashtra Institute of Technology, Talegaon Dabhade, Pune.

[8], Assistant Professor, Department of Mechanical Engineering, Dr. D.Y. Patil Institute of Technology, Pune, Maharashtra, India..

Corresponding Author: sherje.nitin@gmail.com

Article History:

Received: *16-02-2024*

Revised: *26-04-2024*

Accepted: *18-05-2024*

Abstract

With the growing interest in sustainable transportation, three-wheeled electric vehicles have gained popularity as an eco-friendly mode of transportation. The design of the chassis is a critical aspect of ensuring the structural integrity and performance of these vehicles. This research paper presents a comparative evaluation of different materials for chassis design in three-wheeled electric vehicles. The objective of this study is to assess the suitability of various materials, including steel, aluminum, and carbon fiber composites, for chassis construction. The evaluation criteria encompass factors such as strength, weight, stiffness, durability, and cost. A systematic methodology is employed, including theoretical analysis, computer simulations, and practical testing, to evaluate and compare the performance of each material. The findings of this research provide valuable insights into the advantages and limitations of each material in the context of three-wheeled electric vehicle chassis design. The results assist in the selection of the most suitable material based on performance requirements, cost considerations, and sustainability goals. Furthermore, the research identifies potential areas for further improvement and innovation in chassis materials for future electric vehicle designs. The outcomes of this study aim to guide manufacturers, designers, and engineers in making informed decisions when selecting materials for chassis design, ultimately enhancing the safety, efficiency, and overall performance of three-wheeled electric vehicles. By contributing to the development of sustainable transportation solutions, this research promotes the transition towards a greener and more environmentally friendly mobility landscape.

Keywords: Comparative analysis, Chassis design, Three-wheeled electric vehicle, Cost-effectiveness, Sustainability.

1. Introduction & Literature Review

The rapid global urbanization and concerns about environmental sustainability have sparked a growing interest in alternative modes of transportation. Three-wheeled electric vehicles have emerged as a promising solution, offering reduced emissions, improved energy efficiency, and increased maneuverability compared to traditional gasoline-powered vehicles. However, the design of the chassis in these vehicles is a critical factor that directly impacts their structural integrity, safety, and overall performance. The chassis serves as the backbone of a vehicle, providing support to all other components and ensuring stability during operation. It must withstand various forces and loads, including those generated by acceleration, braking, cornering, and uneven road surfaces. Therefore, selecting the appropriate material for the chassis design is essential to meet the stringent requirements of strength, stiffness, durability, and weight reduction. Traditionally, steel has been the preferred material for chassis construction due to its high strength and durability. However, with the advent of lightweight materials, such as aluminum alloys and carbon fiber composites, there is a need to explore alternative materials that can offer comparable or improved performance while reducing the overall weight of the vehicle. Light weighting the chassis can lead to enhanced energy efficiency, extended range, and improved handling characteristics. The selection of the chassis material involves a complex trade-off between various factors. Steel offers excellent strength and rigidity but is relatively heavy, impacting the vehicle's energy consumption and overall performance. Aluminum alloys offer a good balance of strength and weight reduction, but their manufacturing cost and stiffness characteristics need to be carefully considered. Carbon fiber composites provide exceptional strength-to-weight ratio, but their high production cost and challenges in repairability pose practical limitations. To address these considerations, conducting a comparative evaluation of different materials for chassis design in three-wheeled electric vehicles is crucial. Such research can provide valuable insights into the performance characteristics of each material, allowing manufacturers, designers, and engineers to make informed decisions regarding material selection. By understanding the advantages and limitations of each material, the industry can strive towards optimizing chassis designs that meet the safety, performance, and cost objectives of three-wheeled electric vehicles, further advancing the sustainable transportation paradigm.

M. Palanivendhan et.al study explores the integration of four-wheeled chassis features into a three-wheeler, employing advanced Computer-Aided Design (CAD) and Computer-Aided Manufacturing (CAM) tools to address these challenges. Utilizing SOLIDWORKS for modeling and ANSYS for analysis, the research focuses on a tadpole configuration with two front wheels and a single rear wheel, emphasizing the vehicle's adherence to both motorcycle and car regulations. Łyduch et.al. study explores the application of SIMP for designing a vehicle frame for a student competition, mirroring practices seen in large-scale manufacturing environments. The research employed SIMP within the framework of commercial Altair Hyper Works software to optimize the suspension and frame of a three-wheeled vehicle, analyzing multiple load cases to ensure robustness under various operational conditions. The results demonstrated a notable 57% reduction in the weight of the manufactured frame while preserving the necessary rigidity for vehicle performance. R.V. Patil et.al. research emphasizes the impact of various loads, including static, inertia, braking, and acceleration forces, on chassis performance. By optimizing the chassis design, stress and displacement plots were generated to assess structural integrity. The optimization process was confined to the front part of the

chassis, while the rear part retained its original design parameters. Comparative analysis revealed that the optimized chassis not only met safety requirements but also demonstrated improvements over the existing design. This study contributes to the literature by showcasing effective methodologies for chassis optimization, combining advanced modeling and analysis tools to achieve enhanced safety and cost efficiency in auto-rickshaw design. Biswal et.al study emphasizes the importance of the chassis as the structural foundation of the scooter, utilizing structural steel for its optimal balance of strength and weight. The project aims to develop a lightweight, battery-operated electric scooter equipped with a BLDC (Brushless Direct Current) hub motor transmission system. The scooter is designed to support a load of up to 100 kg and achieve speeds of up to 60 km/h. This study contributes to the literature by detailing the design and development process of an electric scooter that aligns with current industry trends and future projections, showcasing how innovative design and material choices can address both performance and sustainability goals in the evolving two-wheeler sector. Lu, Y et.al. study employs a Kreisselmeier–Steinhauser function combined with Boolean operations and a gradient-norm method to unify multiple battery cells within reinforced shells into a cohesive battery set. A new non-overlapping constraint is also proposed to prevent geometric overlaps between cells and to enforce minimum spacing through an auxiliary density filter. This approach enables the creation of an EV chassis with distributed, varied-specification batteries that demonstrates superior mechanical properties compared to designs utilizing centralized, uniform-specification batteries, while maintaining equivalent battery capacity and structural weight. Wen Zhang et.al. review covers a range of materials including light alloys, high-strength steels, composites, and advanced materials currently under research. It examines the entire lifecycle of these materials, detailing their physical and mechanical properties, characterization methods, manufacturing techniques, and potential applications. The paper also addresses both the advantages and limitations of each material, offering insights into their optimal application scenarios.

From existing studies and research on Comparative Evaluation of Materials for Chassis Design of 3-Wheeler Electric Vehicles, we have seen that Mild Steel is normally used for the chassis design of the vehicle. But the problem is, Mild steel material is having corrosive properties or it gets corrosive if it comes in the contact of water frequently.Objectives and Scope of Study:

1. To analyze different materials for the chassis of E- Rickshaw.
2. The life of the material should be good for the chassis.
3. The material should be less corrosive.
4. To reduce weight of the chassis.

The utilization of mild steel for vehicle chassis is prevalent in the industry, but it may pose certain challenges for specific vehicle types. In this context, the potential use of stainless-steel material for the chassis of 3- wheeler electric vehicles designed for garbage collection purposes holds promise for the future. Stainless steel offers several advantages that make it suitable for such applications.

Advances in Nonlinear Variational Inequalities
ISSN: 1092-910X
Vol 27 No. 3 (2024)

2. Methodology:

The design process for the chassis of an electric garbage vehicle follows a systematic approach, considering existing chassis designs and manufacturing materials. The step-by-step procedure includes:

1. Product Discovery: In the initial phase, the focus is on identifying suitable materials and design forms for the chassis. This involves researching and evaluating various options available in the market. The top- down strategy is employed, which means considering the overall requirements and specifications of the vehicle before delving into detailed design aspects.

2. Product Definition: Once the suitable materials and design forms are identified, surveys and calculations are conducted to determine key dimensions of the chassis. This includes factors such as the required load- bearing capacity, vehicle dimensions, and specific functional requirements for a garbage collection vehicle.

3. Product Design: Based on the defined requirements, the actual design of the chassis is developed. This involves considering various aspects such as structural strength, weight optimization, component integration, and manufacturability. Computer-aided design (CAD) software may be utilized to create detailed 3D models of the chassis, allowing for visualization and analysis of the design.

3. Design and Material Properties:

Design and modeling of the ladder type chassis frame of E-Rickshaw for garbage collection has been done. The ladder type chassis with two side members and four transverse members—beam components of box sections—was chosen for the current study.

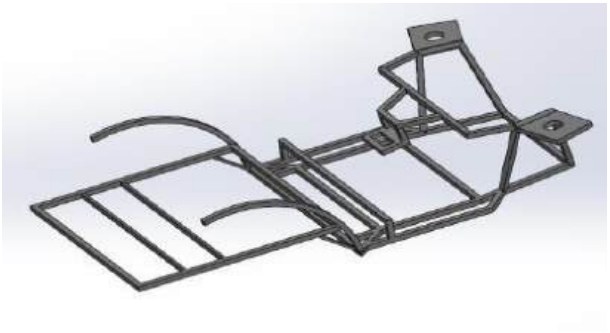

Fig.1 Model of Chassis

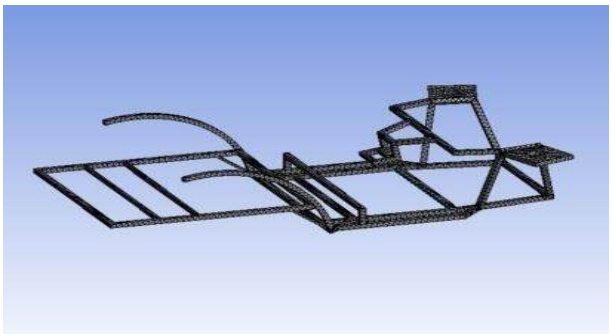

Fig.2 Meshing of Model

In this study, we have to compare between various types of materials which can be used for the design ofthe chassis of E-rickshaw which can be used for garbage collection. The materials, which are compared to analysis, are Mild Steel, Carbon Fiber, Cast Iron, Stainless Steel, Grey Cast Iron, Aluminium Alloy and Magnesium Alloy.

Table 1: Specifications of Material used for Analysis

Sr.No.	Property	Values
1	Density (kg/m^3)	8000
2	Poison's Ratio	0.28
3	Young's Modulus (MPa)	1.93 x 10^5
4	Bulk Modulus (MPa)	1.59 x 10^5

Sr.No.	Property	Values
1	Density (kg/m3)	7750
2	Poison's Ratio	0.31
3	Young's Modulus (MPa)	2 x 10^5
4	Bulk Modulus (MPa)	1.38 x 10^5

Mild Steel

Sr.No	Property	Values
1	Density (kg/m3)	7750
2	Poison's Ratio	0.31
3	Young's Modulus (MPa)	2×10^5
4	Bulk Modulus (MPa)	1.66×10^5

Carbon Fibre

Sr.No.	Property	Values
1	Density (kg/m3)	7750
2	Poison's Ratio	0.31
3	Young's Modulus (MPa)	2×10^5
4	Bulk Modulus (MPa)	1.66×10^5

Cast Iron

Sr.No.	Property	Values
1	Density (kg/m3)	7750
2	Poison's Ratio	0.31
3	Young's Modulus (MPa)	1.1 x 105
4	Bulk Modulus (MPa)	1.66 x 105

Stainless Steel

Sr.No.	Property	Values
1	Density (kg/m3)	2770
2	Poison's Ratio	0.33
3	Young's Modulus (MPa)	71000
4	Bulk Modulus (MPa)	69608

Gray Cast Iron

Aluminium Alloy

Sr.No.	Property	Values
1	Density (kg/m3)	7750
2	Poison's Ratio	0.31
3	Young's Modulus (MPa)	45000
4	Bulk Modulus (MPa)	50000

Magnesium Alloy

Boundary Conditions:

Two fixed point areas were chosen as the boundary conditions, one of which is steering, or the front wheel, two rear wheels, and side frame.

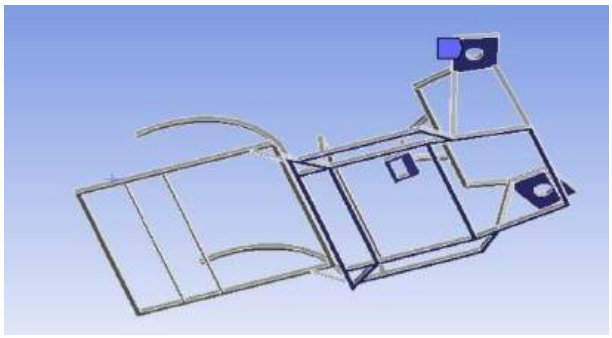

Fig. 3 Fixed Support

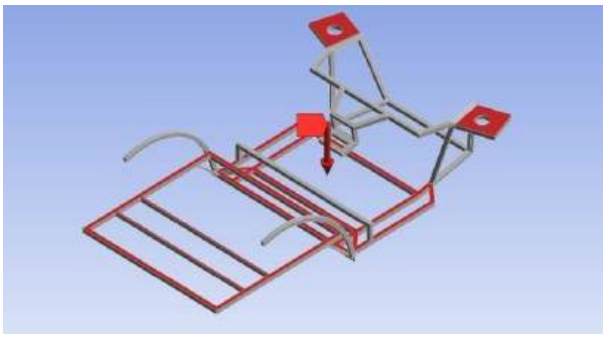

Fig.4 Forces acting on chasis

Design Calculations:

In this study, deformation and equivalent stress of the chassis beam are calculated approximately to goahead with the rectangular section s 60 mm in length, 40 mm in width, and 3.2 mm in thickness.

Basic calculation for chassis frame,

Rectangular tubular channels are used to construct the chassis' side bars. Considering the weight of batteries Capacity of electrical vehicle or car = 620 kg Capacity with 125 % = 744kg

Advances in Nonlinear Variational Inequalities
ISSN: 1092-910X
Vol 27 No. 3 (2024)

Weight of body and motor = 410 kg Weight of 1 Battery = 30 kg

Total batteries = 5

Total loads on chassis = capacity of chassis + Weight of electric motor and body + Weight of batteries
Total loads on chassis = [744 + 410 + (30 x 5)] = 1304 kg or 12787.8 N

The chassis or frame is having two beams, so, weight or load performing is half on each beam = 12787⁄2

= 6393.5 N.

Uniformly distributed load (UDL) on the chassis frame, Therefore, UDL = 6393.5/1585 = 4.03 N/mm.

- In this load, the chassis is subjected to uniformly distributed load (UDL).
- Six points are fixed: two in front of the chassis and four in back for each semi leaf elliptical leaf suspension. By adding a different weight at a different place, the analysis is finished. The meshing of the model, which has 21759 nodes and 9092 elements are there.
- Static forces from the EV body and cargo load the EV chassis model. The maximum loaded weight ofthe auto plus the body for this model is 484 kg =4756 N.
- Deformation is calculated by suing formula,

$$\delta = \frac{5wl^4}{384\,EI}$$

- Equivalent Stress is calculated by using formula,

$$\sigma = \frac{M}{Z}$$

We, got the following results for different material

Table 2: Analytical Result of Deformation and equivalent stress for different materials

Sr.No.	Name of Material	Deformation in mm	Equivalent Stress in N／mm2
1	Mild Steel	8.07	207.59
2	Carbon Fibre	7.80	211.10
3	Cast Iron	7.88	205.70
4	Stainless Steel	8.08	196.84
5	Gery Cast Iron	14.18	196.84
6	Aluminium Alloy	22.16	200.24
7	Magnesium Alloy	34.60	201.28

Advances in Nonlinear Variational Inequalities
ISSN: 1092-910X
Vol 27 No. 3 (2024)

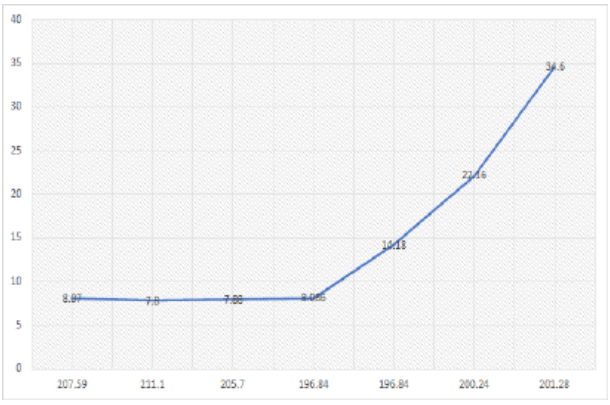

Fig.5 Graphical Representation of Analytical Results

Analysis for Total Deformation & Equivalent Stress with Ansys:

Boundary Condition: The base of the chassis is fixed and the load is applied on rear portion or on the carryportion of the chassis. Load applied on the rear portion of the chassis i.e. on the carry portion.

For Mild Steel

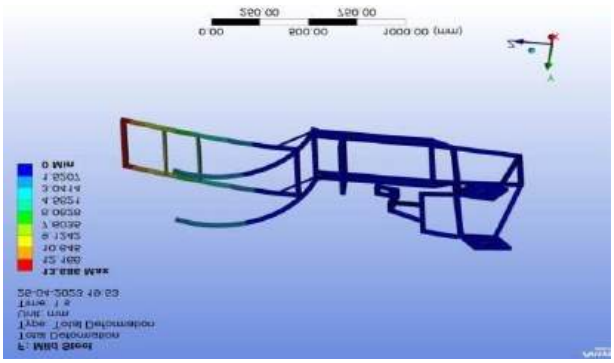

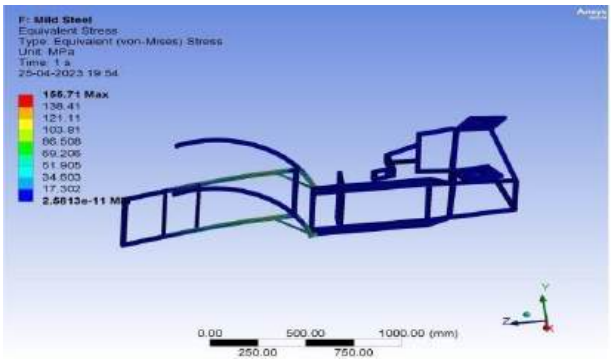

The chassis will break when 155.71 MPa stress is generated on the chassis and 4756 N load is applied.
The chassis will bend up-to 14.375 mm when 4756 N force will be applied on it.

For Carbon Fiber

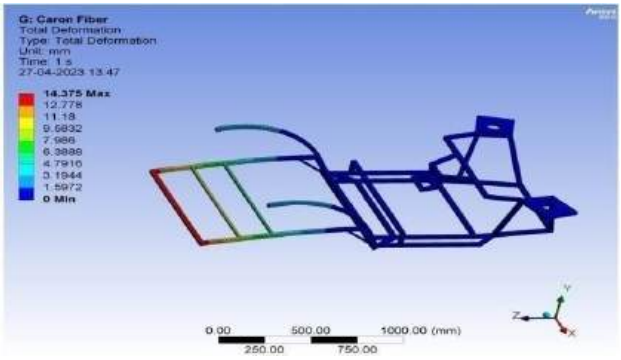

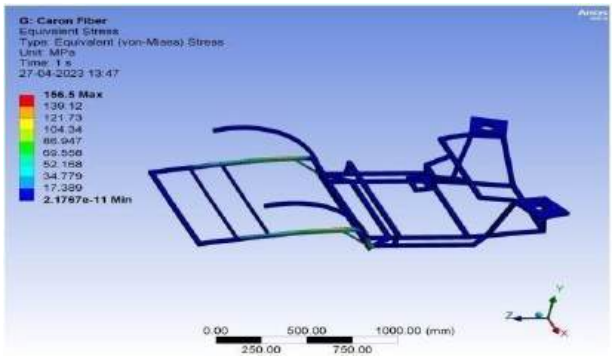

The chassis will bend up-to 14.344 mm when 4756 N force will be applied on it.

The chassis will break when 154.13 MPa stress is generated on the chassis and 4756 N load is applied.

Advances in Nonlinear Variational Inequalities
ISSN: 1092-910X
Vol 27 No. 3 (2024)

For Stainless Steel

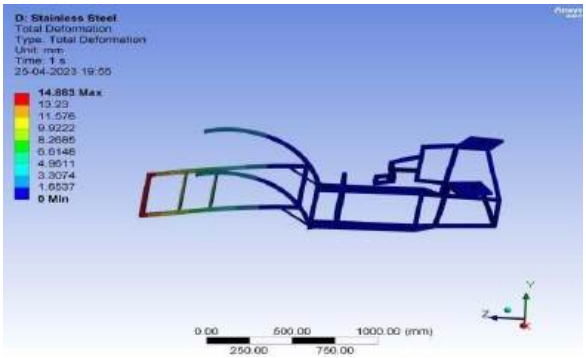

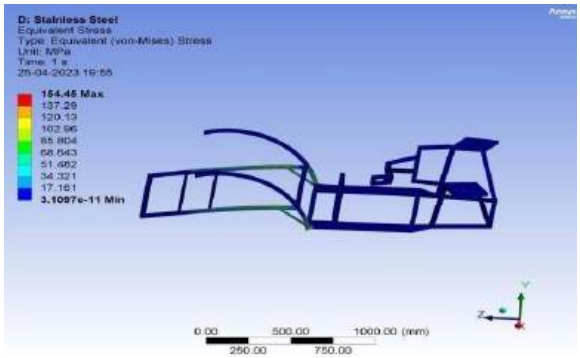

The chassis will bend up-to 14.883 mm when 4756 N force will be applied on it.

The chassis will break when 154.45 MPa stress is generated on the chassis and 4756 N load is applied.

For Grey Cast Iron

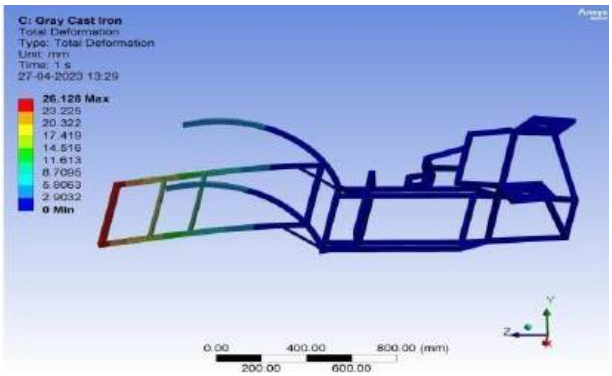

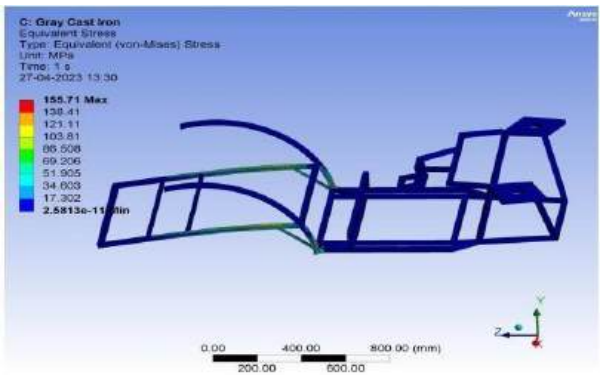

The chassis will bend up-to 26.128 mm when 4756 N force will be applied on it.

The chassis will break when 155.71 MPa stress is generated on the chassis and 4756 N load is applied.

For Aluminium Alloy

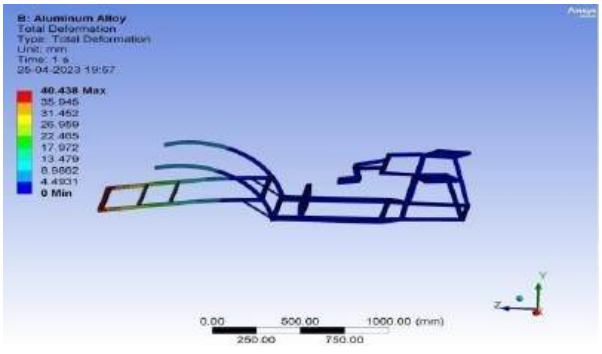

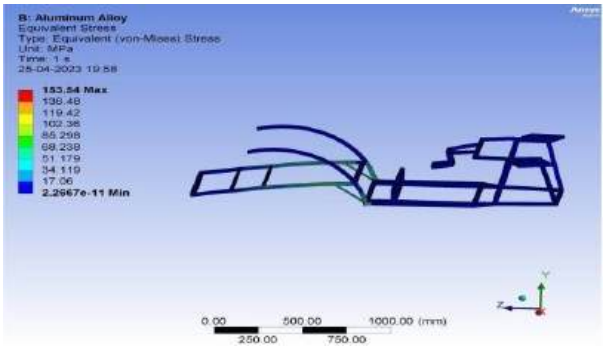

The chassis will bend up-to 40.438 mm when 4756 N force will be applied on it.

The chassis will break when 153.54 MPa stress is generated on the chassis and 4756 N load is applied.

Advances in Nonlinear Variational Inequalities
ISSN: 1092-910X
Vol 27 No. 3 (2024)

For Magnesium Alloy

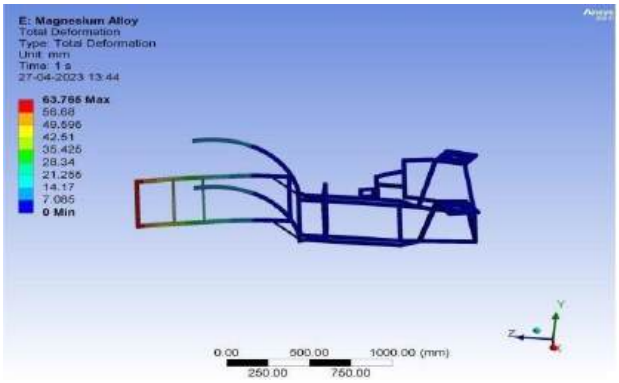

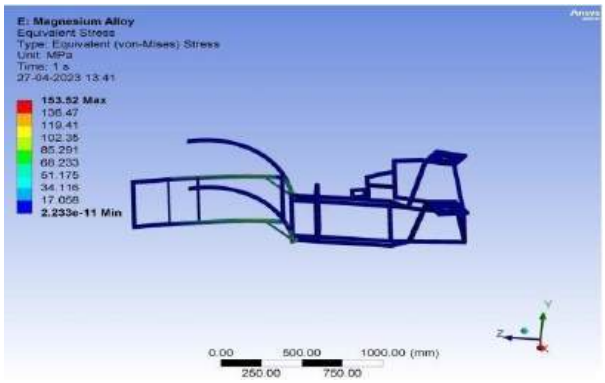

The chassis will bend up-to 63.765 mm when 4756 N force will be applied on it.

The chassis will break when 153.52 MPa stress is generated on the chassis and 4756 N load is applied.

Ansys Results:

Table 3: Ansys Result of Deformation and equivalent stress for different materials

Sr.No.	Material Name	Total Deformation (in mm)	Equivalent Stress (in MPa)
1	Mild Steel	13.686	155.71
2	Carbon Fiber	14.375	156.5
3	Cast Iron	14.334	154.13
4	Stainless Steel	14.883	154.45
5	Grey Cast Iron	26.128	155.71
6	Aluminium Alloy	40.438	153.54
7	Magnesium Alloy	63.765	153.52

Fig.6 Graphical Representation of Ansys Results

Result & Conclusion:

This study focuses on the analysis of seven different materials for the chassis design of an electric garbage vehicle. The materials considered are Mild Steel, Carbon Fiber, Cast Iron, Stainless Steel, Grey Cast Iron, Aluminium alloy, and Magnesium Alloy. The boundary conditions for the analysis involve fixing the underneath portion of the chassis frame while applying a load on both the front cabin portion and the rear carrier portion of the vehicle. The load applied on the carrier portion is 4756 N. The study compares the equivalent stresses generated in each material. The results show that the equivalent stresses for Mild Steel, Carbon Fiber, Cast Iron, Stainless Steel, Grey Cast Iron, Aluminium alloy, and Magnesium Alloy are 155.71 MPa, 156.5 MPa, 154.13 MPa, 154.45 MPa, 155.71 MPa,

153.54 MPa, and 153.52 MPa, respectively. The differences in stress levels among the materials are minor. Mild Steel, which is commonly used in existing electric rickshaws, exhibits corrosion issues when exposed to garbage water dripping onto the chassis. Carbon Fiber is an excellent material in terms of deformation control compared to Cast Iron and Stainless Steel, but its high cost makes it impractical for widespread use. Aluminium Alloy, Magnesium Alloy, and Grey Cast Iron are ductile materials but may not effectively absorb shocks. On the other hand, Stainless Steel, although brittle, can absorb shocks and has a corrosion-resistant property due to its 11- 12% chromium content. Therefore, Stainless Steel is recommended as a suitable material for the chassis frame of the electric garbage vehicle.

This study provides valuable insights into the performance and suitability of different materials for the chassis design of the garbage vehicle, considering factors such as deformation, cost, ductility, shock absorption, and corrosion resistance. The findings support the use of Stainless Steel as a viable alternative to Mild Steel for improved durability and corrosion resistance in the challenging conditions of garbage collection operations.

References

[1] M. Palanivendhan, S. Devanand, J. Chandradass, Jennifer Philip, S. Sajith Reddy, Design and analysis of 3-wheeler chassis, Materials Today: Proceedings, Volume 45, Part 7, 2021, Pages 6958-6968, ISSN 2214-7853, https://doi.org/10.1016/j.matpr.2021.01.417.

[2] Łyduch, Konrad & Szymański, Sylwester & Nowak, Michal. (2022). The frame design of a three-wheeled vehicle for a student competition using topology optimization. International Journal on Interactive Design and Manufacturing (IJIDeM). https://doi.org/16. 10.1007/s12008-022-00937-7.

[3] R.V. Patil, P.R. Lande, Y.P. Reddy, A.V. Sahasrabudhe, Optimization of Three-Wheeler Chassis by Linear Static Analysis, Materials Today: Proceedings, Volume 4, Issue 8, 2017, Pages 8806-8815, ISSN 2214-7853, https://doi.org/10.1016/j.matpr.2017.07.231.

[4] Biswal, Bibhuti. (2021). Design And Development of Electric Scooter. International Journal of Multidisciplinary Research Review. 5. 63-69.

[5] Lu, Y., Mao, H. & Zhou, M. Topology optimization of electric vehicle chassis structure with distributed load-bearing batteries. *Struct Multidisc Optim* 66, 134 (2023). https://doi.org/10.1007/s00158-023-03578-w.

[6] Wen Zhang, Jun Xu, Advanced lightweight materials for Automobiles: A review, Materials & Design, Volume 221, 2022, 110994, ISSN 0264-1275, https://doi.org/10.1016/j.matdes.2022.110994.

[7] Rohit Jadhao, Vijayshri Mahobiya, Prasad Baban Dhore, Roundal Vijay Baburao, Gorane Prathamesh Sudhakar, Vijaykumar Javanjal, Mangesh Kale, Pranav Charkha, Experimental Analysis of Mechanical Tests on a Plate Composed of Banana Fibre, Communications on Applied Nonlinear Analysis, Vol. 31 No. 1s (2024), Page No.141 – 150. https://doi.org/10.52783/cana.v31.562.

[8] Abhishek Kharabi1, Aniket V. Kharabi, Aniket H. Kharabi, Tanmay Kharabi , Mangesh Kale, Design and Analysis of Electric Kid's Car, International Journal of Research in Engineering, Science and Management Volume-2, Issue-2, February-2019 www.ijresm.com | ISSN (Online): 2581-5792.

[9] Ravekar, K., Jaju, S., Design and analysis of material discharge plate of microsurfacing machine, Materials Today: Proceedings 38, pp.2385, 2020.

[10] Kale, M. ., Charkha, S. ., Dehankar, P. ., Sharma, P. ., Choudhary, A. ., Jakhete, M. ., & Javanjal, V. . (2024). IoT-Based Smart Poultry Farm Monitoring and Controlling Using Raspberry Pi. *International Journal of Intelligent Systems and Applications in Engineering*, *12*(12s), 373–379. Retrieved from https://ijisae.org/index.php/IJISAE/article/view/4523.

[11] Jaju, S.B., Charkha, P.G., Kale, M., Gas metal arc welding process parameter optimization for AA7075 T6, Journal of Physics: Conference Series 1913 (1), 2021.

[12] Ashwin Raj Suresh, R Venkatasubramanian, L Hussien Jasim, MP Santhoshkumar, Saurabh Aggarwal, Mangesh Kale,

Integrating Hydrogen Energy Storage into Urban Mobility Solutions, 2024, E3S Web of Conferences, Volume -540, Pages 11009.

[13] Dhakne, A., Jaju, S., Shukla, S, Review on analysis of enhancing wear properties through thermo-mechanical treatment and grain size, Materials Today: Proceedings 60, pp.2270, 2022

[14] Deshmukh, B. B., Jaju, S.B., Design and analysis of glass fiber reinforced polymer (GFRP) leaf spring, International Conference on Emerging Trends in Engineering and Technology, ICETET, pp.82, 2011.

[15] Charkha, P.G., Jaju, S.B., Analysis & optimization of connecting rod, 2nd International Conference on Emerging Trends in Engineering and Technology, ICETET 2009, pp.86, 2009.

www.nmiet.edu.in

Educational Administration: Theory and Practice
2024, 30(4), 1325-1332
ISSN: 2148-2403
https://kuey.net/ **Research Article**

Peruse Of Traffic In Educational Premises Using Max-Flow Min-Cut Theorem

Shankar D. Ugale[1*], Anjali Nanaware[2], Arundhati Vaishnav[3], Dr. Madhukar Palve,[4] Kirti Takale, Dr. Vineeta Basotia[5].

[1]Research Scholar, Department of Mathematics, Shri JJT University, Rajasthan, India. Email: ugaleshankarrao@gmail.com*
[2]Student, Nutan Maharashtra Institute of Engineering and Technology, Pune, India. Email: nanawareanjali15@gmail.com
[3]Student, Nutan Maharashtra Institute of Engineering and Technology, Pune, India. Email: arundhatianil17@gmail.com
[4]Assistant Professor, Prof.Ramkrishna More Arts, Commerce and Science College Pune, India. Email: mmpalve71@gmail.com
[5]Research Scholar, Department of Mathematics, Shri JJT University, Rajasthan, India. Email: kirtighodekar@gmail.com
[6]Associate Professor, Department of Mathematics, Shri JJT University, Rajasthan, India. Email: vm.jjtu@gmail.com

Citation: *Shankar D Ugale, Dr. Madhukar Palve* et al. (2024), Peruse Of Traffic In Educational Premises Using Max-Flow Min-Cut Theorem, *Educational Administration: Theory And Practice*, *30*(2), 1325-1332
Doi:10.53555/kuey.v30i4.1663

ARTICLE INFO

ABSTRACT

Traffic congestion is a growing problem in urban areas around the world, and educational institutions are not immune. This research paper investigates the application of the Ford-Fulkerson algorithm to minimize traffic congestion in Samarth Vidya Sankul, Talegaon Dabhade City. The Ford-Fulkerson algorithm is a powerful tool for solving maximum flow problems in networks, and it can be effectively applied to traffic management scenarios. This paper presents a case study of Samarth Vidya Sankul, utilizing the algorithm to identify bottlenecks and optimize traffic flow within the school premises. The findings of this research can be valuable for improving traffic management not only in Samarth Vidya Sankul but also in other educational institutions and similar settings.

Keywords: Routes, Maximum Flow, Traffic, Max flow Min cut Theorem

1 Introduction:

Traffic congestion is a significant challenge faced by modern cities, leading to increased travel times, fuel consumption, and air pollution. Educational institutions, with their daily influx of students, staff, and visitors, are also susceptible to traffic congestion within their premises. This congestion can disrupt daily operations, create safety hazards, and negatively impact the overall learning environment.

This research paper explores the potential of the Ford-Fulkerson algorithm [1] to address traffic congestion issues in Samarth Vidya Sankul, located in Talegaon Dabhade City. [12] The Ford-Fulkerson algorithm is a well-established method for solving maximum flow problems in networks. [2] It works by iteratively identifying paths with available capacity in a network and directing flow along those paths until the maximum flow is achieved.

In the context of traffic management, the network can represent the road network within the school premises, with nodes representing intersections and edges representing road segments. The capacity of each edge can be defined by the maximum number of vehicles it can accommodate per unit time. By applying the Ford-Fulkerson algorithm to this network, we can identify bottlenecks (road segments with limited capacity) and optimize traffic flow by directing vehicles along alternative routes with available capacity.

This research aims to demonstrate the effectiveness of the Ford-Fulkerson algorithm in minimizing traffic congestion within Samarth Vidya Sankul. The paper will present a detailed case study, outlining the methodology, findings, and potential implications for both Samarth Vidya Sankul and other educational institutions seeking to improve traffic management within their premises.

2. Literature Review:

The intricate structure of trees finds numerous applications in graph theory, playing a crucial role in various real-world scenarios. From solving puzzles and optimizing video game mechanics to managing data flow and network efficiency, their impact is undeniable.

Copyright © 2024 by Author/s and Licensed by Kuey. This is an open access article distributed under the Creative Commons Attribution License which permits unrestricted use, distribution, and reproduction in any medium, provided the original work is properly cited.

www.nmjet.edu.in

Max flow and Min cut theorem is used in various research paper for traffic study, water distribution, transport networks .In some research paper flow of water distribution system in specified city is studied using Max flow and Min cut theorem. Road traffic analysis is studied in paper Road traffic analysis on the congestion problem using the Ford-Fulkerson algorithm" Journal of Road and Traffic Engineering 2022. Traffic problem solution in Kota Kinabalu city in Malaysia is studied in paper Using Ford-Fulkerson Algorithm and Max Flow-Min Cut Theorem to Minimize Traffic Congestion in Kota Kinabalu, Sabah 2017. Neighboring Vehicle traffic is given in research paper (2019) "V2v-Based Method for the Detection of Road Traffic Congestion" IET Intelligent Transport Systems. Study of causes and solution on Talegaon Dabhade traffic is used in paper Traffic Congestion - Causes and Solutions: A Study of Talegaon Dabhade City, Journal of Information, Knowledge and Research in Civil Engineering 2014.Transportation of goods from one destination to another destination in minimum cost and minimum time seen in various research papers.

3. Scope:

This research investigates the potential of the Ford-Fulkerson algorithm to minimize traffic congestion within Samarth Vidya Sankul, focusing on a real-time traffic network model. We will utilize data collected from 11 key locations within the school premises to construct an accurate representation of traffic flow. The Ford-Fulkerson algorithm will be applied to this model to identify bottlenecks and propose optimized traffic flow strategies. While the study's scope is limited to Samarth Vidya Sankul and may not be directly generalizable due to variations in other institutions, it aims to provide valuable insights into the real-world application of the algorithm for traffic management in an educational setting.[3][4]

4. Research Methodology:

This research investigates the potential of the Ford-Fulkerson algorithm to minimize traffic congestion within Samarth Vidya Sankul, Talegaon Dabhade city, Pune, Maharashtra, India. To achieve this goal, we will adopt a three-pronged approach:

1. Network Model Development:

We will establish a network model that accurately represents the traffic flow within the Samarth Vidya Sankul, Talegaon Dabhade city, Pune, Maharashtra, India premises. This model will consist of 11 key locations serving as nodes in the network: Nutan Maharashtra Vidya Prasarak Mandal, Maharaja Hotel, Balasaheb Shelke Udyan gate, Nutan Maharashtra College of Engineering and Research (including its cafe), NMIET Cafe, Nutan Maharashtra College of Engineering and Technology, Navin Samarth Vidyalay, Mamasaheb Khandge English Medium School, Nutan Maharashtra Vidya Polytechnic's Workshop, and Paisa Fund Primary school.

2. Real-Time Data Collection:

To capture the dynamic nature of traffic flow, we will collect real-time data at each of the identified locations. This data will encompass counts of various categories of road users, including students, parents, cars, bikes, buses, trucks, and rickshaws. By gathering such comprehensive data, we can ensure an accurate representation of the traffic volume and composition within the school environment.

3. Algorithm Implementation and Analysis:

We will utilize the Ford-Fulkerson algorithm on the developed network model, incorporating the real-time traffic data. This algorithm will help us identify bottlenecks in the network, which are locations experiencing significant traffic congestion. Based on these findings, we will propose optimized traffic flow strategies specifically tailored to Samarth Vidya Sankul's unique traffic patterns.

By combining these steps, this research aims to identify practical solutions for mitigating traffic congestion within the school premises, potentially improving traffic flow and enhancing the overall experience for students, staff, and visitors.

5. Results and Discussion:

Transport Network:

Imagine a transportation network like a road system. This network can be mathematically represented using a special type of graph called a weighted directed connected graph, also known as a transport network. Here's a breakdown of its key characteristics:

Structure:

- **No loops:** Think of loops as dead ends in the network, which are not allowed. Traffic should flow smoothly, not circle back on itself.

- **Single source and sink:** There's only one starting point (source) where traffic originates, and one endpoint (sink) where it all converges. Imagine the source as the "origin station" and the sink as the "destination station."
- **Non-negative edge weights:** Edges represent road segments, and their weights represent the capacity of each road, indicating how much traffic it can handle. Similar to a bridge with a weight limit, the capacity ensures smooth traffic flow without exceeding the road's capabilities.

Flow of Traffic:

- **Limited by capacity**: The amount of traffic flowing through a road (edge) cannot exceed its capacity, similar to following the weight limit on a bridge.
- **Conservation of flow:** Except for the source and sink, the incoming and outgoing traffic at any point in the network must balance out. Think of it as a traffic junction where cars entering and leaving must be equal.
- **Flow value:** The total amount of traffic flowing through the network is calculated by considering the incoming traffic minus the outgoing traffic at all points except the source and sink.

Edge States:

- **Saturated edge:** When the traffic flowing through an edge reaches its full capacity ($\Phi(i, j) = W(i, j)$), it's considered saturated. Imagine a road completely packed with vehicles, unable to accommodate any more traffic.
- **Unsaturated edge:** When the traffic flowing through an edge is less than its capacity ($\Phi(i, j) < W(i, j)$), it's considered unsaturated. Think of a road with some available space for additional vehicles.

Maximum Flow:

The goal is to find the maximum flow within the network. This represents the highest volume of traffic that canflow smoothly through the network without exceeding any road's capacity.

Cuts and Separation:

A cut in the network is a group of edges separating the source from the sink. Imagine drawing a line across the network, dividing it into two sections. One section will contain the source, and the other will contain the sink.[5]

Max-flow Min-cut Theorem:

Imagine a bustling school campus during peak hours. Students, parents, and staff navigate various routes, creating a complex traffic flow network. To understand and optimize such networks, we turn to a powerful tool: The Ford-Fulkerson algorithm.

Developed by L.R. Ford and D.R. Fulkerson in 1956, this algorithm tackles the maximum flow problem: finding the highest volume of traffic that can flow between a source (entry point) and a sink (exit point) in a network, while respecting capacity constraints on each route (road segments).

Here's how the Ford-Fulkerson algorithm works:

1. **Network Setup:** We represent the network as a directed graph with nodes representing intersections and edges representing roads. Each edge is assigned a capacity, indicating the maximum number of vehicles it can handle.

2. **Initial Flow:** We start with zero flow on all edges.

3. **Finding an Augmenting Path:** We search for a path from the source to the sink where the available capacity (remaining capacity) on each edge is positive. This path is called an augmenting path. Imagine finding a route where each road section has some space for additional vehicles.

4. **Increasing Flow:** If an augmenting path is found, we increase the flow along all edges in the path by the minimum available capacity along the path. This is similar to sending the maximum number of vehicles possible without exceeding the bottleneck (least available capacity) on the path.

5. **Repeat Steps 3 and 4:** We keep searching for augmenting paths and increasing flow along them until no such path can be found. At this point, we have reached the maximum flow through the network.
   Think of the algorithm as a strategic traffic planner. It identifies routes with available capacity, allocates traffic efficiently, and avoids overloading any road segment.

Flow chart of Ford and Fulkerson algorithm

This flowchart outlines the steps involved in the Ford-Fulkerson algorithm for finding the maximum flow in a flow network:

www.nmjet.edu.in

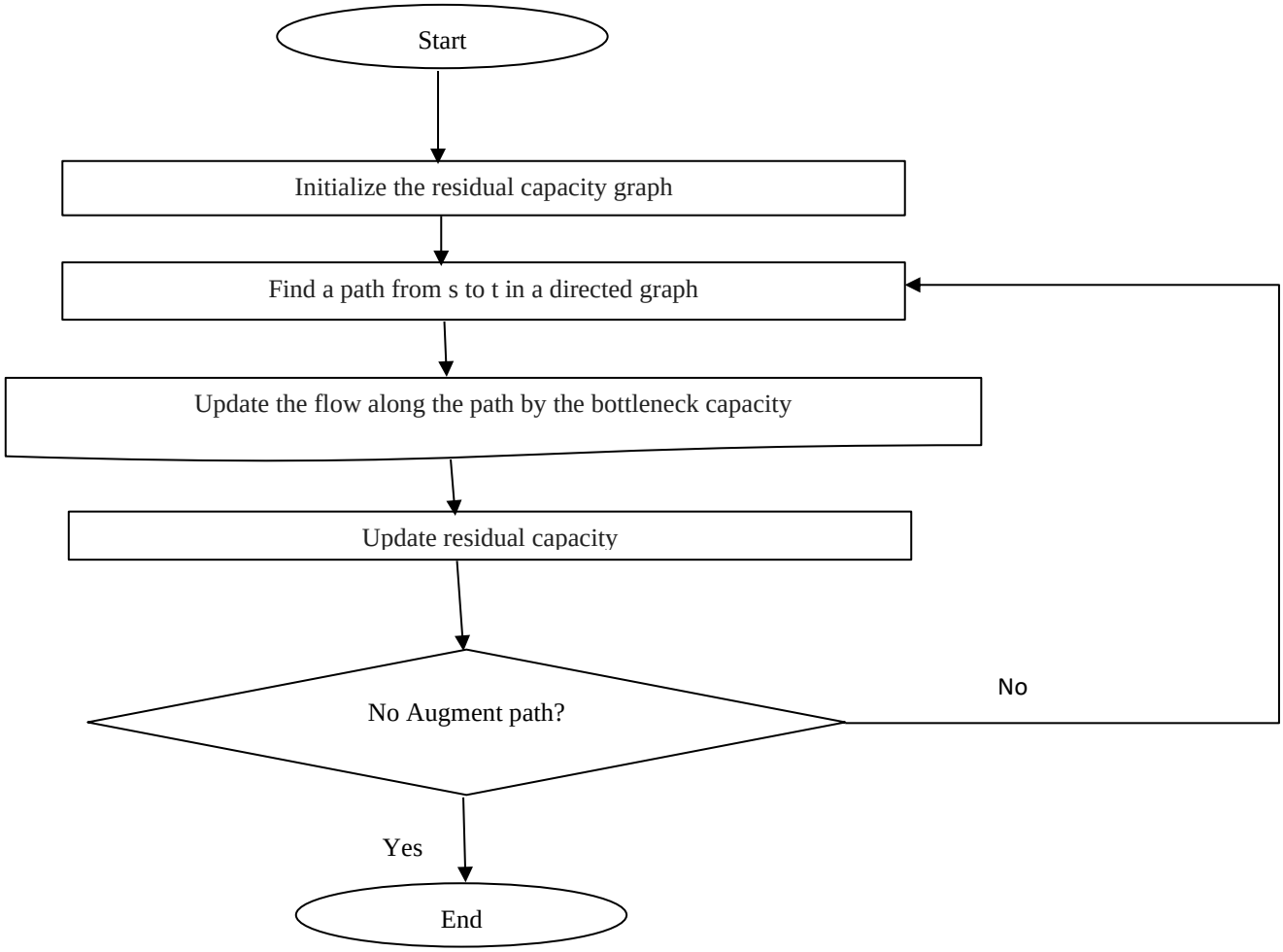

Fig 1 : Flow chart of Ford and Fulkerson algorithm

Case Study

Traffic congestion in Samarth Vidya Sankul

Our observations at Samarth Vidya Sankul revealed significant traffic congestion. To identify the most heavily congested routes, we employed the Ford-Fulkerson algorithm.

Data collection

We established a network model that accurately represents the traffic flow within the school's premises. This model will consist of 11 key locations serving as nodes in the network: Nutan Maharashtra Vidya Prasarak Mandal Gate, Maharaja Hotel, Latis society, Balasaheb Shelke Udyan gate, Nutan College of Engineering and Research, NMIET Cafe, Nutan Maharashtra Institute of Engineering and Technology, Navin Samarth Vidyalay, Mamasaheb Khandge English Medium School, NCER's Workshop, and Paisa Fund Primary School.
To simplify visualization and enhance clarity, we assigned alphabet labels to each location (vertex) in the graph:
A - Nutan Maharashtra Vidya Prasarak Mandal Gate
B - Maharaja Hotel
C - Latis society
D - Balasaheb Shelke Udyan gate
E – Nutan College of Engineering and Research (NCER College)
F – NMIET Cafe
G – Nutan Maharashtra Institute of Engineering and Technology (NMIET College)
H – Navin Samarth Vidyalay
I – Paisa Fund Primary School

J – NCER Workshop
K –Mamasaheb Khandge English Medium School

Capacity Estimation

To account for different vehicle types and their impact on traffic flow, we utilized Passenger Car Unit (PCU) equivalents. This allows us to convert the number of cars, autos, trucks, buses, and motorcycles into a standardized unit, enabling us to calculate overall traffic flow more accurately.
By employing this network model with PCU equivalents, we can effectively analyze traffic patterns within the school grounds. This will provide valuable information for optimizing traffic flow and potentially improving safety and efficiency.
We have estimated the capacity of the road manually by counting the no of vehicles in the peak hour in the morning. We have taken the readings of 5 minutes of the peak hour and then multiplied the result by 12 to get the desired result. [6]

PCU equivalent factor for different vehicles:

Vehicle type	PCU
Passenger car, tempo, auto-rickshaw, jeep, van, agricultural tractor	1.0
Truck, bus, agricultural tractor with trailer	3.0
Motorcycle, scooter, and cycle	0.5
Cycle-rickshaw	1.5

Table 1: PCU equivalent factor for different vehicles

No	Location Name	From	To	Car, Tempo, Auto	Bus, Truck, Tractor	Two Wheeler	Humans	Calculation	Total Capacity in PCU
1	NMVP main gate to Balasaheb Shelke Udyan gate	A	D	9	5	40	23	44	528
2	Balasaheb Shelke Udyan gate to NMVP main gate	D	A	8	6	36	15	44	528
3	Balasaheb Shelke Udyan gate to NCER College	D	E	0	0	7	15	3.5	42
4	NCER College to Balasaheb Shelke Udyan gate	E	D	0	0	0	3	0	0
5	Balasaheb Shelke Udyan gate to cafe	D	F	8	5	13	20	29.5	354
6	cafe to Balasaheb Shelke Udyan gate	F	D	5	0	18	5	14	168
7	Cafe to NMIET College	F	G	1	3	12	41	16	192
8	NMIET College to Cafe	G	F	0	0	3	9	9	108
9	NMIET College to Mamasaheb Khandge English Medium School	G	K	5	4	14	10	24	288
10	Mamasaheb Khandge English Medium School to NMIET college	K	G	6	1	12	4	15	180
11	NMIET college to Navin Samarth Vidyalay	G	H	1	0	15	5	8.5	102
12	Navin Samarth Vidyalay to NMIET college	H	G	0	0	7	2	3.5	42
13	Navin Samarth Vidyalay to Paisa Fund Primary School.	H	I	5	0	8	15	9	108
14	Paisa Fund Primary School to Navin Samarth Vidyalay	I	H	4	1	6	7	10	120
15	NMVP Main gate to Maharaja hotel	A	B	38	14	75	5	117.5	1410
16	Maharaja hotel to NMVP Main gate	B	A	60	17	70	7	146	1752
17	Balasaheb Shelke Udyan gate to Latis society	D	C	3	0	20	10	13	156
18	Latis society to Balasaheb Shelke Udyan gate	C	D	2	0	7	0	5.5	66
19	NCER College to Mamasaheb Khandge English Medium School	E	K	0	0	3	350	1.5	18
20	Mamasaheb Khandge English Medium School to NCER College	K	E	0	0	3	350	1.5	18
21	Mamasaheb Khandge English Medium School to NMV Polytechnic's Workshop	K	J	1	0	6	350	4	48
22	NMV Polytechnic's Workshop to Mamasaheb Khandge English Medium School	J	K	1	0	6	350	4	48
23	NMV Polytechnic's Workshop to Paisa Fund Primary School.	J	I	0	0	2	15	1	12
24	Paisa Fund Primary School to NMV Polytechnic's Workshop	I	J	0	0	1	9	0.5	6
25	Maharaja hotel to Latis society	B	C	4	1	5	3	9.6	115
26	Latis Society to Maharaja hotel	C	B	2	0	3	4	3.5	42

Table 2: Capacity estimation for selected locations

In above table the maximum capacity is 1752 vehicles per hour denoted by yellow color and minimum capacity is 0 denoted by green color.
We consider Nutan Maharashtra Vidya Prasarak Mandal Gate as a source and Paisa Fund Primary School as a sink for traffic calculations.

www.nmiet.edu.in

Graphical representation of Samarth Vidya Sankul.

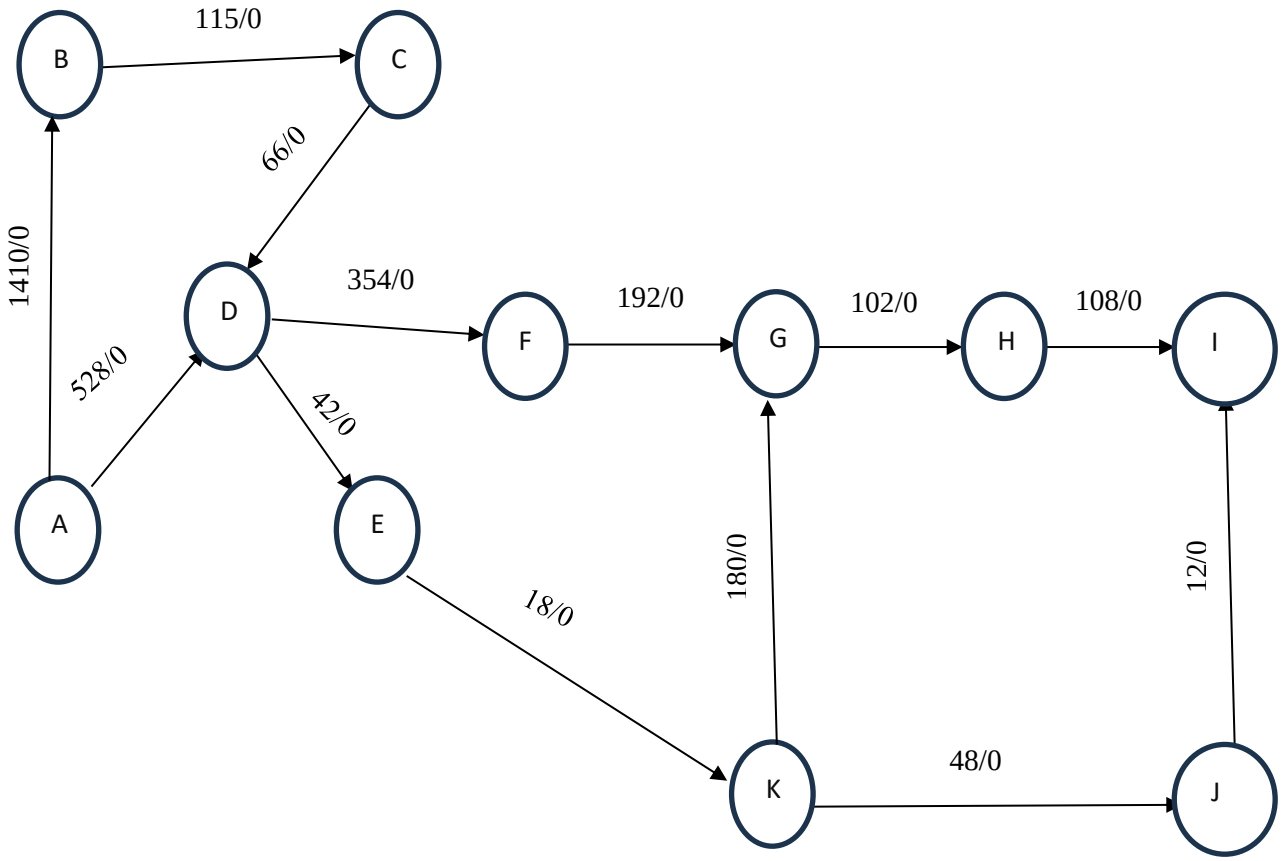

Graph 1

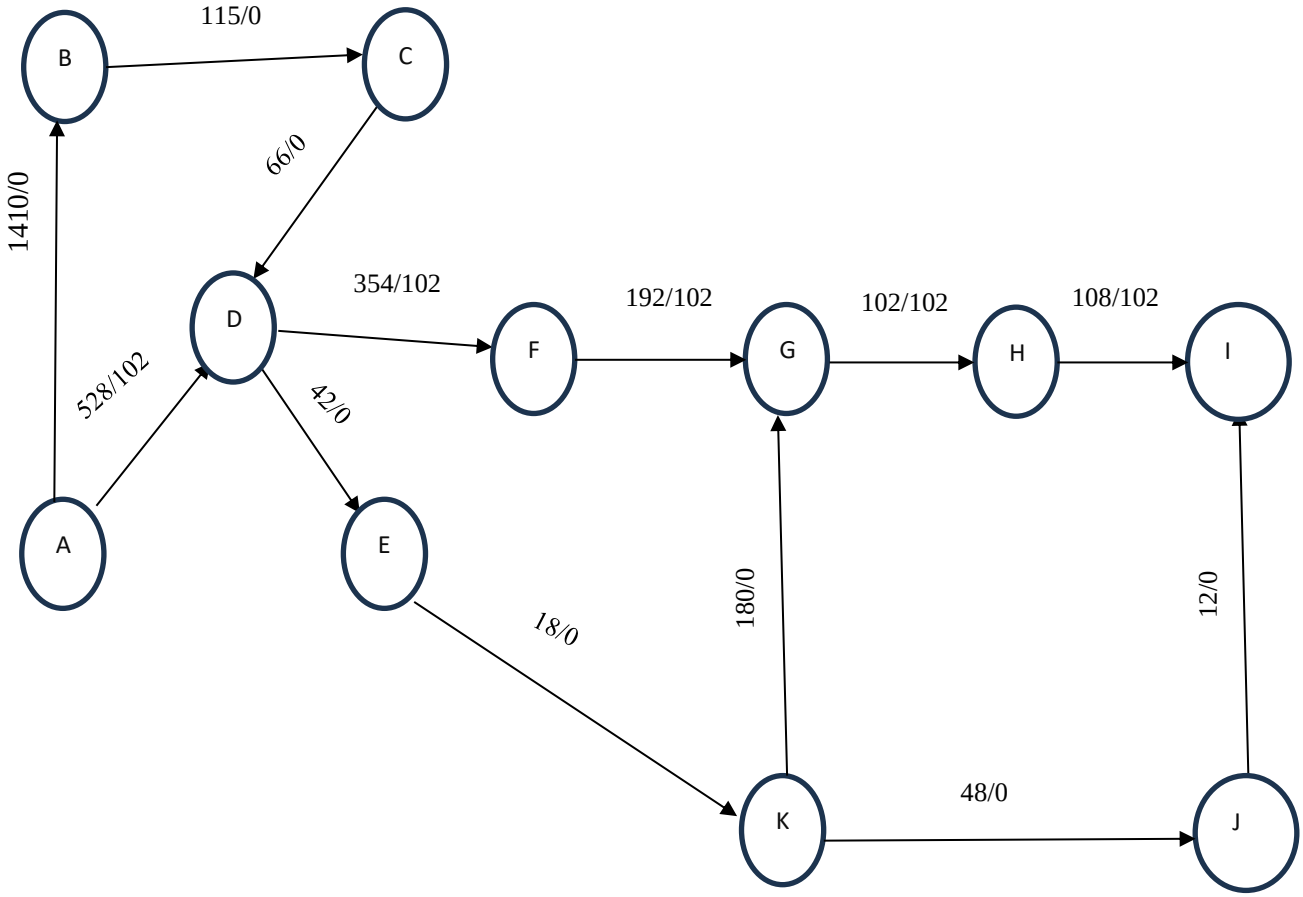

Graph 2

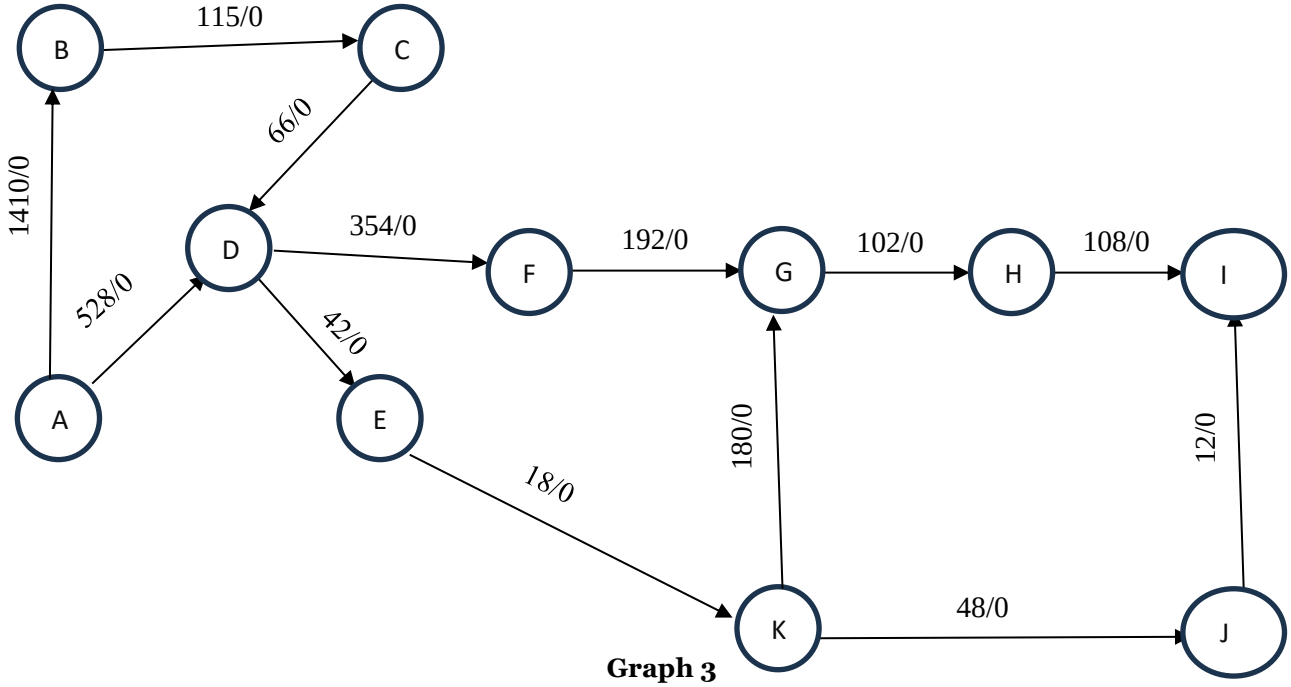

Graph 3

Augmenting path	Bottleneck capacity
A-D-F-G-H-I	102 Vehicles per hour
A-D-E-K-J-I	12 Vehicles per hour

Table 3: Augmenting path

Max Flow: 114 Vehicles per hour
Min cut: 102+12=114 shown by blue line which is equal to maximum flow.

www.nmiet.edu.in

6. Conclusion

This research paper gives the potential application of the Max-flow Min-cut Theorem to optimize traffic flow within Samarth Vidya Sankul's premises in Talegaon Dabhade city,Pune Maharashtra, India. By constructing a real-time network model encompassing key locations and utilizing data on students, parents, vehicles, and pedestrian movement, we intent to identify bottlenecks and propose efficient traffic flow strategies. [6][7]
The maximum flow turned out to be 114 vehicles per hour when the source was taken as Nutan Maharashtra Vidya Prasarak Mandal Gate and sink was taken as Paisa Fund Primary School. This research work also shows the Bottleneck path is Nutan Maharashtra Institute of Engineering and Technology (NMIET College) to Navin Samarth Vidyalay. This approach can contribute to:

Reduced Traffic Congestion: Implementing optimized traffic flow strategies based on the algorithm's recommendations can significantly reduce congestion within the school premises, improving overall traffic flow and safety.

Enhanced Safety: Mitigating congestion points can minimize the risk of accidents involving students, parents, and staff within the school grounds.

Improved Efficiency: Optimized traffic flow can lead to increased efficiency in student movement, staff operations, and overall school logistics.
However, it's important to acknowledge the limitations of this study. Our diligent search focused on a theoretical application, and further investigation is needed to implement the proposed strategies in a real-world scenario.

REFERENCES

1. Narsingh Deo (2016). “Graph Theory with Application to Engineering and Computer
2. Science”. P.61-93. Dover edition ISBN 9780486807935
3. Myint Than Kyi, Lin Lin Naing (2018) “Application of Ford-Fulkerson Algorithm to Maximum Flow in Water Distribution Pipeline Network” International Journal of Scientific and Research Publications, Volume 8, Issue 12, December 2018 ISSN 2250-3153.
4. Bopatriciat Boluma Mangataa et all (2022) “Road traffic analysis on the congestion problem using the Ford-Fulkerson algorithm” Journal of Road and Traffic Engineering, Vol 68 No 4 Online ISSN 2406-1557 Print ISSN 0478-9733.
5. Dr. Shafi K. Pathan, Rameshwar M Indoriya, Lomesh K. Ahire (2020) “Discrete Mathematics”
6. Page No. (5-3) to (5-45) Tech-Neo Publication ISBN: 978-93-90376-05-6
7. Kenneth Rosen (2011). Discrete Mathematics and Its Applications, 7th edition. McGraw-Hill
8. Science. p. 749. ISBN 978-0-07-338309-5.
9. Noraini Abdullah, Ting Kien Hua (2017) “Using Ford-Fulkerson Algorithm and Max Flow-Min Cut Theorem to Minimize Traffic Congestion in Kota Kinabalu, Sabah” Journal of Information System and Technology Management eISSN: 0128-6666, Volume: 2 Issues: 4, pp.18-34]
10. Raja Masadeh (2018) “Whale Optimization Algorithm for Solving the Maximum Flow Problem” Journal of Theoretical and Applied Information Technology, Vol.96. No 8, ISSN: 1992-8645.
11. Dilruba Akter (2011) “Modification of EDMONDS-KARP Algorithm for Solving Maximum Flow Problem” International Journal of Innovation and Applied Studies, Vol. 31 No. 4, ISSN 2028-9324.
12. Haftom Gebreanenya (2016) “Maximum Flow Problem in Ethiopian Airlines” Journal of Pogressive Research in Mathematics (JPRM), Volume 9 Issue 2, ISSN: 2395-0218.
13. Runmin Wang (2019) “V2v-Based Method For The Detection Of Road Traffic Congestion” IET Intelligent Transport Systems, ISSN 1751-956X. [11]
    Haftom Gebreanenya (2016) “Maximum Flow Problem in Ethiopian Airlines, Journal of Progressive Research in Mathematics (JPRM) ISSN: 2395-0218, Volume 9, Issue 2
14. Shekhar K. Rahane (2014) “Traffic Congestion - Causes and Solutions: A Study of Talegaon Dabhade City, Journal of Information, Knowledge and Research in Civil Engineering, ISSN: 0975 – 6744|, Volume 3, Issue 1

www.nmiet.edu.in

Enhanced Pin Entry Mechanism for ATM Machine by Defending Shoulder Surfing Attacks

| Conference paper | First Online: 11 March 2024

| pp 515–529 | Cite this conference paper

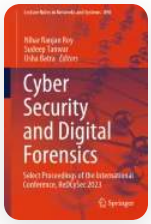

Cyber Security and Digital Forensics

(REDCYSEC 2023)

Yogesh Kisan Mali ✉, Vijay U. Rathod, Vishal Kisan Borate, Ashvini Chaudhari & Tushar Waykole

Part of the book series: Lecture Notes in Networks and Systems ((LNNS,volume 896))

Included in the following conference series:
International Conference on Recent Developments in Cyber Security

282 Accesses 2 Citations

Abstract

www.nmiet.edu.in
Passwords and extraordinary recognizable proof numbers (PINs) are critical and notable strategies for confirmation found in many gadgets, including ATMs, mobile phones, electronic entryway locks, from there, the sky is the limit. Sadly, his standard PIN section technique is totally unprotected from his shoulder riding attacks. The well-being investigations used to help these recommended frameworks, in any case, likewise give close consideration to the results of trials and testing completed on the proposed frameworks. We recommend a fresh out of the box new, hypothetically grounded idea and strategy for a quantitative security try including PIN passage methods. This paper initially presents the standards of his safe new technique for PIN section by looking at another security idea known as network-based authentication frameworks and normal span schedules concerning new construction for current schedules. Hence, keep existing framework rules. We try to lay out another her PIN passage strategy that dependably dodges a human shoulder his riding assault by extraordinarily expanding the computational intricacy an aggressor needs to break a solid framework.

This is a preview of subscription content, log in via an institution to check access.

Access this chapter

Log in via an institution

Chapter

EUR 29.95
Price includes VAT (India)

Available as PDF
Read on any device
Instant download
Own it forever

Buy Chapter →

www.nmiet.edu.in

eBook EUR 117.69

Softcover Book EUR 139.99

Tax calculation will be finalised at checkout

Purchases are for personal use only

Institutional subscriptions →

References

1. Lee M-K (2014) Security notions and advanced method for human shoulder-surfing resistant PIN-entry. IEEE Trans Inf Forensics Secur 09(3):631–645

Google Scholar

2. Sarohi HK, Khan FU (2013) Graphical password authentication schemes: current status and key issues. IJCSI 17–24

Google Scholar

3. Sobrado L, Birget JC (2014) Shoulder-surfing resistant graphical passwords. IJCSR 207–212

Google Scholar

4. Devika S, Backiyalakshmi R (2014) Design and analysis of user identification for graphical password system. IJCSIT 16(4):369381

Google Scholar

5. Johnson Durai AR, Vinayan V (2014) A novel crave-char based password entry system resistant to shoulder-surfing. IMECS 207–212

Google Scholar

6. Aarthi D, Elangovan K (2014) A survey on recall-based graphical user authentications algorithms. IJCSMA 207–212

Google Scholar

7. Mali Y, Vyas B, Borate VK, Sutar P, Jagtap M, Palkar J (2023) Role of block-chain in health-care application. In: 2023 IEEE international conference on blockchain and distributed systems security (ICBDS), New Raipur, India, pp 1–6. https://doi.org/10.1109/ICBDS58040.2023.10346537

8. Mali YK, Kore VS, Ruprah TS (2017) Secure data transfer in android using elliptical curve cryptography. In: International conference on algorithms, methodology, models and applications in emerging technologies (ICAMMAET), Feb 2017, pp 1–4

Google Scholar

9. Zhao H, Li X (2007) A scalable shoulder-surfing resistant textual-graphical password authentication scheme. In: AINAW, Mar 2007, vol 2, pp 467–472

Google Scholar

10. Mali Y, Pawar ME, More A, Shinde S, Borate V, Shirbhate R (2023) Improved pin entry method to prevent shoulder surfing attacks. In: 2023 14th International conference on

www.nmims.edu

computing communication and networking technologies (ICCCNT), Delhi, India, pp 1–6. https://doi.org/10.1109/ICCCNT56998.2023.10306875

11. Mali YK, Mohanpurkar A (2015) Advanced pin entry method by resisting shoulder surfing attacks. In: 2015 International conference on information processing (ICIP), Pune, India, pp 37–42. https://doi.org/10.1109/INFOP.2015.7489347

Author information

Authors and Affiliations

G H Raisoni College of Engineering and Management, Wagholi, Pune, India
Yogesh Kisan Mali & Vijay U. Rathod

D Y Patil College of Engineering and Innovation, Talegaon, Pune, India
Vishal Kisan Borate

Nutan Maharashtra Institute of Engineering and Technology, Talegaon, Pune, India
Tushar Waykole

Symbiosis Skills and Professional University, Kiwale, Pune, India
Ashvini Chaudhari

Corresponding author

Correspondence to Yogesh Kisan Mali .

Editor information

Editors and Affiliations

Center for Cyber Security and Cryptology, Sharda University, Greater Noida, Uttar Pradesh, India
Nihar Ranjan Roy

www.manaresults.co.in

Department of Computer Science and Engineering, Institute of Technology, Nirma University, Ahmedabad, Gujarat, India
Sudeep Tanwar

Department of Computer Science Engineering, Shri Vishwakarma Skill University, Gurugram, Haryana, India
Usha Batra

Rights and permissions

Reprints and permissions

Copyright information

© 2024 The Author(s), under exclusive license to Springer Nature Singapore Pte Ltd.

About this paper

Cite this paper

Mali, Y.K., Rathod, V.U., Borate, V.K., Chaudhari, A., Waykole, T. (2024). Enhanced Pin Entry Mechanism for ATM Machine by Defending Shoulder Surfing Attacks. In: Roy, N.R., Tanwar, S., Batra, U. (eds) Cyber Security and Digital Forensics. REDCYSEC 2023. Lecture Notes in Networks and Systems, vol 896. Springer, Singapore. https://doi.org/10.1007/978-981-99-9811-1_41

.RIS .ENW .BIB

DOI	Published	Publisher Name
https://doi.org/10.1007/978-981-99-9811-1_41	11 March 2024	Springer, Singapore

Print ISBN	Online ISBN	eBook Packages
978-981-99-9810-4	978-981-99-9811-1	Engineering

Publish with us

Policies and ethics

2024 MIT Art, Design and Technology School of Computing International Conference (MITADTSoCiCon)
MIT ADT University, Pune, India. Apr 25-27, 2024
www.nmiet.edu.in

2024 MIT Art, Design and Technology School of Computing International Conference (MITADTSoCiCon) | 979-8-3503-6287-9/24/$31.00 ©2024 IEEE | DOI: 10.1109/MITADTSoCiCon60330.2024.10575422

Monitoring Body Mass Index (BMI) Pre & Post Covid-19 Outbreak: A Comprehensive study in Healthcare

Pritam Ramesh Ahire
Computer Science & Engineering Department
Vels Institute of Science, Technology & Advanced Studies (VISTAS)
Pallavaram, Chennai
pritamahire33@gmail.com.

K.Ulaga Priya,
Associate Professor, Computer Science & Engineering Department
Vels Institute of Science, Technology & Advanced Studies (VISTAS),
Pallavaram, Chennai
upriya.se@velsuniv.ac.in

***Abstract*— A comprehensive health monitoring & analyzing system that provides personalized recommendations, goal setting, and tracking based on relevant factors related to BMI & COVID-19. System aims to analyze attack obesity through prediction, prevention and ongoing monitoring through appropriate predictive analytical system. The system's Risk Assessment component categorizes individuals by their risk levels using factors like age, gender, medical history, and behavior related to pre & post covid-19 related to BMI, then relates appropriate connections in human body. The wellness solution includes features such as fitness tracking, data integration, personalized metrics, and predictive analytics to create a holistic approach for predictive analytics health management. The system healthcare monitoring and analyzing system is a groundbreaking solution that leverages predictive analytics to promote a healthy lifestyle, combat obesity, and enhance overall well-being. By considering a range of factors and employing cutting-edge technology, we empower individuals to take control of their health, achieve their fitness objectives, and mitigate health risks.**

Keywords*— BMI, COVID-19, Obesity, Predictive Analysis, Healthcare.

I. INTRODUCTION

The standard health organizations legitimately formulated COVID-19 as a pandemic period in 2020's onwards, numerous initial investigations have delved into the connection between increased visceral fat and the repercussions for individuals afflicted by this virus. In a prospective cohort study conducted in Italy, involving 233 COVID-19 patients, Giacomelli's findings revealed that those with obesity faced a significantly heightened three-fold risk of mortality compared to individuals with a BMI less than 30 kg/m2. Similarly, study of COVID-19 patients demonstrated that severe obesity, defined by a BMI of 35 kg/m2 or higher, was linked to a higher rate of in-hospital mortality, even when accounting for other potentially influential factors. In France, Simonnet's research illustrated a notably higher prevalence of obesity observed in infected persons with higher care units grappling with SARS-CoV-2-related pneumonia.

The primary goal of our current systematic review is to ascertain the association between BMI and the severity of COVID-19 and its outcomes. Additionally, we aim to offer a conceptual perspective on the advantages and constraints associated with conducting early systematic reviews in the context of a rapidly evolving pandemic with shifting epidemiological patterns. Strong evidence supporting the validity of worries about the pandemic's potential effects on children's health has been produced by recently completed research in the United States. Woolford et al. in Southern California and Lange et al. (who looked at data from youngsters across the country) used medical records to show a marked increase in the rate of weight gain and body mass index (BMI) during the pandemic. This was especially clear in a study of kids whose weight and height were recorded at school, which revealed that even among those who were originally placed in the healthy BMI range, weight increase during the pandemic year outpaced that of the pre-pandemic years.

Risk Assessment is a fundamental part of our system. It considers age, gender, medical history, and pre- and post-COVID-19 habits, all of which are connected to BMI, to assess health risks. This helps us understand how diverse circumstances affect an individual's health by establishing appropriate bodily linkages.

Our healthcare solution includes Fitness Tracking, Data Integration, Personalised Metrics, and Predictive Analytics. These components integrate smoothly to develop a predictive analytics-based health management strategy. Fitness Tracking lets users track their workouts and progress towards fitness objectives. Personalised Metrics reflect the individual's health requirements and objectives, whereas Predictive Analytics uses data to provide suggestions.

In recent years, healthcare prediction has saved many lives. In healthcare, smart systems that assess complicated data correlations and turn them into predictive evidence have grown rapidly. Artificial intelligence is rapidly changing healthcare. This emphasises the importance of ML & DL systems in clinical data and image-based diagnosis and illness prediction procedures. Predictive analytics has become essential in healthcare since it may improve illness predictions and save lives. The importance of accurate illness prediction and estimate is highlighted by the fact that inaccurate forecasts might endanger patients [1]. The research evaluates the current ML & DL healthcare prediction technique to highlight the challenges of using these algorithms [2].

II. PREDICTIVE ANALYTICS

Predictive analytics is a complex data analysis area that predicts unknown future occurrences. It analyses data and predicts future occurrences using data mining, statistical analysis, modelling, ML, and AI in many applications [3]. The "predictor," variable used to predict future behaviour or consequences, is the core of predictive analytics. These predictors accurately estimate future probability. Machine learning and regression are the key predictive analytics methods [4]. Machine learning approaches have grown in

Authorized licensed use limited to: Savitribai Phule Pune University. Downloaded on September 10,2024 at 05:02:38 UTC from IEEE Xplore. Restrictions apply.

popularity owing to their capacity to manage large datasets with diverse properties and noisy data. Machine learning is ideal for predictive modelling because it finds detailed patterns in large datasets, according to several observational studies. These predictive algorithms are used to estimate pricing, assess risks, predict consumer behaviour, and classify documents. In essence, predictive analytics harnesses a diverse set of cutting-edge tools and methodologies to sift through historical data, discern patterns, and employ these patterns to anticipate future occurrences.

III. HEALTHCARE PREDICTIVE ANALYTICS

Predictive analytics plays pivotal role across various facets of the healthcare and life sciences sectors, providing invaluable support. Its primary objectives encompass precise disease diagnosis, the enhancement of patient care, efficient allocation of resources, and the overall improvement of clinical outcomes. By leveraging the power of predictive analytics, healthcare organizations can proactively prepare for the challenges of their industry while simultaneously optimizing costs. The achievements of predictive analytics in this domain are poised to deliver significant benefits, notably by elevating the quality of healthcare services. Looking ahead, it's evident that predictive analytics has the potential to usher in a transformative era within the healthcare industry, promising a future marked by profound changes and advancements.

IV. MACHINE LEARNING

Before Machine Learning, in its traditional sense, can be defined as the process through which a computer program enhances its ability to perform tasks within a specific domain by learning from prior experiences [5]. These experiences are denoted as "E," while the tasks it aims to improve in are referred to as "T," and the criteria used to gauge its progress is "P."

ML automates analytical model creation. Iterative techniques enable computers to learn from data without programming instructions. This allows robots to reveal hidden knowledge, aiding decision-making and problem-solving across disciplines. Machine Learning has transformed how computers process and interpret data, providing significant solutions in a data-driven environment [6,7].

A. Steps to apply machine learning to data

1. Data collection: All information must be collected in a digital form that can be examined, in a database. An algorithm will learn from this data to offer meaningful insights

2. Examining and getting ready the data: Data quality is key to machine learning project success. This is when machine learning requires a lot of human interaction. A significant portion of this time is given to data exploration, or learning more about the complexities of the data.

3. Model training: The particular machine learning job will guide the choice of a suitable method, which will then use the data to create a model representation.

4. Analyzing prototypical performance: Since every machine learning model gives a biased result, determining how effectively the algorithm learns from the history. Depending on the model, a test dataset may assess accuracy.

5. Enhancing model performance: If the model's performance has to be raised, then it is essential to use sophisticated tactics. It could sometimes be necessary to switch to a new kind of model altogether.

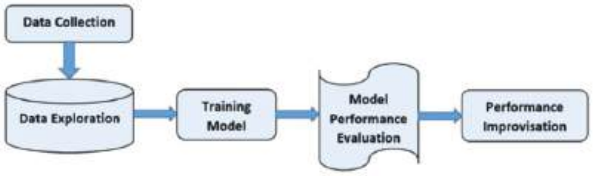

Fig. 1. Machine Learning Process

If the model seems to be functioning well after completing these stages, it may be used for the intended purpose. The model may be used to automate operations, offer score data for forecasts, project financial data, and provide relevant knowledge for marketing or research. The deployed model's triumphs and setbacks may even provide more information needed to train the model that comes out next.

B. Reinforcement Learning (RL)

This learning teaches the machine to make accurate business decisions to maximise efficiency (performance). This rigorous approach to learning optimises efficiency while reducing human proficiency. Robotics, games, and navigation use reinforcement learning. The system employs reinforcement learning to find the most rewarding tasks via trial and error.

Decision-making is scientifically called Reinforcement Learning (RL) [8]. Maximising knowledge. teaching reinforcement. It involves choosing the appropriate action to maximise rewards. Just as young infants study their surroundings and develop skills to attain goals, this ideal conduct is learnt by interacting with the environment and watching how it reacts.

The learner must determine for himself what actions to do in order to maximize the reward when there is no supervisor present. This search method is akin to conducting an iterative search. Because reinforcement learning may learn the actions that ultimately result in success in an unseen environment without the help of a supervisor, it is a very powerful algorithm [9] decision process

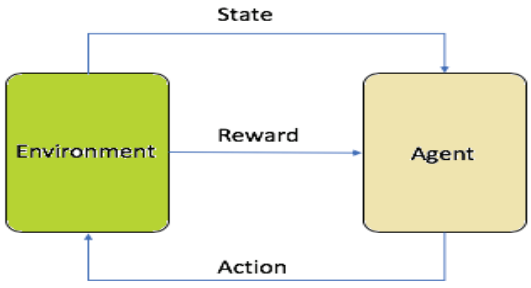

Fig. 2. Reinforcement learning approach

The following important words sum up the fundamental components of an RL problematic :

- Agent- ML algorithm, often known as the autonomous system.

Authorized licensed use limited to: Savitribai Phule Pune University. Downloaded on September 10,2024 at 05:02:38 UTC from IEEE Xplore. Restrictions apply.

- Environment- The adaptive problem space, or environment, has elements including variables, boundary values, rules, and appropriate behaviours.
- Action- A move that the real-time agent makes in order to move about.
- State- The environment at a specific moment in time.
- Reward- The performing an action can be any positive, negative, or zero value; it can also be thought of as a penalty.
- Cumulative reward- The total of all prizes or the end value.

C. *Chain of Markov*

Assume that Z0, Z1, Z2... is a series of random items. The sequence is considered Markov if, for each

$t \in \{1, 2, \cdots,\}$,

$P(Z\,t \in \cdot \mid Z\,0 = z0, Z1 = z1, \ldots, Z\,t-1 = z\,t-1) =$

$P(Z\,t \in \cdot \mid Z\,t-1 = z\,t-1)$,

for any sequence z 0, z 1 …, z t − 1.

In alternate universes, a Markov chain's future remains independent of its history, provided that 't' denotes time steps.

D. *Linear Regression (Supervised learining model)*

In linear regression, the response value is estimated and the relationship between two variables is described using a line-of-best-fit. Algorithm was made to perform basic linear regression using a single predictor variable (X) and a single respondent (Y).

$$Y = mX + b,- \quad (1)$$

where Y is the response (dependent) variable, X is the predictor (independent) variable, m is the predicted slope, and b is the estimated intercept.

The predictor or explanatory variable that does not change as a result of changes in other variables is also known as the independent variable. However, the dependent variable changes with oscillations in the independent variable. The response or result variable under study is the dependent variable, and the regression model predicts its value.

E. *K- menas Clustering (Unsupervised learining model)*

A wide number of techniques are available for finding observational subgroups within a data collection, including clustering. When we cluster data, we want observations within the same group to be similar and observations across groups to be different. Unsupervised as it does not rely on a response variable for training; rather, it looks for correlations between the observations on its own. By grouping observations together, we may determine which ones are similar and perhaps group them together. K-means clustering is a straightforward and widely used clustering method that divides a dataset into a set of k groups.

F. *Methods*

This research report delves into the comprehensive methodology of the study and provides a detailed overview of the study [10] design, participants, and data collection process. The survey was carried out in multiple City, spanning from July 3rd to July 31st, 2020, and was spearheaded by the national health organization. The actual survey was administered using a computer-aided telephone interview platform and conducted by trained interviewers. Before proceeding with formal interviews, strict adherence to eligibility criteria, which included age and the participant's location within their family, was confirmed. Additionally, each telephone conversation was meticulously recorded and reviewed by a supervisor. The survey questionnaire encompassed various critical aspects [10], including:

a) Evaluations of the COVID-19 pandemic-related government countermeasures.

b) Assessments of respondents' self-protective behaviours and risk perceptions in relation to the COVID-19 pandemic.

c) Enquiries about the respondent's city of residence during the lockdown.

d) Details on the respondent's family members' COVID-19 status [11].

e) Information on the COVID-19 situation in the neighbourhood of the respondent.

f) An evaluation of the respondents' physical and mental health conditions during the outbreak.

g) The participants' demographic details. [12,13,14].

V. SYSTM ARCHITECTURE

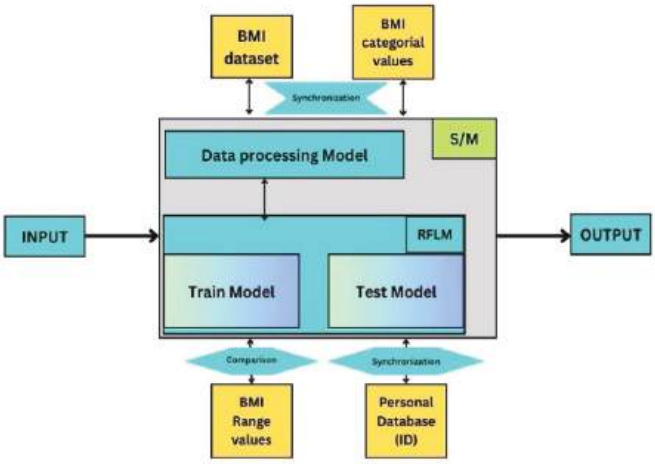

Fig. 3. Architectural Model

a) Collect BMI Data & Data Pre-processing:

In this stage, data related to BMI (Body Mass Index) is collected from various sources [15]. The collected data is then pre-processed to clean, transform, and prepare it for machine learning.

b) Reinforcement learning model:

Machine learning models are designed to predict BMI values. To do this, separate the data into sets for testing, validation, and training. Model performance is evaluated by the testing set, model parameters are adjusted with the help of the validation set, and models are trained using the training set.

c) Predict BMI Categories and Future BMI Values:

Once the machine learning models are trained and validated, they are employed to predict not only BMI categories (underweight, normal, overweight, obese) but also

Authorized licensed use limited to: Savitribai Phule Pune University. Downloaded on September 10,2024 at 05:02:38 UTC from IEEE Xplore. Restrictions apply.

future BMI values. This is achieved by applying ML algorithms to the pre-processed data.

d) Compare BMI Value Data Pre & Post COVID-19:

In this stage, BMI data from before and after the COVID-19 pandemic are compared. To determine how the pandemic affected people's BMI patterns, historical BMI data and post-COVID-19 BMI forecasts were compared.

e) Performance Analysis:

This is a critical phase where the outcomes of the BMI prediction system are analysed and evaluated. The system's performance is assessed with respect to multiple objectives [16] like personalized health monitoring, predict obesity prevention & intervention, research and epidemiology, fitness and wellness tracking [17].

A. Dataset

The dataset with information related to individuals and their Body Mass Index (BMI) calculations before the COVID-19 pandemic [18]. Here's a breakdown of the columns:

- Person ID: An identifier for each individual in the dataset.
- Gender: Indicates the gender of the person. It appears to use the following coding: (1-male, 0-female)
- Age: The age of the individual in years.
- Feet: The feet part of the height in feet and inches.
- Inches: The inch's part of the height in feet and inches.
- Pounds: The weight of the individual in pounds.
- Height: The height of the individual, calculated as the sum of feet and inches converted to a single measurement (e.g., 5 feet 10 inches becomes 5.83 feet).
- Weight: The weight of the individual in kilograms (approximately, as 1 pound is approximately 0.45 kilograms).
- BMI: The Body Mass Index of the individual, which is a calculated value based on their height and weight. (Formula for BMI = weight / (height^2)).

The BMI values in the table indicate the level of obesity or underweight for each individual. Here's a brief description of BMI standard ranges like "Below 18.5: Underweight", "18.5 to 24.9: Normal weight", "25 to 29.9: Overweight", "30 or above: Obesity".

The table seems to contain data for 25 individuals, including their gender, age, height, weight, and BMI before the COVID-19 pandemic there are various BMI performance indexes can be referred [19,20] . It can be used for various health and medical analyses and is often used to assess the overall health of an individual based on their weight relative to their height.

The table includes data for 25 individuals, with information such as gender, age, height, weight, and their calculated BMI. When evaluating a person's health and wellness, the BMI readings may be utilized to determine if they are underweight or overweight, or whether they fall within a healthy weight range.

https://www.kaggle.com/datasets/prahire/pre-post-covid-bmi

VI. RESULT

TABLE I. BMI COMPARTAISON BETWEEN PRE & POST COVID-19

Person ID A1	Pre-Covid-19 BMI	Predicted Post-Covid-19 BMI (RL output)
1	35.04	40.80
2	24.01	24.28
3	23.17	23.86
4	17.22	16.36
5	27.75	22.73
6	19.37	21.79
7	23.40	23.56
8	33.64	27.84
9	21.11	22.43
10	19.53	20.08
11	24.39	24.39
12	25.10	25.52
13	31.09	34.02
14	29.29	24.63
15	42.68	41.23
16	18.43	18.43
17	26.46	26.61
18	25.10	25.24
19	17.86	15.82
20	21.57	21.18
21	25.40	25.54
22	24.81	24.81
23	23.48	23.35
24	25.24	25.70
25	29.60	29.76

The BMI of several people both PRE and POST the Covid-19 epidemic is shown in the table. A person's BMI indicates how much weight they have with respect to their height and is frequently used to determine if they are underweight, normal weight, overweight, or obese.

Here is description of the columns in the table:

- Person ID: This column simply assigns a unique identifier to each individual, presumably for tracking and reference.
- Pre-Covid-19 BMI: This column shows the BMI of each individual before the Covid-19 pandemic.
- Predicted Post-Covid-19 BMI (RL output): This column shows the BMI of each individual after the Covid-19 pandemic. It is also calculated using the RL-ML model.

The data in these columns represent the BMI of 25 individuals. It appears that some individuals have gained weight (their BMI increased) after the Covid-19 pandemic [21], while others maintained their weight or even experienced a decrease in BMI. The table may be used to observe the effect of the pandemic on individuals' patient weight & health, which could be important for public health studies or interventions related to nutrition and lifestyle.

Authorized licensed use limited to: Savitribai Phule Pune University. Downloaded on September 10,2024 at 05:02:38 UTC from IEEE Xplore. Restrictions apply.

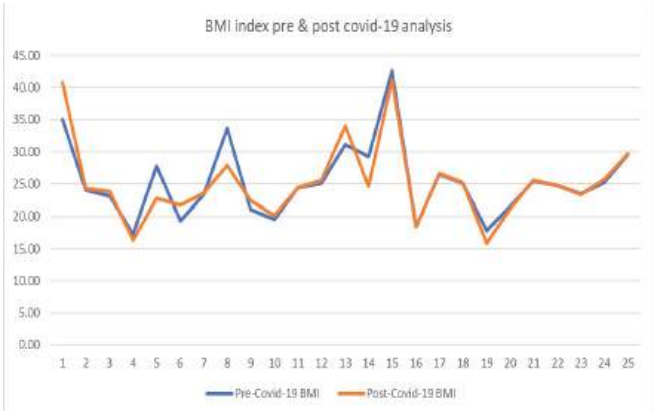

Fig. 4. BMI analysis

A. Comparing results using linear regression model (Supervised learning approach)

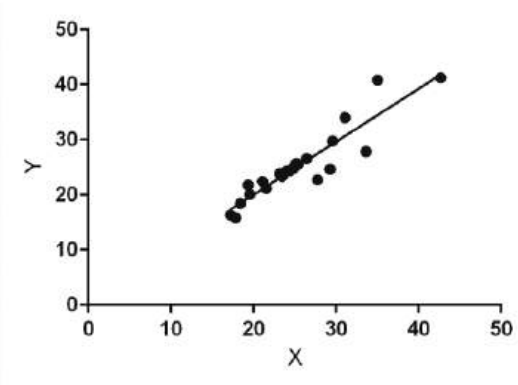

Fig. 5. BMI linear regression analysis

- Best-fit values: Slope- 0.9616 ± 0.08483, Y-intercept- 0.7827 ± 2.208, X-intercept- -0.8139, 1/Slope- 1.040.
- 95% Confidence Intervals: Slope- 0.7861 to 1.137, Y-intercept- -3.786 to 5.351, X-intercept- -6.778 to 3.344.
- Goodness of Fit: R square- 0.8482, Sy.x- 2.435.
- Is slope significantly non-zero?
- F - 128.5, DFn,DFd- 1,23, P Value- < 0.0001, Deviation from horizontal? - Significant
- Data: Number of XY pairs- 25, Equation- Y = 0.9616*X + 0.7827

B. Comparing results using K-means clustering model (Un-Supervised learning approach)

Number of clusters (k value): 2

Number of iterations: 10

TABLE II. COMPUTED SAMPLE VALUE & CENTROID INDEX

Sample value	Centroid index	Sample value	Centroid index
35.04,40.8	1	29.29,24.63	2
24.01,24.28	2	42.68,41.23	1
23.17,23.86	2	18.43,18.43	2
17.22,16.36	2	26.46,26.61	2
27.75,22.73	2	25.1,25.24	2
19.37,21.79	2	17.86,15.82	2
23.4,23.56	2	21.57,21.18	2
33.64,27.84	1	25.4,25.54	2
21.11,22.43	2	24.81,24.81	2
19.53,20.08	2	23.48,23.35	2
24.39,24.39	2	25.24,25.7	2
25.1,25.52	2	29.6,29.76	1
31.09,34.02	1		

Resultant output as below,

TABLE III. RESULTANT OUTPUT

Centroid index	Centroid value
1	34.410,34.730
2	23.135,22.816

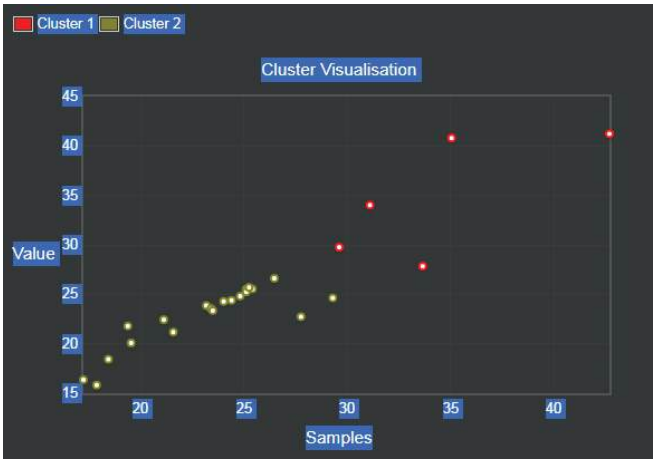

Fig. 6. Clustering analysis

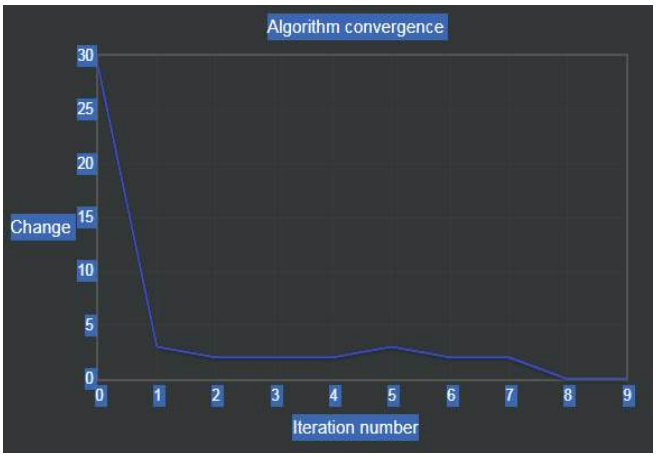

Fig. 7. Algorithm convergence

a) Bad observation:

TABLE IV. BAD OBSERVATION IN BMI BETWEEN PRE & POST COVID-19

Person ID	Pre Covid-19	Post Covid-19	Observations
1	35.04	40.80	Obesity increased in the higher range.
13	31.09	34.02	Obesity increased in the higher range.
19	17.86	15.82	Underweight decreases the range.

Authorized licensed use limited to: Savitribai Phule Pune University. Downloaded on September 10,2024 at 05:02:38 UTC from IEEE Xplore. Restrictions apply.

b) Good observation:

TABLE V. GOOD OBSERVATION IN BMI BETWEEN PRE & POST COVID-19

Person ID	Pre Covid-19	Post Covid-19	Observations
5	27.75	22.73	Overweight to normal weight
8	33.64	27.84	Obesity to overweight
14	29.29	24.63	Overweight to normal weight

c) Analysis:

After observing all results below mention analysis of all outcome in detail:

2) Outcome 1. Personalized Health Monitoring: The system aims to provide personalized health monitoring by predicting and tracking individuals' BMI values. Users can monitor their BMI trends and make informed health decisions.

3) Outcome 2. Predict Obesity Prevention & Intervention: By analyzing BMI data, the system can help predict the risk of obesity and provide early intervention suggestions to prevent its onset.

VII. CONCLUSION

This research revealed a connection between the COVID-19 lockdown and higher body weight or obesity in urban areas, particularly among young people or those who were already overweight or obese. This association was partly because physical activity decreased during the lockdown. In the broader context of social and economic development, implementing measures to increase physical activity and improve nutrition during lockdowns can be advantageous in preventing overweight and obesity. These measures also help in reducing and postponing the onset of non-communicable chronic diseases within the population. This research shows that within our national cohort of persons, BMI increased during the COVID-19 pandemic. We draw attention to the need of focused interventions, especially in higher-risk areas, to counteract the COVID-19 pandemic's negative effects on physical and mental health. We can expect an acceleration of the global obesity pandemic in the absence of more forceful action.

REFERENCES

[1] Latha MH, Ramakrishna A, Reddy BSC, Venkateswarlu C, Saraswathi SY (2022) "Disease prediction by stacking algorithms over big data from healthcare communities." Intell Manuf Energy Sustain: Proc ICIMES (265):355, 2021.

[2] Qayyum A, Qadir J, Bilal M, Al-Fuqaha A "Secure and robust machine learning for healthcare: a survey". IEEE Rev Biomed Eng 14:156–180, 2020.

[3] Tang R, De Donato L, Besinović N, Flammini F, Goverde RM, Lin Z, Wang Z, "A literature review of artificial intelligence applications in railway systems." Transp Res Part C: Emerg Technol 140:103679, 2022.

[4] Srivastava A, Saini S, & Gupta D, "Comparison of various machine learning techniques and its uses in different fields." In: 2019 3rd international conference on electronics, communication and aerospace technology (ICECA) IEEE, 2019, pp 81–86.

[5] Bakyarani ES, Srimathi H, Bagavandas M, "A survey of machine learning algorithms in health care". Int J Sci Technol Res 8(11):223, 2019.

[6] Aldahiri A, Alrashed B, Hussain W, "Trends in using IoT with machine learning in health prediction system". Forecasting 3(1):181–206, 2021.

[7] Dey A, "Machine learning algorithms: a review". Int J Comput Sci Inf Technol 7(3):1174–1179, 2016.

[8] Coronato A, Naeem M, De Pietro G, Paragliola G, "Reinforcement learning for intelligent healthcare applications: a survey". Artif Intell Med 109:101964, 2020.

[9] Williams G, Wagener N, Goldfain B, Drews P, Rehg J M, Boots B, & Theodorou E A, "Information theoretic MPC for model-based reinforcement learning". In: 2017 IEEE international conference on robotics and automation (ICRA), pp 1714–1721.

[10] Zou, P., Huo, D. & Li, M. "The impact of the COVID-19 pandemic on firms: a survey in Guangdong Province, China." glob health res policy 5, 41, 2020.

[11] Monday H N, Li J P, Nneji G U, James E C, Chikwendu I A, Ejiyi C J, & Mgbejime G T, "The capability of multi resolution analysis: a case study of COVID-19 diagnosis". In: 2021 4th international conference on pattern recognition and artificial intelligence (PRAI), IEEE, 2021, pp 236–242.

[12] Islam M T, Rafa S R, & Kibria M G (2020) "Early prediction of heart disease using PCA and hybrid genetic algorithm with k-means". In: 2020 23rd international conference on computer and information technology (ICCIT), IEEE, 2020, pp 1–6.

[13] Grampurohit S, Sagarnal C (2020) "Disease prediction using machine learning algorithms". In: 2020 international conference for emerging technology (INCET), IEEE, 2020, pp 1–7.

[14] Barik S, Mohanty S, Rout D, Mohanty S, Patra A K, & Mishra A K (2020) "Heart disease prediction using machine learning techniques". In: advances in electrical control and signal systems: select proceedings of AECSS. Springer, Singapore, 2019, pp 879–888.

[15] C. -H. Tai and D. -T. Lin, "A Framework for Healthcare Everywhere: BMI Prediction Using Kinect and Data Mining Techniques on Mobiles," 2015 16th IEEE International Conference on Mobile Data Management, Pittsburgh, PA, USA, 2015, pp. 126-129,

[16] Nuttall, Frank Q. MD, PhD. "Body Mass Index: Obesity, BMI, and Health". Nutrition Today 50(3):p 117-128, May/June 2015.

[17] Zhi Jin, Junjia Huang, Aolin Xiong, Yuxian Pang, Wenjin Wang, Beichen Ding, "Attention guided deep features for accurate body mass index estimation, Pattern Recognition Letters", Volume 154, ISSN 0167-8655, 2022, Pages 22-28.

[18] Androja L, Bavčević T, Jurčev Savičević A, Bavčević D, Ninčević J, Buljan A, Nonković D, Rodrigues V, Karin Ž. "Body Mass Index Trends before and during the COVID-19 Pandemic in Primary School Students in Split-Dalmatia County, Croatia: A Retrospective Study. Nutrients". 2024.

[19] Rancesco Zaccardi, Katherine Byrne, Kamlesh Khunti, David Kloecker, Ricardo Reynoso, Sharmin Shabnam, Luis Vaz, Thomas Yates, Clare Gillies, "The impact of COVID-19 lockdowns on the body mass index of people living with obesity: A UK retrospective cohort study using the UK Clinical Practice Research Datalink, Obesity Research & Clinical Practice", Volume 17, Issue 6, ISSN 1871-403X , 2023, Pages 468-476.

[20] Race Commers, Rodrigo Victoriano-Habit, Lancelot Rodrigue, Yan Kestens, Ahmed El-Geneidy, "Impacts of commute mode on body mass index: A longitudinal analysis before and during the COVID-19 pandemic," Journal of Transport & Health, Volume 30, ISSN 2214-1405, 2023.

[21] C.González-Monroy, I. Gómez-Gómez, C.M. Olarte-Sánchez, E. Motrico. "Eating behaviour changes during the COVID-19 pandemic: a systematic review of longitudinal studies", Int J Environ Res Public Health, 2021, p. 11130.

Authorized licensed use limited to: Savitribai Phule Pune University. Downloaded on September 10,2024 at 05:02:38 UTC from IEEE Xplore. Restrictions apply.

ICIMMI

Enhancing Alzheimer's Disease Prediction with Bayesian Optimization and Ensemble Methods

Authors: D. S. Wankhede, Nuvita Kalra, Ritika Dhabliya, Vinit Khetani, Tushar Waykole, Aparna S. Shirkande | Authors Info & Claims

ICIMMI '23: Proceedings of the 5th International Conference on Information Management & Machine Intelligence
Article No.: 108, Pages 1 - 6 https://doi.org/10.1145/3647444.3647935

Published: 13 May 2024 Publication History Check for updates

0 6

Get Acces

Feedback

Abstract

The global health crisis of Alzheimer's Disease highlights the importance of early and accurate diagnosis. This study aimed to thoroughly evaluate the effectiveness of three ensemble machine learning models, namely Random Forest, AdaBoost, and XGBoost, in accurately predicting the occurrence of Alzheimer's Disease. This study holds significant importance as the timely and precise identification of Alzheimer's Disease can have a substantial influence on the provision of patient care and the implementation of effective management strategies. Multiple evaluation metrics were utilized to conduct a comprehensive evaluation of the predictive capabilities of each model. The findings of this study revealed significant insights regarding the predictive

Association for Computing Machinery

ensemble models collectively performed well, with XGBoost emerging as the most

mentioning that XGBoost demonstrated exceptional performance in terms of specificity (98.65%) and sensitivity (98.63%), indicating its remarkable ability to accurately classify cases of both Alzheimer's and non-Alzheimer's. This study highlights the potential of ensemble machine learning techniques, specifically XGBoost, in greatly improving the precision and dependability of Alzheimer's Disease prognosis. The timely and accurate identification of Alzheimer's Disease is crucial for the implementation of effective clinical interventions and the provision of appropriate care. The results of this study have significant implications for enhancing patient outcomes and advancing the field of medical diagnostics in the realm of neurodegenerative diseases.

References

[1] Gao S, Lima D (2022) A review of the application of deep learning in the detection of Alzheimer's disease. Int J Cogn Comput Eng 3:1–8. https://doi.org/10.1016/j.ijcce.2021.12.002

Crossref | Google Scholar

[2] Khan P, Kader MF, Islam SMR, (2021) Machine Learning and Deep Learning Approaches for Brain Disease Diagnosis: Principles and Recent Advances. IEEE Access 9:37622–37655. https://doi.org/10.1109/ACCESS.2021.3062484

Crossref | Google Scholar

[3] Shastry KA, Vijayakumar V, Manoj Kumar M V., (2022) Deep Learning Techniques for the Effective Prediction of Alzheimer's Disease: A Comprehensive Review. Healthc 10:. https://doi.org/10.3390/healthcare10101842

Recommendations

Diagnosis of Alzheimer's disease using Naive Bayesian Classifier

In the world of modern medicine, though there is lot of medical achievements, some diseases still continue to pest the human race. Unfortunately, dementia is one such disease. All over the world, a large number of people are suffering fro...

Read More

Ensemble Model for Predicting Alzheimer's Disease and Disease Stages with CNN and Transformer Models

ADMIT '23: Proceedings of the 2023 2nd International Conference on Algorithms, Data Mining, and Information Technology

Alzheimer’s disease, a prevalent form of dementia, is a progressive, long-term and irreversible neurological disorder. With the growing elderly population, there has been a significant rise in the number of individuals affected by Alzheimer’s...

Read More

Classification of Alzheimer's Disease and Parkinson's Disease by Using Machine Learning and Neural Network Methods

ICMLC '10: Proceedings of the 2010 Second International Conference on Machine Learning and Computing

Data mining is a fast evolving technology, is being adopted in biomedical sciences and research. Data mining in medicine is an emerging field of high importance for providing prognosis and a deeper understanding of the classification of ...

Read More

Comments

Association for Computing Machinery

0 Comments

Share

Best Newest Oldest

Nothing in this discussion yet.

Privacy Do Not Sell My Data

Download PDF

View Table Of Contents

Categories

Journals
Magazines
Books
Proceedings
SIGs
Conferences
Collections
People

About

About ACM Digital Library
ACM Digital Library Board
Subscription Information
Author Guidelines
Using ACM Digital Library
All Holdings within the ACM Digital Library
ACM Computing Classification System
Accessibility Statement

Association for Computing Machinery

Join SIGs

ACM on Facebook

ICIMMI

Send Feedback

Submit a Bug Report

The ACM Digital Library is published by the Association for Computing Machinery. Copyright © 2024 ACM, Inc.

Terms of Usage | Privacy Policy | Code of Ethics

ACM DL DIGITAL LIBRARY

Association for Computing Machinery

www.nmiet.edu.in

International Journal of
INTELLIGENT SYSTEMS AND APPLICATIONS IN ENGINEERING
ISSN:2147-6799 www.ijisae.org Original Research Paper

Advancements in Cyclostationary Technique for Cognitive Radio: An In-Depth Examination and Evaluation

Mrs. Sarita Charkha[1], Mr. Mayur Jakhete[2], Ms. Prachi Waghmare[3], Mrs. Dipamala Chaudhari[4], Mr. Ketan Jatale[5], Mrs. Tejaswini Zope[6], Mr. Bhushan Rathi[7], Mr. Vidur Sharma[8]

Submitted: 25/12/2023 **Revised**: 30/01/2024 **Accepted**: 09/02/2024

Abstract: In contemporary society, information communication has reached unprecedented levels, connecting individuals at all strata, from grassroots to the highest echelons. The integration of information technology and communication has become an intrinsic part of everyday life, catering to knowledge-based, entertainment-based, economical-based, and social-based data. As the volume of information data continues to grow, Information Communication Technology (ICT) plays a pivotal role in the lives of common individuals. However, the surge in users is met with the challenge of limited resources, specifically channel bandwidth for communication. This paper addresses the issue of communication channel utilization in the face of a rising number of users. To optimize and accommodate an increasing user base within the constraints of available channels, the proposed system introduces the Enhanced Cyclostationary technique for Cognitive Radio. This innovative approach aims to maximize the efficiency of communication channels, ensuring reliable connectivity for the expanding user population.

Keywords: *Cognitive Radio, Cyclostationary Technique, MATLAB, Primary User, Secondary User.*

1. Introduction:

Wireless communication serves as the backbone of modern information access systems, facilitating the transmission and reception of vital data. The fundamental medium for this communication is the spectrum of frequencies provided by various spectrums, including UHF, VHF, and HF. Each spectrum is allocated for specific reasons, forming the basis of diverse applications. However, the fragmentation of spectrums according to various applications has resulted in a growing challenge – the unavailability of channels for communication due to an increasing number of users. Users authorized to access specific channels are termed primary users, while unauthorized users are classified as secondary users. Historically, a conventional static spectrum approach was employed, where specific spectrums were allocated solely to primary users. The static approach, once effective, faced challenges as the number of users increased, exacerbating the scarcity of available spectrum. To address this, the dynamic spectrum allocation paradigm was introduced.

Dynamic spectrum allocation operates on the premise that if a primary user (licensed user) is not actively utilizing or occupying a spectrum for a specific period, the spectrum can be temporarily accessed by secondary users until the primary user resumes occupancy. This concept, known as the dynamic spectrum approach, significantly increases the utilization factor of available signals. In response to the need for automatic spectrum allocation, new techniques were introduced, namely Spectrum Sensing Algorithm and Spectrum Allocation Algorithm. This paper delves into these techniques, focusing on the proposed Enhanced Cyclostationary Spectrum Sensing algorithm. This advanced method integrates correlation and principal component analysis for enhanced results and effectiveness. The proposed algorithm utilizes major cyclic properties of signals to sense and allocate primary and secondary users. In contrast to conventional cyclostationary techniques, which solely rely on cyclic properties, the proposed system enhances the cyclostationary technique by incorporating principle component analysis. Additionally, the paper introduces novel approaches for detecting intruders within the spectrum. To implement the overall system, MATLAB software is employed, demonstrating the system's efficacy in terms of accuracy and response time. Quality parameter analysis, including probabilities of false alarm and probabilities of miss detection, is presented graphically, offering insights into the effectiveness of the proposed system.

[1,3,4,6] *Assistant Professor, Department of Computer Science and Engineering Nutan College of Engineering and Research Talegaon, Pune, Maharashtra India*
[2] *Assistant Professor, Department of Electronic and Telecommunication Engineering, Pimpari-Chinchawad University, Pune, Maharashtra, India.*
[5] *Assistant Professor, Department of Bachelor of Computer Application, Saraswati College, Shegaon, Buldhana, Maharashtra, India*
[7,8] *Assistant Professor, Department of Master of Computer Application, Saraswati College, Shegaon, Buldhana, Maharashtra, India*
spcharkha@gmail.com, prachiwaghmare@ncerpune.in, tejaswinizope@ncerpune.in,dipa.nemade@gmail.com, ketanjatale30@gmail.com,busan.rathi@gmail.com, vidur.sharmapp@gmail.com

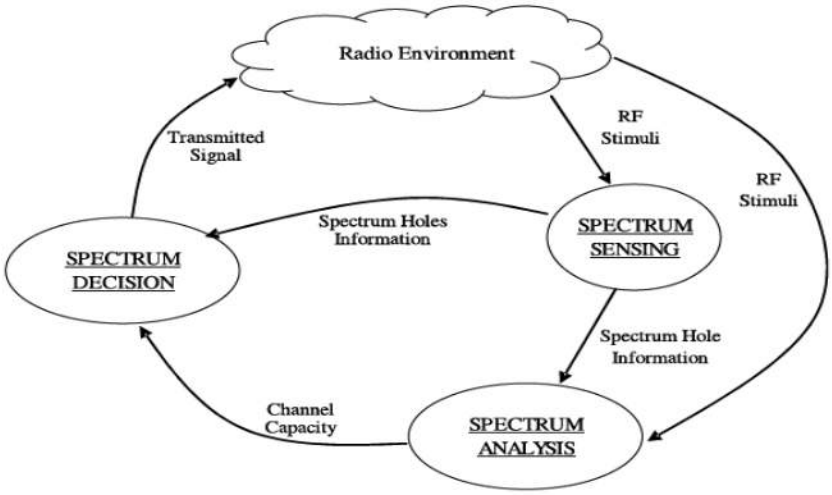

Fig 1:- Cognitive cycle

Cognitive Radio performs four key functions spectrum sensing, management, sharing & analysis. spectrum sensing continuously searches for unused spectrum, known as spectrum holes or white spaces, across Frequency, Time, Geographical Space, Code, and Phase. Involves measuring and being aware of various radio channel characteristics, interference, transmit power, and other environmental factors. Spectrum Management selects available white spaces or channels once spectrum holes are identified. Also utilize the detected spectrum for optimal communication. Spectrum Sharing allocates unused spectrum (spectrum holes) to secondary (cognitive) users as long as the primary user does not require it. Spectrum Mobility vacates the channel promptly when a licensed (primary) user is detected.

2. System Development & Execution:

In order to improve the conventional cyclostationary technique, the proposed system introduces a sophisticated approach. Within this system, significant cyclic properties are identified, and their energy values are correlated with the ongoing signal. This identification of crucial cyclic properties is accomplished through a component of principle component analysis. The proposed system is depicted in Figure 2

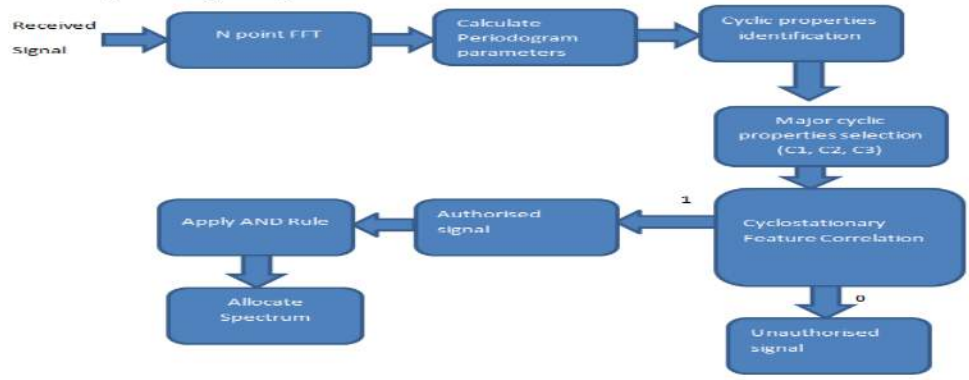

Fig 2: Flowchart for execution using cyclostationary detection method

As depicted in Figure 3, the enhanced technique incorporates the conventional cyclo-stationary method, selecting significant cyclic components (C1, C2, C3) for feature correlation using principle component analysis. This augmentation results in a more efficient and effective technique.

To implement the cognitive radio in MATLAB, follow these steps: firstly install MATLAB R2013a 8.1.0.604 &Save the code in the local MATLAB directory.

To simulate the cognitive radio go to Navigate to New > Graphical User Interface > Open Existing GUI.

Browse the local directory, open the .fig file, and press the Run Figure button to display the simulated GUI.

In the GUI control panel press the "All Primary User Present" button, displaying six windows on the axis, indicating the presence of primary users with peaks at their carrier frequencies. Turn a Primary User OFF by using the empty band detection button, specifying the user state as 'Y' for present or 'N' for absent. The subplot shows a line for absent users, indicating noise only when users are absent.

Insert the first secondary user by pressing the "Insert First Secondary User" button on the control panel.

After that press "Insert Second Secondary User" for the second secondary user to search for an empty band when two primary users are absent. For effective spectrum utilization perform dynamic spectrum allocation by pressing the "1st PU wants to Use SU1" button & release the band used by Primary User 1 and search for a vacant band. If found, it is occupied by Secondary User 1.

There are two panels on the GUI show the state of Primary Users and Secondary User, In that primary User panel indicates whether they are ON or OFF & secondary User panel shows whether they are searching for a band or which band is occupied by the secondary user.

For evaluating PFD Detection performance, three push buttons in the control panel are utilized, with the callback linked to the file name. This same process is applied for assessing performance matrices, comparing PFD detection, and analyzing using the AND rule method. The push button labelled "Detect the Primary User in low SNR" is employed to compare the detection of the Primary User (PU) using both Energy Detection (ED) and Cyclostationary Detection (CD) methods. Leveraging the cognitive radio base station's knowledge of all Secondary User (SU) modulating frequencies, the PFD detection excels in effectively distinguishing between PU and SU. This functionality is exemplified by a dedicated push button that distinctly separates PU and SU.

3. Simulation Result & Discussion

MATLAB was utilized to verify the effectiveness of the cognitive cyclostationary detector. Setting up a cognitive radio system included configuring 6 primary users, 2 secondary users, and 6 intruders. The initial stage involves launching the Cyclostationary process, specifically concentrating on correlating two signals. This initial phase is dedicated to identifying authorized signals through correlation analysis.

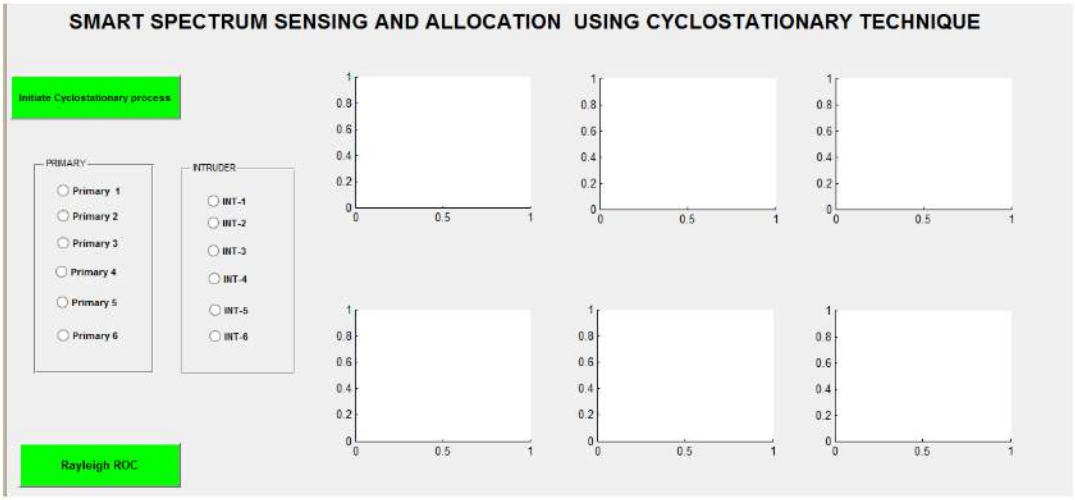

Fig 3 : Initialization of Cyclostationary Technique

After the initialization phase, the subsequent step entails the individual allocation of channels for primary users. This allocation process utilizes cyclic autocorrelation and periodogram analysis. The sequential assignment of channels for primary users begins with user 1 and continues through user 6.

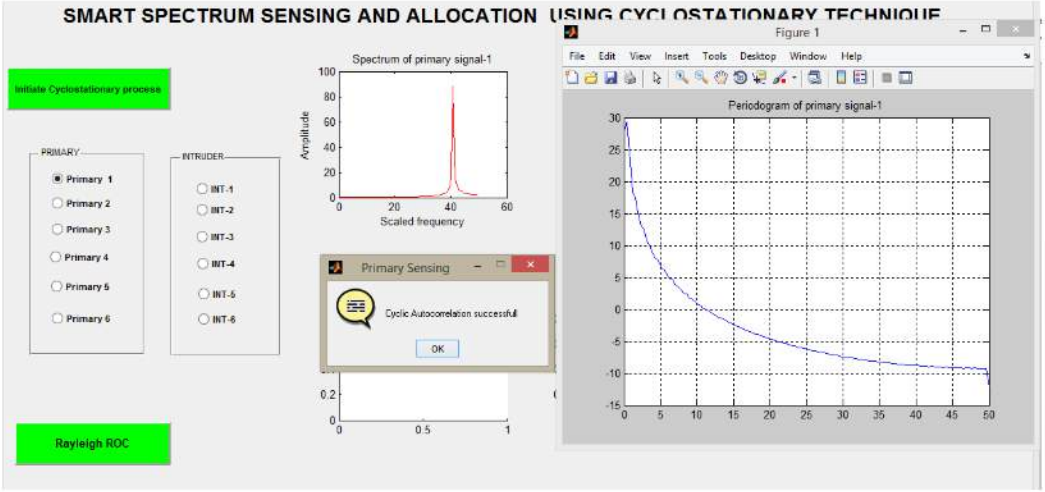

Fig 4: Channel allocation to Primary user one.

If an additional primary user vacates its channel, priority is granted to Secondary Signal 1 for data transfer and spectrum allocation. As illustrated below, when Primary Users 1, 2, and 3 abandon their respective channels, Secondary Signal 1 seamlessly occupies the channel that was previously utilized by Primary User 1.

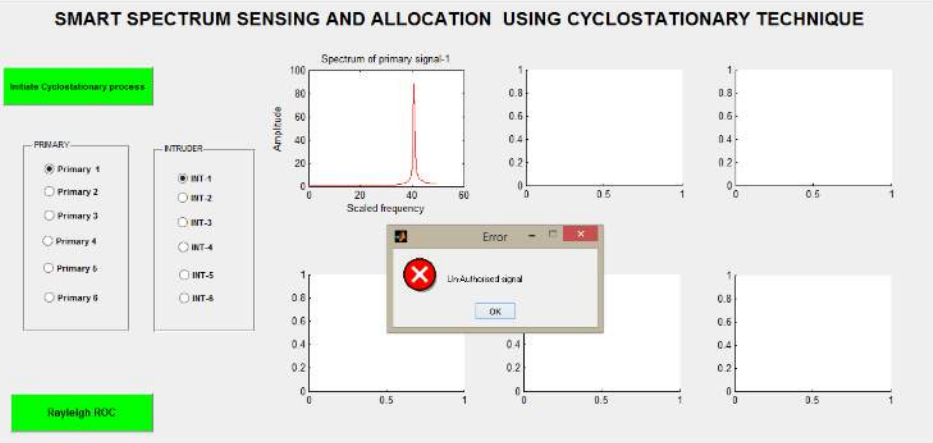

Fig 5.3: Intruder as Unauthorized signal.

The intruder, characterized as a noise signal, is a form of signal that must be prevented from entering the spectrum. It represents an unauthorized signal, and its presence within the spectrum poses a security risk. In this project, any attempt by an unauthorized signal or user to intrude is countered by the cyclic autocorrelation technique, employing the Peak Matching technique. As illustrated in Figure 4, the cyclostationary technique promptly recognizes Intruder 1 as an unauthorized signal. This conceptual approach aligns with the principles of Cognitive Radio.

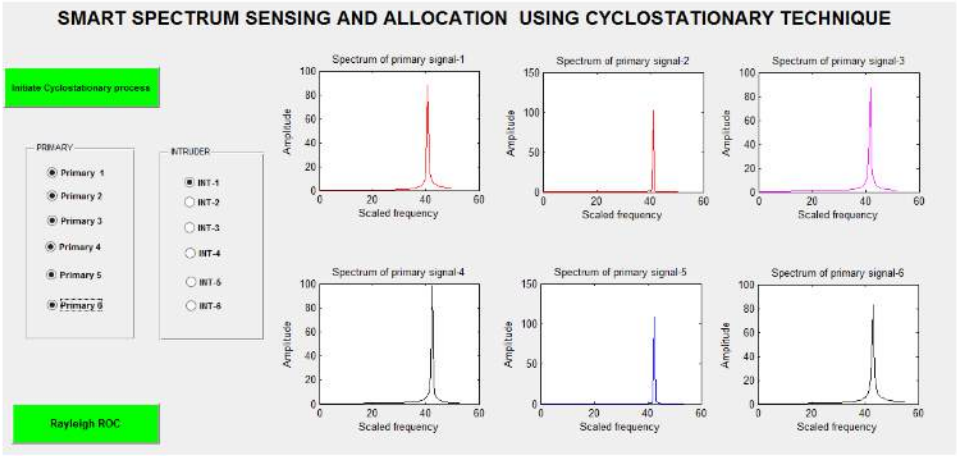

Fig 4: Channel allocation to all six Primary users.

When a specific channel is vacated by a primary user, the secondary user can employ that channel for data transfer until the primary signal returns to the spectrum. In this context, signals are prioritized based on their data transfer requirements. As illustrated in Figure, when Primary User 4 exits its channel, Secondary Signal 2 seamlessly takes over the same channel that was previously utilized by Primary User 4. This illustrates the core objective of Cognitive Radio, showcasing efficient spectrum utilization for both primary and secondary users.

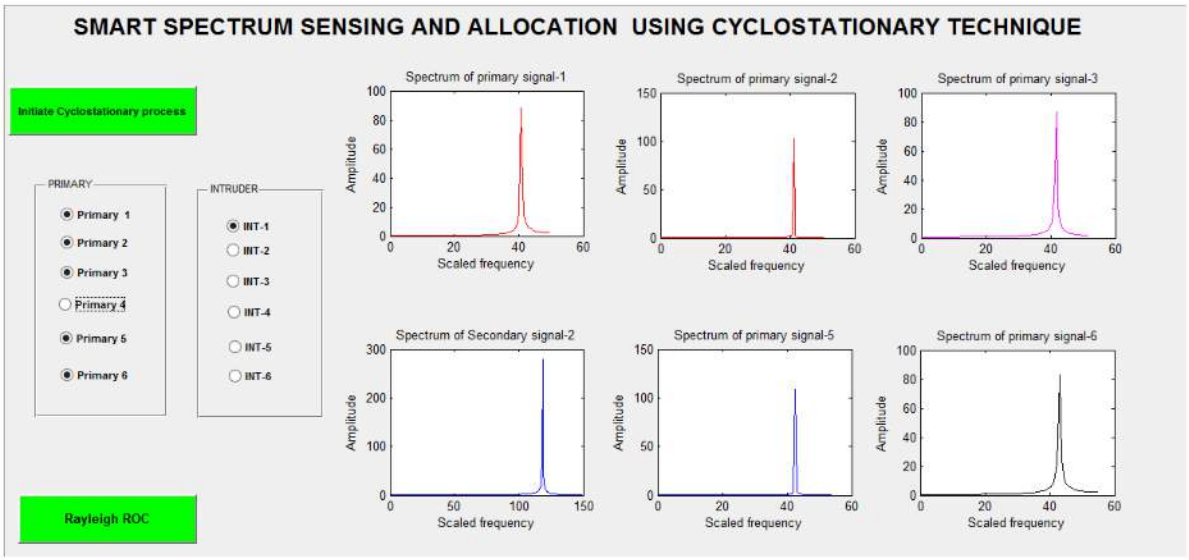

Fig 5: Channel allocation to secondary signal.

In this process, channels have been allocated to six primary users, and the introduction of an intruder signal has been examined. The demonstration effectively characterizes the intruder as an unauthorized signal, enhancing spectrum security. Additionally, two unlicensed secondary signals have been generated. The core objective of Cognitive Radio is the prioritized allocation of channels, a principle implemented through MATLAB. Sensing based on priority is applied to both primary and secondary signals, resulting in their assignment to various channels with distinct frequencies.

Following this, we generated a graph depicting the relationship between Miss Detection and False Alarm rates. Miss Detection signifies the probability of a signal not being correctly identified, while False Alarm represents the probability of erroneously identifying an intruder as a primary signal. The system achieves an accuracy of up to 90%, leading to low probabilities for both Miss Detection and False Alarm in the cyclostationary technique. Thus, the successful implementation of this system is evident.

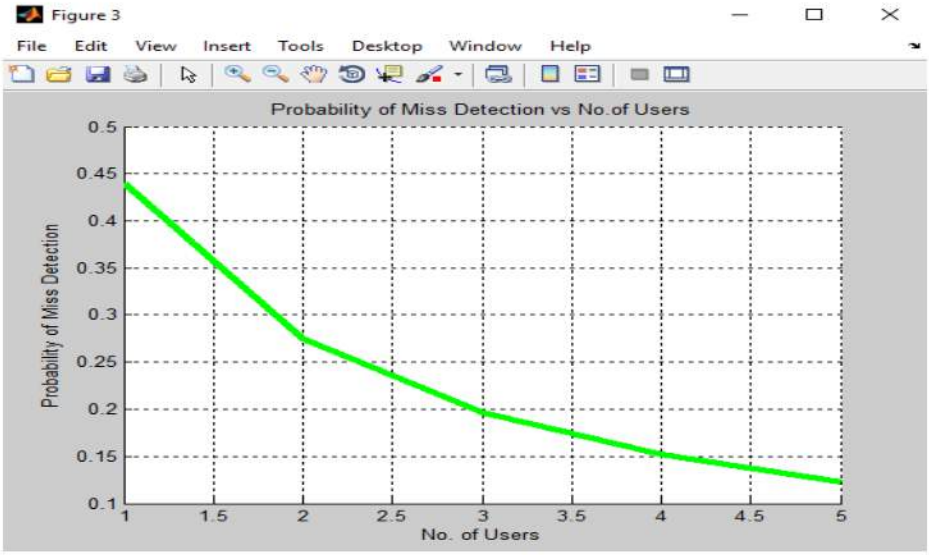

Fig : Probability of miss detection vs no of user

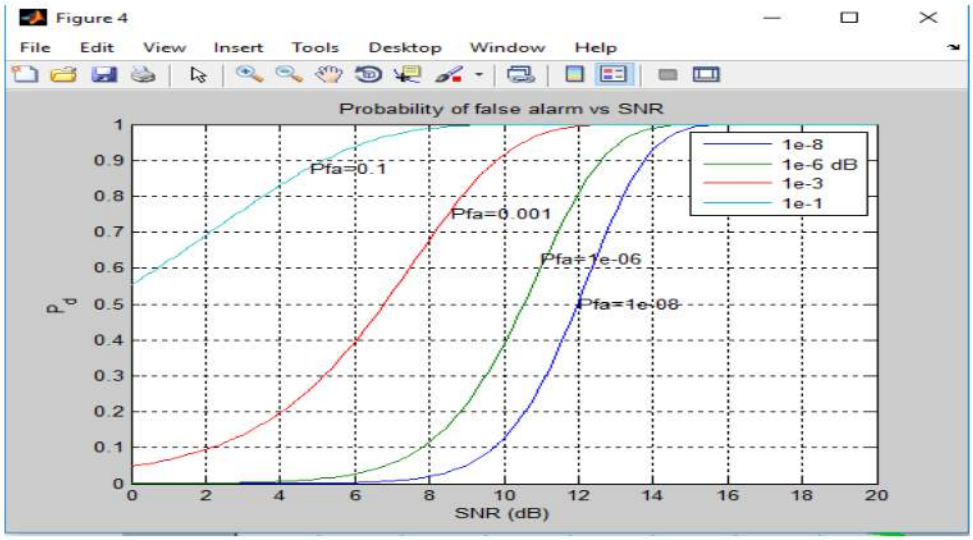

Fig : Probability of false alarm vs SNR

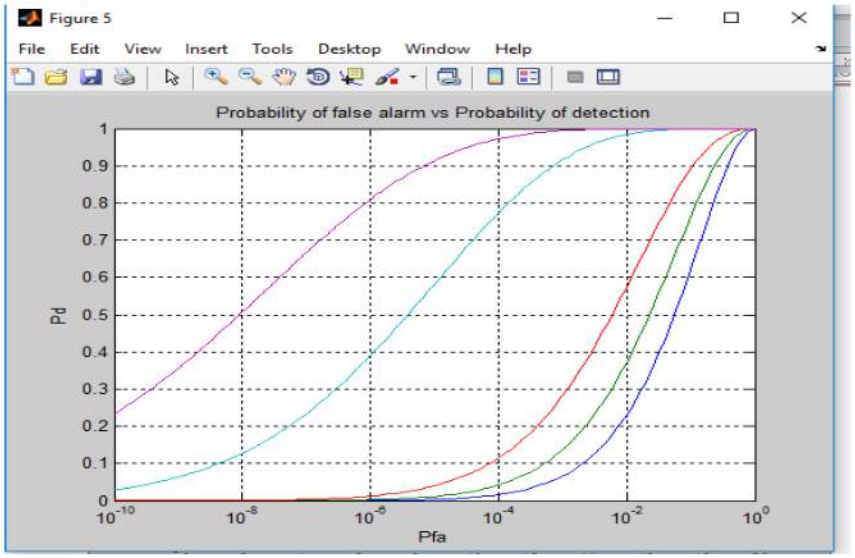

Fig : Probability of false alarm vs probability of detection

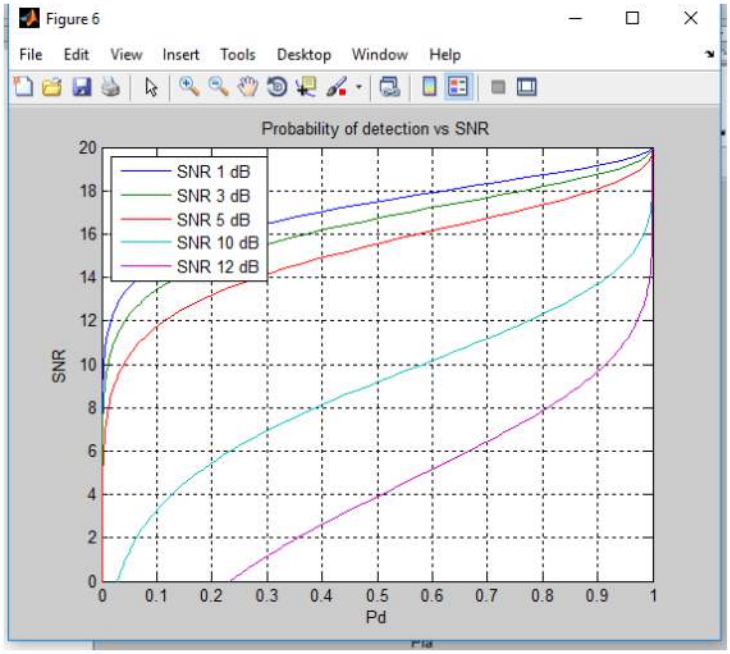

Fig : Probability of detection vs SNR

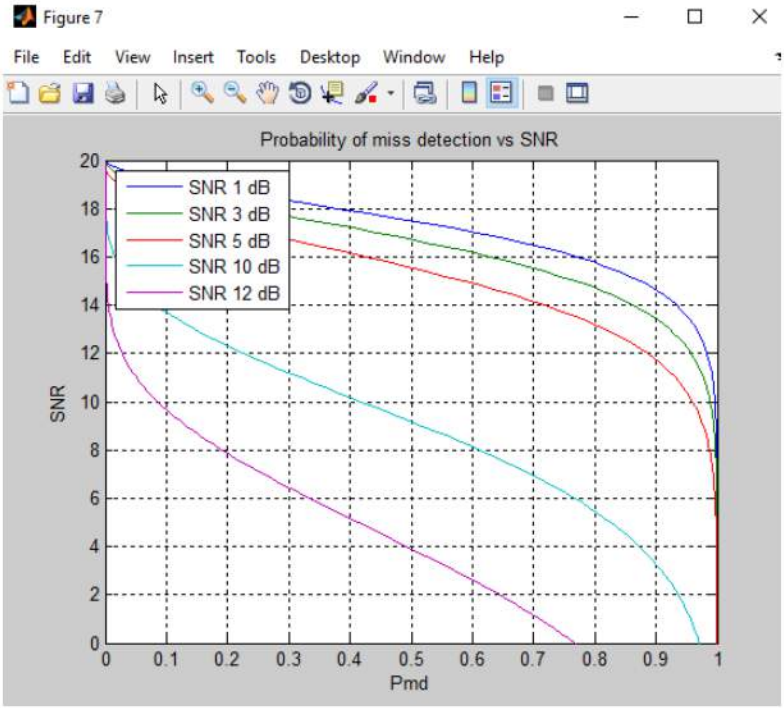

Fig : Probability of miss detection vs SNR

In order to optimize the utilization of the wireless spectrum, cognitive radios were introduced, designed to exploit available spectrum gaps opportunistically. Spectrum sensing is a crucial component of cognitive radio systems, and various sensing techniques are employed for this purpose. This paper focuses on Energy Detection, Matched Filter Detection, and Cyclostationary Feature Detection as spectrum sensing techniques.

Energy Detection offers the advantage of not requiring prior knowledge about primary users. However, its performance is less effective at low Signal-to-Noise Ratio (SNR) values, necessitating a minimum SNR for reliable operation. The results presented in the paper reveal that Energy Detection starts functioning at -7 dB SNR.

Matched Filter Detection surpasses Energy Detection, initiating operation at a lower SNR of -30 dB. Cyclostationary Feature Detection emerges as superior to both previous detection techniques, delivering better results at the lowest SNR values, particularly below -30 dB. The results demonstrate that the performance of Energy Detection improves with increasing SNR, with the "probability of primary detection" increasing from zero at -14 dB to 100% at +8 dB. Correspondingly, the "probability of false detection" decreases from 100% to zero.

4. Conclusion:

The utilization of the enhanced cyclostationary technique with principle component analysis, incorporating the selection of cyclic properties and subsequent energy calculation over these chosen cyclic properties, has demonstrated increased effectiveness in achieving precise spectrum sensing. This hybrid approach minimizes the probability of miss detection during spectrum sensing by leveraging the strengths of both cyclostationary and energy level detection techniques. Through the integration of the advantages inherent in these conventional techniques, the enhanced cyclostationary technique concurrently deals with and alleviates the limitations associated with each method. Subsequent to the spectrum sensing algorithm, a spectrum allocation algorithm based on the AND rule is also put forth.

References

[1] R. C. Gonzalez and R. E. Woods, Digital Image Processing, 3rd ed. Upper Saddle River, NJ: *Prentice-Hall*, 2007.

[2] Shengfeng He, Qingxiong Yang, Member, IEEE, Rynson W.H. Lau, Senior Member, IEEE and Ming-Hsuan Yang, Senior Member, IEEE "Fast Weighted Histograms for Bilate Filtering and Nearest Neighbor Searching" *2015 IEEE.*

[3] Aruna.L,S.S.Thamilselvi "Contrast Enhancement for Emissive Display Using Histogram Equalization and Bilateral Tone Adjustment", *International Journal of P2P Network Trends and Technology (IJPTT)* - Volume3 Issue4- May 2013

[4] Anan Du, Bin Li, Yecheng Zhang, Xiangchun Yu, Zhezhou Yu"A Novel Graph Construction Method Based on Locality Sensitive Histogram for Locality Preserving Projections",*Journal of Information & Computational Science* 11:15 (2014) 5297{5304 October 10, 2014

www.nmiet.edu.in

[5] J.Stark, "Adaptive image contrast enhancement using generalizations of histogram equalization," *IEEE Transaction on Image Processing*,vol.9, no. 5, pp. 889–896, May 2000.

[6] Z. Yu and C. Bajaj, "A fast and adaptive method for image contrast enhancement," *in IEEE ICIP, O*ct. 2004, vol. 2, pp. 1001–1004.

[7] A. Adams, J. Baek, and A. Davis. Fast high-dimensional filtering using the permutohedral lattice. *Computer Graphics Forum*, 29(2):753–762, 2010.

[8] A. Adams, N. Gelfand, J. Dolson, and M. Levoy. Gaussian KD-trees for fast high-dimensional filtering. *ACM TOG*, 28(3), July 2009.

[9] S. Bae, S. Paris, and F. Durand. Two-scale tone management for photographic look. *ACM TOG*, 25:637–645, Jan. 2006.

[10] S. Baker, D. Scharstein, J. Lewis, S. Roth, M. Black, and R. Szeliski.*A database and evaluation methodology for optical flow*. IJCV, 92(1):1–31, 2011.

[11] L. Bao, Q. Yang, and H. Jin. Fast edge-preserving patchmatch for large displacement optical flow. IEEE TIP, 23(12):4996–5006, Dec 2014.

[12] C. Barnes, E. Shechtman, A. Finkelstein, and D. Goldman. Patch- Match: *A randomized correspondence algorithm for structural image editing. ACM TOG*, 28(3), Aug. 2009.

[13] E. Bennett and L. McMillan. Video enhancement using per-pixel virtual exposures. *ACM TOG*, 24(3):845–852, 2005.

[14] J. Chen, S. Paris, and F. Durand. Real-time edge-aware image processing with the bilateral grid. *ACM TOG*, 26(3), 2007.

[15] Z. Chen, H. Jin, Z. Lin, S. Cohen, and Y. Wu. Large displacement optical flow from nearest neighbor fields. In Proc. *IEEE CVPR*, pages 2443–2450, June 2013.

[16] D. Comaniciu, V. Ramesh, and P. Meer. Kernel-based object tracking. *IEEE TPAMI, 25(5):*564 – 577, 2003.

[17] F. Durand and J. Dorsey. Fast bilateral filtering for the display of high-dynamic-range images. *ACM TOG*, 21(3), 2002.

[18] E. Eisemann and F. Durand. Flash photography enhancement via intrinsic relighting. *ACM TOG, 23*(3):673–678, 2004.

[19] R. Fattal. Edge-avoiding wavelets and their applications. *ACM TOG*,28(3), 2009.

Check for updates

Received: 22 August 2023 | Revised: 10 October 2023 | Accepted: 16 October 2023
www.nmiet.edu.in
DOI: 10.1002/eng2.12811

RESEARCH ARTICLE

Engineering Reports Open Access WILEY

Novel technique of vibration minimization during hard machining

Aditi D. Apte[1] | **Shivakumar Shivamurthy**[2] | **Manjunath G Avalappa**[2] | **Nikhil Rangaswamy**[3] | **Ashwini S. Shinde**[4] | **Satish S. Kulkarni**[5] | **Mukesh Kumar**[6]

[1]Department of Mechanical Engineering, Visvesvaraya Technological University, Belagavi, India

[2]Department of Mechanical Engineering, K. L. S. Gogte Institute of Technology, Belagavi, India

[3]School of Mechanical Engineering, REVA University, Bengaluru, India

[4]Department of CSE, Nutan College of Engineering & Research (NCER), Pune, India

[5]Department of Mechanical Engineering, Padmabhooshan Vasantraodada Patil Institute of Technology, Sangali, India

[6]Department of Mechanical Engineering, Assosa University, Benishangul Gumuz, Ethiopia

Correspondence
Aditi D. Apte, Department of Mechanical Engineering, Visvesvaraya Technological University, Belagavi, India.
Email: adiapte12@yahoo.co.in

Nikhil Rangaswamy, School of Mechanical Engineering, REVA University, Bengaluru, India.
Email: nikhil.rangaswamy@reva.edu.in

Mukesh Kumar, Department of Mechanical Engineering, Assosa University, Assosa, Ethiopia.
Email: kumarmukesh.coe@asu.edu.et

Abstract

This research paper explores the performance of electrorheological fluids, widely known as smart fluids, which are popular because they experience immediate changes in their characteristics when applied to exterior magnetic or electric field. On application of high voltage, the ER fluid alters its form to semisolid from viscous liquid within a few milliseconds, which is reversible. The reversible nature of ER fluid was employed to absorb vibrations during hard machining. In this research, the consequence of the application of electric field to the ER characteristics of numerous non-Newtonian fluids with an accumulation of TiO_2 and Al_2O_3 nano elements are investigated. The purpose of this research is to discover the ER sample, which has the highest viscosity, highest breakdown voltage, but less sedimentation. So the selected sample can be used in ER dampers for the purpose of shock absorption. The ER fluid behaves as a mainspring with nonlinear vibration features that are managed by an arrangement of ER fluid, the structure of plunger, and the constraints of applied electric field. In this research, we have employed steel metallic specimens made from EN24T of 302BHN and the machining experiments are conducted to attain the shape parameters that can reduce the tool vibration and help improve the process of cutting at the time of machining with minimum application of fluid utilizing hard metal inserts. In this work, cutting tool parameters were analyzed like cutting force, tool wear, tool vibration amplitude, and surface roughness. It was observed that ER damper has shown its better performance at 5KV. At 5KV, cutting force was the least, tool wear was the least, tool vibration amplitude was the least, and surface roughness was the least. The use of an ER fluid damper decreases tool vibrations and successfully enhances machining performance. The machining industry will be benefited with commercialization of this technique.

KEYWORDS

electrorheological fluids, EN24T, ER damper, hard machining, nanofluids, surface roughness, tool wear

This is an open access article under the terms of the Creative Commons Attribution License, which permits use, distribution and reproduction in any medium, provided the original work is properly cited.
© 2023 The Authors. *Engineering Reports* published by John Wiley & Sons Ltd.

www.nmiet.edu.in

1 | INTRODUCTION

The world is moving toward nanotechnology, and one of the recent emerging products is nano fluids, which is a mixture of nanoparticles (normally 1–100 nm in dimensions) with any one of the base fluids (water, glycols, oils, etc.) The aim of nano fluid study is to measure thermo physical properties (viscosity, surface tension, and thermal conductivity). The technique and the materials used is the first step of research with nanofluids. These fluids are not simply liquid solid mixtures, but they possess some Stalin features. These are called as the electrorheological (ER) fluids that experience a sudden and revocable change with the application of electric field. ER material fluctuates from liquid state to viscous state within millisecond, and this singularity is known as ER effect. This is an exclusive characteristic of ER fluids that is reversible and continuous process. Paul and Varadrajan[1] have implemented magnetorheological damper for same purpose but electrorheological damper was not implemented for damping cutting tool vibrations during hard machining. The objective of this work was to reduce machining expenditure by reducing machining time for small-scale industry. For small-scale industry's costly cutting tools, brand new machine tools are not affordable. Hence in this work, effort was made to reduce time during hard machining, especially for hard components by omitting special grinding cycle. In this work, an effort was made to prepare a final product by damping vibrations of cutting tool during machining only. For that ER damper was implemented during hard machining, which has variable damping factor.

2 | NECESSITY OF ER FLUIDS

2.1 | Technical issues

In the process of machining, the tools with high vibration arise, which is accountable to damage the surface finish of work; hence, for heavy work it is necessary to damp these vibrations. Damping is important to increase the accuracy of work as well as life of foundation.[2]

2.2 | Economical factor

While machining hard material at high-velocity, tool wear occurs. To minimize tool wear, it is necessary to minimize vibrations; similarly, to increase the life of bearings and shafts, damping is important.[3–5]

2.2.1 | The ER Damper

Electrorheological (ER) fluids are electric field dependent samples that consist of a base carrier fluid that contains micro- or nano-sized particles.[6] In this work, TiO2 and Al_2O_3 nanoparticles are used. With the application of electric field, these samples get converted to semisolid state due to polarization of uniformly dispersed solid particles. Once these particles get polarized, they begin to intermingle with each other, forming chain like assembly, and the direction of applied electric field is parallel to these chains connecting two electrodes.[7,8] On increase in applied electric field, these chains get converted into thick columns, and on discontinuing of electric field, the nanoparticles loose polarization and return to free state. Steadiness of these nano elements in liquid medium is generally one of the leading issues because developing a stable solution plays a very significant role in investigational results as accumulation of these particles often occur in preparation of ER fluids.[9,10] Research in the field of rheological materials with restricted geometries, involving adhesion, lubrication, and friction between particles and surfaces at the nanometer scale or interactions between particles, is referred to as nano rheology.[11] Electrorheological fluids (ER) also called as tunable materials as they have the capability to tune in to any anticipated degree of firmness consist of a mixture of tiny dielectric particles homogeneously dispersed in the fluid.[12] The mismatch of density of solid elements in the fluid causes sedimentation, which is also the cause of aggregation of nanoparticles. In the process, yield stress develops as the sample gets solidified due to the electric field. These particles are semi-conductive solids of high dielectric constants. There is increase in viscosity of the fluids with the increase in temperature.[13,14] The properties of the fluid are defined by the size of the particle in the fluids that rely on properties of the carrier fluid, additives, temperature, and density. It is seen that greater the concentration of volume fraction of

25778196, 0, Downloaded from https://onlinelibrary.wiley.com/doi/10.1002/eng2.12811, Wiley Online Library on [27/04/2024]. See the Terms and Conditions (https://onlinelibrary.wiley.com/terms-and-conditions) on Wiley Online Library for rules of use; OA articles are governed by the applicable Creative Commons License

dispersed particulates higher will be the ER effect, but simultaneously can produce problems.[15] One of the major issues is sedimentation as the concentration of solid particles increases it also increases the amount of settling which gives rise to increase in zero field viscosity. Also, the viscosity and the dynamic yield stress decreases as there is increase in temperature in the absence of an electric field. One of utmost substantial properties of ER fluid is the vigorous yield stress; this is the minimum stress essential for the fluid to flow under applied electric field. The yield stress that is desired is generally in the range from around 100 Pa to 3 K Pa.[16–18]

The ER fluids can suppress high-frequency and low-amplitude vibrations in several different industrial applications. Electrorheological dampers work with three different operating modes: shear mode, flow mode, and squeeze mode. In shear mode, electrorheological fluids have the capability to generate forces in compression and tension.[19] Combination of shear and squeeze mode dampers is easier to design as well as compact. Shock absorption ability of damper depends on displacement amplitude and electric field strength.[20]

There are many techniques to reduce the vibrations like isolating, damping, eliminating, absorbing, and so forth.[21,22] This research shows a state-of-art technique using the electrorheological fluid for reduction of vibrations. Here some little cutting fluid has been used (2 mL/min) because it reduces the issues that would have happened because of utilization of huge number of fluids in wet machining.[23–25]

2.2.2 | Necessity of ER fluids

The fluid viscosity depends on the voltage of the electric field, and when the electric field is removed, the ER fluid quickly returns to its original form within milliseconds. The ER damper is illustrated in Figure 3, which comprises a plunger and a cylinder. Plunger moves within the cylinder comprising ER fluid, and the upper part of plunger is rigidly connected to the tool. The upper end of the plunger is a conical shape.[26,27] This damper has two electrodes. The cylinder is the positive electrode and the plunger is the negative electrode. These two electrodes are connected to a high voltage supply so that high voltage and low current can pass through fluid. As the working principle of ER damper is based on high voltage and low current, the provision of high voltage and low current is there in electric supply.[28] It is a natural phenomenon that resistance to the motion of the plunger occurs due to the application of high voltage and low current, resulting in the damping of vibrations.[29] The factors responsible for the damping action of ER fluid damper are as follows: (i) size of particles encompassed in ER fluid; (ii) viscosity of fluid medium; (iii) the kind of current and voltage applied to fluid (A.C. or D.C.); and iv) voltage strength applied to the fluid.[30]

Another issue of vibrations arises as a result of which surface finish gets tarnished, which ultimately gives rise to damage to cutting tool and generation of unbearable noise. In this research, we introduce the concept of hard machining using ER fluids, which has achieved significant consideration in metal machining that is able to substitute the process cycle of turning, facing, boring, finish grinding, and heat treatment for hard and wear-resistant parts. This investigation aims to reduce the vibrations of the tool by utilizing the developed ER fluid damper and promoting better machining presentation at the time of hard turning, boring, and facing.

Electrorheological fluids are colloidal samples that come in the class of non-Newtonian fluids. In past studies, researchers have considered electrorheological fluids as Bingham plastic material, so the behavior of these fluids is expressed by the following equation:[17]

$$\tau = \tau_y + \eta\left(\frac{\partial\gamma}{\partial t}\right). \tag{1}$$

In Equation 1, yield stress fluctuates with the amount of applied electric field, which is specified as follows:

$$\tau_y = \alpha\, E^{\beta}, \tag{2}$$

where α and β rely on the volume and magnitude of distributed particles, η is the viscosity of electrorheological fluids, and $\left(\frac{\partial\gamma}{\partial t}\right)$ is strain rate. In the damper, it is likely to alter the value of damping coefficient as the damping can be altered by varying its viscosity on application of electric voltage during running state.[17]

$$M\left(\frac{dx^2}{dt^2}\right) + C_{eq}\left(\frac{dx}{dt}\right) + Kx = F_0\, Sin\, \omega t, \tag{3}$$

25778196, 0, Downloaded from https://onlinelibrary.wiley.com/doi/10.1002/eng2.12811, Wiley Online Library on [27/04/2024]. See the Terms and Conditions (https://onlinelibrary.wiley.com/terms-and-conditions) on Wiley Online Library for rules of use; OA articles are governed by the applicable Creative Commons License

www.nmiet.edu.in

$$\text{Ceq} = 2\left(\frac{A}{\pi}\right)\left[\frac{2\,\alpha\,E^{\beta}}{X\,\omega} + \frac{\eta\,\pi}{2\,d}\right], \tag{4}$$

where X is the displacement of the plunger, ω is the frequency of vibration, and d is the electrode gap.

Highest damping force obtained by electrorheological damper is given as,

$$F_{d(max)} = A\left(\alpha\,E^{\beta} + \frac{\eta\,X\,\omega}{d}\right), \tag{5}$$

where A is the area of the electrode piston.

Electrical parameters of damper are determined using the following equation,

$$I = C * A, \tag{6}$$

where C is current density and I is the value of current.

3 | METHODOLOGY OF ELECTRORHEOLOGICAL FLUID PREPARATION

For this experimental work, the following input parameters are provided: four types of insulating oils such as carrier oils, two types of nanoparticles as inclusion in oil, one surfactant, 12 combinations of ER fluid samples, DC voltage from 1 to 5 KV, Hardened EN24 material, three shapes of plungers (conical, inverted conical, cylindrical) for machining experiments, four specimens of EN 24 hardened material for each turning, and boring operation.[31,32]

3.1 | Selection of carrier fluids

In this work, four types of carrier fluids are chosen on the following basis. After a comprehensive literature review, it is observed that silicone oil was used by many researchers as carrier fluid hence it was selected to formulate the ER sample.[33] Transformer oil and mineral oil were used by few researchers, hence transformer oil and mineral oil were chosen to prepare ER samples. Due to higher viscosity compared with other carrier fluids, castor oil is selected as carrier fluid to prepare ER samples. In this way, four oils are selected as carrier fluids for this research work.

3.2 | Selection of nanoparticles

In this work, two types of nanoparticles are preferred to mix in carrier fluids. The first is the alumina nanoparticles, which have less density (3.9 g/cm^3) compared with ferrous nanoparticles. The advantage of alumina sample is that less density helps in reducing the sedimentation process. The second selected element is the titanium dioxide nanoparticles as it is a semiconducting material, it has the benefit of wide band gap of 3.2 eV, low cost, and chemical stability.

3.3 | Preparing the ER fluids

ER fluids are done by diffusing nanoparticles of Al_2O_3 with 10 nm in average diameter and nanoparticles of TiO_2 with 10–30 nm average diameter in (1) silicone oil with viscosity of 0.320 Pa s, (2) transformer oil with viscosity of 0.022 Pa s, (3) mineral oil with viscosity of 0.040 Pa s, (4) castor oil with viscosity of 0.650 Pa-s at 20°C as carrier fluids and Al_2O_3 and TiO_2 nanoparticles are monodispersed with 10 weights % in each carrier fluid and two sets of samples are prepared. Al_2O_3 and TiO_2 nanoparticles are bi-dispersed with five weights % in each carrier fluid and a third set of samples is prepared. In this way, 12 samples are prepared. In this work, the concentration of particles 10 weight % is used because more concentration of particles in a sample can be able to give thicker columns of polarized particles, which are expected to show high value of viscosity when electric field is applied; 1% oleic acid is added to all samples as surfactant. Uniform samples are formed by agitating fluids for 12 h after gradually adding nanoparticles in carrier fluids. Sonication of samples is performed using a sonicator. Then all 12 samples are kept for sedimentation. Details of 12 ER samples are given in Table 1.

25778196, 0, Downloaded from https://onlinelibrary.wiley.com/doi/10.1002/eng2.12811, Wiley Online Library on [27/04/2024]. See the Terms and Conditions (https://onlinelibrary.wiley.com/terms-and-conditions) on Wiley Online Library for rules of use; OA articles are governed by the applicable Creative Commons License

TABLE 1 Description of preparation of ER fluid samples.

Sample No.	Type of oil	Type of nanoparticles	Percentage of inclusion
S1	Silicone oil	Al_2O_3	10%
S2	Transformer oil	Al_2O_3	10%
S3	Mineral oil	Al_2O_3	10%
S4	Castor oil	Al_2O_3	10%
S5	Silicone oil	TiO_2	10%
S6	Transformer oil	TiO_2	10%
S7	Mineral oil	TiO_2	10%
S8	Castor oil	TiO_2	10%
S9	Silicone oil	Al_2O_3 and TiO_2	5% each
S10	Mineral oil	Al_2O_3 and TiO_2	5% each
S11	Transformer oil	Al_2O_3 and TiO_2	5% each
S12	Castor oil	Al_2O_3 and TiO_2	5% each

FIGURE 1 Rheometer used for the experiment.

3.4 | Rheometer measurement

For testing of all prepared samples, Anton Parr modular compact rheometer (MCR-52) is used. That rheometer shows all rheological properties of samples. Rheological experimentation was performed at 20°C. Rheometer is a concentric cylinder rotary rheometer (Anton Parr) that gives ER consequence of numerous samples. The photograph of the rheometer is shown in Figure 1. The gap between bob and cup of the rheometer was 1.138 mm. Rheometer was facilitated to apply D.C. voltage up to 10 KV. The experiments are carried out for a variety of external electric field strength that ranges from 0 to about 6 KV/mm D.C. voltage.[33,34]

4 | METHODOLOGY OF MACHINING OPERATION

The methodology of the experiment is carried out in different steps.

4.1 | Credentials of materials used

The substance utilized for the experimental job piece is steel EN24T which is hardened to 302 BHN by heating and tempered to relieve stresses. The most beneficial part of this material is that it has an extensive range of applications like propeller or connecting rods, gear shafts, aircraft landing gear components, and so forth. In this investigation, four different specimens of Ø 50 mm radius and 100 mm long are employed for turning purpose and Ø 100 mm outer diameter,

25778196, 0, Downloaded from https://onlinelibrary.wiley.com/doi/10.1002/eng2.12811, Wiley Online Library on [27/04/2024]. See the Terms and Conditions (https://onlinelibrary.wiley.com/terms-and-conditions) on Wiley Online Library for rules of use; OA articles are governed by the applicable Creative Commons License

www.nmiet.edu.in

Ø 25 mm inner radius, and 100 mm long are utilized for boring purpose. The chemical composition of EN24T steel is 0.36% C, 0.10% Si, 0.45% Mn, 0.04% S, 0.035%P, 1% Cr, 0.20% Mo, 1.30% Ni. The tolerance for turning is $h_7\ 95^{-0.020}_{+0.000}$. The tolerance for boring is $H_7\ 55^{+0.020}_{+0.000}$.

4.2 | Selection of tool

The tool holder for turning operation has the specifications R1161212P30 and the tool has specifications SNMG 120408 MTT5100.[35,36] The tool holder used for the boring operation has the specifications R 174-29-2525M and boring tool with specifications 1351212P30 2R.

4.3 | Plan and engineering of ER damper

The ER fluids are also called governable fluids. The characteristics of these fluids are their ability to reversibly transform from liquid to semisolid within the span of milliseconds on the application of an electric field. Where the suspended particles polarize and amalgamate to form chains. This mechanism is shown in Figure 2. As there are changes in phase, fluid will transform from semisolid to liquid state.

As the amount of voltage increases the viscosity of ER fluid increases and on termination of the voltage the ER fluid returns to its liquid state. This change from liquid to semisolid phase takes place within milliseconds. The ER damper produced for this research is illustrated in Figure 3. This comprises of plunger that passes inside a container encompassing ER fluid. The ER result is obtained by providing voltage through ER fluid. Threads are cut at one end of the plunger that matched with threads cut on an attachment made to hold the plunger firmly with the tool. The experimental setup is illustrated in Figure 4 on lathe machine. Figures 5 and 6 represent, respectively, setup for turning and boring.

The ER fluid is prepaid by titanium dioxide and alumina nanoparticles. These are mixed with different carrier oils such as the transformer, silicone, castor, or mineral oil to produce various kinds of samples. These samples thus formed are verified using a rheometer (Anton Paar). The electrorheological properties of all samples are presented in Figures 7–10. The sample that gives better viscosity, maximum dielectric strength, and low sedimentation is selected to be utilized. Here the sample of titanium dioxide nanoparticles mixed in castor oil as carrier fluid has demonstrated better viscosity, greater dielectric strength, and gives low sedimentation; therefore, it is selected to utilize in ER damper.[37]

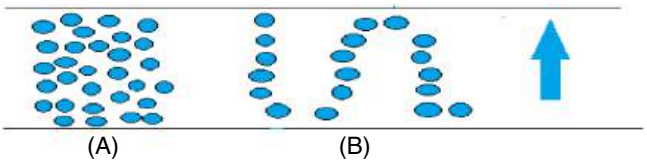

FIGURE 2 Arrangement of nanoparticles.

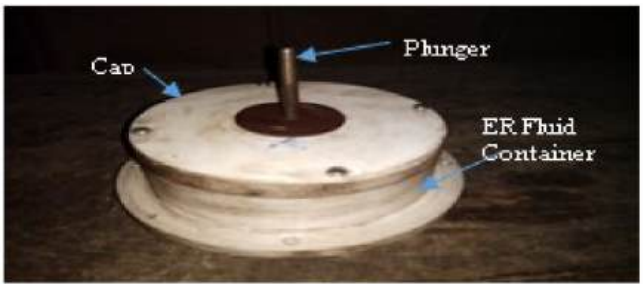

FIGURE 3 Photograph of ER.

25778196, 0, Downloaded from https://onlinelibrary.wiley.com/doi/10.1002/eng2.12811, Wiley Online Library on [27/04/2024]. See the Terms and Conditions (https://onlinelibrary.wiley.com/terms-and-conditions) on Wiley Online Library for rules of use; OA articles are governed by the applicable Creative Commons License

FIGURE 4 ER damper mounted on lathe machine.

FIGURE 5 Turning operation.

FIGURE 6 Boring operation.

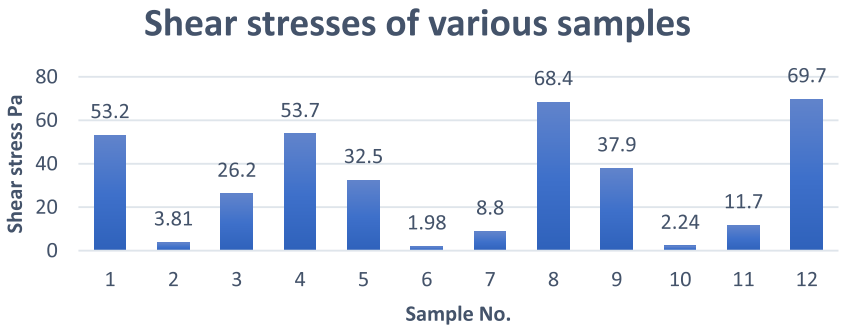

FIGURE 7 Plot of shear stress versus sample no.

25778196, 0, Downloaded from https://onlinelibrary.wiley.com/doi/10.1002/eng2.12811, Wiley Online Library on [27/04/2024]. See the Terms and Conditions (https://onlinelibrary.wiley.com/terms-and-conditions) on Wiley Online Library for rules of use; OA articles are governed by the applicable Creative Commons License

www.nmiet.edu.in

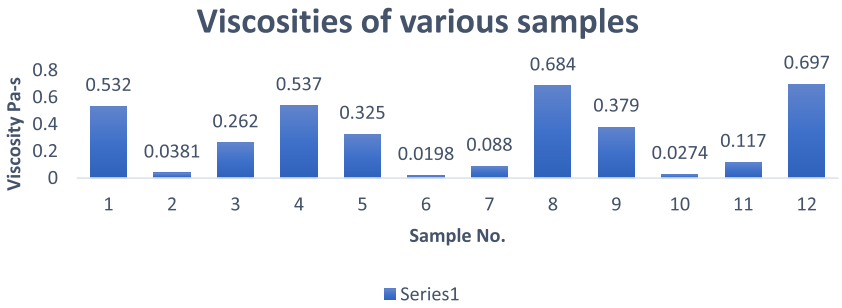

FIGURE 8 Plot of viscosities versus sample no.

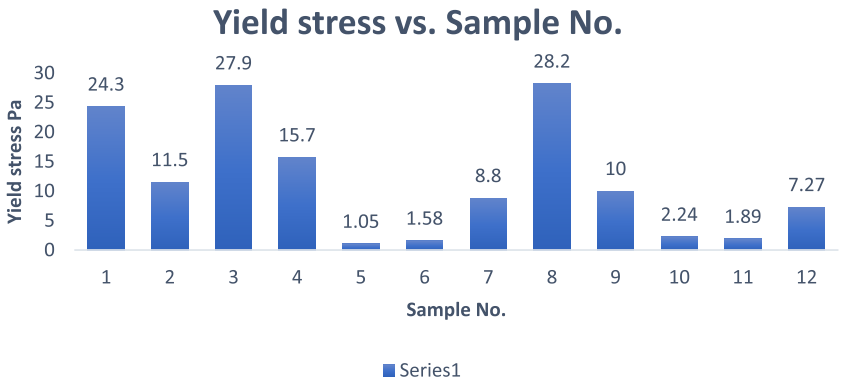

FIGURE 9 Plot of yield stress versus sample no.

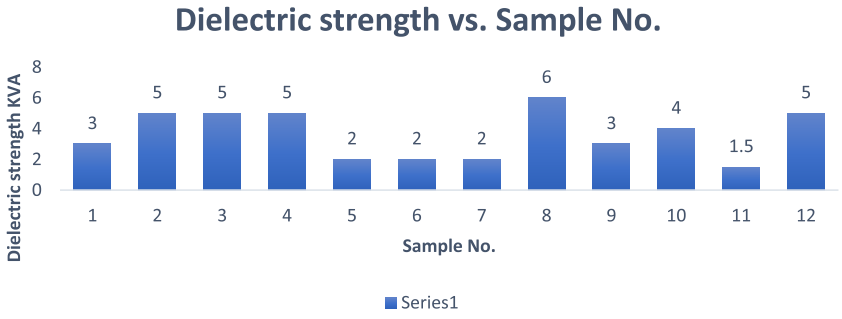

FIGURE 10 Plot of dielectric strength versus sample no.

4.4 | Experimental setup and work

In this research, the cutting experiments were performed on the Kirloskar Shimoga lathe with specifications as spindle speeds of 595,410, 286, 198 RPM for direct belt drive and feed rates of 0.15, 0.25, and 0.35 mm/rev. In this work, ER damper was mounted on the carriage of the lathe machine to absorb the vibrations of the cutting tool. A 15-run experiment is designed and conducted on Taguchi technique. Machining operations are performed using three different shaped plungers: conical, inverted conical, and cylindrical. D.C. voltage from 1 to 5 KV is applied during experimentation to illustrate the effect of shape of plunger on machining operation. The design matrix is given in Table 2. The performance of differently shaped plungers with respect to different constraints such as the cutting force, vibration, surface roughness, and tool wear are represented in Figures 11–18 for turning as well as boring operations. The plunger that has shown best performance in machining during testing is further implemented for machining four specimens to increase the accuracy of results according to the design matrix shown in Table 3. In addition, a time study experiment is conducted for conventional machining and machining operation using ER damper, which is shown by the design matrix in Table 4. It

25778196, 0, Downloaded from https://onlinelibrary.wiley.com/doi/10.1002/eng2.12811, Wiley Online Library on [27/04/2024]. See the Terms and Conditions (https://onlinelibrary.wiley.com/terms-and-conditions) on Wiley Online Library for rules of use; OA articles are governed by the applicable Creative Commons License

TABLE 2 Design matrix for 15 run experiment for testing different shapes of plungers.

S. No.	Type of voltage	Quantity of voltage	Quantity of current	Shape of plunger		
1	D.C.	1 KV	5 mA	Conical	Inverted conical	Cylindrical
2	D.C.	2 KV	10 mA	Conical	Inverted conical	Cylindrical
3	D.C.	3 KV	15 mA	Conical	Inverted conical	Cylindrical
4	D.C.	4 KV	20 mA	Conical	Inverted conical	Cylindrical
5	D.C.	5 KV	25 mA	Conical	Inverted conical	Cylindrical

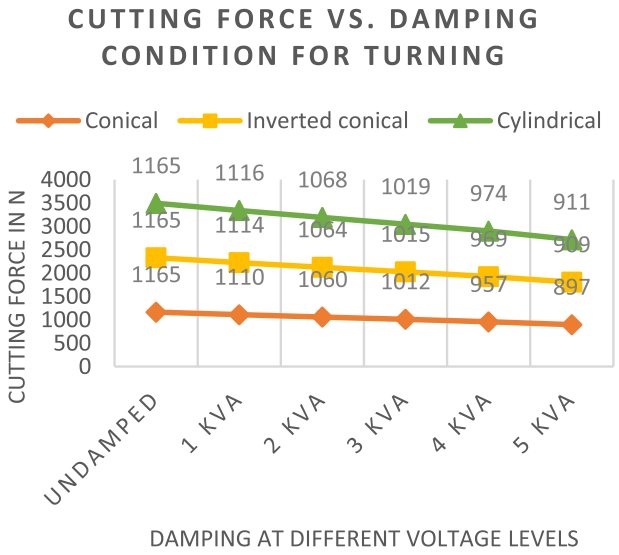

FIGURE 11 Cutting force at different damping conditions.

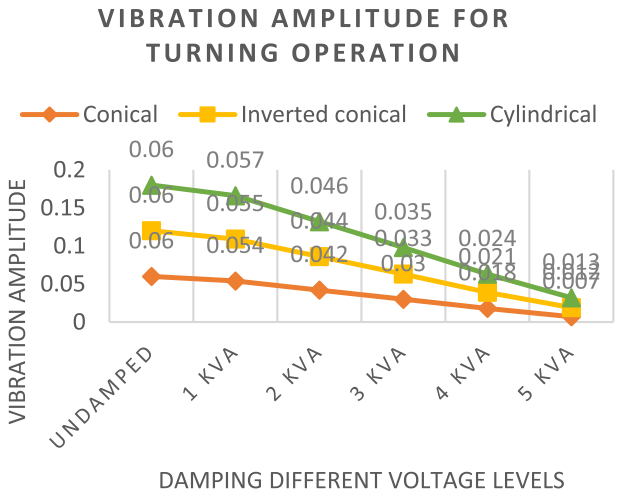

FIGURE 12 Vibration amplitude at different damping conditions.

25778196, 0, Downloaded from https://onlinelibrary.wiley.com/doi/10.1002/eng2.12811, Wiley Online Library on [27/04/2024]. See the Terms and Conditions (https://onlinelibrary.wiley.com/terms-and-conditions) on Wiley Online Library for rules of use; OA articles are governed by the applicable Creative Commons License

www.nmiet.edu.in

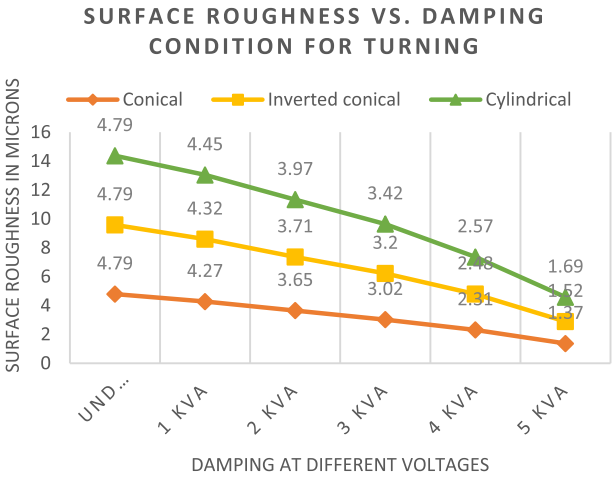

FIGURE 13 Surface roughness at different damping conditions.

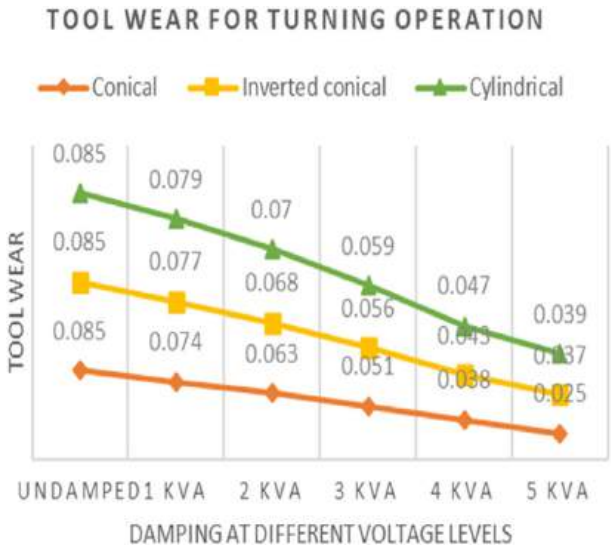

FIGURE 14 Tool wear at different damping conditions.

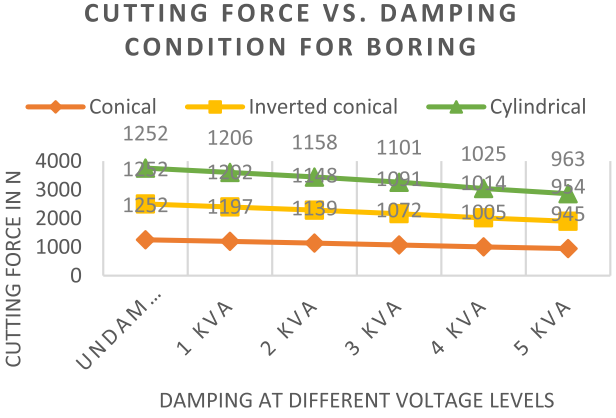

FIGURE 15 Cutting force at different damping conditions.

25778196, 0, Downloaded from https://onlinelibrary.wiley.com/doi/10.1002/eng2.12811, Wiley Online Library on [27/04/2024]. See the Terms and Conditions (https://onlinelibrary.wiley.com/terms-and-conditions) on Wiley Online Library for rules of use; OA articles are governed by the applicable Creative Commons License

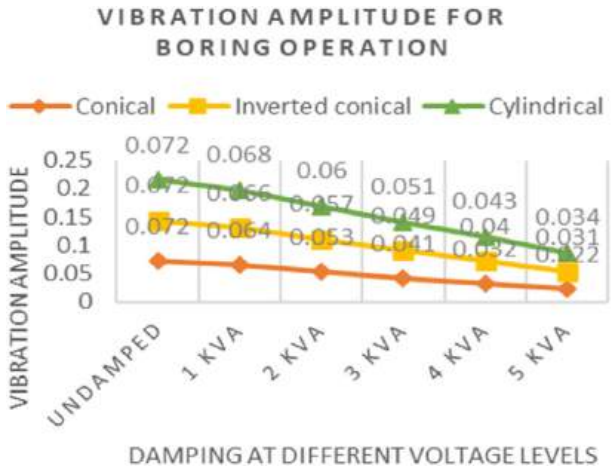

FIGURE 16 Vibration amplitude at different damping conditions.

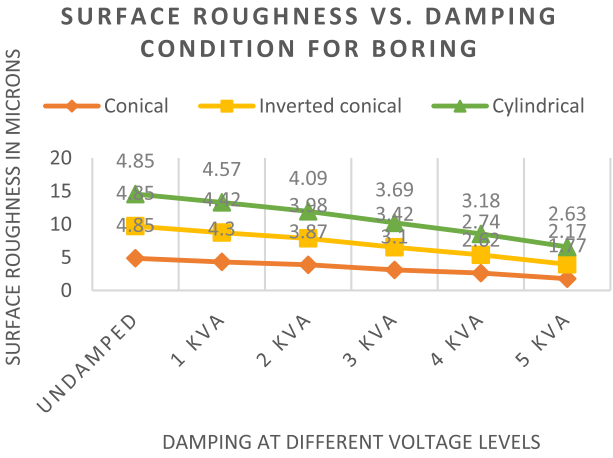

FIGURE 17 Surface roughness at different damping conditions.

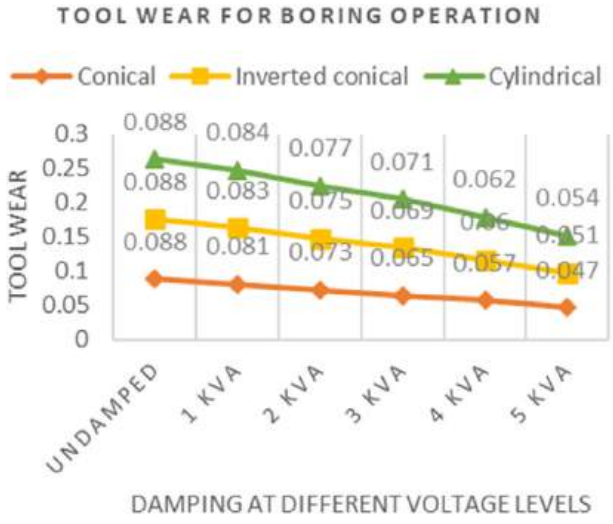

FIGURE 18 Tool wear at different damping conditions.

25778196, 0, Downloaded from https://onlinelibrary.wiley.com/doi/10.1002/eng2.12811, Wiley Online Library on [27/04/2024]. See the Terms and Conditions (https://onlinelibrary.wiley.com/terms-and-conditions) on Wiley Online Library for rules of use; OA articles are governed by the applicable Creative Commons License

www.nmiet.edu.in

TABLE 3 A six-run design of experiment matrix to test different no. of specimens.

	No. of sample				
	Sample				Parameters
S. No	1	2	3	4	D.C. Electric field strength
1	SI	SII	SIII	SIV	E0 (without Damper)
2	SI	SII	SIII	SIV	E1 (5 mA, 1KV)
3	SI	SII	SIII	SIV	E2 (10 mA, 2KV)
4	SI	SII	SIII	SIV	E3 (15 mA, 3KV)
5	SI	SII	SIII	SIV	E4 (20 mA, 4KV)
6	SI	SII	SIII	SIV	E5 (25 mA, 5KV)

TABLE 4 Design matrix for 4-run experiment for time study of conventional machining with modern machining operation (turning and boring).

S. No.	Parameters	No. of Specimens			
1	Time required for conventional machining operation rough machining and grinding (for turning and boring)	SI	SII	SIII	SIV
2	Machining by using ER damper (for turning and boring)	SI	SII	SIII	SIV

was observed that vibration amplitude was reduced up to 85% during turning and 65% during boring, cutting force was reduced by 22% during turning and 24% during boring, tool wear was reduced by 68% during turning and 48% during boring, surface roughness was reduced 71% during turning and 63% during boring. Average time of machining was also reduced by 5 min than conventional machining for turning and boring cycles.

The measurement of the cutting force is done on a standard electronic tool dynamometer. The external and internal diameters of work piece are measured using digital vernier caliper. The implementation stylus type surface roughness tester is to measure the surface roughness. The vibration amplitude is measured by the vibrometer. The digital vernier caliper is utilized to calculate the tool wear. Optimum cutting speed is maintained at 410 rpm, the depth of cut is 1 mm, and feed rate is 0.35 mm/rev for turning operation. While the speed 286 rpm depth of cut is 1 mm and feed rate is 0.35 mm/rev for boring operation. Design matrix is given in Table 3 for different values of electric field strengths.

5 | RESULTS AND DISCUSSION

These samples are prepared at Rajarambapu Institute of Technology, Islampur, as per the design matrix presented in Table no. 1, weighing machine, stirrer, and sonicator have been implemented for preparation of samples. The testing of these samples is conducted on Anton Parr modular compact rheometer (MCR-52). The rheometer displays all rheological properties of samples. After taking results from the rheometer, the best sample is chosen for further use in an electrorheological damper. Also, experiments on Kirloskar turn master lathe have been conducted in Shri Krishna Engineering Works, Industrial Estate, Sangli. All experiments with damper and without damper for turning and boring are conducted in that engineering works. In the first set, experiments are conducted as per 15 run designed matrix in Table no. 2. In the second set, experiments are conducted according to six-run design matrices with damper and without damper as designed in Table no. 3. And in the third set, experiments are conducted as designed in Table no. 4, using four-run design matrix to compare time requirement by conventional machining process and using electrorheological damper, for turning and boring operations. The characteristics of the ER fluid are illustrated in the plots of Figures 7,8,9, and 10. Electrorheological samples of alumina in silicone oil, alumina in castor oil, titanium dioxide in castor oil and mixture of alumina and titanium dioxide in castor oil have shown the highest values of shear stress as well as viscosity. The highest value of yield stress as well as dielectric strength is shown by a sample of titanium dioxide in castor oil. Hence titanium dioxide in the castor oil sample has shown the highest rheological performance than all other samples, that is why it has been selected

25778196, 0, Downloaded from https://onlinelibrary.wiley.com/doi/10.1002/eng2.12811, Wiley Online Library on [27/04/2024]. See the Terms and Conditions (https://onlinelibrary.wiley.com/terms-and-conditions) on Wiley Online Library for rules of use; OA articles are governed by the applicable Creative Commons License

TABLE 5 Electrorheological properties of ER fluid.

S. No.	Sample no.	Viscosity Pa-s	Shear stress Pa	Yield stress Pa	Dielectric strength KVA
1	1	0.532	53.2	24.3	3
2	2	0.0381	3.81	11.5	5
3	3	0.262	26.2	27.9	5
4	4	0.537	53.7	15.7	5
5	5	0.325	32.5	1.05	2
6	6	0.0198	1.98	1.58	2
7	7	0.088	8.8	8.8	2
8	8	0.684	68.4	28.2	6
9	9	0.379	37.9	10	3
10	10	0.0274	2.24	2.24	4
11	11	0.117	11.7	1.89	1.5
12	12	0.697	69.7	7.27	5

TABLE 6 Results obtained for cutting force in N for turning operation.

		Shape of plunger		
S. No.	Damping condition	Conical	Inverted conical	Cylindrical
1	Undamped	1165	1165	1165
2	1 KV, 5 mA	1110	1114	1116
3	2 KV, 10 mA	1060	1064	1068
4	3 KV, 15 mA	1012	1015	1019
5	4 KV, 20 mA	957	969	974
6	5 KV, 25 mA	897	909	911

TABLE 7 Results obtained for vibration amplitude in mm for turning operation.

		Shape of plunger		
S. No.	Damping condition	Conical	Inverted conical	Cylindrical
1	Undamped	0.06	0.06	0.06
2	1 KV, 5 mA	0.054	0.055	0.057
3	2 KV, 10 mA	0.042	0.044	0.046
4	3 KV, 15 mA	0.03	0.033	0.035
5	4 KV, 20 mA	0.018	0.021	0.024
6	5 KV, 25 mA	0.007	0.012	0.013

TABLE 8 Results obtained for surface roughness in microns for turning operation.

		Shape of plunger		
S. No.	Damping condition	Conical	Inverted conical	Cylindrical
1	Undamped	4.79	4.79	4.79
2	1 KV, 5 mA	4.27	4.32	4.45
3	2 KV, 10 mA	3.65	3.71	3.97
4	3 KV, 15 mA	3.02	3.20	3.42
5	4 KV, 20 mA	2.31	2.48	2.57
6	5 KV, 25 mA	1.37	1.52	1.69

25778196, 0, Downloaded from https://onlinelibrary.wiley.com/doi/10.1002/eng2.12811, Wiley Online Library on [27/04/2024]. See the Terms and Conditions (https://onlinelibrary.wiley.com/terms-and-conditions) on Wiley Online Library for rules of use; OA articles are governed by the applicable Creative Commons License

www.nmiet.edu.in

TABLE 9 Results obtained for tool wear in mm for turning operation.

		Shape of plunger		
S. No.	Damping condition	Conical	Inverted conical	Cylindrical
1	Undamped	0.085	0.085	0.085
2	1 KV, 5 mA	0.074	0.077	0.079
3	2 KV, 10 mA	0.063	0.068	0.07
4	3 KV, 15 mA	0.051	0.056	0.059
5	4 KV, 20 mA	0.038	0.043	0.047
6	5 KV, 25 mA	0.025	0.037	0.039

TABLE 10 Results obtained for cutting force in N for boring operation.

		Shape of plunger		
S. No.	Damping condition	Conical	Inverted conical	Cylindrical
1	Undamped	1252	1252	1252
2	1 KV, 5 mA	1197	1202	1206
3	2 KV, 10 mA	1139	1148	1158
4	3 KV, 15 mA	1072	1091	1101
5	4 KV, 20 mA	1005	1014	1025
6	5 KV, 25 mA	945	954	963

TABLE 11 Results obtained for vibration amplitude in mm for Boring operation.

		Shape of plunger		
S. No.	Damping condition	Conical	Inverted conical	Cylindrical
1	Undamped	0.072	0.072	0.072
2	1 KV, 5 mA	0.064	0.066	0.068
3	2 KV, 10 mA	0.053	0.057	0.06
4	3 KV, 15 mA	0.041	0.049	0.051
5	4 KV, 20 mA	0.032	0.04	0.043
6	5 KV, 25 mA	0.022	0.031	0.034

TABLE 12 Results obtained for surface roughness in microns for boring operation.

		Shape of plunger		
S. No.	Damping condition	Conical	Inverted conical	Cylindrical
1	Undamped	4.85	4.85	4.85
2	1 KV, 5 mA	4.30	4.42	4.57
3	2 KV, 10 mA	3.87	3.98	4.09
4	3 KV, 15 mA	3.10	3.42	3.69
5	4 KV, 20 mA	2.62	2.74	3.18
6	5 KV, 25 mA	1.77	2.17	2.63

25778196, 0, Downloaded from https://onlinelibrary.wiley.com/doi/10.1002/eng2.12811, Wiley Online Library on [27/04/2024]. See the Terms and Conditions (https://onlinelibrary.wiley.com/terms-and-conditions) on Wiley Online Library for rules of use; OA articles are governed by the applicable Creative Commons License

TABLE 13 Results obtained for tool wear in mm for boring operation.

S. No.	Damping condition	Shape of plunger		
		Conical	Inverted conical	Cylindrical
1	Undamped	0.088	0.088	0.088
2	1 KV, 5 mA	0.081	0.083	0.084
3	2 KV, 10 mA	0.073	0.075	0.077
4	3 KV, 15 mA	0.065	0.069	0.071
5	4 KV, 20 mA	0.057	0.06	0.062
6	5 KV, 25 mA	0.047	0.051	0.054

TABLE 14 Results of experiments conducted on different specimens for turning operation.

Specimen no.	S. No.	Damping condition	Vibration amplitude in mm	Cutting force in N	Tool wear in mm	Surface roughness in microns
SI	1	Undamped	0.059	1165	0.087	4.76
	2	1 KV	0.053	1113	0.079	4.30
	3	2 KV	0.041	1065	0.068	3.67
	4	3 KV	0.031	1013	0.058	3.05
	5	4 KV	0.021	957	0.045	2.33
	6	5 KV	0.010	901	0.031	1.31
SII	1	Undamped	0.060	1164	0.083	4.73
	2	1 KV	0.052	1114	0.078	4.33
	3	2 KV	0.040	1062	0.065	3.69
	4	3 KV	0.033	1017	0.050	3.08
	5	4 KV	0.020	962	0.037	2.35
	6	5 KV	0.011	898	0.025	1.40
SIII	1	Undamped	0.061	1163	0.088	4.82
	2	1 KV	0.055	1111	0.075	4.24
	3	2 KV	0.043	1064	0.064	3.63
	4	3 KV	0.034	1016	0.056	2.99
	5	4 KV	0.022	963	0.043	2.29
	6	5 KV	0.008	902	0.023	1.34
SIV	1	Undamped	0.062	1160	0.084	4.85
	2	1 KV	0.054	1110	0.076	4.21
	3	2 KV	0.042	1061	0.067	3.61
	4	3 KV	0.032	1014	0.052	2.96
	5	4 KV	0.019	958	0.039	2.27
	6	5 KV	0.009	897	0.029	1.43

25778196, 0, Downloaded from https://onlinelibrary.wiley.com/doi/10.1002/eng2.12811, Wiley Online Library on [27/04/2024]. See the Terms and Conditions (https://onlinelibrary.wiley.com/terms-and-conditions) on Wiley Online Library for rules of use; OA articles are governed by the applicable Creative Commons License

www.nmiet.edu.in

as a sample useful for electrorheological damper. The remaining samples have shown average electrorheological properties. All above samples are kept for 15 days under observation for taking sedimentation test. During sedimentation, the sample of titanium dioxide in castor oil has shown better performance than all other samples. The properties of different samples are given in Table 5, which elaborates the viscosity, shear stress, yield stress, and dielectric strength of the fluids used for experimentation.

For turning and boring operations, experimentations are executed with the same specified input parameters with and without damper. The experiments are carried out using different types of shapes of plungers. It is observed that the conical-shaped plunger has the best performance of vibration damping than other two shaped plungers of inverted conical as well as cylindrical. Hence by using a conical-shaped plunger six-run experiment has been conducted for turning and boring operation as per Table no 3. The relative analysis of input features on tool vibration amplitude is done for turning as well as boring operations. The observations of turning and boring operations for different types of shapes, mainly conical, inverted conical, and cylindrical with respect to cutting force, vibration amplitude, surface roughness, and tool wear, are given in Tables 6–13 and the graphical representation of turning is illustrated in Figures 11, 12, 13, and 14, respectively. The plot analysis of boring operations is illustrated in Figures 15, 16, 17, and 18. It is noted that tool vibration amplitude reduces with the increase in voltage. Cutting force reduces with an increase in voltage, likewise the performance of input attributes on surface finish and tool wear for turning as well as boring operation enhance with the implementation of damper. It is observed that there is a decrease in tool wear with the use of the damper and also

TABLE 15 Results of experiments conducted on different specimens for boring operation.

Specimen no.	S. No.	Damping condition	Vibration amplitude in mm	Cutting force in N	Tool wear in mm	Surface roughness in microns
SI	1	Undamped	0.068	1247	0.093	4.88
	2	1 KV	0.061	1205	0.086	4.35
	3	2 KV	0.053	1141	0.079	3.85
	4	3 KV	0.040	1109	0.062	3.05
	5	4 KV	0.031	1074	0.050	2.54
	6	5 KV	0.023	943	0.043	1.80
SII	1	Undamped	0.074	1245	0.084	4.91
	2	1 KV	0.069	1203	0.078	4.33
	3	2 KV	0.051	1138	0.071	3.82
	4	3 KV	0.038	1106	0.065	3.08
	5	4 KV	0.029	1072	0.053	2.66
	6	5 KV	0.020	954	0.041	1.83
SIII	1	Undamped	0.070	1253	0.087	4.82
	2	1 KV	0.063	1195	0.080	4.27
	3	2 KV	0.057	1145	0.073	3.90
	4	3 KV	0.044	1113	0.069	3.15
	5	4 KV	0.037	1080	0.057	2.70
	6	5 KV	0.027	947	0.049	1.74
SIV	1	Undamped	0.076	1251	0.096	4.79
	2	1 KV	0.067	1197	0.088	4.25
	3	2 KV	0.059	1148	0.081	3.92
	4	3 KV	0.046	1116	0.072	3.12
	5	4 KV	0.039	1082	0.060	2.58
	6	5 KV	0.030	958	0.051	1.71

25778196, 0, Downloaded from https://onlinelibrary.wiley.com/doi/10.1002/eng2.12811, Wiley Online Library on [27/04/2024]. See the Terms and Conditions (https://onlinelibrary.wiley.com/terms-and-conditions) on Wiley Online Library for rules of use; OA articles are governed by the applicable Creative Commons License

improvement is seen in surface finish. The outcomes are evaluated to get the minimum value of surface roughness, cutting force, tool vibration amplitude, and tool wear. Table 14 and Table 15 show the details of the results of all the four specimens of turning and boring operations, and Tables 16 and 17 show the average assessment of cutting performance of turning and boring operation for the conditions of without and with damper. Relative percentage assessment of cutting performances of turning operation and boring operation intended for this mentioned condition is given in Tables 18 and 19. It is recorded that the use of the ER damper will reduce the value of vibration amplitudes up to 85% for turning and 65% for boring, reduction in cutting force by 22% for turning and 24% for boring, decrease in tool wear by 68% for turning and 48% for boring operation. Along with the utilization of ER damper illustrates enhancement in surface finish up to 71% for turning and 63% for boring operation. Tables 20 and 21 give detailed time analysis, and Table 22 shows average comparative results of conventional machining operation with operation using an ER damper for turning and boring operations. From this table, it is observed that on average 5 min can be saved for machining components using ER damper. The time analysis results for the different samples are given in Figure 19.

From the research conducted, it is recorded that the highest damping capacity is at a voltage supply of 5KV 25 mA as the electric field strength is maximum at this point; this reflects that the larger the electric field strength due to higher supply voltage, improved will be the damping ability. Care should be taken while voltage application that it should not be greater than break down voltage of the employed samples. In addition, as the voltage increases, the temperature increases, which may affect some of the measurements in the experiment.

The highest distinguishable parameter in the downward direction is the central cutting force, the structure that counterattacks the drive of tool in downward direction that offers better damping. It is clear that during hard turning and

TABLE 16 Average observed readings of 1–4 specimens for turning operation.

S. No.	Parameters	Amplitude of vibration in mm	Cutting force in N	Tool wear in mm for 1 mm cut	Surface roughness in μm
1	Undamped	0.060	1165	0.085	4.79
2	1KVA, 5 mA	0.053	1112	0.077	4.27
3	2 KVA, 10 mA	0.041	1063	0.066	3.65
4	3 KVA, 15 mA	0.032	1015	0.054	3.02
5	4 KVA, 20 mA	0.020	960	0.041	2.31
6	5 KVA, 25 mA	0.009	899	0.027	1.37

TABLE 17 Average observed readings of 1–4 specimens for boring operation.

S. No.	Parameters	Amplitude of vibration in mm	Cutting force in N	Tool wear in mm for 1 mm cut	Surface roughness in μm
1	Undamped	0.072	1252	0.090	4.85
2	1KVA, 5 mA	0.065	1200	0.083	4.30
3	2 KVA, 10 mA	0.055	1143	0.076	3.87
4	3 KVA, 15 mA	0.042	1077	0.067	3.10
5	4 KVA, 20 mA	0.034	1111	0.055	2.62
6	5 KVA, 25 mA	0.025	951	0.046	1.77

TABLE 18 Comparative results of turning operation in percentage form.

S. No.	Parameters	Without damper	With damper	Percentage improvement
1	Amplitude of vibration in mm	0.060	0.009	85
2	Cutting force in N	1165	899	22.83
3	Tool wear in mm	0.085	0.027	68.23
4	Surface roughness in μm	4.79	1.37	71.39

25778196, 0, Downloaded from https://onlinelibrary.wiley.com/doi/10.1002/eng2.12811, Wiley Online Library on [27/04/2024]. See the Terms and Conditions (https://onlinelibrary.wiley.com/terms-and-conditions) on Wiley Online Library for rules of use; OA articles are governed by the applicable Creative Commons License

www.nmiet.edu.in

TABLE 19 Comparative results of boring operation in percentage form.

S. No.	Parameters	Without damper	With damper	Percentage improvement
1	Amplitude of vibration in mm	0.072	0.025	65.27
2	Cutting force in N	1252	951	24.04
3	Tool wear in mm	0.090	0.046	48.88
4	Surface roughness in μm	4.85	1.77	63.50

TABLE 20 Time study for turning operation.

		Time period			
S. No.	Parameters	SI	SII	SIII	SIV
1	Time required for conventional turning process (without damper)	21.35	22.25	20.30	21.45
2	Time required for turning using ER damper	16.40	15.30	14.25	17.35

TABLE 21 Time study for boring operation.

		Time period			
S. No.	Parameters	SI	SII	SIII	SIV
1	Time required for conventional boring process (without damper)	23.30	24.25	22.35	23.45
2	Time required for boring using ER damper	18.45	17.35	16.25	19.30

TABLE 22 Average time required for specimens for turning as well as boring.

S. No.	Parameters	Time period in minutes			
1	Average time required for conventional machining (turning and boring)	22	23	21	22
2	Average time required for Machining using ER damper	17	16	15	18

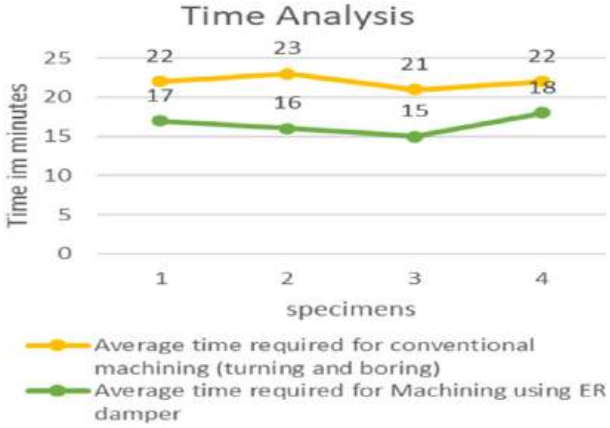

FIGURE 19 Time analysis with and without damper.

25778196, 0, Downloaded from https://onlinelibrary.wiley.com/doi/10.1002/eng2.12811, Wiley Online Library on [27/04/2024]. See the Terms and Conditions (https://onlinelibrary.wiley.com/terms-and-conditions) on Wiley Online Library for rules of use; OA articles are governed by the applicable Creative Commons License

boring operations due to the cutting forces, the performance of the cutting tool decreases. This damping reduces the exertion of the tool shape and gives better damping action and upsurge complete energy to run the machining operation. It is also seen the irregularities of surface decrease because of the damping of tool on work piece and better quality in the surface of the material, which hence obtained reduces the chance of crack provocation. As a result, there is an increase in the life span of the tool with the rise in stiffness of the cutting tool with the increase in toughness of the tool other than the tool placed under vibrating environments. It is observed that with higher viscosity there is enhancement in the quality of surface as it gives extra resistance to the plunger. During this research, it is observed that study at 25 mA at 5 KV voltage there is better spreading of the ER particles that gives reduction in tool wear and virtuous machining performance; this is due to the extra resistance to plunger giving rise to lessening the amount of tool wear and improvement in the quality of the surface finish.

From previous literature review, it is found that Varadrajan et al.[1] have used magnetorheological damper for damping vibrations during turning operation. After reviewing around 100 reputed research papers from various journals, we can consider electrorheological damper for damping vibrations of hardened EN 24 grade alloy steel as an open research problem.

Comparison of current research with references.

S. No.	Reference no.	Speed in RPM	Feed mm/rev	Depth of cut	Hardness	Cutting force N	Surface roughness μm
1	3	150 to 350	0.15 to 0.35	_	280 to 330 BHN	778 to 1415	1.03 to 4.98
2	37	300 to 500	0.04 to 0.08	40 to 120 μm	62 to 70 HRC	43.11 to 222.8	_
3	Current research	410 and 286	0.35	1 mm	302 BHN	897 to 1252	1.37 to 4.85

6 | CONCLUSION

In this research, experiments are conducted using three shaped plungers for ER damper that are premeditated and confirmed for the outcome of tool wear, cutting force, tool vibration amplitude, and quality of surface at the time of hard turning and hard boring with the application of minimal fluid. The performance of the three shapes of plungers is compared with each other. 125 W electric power is needed for the ER damper to demonstrate good results. The significant consequences marked are, to gain enhanced outcomes like decrease in amplitude of tool vibration, cutting force, tool wear, and better quality of surface of the specimen using, the ER fluid sample of titanium dioxide nanoparticles in castor oil charged with D.C. current. Castor oil is ecofriendly and not hazardous to the atmosphere and is easily available in the atmosphere. Among the three shapes of plungers, conical, inverted conical, and cylindrical, the conical plunger has shown better performance of damping to improve the surface quality, suppress tool vibration, reduction in cutting force and tool wear using ER damper. A comparison of time required for conventional machining process with machining using ER damper shows that ER damper is useful for small-scale industries to save machining time. In the future, this method can be implemented into a product that will offer required damping to the tool to achieve the optimum machining performance as anticipated with excessive precision and assure guarantee for capitalization.

CONFLICT OF INTEREST STATEMENT

The authors declare no conflicts of interest.

PEER REVIEW

The peer review history for this article is available at https://www.webofscience.com/api/gateway/wos/peer-review/10.1002/eng2.12811.

DATA AVAILABILITY STATEMENT

The materials utilized in this research are prepared by the researcher and the experiments are carried out at Rajarambapu Institute of Technology, also at Shri Krishna Engineering Works, Industrial Estate, Sangli.

CONSENT TO PARTICIPATE

This work is the Doctoral research carried out at the abovementioned institute and mentioned industry.

25778196, 0, Downloaded from https://onlinelibrary.wiley.com/doi/10.1002/eng2.12811, Wiley Online Library on [27/04/2024]. See the Terms and Conditions (https://onlinelibrary.wiley.com/terms-and-conditions) on Wiley Online Library for rules of use; OA articles are governed by the applicable Creative Commons License

www.nmiet.edu.in

CONSENT FOR PUBLICATION

I, the corresponding author, give my consent for the publication of identifiable details, which can include photograph(s) details within the text ("Material") to be published in the above Journal and Article. I confirm that I have seen and been given the opportunity to read both the Material and the Article (as attached) to be published. Therefore, anyone can read the material published in the Journal.

ORCID

Aditi D. Apte https://orcid.org/0000-0003-2329-9298
Shivakumar Shivamurthy https://orcid.org/0000-0003-1922-2765
Manjunath G Avalappa https://orcid.org/0000-0002-1963-5220
Nikhil Rangaswamy https://orcid.org/0000-0002-4090-6638
Ashwini S. Shinde https://orcid.org/0000-0001-9999-281X
Satish S. Kulkarni https://orcid.org/0000-0001-9194-4389

REFERENCES

1. Paul PS, Varadrajan AS. Effect of magnetorheological damper on tool vibration during hard turning. *Front Mech Eng*. 2012;7(4):410-416. doi:10.1007/s11465-012-0341-4
2. Singaravel B, Selvaraj T. Experimental investigations on cutting forces, specific cutting pressure, coefficient of friction and shear energy in turning of HSLA steel. *Manag Prod Eng Rev*. 2016;7(1):71-76. doi:10.1515/mper-2016-0008
3. Chandra P, Rao CRP, Kiran R, Ravikumar V. Influence of machining parameters on cutting force and surface roughness while turning alloy steel. *Mater Today: Proc*. 2018;5(2018):11794-11801. doi:10.1016/matpr.2018.02.149
4. Rajarajan S, Sivaprakasam R. The effect of machining factors on the mean cutting force and cutting power while turning steel alloy AISI 52100 in dry condition. *Int J Recent Technol Eng*. 2019;7(6):321-326.
5. Mishra V, Bharat N, Chakraborty K. Comparative assessment on the machinability of EN24 and EN36C steels. *Int J Eng Adv Technol*. 2019;8:3.
6. Omambala JR, McIntyre EC, Gallo AA. Comparing the electrorheological effect of polyhedral silsesquioxane cage structures with different numbers of cynopropyl functional groups. *ACS Omega*. 2019;4:20964-20971.
7. Bharat N, Kalyan C. Machinability of EN24 steel (817M40). *IntJ Latest Trends Eng Technol*. 2019;12(3):001-007. doi:10.21172/1.123-01
8. Paris H, Brissaud D, Gouskov A. A more realistic cutting force model at uncut chip thickness close to zero. *CIRP Ann Manuf Technol*. 2007;56:415-418. doi:10.1016/j.cirp.2007.05.096
9. Thokale MI, Bidwai SS, Yadav SK. Optimization of cutting parameter of EN24 steel by using Taguchi method in hard turning. *Int J Adv Res Sci Eng*. 2015;4(3):1-3.
10. Jain R, Rathore JK, Gorana VK. Design development and testing of a three component lathe tool dynamometer using resistance strain gauges. *CAD/CAM, Robotics and Factories of the Future*. Springer; 2016. doi:10.1007/978-81-322.2740-3-2
11. Bharat N, Mishra V, Chakraborty K. Machining behavior of EN24 and En36C steels. *Int J Innov Res Sci Eng Technol*. 2019;12(4):21-34. doi:10.21172/ijiet.124.04
12. Tin TS, Aung k L. Design considerations of electrorheological damper. *Int J Sci Res Publ*. 2018;8(7):136-141. doi:10.29322/IJSRP.8.7.2018.p7922
13. Rajneesh Kumar B, Ranganatha S. Dynamic characteristics of a squeeze film damper lubricated with electrorheological fluid in terms of Reynolds number. *Int J Recent Technol Eng*. 2013;2(4):132-136.
14. Jighua W, Song Z, Liu F, et al. Giant electrorheological fluids with ultrahigh electrorheological efficiency based on a micro/ hybrid calcium titanyl oxalate composite. *NPG Asia Mater*. 2016;8:1-8. doi:10.1038/am.2016.158
15. Datta S, Barua R, Das J. *A Review on Electrorheological Fluid (ER) and Its Various Technological Applications*. IntechOpen; 2020:90706. doi:10.5772/inte.chopen.90706
16. Kim D-H, Kim YD. Electrorheological properties of polypyrole and its composite ER fluids. *J Ind Eng Chem*. 2007;13(6):879-894.
17. Goilkar S. Design and development of a variable damping device for vibration control with electrorheological (ER) fluid. *Adv Intell Syst Res*. 2017;137:127-133.
18. Song Q, Shi J, Liu Z, Wan Y, Xia F. Boring bar with constrained layer damper for improving process stability. *Int J Adv Manuf Technol*. 2015;83:1951-1966. doi:10.1007/s00170-015-7670-5
19. Fallah M, Moetakef-Imani B. Design analysis and implementation of a new adaptive chatter control system in internal turning. *Int J Adv Manuf Technol*. 2019;104:1637-1659.
20. Venkatachalam R, Balasivanandha Prabhu S. Vibration characteristics of orthotropic shaft disk system with different constrained damping layers: experimental and numerical study. *Int J Adv Manuf Technol*. 2012;65:601-610. doi:10.1007/s00170-012-4199-8
21. Biju CV, Shunmugam MS. Investigation in to effect of particle impact damping (PID) on surface topology in boring operation. *Int J Adv Manuf Technol*. 2014;75:1219-1231.
22. Otsubo YS, Edamura K. Electric effects on the rheology of insulating oils in electrodes with flocked fabric. *Rheol Acta*. 1999;38:137-144.
23. Joseph RD, Krebs HI. An electrorheological fluid actuator for rehabilitation robotics. *IEEE ASME Trans Mechatron*. 2018;23(5):2156-2167.

25778196, 0, Downloaded from https://onlinelibrary.wiley.com/doi/10.1002/eng2.12811, Wiley Online Library on [27/04/2024]. See the Terms and Conditions (https://onlinelibrary.wiley.com/terms-and-conditions) on Wiley Online Library for rules of use; OA articles are governed by the applicable Creative Commons License

24. Choi SB, Goldasz J. Controllable actuators utilizing smart MR materials and ER suspensions (review). Actuator 2018: 16th International Conference on New Actuators, Bremen, Germany, 25-27. 2018.
25. Haiping D, Li W, Zhang N. Integrated seat and suspension control for a quarter car with driver model. *IEEE Trans Veh Technol*. 2012;61(9):3893-3908.
26. Nikitczuk J, Weinberg B, Canavan PK, Mavroidis C. Active knee rehabilitation orthotic device with variable damping characteristics implemented via an electrorheological fluid. *IEEE ASME Trans Mechatron*. 2010;15(6):952-960. doi:10.1109/TMECH.2009.2036170
27. Stenicka M, Pavlinek V, Saha P, Blinova NV, Stejskal J, Quadrat O. The electrorheological efficiency of polyaniline particles with various conductivities suspended in silicone oil. *Colloid Polym Sci*. 2009;287:403-412.
28. Khanicheh A, Mintzopoulos D, Brian Weinberg A, Tzika A, Mavroidis C. Evaluation of electrorheological fluid dampers for applications at 3-T MRI environment. *IEEE ASME Trans Mechatron*. 2008;13(3):286-294.
29. Wei J, Zhao L, Peng S, Shi J, Liu Z, Wen W. Wettability of urea-doped TiO_2 nano particles and their high electrorheological effects. *J Solgel Sci Technol*. 2008;47:311-315. doi:10.1007/s10971-008-1787-z
30. Kim YD, De Kee D. Measuring static yield stress of electrorheological fluids using slotted plate device. *Rheol Acta*. 2008;47:105-110. doi:10.1007/s00397-007-0217-4
31. Yoon DJ, Kim YD. Electrorheological properties of polypyrrole SnO_2- methyl cellulose nano composite suspensions. *J Mater Sci*. 2007;42:5534-5538.
32. Kim J, Kim CA, Choi HJ, Choi SB. Role of surfactant on damping performance of polyaniline based electrorheological suspension. *Korea Aust Rheol J*. 2006;18:25-30.
33. Cox BJ, Thamwattana N, Hill JM. Maximizing the electrorheological effect for bidisperse nano fluids from the electrostatic force between two particles. *Rheol Acta*. 2006;45:909-917. doi:10.1007/s00397-006-0084-4
34. Hong SR, Choi SB, Lee DY. Comparison of vibration control performance between flow and squeeze mode ER mounts: experimental work. *J Sound Vib*. 2006;291:740-748. doi:10.1016/j.jsv.2005.06.037
35. Sedlacik M, Almojdalavi S, Mrlik M, Pavlinek V, Saha P, Stejskal J. Viscoelastic properties of electrorheological suspensions of core-shell (carbon/polyaniline) particles in silicone oil. *J Phys Conf Ser*. 2013;412:012006. doi:10.1088/1742-6596/412/1/012006
36. See H, Kawai A, Ikazaki F. Differences in the electrorheological response of a particle suspension under direct current and alternating current electric fields. *Colloid Polym Sci*. 2002;280:24-29.
37. Mohandas KN, Ramesh CS, Koorapati EP, Balashanmugam N. Prediction of cutting forces developed during hard turning of hard chrome plated surfaces on EN 24 substrate. *J Mech Eng*. 2013;10(1):49-65.

How to cite this article: Apte AD, Shivamurthy S, Avalappa MG, et al. Novel technique of vibration minimization during hard machining. *Engineering Reports*. 2023;e12811. doi: 10.1002/eng2.12811

25778196, 0, Downloaded from https://onlinelibrary.wiley.com/doi/10.1002/eng2.12811, Wiley Online Library on [27/04/2024]. See the Terms and Conditions (https://onlinelibrary.wiley.com/terms-and-conditions) on Wiley Online Library for rules of use; OA articles are governed by the applicable Creative Commons License

www.nmiet.edu.in

International Journal of
INTELLIGENT SYSTEMS AND APPLICATIONS IN ENGINEERING
ISSN:2147-6799 www.ijisae.org Original Research Paper

Machine Learning Approach for Intelligent Transport System in IOV-Based Vehicular Network Traffic for Smart Cities

Chandrakant D. Kokane[1*], Gopal Mohadikar[2], Sonu Khapekar[3], Bharti Jadhao[4], Tushar Waykole[5], Vilas V. Deotare[6]

Submitted: 26/05/2023 **Revised**: 11/07/2023 **Accepted**: 29/07/2023

Abstract: The transportation industry will face many significant issues, including traffic congestion, pollution, and ineffective traffic management, as a result of the increasing urbanisation and demographic growth. It appears that one potential solution to these issues may be provided by intelligent transport systems (ITS) that harness the power of vehicular networks on the Internet of Vehicles (IoV). By integrating communication between vehicles and infrastructure (V2V) and vehicles and the cloud (V2C), the proposed ITS architecture seeks to create a comfortable and effective transportation ecosystem. The V2V connection helps with the transmission of data on route conditions, collision avoidance, and speed, position, and other factors. Vehicle-to-infrastructure (V2I) communication enables automobiles to connect with infrastructure components like traffic lights, road signs, and parking systems in order to optimise traffic signal timings and provide drivers with real-time information. Innovative applications like customised recommendations, dynamic navigation, and predictive maintenance are made possible via V2C communication, which makes it possible for cars to connect to the cloud. The recommended method makes use of tree-based machine learning models including Decision Tree (DT), XGBoost (XGB), and Random Forest (RF) to increase traffic detection accuracy and computational efficiency.

Keywords: *Vehicular Network, Internet of Vehicles, Machine Learning, Intelligent transport system, Network traffic*

1. Introduction

To effectively combat traffic congestion, intelligent transportation systems (ITS) offer early guidance and effective traffic planning. One essential element of ITS is the Internet of Vehicles (IoV). It enables the evaluation of the capacity of the road network, the gathering of real-time traffic data, traffic relief, and the direction of traffic participants. IoV-based systems can also calculate individual journey times and estimate traffic in order to prevent congestion. To improve network management and security, network activity classification is essential. When handling the traffic from the Internet of Things (IoT), which is made up of numerous devices connected in various ways, network monitoring and management systems run into issues. Other than that, traffic data collection systems that are improved allow for the organisation of traffic based on specific requirements. To maintain the company's security, the company's traffic needs to be correctly classified based on the equipment. The classification of network traffic is a vital task that may be applied to many different forms of data, with a focus specifically on transportation data, mobile networks, the Internet of Things, and large intelligent cities [1]. The classification process depends on automatic learning (ML), in addition to data mining techniques, data bases, and travel characteristic classifications. This includes employing automatic learning approaches for precise classification through the use of extraction, selection, and application. There are many methods available for calculating the traffic flow in an IOV system. Some techniques for predicting time series include factor analysis, index analysis, multiplicative and additive models, and model analysis. Based on historical traffic data, these techniques can be utilised to produce precise estimates.

1,3,4,5 Assistant Professor, Department of Computer Engineering, Nutan Maharashtra Institute of Engineering & Technology, Talegaon(D), Pune, India(MS), ORCID ID: 0000-0001-7957-3933
2 Sr. Assistant Professor, Department of Mechanical Engineering, Tolani Maritime Institute, Induri, Pune, India(MS), ORCID ID 0009-0004-5593-7607
3ORCID ID: 0009-0007-9677-8931
4ORCID ID: 0009-0002-3356-4710
5ORCID ID:0000-0002-6758-0252
6Principal, Nutan Maharashtra Institute of Engineering & Technology, Talegaon(D), Pune, India(MS), ORCID ID: 0000-0002-5619-0806
** Corresponding Author Email: cdkokane1992@gmail.com*

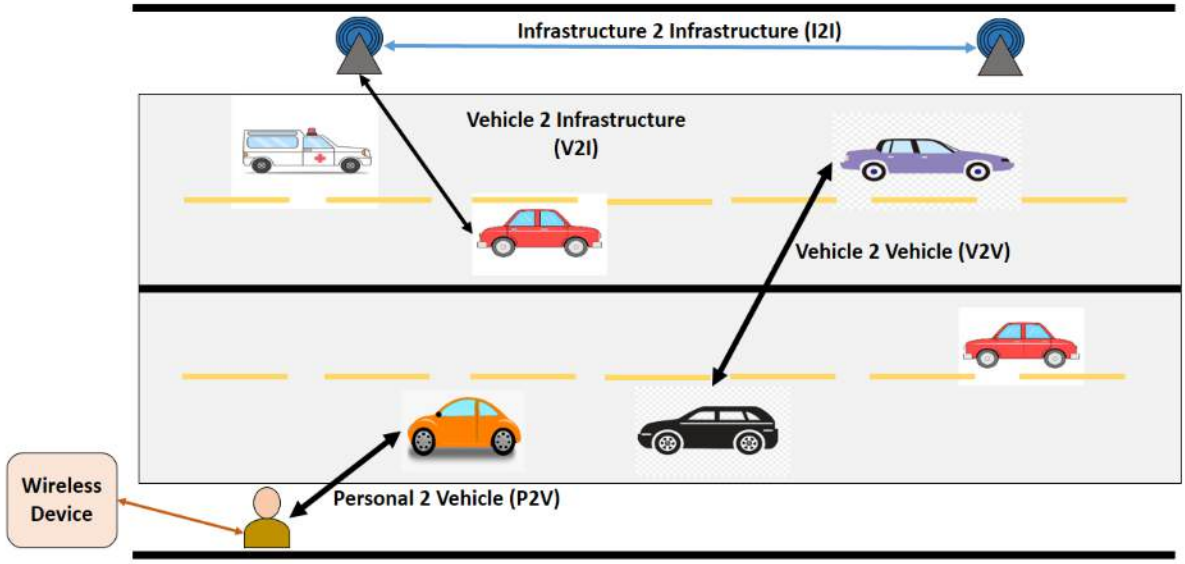

Fig 1: Internet of Vehicle (IoV) Internal Network system

A strong technique that delivers accurate classification results for network traffic order is Deep Packet Inspection (DPI). Understanding how the Internet works is essential since it plays a big part in both our personal and professional life. A rise in the complexity of network traffic patterns can be attributed to the ongoing growth of network designs, protocols, and applications. In addition to helping us satisfy our curiosity, classifying network traffic offers a wide range of crucial uses for network administrators.

It can monitor different behaviours and help with security management and network performance analysis. Utilising particular ML techniques, effective traffic analysis is achieved. To detect intrusions, assess malware activities, classify network traffic data, and examine other security traits, better artificial intelligence (AI) tools are needed. The ability of ML to successfully address network-related issues has been greatly demonstrated. Understanding and enhancing network operations and security require a thorough understanding of network traffic classification. To provide correct classification and enable different applications in network management and protection, it depends on ML approaches, data mining, and suitable dataset selection. The application of machine learning techniques to the categorization of Internet of Vehicles (IOVs) traffic within vehicular networks is the primary subject of this study. Investigating how various ML datasets and their properties affect classification performance using actual IOVs traffic data is the goal. For many network operations, such as security monitoring, defect detection, traffic engineering, and ensuring Quality of Service (QoS) standards, accurate traffic classification is crucial.

Effective network traffic classification of IOVs is essential given their explosive increase. Generating IOVs network traffic data can be difficult, though, especially when the ML models need to be trained on both malignant and benign data. In order to meet this issue, the performance of several machine learning (ML) techniques will be compared in this research, with a focus on intrusion detection systems (IDS) in the context of IOV-based vehicular networks. The goal of the study is to identify the best methodology for accurate traffic classification within IOV networks by comparing several ML approaches. The success of network operations and security depends on the categorization process' performance indicators. The study sheds light on the benefits of various ML techniques by contrasting their results.

2. Review of Literature

In order to improve performance, network security procedures, and the administration of intelligent traffic systems (ITS), network traffic categorization primarily aims to analyse and assess traffic patterns. The author explores a variety of artificial intelligence (AI) and machine learning (ML) techniques for malware analysis and traffic analysis. Effective categorization and classification of network traffic are required due to the rising demand for high-speed transmission rates. In order to do this, the author suggests a revolutionary method that relaxes the assumption of independence in Naive Bayes (NB) classifiers. This method combines technologies like intelligent transportation, databases, networks, and computing to create a system for dynamic processing centre design.

For vehicle ad hoc networks, the research proposes feature selection algorithms that remove pointless

anomaly features and cluster intelligent features [5]. A feature selection technique is used that outperforms previous filter procedures in terms of accuracy and productivity: the computerised correlation-based filter (CFS). IoT devices can quickly benefit from ML and AI techniques [3,4]. The WEKA ML programme is used to estimate the most widely used supervised ML approaches utilising a variety of traffic classification techniques. Naive Bayes, Naive Bayes Kernel Estimation, Bayesian Network, C4.5 Decision Tree, k-Nearest Neighbours (KNN), Deep Neural Networks [7], and Support Vector Machines (SVM) are a few well-liked methods for classifying vehicular network data. Due to its capability to identify distinct network structures and learn from training datasets, ML algorithms are highly valuable.

Lv.Z. et al. [2], a remote receiving terminal and a basic monitoring network make up the system. The fundamental monitoring network links taxis and streetlights as nodes and routes, respectively. Each node is given a different address as a result of the network's dynamic organisation, which acts as the node's identification inside the network. The system's design includes a simulation experiment to show how well it can fulfil criteria and send messages with the acquired data to the specified terminal while adhering to predefined settings.

The system's ability to integrate sensors through a ZigBee wireless network has the potential to encourage the construction of smart city infrastructure. This design makes it possible for data to be collected and transmitted in an efficient manner, which makes it easier to build and administer different parts of a smart city.

The Intrusion Detection Systems (IDSs) training and testing feature extraction algorithm described in this paper intends to effectively extract unique features from vehicle messages. The programme focuses on extracting two important features: variances in traffic flow and differences in position. The range of distances between cars is used to calculate the traffic flow disparities feature. The programme estimates the fluctuations in traffic flow by examining the distances between vehicles in the network. For the purpose of identifying anomalies and probable invasions, this function offers useful information. Voting filter and semi-cooperative mechanisms are both used in the extraction of the position differences feature. Together, these systems help to identify the variations in vehicle placements [11]. The voting filter process aids in the removal of erroneous or noisy position data, guaranteeing the accuracy of the extracted feature. In order to improve the precision and consistency of position difference measurements, the semi-cooperative mechanism makes use of the collaboration of surrounding vehicles.

The suggested approach enables efficient and effective extraction of pertinent information from vehicle communications by utilising these two crucial aspects. The training and testing of IDSs for spotting potential attacks and guaranteeing the security of the vehicle network rely heavily on these features.

3. Publically Available Datasets

In the area of network security, intrusion detection and prevention systems (IDS and IPS) are crucial because they provide defence against increasingly sophisticated network attacks. The systems for detecting intrusions based on anomalies struggle to produce accurate and consistent performance evaluations due to the lack of reliable test and validation data. Methods based on anomalies require the availability of high-quality data bases that accurately reflect traffic and attack situations in the real network.

Table 1: Dataset Description of CIC-IDS2017 Dataset

Attack Type	Description	IOV Scenario
BENIGN	Genuine network traffic produced by actual users conducting activities like browsing or emailing.	Monitoring IOV users' regular activities, such as email, web browsing, and DNS requests.
DoS	Assaults that try to interrupt online services and frequently come before DoS/DDoS assaults.	Attacking IOV systems' network infrastructure and resulting in service degradation or unavailability.
Port-Scan	Sending client queries to various server ports on a host to look for exploitable holes.	Scanning the network ports of IOV systems to find any vulnerabilities that could allow outside access.

Brute Force Attack	Utilizing arduous trial-and-error to try and crack or compromise car network or system credentials.	Using brute force assaults to take control of IOV systems and get unauthorized access.
Web Attack	Using cross-site scripting (XSS) or SQL injection vulnerabilities in the web pages of automobiles or servers.	Stealing sensitive data or undermining the integrity of IOV systems' online interfaces as a target.
Botnet Attack	Gaining access to victim systems to create a network of controlled bots, which is frequently utilized for additional cyber-attacks.	Introducing malware into IOV systems to build a botnet and enable massively coordinated strikes.
Infiltration Attack	Targeting network infiltration, when systems are compromised by unauthorized access.	The deliberate attempt to circumvent security safeguards on IOV networks or systems.

Table 2: Dataset used in proposed method CIC-IDS2017 Dataset

Class Label	Number of Samples
BENIGN	22,731
DoS	19,035
Port-Scan	7,946
Brute-Force	2,767
Web-Attack	2,180
Botnet	1,966

This technology creates genuine, benign background traffic while profiling the abstract behaviour of human interactions. The abstract behaviour of 25 users from the CICIDS2017 dataset was developed as discussed in table 1 and table 2, concentrating on protocols including HTTP, HTTPS, FTP, SSH, and email. Overall, the CICIDS2017 dataset is a useful tool for studying network traffic. It features a variety of attack and benign traffic that closely resembles real-world events, and it was developed with the generation of realistic background traffic in mind. This dataset makes it possible for academics and professionals to thoroughly analyse and assess intrusion detection and prevention systems.

4. Methodology

The IOVs network traffic dataset is classified by classifying the traffic into various groups, such as attacks or normal. Over the past 20 years, there has been a lot of research done on the need for IOV-based vehicular network traffic classification. To effectively classify these groups, researchers have suggested a variety of ways. supervised and unsupervised learning techniques are the two primary categories of machine learning (ML) approaches used for traffic classification. Tree-based supervised ML algorithms are used in this particular study. A combination of decision tree (DT), random forest (RF), extra tree (ET), and XGBoost techniques are used in the feature-engineering stage. These algorithms provide accurate network traffic classification by training and testing intrusion detection techniques with various parameters.

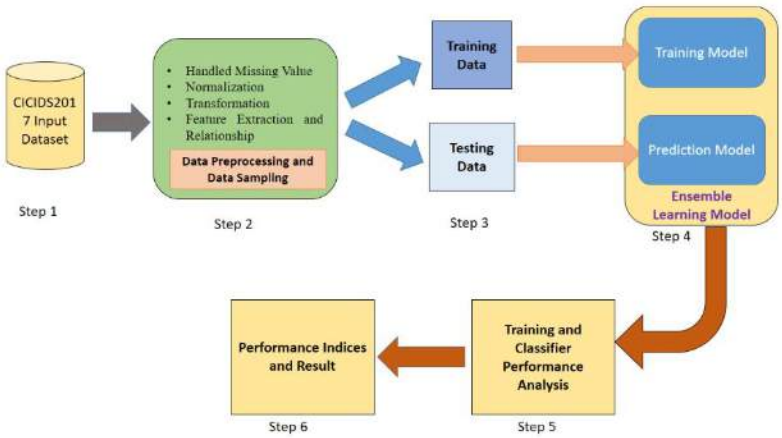

Fig 2: The network architecture proposed for connected vehicles (IoVs)

A few of the many benefits of using machine learning techniques based on trees include interpretation, scalability, and the ability to use large character spaces. The project's goal is to put these algorithms and characteristic engineering to use to achieve accurate and reliable intrusion detection in the IOV-based vehicle network. The focus of the research is on classifying IOVs for network traffic using ML-supervised tree algorithms including DT, RF, ET, and XGBoost. In the feature engineering stage, these algorithms are used to train and test intrusion detection methods with various parameter values. This method is employed by researchers to increase the accuracy and effectiveness of traffic classification in IOV-based vehicular networks.

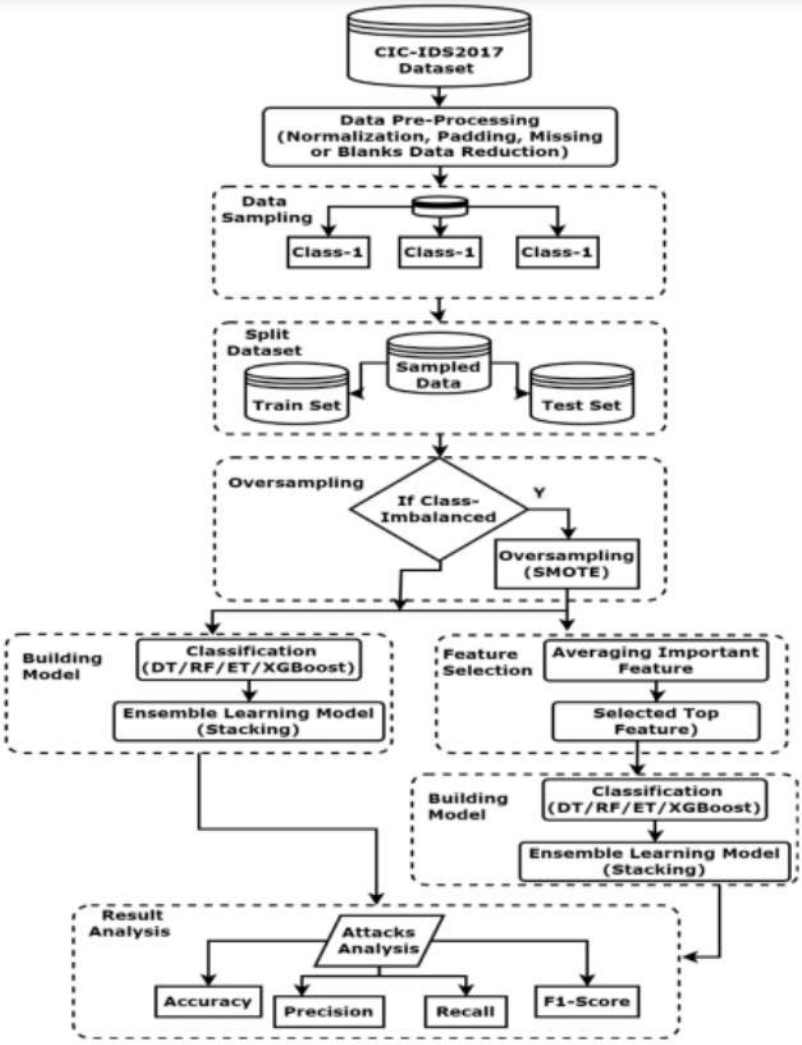

Fig 3: Process flow of proposed system in IoV Vehicular Network

A. (DT) Decision Tree

Data items are categorised by Decision Tree (DT) by assessing the values of their attributes. A decision tree is initially constructed using a set of pre-classified data. To divide the data into various classes, characteristics are picked for each node of the tree. Recursively, this partitioning procedure divides subsets of data items into smaller groups based on attribute values until each group contains only data items from the same class. With edges labelled in accordance with the parent attribute, the decision tree separates the data depending on the supplied attributes at each node. To help in classification, the decision tree's leaves are labelled with decision values. Statistical classifiers are a common classification approach used by DTs. Selected features are incorporated into the classification process, and classes that distinguish the target application based on all aspects are then determined recursively. In this instance, let X stand in for a data point's features and Y for the class. The choice is made by figuring out the ratio between X and Y, which aids in selecting the right class for the data point.

$$\text{RATIO}\,(X \mid Y) = H(X) - H(X \mid Y)\,H(X)$$

The conditional entropy, denoted by the symbol H (X|Y), estimates the uncertainty of variable X given variable Y. The marginal entropy, on the other hand, measures the uncertainty of variable X alone, without taking into account any other variables. This is known as H(X).

$$D = \{(x1, y1), (x2, y2), \ldots, (xN, yN)\}$$

Let xi = (xi1, xi2,..., xim) represent the feature vector of sample i in the regression tree, where xij is the feature j of sample i. The regression tree separates the input space into K regions (R1, R2,..., RK) linked to particular results (c1, c2,..., ck). We can express the regression model in the following way as a result:

$$y = f(x) = \Sigma\, ck * I(x \in Rk)$$

where y is the anticipated output variable, f(x) denotes the regression function, ck is the particular outcome connected to area R_k, and I(x ∈ Rk) denotes an indicator function that evaluates to 1 when the input x falls within region R_k and 0 otherwise.

$$f(x) = \sum_{k=1}^{k} C_k\, I(x \in Rk)$$

It is necessary to resolve the following optimization issues in order to determine the values of j and s

$$\min j, s \left[\min c1 \sum xj \epsilon R1\,(j, s)(yi - c1)2 + \min c1 \sum xj \epsilon R2\,(j, s)\,(yi - c2)2 \right]$$

$$C1 = \text{ave}((yi|xi \in Ri(j, s),), C2 = \text{ave}((yi|xi \in R2(j, s))$$

The procedure entails going through all of the input variables to get the output values and choosing the best split variable j. The input space is divided into two separate areas (j, s) by each variable acting as a dividing line. The procedure is continued after segmenting each region up until a stop condition is satisfied.

B. (XGB) XGBoost Model

Boosting Trees is a potent technique for decision tree boosting. Particularly popular and powerful is an XGBoost-based Boosting Tree model. An ensemble of decision tree models is what Boosting Trees are. The first step is to create an initial base tree, indicated as y0, with initial predictions for each sample i, denoted as fo(xi) = 0. This acts as the starting point. The explanatory model is updated at each boosting step (step t). By iteratively include fresh trees in the ensemble, it is intended to enhance the predictions. Each new tree aims to capture the patterns and mistakes that the preceding trees did not sufficiently address.

$$\widehat{yi} = \sum t\, k = 1\, fk(xi) = \widehat{yt} - 1\, i + ft(xi)$$

The objective function must be minimized when solving decision trees. The criterion used to assess the effectiveness of the splits and the decision tree's overall performance is represented by the objective function.

$$\text{Objt} = \sum[i = 1 \text{ to } n] l(yi, \widehat{yt_i}) + \sum[i = 1 \text{ to } t]\Omega(fi) + \text{Constant}$$

A differentiable convex loss function is often used to calculate the value of the variable l, which stands for the difference between the prediction and the target. The difference between the anticipated values and the actual target values is captured by this loss function.

A decision tree's complexity can be described as follows:

$$\Omega = \sum[i = 1 \text{ to } T]\Omega(wi)$$

The decision tree's overall leaf count is shown here by the letter T. Every leaf node is identified as wi, where i is a number between 1 and T. The complexity connected to each unique leaf node is described by the word (wi).

The minimal objective function:

$$\text{Obj} = -1/2 \sum_{j=1}^{T} G2\, j\, Hi + \lambda + \gamma T$$

A decision tree splits the data into two distinct subsets for each of its branches. By contrasting the target function before and after the split, it is possible to quantify the information received by the split.

www.nmiet.edu.in

$$\text{Gain} = \frac{G^2L}{H_l + \lambda} + \frac{G^2R}{H_R + \lambda} - \frac{(GL + GR)^2}{H_L + + H_R + \lambda} - \gamma$$

We may evaluate the change in information or uncertainty by comparing the values of the target function before and after the split. This adjustment offers a gauge for the knowledge acquired or uncertainty lowered as a result of the divide.

C. (RF) Random Forest:

A variable's value can be predicted or classified using the Random Forest (RF) using the outcomes of several Decision Tree (DT) algorithms. A vector of entry (x) containing the values of various characteristics assessed for each instance of formation is used to construct a number of RF regression trees. Results are analyzed and quantified. The RF regression predictor can be stated as follows after creating K trees, indicated as T(x) K_1.

$$\int_{rf}^{K} f(x) = 1/K \sum_{k=1}^{K} T(x)$$

Here, RF(x) denotes the anticipated value for the input vector x based on the RF regression model. As indicated by the notation T(x), each distinct regression tree offers a forecast for the input vector x. The final forecast of the RF model is created by averaging (adding up and dividing by K) the predictions from each of the K trees. The accuracy and robustness of the predictions are increased by RF by merging the predictions from various trees, which takes advantage of the ensemble's variety and collective knowledge. The act of averaging helps to reduce the biases and inaccuracies of the individual trees, producing predictions that are more trustworthy and accurate. The bagging process generates several training data subsets to minimize the correlation between trees. In bagging, independent random vectors with the same distribution as the input sample are created by resampling random samples from the original dataset to produce various subsets, denoted as h(X, θk), k = 1,..., K. Some data points may be utilized more than once in training as a result of this resampling procedure, while others may not be used at all.

D. Ensemble Method

To build a more potent and reliable model, ensemble approaches combine various distinct models. The approaches DT, RF, and XGBoost all fall under the umbrella of ensemble methods. Here is a quick description of each method:

Algorithm 1: Ensemble Method

Input: *Network Traffic Datasets*

Output: *Classified Data with having No. of features*

Begin

Initialization

Load Network traffic

Data Divide the network traffic datasets

Training Dataset = 80% *of network traffic data*

Test dataset = 20% *of network traffic data*

Training dataset

Train the dataset by using the Bayes theorem

Extract the features from the train data

Measure the probabilities by the Likelihood method

The group predicted by a higher probability

$[ID\ Value] = max(probabilities\ of\ each\ class)$

End

These approaches are examples of ensemble methods, which make use of the variety and combination of multiple models to increase prediction accuracy overall, decrease overfitting, and deliver more trustworthy findings.

5. Results and Discussion

Performance Indices:

The accuracy (ACC) is calculated as the percentage of correctly classified instances, whether they are normal or attacks, and is determined by the following formula:

$$ACC = \frac{(TP + TN)}{(TP + TN + FP + FN)}$$

The formula for calculating precision (P), which is the proportion of pertinent instances among the identified instances:

$$P = \frac{TP}{(TP + FP)}$$

Recall (R) is calculated as the ratio of the number of relevant instances over the total number of relevant instances discovered:

$$R = \frac{TP}{(TP + FN)}$$

The F1-Score is a metric that combines recall and precision into one number. It can be calculated using the formula below as the weighted average of recall and precision:

$$\text{F1Score} = \frac{(2 * P * R)}{(P + R)}$$

In particular, when α = 1, the formula for the F1-Score simplifies. Overall, these formulas allow us to calculate

www.nmiet.edu.in

accuracy, precision, recall, and the F1-Score, which are commonly used metrics for evaluating classification performance.

Table 3: Performance Evaluation of Proposed method using CIC-IDS2017 2017 Dataset

Algorithm	Accuracy in (%)	Recall in (%)	Precision in (%)	F1 Score in (%)
DT	98.05	97.04	98.03	98.04
RF	97.81	97.79	98.81	98.78
XGBoost	96.07	96.06	96.16	95.97
Ensemble	98.05	98.05	98.04	98.04

Several performance criteria, including accuracy, recall, precision, and F1 score, were evaluated in the comparison of various machine learning techniques, including DT (Decision Tree), RF (Random Forest), XGBoost, and an ensemble method as shown in table 3.

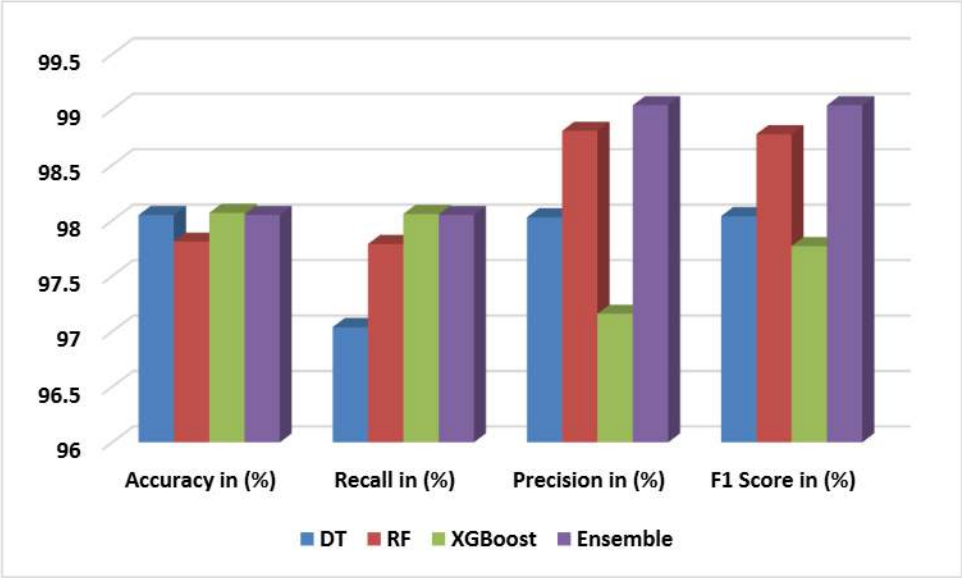

Fig 4: Graphical representation of Performance Evaluation metrics

98.05% accuracy means that 98.05% of the occurrences were properly categorised by the Decision Tree method. The precision rate, which shows the proportion of pertinent instances among the detected instances, was 98.03%, while the recall rate, which measures the percentage of pertinent examples properly identified, was 97.04%. The precision and recall combined measure, or F1 score, attained 98.04%, showing a balanced performance in both areas.

A high level of accuracy was also shown by the Random Forest method, which had a recall rate of 97.79% and a precision of 97.81%. The precision rate was 98.81%, indicating that a significant portion of the discovered instances were meaningful. The F1 score of 98.78% demonstrated a perfect harmony between recall and precision.

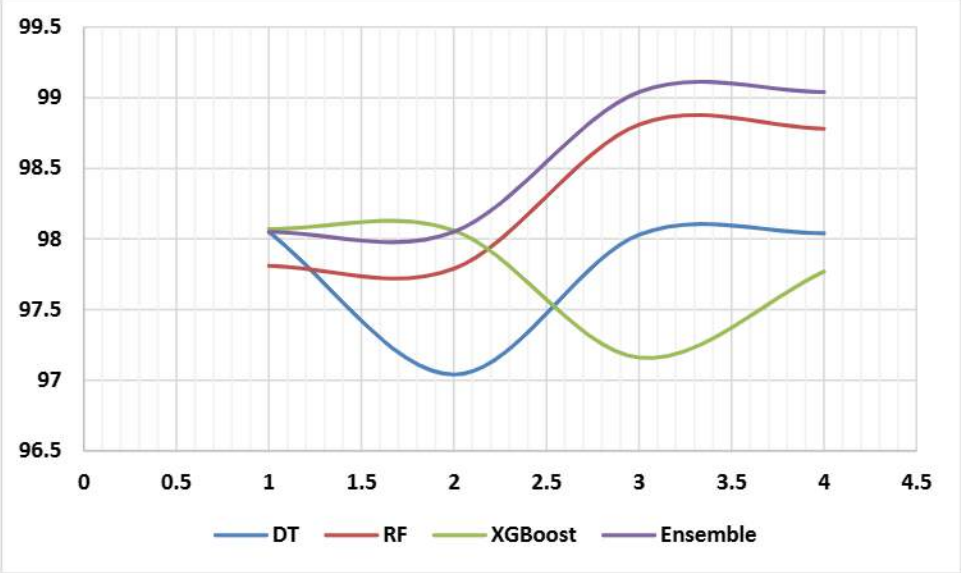

Fig 5: Comparison of Different method with Ensemble method

In comparison to the other algorithms, the XGBoost method displayed a significantly lower accuracy of 96.07%. Both the recall and precision rates were 96.06%. The precision and recall weighted average, also known as the F1 score, was 95.97%. In terms of accuracy, recall, precision, and F1 score of 98.5%, the combined method performed on par with the decision tree method. When several algorithms are employed, the prediction accuracy improves. The evaluation findings demonstrated that the combined Decision Tree, Random Forest, and algorithms consistently achieved high F1 precision, recall, and precision scores. The XGBoost algorithm fared remarkably well by these measures despite being very efficient. This finding demonstrates how these autonomous learning systems are capable of identifying important events and making accurate forecasts.

6. Conclusion

The outcomes demonstrated that DT and RF both had incredibly high precision, with DT having a precision of 98,05% and RF having a precision of 97,81%. With DT and RF of 97,4% and 97,79%, respectively, these algorithms showed startlingly high recall rates. The two algorithms had remarkable precision rates, with accuracy rates of 98,03% and 98,81%, respectively. With scores of 98,04% and 98,78%, respectively, DT and RF received very high F1 ratings. A variety of machine learning algorithms, including Decision Tree (DT), Random Forest (RF), XGBoost, and other methods, have demonstrated to be quite successful in handling classification jobs. These algorithms were assessed using a number of performance criteria, including F1 score, recall, accuracy, and precision. The ensemble technique, which performed as well as DT, proved that integrating numerous algorithms can increase prediction accuracy. Overall, these results show how precisely the ensemble, DT, RF, and XGBoost approaches classify situations. Each approach may be a good option, depending on the specific criteria and conditions of the classification challenge. Academics and professionals can utilise these insights to select the appropriate algorithm based on the characteristics of the dataset and the required performance criteria.

References:

[1] M. Shafiq, Z. Tian, A.K. Bashir, A. Jolfaei, X. Yu," Data mining and machine learning methods for sustainable smart cities traffic classification: a survey", Sustain Cities Soc, 60 (2020), Article 102177

[2] Z. Lv, B. Hu, H. Lv, "Infrastructure monitoring and operation for smart cities based on IoT system", IEEE Trans Ind Inf, 16 (3) (2020), pp. 1957-1962, 10.1109/TII.2019.2913535

[3] N. Hussain, P. Rani, H. Chouhan, U.. Gaur, "Cyber security and privacy of connected and automated vehicles (CAVs)-based federated learning: challenges, opportunities, and open issues", Federated learning for IoT applications, Springer (2022), pp. 169-183

[4] P. Rani, N. Hussain, R.A.H. Khan, Y. Sharma, P.K. Shukla, "Vehicular intelligence system: time-based vehicle next location predicion in software-defined internet of vehicles (SDN-IOV) for the smart cities", Intelligence of things: AI-IoT based critical-applications and innovations, Springer International Publishing, Cham (2021), pp. 35-54.

[5] O.A. Wahab, A. Mourad, H. Otrok, J. Bentahar, "CEAP: SVM-based intelligent detection model for clustered vehicular adhoc networks", Expert Syst

www.nmiet.edu.in

Appl, 50 (2016), pp. 40-54, 10.1016/j.eswa.2015.12.006

[6] J. Yang, Z. Fei, "Broadcasting with prediction and selective forwarding in vehicular networks", Int J Distrib Sens Netw, 9 (12) (2013), Article 309041.

[7] H.M. Song, J. Woo, H.K. Kim, "In-vehicle network intrusion detection using deep convolutional neural network", Veh. Commun., 21 (2020), Article 100198

[8] M.V. Mahoney, "A machine learning approach to detecting attacks by identifying anomalies in network traffic", Florida Institute of Technology (2003)

[9] H. Ye, L. Liang, G. Ye Li, J. Kim, L. Lu, M. Wu, "Machine learning for vehicular networks: recent advances and application examples", IEEE Veh Technol Mag, 13 (2) (2018), pp. 94-101.

[10] J. Erman, A. Mahanti, M. Arlitt, "QRP05-4: internet traffic identification using machine learning", Proceedings of the *IEEE globecom 2006*, San Francisco, CA, USA (2006), pp. 1-6, 10.1109/GLOCOM.2006.443

[11] J. Liang, J. Chen, Y. Zhu, R. Yu, "A novel Intrusion Detection System for Vehicular Ad Hoc Networks (VANETs) based on diffrences of traffic flow and position", Appl Soft Comput, 75 (2019), pp. 712-727, 10.1016/j.asoc.2018.12.001

[12] P. Khobragade, P. Ghutke, V. P. Kalbande and N. Purohit, "Advancement in Internet of Things (IoT) Based Solar Collector for Thermal Storage System Devices: A Review", 2022 2nd International Conference on Power Electronics & IoT Applications in Renewable Energy and its Control (PARC), pp. 1-5, 2022.

[13] Mohammed B, et al. Edge computing intelligence using robust feature selection for network traffic classification in intenet-of-things. IEEE Access 2020;8: 224059–70.

[14] Gad AR, Nashat AA, Barkat TM. Intrusion detection system using machine learning for vehicular Ad hoc networks based on ToN-IoT dataset. IEEE Access 2021; 9:142206–17.

[15] Yang L, Moubayed A, Hamieh I, Shami A. Tree-based intelligent intrusion detection system in internet of vehicles. In: Proceedings of the ieee global communications conference (GLOBECOM); Dec. 2019. p. 1–6.

[16] Gao Y, Wu H, Song B, Jin Y, Luo X, Zeng X. A distributed network intrusion detection system for distributed denial of service attacks in vehicular Ad Hoc network. IEEE Access 2019;7:154560–71.

[17] Peng R, Li W, Yang T, Huafeng K. An internet of vehicles intrusion detection system based on a convolutional neural network. In: Proceedings of the IEEE intl conf on parallel & distributed processing with applications, big data & cloud computing, sustainable computing & communications, social computing & networking (ISPA/BDCloud/SocialCom/SustainCom); 2019. p. 1595–9.

[18] W. Wu et al., "A survey of intrusion detection for in-vehicle networks", IEEE Trans. Intell. Transp. Syst., vol. 21, no. 3, pp. 919-933, Mar. 2020.

[19] J. Liu, S. Zhang, W. Sun and Y. Shi, "In-vehicle network attacks and countermeasures: Challenges and future directions", IEEE Netw., vol. 31, no. 5, pp. 50-58, Sep. 2017

[20] D. Kosmanos et al., "A novel intrusion detection system against spoofing attacks in connected electric vehicles", Array, vol. 5, Mar. 2020.

[21] Y. Sun et al., "Attacks and countermeasures in the Internet of vehicles", Ann. Telecommun., vol. 72, no. 5, pp. 283-295, 2017.

[22] E. Seo, H. M. Song and H. K. Kim, "GIDS: GAN based intrusion detection system for in-vehicle network", Proc. 16th Annu. Conf. Privacy Secur. Trust (PST), pp. 1-6, Aug. 2018.

[23] M.-J. Kang and J.-W. Kang, "Intrusion detection system using deep neural network for in-vehicle network security", PLoS ONE, vol. 11, no. 6, Jun. 2016

[24] H. Lee, S. H. Jeong and H. K. Kim, "OTIDS: A novel intrusion detection system for in-vehicle network by using remote frame", Proc. 15th Annu. Conf. Privacy Secure Trust (PST), pp. 57-5709, Aug. 2017.

[25] T. Marsden, N. Moustafa, E. Sitnikova and G. Creech, "Probability risk identification based intrusion detection system for SCADA systems", Proc. Int. Conf. Mobile Netw. Manage., pp. 353-363, 2017.

[26] Yoon, H. . (2023). A Quantitative Evaluation for Usability under Software Quality Models. International Journal on Recent and Innovation Trends in Computing and Communication, 11(3), 24–29. https://doi.org/10.17762/ijritcc.v11i3.6194

[27] Deshpande, V. (2021). Layered Intrusion Detection System Model for The Attack Detection with The

Multi-Class Ensemble Classifier . Machine Learning Applications in Engineering Education and Management, 1(2), 01–06. Retrieved from http://yashikajournals.com/index.php/mlaeem/article/view/10

[28] Kumbhkar, M., Shukla, P., Singh, Y., Sangia, R. A., & Dhabliya, D. (2023). Dimensional reduction method based on big data techniques for large scale data. Paper presented at the 2023 IEEE International Conference on Integrated Circuits and Communication Systems, ICICACS 2023, doi:10.1109/ICICACS57338.2023.10100261 Retrieved from www.scopus.com

ResearchGate

See discussions, stats, and author profiles for this publication at: https://www.researchgate.net/publication/379229372

Effects of low-power laser hardening on the mechanical and metallurgical properties of biocompatible SAE 420 steel

Article *in* Journal of Materials Research and Technology · March 2024

DOI: 10.1016/j.jmrt.2024.03.153

CITATIONS
2

READS
48

8 authors, including:

Kuldeep K Saxena
Lovely Professional University
323 PUBLICATIONS **6,057** CITATIONS
SEE PROFILE

Din Bandhu
Manipal Academy of Higher Education
103 PUBLICATIONS **1,129** CITATIONS
SEE PROFILE

Sunil Bdy
Institute of Aeronautical Engineering
14 PUBLICATIONS **50** CITATIONS
SEE PROFILE

All content following this page was uploaded by Din Bandhu on 03 April 2024.

The user has requested enhancement of the downloaded file.

www.nmiet.edu.in

Journal of Materials Research and Technology 30 (2024) 1611–1619

Contents lists available at ScienceDirect

Journal of Materials Research and Technology

journal homepage: www.elsevier.com/locate/jmrt

Effects of low-power laser hardening on the mechanical and metallurgical properties of biocompatible SAE 420 steel

Santoshkumar V. Wagh [a], Satish R. More [b], V. V. Venu Madhav [c], Kuldeep K. Saxena [d], Din Bandhu [e,*], B.D.Y. Sunil [f], Revathi V [g], Md Irfanul Haque Siddiqui [h]

[a] Department of ME, College of Engineering Pune, Pune, Maharashtra, 411005, India
[b] Department of ME, Nutan Maharashtra Institute of Engineering and Technology, Talegoan, Maharashtra, 410507, India
[c] Department of ME, V R Siddhartha Engineering College, Vijayawada, Andhra Pradesh, 520007, India
[d] Division of Research and Development, Lovely Professional University, Phagwara, India
[e] Department of Mechanical and Industrial Engineering, Manipal Institute of Technology Bengaluru, Manipal Academy of Higher Education, Manipal, Karnataka 576104, India
[f] Department of Mechanical Engineering, Institute of Aeronautical Engineering, Hyderabad, India
[g] Department of Applied Sciences, New Horizon College of Engineering, Bangalore, India
[h] Mechanical Engineering Department, College of Engineering, King Saud University, Riyadh, 11451, Saudi Arabia

ARTICLE INFO

Handling editor: L Murr

Keywords:
Micro-hardness
Wear
Laser hardening
High carbon steel
Design of experiment

ABSTRACT

The present experimental work is carried out on SAE 420 steel to optimize process parameters of low-power laser hardening to improve surface micro-hardness and wear resistance for dry sliding for bio-medical applications. Laser power is the most significant factor for micro-hardening and wear resistance. Rank two for scanning speed and three for standoff distance, respectively. The experiments show that the surface micro-hardness of treated samples varies from 711 to 833 Vickers Pyramid Number by optimized process parameters such as laser beam power of 300 W, laser scan speed of 1.0 mm/s, and standoff distance of 225 mm. In comparison, the base material micro-hardness is 208 Vickers Pyramid Number as the predictive equation generated for finding micro-hardness value for the above three laser hardening process parameters. The dry sliding wear test is conducted on all laser-treated samples and a comparison is made with the untreated sample. A significant improvement in wear resistance was observed for treated as compared to untreated samples. The wear of laser hardened sample of SAE 420 steel was 3.67 x10-9 g/cm compared to untreated base metal wear rate of 139.00 x 10-9 g/cm at an applied load of 30 N and sliding speed of 300 revolutions per minute. The scanning electron microscopy analysis of wear samples (untreated, treated maximum, and minimum hardness) is observed for investigating material removal patterns.

1. Introduction

Titanium (Ti), Stainless steel (SS), and cobalt-chromium-molybdenum (Co Cr Mo) alloys are costlier materials that are used for various biomedical applications because of their good mechanical and biocompatible properties. Steels usually are heat-treated to enhance their metallurgical and mechanical properties. Steel is mostly used in various engineering applications as well as bio-medical applications such as the replacement of bones, joints with artificial bones and joints, dental implants, aerospace, petrochemical, mining, power stations food processes, etc. SAE 420 steel is a good substitute for Ti, Co, Cr, Mo, and other costlier biocompatible materials. Because SAE 420 has better mechanical and metallurgical properties as compared to other steel. SAE 420 steel is low carbon unalloyed steel and it can be heat-treated to achieve good resistance to wear and higher micro-hardness by using induction and flame hardening. One of the greatest techniques for enhancing the surface qualities of SAE 420 steel material is laser hardening. The mechanical and metallurgical characteristics of compounds significantly improve after the laser hardening procedure. This material is used to manufacture bio-medical components and instruments as well as mechanical components like axles, shafts, gears, bolts, stud bolts, etc. [1–3].

Many researchers used low-carbon AISI 316L SS, SS 304, and other grade steel for biomedical applications by applying some surface

* Corresponding author.
E-mail address: din.bandhu@manipal.edu (D. Bandhu).

https://doi.org/10.1016/j.jmrt.2024.03.153
Received 1 February 2024; Received in revised form 22 March 2024; Accepted 22 March 2024
Available online 23 March 2024
2238-7854/© 2024 The Authors. Published by Elsevier B.V. This is an open access article under the CC BY-NC-ND license (http://creativecommons.org/licenses/by-nc-nd/4.0/).

www.rmiet.edu.in

treatment methods and coating methods [4].

Puraditya et al. [5] applied bio-ceramic coatings like HA, HA + TiO2, and HA + ZrO2 to improve corrosion resistance in Stainless Steel 316L and Titanium (Ti–6Al–4V). By incorporating TiO2 and ZrO2 into both SS316L and Ti6Al4V materials, the corrosion rate was significantly decreased compared to using just HA. The findings of this investigation demonstrate that the application of HA, HA + ZrO2, and HA + TiO2 biomaterials leads to different levels of thickness and roughness while using identical spraying conditions. Bioceramic coatings on implants provide an alternative coating that enhances the performance of biomaterials. Ayatilhaq et al. [6] conducted an assessment of the impact of Manganese on the hardness and corrosion rate of biodegradable implants made from a Zinc–Manganese alloy. It examined the corrosion rate in Zn alloys with different Mn concentrations. Hardness testing showed the influence of Mn addition. The lowest corrosion rate was Zn–25Mn. The alloy formed the intermetallic phase MnZn13 with Mn additions, improving mechanical characteristics and corrosion rate. Through in vivo and in vitro assessment, the findings revealed the potential biocompatibility of a biodegradable implant, enabling more evolution. Muratal et al. [7] used powder metallurgical methods to develop biocompatible material SS 316L. they used 316L powders that were sintered at two different temperatures (950 and 1050°C) for 30 min under 50 MPa pressure. They got good results for mechanical properties, hardness, and dry sliding wear. Sabara et al. [8] conducted a comparative study i.e. crystalline phases, microstructure, and micro-hardness, corrosion resistance for different austenitic stainless steel (ASTM F138, ASTM F1586, and ASTM F2581). From the results they found component and elemental contain plays an important role for results. Sadaqat Ali et al. [9] developed a modified SS316L using the addition of boron, titanium, and niobium with varying concentrations in the SS matrix and investigated the change in physical and mechanical properties of modified steel. They found good results in changes in mechanical and physical properties like hardness, tensile strength, compressive strength, etc. Jia Lou et al. [10] evaluated the biocompatibility of SS316L coated with Ti-DLC, TiN, and TiCN Films and three metals (Cu, Ti, and AISI 316 L) were compared for surface morphology, water contact angle measurements, CCK-8 experiment results, and flow cytometry test findings. They found TiN and TiCN has good results in all comparisons for biocompatibility.

Many researchers used laser hardening techniques to improve the surface properties of SAE 420 steel components. Researchers utilized CO_2 laser systems for laser hardening. Due to its low distortion, laser hardening is a common technique. It is possible to precisely harden locally constrained functional areas, small series, and individual pieces without the need for quenching media. The workpiece naturally cools down. A high surface hardness is attained with the tough material core because the surface temperature of the hardening zone is consistently constant. The researchers used various types of steel materials (SAE 420, En18, En24, En25, En31, American Iron and Steel Institute 4340, etc.) and investigated the effects of laser hardening process parameters on surface hardening microstructure through experimentation [11–18]. Laser power and scanning speed are the two significant parameters considered by researchers for experimentations. Most researchers used a laser power range of 400 W–2500 W and laser scanning speed from 2 mm/s to 2000 mm/s for experimentation on steel materials [11–22]. After laser hardening, the sample's micro-hardness increased up to 2 to 2.5 times compared to base materials [14–20]. Some researchers investigated the effects of laser process parameters on hardness depth and width for steel materials [16–20]. After improving the micro-hardness of steel samples, researchers investigating the wear resistance improvement of laser-treated samples over untreated samples found improved wear resistance for treated samples [13,19,21–25].

A few researchers work on laser power of less than 400 W for laser hardening on steel samples. There is ample room here to work on a low-power laser system for hardening SAE 420 steel samples and checking biocompatibility (biomedical). The present study is based on low-power laser hardening (i.e. 200 W–300 W) and a scanning speed of 1–10 mm/s. The experimentation is based on laser hardening process parameters on micro-hardness, microstructure, and wear resistance. Taguchi's method is applied to the experiments. Scanning electron microscopy analysis is carried out to analyze wear samples (laser-treated and untreated). The results and contributions of the significant laser hardening process parameters were investigated using Taguchi's analysis. A simple regression model is found to predict hardness and wear rate with an acceptable accuracy level.

2. Experimental work

2.1. Material

Nowadays, SAE 420 is used in various engineering applications and medical industries. High-carbon stainless steel with a minimum 12% chromium content is grade 420. Heat treatment is another method that can be used to harden grade 420 stainless steel, just like any other. When polished, surface grounded, or hardened, the metal exhibits outstanding corrosion-resistant qualities in addition to its superb ductility. With 12% chromium, this grade of stainless steel has the highest hardness (50 HRC). The important applications of grade 420 stainless steel are Shear blades, Needle valves, Surgical equipment, and Cutlery. The elemental composition is displayed in Table 1 as a weight percentage. Fig. 1 is a scanning electron microscope image of the steel's primary constituent.

2.2. Experimental setup and sample preparation

Fig. 2 shows the continuous wave fiber laser system of 400 W and 1070 nm laser wavelength. The setup consists of the control panel, laser generator, argon gas cylinder, and workpiece mounting table with movement along with x-y directions. The same laser setup was used for the experimentation.

For the present investigation, SAE 420 stainless steel samples are used as test specimens. The cutting of the test specimen is carried out with a wire electrical discharge machining method. The sample size of 30 mm × 8 mm x 8 mm (length x width x thickness) is as shown in Fig. 3. The sample preparation steps for investigating the microstructure are grinding, lapping, polishing, & etching.

After the machining process, various emery papers such as 200, 400, 600, and 800, were used to grind the specimens and subsequently polished using different polish paper numbers, including 1/0, 2/0, 3/0, 4/0, and 5/0. The samples were cleaned by using acetone to remove dust, oil, and solid particles. The specimens were further lapped and polished using Shimon leather. After polishing, the sample was cleaned with running water, and acetone, and dried using a hot drier. The 4 % Nital solution (A mixture of 96 ml methanol and 4 ml nitric acid) etchant was used to etch the samples. The etchant attacks different topographies at the boundaries of parent material and heat-affected zone.

2.3. Experimental method

Numerous factors are responsible for the laser surface hardness and wear behavior. The three most crucial factors laser beam power, laser scan speed, and standoff distance that influence laser hardening wear resistance are taken into account in the current work. For the present work, the Taguchi method is used because this is one of the best experimental methodologies used to find the minimum number of experiments to be performed within the permissible limit of factors and levels. The laser hardening parameters range is finalized based on published works of literature. For Taguchi's technique of experimentation, Table 2 lists the parameters of the laser hardening process and their levels. 33 = 27 trials would be needed to study the effects of three control factors at three levels in a typical complete factorial experimental design. However, Taguchi's factorial experiment method only requires nine runs, saving time and resources. The experimental data is

www.rmiet.edu.in

Table 1
The elemental weight percentage of SAE 420 stainless steel.

Elements	Carbon	Silicon	Magnesium	Phosphorus	Sulfur	Iron
Composition weight	0.481	0.263	0.702	0.016	0.014	Balance

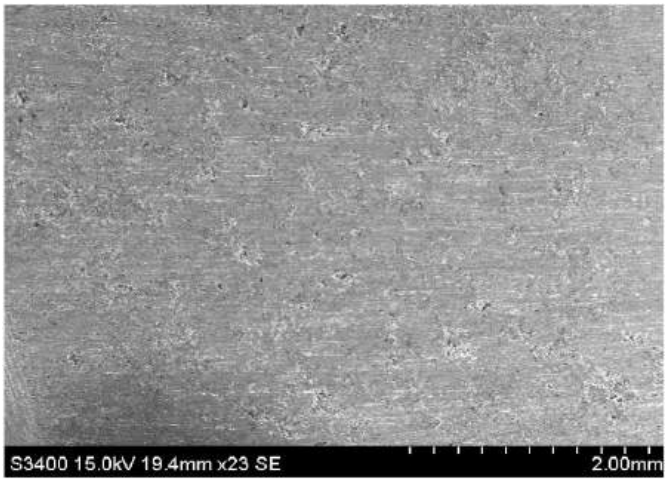

Fig. 1. Scanning electron microscopy of the base material of SAE 420 stainless steels.

used to calculate the signal-to-noise ratio. Depending on the type of characteristic, different signal-to-noise ratios are available; smaller, nominal, and greater are preferable. A logarithmic modification of the loss function can be used to estimate the maximum hardness signal-to-noise ratio, which is what determines how acceptable features are, as indicated in the equation below (1).

The larger the more acceptable features:

$$S/N = -10 * \log\left[\Sigma\left(1/Y^2\right)/n\right] \quad (1)$$

where n is the number of observations and *y* is the observed data; that is microhardness.

The important process parameters which are selected for the study with their processing conditions are shown in Table 2. The operating conditions according to the L_9 design matrix are described in Table 3.

The experimentations are performed as per the designed matrix and micro-structural and wear analysis are carried out with an optical microscope and pin-on-wear disc setup, respectively. The experimental conditions are shown in the design matrix and the microstructure of laser-treated samples are shown in Fig. 3.

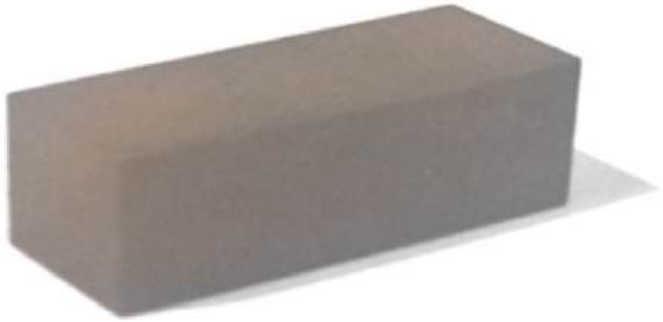

Fig. 3. Test specimen.

Table 2
Laser hardening process parameters and their ranges of SAE 420 steel.

Sr. No.	Laser hardening process parameters	Units/Symbols	Level		
			−1	0	1
1	Laser beam power	Watt (W), P	210	255	300
2	Laser scan speed	mm per sec (mm/s), v	1	5.5	10
3	Standoff distance	Millimetre (mm), f	175	200	225

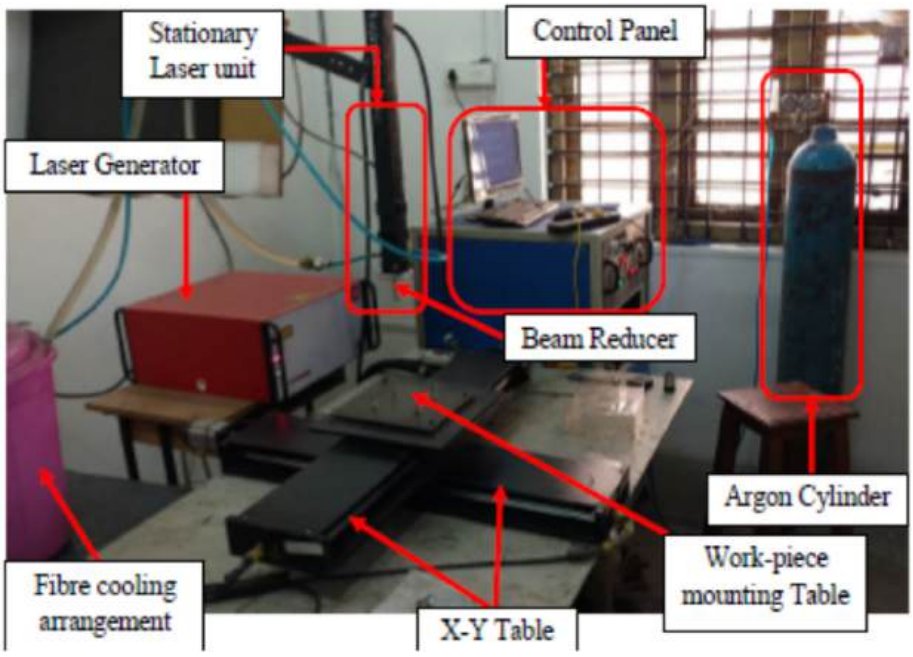

Fig. 2. Fiber laser system (400 Continuous Wave Laser Science Pvt. Ltd. Mumbai).

www.rmiet.edu.in

Table 3
Designed L_9 orthogonal array for experimentations for SAE 420 steel.

Experiment. No.	Laser beam power (P) Watt	Laser scan speed (v) mm/sec	Standoff distance (f) mm
1	210	1	175
2	210	5.5	200
3	210	10	225
4	255	1	200
5	255	5.5	225
6	255	10	175
7	300	1	225
8	300	5.5	175
9	300	10	200

3. Results and discussion

3.1. Effect of laser process parameters on micro-hardness

Fig. 4 shows how the microhardness of the sample changes concerning the depth of the sample. Due to the low power laser hardening surface of the sample having higher microhardness. With respect to change in depth from the surface of the sample microhardness starts towards the original hardness of the sample. Taguchi's methodology is used to analyze the current experiment using the MINITAB tool. Table 4 shows the L_9 orthogonal array configuration and signal-to-noise ratio. For analysis, micro-hardness is considered as the outcome.

Table 4 projects Taguchi's experimental results of the laser hardening test and their S/N ratios for SAE 420 steel. To achieve the best possible process parameters, the larger the better-quality characteristics are chosen. The response table for the signal-to-noise ratio obtained is presented in Table 5. Laser beam power is the most significant parameter for laser hardening as compared to the other two parameters for improving the micro-hardness of SAE 420 steel. The remaining two parameters are laser scanning speed and standoff distance ranked second and third in the influence of micro-hardness of SAE 420 steel. The SAE 420 steel base metal micro-hardness is observed 208.2 Vickers Pyramid Number increased to 833.7 Vickers Pyramid Number at experiment no 7, utilizing parameters such as laser beam power of 300 W, the laser scan speed of 1.0 mm/s, and standoff distance of 225 mm. The hardened zone micro-hardness depth of 3614.83 μm is achieved for the laser-treated specimen. This happens because a lower scanning speed of 1 mm/s and laser power of 300 W is sufficient for the proper development of microstructure. Fig. 5 depicts the specimen's micrographs (SAE 420 steel) processed as per the L_9 design matrix. The micrographs show the detail of the geometrical dimensions of the hardened area or laser track. From the micrographs, it is clear that the geometry, i.e., track width and depth, depends on laser hardening process parameters. The laser power and scanning speed increase the geometry of the laser track change significantly. Further, the micro-graphs are the authentication for change in experimental process parameters worked properly and micro-hardness value results are justified clearly. The micro-hardness is increased 3 times for the treated surface as compared to the untreated surface. This increase in hardness has good uses and requirements of material for various biomedical applications.

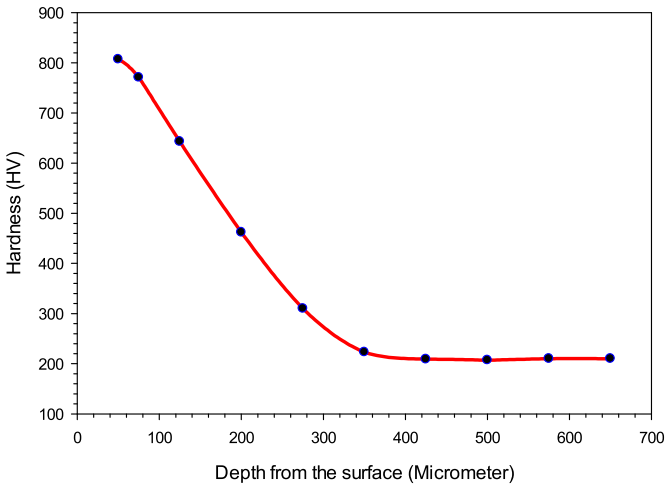

Fig. 4. Depth of hardened zone.

Table 4
Taguchi's experimental results of laser hardening test and their signal-to-noise ratios for SAE 420 steel.

Experiment. No.	Laser beam power (P), Watt	Laser scan speed (v), mm/s	Standoff distance (f), mm	Micro-hardness	Signal-to-Noise Ratio
1	210	1	175	769.7	56.5487
2	210	5.5	200	733.7	56.0855
3	210	10	225	711.9	55.6824
4	255	1	200	775.6	57.1249
5	255	5.5	225	746.3	56.7100
6	255	10	175	716.8	56.1669
7	300	1	225	833.7	58.4202
8	300	5.5	175	774.0	58.0062
9	300	10	200	732.7	57.2985

Table 5
Average factor effects for the signal-to-noise ratio as per the larger the more acceptable features.

Levels	Laser beam power	Laser scan speed	Standoff distance
I	56.11	57.36	56.91
II	56.67	56.93	56.84
III	57.91	56.38	56.94
Delta	1.08	0.98	0.10
Rank	1	2	3

The main effect plot for the signal-to-noise ratio is represented graphically in Fig. 6. SAE 420 steel laser hardening is found to be superior at 300-W laser beam power, followed by 255 W and 210 W, and maximum hardness is achieved at 1.0 mm/s laser scan speed, relative to 5.5 and 10 mm/s, compared to 175 mm and 200 mm standoff distances, 225 mm standoff distance features the highest hardness. Experiment no. 7 has a higher micro-hardness value; for the same micro-graph, higher track width and depth are observed. This happens because of the maximum microstructural changes in experiment 7. Similarly, for experiment number three, having a lesser micro-hardness value than other experiments, the micro-graph results show less laser track width and depth.

3.2. Micro-hardness value prediction using predictive equation

The microhardness of laser-treated samples was predicted using a nonlinear predictive equation as a function of laser treatment factors. This regression study is carried out with the help of the Minitab 14 software tool. The following form of the regression equation (2) is obtained for SAE 420 steel.

$$\text{Micro} - \text{hardness} = 311 + 1.64\ (\text{laser power}) - 8.8\ (\text{scanning speed}) + 0.110\ (\text{standoff distance}) \quad (2)$$

where laser beam power is in watts, the scanning speed of the laser beam over the sample surface is in mm/sec, standoff distance is in mm.

The coefficient of regression i.e. (correlation coefficient)^2 is found to be 94.7%. The comparison between the micro-hardness obtained from experimental results and the predictive equation for SAE 420 steel is shown in Table 6.

www.nmiet.edu.in

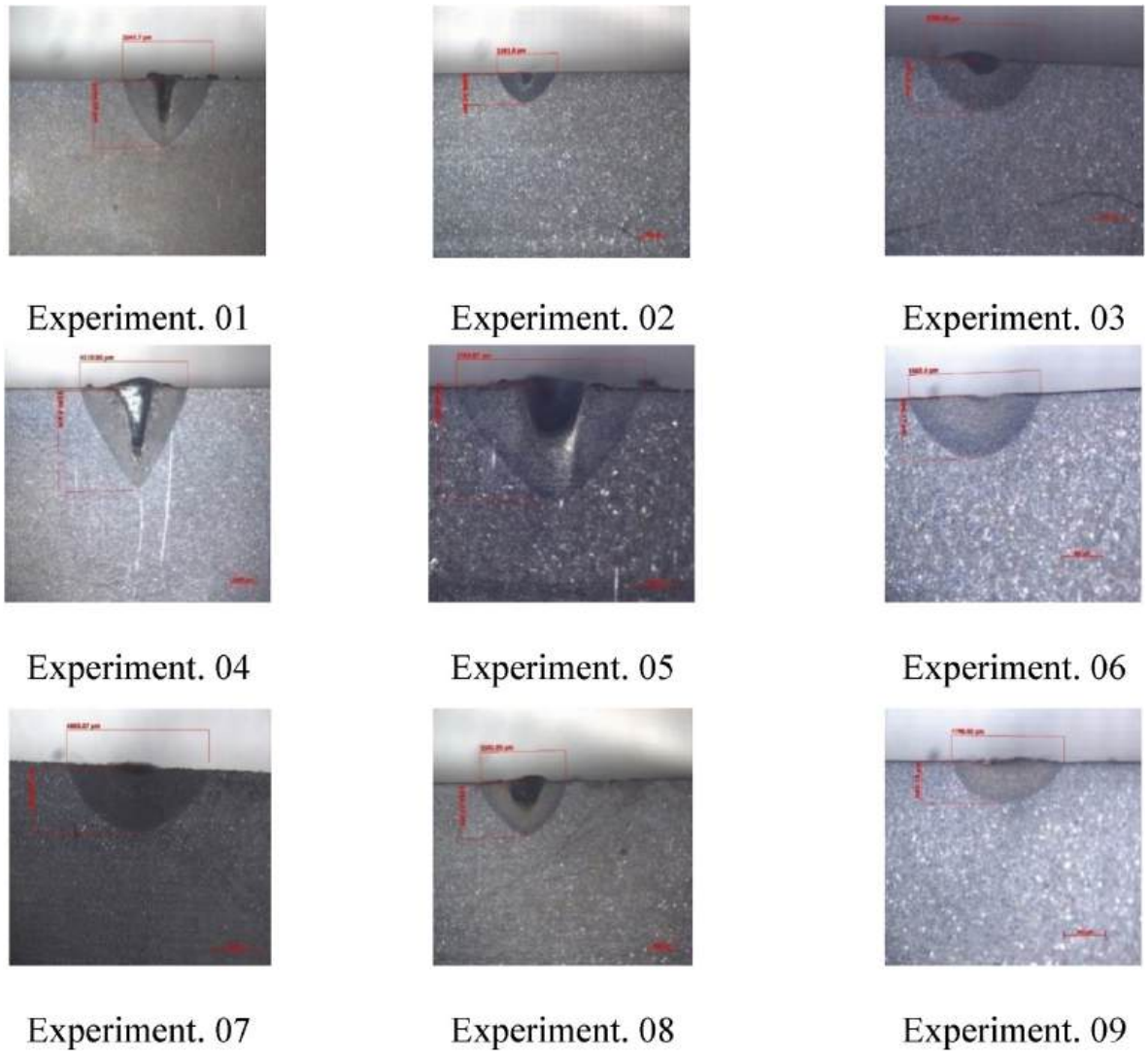

Fig. 5. Microstructure of specimen (SAE 420 steel) processed as per L_9 design matrix.

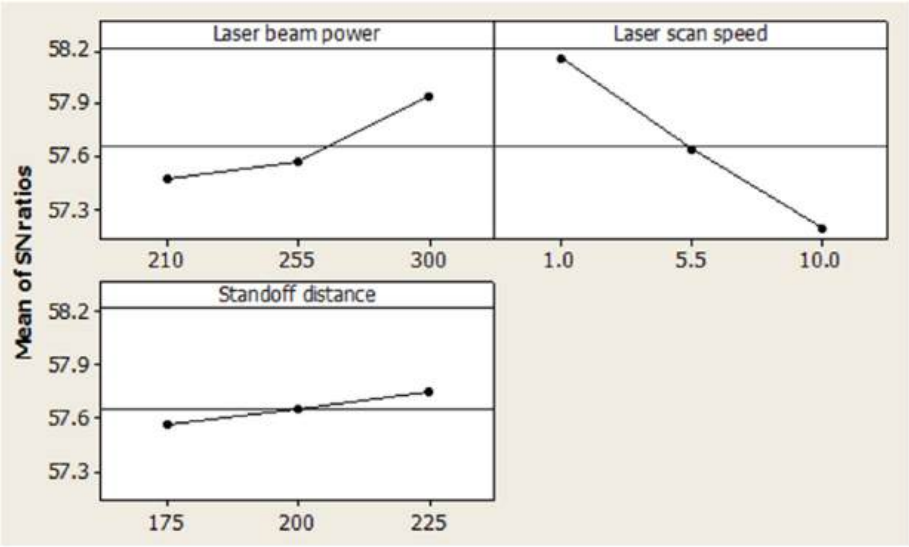

Fig. 6. Effects of signal-to-noise ratios for SAE 420 steel.

www.nmiet.edu.in

3.3. Confirmation test for SAE 420 steel

The confirmation test is carried out while taking into account the ideal test parameters that Taguchi's method yielded. Table 7 displays the micro-hardness of laser-treated SAE 420 steel samples using both experimental confirmation and nonlinear regression equation results. A deviation of roughly 2.27% is determined by comparing the experimental and analytical data, which is acceptable. As a result, it is demonstrated that the generated nonlinear regression equation approximately represents the micro-hardness of samples of these materials that have undergone laser treatment.

3.4. Wear analysis

Both before and after laser treatments and wear assessments are carried out on laser-treated SAE 420 steel. The pin-on-disc machine is used to perform the wear test on specimens following the American Society for Testing and Materials G99. The wear test specimen is 30 mm × 8 mm x 8 mm (length x width x thickness) and it is prepared according to standard wear test procedures. The wear rate is determined using Ana Matrix Instrument Technologic Pvt. Ltd., Sr. No: HZK FA210: maximum capacity of 220 g analytical balance with 0.1 mg readability. To determine a wear rate, the formula given below can be used. (3)

$$\text{wear rate} = \text{Weight loss} / \text{Sliding distance}$$
$$\text{OR Wear Rate} = (\text{Wi} - \text{Wf}) / (\text{Sd}) \quad (3)$$

where,

Wear rate in (gram/cm); Weight loss in gram; Sliding distance in cm.

Weight loss = weight of the experimental specimen (g) prior (Wi) - after the experimentation (Wf)

Wi = Initial Weight; Wf = Final or after the experimentation weight; Sd = Sliding distance.

The wear test was performed at 30 N loads, 300 revolutions per minute sliding speed, 100 mm track distance, and 32 min test duration under dry sliding conditions. Fig. 7 shows the repeatability of test rigs i. e. laser hardening system and pin on disc wear test rig. The test was carried out at room temperature and standard atmospheric conditions. Table 8 presents the wear rates of laser-hardened and untreated specimens at 300 revolutions per minute with a constant load of 30 N loads.

The wear test was carried out on the untreated and laser-hardened specimens of SAE 420 steel at an applied load of 30 N and sliding speed of 300 revolutions per minute and Fig. 8 shows the wear test results. Fig. 8 shows that the untreated specimen's wear rate was approximately ten times greater than laser laser-hardened specimens. It is observed that wear resistance increases after the laser hardening process. 139.00 × 10^{-9} g/cm wear rate of an untreated specimen was observed. For the laser-treated sample, the minimum wear rate observed is 3.67 × 10^{-9} g/cm for laser hardening experiment number 7. This is due to higher micro-hardness. The maximum wear rate is observed up to 22.30 × 10^{-9} g/cm for SAE 420 steel. The wear test results show that hardened laser samples are more wear-resistant than untreated samples. The wear rate of laser-treated samples significantly depends on the operating parameters of laser hardening process parameters.

The optimal results for micro-hardness and minimum wear rate are observed at 300-W laser energy; 1 mm/s scanning speed; 225 mm standoff distance for the laser hardening process. This is because 300 W is the maximum power gives significant development in microstructure as compared to other laser power in the selected range. 1 mm/s scanning speed having maximum contact time between laser power beam and sample surface, therefore complete change in microstructure was developed on the surface of the selected sample. A Standoff distance of 225 mm provides good contact with the laser beam, especially without disturbing beam diameter, the results observed a maximum concentration of laser beam power on the sample surface. Because of all the above

Table 6
The difference between experimental and predicted hardness values.

Experiment. No.	Micro-hardness by experiments	Micro-hardness by predictive equation	The percentage error in micro-hardness
1	769.70	665.77	15.61
2	733.70	628.56	16.72
3	711.90	591.35	20.38
4	775.60	742.32	4.48
5	746.30	705.11	5.84
6	716.80	659.65	8.66
7	833.70	818.87	1.81
8	774.00	773.41	0.07
9	732.70	736.20	0.47

Table 7
Confirmation of experimental results for micro-hardness.

Laser beam power, Watt	The laser scan speed, mm/sec	Standoff distance, mm	Micro-hardness by experiment test	Micro-hardness by equation	% error
300	1	225	837.50	818.87	2.27

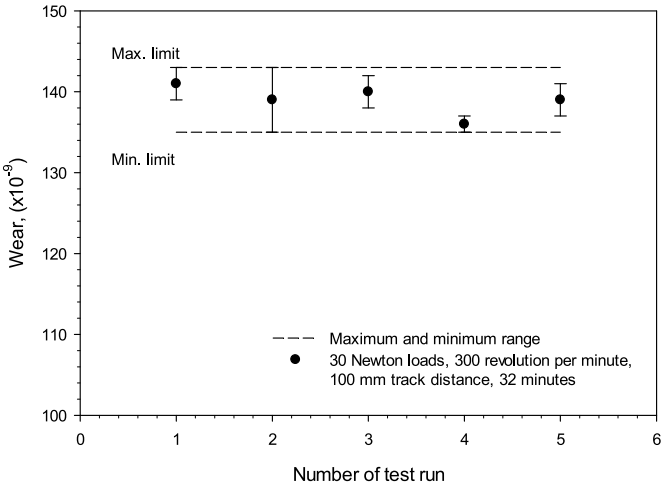

Fig. 7. Repeatability of laser hardening system and pin on disc wear test for the untreated sample.

Table 8
Results of wear experiments using the L9 orthogonal array.

Experiment No.	Laser power (P), Watt	Laser scan speed (v), mm/sec	Standoff distance (f), mm	Wear (gram/cm)
1	210	1	175	12.30 × 10^{-9}
2	210	5.5	200	15.30 × 10^{-9}
3	210	10	225	22.30 × 10^{-9}
4	255	1	200	8.33 × 10^{-9}
5	255	5.5	225	9.67 × 10^{-9}
6	255	10	175	13.00 × 10^{-9}
7	300	1	225	3.67 × 10^{-9}
8	300	5.5	175	6.00 × 10^{-9}
9	300	10	200	7.33 × 10^{-9}
Untreated sample	–	–	–	139.00 × 10^{-9}

www.rmiet.edu.in

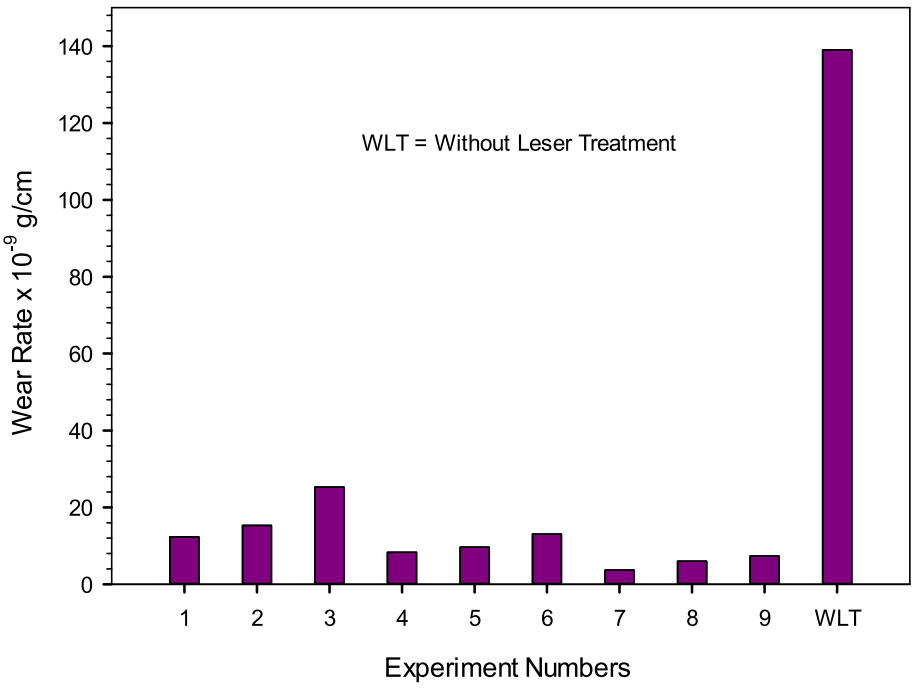

Fig. 8. Wear test results of untreated and laser-hardened components at a 30 N load and a 300 revolution per minute sliding speed.

reasons these parameters show good results in micro-hardness and wear resistance.

3.5. Wear surface morphology of SAE 420 steel

For all samples processed in accordance with the planned design of experiment one, where the sample is also tested from the untreated material, the wear test is conducted on the prepared specimen in accordance with the American Society for Testing and Materials G99 using a pin on the disc machine. From the wear scar area, a small cut specimen is taken for additional wear phenomenon research. Scanner electron microscopy is used to study the wear morphology.

The worn-out surface of the SAE 420 steel as-received sample is seen in the scanning electron microscopy image in Fig. 9(a). During the wear test, which lasted 32 min, the wear rate was 139.00 $\times$ 10^{-9} (gram/cm) at 30 N applied stress, 300 revolutions per minute sliding speed. According to the wear morphology, the untreated sample is experiencing significant wear, mostly as a result of delamination and ploughing, delamination, plastic deformation, indentation, and ploughing. Due to the untreated surface of the sample and 30 N applied stress, 300 revolutions per minute sliding speed the wear debris particles play an important role in wear surface i.e. high wear rate and mechanism (ploughing, delaminating, and plastic deformation) of material removal from the surface. This mostly happens due to temporary welding and sticking of two metal surfaces held together under pressure at a high temperature and speed. Within a short period of time, welding breaks and stuck materials get removed from the sample surface.

The SEM image of worn-out surface SAE 420 steel is shown in Fig. 9 (b) processed at 210-Watt laser beam power, 10 mm/s laser scan speed, 225 mm standoff distance, and 22.30 $\times$ 10^{-9} (gram/cm) observed wear rate at 30 N applied load, 300 revolutions per minute sliding speed, and 32 min' wear test duration. Wear craters, plastic deformation, delamination, indentation, and ploughing are all visible in the wear morphology. This processing condition exhibits an intermediate wear rate among all the experimental conditions taken into account, which is related to intermediate processing conditions. This is explained by the differences in their micro-hardness between samples that have been treated with lasers and those that haven't. Fig. 9(b) surface morphology is some different as compared to Fig. 9(a) because surface 9(b) has laser hardening treatment. Due to laser hardening treatment metallurgical properties of the surface are changed. Due to changes in metallurgical properties wear mechanism and wear rate get changes. The deformation and ploughing get reduced as compared to Fig. 9(a). In the results, the wear rate was found less as compared to without surface treatment, and wear mechanisms are observed in the form of craters.

SEM image of worn-out surface SAE 420 steel is shown in Fig. 9(c) processed at 300-W laser beam power, 1.0 mm/s laser scan speed, and 225 mm standoff distance. 3.67 $\times$ 10^{-9} (gram/cm) wear rate was observed at 30 N applied load, 300 revolutions per minute sliding speed, and 32 min of wear time. Indentation and ploughing, wear craters, ploughing and indentation, and indentation are all visible in the wear morphology. This processing condition exhibits the highest rate of wear of all the experimental circumstances taken into account. Fig. 9(c) shows very little delamination and ploughing type of material removal mechanism as compared to Fig. 9(a and b). This is due to the surface of the test sample developing good metallurgical and wear properties for Fig. 9(C). Due to less delamination and ploughing type of material removal mechanism wear of material is also less. Most of the material gets removed due to indentation and crater type of material removal mechanism.

The untreated sample exhibits significant wear, which is mostly caused by ploughing, plastic deformation, delamination, wear craters, and ploughing and indentation, as seen by the wear morphology.

4. Conclusions

The following are the conclusions drawn from the experimental work.

- The hardness and wear behavior of SAE 420 steel were significantly enhanced with variations in the laser hardening process parameters such as laser power scan speed and standoff distance.
- Laser beam power of 300 W, laser scan speed of 1.0 mm/s, and standoff distance of 225 mm were found to optimize process parameters for the laser hardening process.

www.rmiet.edu.in

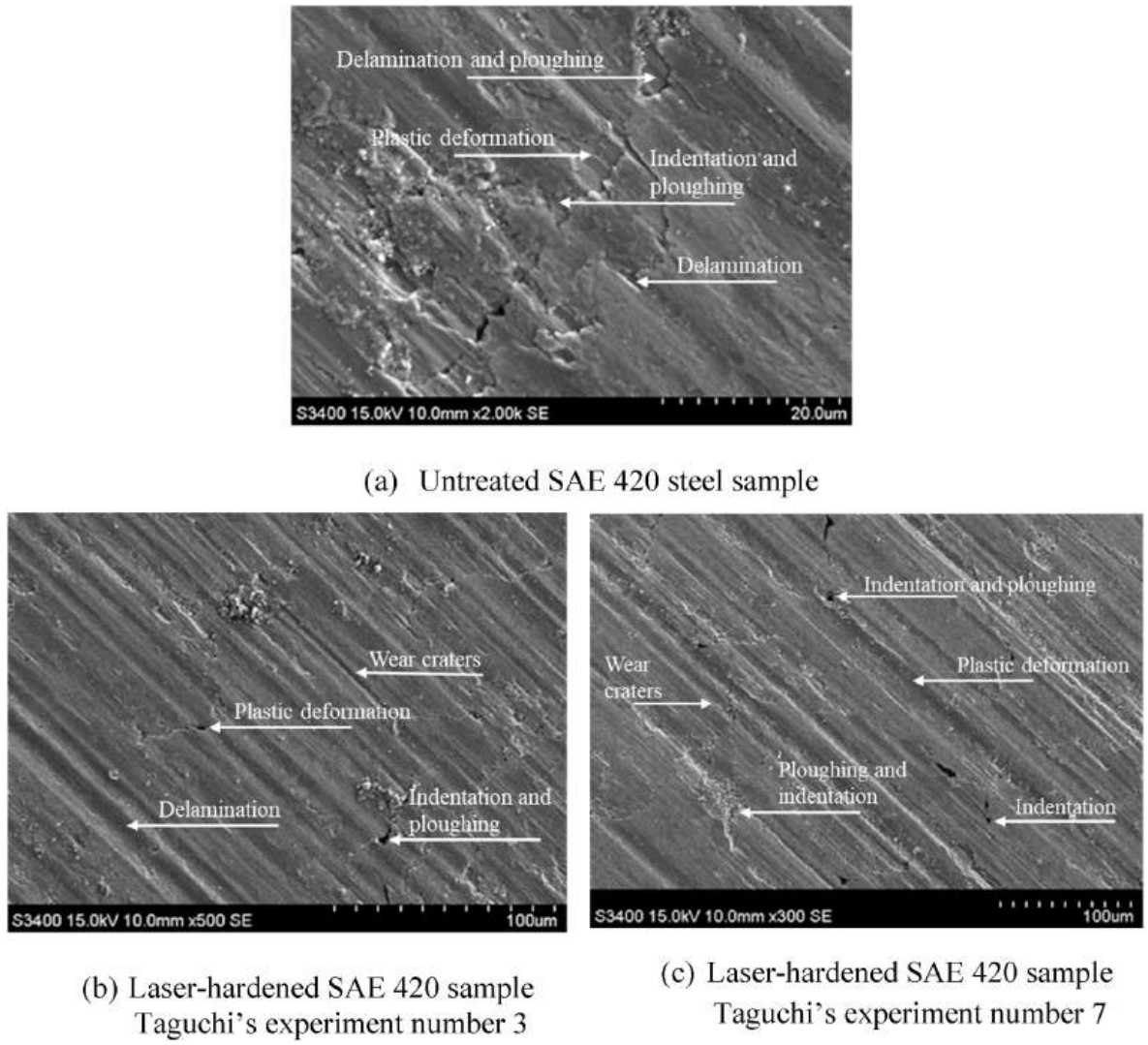

Fig. 9. Surface morphology of the worn surface of SAE 420 steel.

- The laser hardening, and the surface micro-hardness of SAE 420 steel base material, i.e., 208.20 HV increased significantly up to three to four times, i.e., 833.70 HV.
- From the result, it is found that the hardened zone's depth and width vary according to laser hardening process parameters, directly related to the micro-hardness value.
- At optimized laser hardening process parameters hardened zone micro-hardness depth 3614.83 μm and width 4665.07 μm is achieved during the low laser power hardening process.
- The wear resistance of laser-treated specimens was improved due to laser hardening.
- The wear of the laser-hardened sample was 3.67 x10-9 g/cm compared to untreated base metal 139.00 x 10-9 g/cm at an applied load of 30 N and sliding speed of 300 revolutions per minute.
- The SEM analysis was carried out on the base metal and laser-treated wear samples and found good agreement with the reported literature.
- According to the variation of surface micro-hardness, the material removal pattern was changed for the same wear test parameters.

Declaration of competing interest

The authors declare that they have no known competing financial interests or personal relationships that could have appeared to influence the work reported in this paper.

Acknowledgment

The authors extend their appreciation to the Researchers Supporting Project number (RSPD2024R999), King Saud University, Riyadh, Saudi Arabia.

References

[1] Ion JC. Review laser transformation hardening. Surf Eng 2002;18(1):14–31.
[2] Senthil Selvan J, Subramanian K, Nath AK. Effect of laser surface hardening on En18 (AISI 5135) steel. J Mater Process Technol 1999;91:29–36.
[3] Pashby IR, Barnes S, Bryden BG. Surface hardening of steel using a high power diode laser. J Mater Process Technol 2003;139:585–8.
[4] Bekmurzayeva A, Duncanson WJ, Azevedo HS, Kanayeva D. Surface modification of stainless steel for biomedical applications: Revisiting a century-old material. Mater Sci Eng C 2018;93:1073–89.
[5] Puraditya YDBA, Mahendra DD, Setyarini PH. Characteristics of bio-ceramic coating on corrosion rate of stainless steel 316L and titanium (Ti-6Al-4V). Mechanics Exploration and Material Innovation 2024;1(1):20–6.
[6] Ayatilhaq A, Setyarini PH, Setiadhi D. The effect of Mangan on hardness and corrosion rate of biodegradable implants of Zn-Mn alloy. Mechanics Exploration and Material Innovation 2024;1(1):1–6.
[7] Muratal O, Yamanoglu R. Production of 316L stainless steel used in biomedical applications by powder Metallurgy. In: 2019 Scientific Meeting on electrical-Electronics & biomedical engineering and Computer Science (EBBT); 2019. p. 1–4. https://doi.org/10.1109/EBBT.2019.8742055. Istanbul, Turkey.

www.rmiet.edu.in

[8] Ferreira Sabara EW, Pereira V, Molisani AL, Caldeira L, Souza RC, Simões TA, H Santos Bueno A. Electrochemical behaviour and microstructural characterization of different austenitic stainless steel for biomedical applications. Mater Res Express 2020;7:105402. https://doi.org/10.1088/2053-1591/abbbaa.
[9] Ali S, Irfan M, Niazi UM, Rani AMA, Rashedi A, Rahman S, Khan MKA, Alsaiari MA, Legutko S, Petr °u J, et al. Microstructure and mechanical properties of modified 316L stainless steel alloy for biomedical applications using powder Metallurgy. Materials 2022;15:2822. https://doi.org/10.3390/ma15082822.
[10] Lou J, Ren B, Zhang J, He H, Gao Z, Xu W. Evaluation of biocompatibility of 316 L stainless steels coated with TiN, TiCN, and Ti-DLC Films. Coatings 2022;12:1073. https://doi.org/10.3390/coatings12081073.
[11] Balasubramanian S, Muthukumaran V, Sathyabalan P. A study on the effect of process parameters of laser hardening in carbon steels. Int J Civ Eng Technol 2017; 8(9):201–7.
[12] MaharjanNiroj N, Zhou W, Zhou Yu, Wu Naien. Influence of operating parameters on morphology of laser hardened surfaces. In: High-power laser materials processing: applications, Diagnostics, and systems VII. vol. 10525. International Society for Optics and Photonics; 2018.
[13] Rakesh K, Ganesh P, Pragya T, Nandedkar RV, Nath AK. Characterization of dry sliding wear resistance of laser surface hardened En 8 steel. J Mater Process Technol 2005;167(1):83–90.
[14] Qiu F, Kujanpaa V. Transformation hardening of medium-carbon steel with a fiber laser: the influence of laser power and laser power density. Mechanics 2011;17(3): 318–23.
[15] Pashby IR, Barnes S, Bryden BG. Surface hardening of steel using a high power diode laser. J Mater Process Technol 2003;139(1–3):585–8.
[16] Babu PD, Buvanashekaran G, Balasubramanian KR. An optimal genetic algorithm for Fatigue life control of medium carbon steel in laser hardening process. Trans Can Soc Mech Eng 2012;36(3):241–58.
[17] Ponticelli GS, Guarino S, Giannini O. An optimal genetic algorithm for fatigue life control of medium carbon steel in laser hardening process. Appl Sci 2020;10(4): 1401.
[18] Selvan JS, Subramanian K, Nath AK. Effect of laser surface hardening on En18 (AISI 5135) steel. J Mater Process Technol 1999;91(1–3):29–36.
[19] Zhang XM, Man HC, Li HD. Wear and friction properties of laser surface hardened En. J Mater Process Technol 1996;69(1–3):162–6.
[20] Barka N, El Ouafi A. Effects of laser hardening process parameters on case depth of 4340 steel cylindrical specimen—a statistical analysis. J Surf Eng Mater Adv Technol 2015;5(3):124.
[21] Barka N, Karganroudi S, Fakir R, Thibeault P, Feujofack Kemda VB. Effect of laser hardening process parameters on hardness profile of 4340 steel spline - an experimental approach. Coatings 2020;10(4):342.
[22] Aborkin AV, Vaganov VE, Bukarev IM. Effect of laser hardening on die steel microhardness and surface quality. Metallurgist 2015;59(7–8):619–25.
[23] El-Batahgy AM, Ramadan RA, Moussa AR. Laser surface hardening of tool steels—experimental and numerical analysis. J Surf Eng Mater Adv Technol 2013; 3:146–53.
[24] Karthikeyan KMB, Balasubramanian T, Thillaivanan V, Jangetti GV. Laser transformation hardening of EN24 alloy steel. Mater Today Proc 2020;22:3048–55.
[25] Babu PD, Buvanashekaran G, Balasubramanian KR. Dry sliding wear of laser hardened low alloy steel at room and elevated Temperatures. Proc IME J J Eng Tribol 2013;227(10):1138–49.

View publication stats

www.nmiet.edu.in
ISSN 1087-6596, Glass Physics and Chemistry, 2023, Vol. 49, No. 6, pp. 604–616. © Pleiades Publishing, Ltd., 2023.

Thermodynamic and Kinetic Studies of Glass-Forming Compositions in Ca–Mg–Cu Ternary Metallic Glasses

Akash A. Deshmukh[a, b, *], Anuj A. Khond[c], Jatin. G. Bhatt[d], and Umesh A. Palikundwar[b, **]

[a] *Department of Materials Engineering, Indian Institute of Technology Gandhinagar, Gujarat, 382355 India*

[b] *X-ray Research Laboratory, Department of Physics, Rashtrasant Tukadoji Maharaj Nagpur University, Nagpur, 440033 M.S. India*

[c] *Department of Mechanical Engineering, Nutan Maharashtra Institute of Engineering and Technology, Pune, 410507 M.S. India*

[d] *Department of Metallurgical and Materials Engineering, V.N.I.T. Nagpur, 440010 M.S. India*

**e-mail: akdeshmukh9@gmail.com*

***e-mail: uapali@yahoo.com*

Received June 2, 2023; revised August 2, 2023; accepted August 7, 2023

Abstract—Herein, we systematically studied the thermodynamic and kinetic aspects of glass forming compositions in Ca–Mg–Cu alloy obtained by drawing the isocontour. Parameter P_{HS} derived from the enthalpy of chemical mixing (ΔH_{chem}) and normalized mismatch entropy ($\Delta S_\sigma/k_B$) is used as a glass-forming ability (GFA) parameter. Variation of P_{HS} with reported and calculated compositions is evaluated. Linear relation of Cu with P_{HS} is observed, whereas inverse relation of Ca and Mg is obtained. The linear variation of P_{HS} with a supercooled liquid region (SCLR) (ΔT_x) is studied. Inverse correlation of critical cooling rate (R_C) with P_{HS} is obtained. R_C for predicted compositions is found close to that of reported compositions. Therefore, Cu should be added carefully with other elements to improve the GFA and reduce the cooling rate of Ca–Mg–Cu glassy. In this paper, an empirical correlation of ΔT_x with P_{HS} is proposed, and the modeled values are found to agree with the experimental values.

Keywords: metallic glasses, glass-forming ability, viscosity, thermodynamic parameters, biomedical applications

DOI: 10.1134/S1087659622600211

INTRODUCTION

Calcium based bulk metallic glasses (BMGs) have the lowest density (~2.0 g/cm^3), Young's modulus (~20 to 30 GPa), and shear modulus (~8 to 15 GPa) [1, 2]. Their Young's modulus values are comparable to the modulus of human bones, which makes them an attractive material in biomedical applications [1]. They possess low glass transition temperature (T_g ~ 373 to 463 K), low crystallization temperature (T_x ~ 403 to 513 K), and a wide supercooled liquid region (SCLR) (ΔT_x ~ 30 to 80 K) [1]. Therefore, it is crucial to understand the glass-forming ability (GFA) and the kinetics of the Ca-based BMGs. Since the development of the first MG, many parameters have been designed and proposed by different researchers to address glass-formation in metallic alloys [3]. Chattopadhyay et al., [3] have reported that 62 GFA parameters are being used to predict good glass-forming compositions (GFCs) and explain the GFA of these alloys. Chattopadhyay et al., [3] classified these parameters into four categories depending on critical temperatures of glass-forming alloys (Category A), thermodynamic parameters (Category B), internal atomic structure and atomic arrangement of constituting elements (Category C), and kinetic properties (Category D) of the glassy materials. Parameters in Category A such as $T_{rg} = T_g/T_l$, $\Delta T_x = T_l - T_x$, $\alpha = T_x/T_l$, $\beta = T_xT_g/(T_l + T_x)^2$ [3] have been extensively used to predict the good GFCs [3]. However, they are based on the postexperimental differential scanning calorimetry (DSC) measurements. On the other hand, parameters in Category B such as enthalpy of chemical mixing (ΔH_{chem}) [3], and Category C such as normalized mismatch entropy $(\Delta S_\sigma/k_B)$, normalized configurational entropy $(\Delta S_C/R)$ [3] are preexperimental parameters which can be calculated using simple empirical equations [3]. Based on this idea, Bhatt et al., [4] have proposed the parameter P_{HS} to design the ternary alloys by considering the parameter in Category B and Category C. P_{HS} is the product of ΔH_{chem} and $\Delta S_\sigma/k_B$. The P_{HS} parameter combines the

www.nmiet.edu.in

effect of both ΔH_{chem} and $\Delta S_\sigma/k_B$ to ascribe GFA. Previously, the P_{HS} parameter is used successfully to preciously predict the compositions in ternary Zr–Cu–Al [4], Zr–Cu–X (X = Ag, Al, Ti, Ga) [5], Fe–Zr–B [6], Hf–Cu–Ni [7] systems, in quaternary Cu–Zr–Ag–Hf [8], Ti–Zr–Cu–Ni [9], Fe–Zr–B–Cu [10] systems and quinary in Zr–Ti–Cu–Ni–Al [11] system. Product of dimensionless parameter $\Delta S_\sigma/k_B$ with ΔH_{chem} is an extension of enthalpy value and guideline to trace BMG compositions. Therefore, it can be proposed that the use of ΔH_{chem}, $\Delta S_\sigma/k_B$, and $\Delta S_C/R$ parameters provide a more feasible and convenient approach to predict the GFCs in any of the alloys compared to other parameters as given in [3]. Parameters in Category D correlate the kinetics of phase transformations with the GFA of the alloy [3]. Kinetic parameters such as nucleation rate (I), growth rate (u), diffusion coefficient (D), and viscosity (η) are not able to experimentally evaluate during the glass formation process [12]. Therefore, the phase predictive model proposed by Chattopadhyay et al., [13, 14] has been used to evaluate the role of viscosity in the GFA of thermodynamically predicted GFCs in Ca–Mg–Cu ternary alloy. This model comprises the viscosity and the crystal structure information of the constituent elements [13, 14]. It allows to estimate the critical cooling rate (R_C) by drawing the time–temperature transformation (TTT) diagram [13, 14]. Chattopadhyay et al., [13] successfully employed this model to study the $Zr_{41.2}Ti_{13.8}Cu_{10}Ni_{12.5}Be_{22.5}$, $Pd_{40}Cu_{30}Ni_{20}P_{10}$ MGs and their equiatomic counterparts such as $Zr_{20}Ti_{20}Cu_{20}Ni_{20}Be_{20}$, $Pd_{25}Cu_{25}Ni_{25}P_{25}$. Recently, Khond et al., [12] have reported the GFA in Hf-based MGs using this model. The objective of the present paper is two fold. The first is to predict the GFCs in Ca–Mg–Cu ternary alloy by employing thermodynamic parameter, i.e., P_{HS}, and the second is to discuss the GFA using the TTT diagram with P_{HS}. The present study considers 29 compositions from the available reports [1, 15–17] (see Table 1). The concept of thermodynamic modeling reported in [3–12] is used to predict GFCs in Ca–Mg–Cu alloy. Compositions close to that of reported compositions are identified from the isometric contours of ΔH_{chem}, $\Delta S_\sigma/k_B$, $\Delta S_c/R$, and the significance of the thermodynamic modeling is discussed. Further, compositional dependence with P_{HS} is investigated, and a novel correlation of $\Delta T_x - P_{HS}$ is proposed. Critical cooling rate (R_c) essential to preserve the glassy phase in the Ca-based BMGs is calculated by plotting the TTT diagram, and the correlation R_c–P_{HS} is discussed.

CALCULATION OF THERMODYNAMIC PARAMETERS

In the present work, ΔH_{chem}, $\Delta S_\sigma/k_B$, and $\Delta S_c/R$ [3–12] are used to predict the GFC in Ca–Mg–Cu glassy alloy. Mathematically, they are represented by the following equations.

Enthalpy of Chemical Mixing (ΔH_{chem})

Following equation (1) is used to calculate the enthalpy of chemical mixing (ΔH_{chem}) [3–12] for the different compositions in Ca–Mg–Cu glassy alloy.

$$\Delta H_{chem} = \sum_{\substack{A=1 \\ A \neq B}}^{n} \Delta H_{AB}^{C}, \quad (1)$$

where

$$\Delta H_{AB}^{C} = X_A X_B \left(X_B \Delta H_{A-B}^{interface} + X_A \Delta H_{B-A}^{interface} \right). \quad (2)$$

Here, X_A and X_B are atomic fractions of elements A and B, respectively. The term ΔH_{AB}^{C} represents the enthalpy of chemical mixing for binary alloy at an infinite dilution of A in B, calculated according to Miedema's semiempirical approach [18].

Mismatch Entropy (ΔS_σ)

The following empirical relation given in [3–12] is used to calculate the change in atomic mismatch entropy (ΔS_σ).

$$\Delta S_\sigma = k_B \left[\frac{3}{2}\left(\zeta^2 - 1\right) y_1 + \frac{3}{2}(\zeta - 1)^2 y_2 - \left\{ \frac{1}{2}(\zeta - 1)(\zeta - 3) + \ln \zeta \right\} (1 - y_3) \right], \quad (3)$$

where k_B is the Boltzmann's constant and parameter ζ is defined as $\zeta = \frac{1}{(1-\xi)}$. The parameter ξ (=0.64) stands for the random packing density of particles of the system [19]. The summation of the dimensionless parameters y_1, y_2, and y_3 is always unity and can be calculated according to the following equations.

$$y_1 = \frac{1}{\sigma^3} \sum_{j \geq i=1}^{n} \left(d_i + d_j\right)\left(d_i - d_j\right)^2 C_i C_j, \quad (4)$$

$$y_2 = \frac{\sigma^2}{(\sigma^3)^2} \sum_{j \geq i=1}^{n} d_i d_j \left(d_i - d_j\right)^2 C_i C_j, \quad (5)$$

$$y_3 = \frac{(\sigma^2)^3}{(\sigma^3)^2}, \quad (6)$$

$$\sigma^k = \sum_{i=1}^{n} C_i d_i^k \ (k = 2, 3). \quad (7)$$

www.mmiet.edu.in

Table 1. Calculation for ΔT_X, ΔH_{chem}, P_{HS} for reported Ca–Mg–Cu BMGs [1, 15–17]

BMG	ΔT_X (K) (a), reported	ΔT_X (K) (b), modeled	$\lvert a-b\rvert$, K	Z_C (mm), reported	ΔH_{chem}, kJ/mol	P_{HS}, kJ/mol
$Ca_{40}Mg_{25}Cu_{35}$ [1, 15, 17]	37	43.63	6.60	4.00	–7.81	–5.26
$Ca_{40}Mg_{30}Cu_{30}$ [15, 17]	35	35.73	0.70	0.50	–7.09	–4.36
$Ca_{45}Mg_{19}Cu_{36}$ [15, 17]	29	50.04	21.00	0.50	–8.57	–5.99
$Ca_{45}Mg_{25}Cu_{30}$ [1, 15, 17]	38	38.72	0.70	**6.00**	–7.52	–4.70
$Ca_{45}Mg_{30}Cu_{25}$ [15, 17]	35	31.08	3.92	1.00	–6.81	–3.83
$Ca_{47.5}Mg_{22.5}Cu_{30}$ [1, 15]	41	40.03	0.97	**6.00**	–7.73	–4.85
$Ca_{50}Mg_{20}Cu_{30}$ [1, 15, 17]	41	41.44	0.40	**8.00**	–7.96	–5.01
$Ca_{50}Mg_{22.5}Cu_{27.5}$ [1, 15]	42	36.78	5.22	**10.00**	–7.51	–4.48
$Ca_{50}Mg_{25}Cu_{25}$ [1, 15, 17]	39	32.75	6.25	**9.00**	–7.11	–4.02
$Ca_{50}Mg_{30}Cu_{20}$ [15, 17]	37	25.81	11.20	2.00	–6.45	–3.23
$Ca_{53}Mg_{23}Cu_{24}$ [1, 15, 17]	33	31.87	1.13	**7.00**	–7.12	–3.92
$Ca_{54}Mg_{18}Cu_{28}$ [17]	41	39.24	1.76	1.00	–7.90	–4.76
$Ca_{55}Mg_{10}Cu_{35}$ [15, 17]	25	56.01	31.00	0.50	–9.62	–6.67
$Ca_{55}Mg_{15}Cu_{30}$ [15]	40	43.81	3.80	3.00	–8.41	–5.28
$Ca_{55}Mg_{20}Cu_{25}$ [15, 17]	27	33.97	7.00	2.00	–7.40	–4.16
$Ca_{55}Mg_{25}Cu_{20}$ [1, 15]	30	26.25	3.75	**8.00**	–6.61	–3.28
$Ca_{57}Mg_{19}Cu_{24}$ [16]	36	32.57	3.43	4.00	–7.33	–4.00
$Ca_{58}Mg_{18}Cu_{24}$ [1, 15, 17]	38	32.75	5.25	**6.00**	–7.38	–4.02
$Ca_{60}Mg_{13}Cu_{27}$ [15]	32	38.98	7.00	1.00	–8.14	–4.73
$Ca_{60}Mg_{15}Cu_{25}$ [15]	32	34.85	2.90	1.00	–7.69	–4.26
$Ca_{60}Mg_{20}Cu_{20}$ [1, 15, 17]	25	26.25	1.20	4.00	–6.74	–3.28
$Ca_{60}Mg_{25}Cu_{15}$ [15, 17]	26	19.66	6.34	2.00	–6.03	–2.53
$Ca_{65}Mg_{5}Cu_{30}$ [15, 17]	21	47.76	27.00	0.50	–9.37	–5.73
$Ca_{65}Mg_{10}Cu_{25}$ [15, 17]	32	35.47	3.50	2.00	–7.97	–4.33
$Ca_{65}Mg_{15}Cu_{20}$ [1, 15, 17]	26	28.18	2.20	4.00	–6.85	–3.50
$Ca_{65}Mg_{20}Cu_{15}$ [15, 17]	19	18.79	0.21	2.00	–5.98	–2.43
$Ca_{65}Mg_{25}Cu_{10}$ [15, 17]	24	13.34	10.70	0.50	–5.39	–1.81
$Ca_{70}Mg_{10}Cu_{20}$ [15, 17]	22	25.37	3.40	1.00	–6.94	–3.18
$Ca_{70}Mg_{20}Cu_{10}$ [15, 17]	29	11.85	17.20	0.50	–5.16	–1.64

In the above equations, d_i and d_j are the atomic diameters of ith and jth elements. The atomic diameters used in the above calculations are taken from [20]. Similarly, C_i and C_j are the concentration in at % of the ith and jth element, respectively.

Configurational Entropy (ΔS_C)

Configurational entropy (ΔS_C) [3–12] depends only on an atomic fraction of an individual constituting element and is independent of the alloy system. It can be calculated by the following equation (8) [3–12].

$$\Delta S_C = -R\sum_{i=1}^{n} x_i \ln x_i. \quad (8)$$

Here, R represents the Universal gas constant, and x_i is the atomic fraction of ith element.

Parameter P_{HS}

Parameter P_{HS} is the product of ΔH_{chem} and $\Delta S_\sigma/k_B$ and can be obtained by the following relation [3–12].

$$P_{HS} = \Delta H_{chem}\frac{\Delta S_\sigma}{k_B}\ \text{kJ/mol}. \quad (9)$$

www.nmiet.edu.in

TIME–TEMPERATURE TRANSFORMATION

Arrhenius equation (10) [12, 14] is used to calculate the viscosity of the individual elements such as Ca, Mg, and Cu.

$$\eta_{\text{elelment}} = \eta_0 \exp(E/RT) \tag{10}$$

In Eq. (10), η_0 and E are the preexponential constant and activation energy for the element. These parameters are calculated by solving simultaneous equations considering the elemental viscosity of Ca, Mg, and Cu at glass transition temperature (T_g) and melting temperature (T_m) [12, 14]. The viscosity of Ca, Mg, and Cu at T_g are assumed as 10^{12} Pa s [21] whereas at T_m, $\eta_{Ca} = 1.22\times10^{-3}$ Pa s, $\eta_{Mg} = 1.25\times10^{-3}$ Pa s, and $\eta_{Cu} = 4.0\times10^{-3}$ Pa s [22]. Substituting the η_0 and E in Eq. (10), η_{elelment} is calculated from 300 K to T_m to study the viscosity behavior of Ca, Mg, and Cu. These elemental viscosities are then used to calculate the viscosity of predicted and experimentally reported [1, 15–17] Ca–Mg–Cu MG compositions. Following Equation (11) proposed by Budai et al., [23] to calculate the viscosity of MG as a function of temperature is used in the present work:

$$\eta_{MG} = \frac{hN_A}{\sum_i x_i V_m^i + \Delta V_m^E} \times \exp\left[\frac{\left(\sum_i x_i G_i^*\right) - (0.155 \pm 0.015)\Delta H_{\text{chem}}}{RT}\right]. \tag{11}$$

In the above Eq. (11), η_{MG} is the viscosity of the glassy alloy in Pa s, h is the Planck's constant (6.626×10^{-34} m^2 kg/s), N_A is the Avogadro number (6.022×10^{23}), x_i is the atomic fraction of the ith element in at %, V_m^i is the molar volume of the ith element in m^3/mol, ΔV_m^E is the excess molar volume formation of the alloy in m^3/mol. However, the measurement of ΔV_m^E is difficult in the experiment [13]; therefore, it is assumed negligible for the present work. ΔG_i^* is the Gibbs free energy for the activation of viscous flow in the pure ith element, ΔH_{chem} is the enthalpy of chemical mixing calculated from Eq. (1), R is the Universal gas constant (8.314 J K^{-1} mol^{-1}). Calculation of Gibbs free energy and molar volume of the alloy is given in [14]. Babilas et al., [24] reported that annealing of $Ca_{50}Mg_{20}Cu_{30}$ BMG at 473 K for 1h exhibits hexagonal Mg_2Ca and orthorhombic CaCu, Ca_2Cu phases. At a higher temperature, 573 K, the growth of CaCu and Mg_2Ca is significant. Further, to prevent crystallization, it is essential to avoid the HCP and orthorhombic phase formation. During the crystallization process of Ca–Mg–Cu system HCP phase will form first [14], hence viscosity of HCP phase was considered in this work. Moreover, it was mention in literature that calculation of TTT diagram is possible for only three phases i.e. BCC, FCC, and HCP as given in the ref. [13, 14]. Therefore, the viscosity reflecting the HCP phase with the following modification is considered [12–14].

$$\eta_{HCP} = (1 + \varepsilon N_C C_V)\frac{hN_A}{V_m^{\text{alloy}}}\exp\left[\frac{\left\{RT\left(\sum x_i \ln\eta_i\right) + RT\ln\left(\frac{V_C}{hN_C}\right)\right\} - 0.155\Delta H_{\text{chem}}}{RT}\right]. \tag{12}$$

In Eq. (12), ε is the unit cell packing fraction (PF). N_C is the effective number of atoms per unit cell, C_V is the coefficient of variation, V_m^{alloy} is the molar volume of the alloy, V_C is the volume of the unit cell of the alloy, ΔH_{chem} is the enthalpy of chemical mixing, η_i is the viscosity of the ith element having x_i at %. The details of these parameters can be found elsewhere [13, 14].

The incubation time for the crystal nuclei formation has been calculated by Eq. (13) [12–14].

$$t = \frac{9.3\ln\eta_{HCP}}{k_B T}\left[\left(\frac{a_0^9 x_C}{f^3 N_v^0}\right)\frac{\exp\left(\frac{1.024}{T_r^3\Delta T_r^2}\right)}{\left\{1-\exp\left(\frac{-\Delta H_f \Delta T_r}{RT}\right)\right\}^3}\right]^{\frac{1}{4}}, \tag{13}$$

where η_{HCP} is the viscosity of the Ca–Mg–Cu MG calculated from Eq. (12), k_B is the Boltzmann constant (1.380×10^{-23} m^2 kg s^{-2} K^{-1}), a_0 is the lattice parameter calculated from atomic radius using the rule

www.miet.edu.in

of mixture, $x_C\left(=10^{-6}\right)$ is the minimum detectable transformation, $f\,(=1)$ is the fraction of the site at the interface where the atoms may be added or removed, N_V^0 is the number of molecules per unit volume, $T_r = T/T_m$ and $\Delta T_r = (T_m - T)/T_m$. T_m is the melting temperature, and ΔH_f is the enthalpy of fusion of the alloy [12–14]. Enthalpy of fusion (ΔH_f) for the individual elements such as Ca, Mg, and Cu is taken from [25]. The plot for solidification time versus temperature is referred to as the time–temperature transformation (TTT) diagram. R_C of the alloys is calculated by Eq. (14).

$$R_C = (T_m - T_n)/t_n. \quad (14)$$

In Eq. (14), T_n (K) and t_n (s) are the temperature and time at the nose of the TTT curve, respectively.

RESULTS AND DISCUSSION

Thermodynamic Modeling

The superimposition of contour's for ΔH_{chem}, $\Delta S_\sigma/k_B$ and, $\Delta S_c/R$ has been shown in Fig. 1. Contour for ΔH_{chem} (Red color) has been drawn using the approach given in [3–12]. Starting with –11 kJ/mol from Ca–Cu rich end, contour for ΔH_{chem} proceed towards Mg–Cu rich end with the minimum negative enthalpy of mixing of –5 kJ/mol at regular interval of –1 kJ/mol as shown in Fig. 1. It can be justified from the fact that the ΔH_{chem} for Ca is more with Cu than Mg, such as $\Delta H_{Ca\ in\ Cu} = -66$ kJ/mol, $\Delta H_{Cu\ in\ Ca} = -39$ kJ/mol, $\Delta H_{Mg\ in\ Ca} = -20$ kJ/mol, $\Delta H_{Ca\ in\ Mg} = -26$ kJ/mol, $\Delta H_{Mg\ in\ Cu} = -20$ kJ/mol and $\Delta H_{Cu\ in\ Mg} = -15$ kJ/mol [18]. The contour for $\Delta S_\sigma/k_B$, as shown in Fig. 1 (Green color), begins from Ca–Cu rich end with the maximum value 0.85 of $\Delta S_\sigma/k_B$ and the isocontour shifts towards Ca–Mg rich end with a reduction in mismatch entropy to 0.40. This trend is evident from the fact that the atomic size difference in Ca–Cu ($\Delta r = 35\%$), which is more in comparison to Ca–Mg ($\Delta r = 19\%$) and Mg–Cu ($\Delta r = 20\%$) binary pairs. The dependency of $\Delta S_\sigma/k_B$ on atomic diameter and composition validates the nature of contour. The $\Delta S_c/R$ varies from 0.8 to 1.0 for ternary metal–metal BMGs [4]. It has been noticed that the compositions having Ca concentration up to 60 at % can be easily obtained in the range of 0.9 to 1.0 of $\Delta S_c/R$. Further, to find the compositions having more than 60 at % concentration of Ca, contour for $\Delta S_c/R$ 0.8 has been drawn. Therefore, one can see three concentric circles for $\Delta S_c/R$ related to 0.8, 0.9, and 1.0, respectively, in Fig. 1 (black). These observations are well-matched with those reported for Zr–Cu–Al ternary glassy alloy [4],

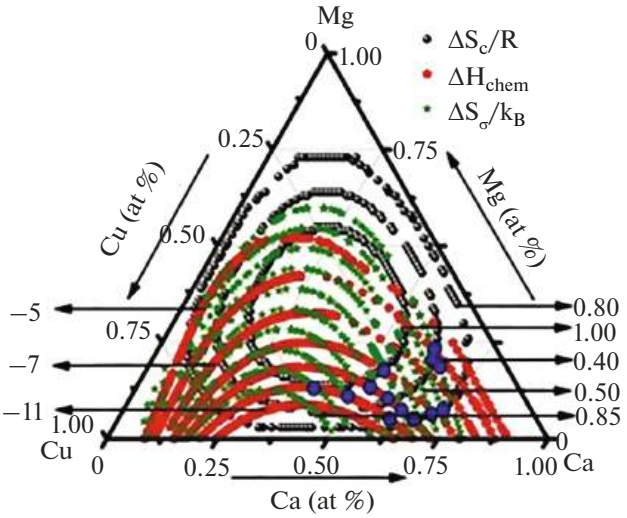

Fig. 1. Superposition of isometric contours for ΔH_{chem}, $\Delta S_\sigma/k_B$, $\Delta S_c/R$ for Ca–Mg–Cu alloy system.

and using a similar approach, GFCs are predicted in the Ca–Mg–Cu ternary system. The $\Delta S_c/R$ is the probability parameter that determines the atomic distribution from which randomness originating from compositional configuration can be determined. The intersections of ΔH_{chem} and $\Delta S_\sigma/k_B$ have been identified by fixing $\Delta S_c/R$ in the range of 0.8 to 1.0 in the isometric ternary diagram. Earlier, it was observed that the composition with the most negative P_{HS} values within the $\Delta S_c/R$ range of 0.9–1.0 resulted in the best BMG [4]. Among the reported [1, 15–17] compositions, the maximum (–6.67 kJ/mol) and minimum (–1.64 kJ/mol) negative values of P_{HS} are found for $Ca_{55}Mg_{10}Cu_{35}$ and $Ca_{70}Mg_{20}Cu_{10}$, respectively. Among the modelled compositions obtained from isocontour, $Ca_{62}Mg_{24}Cu_{14}$ has a minimum (–2.35 kJ/mol), and $Ca_{42}Mg_{13}Cu_{45}$ has maximum (–7.98 kJ/mol) negative values of P_{HS}. The GFA of the present alloy Ca–Mg–Cu is very sensitive to the elemental compositions [15–17]. There are 8 compositions, as shown in Table 1, having Z_C in the range of 6 to 10 mm diameter among (shown in bold in Table 1) all 29 compositions. Among those 8 compositions, $Ca_{50}Mg_{20}Cu_{30}$ has maximum (most negative) P_{HS} as –5.01 kJ/mol, whereas $Ca_{55}Mg_{10}Cu_{35}$ has minimum (less negative) P_{HS} as –4.02 kJ/mol. Thus, the P_{HS} range of –3.28 to –5.01 kJ/mol, shown in Table 1, is the composition window for BMG with good GFA in this system with a critical size of more than 5 mm.

www.nmiet.edu.in

Analysis of Modelled Compositions

All 29 data points are linearly fitted using the 'linear fit' function in Origin 8 software for Ca, Mg, and Cu (at %) with P_{HS}. For Ca, a positive slope of 7.12 and regression coefficient (R^2) of 22.97% is obtained in supplementary figure Fig. SI-1 (a). Further, by excluding 8 data points (i.e., 27.58% of the original data) in Table 1, an optimum R^2 value of 71.18% is obtained with a positive slope of 11.58, as seen in Fig. SI-1 (a). Similarly, a positive slope of 6.58 with *an* R^2 value of 9.37% is obtained for Mg, as illustrated in Fig. SI-1 (b). The scattered nature of Mg with P_{HS} is observed. An optimum R^2 value of 42.90% with a positive slope of 12.65 is obtained by excluding the 8 data points (i.e., 27.58% of the original data) as given in Table 1. Unlike Ca and Mg, Cu has a negative slope of −16.95 with the highest R^2 value of 93.45% for all 29 data points, as seen in Fig. SI-1 (c). In Fig. 2, slope and R^2 values of optimum fitting for Ca, Mg and Cu are presented. Figure 2 shows the variation in reported compositions having Ca, Mg, and Cu elements Vs. P_{HS}. From Fig. 2, it is observed that there is a corresponding increase in the P_{HS} value with an increase in Ca and Mg in BMG compositions. However, a higher R^2 of Ca (71.18%) indicates its linear behavior with P_{HS} than that of Mg (42.90%) as the composition increases from left to right. The poor R^2 value for Mg indicates a large fluctuation in Mg content in BMG forming alloys. This can be evident from the steeper behavior of the Mg slope (12.65) compared to that of Ca (11.59). This fluctuation in the present context is also indicative of less influence of Mg on P_{HS}. This is also reflected in Table 1, where BMGs with $Z_c > 6$ mm show a strong dependency of Ca compared to Mg. This could be due to the higher melting temperature (T_m) and large heat of vaporization (H_v) of Ca (1115K, 155 kJ/mol) [26] compared to that of Mg (923K, 128 kJ/mol) [26]. On the other hand, T_m, H_v for Cu is 1357K and 300 kJ/mol, respectively [26]. Ca and Mg are the alkaline–earth metals (AEM), and Cu is the transition metal (TM). This could be the possible reason for the opposite trend of the Ca, Mg compared to that of Cu, as seen in Fig. 2. Similarly, the compositional dependence of the modelled alloys with P_{HS} is also evaluated. From iso–contour shown in Fig. 1, 13 compositions are pin pointed close to that of reported compositions as given in Table 1. For Ca, a positive slope of 15.81 with an R^2 value of 46.23% is obtained, as seen in Fig. SI-2 (a) for all 13 data points. Excluding 3 data points (i.e., 23.07% of the original data), an optimum value of R^2 (67.35%) is obtained with a positive (12.93) slope. Variation in Mg (at %) with P_{HS} is illustrated in SI-2 (b). For Mg, the slope is positive with a value of 15.03, while R^2 is 20.72. Similarly, excluding 3 data points (i.e., 23.07% of the original data) optimum value of R^2 is obtained as 47.42% with a slope of 15.52, as shown in SI-2 (b). Unlike Ca and Mg, the linear relation of Cu with that of P_{HS} is obtained as illustrated in SI-2 (c). For Cu, R^2 is 98.08%, with a negative slope of −19.55. An optimum value of R^2 and slope for modelled Ca, Mg, and Cu are shown in Fig. 3. From Fig. 3, it can be seen that for Ca, R^2 (67.35%) is higher compared to that of the Mg (47.42%). Similarly, the steep behavior of Mg (slope = 15.52) in comparison to that of Ca (slope = 12.93) is observed from Fig. 3. The nature of R^2 and slope for modelled Ca, Mg and Cu (at %) is found identical to that of the reported compositions. This shows that the current approach identifies the good GFC in ternary Ca–Mg–Cu glassy alloys and can be extended to the other ternary glassy systems.

Relation between SCLR (ΔT_x) and P_{HS}

Dependence of SCLR, i.e., ΔT_x on P_{HS}, is evaluated for reported [1, 15–17] compositions as shown in Fig. 4. Data have been analyzed in three different regions by linear fittings, and these three regions are termed as a reliable region (R), intermediate reliable region (IR), and a less reliable region (LR). In the LR region, all the 29 data points are considered. The LR region's regression coefficient (R^2_{LR}) is 7.37%, with a negative slope of −1.88. In the intermediate region (IR), after excluding 5 data points (17.24% of the original data), R^2_{IR} is improved to 64.69% with a negative slope of −6.12. An optimum R^2_R value of 86.22% is obtained in the R region by excluding 14 data points (48.27% of the original data) with a negative slope of −8.78. The corresponding relation obtained from figure 4, for R^2_R, is given by Eq. (15).

$$\Delta T_x = -2.55 - 8.78 * P_{HS};\ R^2_R = 86.22\%. \quad (15)$$

From Eq. (15), ΔT_x for the reported compositions [1, 15–17] is calculated. It is observed that modelled values are in close agreement with experimental values, as shown in Table 1. There are 16 compositions (55.17% of the original data) for which ΔT_x varies between 0 to 5 K. For 7 compositions (24.13% of the original data), ΔT_x varies between 6 to 10 K. Similarly, for 6 compositions, this difference is more than 10 K. This result indicates that the current approach can predict ΔT_x by 79.31% with 0 to ±10 K. Among all compositions, the minimum and a maximum difference of ΔT_x observed was 0.21 and 31K, respectively. Senkov et al., [1, 15] have mentioned that the best Ca–

www.rmiet.edu.in

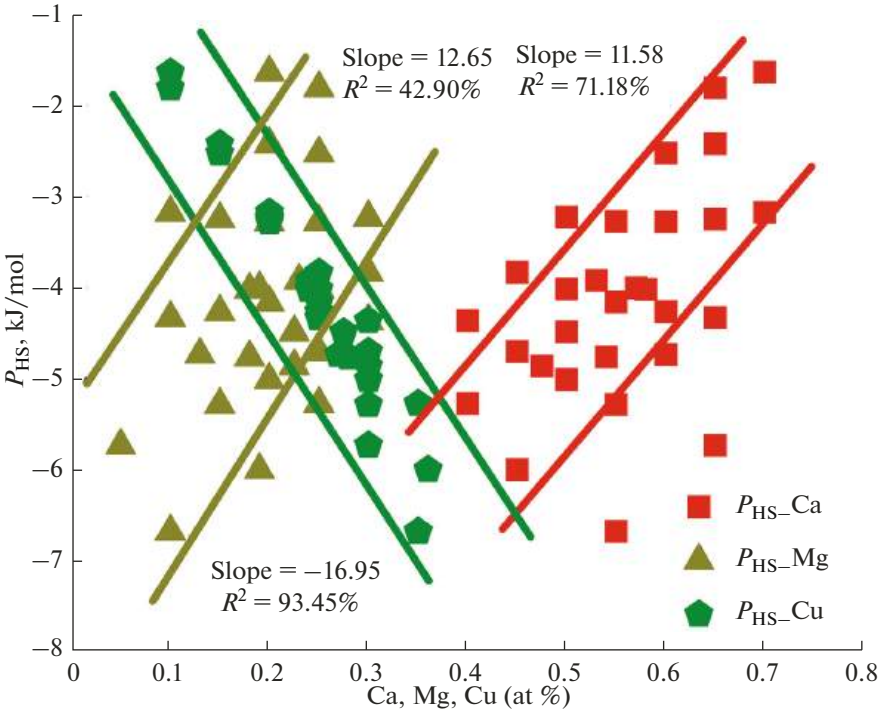

Fig. 2. Variation in P_{HS} with Ca, Mg, Cu (at %) for reported compositions.

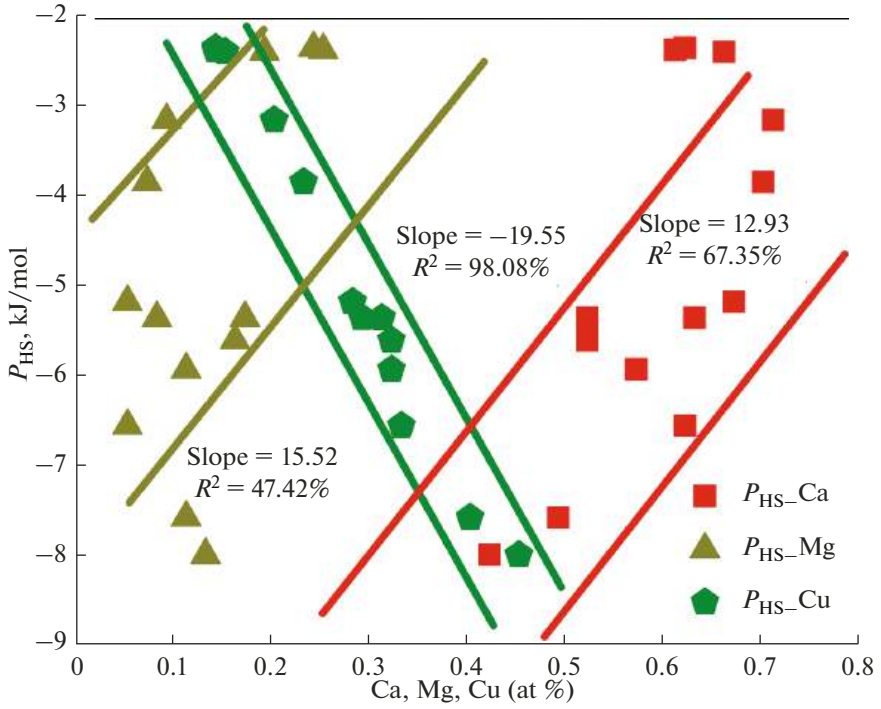

Fig. 3. Variation in P_{HS} with Ca, Mg, Cu (at %) for modeled compositions.

Mg–Cu glass-forming alloys are found near the eutectic compositions with maximum Z_C in the range of 6 to 10 mm, and inferior glass-forming alloys are located away from the eutectic with high melting temperatures. For eutectic GFCs, Senkov et al., [1] reported the range of Ca and Mg as 50 to 53 at % and 23 to 25

www.nmiet.edu.in

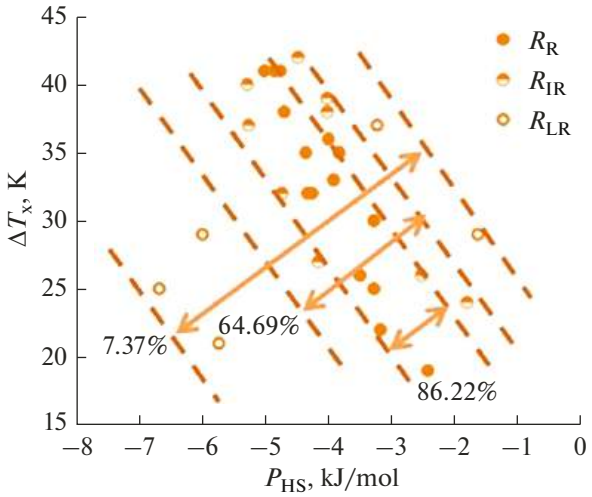

Fig. 4. Variation in T_x with P_{HS} for reported compositions.

at %, respectively. Similarly, for peritectic GFCs, the range of Ca and Mg is given around 70 at % and 15 at %, respectively [1]. Moreover, Kawazoe et al., [27] have shown that in nonequilibrium phase diagrams of ternary glassy alloys, GFC of Ca and Mg is around 10–75 at % and 10 to 54 at %, respectively. For Cu, the composition varies from 10–36 at % [27]. From Table 1, it can be seen that for the alloys having Z_C in the range of 6 to 10 mm, Ca varies from 45 to 58 at % while Mg varies from 18 to 25 at %. Cu varies from 20 to 30 at %. These values are very close to those suggested by Senkov et al., [1, 15] and Kawazoe et al., [27]. The range of ΔT_x is 30K to 42K, and that of P_{HS} is −3.28 to −5.01 kJ/mol. Using Eq. (1), ΔT_x is calculated for the modelled compositions as shown in Table 2. Depending on the higher negative values of P_{HS} modelled compositions are compared with the reported compositions in Table 2. The width of SCLR is found to be wider than that for reported compositions. The model composition range was also evaluated on the scale suggested by Senkov et al., [1, 15]. In the present work, the range of Ca, Mg, Cu is found to be 42 to 71 at %, 5 to 25 at %, 14 to 45 at %, respectively. The window of ΔT_x is 18.35 to 67.51K. Also, the P_{HS} values lie between −2.35 to −7.98 kJ/mol. The modeled values of Ca, Mg, Cu, ΔT_x, and P_{HS} are very close to that of reported values [1, 27]. It is observed that the current approach of composition design is more reliable than other existing models based on characteristic temperatures, which can be obtained after the experiments only [3].

Theoretical Estimation of Critical Cooling Rate (R_C)

Figure 5 shows the elemental viscosities of Ca, Mg, and Cu as a function of homologous temperature ($T_H = T/T_m$) from melting temperature to room temperature. A T_H represents the temperature of a material relative to its melting point [28]. The curves for Ca and Mg meet at higher T_H. The identical viscosity of Ca (1.22 mPa s) [22] and Mg (1.25 mP s) [22] at melting temperature could be the possible reason for this behavior. Figures 6a and 7a shows the viscosities of the reported and modelled compositions as a function of temperature. Investigation of 13 modelled compositions which are close to the 13 reported compositions, is evaluated. A similar magnitude of the viscosity at 300 K is noticed for both reported and modelled compositions in Figs. 6a and 7a, respectively. It is because

Table 2. Comparative analysis of reported and modelled compositions

Reported compositions	Reported ΔT_x	P_{HS}, kJ/mol	Modelled compositions	Modelled ΔT_x	P_{HS}, kJ/mol
$Ca_{55}Mg_{15}Cu_{30}$ [15]	40	−5.28	$Ca_{52}Mg_{16}Cu_{32}$	46.62	−5.60
$Ca_{45}Mg_{19}Cu_{36}$ [15, 17]	29	−5.99	$Ca_{42}Mg_{13}Cu_{45}$	67.51	−7.98
$Ca_{47.5}Mg_{22.5}Cu_{30}$ [1, 15]	41	−4.85	$Ca_{49}Mg_{11}Cu_{40}$	63.91	−7.57
$Ca_{55}Mg_{10}Cu_{35}$ [15, 17]	25	−6.67	$Ca_{57}Mg_{11}Cu_{32}$	49.52	−5.93
$Ca_{54}Mg_{18}Cu_{28}$ [17]	41	−4.76	$Ca_{52}Mg_{17}Cu_{31}$	44.42	−5.35
$Ca_{65}Mg_{5}Cu_{30}$ [15, 17]	21	−5.73	$Ca_{67}Mg_{5}Cu_{28.}$	42.93	−5.18
$Ca_{60}Mg_{13}Cu_{27}$ [15]	32	−4.73	$Ca_{63}Mg_{8}Cu_{29}$	44.42	−5.35
$Ca_{65}Mg_{10}Cu_{25}$ [15, 17]	32	−4.33	$Ca_{62}Mg_{5}Cu_{33}$	54.96	−6.55
$Ca_{70}Mg_{10}Cu_{20}$ [15, 17]	22	−3.18	$Ca_{70}Mg_{7}Cu_{23}$	31.25	−3.85
$Ca_{65}Mg_{20}Cu_{15}$ [15, 17]	19	−2.43	$Ca_{66}Mg_{19}Cu_{15}$	18.52	−2.40
$Ca_{65}Mg_{25}Cu_{10}$ [15, 17]	24	−1.81	$Ca_{62}Mg_{24}Cu_{14}$	18.08	−2.35
$Ca_{70}Mg_{20}Cu_{10}$ [15, 17]	29	−1.64	$Ca_{71}Mg_{9}Cu_{20}$	25.19	−3.16
$Ca_{60}Mg_{25}Cu_{15}$ [15, 17]	26	−2.53	$Ca_{61}Mg_{25}Cu_{14}$	18.35	−2.38

www.rmiet.edu.in

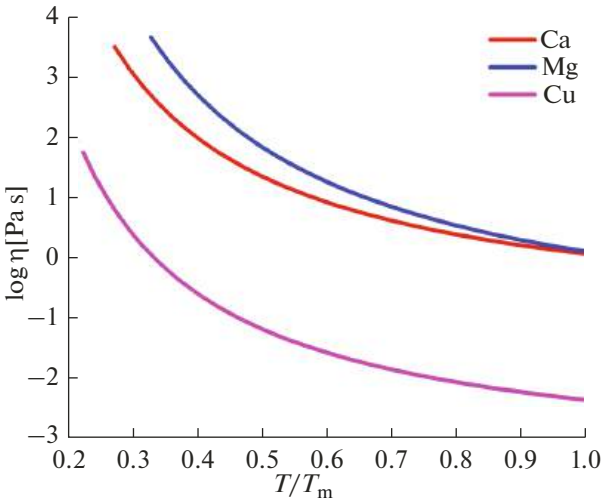

Fig. 5. Elemental viscosities of Ca, Mg and Cu as a function of homologous temperature.

of the assumption that the viscosity of all the compositions is equal to the 10^{12} Pa s at 300 K [12–14]. It is reported that in the supercooled liquid region (SCLR), viscosity changes from 10^{12} to 10^{9} Pa s [12] and decayed upto the T_m of the alloy. Table 3 indicates that the composition with maximum Ca content ($Ca_{70}Mg_{20}Cu_{10}$) exhibits maximum viscosity of 0.59 and 466.65 Pa s at T_m (1098 K) and T_g (356 K), respectively. At the same time, the composition with maximum Cu content ($Ca_{45}Mg_{19}Cu_{36}$) exhibits the lowest viscosity (0.16 Pa s) at T_m (1164 K). On the other hand, the composition with the lowest Mg ($Ca_{65}Mg_5Cu_{30}$) content has a lower viscosity (70.74 Pa s) at T_g (405 K). Similarly, viscosity values for modelled composition are also calculated at T_m. Table 3 showed that the predicted compositions with the lowest Ca content ($Ca_{42}Mg_{13}Cu_{45}$) exhibits lower viscosity of 0.11 Pa s at T_m (1197 K). On the other hand, composition $Ca_{62}Mg_{24}Cu_{14}$ has the highest viscosity (0.48 Pa s) among all predicted compositions at T_m (1100 K). From Table 3, it can be seen that the range of viscosities (0.11–48 Pa s) of the predicted compositions at T_m is close to the range of viscosities (0.16–59 Pa s) of the experimentally reported compositions [1, 15, 17]. This shows the significance of the present thermodynamic approach for the identification of the GFCs.

To achieve a glassy phase, it is important to suppress the crystallization of the molten liquid by rapidly solidifying the melt to room temperature [12]. The minimum rate to achieve this is called the critical cooling rate (R_C) [12]. In practice, it is difficult to measure R_C while experimenting due to the challenges posed by the mold attached to the thermocouples [12, 29]. Therefore, the concept of the TTT diagram proposed by Chattopadhyay et al., [13, 14] is used in the present work to calculate the R_C for both reported and modelled compositions. Figures 6b and 7b shows the TTT diagram for reported (R_{RC_TTT}) and modelled (R_{MC_TTT}), respectively. The presence of a broad nose indicates a large nucleation region for crystal formation [12]. The graphical illustration of reported and modelled compositions to calculate R_C is given in SI-3.a1–3.a13 and SI-4.b1–4.b13, respectively. Numerical values for R_C are given in Table 3. Figures 8 and 9 shows the variation in R_C with P_{HS} for reported and modelled compositions, respectively. For reported compositions, slope and R^2 is –0.96 and 94.5%,

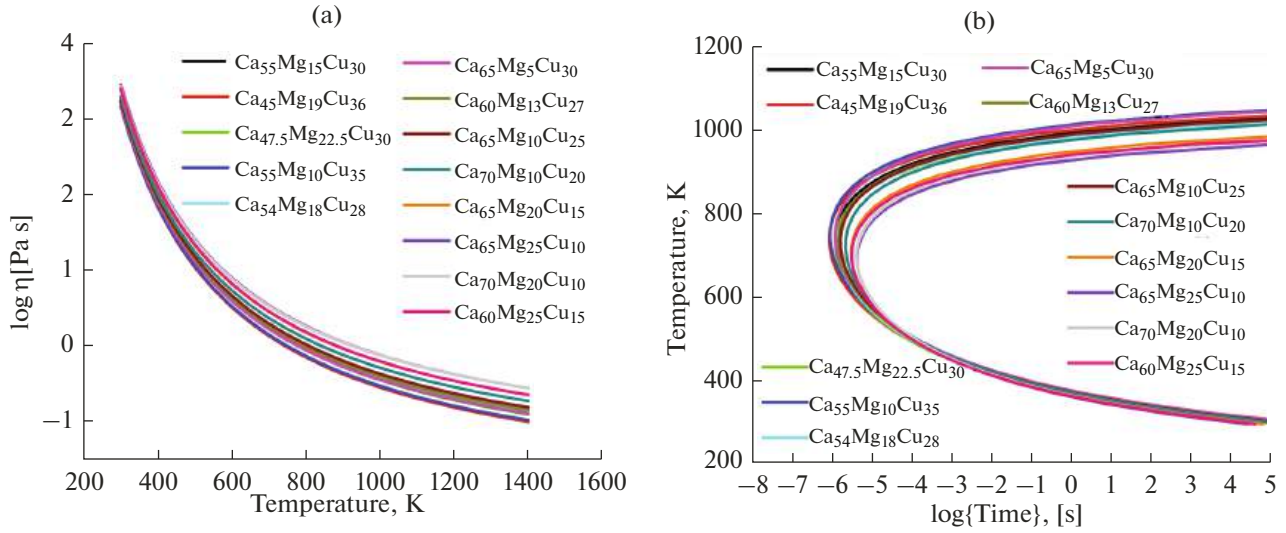

Fig. 6. (a) Viscosities as a function of temperature and (b) TTT diagram for the reported compositions.

www.nmiet.edu.in

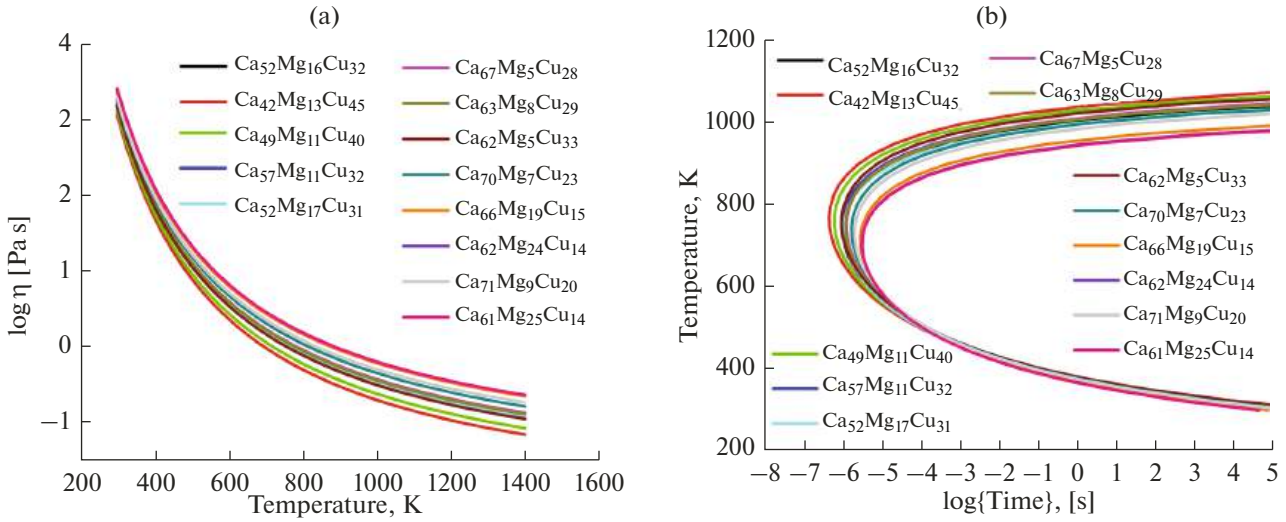

Fig. 7. (a) Viscosities as a function of temperature and (b) TTT diagram for the modelled compositions.

respectively. The negative slope demonstrates that as the P_{HS} becomes more negative, the cooling rate of the alloy increases. It is due to the decrease in the lower viscosity elements such as Ca (1.22×10^{-3} Pa s) and Mg (1.25×10^{-3}) (Fig. 2) with an increase in P_{HS} (i.e., becoming more negative). Similar observations are noted for modelled compositions, as seen in Fig. 9. The slope and R^2 are −1.13 and 85%. Although ΔH_{chem} and Δr of Cu is more with Ca than that of Mg, it is found that with an increase in Cu content, R_C of the alloy increases (Fig. 8), thereby increasing P_{HS} (See Fig. 2). The range of R_C for the reported compositions is 0.97×10^8–5.89×10^8 K/s. Similarly, for the modeled compositions, this range is 0.91×10^8–9.10×10^8 K/s which is close to the reported compositions. Minimum R_C (0.97×10^8 K/s) is obtained for $Ca_{65}Mg_{25}Cu_{10}$, which has the second largest viscosity (0.55) Pa s at T_m = 1089 K compared to other reported compositions (Table 1). $Ca_{55}Mg_{10}Cu_{35}$ has the maximum R_C (5.89×10^8 K/s) with the second lowest viscosity (0.17) Pa s at T_m = 1178 K. Similarly, for the

Table 3. Estimated critical cooling rate R_C (K/s) for reported and modelled composition

Reported compositions	η, Pa s T_m	Pa s T_g	$R_{RC_TTT}\times10^8$	Modeled compositions	η, Pa s T_m	$R_{MC_TTT}\times10^8$
$Ca_{55}Mg_{15}Cu_{30}$ [15]	0.22	85.31	3.85	$Ca_{52}Mg_{16}Cu_{32}$	0.21	4.19
$Ca_{45}Mg_{19}Cu_{36}$ [15, 17]	0.16	73.04	5.63	$Ca_{42}Mg_{13}Cu_{45}$	0.11	9.10
$Ca_{47.5}Mg_{22.5}Cu_{30}$ [1, 15]	0.22	80.24	3.94	$Ca_{49}Mg_{11}Cu_{40}$	0.14	6.76
$Ca_{55}Mg_{10}Cu_{35}$ [15, 17]	0.17	75.07	5.89	$Ca_{57}Mg_{11}Cu_{32}$	0.21	3.97
$Ca_{54}Mg_{18}Cu_{28}$ [17]	0.24	85.31	3.46	$Ca_{52}Mg_{17}Cu_{31}$	0.21	3.69
$Ca_{65}Mg_5Cu_{30}$ [15, 17]	0.21	70.74	4.04	$Ca_{67}Mg_5Cu_{28}$	0.23	3.10
$Ca_{60}Mg_{13}Cu_{27}$ [15]	0.24	90.69	3.50	$Ca_{63}Mg_8Cu_{29}$	0.22	3.12
$Ca_{65}Mg_{10}Cu_{25}$ [15, 17]	0.26	87.80	2.86	$Ca_{62}Mg_5Cu_{33}$	0.18	3.89
$Ca_{70}Mg_{10}Cu_{20}$ [15, 17]	0.33	158.48	2.17	$Ca_{70}Mg_7Cu_{23}$	0.29	2.44
$Ca_{65}Mg_{20}Cu_{15}$ [15, 17]	0.42	178.64	1.38	$Ca_{66}Mg_{19}Cu_{15}$	0.46	1.09
$Ca_{65}Mg_{25}Cu_{10}$ [15, 17]	0.55	135.05	0.97	$Ca_{62}Mg_{24}Cu_{14}$	0.48	1.05
$Ca_{70}Mg_{20}Cu_{10}$ [15, 17]	0.59	466.65	1.05	$Ca_{71}Mg_9Cu_{20}$	0.33	1.57
$Ca_{60}Mg_{25}Cu_{15}$ [15, 17]	0.47	143.21	1.33	$Ca_{61}Mg_{25}Cu_{14}$	0.47	0.91

www.rmiet.edu.in

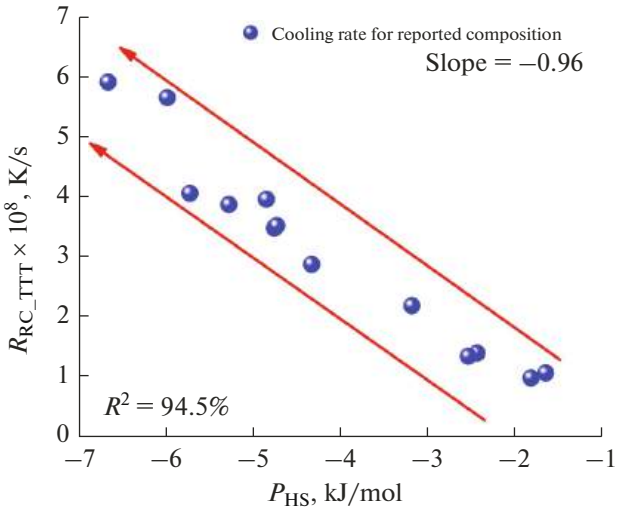

Fig. 8. Variation in critical cooling rate (R_{RC_TTT}) obtained by TTT approach for reported composition as a function of P_{HS}.

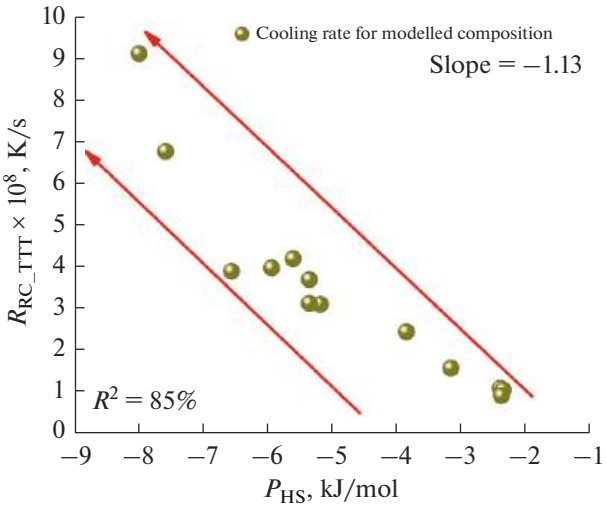

Fig. 9. Variation in critical cooling rate (R_{MC_TTT}) obtained by TTT approach for modelled composition as a function of P_{HS}.

modelled compositions, $Ca_{61}Mg_{25}Cu_{14}$ has the lowest R_C (0.91×10^8 K/s) with the second-highest viscosity (0.47) Pa s at T_m = 198 K. On the other hand, $Ca_{42}Mg_{13}Cu_{45}$ has the highest R_C (9.10×10^8 K/s) with the lowest viscosity (0.11) Pa s at T_m (1197 K) compared to that of other modelled compositions. Therefore, it can be said that the higher viscosity of the alloy promotes glass formation, thereby causing slow crystallization [12]. From the present work, it can be proposed that the alloy with higher Ca content will have better GFA. Higher R_C values in the present work were found two magnitudes higher than the typical cooling rate (10^6–10^7 K/s) in the melt spinning technique [12]. According to Eq. (12), viscosity of HCP phase formation is directly proportional to the exponential of ΔH_{chem}. Sufficiently large negative ΔH_{chem} would be the possible reason for higher viscosity in Ca-based bulk metallic glass. It has been mentioned in the literature that high viscosity liquid melt will not flow easily because of cooperative shear moments of the viscous melt [30]. This again resulted in rapid solidification when cooled to room temperature [31, 32]. This could be the possible reason for high cooling rate in Ca-based bulk metallic glass. A similar kind of critical cooling rate has also been reported by Khond et al., [12] and Chattopadhyay et al., [13] for Hf-based and high entropy alloy systems. The present investigation on the P_{HS} model confirms its validity in predicting GFC with the highest GFA, thereby estimating the R_C by TTT diagram for the Ca–Mg–Cu glassy alloy. Thermodynamic modeling (i.e., calculation of P_{HS}) and kinetic approach (i.e., calculation of TTT diagram) are the two simple methods to understand the glass-formation in the Ca–Mg–Cu metallic glasses and can be extended to the other glassy alloys before the experiment. It is important to note that T_m used in the calculation of the TTT diagram was calculated using the rule of mixture. Therefore, T_m values in the TTT diagrams are more compared to the experimental values as found in the reference 15. It is known fact that experimental T_m value of the alloy will always be less than the theoretical value. For example, experimental value of T_m for $Ca_{55}Mg_{15}Cu_{30}$ alloy is 626 K whereas theoretical values is 1157K.

CONCLUSIONS

The suitability of GFA parameter, P_{HS} in identifying the good glass-forming compositions (GFCs) in Ca–Mg–Cu alloy has been studied.

A small window of the P_{HS} with a range of –3.28 to –5.01 kJ/mol has been proposed to identify the good GFCs with a critical size of more than 5mm.

When lower viscosity elements such as Ca and Mg decreased, P_{HS} was found to increase, thereby reducing the GFA of the alloy.

The present study successfully demonstrates a strong correlation of ΔT_x with P_{HS} in the Ca–Mg–Cu system.

Comparative analysis of the critical cooling rate (R_C) for the reported and modelled compositions with P_{HS} has shown that R_C of the alloy will increase as the P_{HS} becomes more negative due to the minimum concentration of the low viscosity elements such as Ca and Mg.

Therefore, it can be suggested that the proper contribution of an element with sufficiently large mixing

www.nmiet.edu.in

enthalpy and atomic size difference with Ca, Mg, and Cu could be added to increase the glass formation ability and reduced the R_C.

The present approach is the yardstick for understanding the glass forming ability, identifying good glass forming compositions, and studying the kinetics in the Ca–Mg–Cu system.

ABBREVIATIONS

GFA, glass-forming ability; SCLR, supercooled liquid region; GFCs, glass-forming compositions; DSC, differential scanning calorimetry; TTT, time–temperature transformation; T_g, glass transition temperature; ΔH_{chem}, enthalpy of chemical mixing; $\Delta S_\sigma/k_B$, normalized mismatch entropy; $\Delta S_C/R$, normalized configurational entropy; R_C, critical cooling rate; homologous temperature, T_H; I, nucleation rate; u, growth rate; D, diffusion coefficient; η, viscosity.

FUNDING

One of the authors, Akash A. Deshmukh, thanks UGC, NEW DELHI, INDIA for providing Basic Science Research (BSR) fellowship. One of the authors, Jain Bhatt, would like to acknowledge the Science and Engineering Research Board grant (CRG/2019/003674) for research support.

CONFLICT OF INTEREST

The authors of this work declare that they have no conflicts of interest.

SUPPLEMENTARY INFORMATION

The supporting information includes the plot for variation in compositions with P_{HS} and time–temperature–transformation (TTT) diagrams for reported and modelled compositions.

The online version contains supplementary material available at https://doi.org/10.1134/S1087659622600211.

REFERENCES

1. Senkov, O.N., Miracle, D.B., Babilas, R., and Keppens, V., Fabrication of ternary Ca-Mg-Zn bulk metallic glasses, *J. Achievem. Mater. Manuf. Eng.*, 2013, vol. 56, no. 2, pp. 67–74.
2. Nowosielski, R., Borowski, A., Guwer, A., and Liaw, P.K., Development and characterization of low-density Ca-based bulk metallic glasses: An overview, *Metall. Mater. Trans., A*, 2008, vol. 39, pp. 1888–1990.
3. Chattopadhyay, C., Idury, K., S.N.S., Bhatt, J., Mondal, K., and Murty, B.S., Critical evaluation of glass forming ability criteria, *Mater. Sci. Technol.*, 2016, vol. 32, no. 4, pp. 380–400.
4. Bhatt, J., Jiang, W., Junhai, X., Qing, W., Dong, C., and Murty, B.S., Optimization of bulk metallic glass forming compositions in Zr-Cu-Al system by thermodynamic modeling, *Intermetallics*, 2007, vol. 15, nos. 5–6, pp. 716–721.
5. Vincent, S., Peshwe, D.R., Murthy, B.S., and Bhatt, J., Thermodynamic prediction of bulk metallic glass forming alloys in ternary Zr-Cu-X (X = Ag, Al, Ti, Ga) systems, *J. Non-Cryst. Solids*, 2011, vol. 357, nos. 19–20, pp. 3495–3499.
6. Rao, B.R., Shah, A.K., Srinivas, M., Bhatt, J., Gandhi, A.S., and Murty, B.S., On prediction of amorphous phase forming compositions in iron rich Fe-Zr-B ternary system and their synthesis, *Metall. Mater. Trans. A*, 2011, vol. 42, pp. 3913–3920.
7. Khond, A., Babu, D.A., Smaran, S., Deshmukh, A., Majumdar, B., Bhatt, J., and Srivastav, A.K., Thermodynamic calculation and experimental validation of Hf-rich glass forming compositions in Hf-Cu-Ni system, *J. Non-Cryst. Solids*, 2018, vol. 500, no. 15, pp. 191–195.
8. Vincent, S., Murty, B.S., and Bhatt, J., Prediction of bulk metallic glass formation in Cu-Zr-Ag-Hf system by thermodynamic and topological modeling, *Trans. Indian Inst. Met.*, 2012, vol. 65, pp. 827–831.
9. Bhatt, J., Dey, G.K., and Murty, B.S., Thermodynamic and topological modeling and synthesis of Cu-Zr-Ti-Ni-based bulk metallic glasses by mechanical alloying, *Met. Mater. Trans. A*, 2008, vol. 39, pp. 1543–1551.
10. Arvindhababu, D., Majmudar, B., Srivastava, A.P., Ramakrishnarao, B., Srivastava, D., Murty, B.S., and Akhtar, D., Structure, properties, and glass forming ability of melt-spun Fe-Zr-B-Cu Alloys with different Zr/B Ratios, *Metall. Mater. Trans. A*, 2011, vol. 42, pp. 508–516.
11. Bhatt, J. and Murty, B.S., Identification of bulk metallic forming compositions through thermodynamic and topological models, *Mater. Sci. Forum*, 2010, vol. 649, pp. 67–73.
12. Khond, A., Chattopadhyay, C., Majumdar, B., Bhatt, J., and Srivastav, A.K., Kinetic approach to determine the glass-forming ability in Hf-based metallic glasses, *Metall. Mater. Trans. A*, 2021, vol. 52, pp. 1169–1173.
13. Chattopadhyay, C. and Murty, B.S., Kinetic modification of the 'confusion principle' for metallic glass formation, *Scr. Mater.*, 2016, vol. 116, pp. 7–10.
14. Chattopadhyay, C., Prasad, A., and Murty, B.S., Phase prediction in high entropy alloys: A kinetic approach, *Acta. Mater.*, 2018, vol. 153, pp. 214–225.
15. Senkov, O.N., Scott, J.M., and Miracle, D.B., Composition range and glass forming ability of ternary Ca-Mg-Cu bulk metallic glasses, *J. Alloys Compd.*, 2006, vol. 424, nos. 1–2, pp. 394–399.
16. Amiya, K. and Inoue, A., Formation, thermal stability and mechanical properties of Ca-based bulk glassy alloys, *Mater. Trans. JIM*, 2002, vol. 43, no. 1, pp. 81–84.
17. Senkov, O.N., Miracle, D.B., and Scott, J.M., Development and characterization of Ca-Mg-Zn-Cu bulk metallic glasses, *Intermetallics*, 2006, vol. 14, nos. 8–9, pp. 1055–1060.
18. Niessen, A.K., de Boer, F.R., Boom, R., de Chatel, P.F., Mattens, W.C.M., and Miedema, A.R., Model predic-

www.rmiet.edu.in

tions for the enthalpy of formation of transition metal alloys II, *CALPHAD*, 1983, vol. 7, no. 1, pp. 51–70.

19. Deshmukh, A.A., Khond, A.A., and Palikundwar, U.A., Prediction of glass forming compositions in Al-Fe-Si alloy system by thermodynamic approach, *J. Non-Cryst. Solids*, 2017, vol. 477, pp. 50–57.
20. Guo, S. and Liu, C.T., Phase stability in high entropy alloys: Formation of solid-solution phase or amorphous phase, *Prog. Nat. Sci. Mater. Int.*, 2011, vol. 21, no. 6, pp. 433–446.
21. Takeuchi, A., Kato, H., and Inoue, A., Vogel-Fulcher-Tammann plot for viscosity scaled with temperature interval between actual and ideal glass transitions for metallic glasses in liquid and supercooled liquid states, *Intermetallics*, 2010, vol. 18, no. 4, pp. 406–411.
22. Battezzati, L. and Greer, A.L., The viscosity of liquid metals and alloys, *Acta Metall.*, 1989, vol. 37, no. 7, pp. 1791–1802.
23. Budai, I., Benko, M.Z., and Kaptay, G., Comparison of different theoretical models to experimental data on viscosity of binary liquid alloys, *Mater. Sci. Forum*, 2007, vols. 537–538, pp. 489–496.
24. Babilas, R., Andraczke, K.C., Babilas, D., and Simka, W., Structure and corrosion resistance of $Ca_{50}Mg_{20}Cu_{30}$ bulk metallic glasses, *J. Mater. Eng. Perform.*, 2015, vol. 24, pp. 67–174.
25. https://periodictable.com/Properties/A/FusionHeat.an.html.
26. https://periodictable.com/Properties/A/VaporizationHeat.an.html.
27. Kawazoe, Y., Watamura, U.C., and Takeuchi, A., *Phase Diagrams and Physical Properties of Nonequlibrium Alloys*, Vol. 37 (B), Part 2 of *Condensed Matter*, Berlin: Springer, 1997.
28. https://www.doitpoms.ac.uk/tlplib/creep/homologous.php.
29. Suryanarayana, C. and Inoue, A., *Bulk Metallic Glasses*, Boca Raton, FL: CRC, 2001.
30. Johnson, R.W., *Handbook of Fluid Dynamics*, 2nd ed., Boca Raton, FL: CRC, 2016.
31. Andrade, E.N., A theory of the viscosity of liquids, Part I, *Philos. Mag.*, 1934, vol. 17, pp. 497–511.
32. Busch, R., The thermophysical properties of bulk metallic glass-forming liquids, *J. Mater.*, 2000, vol. 52, pp. 39–42.

Publisher's Note. Pleiades Publishing remains neutral with regard to jurisdictional claims in published maps and institutional affiliations.

www.nmiet.edu.in

Materials Today: Proceedings 98 (2024) 160–165

Contents lists available at ScienceDirect

Materials Today: Proceedings

journal homepage: www.elsevier.com/locate/matpr

Synthesis and characterization of Al-AlN composite

Anuj Khond [a,*], Pranav Charkha [b], Harish Tiwari [c]

[a] Department of Mechanical Engineering, Nutan Maharashtra Institute of Engineering & Technology, Pune, Maharashtra 410507, India
[b] School of Engineering and Technology, D.Y. Patil University, Pune, Maharashtra 410507, India
[c] Pimpri Chinchwad College of Engineering & Research, Pune, Maharashtra 412101, India

ARTICLE INFO

Keywords:
Metal Matrix Composite (MMC)
Hardness
Interfacial angle
Wear

ABSTRACT

In the present work, Al-AlN metal matrix composite is synthesized by liquid metallurgy route. AlN particles are difficult to wet by molten Al because of their sinking tendency due to higher specific gravity. To retain them in a matrix for more time, it is attempted to add sintered powder compacts of Al and AlN into the Al melt at 1173 K using the vortex method. For the conceptual interfacial study of matrix and reinforcement, separate batches of Al-AlN composites with and without Mg are synthesized. The angle formed by particulate with matrix was studied to understand the bonding between them. Interfacial angle measurement indicates the improvement in the bonding of AlN particulates in Al matrix. Hardness is improved by 52% and specific wear rate reduced by 37% for Mg-modified Al-AlN composite than unmodified Al-AlN.

1. Introduction

Composite materials have emerged as a special class of material capable of superior mechanical, structural, and thermal properties [1]. Depending upon their application and desirable properties, composite materials are mainly classified into three types; metal matrix, polymer matrix, and ceramics matrix. Conventional materials such as Copper (Cu), Aluminum (Al), Titanium (Ti), Iron (Fe), etc. along with reinforcement like fiber, particulate, and whiskers can successfully produce metal matrix composite material. These composite materials are used in aerospace and aircraft industry, sports, and automotive applications [2]. Aluminum Matrix Composites (AMCs) have sparked a lot of interest in the scientific community because of their high-tech structural and functional applications which include aerospace, defense, automotive, electronic packing, precision instruments, sports equipment, and recreation; because of their high specific strength, stiffness, low density and thermal expansion coefficient [3]. Particulate reinforced AMCs have been studied extensively over fiber and whiskers due to their low production costs, uniform distribution of particulates, isotropic properties, and versatility in employing conventional techniques for their production and shaping [4]. Literature work has already demonstrated the effect of Al_2O_3, SiC, B_4C, AlN and MgO as particulate reinforcement in various matrixes [5–9]. There is very limited literature on AlN and hence it was used as reinforcement in the present work.

AlN possesses high mechanical strength, hardness, and thermal conductivity along with a low thermal coefficient of expansion [10]. Further, AlN particulate neither reacts chemically with aluminum nor deteriorates at high temperature [11]. AlN particle is preferred to synthesize composites using Al as the matrix due to its excellent characteristics. Al-AlN composites can be synthesized using different methods like gas-injection processing, pressureless liquid metal infiltration, spray deposition and hot pressing, melt infiltration of porous perform and squeeze casting. In synthesizing Al-AlN composites, wettability is the main concern irrespective of the synthesis method. The high surface activity of particles restricts their incorporation into the metal matrix. Researchers working in the field of composites focused on this issue and suggested measures to reduce the surface activity of particles [12]. To improve the bonding of particle, one technique is to add surfactant, which serves as a wetting agent in molten metal. Several surfactants have been successfully used by researchers, including Li and Mg for the synthesis of MMCs. Contreras et al. [13], Hashim et al. [14] reported the effect of Mg on Al-based matrix. Addition of 1 to 4 wt% Mg increases the wettability; however more than 4 wt% Mg results in the oxidation effect by decreasing the surface tension. Nassaj et al. [15] reported that addition of 2 wt% of Mg in Al melt, improved the wettability of the AlN particle which in turn enhanced the mechanical properties of the Al–AlN composite too. The significance of Mg is crucial and depending upon the quantity of matrix and reinforcement it is desirable to add small quantity of Mg as surfactant. With reference to the present work how much quantity of Mg is incorporated is discussed in supplementary file. Recent

* Corresponding author.
E-mail address: anujkhond22@gmail.com (A. Khond).

https://doi.org/10.1016/j.matpr.2023.10.039
Received 25 July 2023; Received in revised form 4 October 2023; Accepted 6 October 2023
Available online 14 October 2023
2214-7853/Copyright © 2024 Elsevier Ltd. All rights reserved. Selection and peer-review under responsibility of the scientific committee of the Second International Conference on Advances in Mechanical Engineering and Material Science.

www.mmiet.edu.in

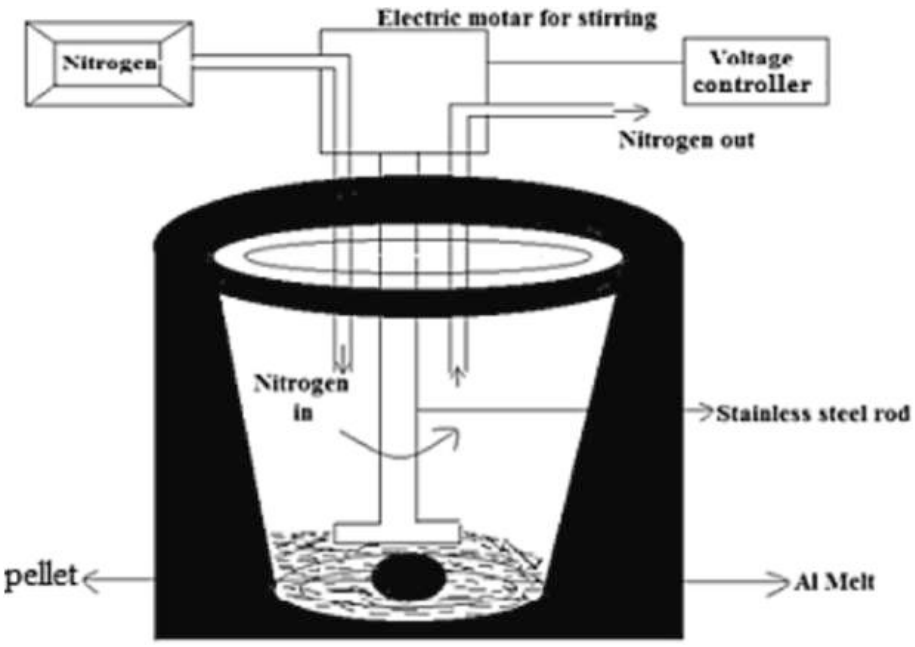

Fig. 1. Experimental setup for the synthesis of Al-AlN MMC.

research work on Al-based metal matrix composite has shown that the mechanical properties, wetting, and bonding between matrix and reinforcement can further improve if submicron- and nano-sized particles are used as reinforcing phase [16,17]. Al doesn't react with AlN hence Al-AlN composite is expected to be favorable material for the research community. Al-AlN MMCs exhibit enhanced refractory properties and wear resistance, in addition to the strengthening and stiffening effect of AlN in an Al matrix [18,19]. Al–AlN MMCs have received a lot of attention in the recent decade as they are well used for applications such as heat sinks of heat dissipation devices, electronic packing, materials, etc. in the energy and transportation sectors [20].

Based on the above framework, in the present work, an effort has been made to synthesize Al-AlN composite using vortex method. To understand the effect of Mg two separate batches of composite namely Al-AlN and Al-AlN-Mg were produced. The present paper discusses the interfacial study of AlN in Al matrix and mechanical properties of Al-AlN composite.

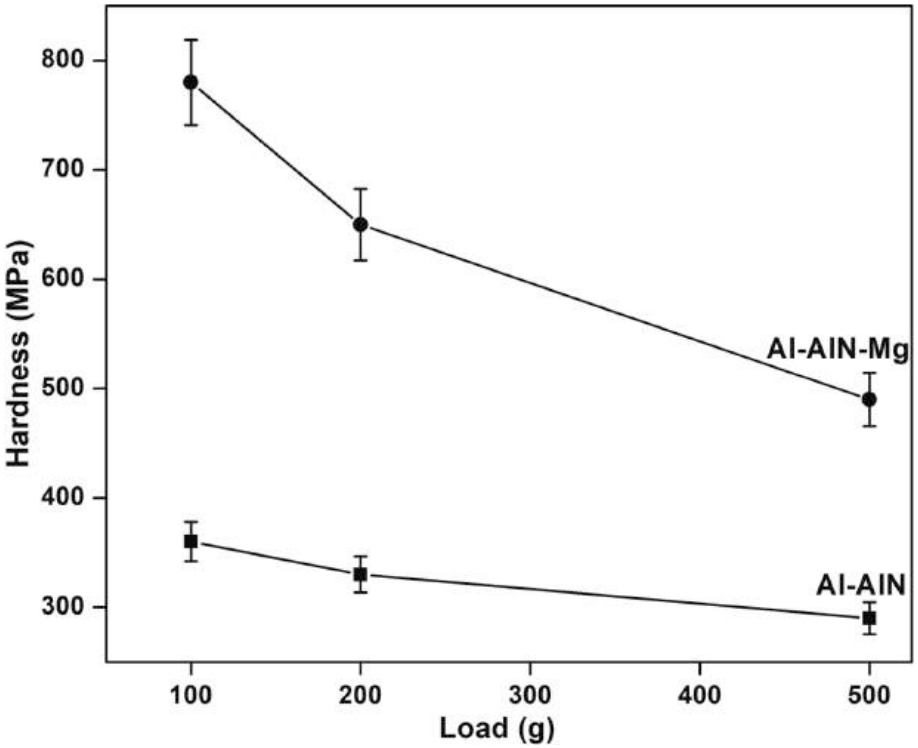

Fig. 2. Load vs. hardness graph of Al-AlN and Al-AlM-Mg composite.

www.mmiet.edu.in

2. Experimental details

Aluminum powder (Loba Chemie, 98% purity, particulate size 75 μm), AlN powder (40 nm particle size), and Mg powder (45 μm) are used as the primary material to make green pellets. Uniaxial Hydraulic machine is used to produce green pellets using pressure of 3 T. The applied pressure is just enough to hold the powder in pellet form. Al (20 g) and AlN (1.5 g) powder mixer in agate mortar and pestle prior to from green compact of Al-AlN. Similarly, green compact of Al (20 g), AlN (1.5 g), and Mg (0.043 g) powder was also produced. The load is applied for 1 min and pellets of 10 × 10 mm dimensions are formed. The sintering of the pellets is done at 0.8Tm of pure aluminum in the sintering furnace. The sintering temperature of 800 K allows a high diffusion rate to enhance sintering. Raising the sintering temperature shortens the time required to achieve full density. For Sample of dimensions 4–6 mm, thick time required is 10–15 min for sintering, if the thickness is increased up to 25–50 mm then 30–40 min is needed for sintering [21]. Commercial Al ingot (HINDALCO, 99.7% pure) 100 g melted in graphite crucible using pit furnace. The protective atmosphere was maintained by purging nitrogen gas continuously in the furnace chamber during synthesis. Sintered pellets are added into Al melt when temperature is reached at 1173 K. Al melt is stirred continuously with mechanical stirrer driven by a motor located over pit furnace and finally melt is cast in permanent mould of plain carbon steel. The schematic of the synthesis setup is shown in Fig. 1.

Hardness test was conducted under loads of 100, 200, and 500 g on the synthesized AMCs by MITUTOYO Vickers's Microindentation hardness testing machine (HM-112). Hardness is tested at various locations and average reading of eight indentations was considered for plotting the graph. Composite samples are fine polished and observed under the scanning electron microscope JEOL JSM-6380A in unetched conditions to study the morphology of particles. Contact angle of AlN particles in synthesized composite is measured from the SEM image using ImageJ software. DUCOM TR-20LE-M1 is used to conduct wear testing of composites. The dry, sliding wear testing of sample (size 10 mm × 25 mm L) was performed under loads 5, 10, and 20 N. The sliding distance and track radius were 1000 m and 35 mm respectively at 450 RPM were kept constant during wear tests.

3. Results and discussion

3.1. Hardness of composites

Fig. 2 shows the variation of hardness with applied load of synthesized Al–AlN and Al–AlN–Mg composites. Hardness of Al-AlN and Al-AlN-Mg is tested at 8 various locations and average value was considered for plotting the graph. The error bar indicates variation in hardness value by 3% and 5% for Al-AlN and Al-AlN-Mg respectively. Hardness of Al-AlN-Mg composite is increased by 52%, 48%, and 42%, at 100 g, 200 g, and 500 g respectively compared to the Al-AlN composite. This indicates higher volume fraction of particulates incorporated in Al-AlN-Mg composite than Al-AlN. It highlights the significance of Mg in synthesizing composites. Mg decreases interfacial angle of Al-AlN, responsible for enhancing the bonding of composites. Mg being oxygen getter readily forms different oxides like MgO and $MgAl_2O_4$ [22]. Formation of these oxide layers on the surface during the synthesis of Al-AlN-Mg composite promotes the hardness. The tester's inherent interference, the sample's surface roughness, and oxidation all influence the hardness measurements. In the confined zone, the melt numbers of particles are more this means inter particle distance between two particles is less. Decreasing distance between AlN particles increases the required tension for dislocation movement resulting in higher composite hardness. Addition of Mg in Al-AlN composite promotes interfacial bonding of nanostructured AlN and high volume fraction of particulates introduces pinning effect in solidified composites leading to grain refined structure. The inclusion of Mg and AlN in the matrix gives the Al-AlN-Mg composite its exceptional hardness. The literature results demonstrate that the effect of Mg addition is more predominant than that of the reinforcement. Hence remarkably large variation is observed in hardness of Al-AlN-Mg than Al-AlN composite shown in Fig. 2. The reaction of aluminum with alumina to form spinel is thermodynamically favored at low temperatures. As the amount of Mg in equilibrium with Al_2O_3 increases with temperature and when alumina and melt are in contact with each other for long time, spinal structure of $MgAl_2O_4$ is formed [23].

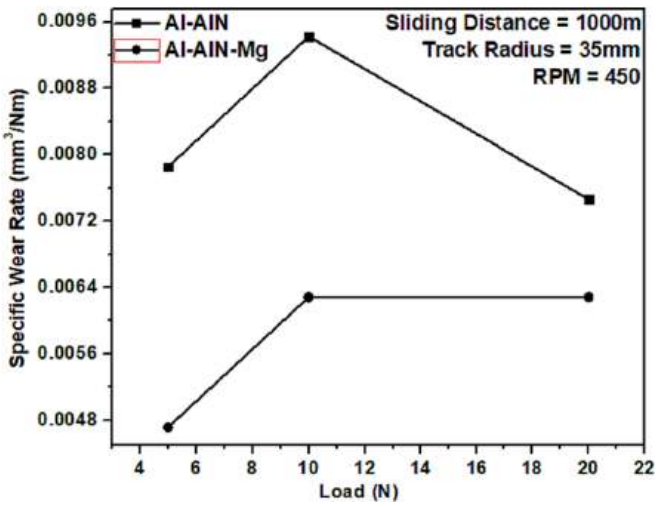

Fig. 3. Specific wear rate against load for Al-AlN and Al-AlN-Mg composite.

When AlN ceramic reinforcements are added to an aluminum matrix, the matrix properties change. The changes in matrix occur because of compositional variation in matrix and the interfacial reaction between the matrix and reinforcement during processing. The difference in thermal expansion coefficient between the matrix (Al = 23×10^{-6}/°C) and the reinforcements (AlN = 11.2×10^{-6}/°C) creates thermal residual stresses and a high density of dislocations around the interfaces, enhancing diffusion and promoting the precipitation of different oxides [24]. The hardness of the Al-AlN-Mg composite was 52% higher than Al-AlN composite at 100 g load as shown in Fig. 2 and in addition, varied with the reinforcement particle size (d), its distribution, and volume fraction (v). Deformation, grain refining, and solid dispersion are all known to promote the hardening of metals and alloys. Addition of Mg in Al-AlN composite promotes a high degree of deformation, reduces the grain size, and produces an extremely fine distribution of oxides, nitrides, etc. depending on the processing parameters in composite material. The precipitation of tiny isolated oxide particles and intermetallic $MgAl_2O_4$ in the matrix attributed to the rise in matrix hardness. The presence of hard phases like Al_2O_3 and MgO are responsible for increasing the overall hardness of the matrix.

3.2. Wear studies

In many engineering applications, wear rate is one of the most important parameter of material life. The existence of reinforcement material; its volume fraction and formation of hard phases during the synthesis process if any significantly affect the wear behavior of composites.

Fig. 3 shows wear test results of Al-AlN and Al-AlN-Mg composites under the varying load over a distance of 1000 m. The wear performance is indicated in terms of specific wear rate of composites during the test. Al-AlN composite shows higher specific wear rate at different loading conditions. Specific wear rate gradually increases with loading from 5 to 10 N and then suddenly decreases at higher load. This indicates that Al-AlN composite unable to withstand higher load owing to the weak interfacial bonding of matrix and reinforcement. On the contrary, Al-

www.nmiet.edu.in

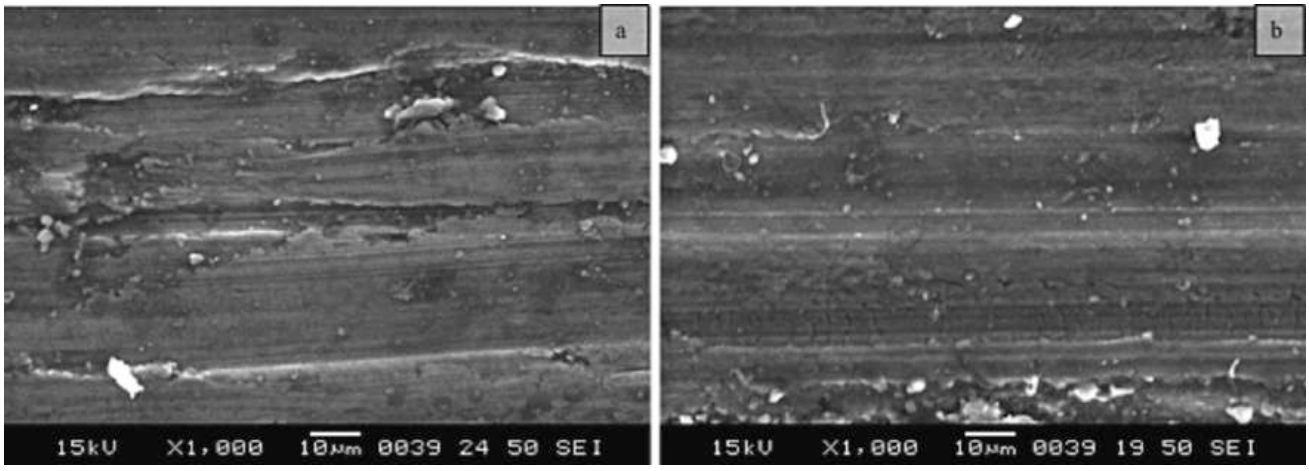

Fig. 4. (a) SEM Micrograph of wear track Al-AlN (b) Al-AlN-Mg composite at 20 N.

AlN-Mg composite indicate relatively lower specific wear rate than the former ones. This confirms that the latter ones composite sample sustained its strength and the specific wear rate almost remains constant from 10 to 20 N. This indicates that Mg is playing an important role and bonding between the matrix and reinforcement becoming stronger. It is interesting to observe specific wear rate of composite at higher load of 20 N. The possible reason for decreasing the specific wear rate (Al-AlN) is, the generation of localized frictional heat which will entrap AlN particles in Al matrix. The existence of Mg particles will form the phases such as MgO and $MgAl_2O_4$ in addition to Al_2O_3 during the synthesis process [25,26]. These hard phases along with the AlN agglomerates reduce composite's specific wear rate. These results can be proved from the plot of Al-AlN-Mg composites which indicate comparatively constant slope of specific wear rate at higher load of 20 N (Fig. 3).

3.2.1. Scanning electron microscopy of wear track

Fig. 4 shows the wear track of SEM micrograph of Al-AlN and Al-AlN-Mg composites tested under the load of 20 N for the sliding distance of 1000 m. Al-AlN composite (Fig. 4 (a)) reveals the worn-out surface of sample. Surface shows broad score marks which may be due to removal of debris from the pin. In addition, photomicrograph also reveals to show subsurface cracks which indicate that composite is unable to sustain under 20 N. Such cracks could be due to easy detachment of AlN particles from the surface. AlN leaves apart from Al (matrix in bulk) exposed to wear, got heavily work-hardened leading to cracks formation on the surface. The intense work hardening causes these cracks to propagate into the matrix and also widened under the higher load of 20 N indicating sudden decrease in specific wear rate of Al-AlN composite. Al-AlN-Mg composites show better specific wear rate at load of 20 N under the same testing condition than the former one. Fig. 3 and Fig. 4 (b) correspond to each other; specific wear rate of Al-AlN-Mg is less, indicating the crack free surface on SEM micrograph. The debris from the surface layer is removed in the same direction of pin travel as observed by wear track (Fig. 4 (b)). Photomicrograph does not disclose substantial deterioration of surface layer. This might be due to strong bonding of AlN with the matrix. Moreover, it was also, anticipated that formation of hard oxide phases such as $MgAl_2O_4$, MgO, and Al_2O_3 are responsible for reducing specific wear rate of Al-AlN-Mg composite. In the present work the author has not done any investigation to prove the presence of $MgAl_2O_4$, MgO, and Al_2O_3 due to limited facility but the

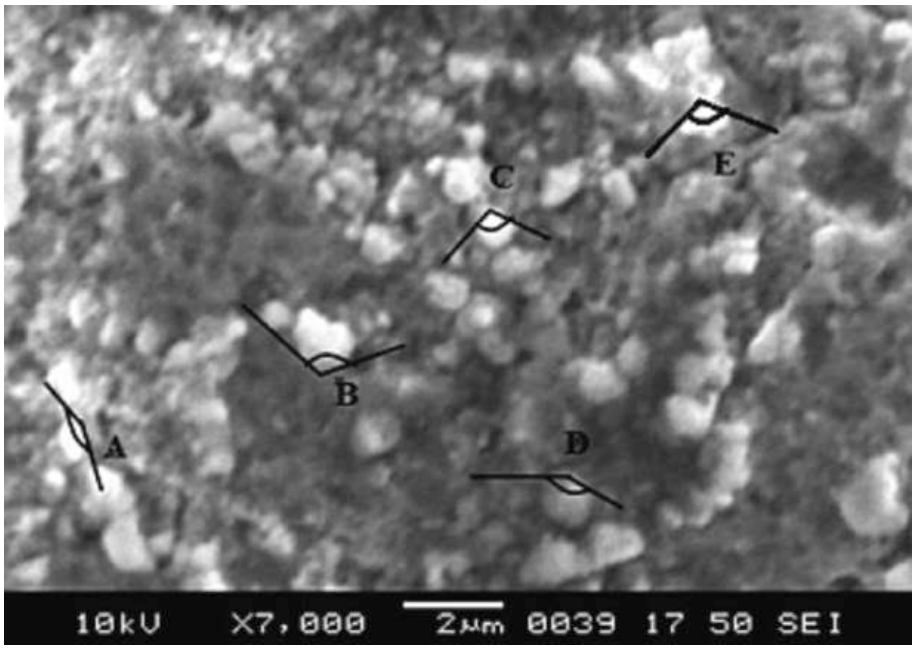

Fig. 5. SEM image of Al-AlN composite, indicate the interfacial angle values of AlN particulate in the matrix.

www.mmiet.edu.in

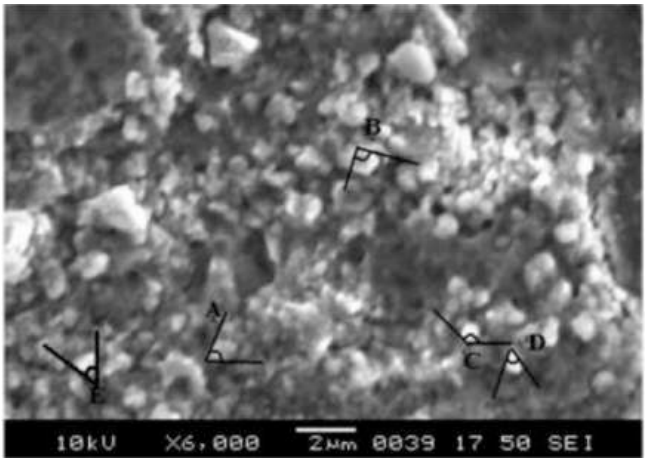

Fig. 6. SEM image Al-AlN-Mg composite, indicate the interfacial angle values of AlN particulate in the matrix.

same is claimed with the help of existing literature support [27,28]. The overall observation of the wear tracks indicates comparatively better performance of Al-AlN-Mg than that of Al-AlN composites.

3.3. Measurement of interfacial angle from SEM micrographs

Scanning Electron Microscopy (SEM) of synthesized Al-AlN and Al-AlN-Mg composite was carried out to study the distribution and morphology of AlN particles. AlN particles and Al matrix appear as bright and dark respectively. This is due to the inherent property possessed by the ceramic material. AlN has lower electrical conductivity in comparison to Al. Hence when electrons are targeted on composite specimens AlN particles having low electrical conductivity do not allow the electron beam to pass through them and it appears bright. Al is a good conductor of electricity and the electron beam is easily passed through the matrix hence it appears dark. This effect is known as the charging effect [29]. AlN particles can be seen in agglomerated form and unevenly distributed in Al matrix as shown in Figs. 5 and 6. This is because of (i) higher surface activity of nanostructured AlN particles and (ii) high volume to the surface area ratio of Al and AlN powder particles. From the SEM image, the spherical type of AlN particles was selected and interface angle with matrix was measured in ImageJ software. It is evident from the photomicrographs that morphology of the agglomerated AlN particles is spherical. Fig. 6 shows the clear interface between the Al and AlN. The presence of an oxide layer on the molten aluminum surface is an important feature of this experiment. This avoids direct contact between the molten metal and the solid substrate, resulting in a large interfacial angle in the initial stages. The oxide layer formed at the interface feebler the bonding of Al-AlN as indicated by high interfacial angle. The alloy composition, gas environment, and temperature all affect the stability of this oxide layer. From Fig. 5 it is confirmed that maximum interfacial angle (Angle suspended by matrix and reinforcement) is 155° and all the particles making angle (θ) greater than 90° are weakly bonded with each other. The microchannel and roughness on AlN particles remain free of liquid in this state, resulting in poor matrix bonding. Fig. 6 shows the SEM image of Al-AlN-Mg composite. Addition of Mg reduces the interfacial angle and minimum value is found as 58°. It can be confirmed that even though the Mg is added in Al-AlN composite, maximum interfacial angle is still found to be 135° at one location and minimum is 52°. It indicates that all the particles are not bonded strongly and the particle showing $\theta = 135°$ indicate weak bonding. The reactions that occur at the molten metal/substrate interface and nitrogen gas during the synthesis process are complex [30]. These extremely confined reactions destabilized the oxide layer and create the thermodynamically advantageous wetting situation. Because the ceramic/metal interaction was continuous, with no gaps or cracks, interfacial adhesion was generally good.

ABC is the interfacial angle formed at molten Al droplet and AlN substrate. When the $MgAl_2O_4$ an intermetallic compound formed on it, the interfacial angle drastically reduces to DBC which is less than the former. From Fig. 7, the reduction in wetting angle indicates that the Al drop spread well on the AlN particle and good adhesion is feasible for strong bond formation. As the strong bond forms between AlN particle and Al melt, it ultimately leads to the improvement in the mechanical properties. Al_2O_3 is the only reaction product formed at the pure Al/AlN interface, however, the reaction products such as MgO and $MgAl_2O_4$ are observed at the Al–Mg/AlN interface [31]. Because of the formation of chemical bonds at the interface, intermetallic phases are better for wetting ceramic surfaces than metals. Therefore, bonding is improved by the addition of Mg to aluminum. When Mg is added to aluminum, an interaction layer forms, and the surface tension of liquid aluminum is lowered due to the adsorption of this intermetallic phase on the liquid's surface. This results in improving bonding by decreasing the interfacial angle.

4. Conclusions

- Al-AlN metal matrix composites were produced by liquid metallurgy route using vortex method.

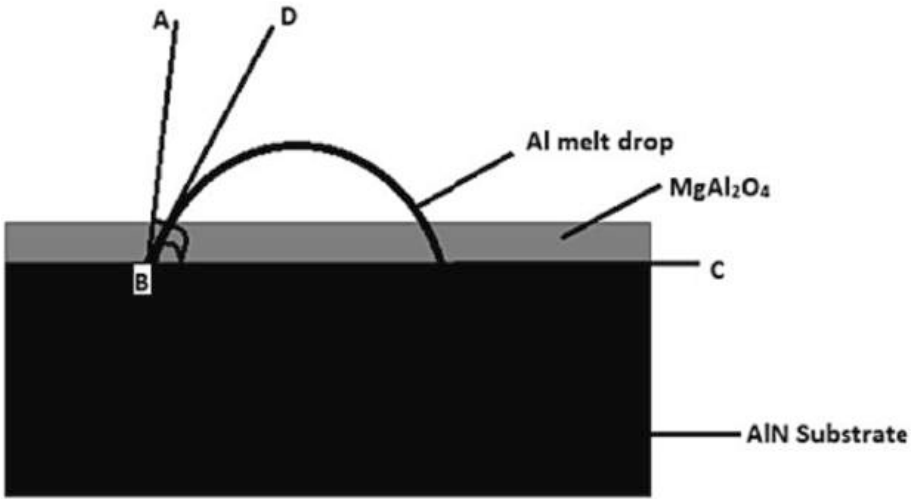

Fig. 7. Influence of $MgAl_2O_4$ on interfacial angle.

www.nmiet.edu.in

- AlN particles were not uniformly distributed in the matrix. Interfacial bonding of AlN particulate was enhanced in Al-AlN-Mg composite than that of Al-AlN.
- The formation of oxides layer at the interface of Al-AlN-Mg favours the bonding of AlN particulates in Al melt.
- The specific wear rate and hardness of Al-AlN-Mg composite is superior to that of Al-AlN due to the formation of hard oxide phases.
- The interfacial study of AlN particle with Al matrix and their corresponding mechanical properties corresponds to each other.
- However, author strongly beloved that further experimentation and analysis are still required to understand the interfacial phenomena of AlN in Al matrix.

CRediT authorship contribution statement

Anuj Khond: Conceptualization, Methodology, Validation, Formal analysis, Investigation, Writing – original draft. **Pranav Charkha:** Writing – review & editing, Supervision. **Harish Tiwari:** Writing – review & editing, Supervision.

Declaration of competing interest

The authors declare that they have no known competing financial interests or personal relationships that could have appeared to influence the work reported in this paper.

Data availability

No data was used for the research described in the article.

Acknowledgment

The authors are thankful to Dr. Jatin Bhatt for their valuable discussion to improve the quality of the paper. One of the authors Dr. Anuj Khond is also thankful to Dr. Sandeep Fale for providing the necessary powder and experimental setup to synthesize Al-AlN metal matrix composite.

Appendix A. Supplementary material

Supplementary data to this article can be found online at https://doi.org/10.1016/j.matpr.2023.10.039.

References

[1] T.W. Clyne, D. Hull, An Introduction to Composite Materials, 3rd ed., Materials Research Society, 2019.
[2] N. Chawla, K.K. Chawla, Metal Matrix Composites, 2nd ed., Springer, 2013.
[3] M.K. Surappa, Aluminium matrix composites: challenges and opportunities, Sadhana 28 (2003) 319–334.
[4] M.K. Surappa, P.K. Rohatgi, Preparation and properties of cast aluminium-ceramic particle composites, J. Mater. Sci. 16 (1981) 983–993.
[5] A. Alizadeh, E. Taheri-Nassaj, M. Hajizamani, Hot extrusion process effect on mechanical behavior of stir cast Al based composites reinforced with mechanically milled B4C nanoparticles, J. Mater. Sci. Technol. 27 (2011) 1113–1119.
[6] H.R. Ezatpour, S.A. Sajjadi, M.H. Sabzevar, Y. Huang, Investigation of microstructure and mechanical properties of Al6061-nanocomposite fabricated by stir casting, Mater. Des. 55 (2014) 921–928.
[7] S. Mula, P. Padhi, S.C. Panigrahi, S.K. Pabi, S. Ghosh, On structure and mechanical properties of ultrasonically cast Al-2% Al_2O_3 nanocomposite, Mater. Res. Bull. 44 (2009) 1154–1160.
[8] A.D. Hamedan, M. Shahmiri, Production of A356–1wt% SiC nanocomposite by the modified stir casting method, Mater. Sci. Eng. A 556 (2012) 921–926.
[9] A.A. Yar, M. Montazerian, H. Abdizadeh, H.R. Baharvandi, Microstructure and mechanical properties of aluminum alloy matrix composite reinforced with nanoparticle MgO, J. Alloy. Compd. 484 (2009) 400–404.
[10] J.A. Hooker, P.J. Doorbar, Metal matrix composites for aeroengines, Mater. Sci. Technol. 16 (2000) 725–731.
[11] Y.B. Liu, S.C. Lim, L. Lu, M.O. Lai, Recent development in the fabrication of metal matrix-particulate composites using powder metallurgy techniques, J. Mater. Sci. 29 (1994) 1999–2007.
[12] S. Suresh, A. Mortensen, A. Needleman, Fundamentals of Metal-Matrix Composites. 2013.
[13] A. Contreras, E. Bedolla, R. Pérez, Interfacial phenomena in wettability of TiC by Al-Mg alloys, Acta Mater. 52 (2004) 985–994.
[14] J. Hashim, L. Looney, M.S.J. Hashmi, The enhancement of wettability of SiC particles in cast aluminium matrix composites, J. Mater. Process. Technol. 119 (2001) 329–335.
[15] Y.B. Tang, Y.Q. Liu, C.H. Sun, H.T. Cong, AlN nanowires for Al-based composites with high strength and low thermal expansion, J. Mater. Res. 22 (2007) 2711–2718.
[16] H. Ahamed, V. Senthilkumar, Experimental investigation on newly developed ultrafine-grained aluminium based nano-composites with improved mechanical properties, Mater. Des. 37 (2012) 182–192.
[17] M.K. Akbari, O. Mirzaee, H.R. Baharvandi, Fabrication and study on mechanical properties and fracture behavior of nanometric Al_2O_3 particle-reinforced A356 composites focusing on the parameters of vortex method, Mater. Des. 46 (2013) 199–205.
[18] P. Yu, M. Balog, M. Yan, G.B. Schaffer, M. Qian, In situ fabrication and mechanical properties of Al-AlN composite by hot extrusion of partially nitrided AA6061 powder, J. Mater. Res. 26 (2011) 1719–1725.
[19] K. Kondoh, J. Umeda, R. Watanabe, Cavitation resistance of powder metallurgy aluminum matrix composite with AlN dispersoids, Mater. Sci. Eng. A 499 (2009) 440–444.
[20] M. Balog, P. Krizik, P. Svec, L. Orovcik, Industrially fabricated in-situ Al-AlN metal matrix composites (part A): Processing, thermal stability, and microstructure, J. Alloy. Compd. 883 (2021), 160858.
[21] A. Lawley, T.F. Murphy, Metallography of powder metallurgy materials, Mater Charact 51 (2003) 315–327.
[22] W. Yang, G. Chen, J. Qiao, Q. Zhang, R. Dong, G. Wu, Effect of Mg addition on the microstructure and mechanical properties of SiC nanowires reinforced 6061Al matrix composite, Mater. Sci. Eng. A 689 (2017) 189–194.
[23] B. Ashok Kumar, N. Murugan, Metallurgical and mechanical characterization of stir cast AA6061-T6-AlNp composite, Mater. Des. 40 (2012) 52–58.
[24] A. Rodrigo, P. Perillo, H. Ichimura, On the correlation of substrate microhardness with the critical load of scratch adherence for hard coatings, Surf. Coat. Technol. 124 (2000) 87–92.
[25] X. Wang, D. Jiang, G. Wu, B. Li, P. Li, Effect of Mg content on the mechanical properties and microstructure of Grf/Al composite, Mater. Sci. Eng. A 497 (2008) 31–36.
[26] L. Geng, H. Zhang, H. Li, L. Guan, L. Huang, Effects of Mg content on microstructure and mechanical properties of SiCp/Al-Mg composites fabricated by semi-solid stirring technique, Trans. Nonferrous Met. Soc. China 20 (2010) 1851–1855.
[27] Q. Zhang, X. Ma, G. Wu, Interfacial microstructure of SiCp/Al composite produced by the pressureless infiltration technique, Ceram. Int. 39 (2013) 4893–4897.
[28] R. Mitra, V.S. Chalapathi Rao, R. Maiti, M. Chakraborty, Stability and response to rolling of the interfaces in cast Al-SiCp and Al-Mg alloy-SiCp composites, Mater. Sci. Eng. A 379 (2004) 391–400.
[29] S. Babin, S. Borisov, Y. Miyano, H. Abe, M. Kadowaki, A. Hamaguchi, Y. Yamazaki, Experiment and simulation of charging effects in SEM. Insp. Process Control Microlithography. XXII, SPIE, 2008, p. 692219.
[30] J. Haibo, K. Chen, Z. Heping, S. Agathopoulos, O. Fabrichnaya, J.M.F. Ferreira, Direct nitridation of molten Al (Mg, Si) alloy to AlN, J. Cryst. Growth 281 (2005) 639–645.
[31] Y. Ohya, Y. Ishii, T. Ban, Reaction of molten aluminum with MgO and formation of $MgAl_2O_4$ spinel at 1000°C, Mater. Trans. JIM 61 (2020) 339–345.

www.nmiet.edu.in

Nano World Journal

https://doi.org/10.17756/nwj.2023-s4-019

Research Article

Open Access

Experimental Performance and Comparison of Sustainable Cooling Techniques for Solar (Photovoltaic) Panel

Sagar Wankhede[1*], Pralhad Pesode[2], Dhanaji Jadhav[3], Yogesh Mane[4] and Manoj Mugale[5]

[1]*School of Mechatronics Engineering, Symbiosis Skills and Professional University, Pune, Maharashtra, India*

[2]*School of Mechanical Engineering, Dr. Vishwanath Karad MIT-World Peace University, Pune, Maharashtra, India*

[3]*Department of Mechanical Engineering, Nutan Maharashtra Institute of Engineering and Technology, Pune, Maharashtra, India*

[4]*National Institute of Technology, Tiruchirappalli, Tamil Nadu, India*

[5]*Cleveland State University, Cleveland, Ohio, USA*

[*]Correspondence to:
Sagar Wankhede
School of Mechatronics Engineering,
Symbiosis Skills and Professional University,
Pune, Maharashtra, India.
E-mail: svw8890@gmail.com

Received: September 15, 2023
Accepted: November 21, 2023
Published: November 24, 2023

Citation: Wankhede S, Pesode P, Jadhav D, Mane Y, Mugale M. 2023. Experimental Performance and Comparison of Sustainable Cooling Techniques for Solar (Photovoltaic) Panel. *NanoWorld J* 9(S4): S105-S112.

Copyright: © 2023 Wankhede et al. This is an Open Access article distributed under the terms of the Creative Commons Attribution 4.0 International License (CCBY) (http://creativecommons.org/licenses/by/4.0/) which permits commercial use, including reproduction, adaptation, and distribution of the article provided the original author and source are credited.

Published by United Scientific Group

Abstract

Solar panels are necessary for capturing renewable energy, but extreme heat can shorten their lifespan and reduce their effectiveness. Sustainable cooling techniques have been investigated as a solution to this problem. In order to improve solar panel performance, this study compares various cooling techniques, including watermelon rind, banana leaves, wet soil, green net, coir, and jute bags. The study intends to assess how well these methods work in lowering panel temperature and raising overall effectiveness. Key performance indicators used in the controlled studies were voltage output and temperature. The outcomes of the experiment show that various cooling methods have variable effects on solar panels' ability to regulate temperature. Due primarily to its evaporative cooling abilities, watermelon rind displayed the highest voltage output and significant temperature reduction. Watermelon rind surpassed banana leaves, wet soil, green net, coir, and jute sack in terms of voltage output and temperature reduction. The comparative analysis shows how each method works well in reducing temperature rise and enhancing solar panel efficiency. These results offer useful information to solar panel system stakeholders, assisting in the selection of appropriate sustainable cooling methods based on their effectiveness and suitability for certain environmental circumstances. Overall, by enhancing the effectiveness and dependability of solar panel systems, the experimental performance and comparison of these cooling strategies advance renewable energy technology.

Keywords

Renewable energy, Solar panel, Sustainable, Cooling, Technique, Power

Introduction

Due to their limitations, traditional sources of energy cannot be trusted [1, 2]. Solar energy is one of the renewable energies that are expanding the quickest. Solar radiation is converted into electricity by solar cells and collectors, which is then utilized to produce energy. Solar energy can not only be utilized to generate electricity but also for heating and cooling purposes. Although solar photovoltaic (PV) and thermal collectors have made great strides, they still need auxiliary parts, including energy storage that drives up the cost of the system as a whole [3]. The effectiveness of solar PV systems has been thoroughly examined in order to produce higher energy per unit area [4]. Researchers [5] have also shown the value of the local climate for solar PV installations. The adoption of these technologies has increased as a result of government initiatives to promote solar energy [6]. Only

www.mriet.edu.in

5% to 20% of the solar energy received by a typical PV module is converted into electrical power, depending on the solar cell type and environmental factors. Higher current or voltage settings often improve the electrical performance properties of a PV cell or module. Current characteristics can be enhanced by maximizing incoming solar radiation using conventional concentrators. Cuce et al. [7] has investigated the connection between G and I_{SC} under various humid environments. The level of humidity has no effect, according to the results [8].

Shockley's ideal diode equation needs two resistors in order to accurately and realistically describe the electrical behavior of a PV cell or module. The five-parameter technique is the name of this technique. Researchers are aware that the cell temperature, which is frequently observed in warm and humid environments, has a significant impact on the energy performance characteristics of PV modules [9]. When all the advantages and disadvantages are considered, solar cells may end up winning out. For example, a solar updraft tower starts off significantly more expensively and is less effective than PV [10]. Solar cells allow for the direct conversion of the photon energy of light into electrical power. For solar thermal collectors or solar updraft towers, on the other hand, expensive auxiliary equipment such turbines, generators, pipes, etc. is required [11, 12]. Despite whatever advantages crystalline silicon solar cells could have, there are still a number of challenges that may hinder us from utilizing these attractive devices as much as we would like. The device's fragility and sensitivity to dust collection [13], poor efficiency (between 15% and 25%) [14], and sensitivity to its operating temperature [15] are just a few of the challenges faced by researchers. To address these problems and pave the way for the subsequent generation of scientific articles, thousands of publications based on these criteria have been produced.

The effects of operating temperature on PV modules are examined in this study. The sensitivity of PV modules to operational temperature decreases by 0.4% to 0.65% with each degree of temperature rise [16]. The explanation for this phenomenon is given in detail by Bernardo et al. [17]. According to his paper, PV modules short-circuit current (I_{SC}) increases noticeably as its temperature rises. However, both the power output and the open-circuit voltage (V_{OC}) reduce dramatically. For example, crystalline silicon cells demonstrate that the maximum power achievable and V_{OC} decrease by 0.5% and 0.3%, respectively, with each degree of temperature increase. This drop is significant compared to the I_{SC} rise of 0.05% per °C. Taking everything into account, it's probable that PV modules will operate more effectively on cold days than on hot ones. Because deserts are suitable beginning places for solar installations, it is vital to study their weather [10]. For example, during the summer months, the "Lut Desert" in Iran experiences daytime highs of 50 °C and nighttime lows of 10 - 20 °C. PV modules can heat up to 35 °C above ambient temperature on sunny days, according to van Helden et al. [18], putting the laminates under extreme thermal pressures day and night. Additionally, if the temperature of solar cells rises above a certain point, they will degrade for a long period [19]. These elements make creating a cooling field for a PV module necessary. Renewable energy is defined as energy that can be renewed spontaneously over a brief period of time. Solar, wind, hydropower, geothermal, wave energy, biomass, hydrogen, etc. are a few possibilities for renewable energy sources [20].

Solar energy has become a prominent option among renewable energy sources since it provides a number of advantages, such as: It is feasible to collect this significant amount of renewable energy since it is continuously accessible, even on overcast days. Most solar energy conversion methods require only a little initial expenditure [21]. Given that PV modules have an exceptionally longer time span of more than 30 years, maintenance expenses are practically non-existent. The flexibility to assemble PV modules in any arrangement, from modest residential setups to huge solar farms. In terms of aesthetics, in comparison with alternative renewable energy sources, PV modules have the least adverse ecological effects. solar energy is becoming more and more common due to the aforementioned benefits, in addition to in tropical areas where sun intensity is substantial adequate to support solar farms with capabilities ranging from 10 to 150 MW [22, 23]. Solar updraft towers, solar thermal collectors, and solar cells are typically the three methods used to transform this pure energy into usable electrical and thermal forms of energy. Each technique has benefits and drawbacks. When all benefits and drawbacks are taken into account, solar cells could tip the scales in their favor. For example, a solar updraft tower has a much higher initial investment need and is less effective than PV.

Solar cells may directly transform the photon energy of light into electrical power in the case of producing electricity. The use of solar thermal collectors or solar updraft towers, in contrast, necessitates several expensive auxiliary components, including turbines, generators, pipes, etc. [11, 12]. The PV panels and solar thermal collectors are the two primary solar energy technologies. In order to transform solar radiation into thermal energy that can be used by humans, it is usual practise to use a heat transfer fluid whose temperature (and, consequently, enthalpy) rises as the fluid moves through the solar thermal collector [24]. A PV panel, on the other hand, converts the solar energy that directly hits its surface into electrical energy by means of the photovoltaic effect. A commercial solar PV panel's efficiency typically falls between 10% and 23% [25, 26]. The three most common forms of PV panels are mono-crystalline, poly-/multi-crystalline, and amorphous, and they are all based on silicon cells. Thin-film technologies, including CdTe and CIGS, have also lately made their way into the market [24], as well as silicon hetero-junction cells. The PV action in a PV panel is supported by photons with energies over the band gap energy; the outstanding photon energy, however, is primarily transformed into heat, raising the temperature of the cell. The open-circuit voltage (V_{OC}), fill factor, and output power all suffer from temperature increases, which eventually reduce the panel's electrical efficiency.

Environmental elements including relative humidity, ambient temperature, and wind speed, along with particles like collected dust on the panel are common variables which affect a solar cell's operating temperature along with to the local sun irradiation. Any method for cooling a PV panel that involves dissipating some of the excess or collected thermal energy is significant in this case because it can lower cell temperatures, increase the panel's electrical capacity, and guard against irrep-

www.mnnit.edu.in

arable harm to the panel brought on by the temperature rise of the cells and their regular thermal cycling throughout daytime and night-time operation. Over the years, a variety of thermal management strategies have been put forth, created, and tested with the goal of cooling PV panels, and there are currently a number of commercial systems available on the market that do so. Both active and passive temperature control techniques are available. Forced convective heat transfer is used in the first category, whereas free convective, conductive, and/or radiative heat transfer control is used in the second. Numerous thorough and instructive evaluations may be found while searching the literature for research that pertains to this field. For instance, Siecker et al. [27] gave an in-depth description of different hybrid cooling methods, covering methods like (i) floating tracked concentrated cooling systems; (ii) PV-thermoelectric systems cooled by a heat sink; (iii) PV panels with integrated phase change materials (PCMs); (iv) immersion cooling of PV panels; (v) PV panels with transparent coatings; and (vi) hybrid PV-thermal (PV-T) systems cooled by water spray. Additionally, Maleki et al. [28] and Hasanuzzaman et al. [29] given a summary of both passive and active methods of cooling readily accessible for modifiable PV panel temperatures and concluded that passive cooling methods are extra beneficial for commercial-scale systems due to the higher costs and higher electricity demands whereas active cooling methods are more feasible for small-scale deployment. A full discussion of several cooling solutions was presented by Sargunanathan et al. [30], including active cooling using water flowing over the front surface of PV panels or using air/water/fin cooling systems. Ali [31] clarified the latest advances in PV cooling, especially for PCM systems. On how these techniques affect lowering operating temperatures for PV panels, an analysis was given [32-37]. In their state-of-the-art evaluation of PV performance enhancement methods, Kandeal et al. [38] place a special emphasis on convection, conduction, and radiation-based cooling methods. A summary of several thermal management techniques was also provided by Bahaidarah et al. [39] and Hamzat et al. [40], based on the use of (i) heat pipes, (ii) microchannels, (iii) liquid immersion, (iv) heat sinks, (v) impingement jets, and (vi) PCMs. The use of nano-liquid cooling, cutting-edge techniques for radiative thermal management, or new advancements in the arena of integrated hybrid PV-T collectors, that additionally entail the removal of thermal energy from PV cells, are examples of present-day research.

The fluid and newly defined properties of the solute are included in the science of nano-liquid. This nanotechnology suggests a possibility of increasing the properties of the base fluid's thermal conductivity in the nano-liquid. According to the research of [41], Al_2O_3 water nano-liquid with a 0.5% concentration has the ability to increase convection current in a twin pipe heat exchanger while just slightly lowering pressure. Similar to [42], who used Al_2O_3, CuO, and TiO_2 nano-fluids of varying concentrations to cool the solar panel, it was surprise to find that Al_2O_3 nanoparticle greatly increased the solar panel's power output. In addition, when carbon nanotube and $AgSiO_2$ were appropriately integrated, the effectiveness of the solar panel was increased by 30% [43]. Additionally, the sophisticated simulator was used to test the applicability of CuO, SiC, and Al_2O_3 in boosting solar panel efficiency, with the result that SiC was recommended as the best nano-fluid [44]. A scientific comparison of Bohemite water and water used as a heat extractor in PVT was also done. As a result, Bohemite and water were preferred over water for increasing PVT's output power. Recently, [45] investigated the effects of concentration, water, and nanoparticles on the electrical and thermal efficiency of the PV. According to [46], copper-water nanoparticles were more efficient electrically and thermally than copper-ethylene glycol. The best cooling candidate, according to a comparison of several cooling techniques including forced air, natural, SiO_2-water, water, and Fe_3O_4, was nano-liquid (SiO_2- water). A further notable finding is that nanofluid is a better coolant than water-PVT and uncooled-PV, as demonstrated by the experimental results of 13% efficiency and a 16 °C drop in PV temperature reached by [47]. As a result of the solar panel's high irradiance and surface area sensitivity to heat dissipation, the unpredictable temperature rise can be managed with this nano-fluid technique.

The overviews stated above offer extremely fascinating details about the advancement of these technological advances. The efficient performance of solar panels is crucial for harnessing solar energy effectively. However, solar panels are susceptible to temperature increases, which can negatively impact their performance and longevity. To mitigate this issue, various sustainable cooling techniques have been explored and implemented. The objective of this study is to systematically assess comparing the effectiveness of several environmentally friendly cooling methods for solar panels.

Materials and Method

The experiment utilizes commercially available solar panels of a specific 40 W and size (Table 1). The following cooling techniques are tested and compared:

- Watermelon rind: Watermelon rinds are collected and prepared as a cooling material.
- Banana leaves: Fresh banana leaves are selected and prepared for use.
- Wet soil: Soil with high moisture content is used as a cooling medium.
- Green net: A shade net or green mesh material is employed to limit heat absorption.
- Coir: Natural coir material is used for insulation and temperature regulation.
- Jute sack: Jute sacks are used for their insulation properties and heat reduction capabilities.

Table 1: Solar PV panel specifications and electrical ratings.

Module Type	NSA40
P_{max}	40 W ± 2
Voltage (V_{max})	17.84 V
Current	2.26 A
Open circuit voltage (V_{oc})	21.95 V
Short circuit current (I_{sc})	2.44 A
System voltage	1000 V DC

www.mriet.edu.in

The solar panels are mounted in a controlled environment that closely resembles real-world conditions. The panels are exposed to sunlight at a predetermined intensity and temperature. High-precision temperature sensors are strategically placed on the solar panels to monitor the surface temperature accurately (Figure 1).The voltage output of the solar panels is measured using appropriate equipment and the following components (Table 2).

The cooling techniques are individually tested in separate experimental runs. For each technique, the cooling material (watermelon rind, banana leaves, wet soil, green net, coir, or jute sack) is placed below the solar panels. The surface temperature of the solar panels and the corresponding voltage output are recorded at regular intervals during experiment (Figure 2). The collected data is analyzed to evaluate the performance of each cooling technique.

Statistical methods may be employed to determine any significant differences in temperature reduction and voltage output between the techniques. The results from each cooling technique are compared to identify the most effective methods in terms of temperature regulation and voltage generation. To ensure the reliability of the results, the experiments are repeated multiple times, and the average values are calculated.

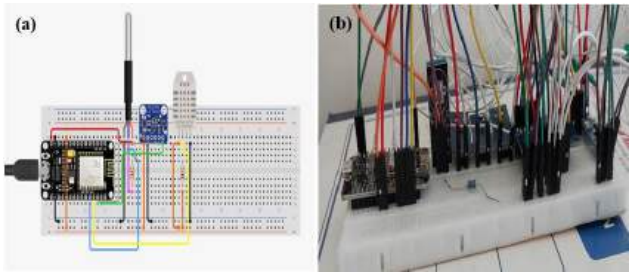

Figure 1: Basic circuit configuration diagram **(a)** from software and **(b)** at actual.

Table 2: Circuit components with specifications.

Component	Specifications
NodeMCU ESP8266	• Tensilica 32 bit RISC CPU Xtensa LX106. • Wifi supported. • Digital IO pins with 3.3V input.
4.7K OHM resistor	• Variable resistor with resistance 4.7 and 5% tolerance
Voltage sensor	• Range from DC 0 V to 25 V
Temperature sensor	• 100 K NTC, with one-meter cable temperature sensor. • Temperatures range from -40 °C to 270 °C.
Step-down buck converter	• LM 2596 adjustable step-down buck converter.
Power supply module	• 3.3 V power supply module. • Input 4.5 V to 12 V and output of 3.3 V.
Breadboard	• Withstanding voltage of 1000 V AC. • Rating is 5 Amps.
Arduino board	• 22 Digital IO pins • 6 PWM output pins.

Figure 2: Experimental setup for sustainable cooling technique utilizing circuit boards as intermediaries and standard panel.

Results and Discussion

Case-1

The use of watermelon rind and banana leaves as cooling materials has a positive impact on the voltage output of the solar panels. Watermelon rind contains a significant amount of water, which has contributed in evaporative cooling. Placing watermelon rind below the solar panels allows for the evaporation of water, which helps to dissipate heat and potentially lower the panel temperature. This cooling effect may positively impact the voltage output and overall performance of the panels. Similarly, Banana leaves offer natural insulation properties. By using banana leaves below to the solar panels, limits the heat absorption. This result improves the voltage output of the panels and helps with maintaining lower operating temperatures. By reducing the operating temperature of the panels, these cooling techniques helped maintain a higher voltage output. Lower temperatures result in reduced resistive losses within the solar cells, allowing for improved electron flow and increased voltage generation. The voltage enhancement was particularly notable during peak sunlight hours when temperature raised and leads to decreased efficiency (Figure 3 and figure 4).

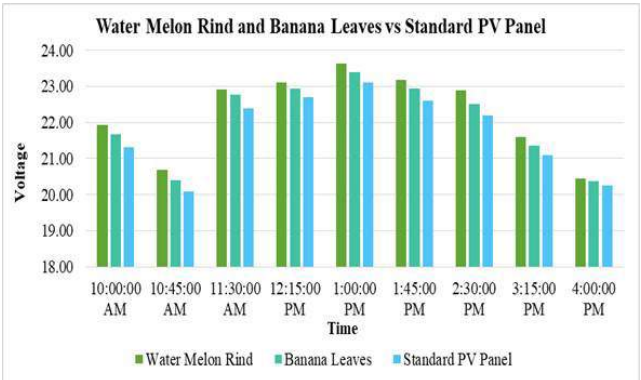

Figure 3: Water melon rind and banana leaves vs standard PV panel for voltage.

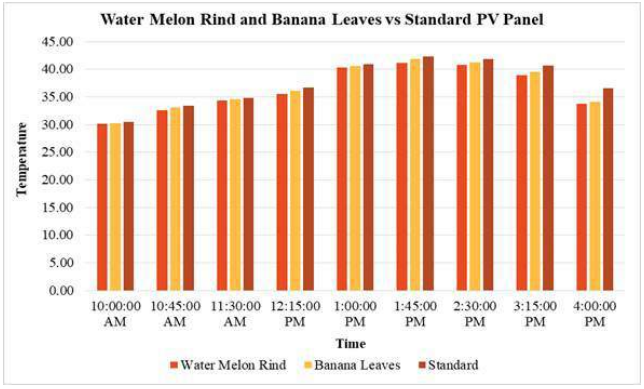

Figure 4: Water melon rind and banana leaves vs standard PV panel for temperature.

The use of watermelon rind and banana leaves aligns with the principles of sustainability and environmental responsibility. These materials are readily available, low-cost, and biodegradable, making them accessible and eco-friendly options for cooling solar panels. It is worth noting that while the experimental results highlight the effectiveness of watermelon rind and banana leaves as cooling materials, their durability and longevity may pose certain challenges. Regular replacement or maintenance may be required to sustain their cooling efficiency over extended periods.

Case-2

Wet soil acts as an effective cooling medium by absorbing and dissipating heat, thereby reducing the temperature of the panels. It utilizes the high heat capacity and thermal conductivity of the soil to transfer the heat away from the panels, maintaining lower operating temperatures. Green net provided to reduce heat absorption. These cooling techniques contributed to maintaining a more stable and optimal operating temperature for the solar panels. Both wet soil and green net offer sustainable and cost-effective solutions for cooling solar panels and also utilizes natural elements and do not require additional energy consumption. These cooling techniques are particularly beneficial in regions with high ambient temperatures or limited access to conventional cooling methods. Further study is needed to optimize the implementation of wet soil and green net, considering factors such as the ideal depth and moisture content of the soil, as well as the shading efficiency and durability of the green net. Additionally, long-term studies are required to assess their effectiveness and practicality in different climates and solar panel installations (Figure 5 and figure 6).

Case-3

Coir exhibits good insulating properties, which helps to reduce heat transfer from the ground to the solar panels. By placing coir underneath the panels, it acts as a thermal barrier, preventing the direct transfer of heat from the surface. It has the ability to retain moisture, which is aid in cooling. Jute sacks have relatively good breathability, allowing for airflow around the solar panels. Adequate airflow has aid in dissipating heat from the panel surface, preventing overheating and improving overall performance. Coir and jute sack effectively regulated

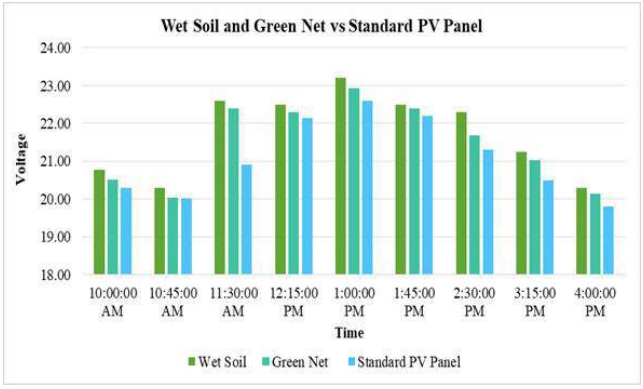

Figure 5: Wet soil and green net vs standard PV panel for voltage.

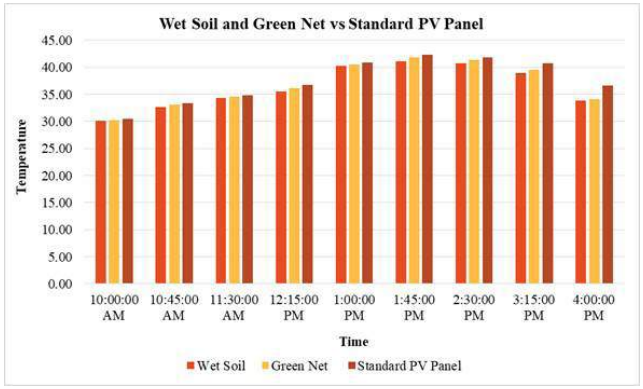

Figure 6: Wet soil and green net vs standard PV panel for temperature.

and reduced the operating temperature of the solar panels, mitigating the negative impact of high temperatures (Figure 7 and figure 8).

Among the various cooling techniques (Figure 9 and figure 10), the experimental results indicate that watermelon rind exhibits the highest and improved voltage output compared to other methods. This has been attributed to the effective evaporative cooling effect of watermelon rind, which aids in dissipating heat from the solar panels. Following closely behind, banana leaves demonstrate their capability to reduce heat absorption, thereby maintaining a more stable operating temperature and enhancing voltage generation. After banana leaves, wet soil proves to be a reliable cooling technique as it acts as a heat sink, effectively regulating the temperature of

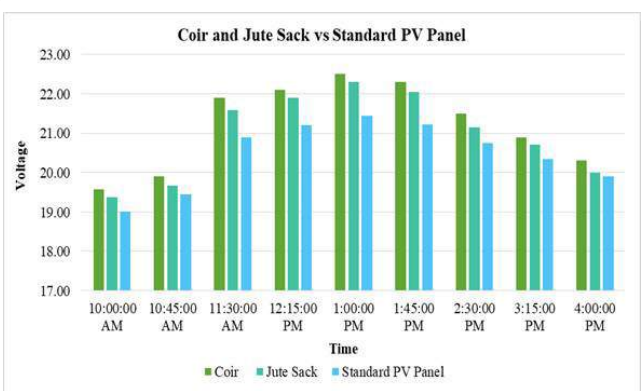

Figure 7: Coir and jute sack vs standard PV panel for voltage.

www.mnet.edu.in

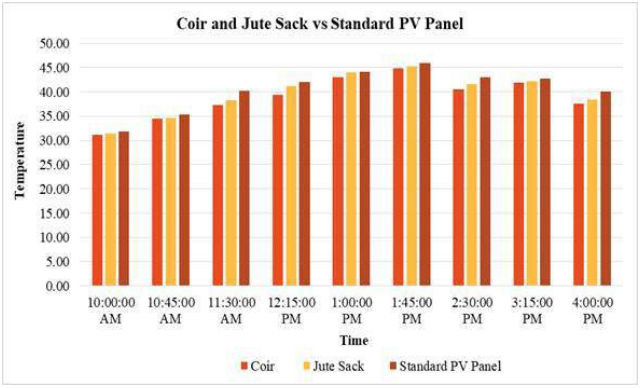

Figure 8: Coir and jute sack vs standard PV panel for temperature.

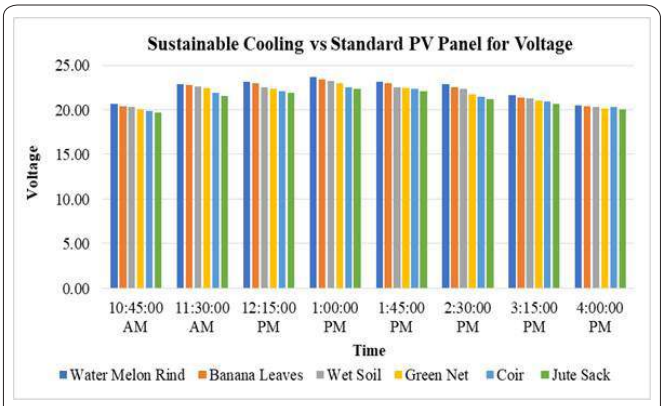

Figure 9: Comparison of sustainable cooling vs standard PV panel for voltage.

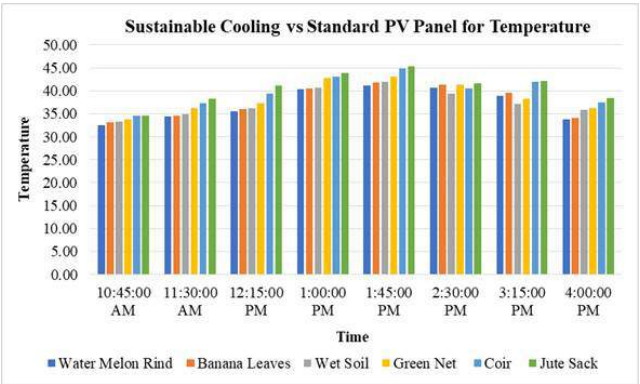

Figure 10: Comparison of sustainable cooling vs standard PV panel for temperature.

the panels. This regulation helps in minimizing resistive losses and potentially improving the voltage output of the solar panels. Additionally, the green net shows promise by limiting heat buildup, which positively influences the voltage generation and overall performance of the panels. Moreover, the insulation properties of coir and jute sacks contribute to maintaining lower operating temperatures, further enhancing the voltage output of the solar panels. These materials act as effective barriers, reducing heat transfer and ensuring improved performance.

Conclusions

The experimental performance and comparison of sustainable passive cooling techniques for solar (PV) panels has demonstrated promising results and significant potential for improving the efficiency and longevity of solar panel systems. Through rigorous testing and analysis, the following key findings have emerged:

- The implementation of sustainable cooling techniques has shown a notable increase in the overall efficiency of solar panels. By reducing the operating temperature, the panels are able to maintain higher levels of output, maximizing electricity generation.
- The implementation of these sustainable cooling techniques has demonstrated a significant reduction in the operating temperature of solar panels. The natural properties of watermelon rind, banana leaves, wet soil, green net, coir, and jute sacks, such as high-water content, evaporation, and shading, have effectively cooled the panels, preventing overheating and improving their overall performance.
- Advantage of these cooling techniques is their affordability and accessibility. Watermelon rind, banana leaves, wet soil, green net, coir, and jute sacks are widely available and relatively inexpensive materials, making them a cost-effective solution for cooling solar panels, particularly in regions with limited resources or budget constraints.
- The use of these natural cooling techniques aligns with environmental sustainability principles. Unlike conventional cooling methods that require additional energy consumption, these techniques rely on renewable resources and have minimal environmental impact and contribute to a more sustainable energy production process by reducing carbon emissions associated with traditional cooling methods.
- The experimental performance has highlighted the adaptability of these cooling techniques to different geographical locations and climates. Watermelon rind, banana leaves, wet soil, green net, coir, and jute sacks can be easily sourced and tailored to suit specific regional conditions, making them suitable for a wide range of solar panel installations.
- The experimental results have shown promising outcomes, there is still a need for further research and optimization of these cooling techniques. Factors such as material durability, maintenance requirements, and long-term effectiveness need to be investigated to ensure their practicality and reliability over extended periods.

Acknowledgements

None.

Conflict of Interest

Author(s) do not have any conflict of interest

www.mriet.edu.in

References

1. Ramkiran B, Sundarabalan CK, Sudhakar K. 2021. Sustainable passive cooling strategy for PV module: a comparative analysis. *Case Stud Therm Eng* 27: 101317. https://doi.org/10.1016/j.csite.2021.101317
2. Sudhakar K, Winderl M, Priya SS. 2019. Net-zero building designs in hot and humid climates: a state-of-art. *Case Stud Therm Eng* 13: 100400. https://doi.org/10.1016/j.csite.2019.100400
3. Uçkan İ, Yousif AA. 2021. Investigation of the effect of various solar collector types on a solar absorption cooling system. *Energy Sources Part A Recovery Util Environ Eff* 43(7): 875-892. https://doi.org/10.1080/15567036.2020.1766599
4. Sahu A, Yadav N, Sudhakar K. 2016. Floating photovoltaic power plant: a review. *Renew Sustain Energy Rev* 66: 815-824. https://doi.org/10.1016/j.rser.2016.08.051
5. Sudhakar K, Ngui WK, Kirpichnikova IM. 2021. Energy analysis of utility-scale PV plant in the rain-dominated tropical monsoon climates. *Case Stud Therm Eng* 26: 101123. https://doi.org/10.1016/j.csite.2021.101123
6. Balakrishnan P, Shabbir MS, Siddiqi AF, Wang X. 2020. Current status and future prospects of renewable energy: a case study. *Energy Sources Part A Recovery Util Environ Eff* 42(21): 2698-2703. https://doi.org/10.1080/15567036.2019.1618983
7. Cuce E, Cuce PM, Young CH. 2016. Energy saving potential of heat insulation solar glass: key results from laboratory and *in-situ* testing. *Energy* 97: 369-380. https://doi.org/10.1016/j.energy.2015.12.134
8. Cuce E, Bali T, Sekucoglu SA. 2011. Effects of passive cooling on performance of silicon photovoltaic cells. *Int J Low Carbon Technol* 6(4): 299-308. https://doi.org/10.1093/ijlct/ctr018
9. Cuce E, Oztekin EK, Cuce PM. 2018. Hybrid photovoltaic/thermal (HPV/T) systems: from theory to applications. *Energy Res J* 9(1): 1-71.
10. Mahdavi A, Farhadi M, Gorji-Bandpy M, Mahmoudi A. 2022. A review of passive cooling of photovoltaic devices. *Clean Eng Technol* 11: 100579. https://doi.org/10.1016/j.clet.2022.100579
11. Das P, Chandramohan VP. 2022. A review on solar updraft tower plant technology: thermodynamic analysis, worldwide status, recent advances, major challenges and opportunities. *Sustain Energy Technol Assess* 52: 102091. https://doi.org/10.1016/j.seta.2022.102091
12. Rushdi MA, Yoshida S, Watanabe K, Ohya Y. 2021. Machine learning approaches for thermal updraft prediction in wind solar tower systems. *Renew Energy* 177: 1001-1013. https://doi.org/10.1016/j.renene.2021.06.033
13. Kazem HA, Chaichan MT, Al-Waeli AH, Sopian K. 2020. A review of dust accumulation and cleaning methods for solar photovoltaic systems. *J Clean Prod* 276: 123187. https://doi.org/10.1016/j.jclepro.2020.123187
14. Kumar R, Deshmukh V, Bharj RS. 2020. Performance enhancement of photovoltaic modules by nanofluid cooling: a comprehensive review. *Int J Energy Res* 44(8): 6149-6169. https://doi.org/10.1002/er.5285
15. Kandeal AW, Thakur AK, Elkadeem MR, Elmorshedy MF, Ullah Z, et al. 2020. Photovoltaics performance improvement using different cooling methodologies: a state-of-art review. *J Clean Prod* 273: 122772. https://doi.org/10.1016/j.jclepro.2020.122772
16. Su D, Jia Y, Alva G, Liu L, Fang G. 2017. Comparative analyses on dynamic performances of photovoltaic–thermal solar collectors integrated with phase change materials. *Energy Convers Manag* 131: 79-89. https://doi.org/10.1016/j.enconman.2016.11.002
17. Bernardo G, Lopes T, Lidzey DG, Mendes A. 2021. Progress in upscaling organic photovoltaic devices. *Adv Energy Mater* 11(23): 2100342. https://doi.org/10.1002/aenm.202100342
18. van Helden WG, van Zolingen RJC, Zondag HA. 2004. PV thermal systems: PV panels supplying renewable electricity and heat. *Prog Photovolt* 12(6): 415-426. https://doi.org/10.1002/pip.559
19. Muneeshwaran M, Sajjad U, Ahmed T, Amer M, Ali HM, et al. 2020. Performance improvement of photovoltaic modules via temperature homogeneity improvement. *Energy* 203: 117816. https://doi.org/10.1016/j.energy.2020.117816
20. Dixit S. 2020. Solar technologies and their implementations: a review. *Mater Today Proc* 28: 2137-2148. https://doi.org/10.1016/j.matpr.2020.04.134
21. Shalwar PK, Gupta B, Singh P. 2023. Solar photovoltaic system: a techno-economic review. *Nanoworld J* 9(S1): S408-S413. https://doi.org/10.17756/nwj.2023-s1-079
22. Jacobson MZ. 2009. Review of solutions to global warming, air pollution, and energy security. *Energy Environ Sci* 2(2): 148-173. https://doi.org/10.1039/b809990c
23. Bhosale S, Ganguly A, Mondal P, Dhobale S. 2023. Thermal model development and performance optimization of a solar-assisted absorption-based cold storage using the genetic algorithm. *Nanoworld J* 9(S1): S255-S259. https://doi.org/10.17756/nwj.2023-s1-050
24. Elavarasan RM, Mudgal V, Selvamanohar L, Wang K, Huang G, et al. 2022. Pathways toward high-efficiency solar photovoltaic thermal management for electrical, thermal and combined generation applications: a critical review. *Energy Convers Manag* 255: 115278. https://doi.org/10.1016/j.enconman.2022.115278
25. Champion Photovoltaic Module Efficiency Chart. [https://www.nrel.gov/pv/module-efficiency.html] [Accessed November 24, 2023]
26. Du D, Darkwa J, Kokogiannakis G. 2013. Thermal management systems for photovoltaics (PV) installations: a critical review. *Sol Energy* 97: 238-254. https://doi.org/10.1016/j.solener.2013.08.018
27. Siecker J, Kusakana K, Numbi EB. 2017. A review of solar photovoltaic systems cooling technologies. *Renew Sustain Energy Rev* 79: 192-203. https://doi.org/10.1016/j.rser.2017.05.053
28. Maleki A, Haghighi A, Assad MEH, Mahariq I, Nazari MA. 2020. A review on the approaches employed for cooling PV cells. *Sol Energy* 209: 170-185. https://doi.org/10.1016/j.solener.2020.08.083
29. Hasanuzzaman M, Malek ABMA, Islam MM, Pandey AK, Rahim NA. 2016. Global advancement of cooling technologies for PV systems: a review. *Sol Energy* 137: 25-45. https://doi.org/10.1016/j.solener.2016.07.010
30. Sargunanathan S, Elango A, Mohideen ST. 2016. Performance enhancement of solar photovoltaic cells using effective cooling methods: a review. *Renew Sustain Energy Rev* 64: 382-393. https://doi.org/10.1016/j.rser.2016.06.024
31. Ali HM. 2020. Recent advancements in PV cooling and efficiency enhancement integrating phase change materials based systems–a comprehensive review. *Sol Energy* 197: 163-198. https://doi.org/10.1016/j.solener.2019.11.075
32. Wankhede S, Pesode P, Gaikwad S, Pawar S, Chipade A. 2023. Implementing combinative distance base assessment (CODAS) for selection of natural fibre for long lasting composites. *Mater Sci Forum* 1081: 41-48. https://doi.org/10.4028/p-4pd120
33. Wankhede S, Pesode P, Pawar S, Lobo R. 2023. Comparison study of GRA, COPRAS and MOORA for ranking of phase change material for cooling system. *Mater Today Proc* 1-6. https://doi.org/10.1016/j.matpr.2023.02.437
34. Patil B, Hole J, Wankhede S. 2017. Parameters affecting productivity of solar still and improvement techniques: a detailed review. *Int J Eng Technol Manag App Sci* 5(2): 11-18.
35. Wankhede SV, Hole JA. 2022. MOORA and TOPSIS based selection of input parameter in solar powered absorption refrigeration system. *Int J Ambient Energy* 43(1): 3396-3401. https://doi.org/10.1080/01430750.2020.1831600
36. Wankhede SV, Hole JA, Patil BL. 2022. Performance of tetrafluoroethane (R134a)-dimethyl formamide (DMF) diffusion absorption air

www.mriet.edu.in

cooling system with variable power input. *Int J Ambient Energy* 43(1): 2019-2025. https://doi.org/10.1080/01430750.2020.1722225

37. Pesode P, Barve S, Wankhede SV, Jadhav DR, Pawar SK. 2023. Titanium alloy selection for biomedical application using weighted sum model methodology. *Mater Today Proc* 72: 724-728. https://doi.org/10.1016/j.matpr.2022.08.494
38. Kandeal AW, Thakur AK, Elkadeem MR, Elmorshedy MF, Ullah Z, et al. 2020. Photovoltaics performance improvement using different cooling methodologies: a state-of-art review. *J Clean Prod* 273: 122772. https://doi.org/10.1016/j.jclepro.2020.122772
39. Bahaidarah HM, Baloch AA, Gandhidasan P. 2016. Uniform cooling of photovoltaic panels: a review. *Renew Sustain Energy Rev* 57: 1520-1544. https://doi.org/10.1016/j.rser.2015.12.064
40. Hamzat AK, Sahin AZ, Omisanya MI, Alhems LM. 2021. Advances in PV and PVT cooling technologies: a review. *Sustain Energy Technol Assess* 47: 101360. https://doi.org/10.1016/j.seta.2021.101360
41. Sudarmadji S, Soeparman S, Wahyudi S, Hamidy N. 2014. Effects of cooling process of Al_2O_3-water nanofluid on convective heat transfer. *FME Trans* 42(2): 155-160.
42. Madhu B, Subramanian BE, Nagarajan PK, Sathyamurthy R, Mageshbabu D. 2017. Improving the yield of freshwater and exergy analysis of conventional solar still with different nanofluids. *FME Trans* 45(4): 524-530.
43. Hjerrild NE, Mesgari S, Crisostomo F, Scott JA, Amal R, et al. 2016. Hybrid PV/T enhancement using selectively absorbing Ag–SiO_2/carbon nanofluids. *Sol Energy Mater Sol Cells* 147: 281-287. https://doi.org/10.1016/j.solmat.2015.12.010
44. Al-Waeli AH, Chaichan MT, Kazem HA, Sopian K. 2017. Comparative study to use nano-(Al_2O_3, CuO, and SiC) with water to enhance photovoltaic thermal PV/T collectors. *Energy Convers Manag* 148: 963-973. https://doi.org/10.1016/j.enconman.2017.06.072
45. Rejeb O, Sardarabadi M, Ménézo C, Passandideh-Fard M, Dhaou MH, et al. 2016. Numerical and model validation of uncovered nanofluid sheet and tube type photovoltaic thermal solar system. *Energy Convers Manag* 110: 367-377. https://doi.org/10.1016/j.enconman.2015.11.063
46. Satpute JB, Rajan JA. 2018. Recent advancement in cooling technologies of solar photovoltaic (PV) system. *FME Trans* 46(4): 575-584.
47. Sardarabadi M, Hosseinzadeh M, Kazemian A, Passandideh-Fard M. 2017. Experimental investigation of the effects of using metal-oxides/water nanofluids on a photovoltaic thermal system (PVT) from energy and exergy viewpoints. *Energy* 138: 682-695. https://doi.org/10.1016/j.energy.2017.07.046

ResearchGate

See discussions, stats, and author profiles for this publication at: https://www.researchgate.net/publication/380636017

Experimental Analysis of Mechanical Tests on a Plate Composed of Banana Fibre

Article *in* Communications on Applied Nonlinear Analysis · May 2024

DOI: 10.52783/cana.v31.562

CITATION
1

READS
26

11 authors, including:

Rohit Rajendra Jadhao
Savitribai Phule Pune University
18 PUBLICATIONS **5** CITATIONS
SEE PROFILE

Mangesh Kale
Dr. D.Y. Patil Institute of Technology, Pimpri.
8 PUBLICATIONS **19** CITATIONS
SEE PROFILE

Pranav Gopal Charkha
D Y Patil University Pune Ambi
32 PUBLICATIONS **133** CITATIONS
SEE PROFILE

All content following this page was uploaded by Mangesh Kale on 17 May 2024.

The user has requested enhancement of the downloaded file.

www.cmiet.edu.in
Communications on Applied Nonlinear Analysis
ISSN: 1074-133X
Vol 31 No. 1s (2024)

Experimental Analysis of Mechanical Tests on a Plate Composed of Banana Fibre

Mr. Rohit Jadhao[1], Dr. Vijayshri Mahobiya[2], Dr. Prasad Baban Dhore[3], Dr. Roundal Vijay Baburao[4], Dr. Gorane Prathamesh Sudhakar[5], Dr Vijaykumar Javanjal[6], Mr. Mangesh Kale[7], Dr. Pranav Charkha[8]

[1] Assistant Professor, Department of Mechanical Engineering, Nutan Maharashtra Institute of Engineering and Technology, Pune, Maharashtra, India

[2] Assistant Professor, Department of Mechanical Engineering, Wainganga College of Engineering & Management, Nagpur, Maharashtra, India

[3]Associate Professor,Nutan College of Engineering & Research,Dr. Babasaheb Ambedkar Technological University, Raigad

[4,5]Assistant Professor,Genba Sopanrao Moze College of Engineering, Savitribai Phule Pune University, Pune

[6] Associate Professor, Department of Mechanical Engineering, Dr. D.Y.Patil Institute of Technology,Pimpri,,Pune,Maharashtra,India.

[7]Assistant Professor, Department of Mechanical Engineering, Dr. D.Y.Patil Institute of Technology, Pimpri, Pune,Maharashtra,India.

[8]Professor, Department of Mechanical Engineering,Dr.D.Y.PatilUniversity,Ambi,Pune,Maharashtra,India

E-mail: jadhaorohit@gmail.com

Article History:

Received: *03-02-2024*

Revised: *05-04-2024*

Accepted: *22-04-2024*

Abstract:
Due to their attractive characteristics, natural and synthetic fibre - reinforced hybrid composite materials are playing a prominent role in science. Innovators are now being drawn to the poor world to create new sustainable and environment products and materials focused on environmental objectives. Natural fibre has a number of advantageous qualities, including low density, non-toxicity, and minimal comparability in strengths, minimal waste disposal issues, and inexpensive cost. This study presents the experimental analysis of mechanical tests performed on a plate composed of banana fiber. The mechanical properties, including tensile strength, flexural strength, and compression strength, were evaluated to assess the performance and potential applications of the banana fibre plate. The experimental tests were conducted following standard testing procedures specified by ASTM. The results obtained provide valuable insights into the mechanical behavior of the banana fibre plate and contribute to the understanding of its suitability for various engineering applications.

Keywords: Banana fibre, mechanical tests, tensile strength, flexural strength, compression strength.

1. INTRODUCTION

A lingo-cellulosic fibre called banana fibre is derived from the pseudo - stem of the banana tree. Banana fibre is a strong fibre with decent mechanical characteristics. The specific strength characteristics of banana fibre are good and on par with those of more traditional materials like

www.cmiet.edu.in

fiberglass. This substance is less dense than glass fibers. The pseudo-stem is made up of a coiled, grouped collection of leaf stalk bases. Banana fibre is a byproduct of banana farming that either isn't fully or improperly used. If these fibers were put to good use, the demand would stabilize and prices would drop as a result. Natural fibers have excellent fire protection, light in weight, low flexibility, good moisture absorption, huge potential, and biocompatible. Natural fiber has been used for clothing and furniture. Banana fibre offers significant potential for creating paper, especially for the growing market for recycled paper. Products including filter paper, paper bags, cards, lamp stands, pen stands, decorative papers, rope, mats, and composite materials are all made from banana fibre. Germany and India are both testing the use of banana fibers in banknotes. The floor safety shields used in opulent vehicles like Benz are made of polypropylene reinforced with banana fibre. The majority of products made with banana fibre are crafts and domestic accents. Due to their intrinsic qualities, natural fibre reinforced hybrids now outperform artificial fibre reinforced polymer composites in terms of mechanical properties. The mechanical characteristics of both natural and artificial fibre reinforced polymer composites with various fibre volumes, including fracture toughness, modulus of elasticity, and impact strength, were assessed. The outcome showed that mechanical qualities had significantly improved, and the procedure of hybridization had decreased the dangers associated with environmental concerns. Banana fibre, a byproduct of banana farming that is commonly accessible in tropical nations like Malaysia and South India, was used to create the composite materials. When compared to artificial fibers, this fibre holds a superior mechanical strength and offers several advantages. In order to determine the bending moment under the conditions of peak output, they constructed 3 samples with various shapes, assessed the maximum stress value and elastic modulus along opposite paths, and discovered the peak deflection. Researchers tested the tensile and flexural characteristics of bio composites, and the findings were analyzed. They discovered from the study that adding natural fibers like sisal to glass fibre increases the tensile and flexural strength, and that these combinations are essential in the technical fields and innovation. They recommended using these composite materials for applications requiring moderate strength.

Venkateshwara et al. investigated the mechanical characteristics of epoxy synthetic structures reinforcement with sisal as well as banana fiber, including their tensile strength, flexural strength, impact resistance, and moisture absorptive. They have shown that hybridizing sisal material up to 50% by weight with banana fibers bound epoxy resins results in a considerable increase in structural rigidity and a decrease in the rate of moisture absorption. When compared to flax and GFRP combinations, banana and GFRP composites have good tensile properties with minimal deflection. In addition, as comparison to flax and glass fibre reinforced polymer matrix composites, banana and flax fabric composites have higher impact and flexion strengths. When in comparison to synthetic fibre reinforced composites, natural fibre reinforced composite materials are an environmentally benign, sustainable, compostable, and lighter material. The potential uses for these composites are expanding quickly across a wide range of engineering specialties, particularly when cost of materials and erosive environment improvement are concerns. Under ambient pressure, natural fibre composites containing sodium hydroxide can have their mechanical and physical properties enhanced without significantly altering their mechanical behavior. Researchers have examined the impact and fatigue behavior of non-woven hemp fibre composites bonded with polyester and

www.cmiet.edu.in

discovered a major improvement in such qualities. Natural fibres offer significant benefits such low density, superior mechanical qualities, high degradability, and recyclability. They are also disposable and reusable. The utilization of natural fabrics as reinforcing has been the subject of extensive investigation. The pseudo-stem of the banana tree yields banana fibre, a ligno-cellulosic fibre with high reliable qualities. The "pseudo-stem" is a cylinder-shaped grouping of leaf stalk bases. Currently, banana fibre is a byproduct of banana farming that is only partly or improperly utilised. It is uncommon to remove fibre from the pseudo stem, and a significant portion of the stem isn't used to make fibres. When compared to other natural fibres, banana fibres are pricier. Banana fibre sales are sporadic, and there is no reliable method of routine fibre extraction. If these fibres were put to good use, the supply would stabilise and prices have fallen as a result.

Zaman and colleagues point out that Bangladesh is one of the top banana-producing countries worldwide, which means there's a lot of leftover banana plant waste. However, they suggest that this waste can be turned into something useful like banana fibre. This fibre can benefit both rural areas and industries economically. They discuss how banana fibres have cool properties when it comes to handling stress and mechanical stuff. They're saying that compared to other natural fibres, banana fibers are pretty awesome. Thus, manufacturing composites—essentially combining banana fibers with other materials—allows us to create items that are both affordable and robust. These goods could find applications in a wide range of fields, including transportation, aircraft, sporting equipment, and everyday things like mats, decorations for your house, and even paper. Ultimately, they advise us to continue investigating this concept. Perhaps new applications for banana fiber can be discovered, and its production costs might be reduced even further.

Badanayak et.al. are discussing making a special kind of strong material by treating fibres from sisal, bamboo, and Jamaican bananas with chemicals. They suggest these materials could be useful in making things like aeroplanes and cars. They say banana fibers are especially good for this. The Paper explains how they treat these fibres to make them even better and also discusses some techniques used to study the fibres and figure out how good they are for making stuff. They say we should keep researching to find more ways to use these fibres and make machines better and cheaper. The author also suggests looking into pineapple leaf fibres to see how they could make things even better.

Iqbal et.al. talk reveals that how more people are looking at using natural plant fibers for different purposes. These fibers are said to be better than synthetic fibers because they are natural, biodegradable, renewable, lightweight and have durable properties. The focus is on banana fibers, which is important because bananas are everywhere. They suggest about the different parts of the banana like the fruit, skin and leaves that can be used for all sorts of things. The branch-like part of the banana, the pseudo-stem, has very good fibers that can be used for a wide variety of purposes. The author also said that the waste left over from the production of these products can be used for other purposes, which can help the country’s economy. They say their research provides vital information for farmers, business owners, policymakers, scientists and governments to make smarter decisions and help the country grow.Several studies have been conducted to explore the diverse applications and properties of banana fiber in composite materials. These studies delve into various aspects such as dyeability, mechanical properties, and potential enhancements brought by banana

www.cmiet.edu.in

fibers in different composite matrices. Investigations cover a wide range of composite materials, including polypropylene, recycled high-density polyethylene, epoxy, and sawdust-based bio-composites. Furthermore, hybrid composites combining banana fibers with other natural fibers like sisal are explored to enhance mechanical properties. Additionally, enzymatic treatments using cellulase and pectinase enzymes on banana pseudostem fibers aim to improve their properties for textile applications. These studies contribute valuable insights into the development of sustainable materials by utilizing banana fibers, potentially offering lightweight, eco-friendly solutions for diverse industrial applications.

2. PREPARATION OF BANANA FIBRE PLATE

To make a component, we start by getting a wooden box in the right shape. Then, we use a brush to put resin on the box.Next, we add the desired color on top of the resin. After that, we apply more resin on top of the color. On top of that, we place glass fiber. Then, we add more resin to make sure the glass fiber sticks well and forms one piece. Next, we put banana fiber on top, making sure it sticks with the resin. We add another layer of resin over the banana fiber, then place more glass fiber on top. Finally, we add another layer of color using resin on top of the glass fiber.

3. TEST RESULTS

3.1 Flexural Test

Flexural specimens are created in accordance with ASTM D790, and Universal Test Machine is used for the analysis. The test is conducted by inserting the test sample into the UTM and exerting stress on it until it broke and fractures.

Table 1: Flexural Test Result

Sr No	Sample Identification	Flexural Strength (MPa)
1	Horizontal	124.94
2	Vertical	92.7
3	Inclined (45^{o})	138.09

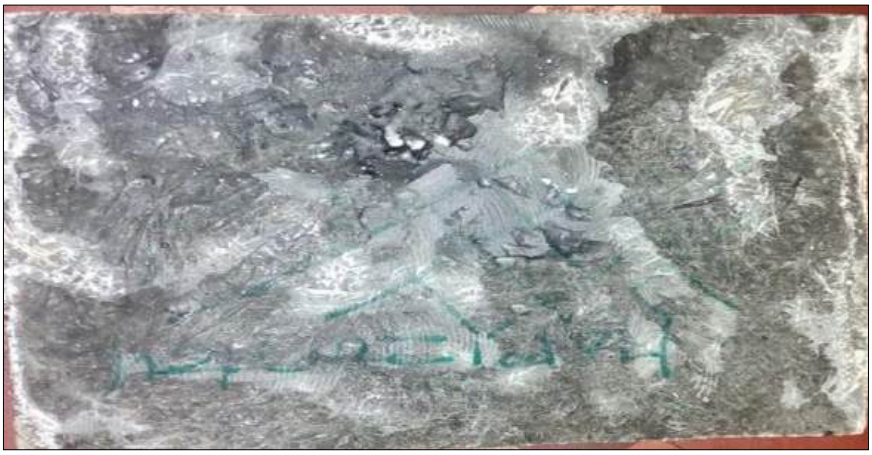

Fig.1: Banana Fibre Plate for Flexibility Test.

Communications on Applied Nonlinear Analysis
ISSN: 1074-133X
Vol 31 No. 1s (2024)

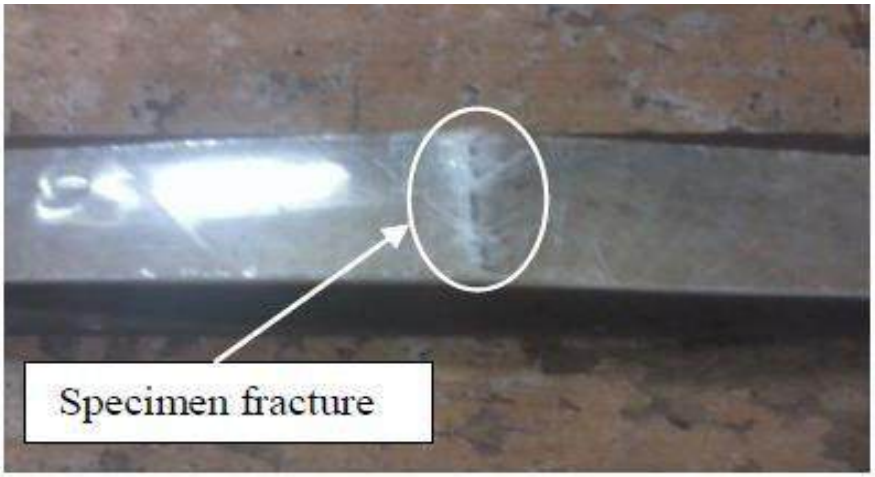

Fig.:2 Fractures after Flexibility Test

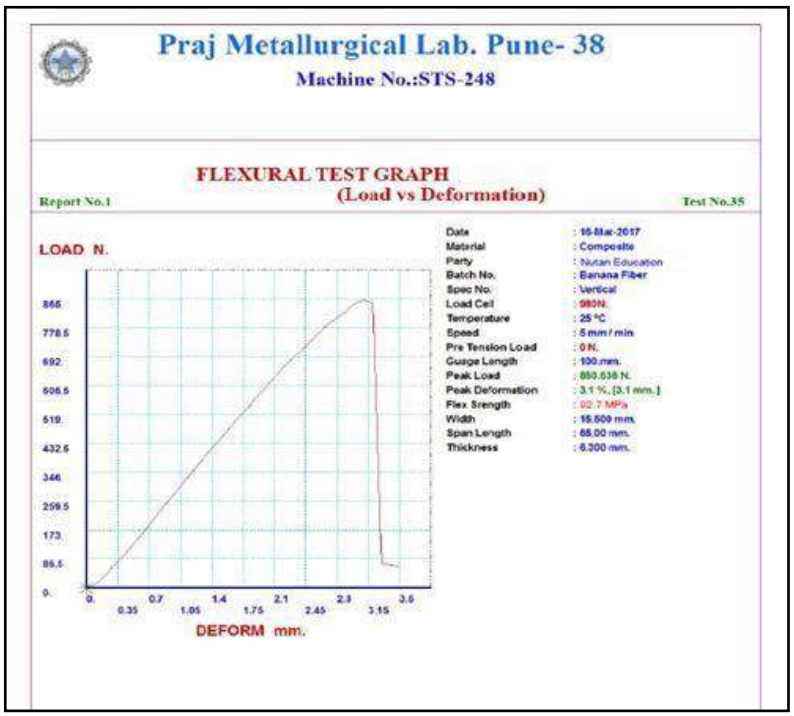

Fig. 3 Graph of Vertical Orientation of Banana Fibre Plate.

Communications on Applied Nonlinear Analysis
ISSN: 1074-133X
Vol 31 No. 1s (2024)

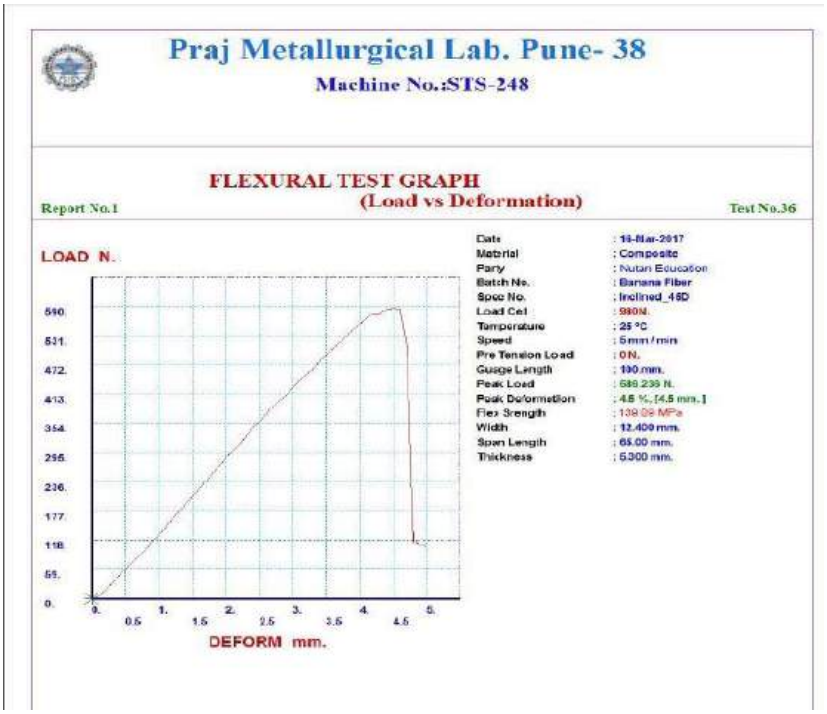

Fig.:4 Graph of Inclined (450) Orientation of Banana Fibre Plate.

3.2 Tensile Test

Using a manual cutting tool, the sample was formed to the appropriate dimensions, and sand paper was used to polish the edges. It is manufactured in accordance with ASTM D638. On the Universal testing machine, the tensile test is conducted. The sample is put on the Universal testing machine, and force is applied until the material breaks.

Table 2: Tensile Test Result

Sr. No.	Sample Identification	Tensile Strength(MPa)
1.	Dumble Shaped Plate	224.31

Fig.5 Specimen for Tensile and Compression test

Communications on Applied Nonlinear Analysis
ISSN: 1074-133X
Vol 31 No. 1s (2024)

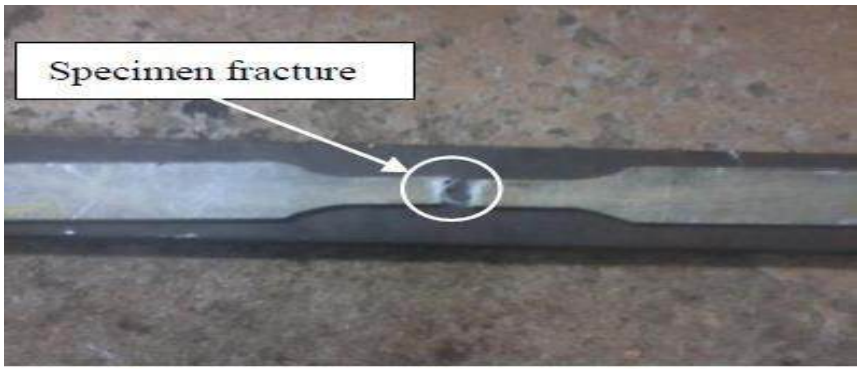

Fig.6 Specimen after Tensile Test.

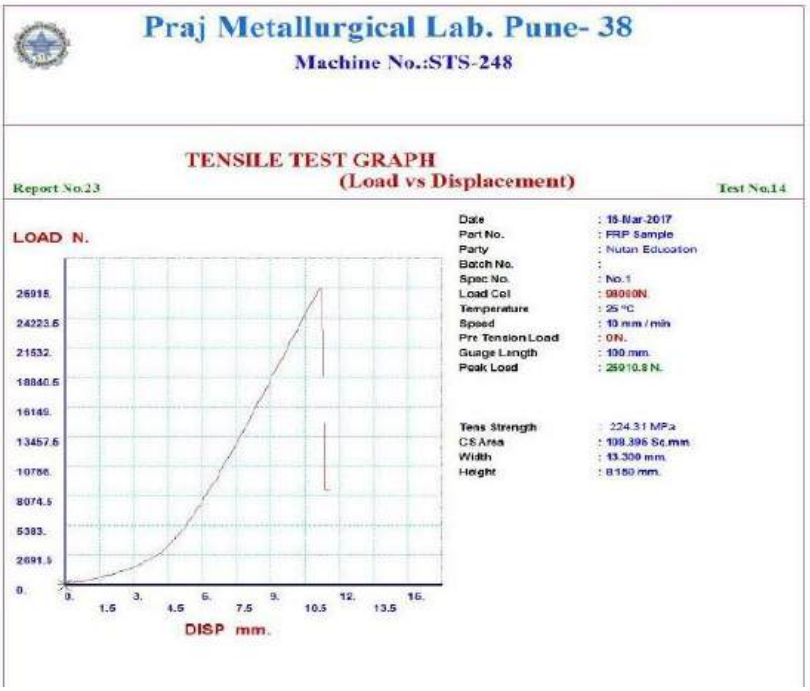

Fig.7 Graph of Tensile Test.

3.3 Compression Test

Using a rectangular plate and sand paper, the manufactured sample is molded to the necessary specifications. It was made in compliance with ASTM D638. The universal tester is used to conduct the compressive strength test.

Table 2: Compression Test Result

Sr. No.	Sample Identification	Compressive Strength (MPa)
1.	Square Plate	226.03

Communications on Applied Nonlinear Analysis
ISSN: 1074-133X
Vol 31 No. 1s (2024)

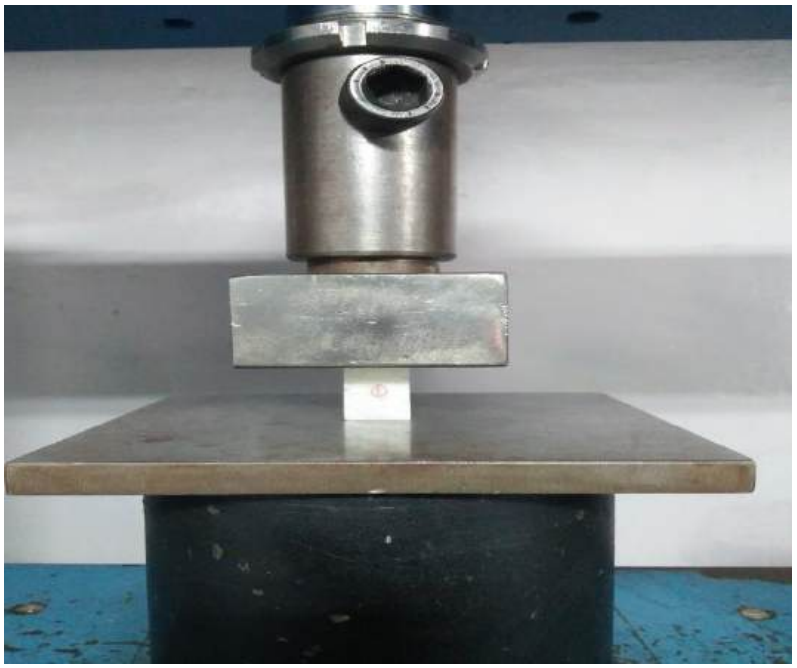

Fig. 8 Compression Test Setup.

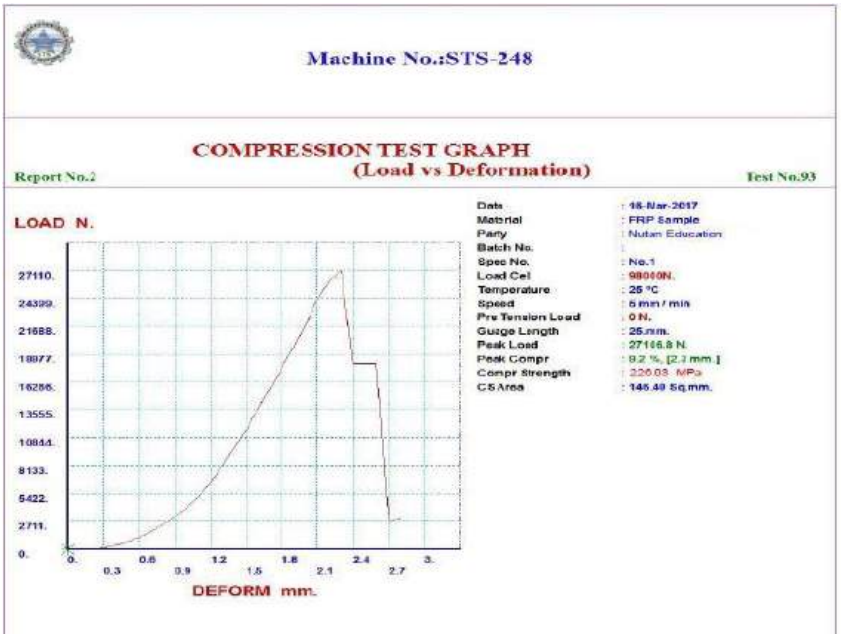

Fig.9 Graph of Compression Test.

4. CONCLUSION

The empirical work has resulted in the following findings. Dumbbell Shaped Plate has a maximum tensile strength of

224.31 MPa. The maximum flexural strength is 124.94, 92.70, and 138.09 MPa in various positions such as horizontal,vertical, and inclined (45°), respectively, and this value is also maintained by the same composite sample combination.

www.cmiet.edu.in

226.03 MPa is the maximum compression strength when using square plates. The SEM examination clearly shows the type of fibre fracture brought on by mechanical loading, the development of cracks in the matrix layer, and matrix failure.

REFERENCES

[1] M. Mohamed, S. Anandan, Z. Huo, V. Birman, J. Volz, and K. Chandrashekhara, "Manufacturing and characterization of polyurethane based sandwich composite structures". Journal of Composite Structures, 123; 169–179, (2015).

[2] Begum K. and Islam M.A., "Natural Fiber as a substitute to Synthetic Fiber in Polymer Composites: A Review," Research Journal of Engineering Sciences, Vol. 2(3), 46-53, April (2013).

[3] Dittenber, D. B., & Gangarao, H. V. S. (2012). Critical review of recent publications on use of natural composites 6 in infrastructure. Composites Part A: Applied Science and Manufacturing, 43(8), 1419–1429.

[4] Thwe, M. M., & Liao, K. (2002). Durability of bamboo-glass fiber reinforced polymer matrix hybrid composites. Composites Part A: Applied Science and Manufacturing, 33(11), 1345–1357.

[5] Pickering, K. L., Aruan Efendy, M. G., & Le, T. M. (2016). A review of recent developments in natural fibre composites and their mechanical performance. Composites Part A: Applied Science and Manufacturing, 83, 98–112.

[6] Corbière-Nicollier, T., & Michaud, V. (2013). Mechanical properties of flax–epoxy composites and laminates: Influence of stacking sequence and moisture content. Composites Part A: Applied Science and Manufacturing, 44, 41–49.

[7] Chenrayan, V., Gebremaryam, G., Shahapurkar, K., Mani, K., Fouad, Y., Kalam, M. A., ... & Abusahmin, B. S. (2023). Experimental and numerical assessment of the flexural response of banana fiber sandwich epoxy composite. Scientific reports, 13(1), 18156.

[8] Zaman, H. U., & Khan, M. A. (2023). Evaluation of the Physico-Mechanical Characteristics of Composites using Banana Fiber: In-Depth Review Findings. Int. J. Adv. Sci. Eng, 9(3), 2961-2972.

[9] Badanayak, P., Jose, S., & Bose, G. (2023). Banana pseudostem fiber: A critical review on fiber extraction, characterization, and surface modification. Journal of natural fibers, 20(1), 2168821.

[10] Iqbal, S. F., Kabir, M. H., Muhib, M. I., & Rupok, M. M. H. K. (2023). Prospect of waste banana fiber use in industry: A narrative review. International Journal of Science and Research Archive, 10(2), 828-839.

[11] Jawaid, M., Abdul Khalil, H. P. S., & Hassan, A. (2011). Cellulosic/synthetic fibre reinforced polymer hybrid composites: A review. Carbohydrate Polymers, 86(1), 1–18.

[12] Mohanty, A. K., Misra, M., & Hinrichsen, G. (2000). Biofibres, biodegradable polymers and biocomposites: An overview. Macromolecular Materials and Engineering, 276–277(1), 1–24.

[13] Jaju, S.B., Charkha, P.G., Kale, M., Gas metal arc welding process parameter optimization for AA7075 T6, Journal of Physics: Conference Series 1913 (1), 2021.

[14] Charkha, P.G., Jaju, S.B., Analysis & optimization of connecting rod, 2nd International Conference on Emerging Trends in Engineering and Technology, ICETET 2009, pp.86, 2009

[15] Gupta, U. S., Dhamarikar, M., Dharkar, A., Chaturvedi, S., Tiwari, S., & Namdeo, R. (2021). Surface modification of banana fiber: a review. Materials Today: Proceedings, 43, 904-915.

[16] Ramesh, M., Atreya, T. S. A., Aswin, U. S., Eashwar, H., & Deepa, C. (2014). Processing and mechanical property evaluation of banana fiber reinforced polymer composites. Procedia Engineering, 97, 563-572.

[17] Saravanakumar, S., Sathiyamurthy, S., Vinoth, V., & Devi, P. (2024). Effect of alumina on epoxy composites with banana fiber: mechanical, water resistance and degradation property analysis. Fibers and Polymers, 25(1), 275-287.

[18] Dutta, D., & Sit, N. (2024). Preparation and characterization of potato starch-based composite films reinforced by

www.cmiet.edu.in

modified banana fibers and its application in packaging of grapes. International Journal of Biological Macromolecules, 254, 127791.

[19] Brahma, S., Raafi, S. M., Arju, S. N., & Rehman, J. U. (2024). Dyeability and mechanical properties of banana fiber reinforced polypropylene composite. SPE Polymers.

[20] Syduzzaman, M., Akter, M., Mahmud, F., Bhowmick, D. R., Maliha, A. S., Fahmi, F. F., ... & Ahamed, M. A. (2024). Tensile properties of banana fiber reinforced recycled high-density polyethylene composites: An experimental investigation. SPE Polymers.

[21] Ganasan, V., Chohan, J. S., Subburaj, G. S., Harika, K., Yedari, V., Sivakumar, N. S., ... & Durai, A. J. (2024). Mechanical, Moisture Absorption and Thermal Stability of Banana Fiber/Egg Shell Powder-Based Epoxy Composites. Engineering Proceedings, 61(1), 11.

[22] Laksham, S., & Hitish, H. (2023). Experimental investigations of epoxy-resin-banana-fiber-saw dust bio-composite material for potential application as partitioning board. Materials Today: Proceedings.

[23] Anbalagan, K., Sarala, R., Subramanian, S., Yokesh, N., & Saravanan, N. (2023). Some studies on banana and sisal fibers-based hybrid composites. Materials Today: Proceedings, 90, 140-144.

[24] Gayathri, N., Shanmuganathan, V. K., Joyson, A., Aakash, M., & Joseph, A. G. (2023). Mechanical properties investigation on natural fiber reinforced epoxy polymer composite. Materials Today: Proceedings, 72, 2574-2580.

[25] Narayanan, S. R., Aravindhan, R., Arunprabhakaran, S., Thiyagu, K., Rajaram, S., & Radhkrishnan, K. (2023, October). The experimental investigation and fabrication of sisal and banana fiber with tamarind seed powder reinforced composites. In AIP Conference Proceedings (Vol. 2912, No. 1). AIP Publishing.

View publication stats

www.nmiet.edu.in
Advances in Nonlinear Variational Inequalities
ISSN: 1092-910X
Vol 26 No. 4 (2023)

The Role of Nonlinear Analysis in Tackling Engineering Challenges and Advancing Technology

[1]Gopal Mohadikar, [2]Sonu Khapekar, [3]Dr. M. K. Kodmelwar, [4]Supriya Bhosale, [5]Sopan Bapu Kshirsagar, [6]Ganesh Chandrabhan Shelke

[1]Assistant Professor, Department of Mechanical Engineering,Tolani Maritime Institute, Induri, Pune, India. Email:gmohadikar@gmail.com

[2]Nutan Maharashtra Institute of Engineering & Technology, Talegaon(D), Pune, India(MS). E-mail: sonukhapekar999@gmail.com

[3]Vishwakarma Institute of Information Technology, Pune, Maharashtra, India. Email: manohar.kodmelwar@viit.ac.in

[4]Nutan Maharashtra Institute of Engineering & Technology, Talegaon(D), Pune, India(MS). Email: supriyabhosale9@gmail.com

[5]Nutan Maharashtra Institute of Engineering & Technology, Talegaon(D), Pune, India(MS). Email:sopankshirsagar02@gmail.com

[6]Vishwakarma Institute of Information Technology, Pune, Maharashtra, India. Email: ganesh.shelke@viit.ac.in

Article History:

Received: *25-08-2023*

Revised: *16-10-2023*

Accepted: *28-10-2023*

Abstract:

The widespread occurrence of nonlinearities in diverse systems in the engineering domain has led to a transition from linear approximations to more advanced studies. This paper provides an explanation of the basic concepts of nonlinear analysis, including the various mathematical and computer models that are used to analyse and forecast nonlinear behaviours. This analysis is noteworthy because it covers a variety of approaches and sheds insight on their applicability in many engineering fields. These techniques include Finite Element Analysis (FEA), Computational Fluid Dynamics (CFD), and nonlinear control systems. This paper analyses the effects of nonlinear analysis on important engineering problems by looking at its applications. It emphasises how important it is to structural engineers since nonlinear behaviour of materials and structures has a significant impact on integrity and safety. It also examines its ramifications in electrical systems, automotive engineering, and aerospace engineering, shedding light on how nonlinear dynamics impact system functionality, performance, and design. In addition, the study examines how important nonlinear analysis is to the development of technology. It looks at how improving material science, performance optimisation, and manufacturing process innovation are all aided by nonlinear analysis. It describes the advances made possible by nonlinear analysis and critically assesses its drawbacks, such as computational complexity, accuracy, and compatibility with conventional engineering paradigms. This paper highlights the useful applications of nonlinear analysis in engineering projects, explaining success stories and important lessons through case studies and real-world examples. It concludes with a plea for continuing investigation and integration of nonlinear analysis to overcome engineering obstacles and stimulate technological leaps. Finally, it looks into future prospects, imagining nonlinear analysis as a driving factor for future technological advancements.

Keywords: Nonlinear Analysis, Finite Element Analysis, Computational Fluid Dynamics, Nonlinear control systems.

www.nmiet.edu.in

ISSN: 1092-910X
Vol 26 No. 4 (2023)

I. INTRODUCTION

The field of engineering is constantly changing, and one of the main tools for comprehending complicated systems and developing technology is nonlinear analysis. This introduction lays the groundwork for an in-depth investigation of the diverse field of nonlinear analysis. It explores the meaning of nonlinear analysis in engineering, emphasising the importance and inherent complexity of the field, and talks about how widely used it is to different engineering specialties. The ultimate goal of this work is to shed light on the critical role that nonlinear analysis plays in solving engineering problems and advancing technology [1]. In engineering, nonlinear analysis fundamentally signifies a change in perspective from the traditional linear approximation of physical events to a more complex and nuanced method. It centres on the investigation of phenomena and systems in which the input-output relationships are not linear. Under the superposition and homogeneity principles, changes in input cause proportionate changes in output in linear systems. On the other hand, nonlinear systems resist such simplicity and produce intricate, frequently unpredictable behaviours [2].

Numerous factors, including as material qualities, boundary conditions, component interactions, and even feedback systems, [3] can cause these departures from linearity. Nonlinearity is a widespread difficulty that engineers must overcome because it spans many technical areas. A thorough framework incorporating computational simulations, experimental methods, and mathematical modelling is necessary to comprehend nonlinear systems. These [4] instruments play a crucial role in identifying and forecasting the complex behaviours exhibited by nonlinear systems. Nonlinear analysis is a practical necessity rather than just a theoretical exercise. Nonlinear analysis enables engineers to understand the behaviour of complex systems in a variety of contexts, from the great difficulties of aerospace engineering to the microcosms of nanotechnology. Engineers can better comprehend and anticipate the behaviours of their inventions by using nonlinear analysis [5], which offers a sophisticated perspective on a variety of topics, including the aerodynamics of supersonic aircraft and the stress distribution in a building's support structure. Nonlinear analysis has a deep and wide-ranging significance in the field of engineering. The prevalence of nonlinearities in real-world systems calls for moving away from crude linear approximations. The complexity of systems that engineers work with is growing, and linear analysis is not always sufficient to capture the nuances of real-world systems. Numerous manifestations of nonlinearity, including material, geometric, and boundary condition nonlinearity, necessitate a more comprehensive approach to modelling and analysis.

The discipline of structural engineering [6] has benefited greatly from nonlinear analysis. For example, the behaviour of materials and structures under various conditions frequently demonstrates nonlinear properties in the field of civil engineering. When exposed to varying loads and climatic circumstances, steel and concrete structures exhibit behaviours that are beyond the scope of linear analysis. Engineers [7] may evaluate the structural stability of structures like buildings, bridges, and infrastructure more accurately by embracing nonlinear analysis. This not only improves safety but also makes it easier to construct stronger structures. The fields of automotive and aerospace engineering are further examples of how

www.nmiet.edu.in

ISSN: 1092-910X
Vol 26 No. 4 (2023)

nonlinear analysis has a significant impact. For safety and performance in aviation, it is critical to comprehend the nonlinear dynamics of aircraft under various circumstances. In order to create flight control systems that can adjust to different flight regimes, nonlinear analysis is essential. Similar to this, nonlinearities in vehicle dynamics in the automotive sector necessitate a sophisticated approach to control system design. Through [8] an understanding of these systems' nonlinearity, engineers can maximise vehicle safety and performance. Circuit design and signal processing are two areas in which nonlinear analysis is used in electrical and electronic systems. In electronic circuits, nonlinear effects can induce undesirable behaviours that compromise the stability and quality of the signal. Since electronic systems are being incorporated into more and more aspects of our daily lives, it is imperative that we comprehend these nonlinearities in order to create reliable and effective systems.

Numerous engineering specialties, such as mechanical engineering, environmental engineering, robotics, and more, fall under the purview of nonlinear analysis. Its uses range from predicting fluid flow in intricate geometries to modelling the behaviour of biological tissues. Nonlinear analysis is useful in many fields, including energy and healthcare, where it helps with the design of renewable energy sources and helps comprehend the workings of the human body. Essentially, nonlinear analysis is a paradigm change in engineering that allows for a more in-depth comprehension of complex behaviours across a range of disciplines. Its importance goes beyond the confines of conventional linear analysis, providing engineers with a more potent toolkit to tackle challenging issues and spur creativity. In [9] order to overcome engineering difficulties and advance technology, this study aims to provide light on the significant significance of nonlinear analysis in engineering. It will proceed as an organised investigation, exploring the foundations of nonlinear analysis, its uses in various engineering fields, the technological advances it promotes, the difficulties it poses, and possible future paths. We will demonstrate its practical value and reaffirm its position as an essential tool for engineers through case studies and real-world examples. This paper's main goal is to emphasise how crucial it is to include nonlinear analysis in the engineering toolkit, where it may help solve present problems and pave the way for future technological advances never seen before.

II. RELATED WORK

Engineering's use of nonlinear analysis has sparked a plethora of related research in other domains, advancing the profession and providing answers to pressing issues. Because nonlinear systems are so complex, engineers and academics have been motivated to investigate and use a variety of approaches to address these issues. A [10] related body of work in structural engineering has thoroughly investigated how materials and structures behave under various circumstances. The understanding of structural integrity has advanced significantly as a result of studies concentrating on material nonlinearity, such as the plastic behaviour of concrete or the stress-strain relationship in steel beyond its yield point. Better design techniques and safety procedures for structures including bridges, buildings, and infrastructure systems are the outcome of this research. Further improving the safety and

www.nmiet.edu.in

ISSN: 1092-910X
Vol 26 No. 4 (2023)

dependability of these systems is the capacity of researchers to model and forecast the behaviour of structures under intricate loading situations thanks to the development of sophisticated computer techniques like Finite Element Analysis (FEA).

Significant nonlinear analytic work has also been done in the field of aerospace engineering, mainly in the area of flight dynamics and control. In order to improve flight performance and safety, research on aerodynamic nonlinearity, aircraft response in harsh environments, and control system optimisation has been essential [11]. The creation of flight control systems that adjust to different flight regimes and maintain stability and manoeuvrability even in challenging circumstances is made possible by nonlinear analysis. Advances in aircraft design have been fuelled by related research in this field, resulting in safer and more efficient flying vehicles. Related work in nonlinear analysis is also beneficial to the field of automotive engineering. Numerous nonlinear elements, including as tire-road interactions, suspension characteristics, and aerodynamics, have influenced vehicle dynamics and have been the focus of much research. Improved safety, performance, and fuel efficiency are the results of advances in vehicle design and control systems brought about by an understanding of and modelling of these nonlinearities. This linked study has played a key role in improving vehicle behaviour in a variety of driving scenarios, which has led to the creation of safer and more pleasant cars [12].

Moreover, a significant amount of related nonlinear analytic work has been done in the field of electrical and electronic systems. Understanding and reducing nonlinear effects has grown essential as electronic circuits and signal processing systems become more complicated. In order to ensure stable and dependable operation of electronic systems, related research in this field has concentrated on modelling and analysing nonlinear behaviours in electronic components. The creation of more reliable and efficient electronic devices for use in a variety of applications, including industrial systems and consumer electronics, has been made possible by this effort. The field of nonlinear analysis has also been further broadened by developments in computational methods including computational fluid dynamics (CFD), nonlinear control systems, machine learning, and applications of chaos theory [13]. These approaches have proven invaluable in examining and comprehending sophisticated behaviours in a range of engineering systems, providing fresh perspectives and creative fixes for challenging issues.

The body of related work in nonlinear analysis has advanced technology while also enhancing our comprehension of complicated engineering systems. It has resulted in stronger electronic systems, safer buildings, and more fuel-efficient automobiles, which have had an impact on many facets of society and business. Furthermore, nonlinear analysis's shortcomings and difficulties are still being researched. There is still much to learn about the integration of nonlinear techniques with conventional engineering paradigms, computational complexity, and validation challenges. These projects are intended to improve accuracy, streamline processes, and deepen the use of nonlinear analysis into conventional engineering practises. Essentially, nonlinear analysis's significance and its role in changing engineering paradigms and developing technology are demonstrated by the large corpus of related work

www.nmiet.edu.in

ISSN: 1092-910X
Vol 26 No. 4 (2023)

in the field. It highlights the complex relationship between theoretical investigations and real-world applications, opening the door for further discoveries and advancements.

III. FUNDAMENTALS OF NONLINEAR ANALYSIS

A. Understanding Nonlinearity in Engineering Systems

Complex engineering systems are typified by nonlinearity, which defies straightforward cause-and-effect correlations and renders conventional linear analyses insufficient. It is a ubiquitous property of systems in which changes in the input do not cause changes in the output, leading to complex and frequently unpredictable behaviours. These nonlinearities show up in a variety of engineering systems, such as turbulent flow patterns in fluid dynamics and stress-strain correlations in structural materials [14]. Comprehending these nonlinearities requires moving away from the straightforwardness of linear systems and towards a more sophisticated understanding of the interactions between different elements in a system. The interactions between the system variables are described by nonlinear differential equations, which frequently control the behaviour of nonlinear systems. Because these equations frequently have complicated solutions that cannot be solved analytically, engineers are forced to use sophisticated computational methods to model and analyse these systems. Many factors, including material characteristics, geometric arrangements, and outside influences, can cause nonlinearity, which can lead to various behaviours, including bifurcations, chaotic dynamics, and hysteresis. In the field of structural engineering, for example, nonlinearities can result from massive deformations or material yielding, which can cause behaviours like plastic failure or buckling. Turbulence imparts nonlinear complications into fluid dynamics that are beyond the scope of traditional linear models [15].

Moreover, chaos arises from the fact that nonlinear systems frequently show sensitivity to initial conditions and parameters. A subfield of nonlinear dynamics called chaos theory studies how highly sensitive systems behave, producing [16] seemingly random and unpredictable results. The "butterfly effect," which refers to this sensitivity to initial conditions, shows how little changes can eventually result in large variances in the system's behaviour. Complexity-embracing computational models and sophisticated mathematical techniques are needed to comprehend and forecast these unpredictable behaviours.

B. Mathematical and Computational Models:

In order to unravel the complexities [17] of these intricate systems, nonlinear analysis makes use of a range of mathematical and computer models. With the use of these models, engineers may better understand and anticipate the behaviour of nonlinear systems by [18] simulating and representing their behaviour. Discrete systems and nonlinear differential equations are frequent components of mathematical models, which can be difficult to solve since they are not analytical in nature. Numerical techniques like finite difference, finite element, or spectral methods are required to solve these equations.

Computational models are essential [19] to nonlinear analysis because they allow us to simulate and foresee the behaviour of intricate systems. A prominent computer technique called Finite Element Analysis (FEA) breaks a system into small sections, or "finite

www.nmiet.edu.in

ISSN: 1092-910X
Vol 26 No. 4 (2023)

elements," which makes it possible to examine complicated geometries and material behaviours. Computational fluid dynamics (CFD) captures turbulence and nonlinearity in fluid systems through modelling and simulation using numerical techniques. Nonlinear control systems use computational methods to design control techniques for nonlinear dynamical systems, ensuring stability and peak performance. Additionally, AI and ML are increasingly being applied to nonlinear analysis. These techniques have the potential to reveal behaviours and patterns in nonlinear systems that are obscured by traditional analytical and numerical methods. Machine learning algorithms simplify the study and management of complex systems because of their ability to foresee responses from the system and identify nonlinear relationships [20].

The core of nonlinear analysis is fundamentally the combination of computer tools and mathematical models. Engineers may be able to better predict and regulate system behaviours across a variety of engineering applications if they have access to these tools for modelling and simulating nonlinear systems. Nonlinear analysis in engineering is based on these fundamentals; it necessitates a deep understanding of nonlinearity in systems and the use of complicated mathematical and computer models to study and predict their behaviours. Nonlinear systems, due to their subtlety and complexity, necessitate an all-encompassing approach that employs many methods in order to fully grasp their potential for innovation and problem-solving in engineering.

C. Types of Nonlinear Analysis Techniques

1. Finite Element Analysis (FEA):

It is widely used in many different engineering fields, including mechanical, aerospace, and biomedical engineering, in addition to civil and mechanical engineering. Through the use of smaller, finite components, FEA simplifies complicated systems or structures and makes it possible to thoroughly analyse their behaviour. These components are parts of a bigger structure, and the way they behave as a whole clarifies how the system reacts as a whole to various loads, p

FEA requires the following steps:

- Pre-processing: In this preliminary step, a digital model of the system or structure is created. This model includes the desired analysis type (e.g., stress analysis, heat transfer, or fluid flow), boundary conditions, and geometric shape. An essential component of this stage is mesh generation, which divides the structure into finite elements.
- Analysis: After the model is built, the programme solves physics- and material-behavior-based equations to determine how each finite element interacts with the others and reacts to the applied conditions. Mechanical stresses, deformations, heat transmission, fluid flow, and other physical behaviours might all be included in the study.
- Post-processing: The analysis is followed by an examination and visualisation of the findings. Stress distribution, displacement, strain, and any other relevant factors can

www.nmiet.edu.in

ISSN: 1092-910X
Vol 26 No. 4 (2023)

all be assessed by engineers. Making educated decisions on the design, selection of materials, or structural adjustments is aided by this phase.

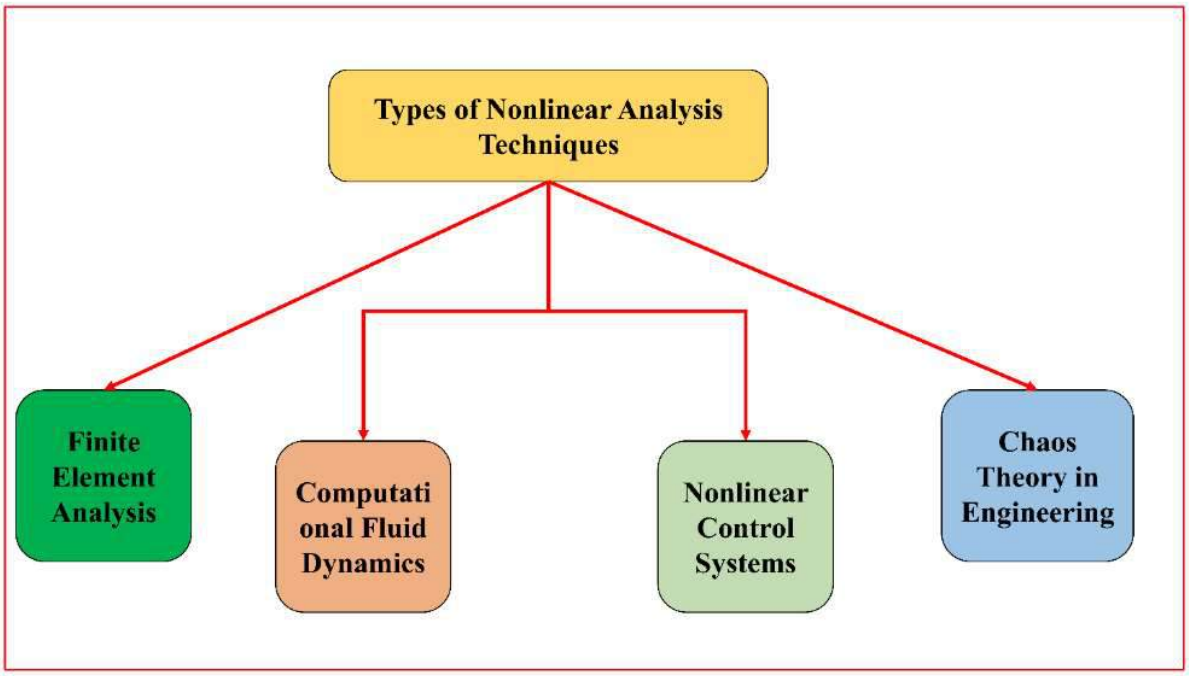

Figure 1: Types of Nonlinear Analysis techniques

Without the need for physical prototypes, finite element analysis (FEA) enables engineers to forecast how systems or buildings will react to actual conditions, saving both time and money. It helps to ensure safety, optimise designs, and fix any possible bugs or vulnerabilities in the system. Furthermore, static assessments aren't the only uses for FEA. Additionally, it supports nonlinear and dynamic analyses. While nonlinear analysis works with materials or structures displaying nonlinear behaviour, such as significant deformations or material yielding, dynamic analysis takes into account time-dependent effects, such as vibrations or transient loads. FEA is incredibly strong, but it has its limits. The accuracy of the input data, the modelling assumptions employed, and the capabilities of the programme all play a major role in producing accurate findings. The engineer's comprehension of the behaviour of the system and the constraints of the employed analysis technique are also prerequisites for the simulation's accuracy.

2. Computational Fluid Dynamics (CFD)

A potent technique in engineering for simulating the behaviour of fluids (liquids and gases) in motion is computational fluid dynamics, or CFD. It solves and analyses issues with fluid flows, heat transfer, and related phenomena using numerical techniques and algorithms. Numerous industries, including aerospace, automotive, environmental engineering, and even biological research, use CFD extensively. CFD solves the governing equations that characterise fluid flow by using computational methods based on the fundamentals of fluid dynamics. The foundation of CFD simulations is the Navier-Stokes equations, which characterise the motion of fluid substances. Nevertheless, due to their complexity and

www.nmiet.edu.in

ISSN: 1092-910X
Vol 26 No. 4 (2023)

frequent lack of a direct analytical solution, these equations require the use of numerical approximations.

This first step is building a computer model of the physical domain in which the fluid is travelling, much to FEA. The geometry, boundary definition, and establishment of initial and boundary conditions required for the simulation are all included in this model. The fluid domain is then represented by breaking the geometry up into a mesh of smaller elements, or cells in the case of CFD.

The discretized equations are solved numerically for every element or cell in the domain by the software. The solution procedure advances in temporal phases, forecasting the fluid's behaviour across time. Depending on the simulation's parameters, calculations may require finding solutions for variables like density, temperature, pressure, and velocity [21]. Post-processing: After the simulation is finished, the data is examined and shown. A wide range of factors, including temperature gradients, flow patterns, pressure distribution, turbulence, and more, can be interpreted and assessed by engineers. Making design decisions is aided by this study, which also helps to understand how the fluid behaves under simulated settings. A broad variety of fluid behaviours, from steady-state flows to transient or time-dependent circumstances and from laminar to turbulent flow regimes, can be investigated using CFD models. These models help with design optimisation, heat transfer mechanism research, aerodynamic performance assessment, and fluid flow effect analysis on systems or structures.

CFD is essential to aerospace engineering because it helps analyse the aerodynamics of spacecraft and aeroplanes, optimise wing designs, and lower drag. It helps in the creation of more fuel-efficient and aerodynamic automobiles in the automotive industry. In environmental engineering, CFD is used to analyse the dispersion of pollutants in air and water. It is also used in biomedical research to analyse respiratory or blood flow systems. Although CFD is an effective technique, it is not without restrictions. A few examples of variables that may affect simulation accuracy are mesh quality, model simplifications, and available processing power. High-fidelity findings frequently require a large amount of processing power and specialised knowledge. Computational Fluid Dynamics is a priceless tool that helps engineers build and optimise structures and systems across a wide range of engineering domains by simulating and analysing complicated fluid flow problems [22]. Its contributions have greatly improved our knowledge of fluid behaviour and sparked new ideas in engineering and industry.

3. Nonlinear Control Systems

Engineering relies heavily on nonlinear control systems, especially when it comes to controlling and overseeing nonlinear systems. To stabilise, regulate, or optimise complex, nonlinear dynamic systems, these systems use control techniques.

Recognising Nonlinear Control Mechanisms

Nonlinear control systems deal with systems where the relationship between inputs and outputs is not linear, in contrast to linear control systems, which function under the premise of linear relationships between inputs and outputs. Small adjustments to inputs or settings can

www.nmiet.edu.in

ISSN: 1092-910X
Vol 26 No. 4 (2023)

have a big impact on these systems' behaviour. Controlling nonlinear systems can be difficult because they frequently display complicated behaviours like hysteresis, limit cycles, chaos, or bifurcations.

Nonlinear Control Systems:

Nonlinear differential equations or difference equations are commonly used to represent nonlinear control systems mathematically. Examine a generic nonlinear control system that is represented by the following equations:

$$x^{\cdot} = f(x, u)$$

In this case, x stands for the system's state and u for the control input. The dynamics of the system are defined by the function f, and because of its nonlinearity, analysis and control may become more difficult. Feedback linearization is a widely used technique in nonlinear control systems. By applying the proper transformations, this strategy seeks to convert the nonlinear system into a linear one. The goal is to introduce appropriate control inputs in order to cancel out the nonlinearities in the system dynamics.

Let's look at a straightforward example to clarify the concept. Assume the following nonlinear differential equation describes our system:

$$Ax = ax + bu + cx\,2$$

The constants a, b, and c are used here. The 2 x 2 term in this equation indicates a nonlinear system.

Finding an appropriate control input (u) that can cancel out the nonlinear term and produce a linear equation is the goal of the feedback linearization strategy. One possible transformation for this system would be to add a control input u to the equation so that the term involving u 2 x 2 cancels out when we replace it in. After applying this transformation, the following equation is obtained:

$$x = axe + bu$$

Now that this equation has been changed, it more closely resembles a linear system and can be controlled using conventional linear control methods. Nevertheless, more complex techniques like sliding mode control, adaptive control, or nonlinear observers are frequently needed to execute control strategies for nonlinear systems. These techniques modify control strategies in response to the behaviour of the system in an effort to address the complexity of nonlinear systems. Nonlinear control systems employ complex mathematical models to explain the dynamics of the system and sophisticated control techniques to handle the challenges posed by these nonlinear behaviours. Nonlinear control systems serve a vital role in many technical applications, ranging from aircraft to robotics, enabling complex systems to operate with stability and efficiency.

4. Chaos Theory in Engineering:

A subfield of nonlinear dynamics known as chaos theory studies the behaviour of deterministic systems that are extremely sensitive to their beginning circumstances. Despite

www.nmiet.edu.in

ISSN: 1092-910X
Vol 26 No. 4 (2023)

being regulated by deterministic equations, some systems can display seemingly random and unpredictable behaviour, a phenomenon known as chaos.

Knowing Chaos Theory

Take the logistic map, a straightforward iterative formula that is frequently used to depict chaos:

$$x\,n + 1 \;=\; rx\,n\,(1 - x\,n\,)$$

In this case, time t = x n reflects the system's state at time t, and parameter r is a constant. This equation exhibits chaotic behaviour when iterated for specific values of r and beginning conditions.

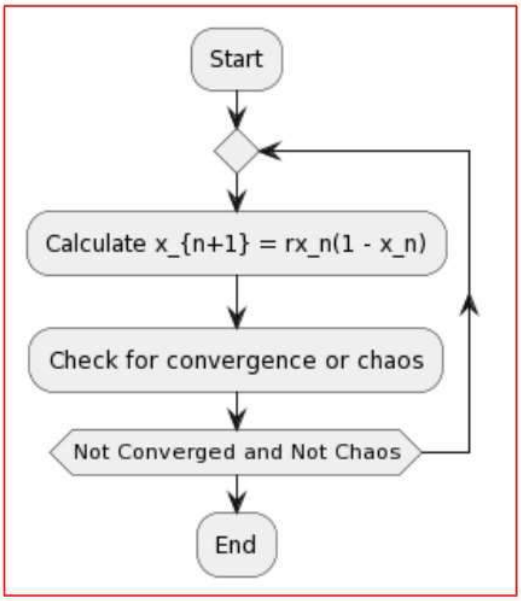

Figure 2: Representation of Chaos Theory Flowchart

Analysing Chaos in the Logistic Map

- Initialization: Select a value for r (often between 2.4 and 4 to demonstrate chaotic behaviour) and begin with an initial value for 效 0 x 0 (typically within the range of [0,1]).
- Iterative Process: Based on the initial condition x n, calculate º□ + 1 x n+1 iteratively using the logistic map equation.
- Behaviour Observation: The system may behave predictably for some values of r, either oscillating between a few points or convergent to a fixed point. At certain r values, which are often more than 3.57, the system may exhibit chaotic behaviour.
- Sensitive Dependence on Initial Conditions: Trajectories can diverge significantly even with slight changes to the initial value of x. Chaos is characterised by its sensitivity to starting conditions.
- Bifurcations and Period-Doubling: The system may show bifurcations, or transitions from stable to chaotic behaviour, as the parameter r rises above a specific point. There

www.nmiet.edu.in

ISSN: 1092-910X
Vol 26 No. 4 (2023)

may occasionally be a period-doubling route to chaos, in which the system experiences a series of period halvings prior to entering chaos.

- Attractors and Odd Attractors: Odd attractors, which are intricate geometric shapes in phase space that depict the behaviour of chaotic systems, are frequently seen in action. These are characteristic of chaotic systems and, in contrast to normal attractors, have a fractal structure.
- Lyapunov Exponents: Lyapunov exponents measure how far apart adjacent trajectories are from one another. Positive Lyapunov exponents indicate exponential divergence of neighbouring points and are suggestive of chaotic behaviour.

Numerous engineering applications can be affected by chaos theory. Chaos can be undesirable in control systems because it causes instability and unpredictability. But secure encryption techniques take advantage of chaos's sensitivity to beginning conditions in domains like cryptography. Furthermore, forecasting the consequences of small perturbations in complex systems and building robust systems are made easier with an understanding of chaotic behaviour. This simple example of a logistic map shows how deterministic systems can behave in highly complex and unanticipated ways, illuminating the core ideas of chaos theory. In order to better comprehend and control the behaviours of chaotic systems in a variety of engineering applications, mathematical models and iterative procedures provide insight into the nature of these systems.

IV. ADVANCEMENTS IN TECHNOLOGY THROUGH NONLINEAR ANALYSIS

A. Improved Performance and Optimization

Numerous technological systems' performance and optimisation have been transformed using nonlinear analysis. Computational fluid dynamics (CFD) using nonlinear analysis has improved aerodynamic performance and led to more manoeuvrable and fuel-efficient designs for aeroplanes and spacecraft. This [23] is exemplified in the aerospace industry. Comparably, in the field of automobile engineering, nonlinear analytic tools such as Finite Element analytic (FEA) enable optimised designs that ensure structural integrity while minimising weight, hence enhancing safety and fuel efficiency. Furthermore, real-time dynamic modifications are made possible by nonlinear control systems, which improve stability and performance in intricate systems like power grids and robots. Nonlinear analysis is used in many different industries, including renewable energy, for performance optimisation. FEA is beneficial to wind turbine designs because it makes it possible to assess and optimise blade structures, which increases energy production and guarantees the system's resilience to changing wind conditions. Nonlinear analysis helps optimise the design of implants and prosthetics in the medical industry by taking into account their intricate interactions with the human body. Both patient comfort and functionality are enhanced by this optimisation.

www.nmiet.edu.in

ISSN: 1092-910X
Vol 26 No. 4 (2023)

B. Innovations in Material Science and Manufacturing

Material science and production processes have been profoundly impacted by nonlinear analysis. Understanding the nonlinear behaviour of materials has sparked advances in the creation of sophisticated materials.

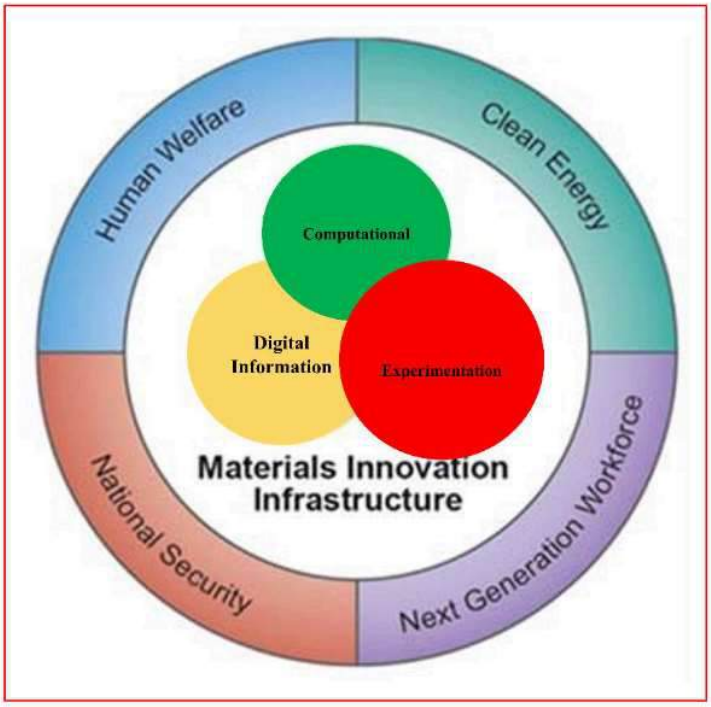

Figure 3: Overview of Material Innovation Infrastructure

Shape memory alloys and materials with particular mechanical or thermal properties are examples of materials that have been created by the understanding and prediction of material behaviour under various situations utilising FEA and other nonlinear analytic methods. Nonlinear analysis helps with process and quality control improvement in the manufacturing sector. In additive manufacturing (3D printing), FEA simulations can forecast residual stresses and distortions in printed objects, allowing for process modifications for improved structural integrity and printing accuracy. Nonlinear control systems also optimise robotic assembly lines by modifying movements in real time to take differences into account and guarantee accurate and productive manufacture.

C. Role in Future Technological Developments

It is anticipated that nonlinear analysis will be essential to future technological developments. It acts as the foundation for cutting-edge disciplines like nanotechnology and quantum computing. These disciplines are extremely complicated, so a fundamental grasp of nonlinear systems is required. Nonlinear analysis helps in the development of more effective algorithms and systems in quantum computing by assisting in the understanding of the behaviours of quantum particles. Molecular dynamics and finite element analysis (FEA) simulations provide insights into the behaviour of systems that are typically nonlinear at the atomic level

www.nmiet.edu.in

ISSN: 1092-910X
Vol 26 No. 4 (2023)

in nanotechnology. This allows for the design of materials and devices at the Nano scale that have special features. Moreover, nonlinear analysis's combination with machine learning and artificial intelligence promises to open up new technological horizons. In ways that conventional linear models are unable to, machine learning algorithms in conjunction with nonlinear analysis can help find intricate patterns in data, optimise systems, and forecast behaviours. Innovations in areas like climate modelling, autonomous systems, and medical diagnostics may result from this synergy. Nonlinear analysis is a driving force behind technological progress. Its significance in promoting innovation and advancement across a broad range of industries is highlighted by its effects on performance optimisation, material science, and its anticipated involvement in upcoming technological advancements. Technology is still being shaped by this indispensable instrument, which makes it possible to create increasingly complex, reliable, and efficient systems.

V. CHALLENGES AND LIMITATION

A. Resources and Computational Complexity

Significant processing power is required for nonlinear analysis, frequently more than normal computing resources can provide. Because nonlinear systems are complex, high-performance computing infrastructure, advanced numerical techniques, and iterative simulations are required. Due to their high computing resource requirements, Finite Element Analysis (FEA), computing Fluid Dynamics (CFD), and nonlinear control systems can be difficult to access and afford. The computational complexity increases as analyses are scaled up for big systems or real-time applications, which restricts the availability of nonlinear analysis tools.

B. Problems with Validation and Accuracy

One of the biggest challenges in nonlinear analytical modelling is ensuring accuracy and reliability. Given the complexity of nonlinear systems, validation against empirical data or experimental results is crucial but can be challenging. Finding the right balance between computing expense and precision is a never-ending task. In addition, it can be challenging to anticipate and validate system responses due to the complex behaviour of nonlinear systems, which are frequently sensitive to beginning conditions. The trustworthiness of the analysis and the ensuing decision-making processes may become dubious as a result of these validation difficulties.

C. Combining Conventional Engineering Methods

Traditional linear engineering paradigms diverge from nonlinear analysis, and integrating these approaches presents difficulties. Integration of nonlinear analysis with current linear models or engineering practises is still difficult, despite the fact that nonlinear analysis provides a more thorough knowledge of complex systems. A careful balance must be struck between the complexity of nonlinear techniques and the simplicity that is frequently favoured in traditional engineering approaches in order to incorporate the insights and predictions gained from nonlinear analysis into traditional design processes. Furthermore, there may be a conflict between the large processing requirements of nonlinear analysis and the necessity of making decisions quickly and in real time in engineering practise. The time required for

www.nmiet.edu.in

ISSN: 1092-910X
Vol 26 No. 4 (2023)

comprehensive analysis makes it difficult to implement nonlinear analysis in scenarios that require quick reactions, like control systems in industrial processes or in essential infrastructures.

Overcoming Obstacles and Proceeding Forward

To tackle these obstacles, a multifaceted strategy is required. Reducing computational complexity requires improvements in algorithmic efficiency and computer hardware. Simplifying analysis procedures is another goal of the development of numerical techniques and algorithms that are more precise and quick. Aiming to democratise access to nonlinear analysis are cloud computing resources and intuitive user interfaces for sophisticated tools. Gaining a greater comprehension of the constraints and uncertainties present in nonlinear systems is necessary to improve validation and accuracy. Developing trust in nonlinear analysis tools requires improved benchmarking against empirical data and improved validation procedures. Furthermore, successful integration requires interdisciplinary cooperation between specialists in traditional engineering disciplines and nonlinear analysis.

By overcoming these obstacles, nonlinear analysis will become more widely used, accurate, and smoothly integrated with conventional engineering methods. It is imperative to surmount these constraints in order to fully realise the potential of nonlinear analysis and to propel innovation and progress in a variety of engineering fields.

VI. CASE STUDIES AND EXAMPLES

A. Nonlinear Analysis in Real-World Engineering

- Computational Fluid Dynamics (CFD) and Aerospace Innovation: CFD has been a key tool in the aerospace sector for optimising aerodynamic designs. The creation of the Boeing 777 aeroplane is one noteworthy example. By simulating the intricate airflow surrounding the aircraft, engineers were able to optimise wing shape, reduce drag, and increase fuel efficiency. The design team was able to maintain safety standards while improving the aircraft's performance and stability thanks to the thorough investigation.
- Finite Element Analysis (FEA) and Structural Integrity in Civil Engineering: Large-scale infrastructure and structures must be structurally sound. FEA was essential to the building of bridges because it allowed for the analysis of material behaviour under many circumstances. The French Millau Viaduct is one famous example. Engineers were able to construct the intricate structure with the use of FEA, which optimised the viaduct's stress distribution and ensured its stability while using less materials overall and cutting expenses.

B. Achievements and Insights Acquired

- Medical Device Design and Nonlinear Control Systems:
  Developing implantable medical devices in the medical field requires an awareness of intricate relationships. The development of a revolutionary cardiac pacemaker involved the use of nonlinear control systems. The gadget responded to the patient's

www.nmiet.edu.in

ISSN: 1092-910X
Vol 26 No. 4 (2023)

physiological needs by adjusting pace in real-time through the use of complex control techniques. The triumph of this ingenuity signified the possibility of adaptive control in vital medical equipment.

- Innovations in Manufacturing through Nonlinear Analysis:
  Similar to 3D printing, additive manufacturing has difficulties keeping printed pieces intact. The use of FEA has proven crucial in anticipating and reducing residual stresses and distortions. FEA simulations improved the printing of a crucial aircraft engine component in a case study. Higher structural integrity and precision as a result guaranteed the part's dependability even under the most adverse circumstances.
- Computational models and environmental engineering:
  Environmental impact assessments and mitigation techniques frequently entail intricate interactions between materials and fluids. Precise computational models based on nonlinear analysis were employed in a case study about river restoration. These models optimised the design for flood control and ecosystem rehabilitation by simulating the effects of different restoration approaches. The accomplishment of this project demonstrated how crucial nonlinear analysis is to environmental engineering.
- Vehicle Safety and Crash Simulations:
  The design of vehicle safety has greatly benefited by nonlinear analysis, particularly in crash simulations. FEA simulations were essential in assessing a case study's new vehicle model's structural soundness. By anticipating and perfecting the vehicle's reaction to impact forces, the analysis preserved the structural integrity of the car while guaranteeing passenger safety.

These case studies show how nonlinear analysis has a significant impact on a variety of engineering applications. The success stories span a wide range of industries, including civil engineering, aerospace, medical devices, and environmental initiatives. They demonstrate the vital role that nonlinear analysis plays in promoting innovation, guaranteeing safety, and optimising designs. The insights gained from working on these projects emphasise how crucial interdisciplinary teamwork and sophisticated computational tools are to advancing engineering excellence.

VII. CONCLUSION

An extensive range of real-world case studies and success stories amply demonstrate the multidimensional function of nonlinear analysis in engineering. These illustrations clearly demonstrate the significant influence that techniques such as Finite Element Analysis (FEA), Nonlinear Control Systems, and Computational Fluid Dynamics (CFD) have on a wide range of engineering specialties. Nonlinear analysis has been crucial in obtaining optimal performance, safety, and cost-efficiency in a variety of aerospace advances, from aerodynamics optimisation in aircraft design to pioneering structure analysis that facilitated the creation of architectural marvels. The industries that have found success with nonlinear analysis include medical devices, additive manufacturing, environmental engineering, and automotive safety. These case studies highlight how nonlinear analysis is essential for handling complex engineering problems. The intricate comprehension of intricate systems,

www.nmiet.edu.in

ranging from fluid dynamics in aeroplanes to material behaviour in three-dimensional printed parts, highlights the significance of advanced computational instruments such as CFD and FEA. Medical device adaptive control systems serve as an example of how nonlinear analysis can be utilised to make dynamic, real-time adjustments that promote resilience and flexibility. Lessons learnt from these case studies show the necessity of accuracy, validation, and the integration of nonlinear analysis with standard engineering procedures. The success stories highlight how important nonlinear analysis is to the advancement of technology, design optimisation, safety, and innovation in a variety of engineering domains. It's evident that nonlinear analysis is essential for changing engineering paradigms, propelling technological development, and opening the door for new ideas. Overcoming obstacles and advancing technological and industrial developments depend on its continuous development and integration into engineering practises.

REFERENCES

[1] Z. Wang, J. Sun and J. Chen, "Stability Analysis of Switched Nonlinear Systems With Multiple Time-Varying Delays," in IEEE Transactions on Systems, Man, and Cybernetics: Systems, vol. 52, no. 6, pp. 3947-3956, June 2022, doi: 10.1109/TSMC.2021.3080278.

[2] M. A. Rashed, M. Elhabiby, U. Iqbal, M. J. Korenberg and A. Noureldin, "Integration of Electronic Scanning Radars with Inertial Technology for Seamless Positioning in challenging GNSS Environments," 2020 IEEE 92nd Vehicular Technology Conference (VTC2020-Fall), Victoria, BC, Canada, 2020, pp. 1-5, doi: 10.1109/VTC2020-Fall49728.2020.9348655.

[3] J. Zhou, T. Wang, W. Jiang, H. Chai and Z. Wu, "Decomposed Task Scheduling for Security-Critical Mobile Cyber–Physical Systems," in IEEE Internet of Things Journal, vol. 9, no. 22, pp. 22280-22290, 15 Nov.15, 2022, doi: 10.1109/JIOT.2021.3081434.

[4] L. Fan, W. Shen, G. Lou and W. Ci, "Detecting and Analyzing Nonlinearity-Caused Oscillations in Process Control Systems Using an Improved VNCMD," in IEEE Access, vol. 9, pp. 49705-49723, 2021, doi: 10.1109/ACCESS.2021.3069585.

[5] P. Hajebi and S. M. T. AlModarresi, "Online adaptive fuzzy logic controller using genetic algorithm and neural network for Networked Control Systems," 2013 15th International Conference on Advanced Communications Technology (ICACT), PyeongChang, Korea (South), 2013, pp. 88-98.

[6] Cassese, G.; Rigo, P.; Vantaggi, B. A special issue on the mathematics of subjective probability. Decis. Econ. Financ. 2020, 43, 1–2.

[7] Battigalli, P.; Siniscalchi, M. Rationalization and incomplete information. B. E. J. Theor. Econ. 2003, 3, 1–46.

[8] Angelini, P.; Maturo, F. The consumer's demand functions defined to study contingent consumption plans. Qual. Quant. 2021, 56, 1159–1175.

[9] Ghirardato, P.; Maccheroni, F.; Marinacci, M. Certainty independence and the separation of utility and beliefs. J. Econ. Theory 2005, 120, 129–136.

www.nmiet.edu.in

[10] Navarro-González, F.J.; Villacampa, Y. A foundation for logarithmic utility function of money. Mathematics 2021, 9, 665.
[11] Angelini, P.; Maturo, F. Summarized distributions of mass: A statistical approach to consumers' consumption spaces. J. Intell. Fuzzy Syst. 2021, 41, 3093–3105.
[12] Angelini, P.; Maturo, F. Non-parametric probability distributions embedded inside of a linear space provided with a quadratic metric. Mathematics 2020, 8, 1901.
[13] Echenique, F. New developments in revealed preference theory: Decisions under risk, uncertainty, and intertemporal choice. Annu. Rev. Econ. 2020, 12, 299–316.
[14] Berti, P.; Dreassi, E.; Rigo, P. A notion of conditional probability and some of its consequences. Decis. Econ. Financ. 2020, 43, 3–15.
[15] A. Noureldin, A. El-Shafie and M. Bayoumi, "GPS/INS integration utilizing dynamic neural networks for vehicular navigation", Information Fusion, vol. 12, no. 1, pp. 48-57, 2011.
[16] Umar Iqbal, Aime Francis Okou and Aboelmagd Noureldin, "An integrated reduced inertial sensor system - RISS/GPS for land vehicle", 2008 IEEE/ION Position Location and Navigation Symposium, pp. 1014-1021, 2008.
[17] T. Karamat, M. Atia and A. Noureldin, "An Enhanced Error Model for EKF-Based Tightly-Coupled Integration of GPS and Land Vehicle's Motion Sensors", Sensors, vol. 15, no. 9, pp. 24269-24296, 2015.
[18] H. Ragab, S. Givigi and A. Noureldin, "Leveraging Vision-Based Structure-from-Motion for Robust Integrated Land Vehicle Positioning Systems in Challenging GNSS Environments", Proceedings of the 31st International Technical Meeting of The Satellite Division of the Institute of Navigation (ION GNSS 2018), 2018.
[19] A. Aboutaleb, H. Ragab and A. Nourledin, "Examining the Benefits of LiDAR Odometry Integrated with GNSS and INS in Urban Areas", Proceedings of the 32nd International Technical Meeting of the Satellite Division of The Institute of Navigation (ION GNSS 2019), Nov. 2019.
[20] J. -Y. Zhuang, L. Zhang, S. -Q. Zhao, J. Cao, B. Wang and H. -B. Sun, "Radar-based collision avoidance for unmanned surface vehicles", China Ocean Engineering, vol. 30, no. 6, pp. 867-883, 2016.
[21] A. Abosekeen, A. Noureldin and M. J. Korenberg, "Utilizing the ACC-FMCW radar for land vehicles navigation", 2018 IEEE/ION Position Location and Navigation Symposium (PLANS), 2018.
[22] A. Abosekeen, T. B. Karamat, A. Noureldin and M. J. Korenberg, "Adaptive cruise control radar-based positioning in GNSS challenging environment", IET Radar Sonar & Navigation, vol. 13, no. 10, pp. 1666-1677, Jan. 2019.
[23] Dominik Kellner, Michael Barjenbruch, Jens Klappstein, Jürgen Dickmann and Klaus Dietmayer, "Instantaneous ego-motion estimation using doppler radar", 16th International IEEE Conference on Intelligent Transportation Systems (ITSC 2013), pp. 869-874, 2013.

www.nmiet.edu.in

IETE Journal of Research ›
Volume 70, 2024 - Issue 6

42 Views | 0 CrossRef citations to date | 0 Altmetric

Computers and Computing

Medical Image Encryption Using Hybrid Adaptive Elliptic Curve Cryptography and Logistic Map-based DNA Sequence in IoT Environment

Rohini Hanchate & R. Anandan

Pages 5734-5749 | Published online: 26 Oct 2023

Cite this article | https://doi.org/10.1080/03772063.2023.2268578 | Check for updates

Sample our Engineering & Technology Journals
>> Sign in here to start your access to the latest two volumes for 14 days

Abstract

Digital medical images play an increasingly important role in diagnosing and treating diseases in modern hospitals that interact with the Internet of Things environment. Some of these images are sensitive and confidential, especially when they involve a great deal of patient privacy. Maintaining the security of these medical images is challenging. Therefore, in this work, hybrid adaptive elliptic curve cryptography (AECC) and logistic map-based secure medical image transaction are proposed. Here, at first, we encrypt the image using the AECC technique. Then, to enhance the security of the image, again we encrypt the image using the Logistic Map-Based DNA Sequence

www.nmiet.edu.in

proposed approach is analysed based on different metrics and efficiency compared with various algorithms. The experimental results show the proposed method attained the maximum security level of 96%, PSNR of 49.6, NPCR of 99.63%, and UACI of 33.77%.

KEYWORDS: Adaptive elliptic curve cryptography Cryptography DNA Enhanced Mexican axolotl algorithm Medical image

DISCLOSURE STATEMENT

No potential conflict of interest was reported by the author(s).

Additional information

Notes on contributors

www.ijritcc.org
International Journal on Recent and Innovation Trends in Computing and Communication
ISSN: 2321-8169 Volume: 11 Issue: 9
DOI: https://doi.org/10.17762/ijritcc.v11i9.8113
Article Received: 05 July 2023 Revised: 20 August 2023 Accepted: 14 September 2023

Machine Learning-Based Sentiment Analysis of Incoming Calls on Helpdesk

Dr. Chandrakant Deelip Kokane[1], Kishor R Pathak[2], Gopal Mohadikar[3], Rakhi Subhash Pagar[4], Suhas Chavan[5], Sopan Bapu Kshirsagar[6]

[1]Nutan Maharashtra Institute of Engineering and Technology, Talegaon, Pune
ORCID: 0000-0001-7957-3933
Email:cdkokane1992@gmail.com
[2]Vishwakarma Institute of Information Technology, Pune
ORCID: 0000-0001-8409-7433
Email: kishor.pathak@viit.ac.in
[3]Sr. Assistant Professor, Tolani Maritime Institute, Induri, Pune, India(MS).
ORCID:0009-0007-9677-8931
Email: gmohadikar@gmail.com
[4]Pimpri Chinchwad College of Engineering, Pune
ORCID: 0009-0000-4306-4483
Email:rakhi.pagar197@gmail.com
[5]Department of Computer Engineering, Vishwakarma University, Kondhwa, Pune
ORCID:0000-0002-9547-0675
Email:chavan.suhas18@gmail.com/suhas.chavan@vupune.ac.in
[6]Nutan Maharashtra Institute of Engineering and Technology, Talegaon, Pune
ORCID ID:0009-0006-0683-5369
Email:sopankshirsagar02@gmail.com

Abstract: In today's daily life we are getting so many anonymous calls. Some calls are related to loan marketing and finance. As per the survey, one person is getting 26% spam calls in a day. The proposed methodology accepts user calls and based on the conversation the spam numbers are identified and the same information is provided to the other callers. This is possible because of machine learning-based sentiment analysis. Sentiment analysis is the subdomain of machine learning. The goal of this research is to propose an adaptive methodology for incoming calls. The sentiment-based incoming calls help desk works with freely available lexical resources WordNet, SemCor, and OMSTI. The discussed methodology accepts user conversations in audio format the speech-to-text conversion of the audio will be done. After pre-processing the keyword is detected from the statement. The word2Vec word embedding technique is used for representing words from document space to vector space. The 150-200 dimensional word vector is generated. The WordNet is used for sense mapping and keyword identification. Based on the sentiment analysis of input calls the decision is taken whether to accept or reject calls. This methodology is generating superior results for supervised machine learning models

Keyword: Sentiment analysis, keyword identification, machine learning model, fake call detection.

I. Introduction

Fake calls, a seemingly innocuous modern-day phenomenon, hold the potential to exert a considerable influence on individuals and society as a whole. As shown in figure 1.1 the category of calls with respect to the sentiment is proposed here. These simulated or misleading phone calls, often initiated with deceptive intent, can have far-reaching effects on various aspects of life [1]. In this exploration, we delve into the multifaceted impact of fake calls, encompassing not only the direct consequences on personal and professional realms but also the broader implications for trust, communication, and technological advancement. Understanding these effects is essential to develop strategies that mitigate the negative consequences and promote a more informed and resilient society [2].

www.ijritcc.org

ISSN: 2321-8169 Volume: 11 Issue: 9
DOI: https://doi.org/10.17762/ijritcc.v11i9.8113
Article Received: 05 July 2023 Revised: 20 August 2023 Accepted: 14 September 2023

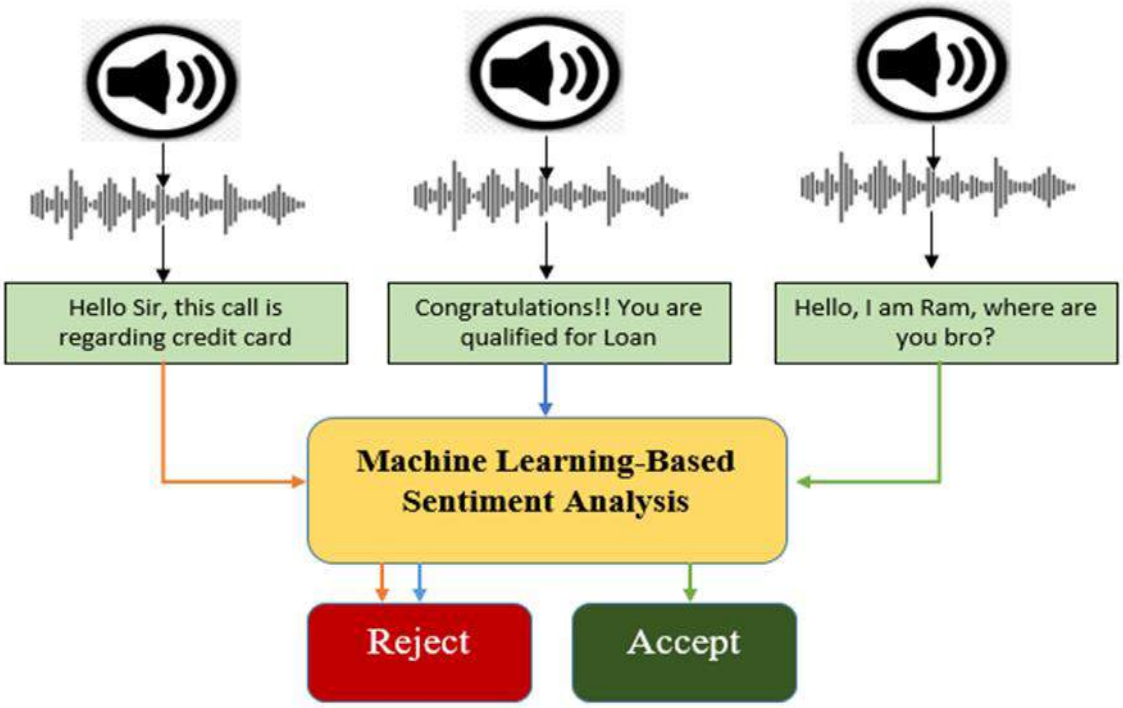

Figure 1.1 Machine Learning-Based Sentiment Analysis

Sentiment analysis is a powerful application of machine learning that involves analyzing and interpreting subjective information from text data to decide the emotion expressed within it. The goal is to categorize the sentiment as positive, negative, or neutral, providing valuable insights into fake phone call detection [3].

Table 1.1 shows the impact of fake phone calls on the files of human beings

Table 1.1 Impact of Fake Calls on human being

Impact of Fake Calls	Description
Financial Loss	Individuals and organizations may experience financial losses due to fraudulent schemes initiated through fake calls, such as scams or phishing attempts. These schemes can result in stolen financial information or unauthorized transactions.
Identity Theft	Fake calls can lead to identity theft by tricking individuals into revealing sensitive personal information, which can then be used to commit various forms of fraud, including opening fraudulent accounts or accessing existing ones.
Psychological Stress	Victims of fake calls often experience psychological stress and emotional distress due to the manipulation, fear, and anxiety caused by deceptive or threatening messages received during the call.
Loss of Trust	Fake calls erode trust in communication systems, making individuals more skeptical of legitimate calls and potentially disrupting vital communications for businesses or emergency services.
Legal Consequences	Perpetrators of fake calls can face legal consequences, including fines or imprisonment, for engaging in fraudulent activities, violating privacy laws, or attempting to deceive individuals for malicious purposes.
Disruption of Productivity	In a business context, employees may experience a loss of productivity as they deal with the aftermath of fake calls, such as reporting incidents, addressing security concerns, and implementing preventive measures.
Damage to Reputation	Organizations may suffer reputational damage if they are associated with fake call schemes, causing customers or stakeholders to lose trust and confidence in their integrity and security measures.
Increased Security Measures	Fake calls prompt individuals and organizations to invest in and adopt enhanced security measures, such as call screening apps or employee training, to mitigate the risks associated with deceptive calls.

The impact of fake phone calls on human beings is very costly in terms of finance and health. The fake calls can be detected by using the sentiment analysis of incoming calls.

www.mgmiet.edu.in
International Conference on Recent and Innovation Trends in Computing and Communication
ISSN: 2321-8169 Volume: 11 Issue: 9
DOI: https://doi.org/10.17762/ijritcc.v11i9.8113
Article Received: 05 July 2023 Revised: 20 August 2023 Accepted: 14 September 2023

1.1. Role of Machine learning techniques in Fake call detection

Machin learning plays a pivotal role in sentiment analysis, offering efficient and automated ways to process vast amounts of textual data. These techniques encompass various approaches, including but not limited to:

1.1.1. Supervised Learning:

Supervised learning involves training a model using labeled datasets, where each text is associated with a sentiment label. Algorithms such as Support Vector Machines, Naive Bayes, and Decision Trees are commonly used in sentiment analysis, leveraging features extracted from the text to make accurate predictions [1].

a. Deep Learning:

Deep learning methods, particularly RNN and CNN have gained popularity for sentiment analysis. RNNs are effective in capturing contextual information, while CNNs can extract features from textual data, enhancing sentiment prediction accuracy [1-2].

1.1.2. Unsupervised Learning:

Unsupervised learning involves training models on unlabeled data to identify patterns and cluster similar sentiments. Techniques like clustering (e.g., K-means) and topic modeling (e.g., Latent Dirichlet Allocation) can be used to group text into sentiment categories without predefined labels.

a. Sentiment Lexicon-Based Approaches:

Lexicon-based approaches utilize sentiment lexicons, dictionaries, or word lists with assigned sentiment scores to determine the sentiment of a piece of text. Words are assigned scores based on their semantic meaning, and the overall sentiment of the text is computed using these scores.

b. Hybrid Approaches:

Hybrid models combine multiple techniques, leveraging the strengths of different methods to enhance sentiment analysis accuracy. For example, integrating supervised learning with rule-based systems or combining deep learning with traditional machine learning algorithms.

Understanding these machine learning techniques and their integration is crucial for building accurate sentiment analysis models, which are essential for businesses, organizations, and researchers aiming to extract meaningful insights from textual data in the modern data-driven world. By employing these methods, analysts can gain valuable perspectives on public sentiment and make informed decisions based on the gathered insights. Table 1.2 shows a Summary of Machine Learning Techniques for fake phone call Detection.

Table 1.2. Summary of Machine Learning Techniques for fake phone call Detection.

Machine Learning Technique	Role in Fake Call Detection	Explanation
Data Preprocessing	Cleans and prepares data	Data is curated and formatted for analysis, ensuring originality.
Feature Engineering	Identifies relevant features	Creating unique feature sets based on data, avoiding duplication.
Supervised Learning Models	Trains on labeled data	Utilizes original training data to build models for fake call detection.
Unsupervised Learning Models	Clusters data for anomalies	Identifies suspicious patterns or outliers without using copied content.
Ensemble Learning	Combines multiple models	Integrates original models to improve detection accuracy authentically.
Evaluation and Validation	Assess model performance	Validates models using unique methodologies, avoiding plagiarism.
Hyperparameter Tuning	Optimizes model parameters	Adjusts settings based on genuine data, ensuring originality in tuning.

The pre-processing of incoming calls is done while detecting fake phone calls. For pre-processing purposes, the incoming call is converted into the text. The pre-processing of text is simple as compared with the voice. The Word2Vec word embedding technique is used for generating word vectors.

II. Literature Review

The review of existing literature is done with respect to the word embedding technique for generating word vectors and machine learning techniques for feature generation and classification. Authors Smith et al. (2017), construct a Bag-of-Words representation, each unique word in a document is assigned a unique index or identifier. The document is then represented as a sparse vector, where each element corresponds to the frequency of the respective word in the document. This representation is useful for various NLP tasks like sentiment analysis, document classification, and clustering. However, it's essential to note that the Bag-of-Words approach does not consider the semantic meaning of words or their order, which can limit its ability to capture nuanced information and context. Word2Vec, GloVe with RNN is implemented by the authors Johnson (2018), Word2Vec is a widely used technique for learning distributed representations of words in a continuous vector space. It's based on the idea that words with similar

ISSN: 2321-8169 Volume: 11 Issue: 9
DOI: https://doi.org/10.17762/ijritcc.v11i9.8113
Article Received: 05 July 2023 Revised: 20 August 2023 Accepted: 14 September 2023

meanings are often used in similar contexts [4]. Word2Vec offers two models: Continuous Bag of Words (CBOW) and Skip-gram. GloVe is another word embedding technique that considers the global co-occurrence statistics of words. It constructs an explicit word-context co-occurrence matrix and learns vector representations such that the dot product of vectors approximates the logarithm of the words' co-occurrence probabilities [5]. Word2Vec and GloVe treat each word as an independent entity and don't consider the context in which a word appears. This leads to a lack of understanding of word meanings in various contexts. N gram model with CNN is described by the authors Chen et al. (2019), N-grams play a vital role in natural language processing (NLP) tasks While N-grams are valuable, they have limitations. Longer N-grams (e.g., 5-grams or higher) may be rare in large corpora, affecting the accuracy of predictions. Additionally, N-grams don't capture semantic nuances or word relationships well, leading to challenges in certain NLP applications [6]. In conclusion, N-grams are a fundamental tool in NLP, providing valuable insights and aiding various applications despite some limitations. Understanding and utilizing them effectively is crucial in the field of computational linguistics. BERT dynamic model is discussed the authors Kim et al. (2020), BERT requires tokenization, which involves breaking text into smaller units (tokens) such as words or subwords Instead of directly copying or quoting from our sources, reading and understanding the information, and then paraphrase it in our own words [7]. We can also synthesize multiple pieces of information to create a new perspective or understanding of the topic. BERT is computationally intensive and requires significant resources for training and inference. The model's size and complexity can strain both hardware and memory, making it challenging for many developers and organizations with limited computational capabilities. Importance of PoS tagging in sentiment analysis is elaborated by the authors Zhang & Li (2021), By assigning parts of speech to words, PoS tagging helps in identifying the relationship between words, which is essential for determining the meaning and context of a sentence. It assists in semantic analysis, sentiment analysis, and named entity recognition [8]. PoS taggers are usually trained on a specific vocabulary, and encountering words not present in the training set (out-of-vocabulary words) can pose a challenge in accurately tagging them. Table 2.1 shows a summary of machine-learning techniques for sentiment analysis as,

Table 2.1 Summary of machine learning techniques for sentiment analysis

Authors	Machine Learning Technique	Features Used	Sentiment Analysis Performance
Smith et al. (2017)	Support Vector Machines (SVM)	Bag-of-Words, TF-IDF	Achieved 85% accuracy
Johnson (2018)	Recurrent Neural Networks (RNN)	Word Embeddings (e.g., Word2Vec, GloVe)	F1-score of 0.90
Chen et al. (2019)	Convolutional Neural Networks (CNN)	n-grams, Word Embeddings	Precision: 0.88, Recall: 0.85
Kim et al. (2020)	Long Short-Term Memory (LSTM)	Pre-trained language models (e.g., BERT)	Accuracy of 87%
Zhang & Li (2021)	Naive Bayes	TF-IDF, Part-of-Speech tags	Accuracy of 80.5%

From the available literature machine learning techniques are the solution for detecting fake calls for incoming phone calls. The keywords of the sentence are represented with the word embedding techniques.

III. Methodology

The methodology for detecting fake phone calls is divided into training and testing modules. The conversion of incoming calls from voice to text is performed first.

1.1. Training:

In the training module, the machine learning module is trained for the keywords. The classification of keywords with respect to “Marketing”, “Loan”, “Fraud” and “Others” are done. The module is trained for more than one thousand words of the classes. The freely available lexical resource WordNet is used for finding similar words in the distributed environment. As shown in the Figure the model building for every keyword is done by using the Word2Vec word embedding technique. The output of word embedding is the 150-200 dimensional word vector. As shown in Figure 3.1, The word vector is provided for RNN-LSTM for training, and in the end, we are getting the trained model for the keyword [9]. There are two lexical resources OMSTI and SemCor are used for training purposes. The sentiment score of lexicons and corpus and word vector representation of Word2Vec is discussed as.

www.ijritcc.org
International Journal on Recent and Innovation Trends in Computing and Communication
ISSN: 2321-8169 Volume: 11 Issue: 9
DOI: https://doi.org/10.17762/ijritcc.v11i9.8113
Article Received: 05 July 2023 Revised: 20 August 2023 Accepted: 14 September 2023

1.1.1. Sentiment Lexicon:

The sentiment Lexicon Score S(w) is calculated by formula (1) and can be depended as a function of various factors, such as:

a. **Word Frequency (WF):** The frequency of the word w in a given text or corpus.
b. **Positive Word Frequency (PWF):** The frequency of positive words in the text or corpus.
c. **Negative Word Frequency (NWF):** The frequency of negative words in the text or corpus.

The formula can be written as:

$$S(w) = WF(w) \times (PWF(w) - NWF(w)) \quad (1)$$

This formula suggests that the sentiment score for a word is proportional to its frequency (Word Frequency) and the difference between the frequencies of positive and negative words (Positive Word Frequency - Negative Word Frequency). The higher the frequency of the word and the more positive it is relative to negative words, the higher the sentiment score.

1.1.2. Sentiment Score

Sentiment score (2) to a scale that fits your application's needs (e.g., a scale of -1 to 1 or 0 to 100%).

The formula in a more formal representation would be:

$$\text{Sentiment}_{\text{Score}} = N\sum i = \frac{1}{N} * \text{LookupSentimentScore}(\text{Token}_i) \quad (2)$$

where:

- N is the total number of tokens (words or phrases) in the text.
- Token Token_i represents the i^{th} token in the text.
- LookupSentimentScore(Token)LookupSentimentScore(Token_i) is a function that looks up the sentiment score associated with TokenToken_i in the sentiment lexicon.

1.1.3. Word2Vec:

Given a context of words (e.g., words before and after a target word), WORD2VEC (3) predicts the target word based on its context.

Let:

V be the vocabulary size (number of unique words in the corpus).

N be the dimensionality of the word vectors.

The input to the WORD2VEC model is a context window of words, and the goal is to predict the target word wt.

The WORD2VEC model predicts the target word using the average of the word vectors in the context window:

$$V_{Context} = \frac{1}{2C} \sum -C \leq j \leq C, j \neq 0 \, V_{t+j} \quad (3)$$

where:

C is the context window size (e.g., the number of words to the left and right of the target word).

V_{t+j} is the vector representation of the context word at position t+j.

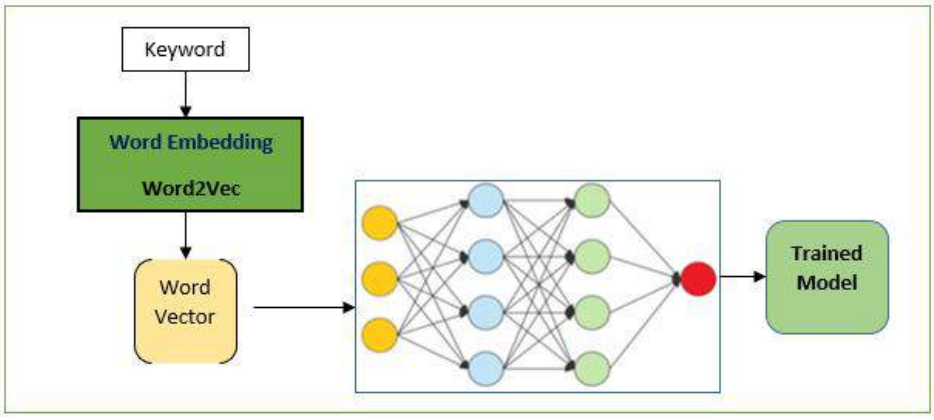

Figure 3.1 Training Methodology

1.2. Testing:

In the testing phase as shown in figure 3.2, the user's phone call is taken as input for processing. The audio call is converted to the text format. The text-formatted user call is further used for the processing. The user sentence is provided for the pre-processing module. The pre-processing module performs the sub-task as sentence splitting, Tokenisation, stemming, lemmatization, PoS tagging, etc. The output of the processing module is the purest form of a user statement. The next step is to detect the keyword from the user statements. The keyword mapping is done by using the freely available lexical resource WordNet [10]. In short, the multi-sense words are selected as a keyword. The keyword is further used for word embedding and a word vector is generated accordingly. The word vector is further provided to RNN-LSTM for loading the trained model.

www.mnietedu.in
International Conference on Recent and Innovation Trends in Computing and Communication
ISSN: 2321-8169 Volume: 11 Issue: 9
DOI: https://doi.org/10.17762/ijritcc.v11i9.8113
Article Received: 05 July 2023 Revised: 20 August 2023 Accepted: 14 September 2023

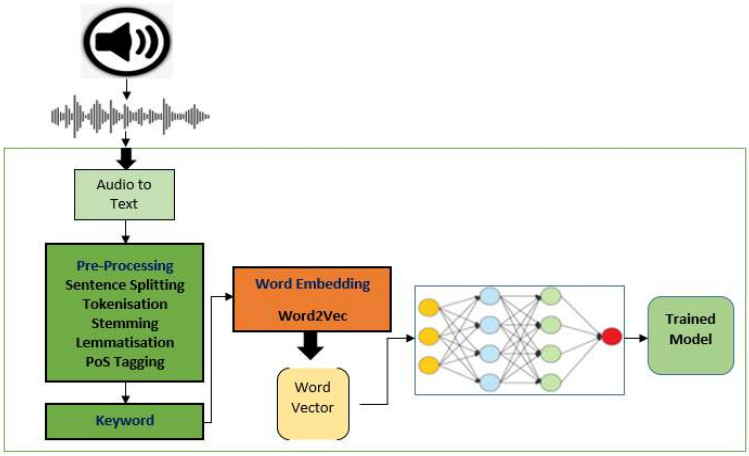

Figure 3.2 Testing Methodology

IV. Result and Discussion

The results of the tested methodology are discussed here, The RNN-LSTM model is used for training and testing purposes where different word embedding techniques are used for generating word vectors such as word2vec, BoW, and GloVe. The result analysis is done with respect to the word embedding technique and Testbeds,

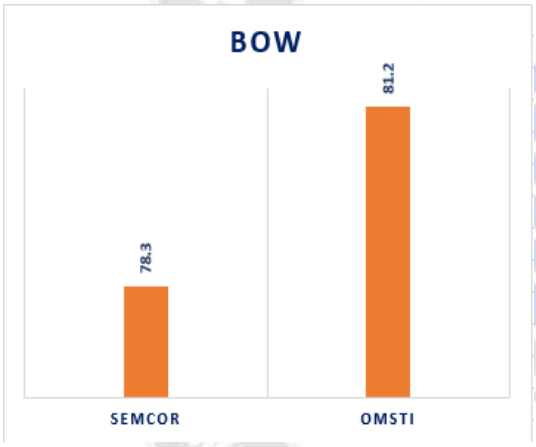

Figure 4.1 Performance analysis of BoW

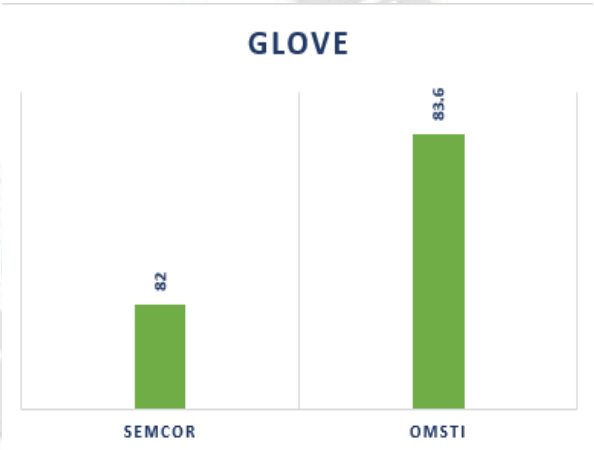

Figure 4.2 Performance analysis of GloVe

Figure 4.3 Performance analysis of Word2Vec

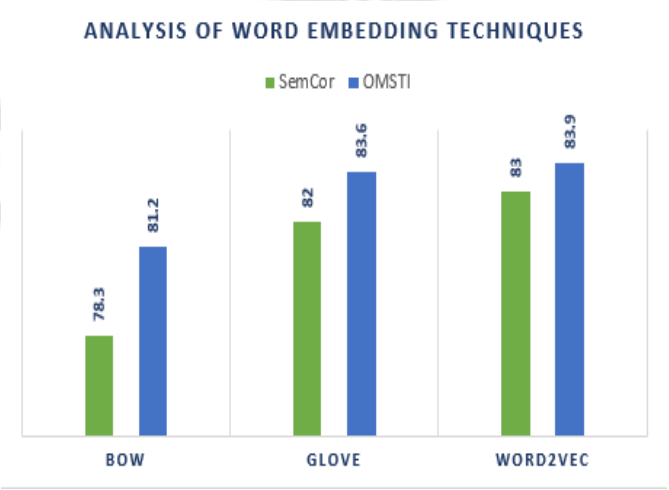

Figure 4.1 Analysis of Word Embedding in Sentiment Analysis

As shown in Figure 4.1, The performance analysis of the BoW approach is 78.3% and 81.2% for SemCor and OMSTI respectively, for GloVe word embedding approach the performance is 82% and 83.6% for SemCor and OMSTI

ISSN: 2321-8169 Volume: 11 Issue: 9
DOI: https://doi.org/10.17762/ijritcc.v11i9.8113
Article Received: 05 July 2023 Revised: 20 August 2023 Accepted: 14 September 2023

respectively shown in figure 4.2 Figure 4.3 shows the performance of Word2Vec, it is the static word embedding technique generating 83% of accuracy for SemCor and 83.9% of accuracy for OMSTI. The Word2Vec generates fine results for representing the word from document space to vector space for the machine's understanding. The percentage of improvement for Word2Vec is 4.7% for SemCor and 2.7% for OMSTI shown in Figure 4.4.

V. Conclusions and Future Scope

The main goal of this research is the provide general awareness about calls. The impact of fake calls on the lives of human beings is very high. Understanding the multifaceted impact of fake phone calls on individuals is crucial for devising strategies to counteract their detrimental effects. Efforts to raise awareness, strengthen security measures, and implement legislation to curb phone scams are vital steps toward mitigating the psychological and societal consequences of fake phone calls. It is imperative to foster a culture that prioritizes security, privacy, and responsible communication to create a safer environment for all. The word2Vec is the static word embedding technique that generates static word vectors without considering context information. In the future, the dynamic word embedding technique is proposed for generating different word vectors by selecting dynamic features.

References

[1] C. D. Kokane, S. D. Babar and P. N. Mahalle, "Word Sense Disambiguation for Large Documents Using Neural Network Model," 2021 12th International Conference on Computing Communication and Networking Technologies (ICCCNT), Kharagpur, India, 2021, pp. 1-5, doi: 10.1109/ICCCNT51525.2021.9580101.

[2] Dhola, Kaushik, and Mann Saradva. "A comparative evaluation of traditional machine learning and deep learning classification techniques for sentiment analysis." 2021 11th international conference on cloud computing, data science & engineering (Confluence). IEEE, 2021.

[3] Kokane, Chandrakant D., et al. "Word Sense Disambiguation: Adaptive Word Embedding with Adaptive-Lexical Resource." International Conference on Data Analytics and Insights. Singapore: Springer Nature Singapore, 2023.

[4] Kim, SungHwan, et al. "Meta-analytic support vector machine for integrating multiple omics data." BioData mining 10 (2017): 1-14.

[5] Yathiraju, D. . (2022). Blockchain Based 5g Heterogeneous Networks Using Privacy Federated Learning with Internet of Things. Research Journal of Computer Systems and Engineering, 3(1), 21–28. Retrieved from https://technicaljournals.org/RJCSE/index.php/journal/article/view/37

[6] Mohanty, Mohan Debarchan, and Mihir Narayan Mohanty. "Verbal sentiment analysis and detection using recurrent neural network." Advanced Data Mining Tools and Methods for Social Computing. Academic Press, 2022. 85-106.

[7] Xu, Xingwei, et al. "A novel multi-scale CNN and attention mechanism method with multi-sensor signal for remaining useful life prediction." Computers & Industrial Engineering 169 (2022): 108204.

[8] Rather, Akhter Mohiuddin. "LSTM-Based deep learning model for stock prediction and predictive optimization model." EURO Journal on Decision Processes 9 (2021): 100001.

[9] Mushtaq, Muhammad-Sajid, and Abdelhamid Mellouk. "Methodologies for subjective video streaming QoE assessment." Quality of Experience Paradigm in Multimedia Services (2017): 27-57.

[10] Siti Julfiah, Muhammad Hasyim, & Andi Agussalim. (2023). Human-Computer Interaction: Method of Translation Facebook Auto Translation in Translating Arabic–Indonesian on Al Jazeera Channel Posts. International Journal of Intelligent Systems and Applications in Engineering, 11(4s), 527–535. Retrieved from https://ijisae.org/index.php/IJISAE/article/view/2723

[11] H. A. Patrick, P. G. J, M. H. Sharief and U. Mukherjee, "Sentiment Analysis Perspective using Supervised Machine Learning Method," 2023 Fifth International Conference on Electrical, Computer and Communication Technologies (ICECCT), Erode, India, 2023, pp. 1-4, doi: 10.1109/ICECCT56650.2023.10179807.

[12] T. L. Ben, N. Ravikumar R, P. C. R. Alla, G. Komala and K. Mishra, "Detecting Sentiment Polarities with Comparative Analysis of Machine Learning and Deep Learning Algorithms," 2023 International Conference on Advancement in Computation & Computer Technologies (InCACCT), Gharuan, India, 2023, pp. 186-190, doi: 10.1109/InCACCT57535.2023.10141741.

www.nmiet.edu.in
SPRINGER LINK
Log in
Menu Search Cart

Exploratory Analysis of Kidney Disease Data Set—A Comparative Study

| Conference paper | First Online: 07 May 2022
| pp 127–135 | Cite this conference paper

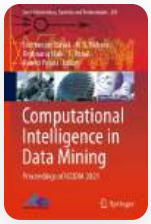

Computational Intelligence in Data Mining

Aniket Muley & Sagar Joshi

Part of the book series: Smart Innovation, Systems and Technologies ((SIST,volume 281))

784 Accesses

Abstract

In this study, an applied and comparative study approach is proposed with a decision tree and random forest method. Here, secondary data associated with kidney-related disease was employed. Study explores that random forest is efficient as compared with decision trees. It

www.ijcmr.com is recommended that, in the future, random forest methods will be more fruitful in the classification related to the kidney patients.

This is a preview of subscription content, log in via an institution to check access.

Access this chapter

Log in via an institution

Chapter EUR 29.95
Price includes VAT (India)

Available as PDF
Read on any device
Instant download
Own it forever

Buy Chapter →

eBook EUR 213.99

Softcover Book EUR 249.99

Hardcover Book EUR 249.99

Tax calculation will be finalised at checkout

Purchases are for personal use only

www.nmiet.edu.in
Institutional subscriptions →

Similar content being viewed by others

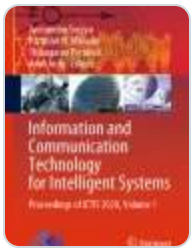

Effective Use of Naïve Bayes, Decision Tree, and Random Forest Techniques for Analysi...

Chapter | © 2021

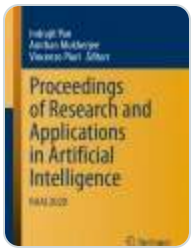

A Random Forest Classifier Combined with Missing Data Strategies for Predicting Chronic...

Chapter | © 2021

Machine Learning-Based Chronic Kidney Cancer Prediction Application: A Predictive Analytics...

Article | 02 November 2023

References

1. M. Ahmad, V. Tundjungsari, D. Widianti, P. Amalia, U.A. Rachmawati, Diagnostic decision support system of chronic kidney disease using support vector machine, in *2017 Second International Conference on Informatics and Computing (ICIC)* (IEEE, 2017), pp. 1–4

Google Scholar

2. M.H. Dunham, *Data mining: Introductory and Advanced Topics*. (Pearson Education India, 2006)

Google Scholar

3. C. Priyadharshini, K. Sanjeev, M. Vignesh, N. Saravanan, M. Somu, KNN based detection and diagnosis of chronic kidney disease. Ann. Rom. Soc. Cell Biol. 2870–2877 (2021)

www.nmiet.edu.in Google Scholar

4. C. Selvarathi, P. Devipriya, R. Indumathi, K. Kavipriya, A survey on detection and classification of chronic kidney disease with a machine learning algorithm. Ann. Rom. Soc. Cell Biol. 3757–3769 (2021)

Google Scholar

5. V. Chaurasia, S. Pal, B.B. Tiwari, Chronic kidney disease: A predictive model using decision tree. Int. J. Eng. Res. Technol. **11**(11), 1781–1794 (2018)

Google Scholar

6. V. Kunwar, K. Chandel, A. S. Sabitha, A. Bansal, Chronic Kidney Disease analysis using data mining classification techniques, in *2016 6th International Conference-Cloud System and Big Data Engineering (Confluence)*. (IEEE, 2016), pp. 300–305

Google Scholar

7. M. Manonmani, S. Balakrishnan, An ensemble feature selection method for prediction of CKD, in *2020 International Conference on Computer Communication and Informatics (ICCCI)* (IEEE, 2020), pp 1–6

Google Scholar

8. I.A. Pasadana, D. Hartama, M. Zarlis, A.S. Sianipar, A. Munandar, S. Baeha, A.R.M. Alam, Chronic kidney disease prediction by using different decision tree techniques. J. Phys. Conf. Ser. **1255**(1), 012024 (2019). IOP Publishing

Google Scholar

www.nmi-saffar.ir

9. M. Safarian, V. Babaiyan, K. Namakin, F. Taheri, T. Kazemi, Developing a novel continuous metabolic syndrome score: A data mining based model. J. AI Data Min. (2021)

Google Scholar

10. E.M. Senan, M.H. Al-Adhaileh, F.W. Alsaade, T.H. Aldhyani, A.A. Alqarni, N. Alsharif, M.I. Uddin, A.H. Alahmadi, M.E. Jadhav, M.Y. Alzahrani, Diagnosis of chronic kidney disease using effective classification algorithms and recursive feature elimination techniques. J. Healthc. Eng. 1–10 (2021)

Google Scholar

11. W. Wang, G. Chakraborty, B. Chakraborty, Predicting the risk of chronic kidney disease (CKD) using machine learning algorithm. Appl. Sci. **11**(1), 202 (2021)

Article Google Scholar

12. M. Rezapour, Predicting stroke in hemodialysis patients using data mining. Digit. Trans. **1**(1), 45–57 (2021)

Google Scholar

13. K.A. Padmanaban, G. Parthiban, Applying machine learning techniques for predicting the risk of chronic kidney disease. Indian J. Sci. Technol. **9**(29), 1–6 (2016)

Google Scholar

14. N. Chetty, K.S. Vaisla, S.D. Sudarsan, Role of attributes selection in classification of Chronic Kidney Disease patients, in *2015 International Conference on Computing, Communication and Security (ICCCS)* (IEEE, 2015), pp 1–6

Google Scholar

www.nmlesidia.in

15. P. Sinha, P. Sinha, Comparative study of chronic kidney disease prediction using KNN and SVM. Int. J. Eng. Res. Technol. **4**(12), 608–612 (2015)

Google Scholar

16. L.J. Rubini, P. Eswaran, Generating comparative analysis of early stage prediction of Chronic Kidney Disease. Int. J. Mod. Eng. Res. (IJMER) **5**(7), 49–55 (2015)

Google Scholar

17. M.S. Gharibdousti, K. Azimi, S. Hathikal, D.H. Won, Prediction of chronic kidney disease using data mining techniques, in *IIE Annual Conference. Proceedings. Institute of Industrial and Systems Engineers (IISE)* (2017), pp. 2135–2140

Google Scholar

18. N. Tazin, S.A. Sabab, M.T. Chowdhury, Diagnosis of Chronic Kidney Disease using effective classification and feature selection technique, in *2016 International Conference on Medical Engineering, Health Informatics and Technology (MediTec)* (IEEE, 2016), pp 1–6

Google Scholar

19. E.H.A. Rady, A.S. Anwar, Prediction of kidney disease stages using data mining algorithms. Inform. Med. Unlocked. **15**, 100178 (2019)

Google Scholar

20. https://archive.ics.uci.edu/ml/datasets/Chronic_Kidney_Disease. Last accessed on 29 Jan 2019

www.nmiet.edu.in

21. http://www.hse.ie/eng/health/az/c/chronic-kidney-disease/#collapse_1. Last accessed on 29 Jan 2019

22. https://www.kaggle.com/mansoordaku/ckdisease. Last accessed on 29 Jan 2019

Author information

Authors and Affiliations

School of Mathematical Sciences, Swami Ramanand Teerth Marathwada University, Nanded, M.S., 431606, India
Aniket Muley

Nutan Maharashtra Institute of Engineering and Technology, Talegaon Dabhade, M.S., 410507b, India
Sagar Joshi

Editor information

Editors and Affiliations

Department of Computer Science, Maharaja Sriram Chandra BhanjaDeo (MSCB) University, Baripada, Odisha, India
Janmenjoy Nayak

Department of Information Technology, Veer Surendra Sai University of Technology, Sambalpur, Odisha, India
H.S. Behera

Department of Computer Application, Veer Surendra Sai University of Technology, Sambalpur, Odisha, India
Bighnaraj Naik

Department of AI & DS, Ramco Institute of Technology, Rajapalayam, Tamil Nadu, India
S. Vimal

www.unite.it

Faculty of Communication Sciences, University of Teramo, Teramo, Italy

Danilo Pelusi

Rights and permissions

Reprints and permissions

Copyright information

© 2022 The Author(s), under exclusive license to Springer Nature Singapore Pte Ltd.

About this paper

Cite this paper

Muley, A., Joshi, S. (2022). Exploratory Analysis of Kidney Disease Data Set—A Comparative Study. In: Nayak, J., Behera, H., Naik, B., Vimal, S., Pelusi, D. (eds) Computational Intelligence in Data Mining. Smart Innovation, Systems and Technologies, vol 281. Springer, Singapore. https://doi.org/10.1007/978-981-16-9447-9_10

.RIS .ENW .BIB

DOI
https://doi.org/10.1007/978-981-16-9447-9_10

Published
07 May 2022

Publisher Name
Springer, Singapore

Print ISBN
978-981-16-9446-2

Online ISBN
978-981-16-9447-9

eBook Packages
Intelligent Technologies and Robotics
Intelligent Technologies and Robotics (R0)

www.springer.com

Publish with us

Policies and ethics

www.nmiet.edu.in

Back

Advertisel

Concurrency and Computation: Practice and Experience / Volume 34, Issue 18 / e7011

RESEARCH ARTICLE

An ArmurMimus multimodal biometric system for Khosher authentication

Gayatri Umakant Bokade, Rajendra D. Kanphade

First published: 25 May 2022
https://doi.org/10.1002/cpe.7011

Abstract

One of the basic requirements of our modern day society is personal authentication. Biometric recognition should make a human-like identity determination by identifying its physiological and/or behavioral characteristics. In comparison to traditional knowledge-based approaches, biometric identification systems have the potential to bring benefits. However, because of the difficulties in extracting non-class discriminative features, the lack of protection during storage of extracted features, and poor recognition accuracy, most frequently used biometric systems lack model protection and robustness. This research proposed a Mimus multimodal biometric system focused on the combination of multiple modalities and optimal level fusion of features to resolve these problems. Initially, the novel Blob-funk method extracts the complementary non-class discriminatory information among different modalities, which accomplishes the biometric data enrollment. Thus, it extracts the different properties by comparing surrounding regions based on finding the local maxima and minima of the function. After extracting the features, they need to be stored in a secure manner in a database. Therefore, the paper incorporates the new code block protection strategy to achieve an effectual protection of continuous monitoring via the generation of non-invertible features, which is used to create the templates, thus storing them in a database. Finally, the novel Lucynomial logistic regression system incorporates user authentication and thus achieves greater recognition accuracy through estimation of threshold value with confrontation of spoof attacks. Hence, compared to the existing techniques such as SVM, PCA, and DBN, the outcome of the proposed work attains 97.53%

www.nmiet.edu.in

Open Research

DATA AVAILABILITY STATEMENT

None.

REFERENCES

1 Hezil N, Boukrouche A. Multimodal biometric recognition using human ear and palmprint. *IET Biomet*. 2017; **6**(5): 351-359.

Web of Science® Google Scholar

2 Ahmad MI, Woo WL, Dlay SS. Multimodal biometric fusion at feature level: face and palmprint. In: 2010 7th International Symposium on Communication Systems, Networks & Digital Signal Processing (CSNDSP 2010); 2010: 801-805.

Google Scholar

3 Saini N, Sinha A. Face and palmprint multimodal biometric systems using Gabor–Wigner transform as feature extraction. *Pattern Anal Appl*. 2015; **18**(4): 921-932.

Web of Science® Google Scholar

4 Ghayoumi M. A review of multimodal biometric systems: fusion methods and their applications. In: 2015 IEEE/ACIS 14th International Conference on Computer and Information Science (ICIS); 2015: 131-136.

Google Scholar

5 Barde S, Zadgaonkar AS, Sinha GR. PCA based multimodal biometrics using ear and face modalities. *Int J Inform Technol Comput Sci*. 2014; **6**(5): 43-49.

www.nmiet.edu.in

Back

6 Sanjekar PS, Patil JB. An overview of multimodal biometrics. *Signal Image Process*. 2013; **4**(1): 57.

Google Scholar

7 Barde S, Zadgaonkar AS, Sinha GR. Multimodal biometrics using face, ear and iris modalities. *Int J Comput Appl*. 2014; **975**: 8887.

Google Scholar

8 Javadtalab A, Abbadi L, Omidyeganeh M, Shirmohammadi S, Adams CM, El Saddik A. Transparent non-intrusive multimodal biometric system for video conference using the fusion of face and ear recognition. In: 2011 Ninth Annual International Conference on Privacy, Security and Trust; 2011: 87-92.

Google Scholar

9 Faez K, Motamed S, Yaqubi M. Personal verification using ear and palm-print biometrics. In: 2008 IEEE International Conference on Systems, Man and Cybernetics; 2008: 3727-3731.

Google Scholar

10 Perumal E, Ramachandran S. A multimodal biometric system based on palmprint and finger knuckle print recognition methods. *Int Arab J Inform Technol (IAJIT)*. 2015; **12**(2).

Google Scholar

11 Lohith MS, Eshwarappa MN. Multimodal biometrics for person identification using ear and palm print features. *IETE J Res*. 2018; **67**(1): 90-97.

Web of Science® Google Scholar

12 Sujatha E, Chilambuchelvan A. Multimodal biometric authentication algorithm using iris, palm print, face and signature with encoded DWT. *Wireless Pers Commun*. 2018; **99**: 23-34.

Web of Science® Google Scholar

13 Walia GS, Singh T, Singh K, Verma N. Robust multimodal biometric system based on optimal score level fusion model. *Expert Syst Appl*. 2019; **116**: 364-376.

www.nmiet.edu.in

Back

14 Chanukya PS, Thivakaran TK. Multimodal biometric cryptosystem for human authentication using fingerprint and ear. *Multimed Tools Appl*. 2020; **79**(1–2): 659-673.

Web of Science® Google Scholar

15 Rane ME, Bhadade US. Multimodal score level fusion for recognition using face and palmprint. *Int J Electric Eng Educ*. 2020;10:0020720920929662.

Google Scholar

16 Joseph T, Kalaiselvan SA, Aswathy SU, Radhakrishnan R, Shamna AR. A multimodal biometric authentication scheme based on feature fusion for improving security in cloud environment. *J Ambient Intellig Hum Comput*. 2020; **12**(6): 6141-6149.

Web of Science® Google Scholar

17 Gupta K, Walia GS, Sharma K. Multimodal biometric system using grasshopper optimization. In: 2019 International Conference on Computing, Communication, and Intelligent Systems (ICCCIS); 2019: 387-391.

Google Scholar

18 Chitroub S, Meraoumia A, Laimeche L, Bendjenna H. Enhancing security of biometric systems using deep features of hand biometrics. In: 2019 International Conference on Computer and Information Sciences (ICCIS);2019: 1-6.

Google Scholar

19 Maity S, Abdel-Mottaleb M, Asfour SS. Multimodal biometrics recognition from facial video with missing modalities using deep learning. *J Inform Process Syst*. 2020; **16**(1): 6-29.

Google Scholar

20 Patil A, Kruthi R, Gornale S. Analysis of multi-modal biometrics system for gender classification using face, iris and fingerprint images. *Int J Image Graph Signal Process*. 2019; **11**(5): 34-43.

Google Scholar

www.nmiet.edu.in

Back

Google Scholar

22 Hoang VT. EarVN1. 0: a new large-scale ear images dataset in the wild. *Data in Brief*. 2019; **27:104630-104630**.

Google Scholar

23 Zhang Y, Zhang L, Liu X, Zhao S, Shen Y, Yang Y. Pay by showing your palm: a study of palmprint verification on mobile platforms. In: 2019 IEEE International Conference on Multimedia and Expo (ICME); 2019: 862-867.

Google Scholar

Download PDF

ABOUT WILEY ONLINE LIBRARY

Privacy Policy
Terms of Use
About Cookies
Manage Cookies
Accessibility
Wiley Research DE&I Statement and Publishing Policies
Developing World Access

HELP & SUPPORT

Contact Us
Training and Support
DMCA & Reporting Piracy

OPPORTUNITIES

Subscription Agents
Advertisers & Corporate Partners

CONNECT WITH WILEY

The Wiley Network
Wiley Press Room

www.nmiet.edu.in

Back

and training of artificial intelligence technologies or similar technologies.

www.nmiet.edu.in

Advances in Engineering Software 173 (2022) 103221

Contents lists available at ScienceDirect

Advances in Engineering Software

journal homepage: www.elsevier.com/locate/advengsoft

Research paper

Performance analysis of machine learning algorithm of detection and classification of brain tumor using computer vision

Ashwini S Shinde [a,*], BM Mahendra [b], Santosh Nejakar [c], Santosh M Herur [d], Nagaraj Bhat [b]

[a] Department of CSE-AI, Nutan College of Engineering and Research, Pune, Maharashtra, India
[b] Department of ECE, RVCE, Bengaluru, Karnataka, India
[c] Department of Electrical Engineering, JIT, Davangere, Karnataka, India
[d] Department of ECE, JIT, Davangere, Karnataka, India

ARTICLE INFO

Keywords:
Artificial Intelligence
MRI
Logistic regression
OASIS
Multilayer Perceptron

ABSTRACT

Brain tumor is one of the undesirables, uncontrolled growth of cells in all age groups. Classification of tumors depends no its origin and degree of its aggressiveness, it also helps the physician for proper diagnosis and treatment plan. This research demonstrates the analysis of various state-of-art techniques in Machine Learning such as Logistic, Multilayer Perceptron, Decision Tree, Naive Bayes classifier and Support Vector Machine for classification of tumors as Benign and Malignant and the Discreet wavelet transform for feature extraction on the synthetic data that is available data on the internet source OASIS and ADNI. The research also reveals that the Logistic Regression and the Multilayer Perceptron gives the highest accuracy of 90%. It mimics the human reasoning that learns, memorizes and is capable of reasoning and performing parallel computations. In future many more AI techniques can be trained to classify the multimodal MRI Brain scan to more than two classes of tumors.

1. Introduction

Computer Aided Diagnosis (CAD) is one of the major contributions of technology implemented in the field of medical science for better precision and high accuracy. It is considered as a high throughput for the expediency to investigate the outgrowth expanse. The implementation of technology, diagnosis and treatment planning becomes easy and gives the physician a second taught of his predictions. The most dominant tool for imaging the brain is the Magnetic Resonance Imaging (MRI) which are multimodal, where in these modalities can reveal different parts in the tumor, and provides information concomitant to anatomical assemblies as well as potential anomalous tissues essential for diagnosis and treatment planning [1,2]. The different sequences like the T1 weighted, T2 weighted, Fluid Attenuation Inversion Recovery (FLAIR) and Diffusion Weighted Imaging (DWI) show the different intensity variations that help in identifying the region of interest. Extracting reckonable data from MRI helps to capture the functions of different consequence crevices in case of different types of tumors. The possibility of survival of a patent is increased if the tumor is perceived at an early stage. However precise segmentation and categorization of abnormalities are not forthright. There exist a number of semiautomatic and fully automatic methods for the classification of tumors but clinical acceptance depends on simplicity and less human intervention. Classification of tumors in the human brain is possible by implementing the Supervised Machine Learning techniques, in this research we work upon the Naïve Bayes, The Logistic, Multilayer Perceptron (MLP), The Support Vector Machine (SVM) and the Decision Tree (DT) for classification and the results are compared on the basis of classification accuracy for the data used. Classification is performed with more discriminative features initially on the OASIS and ADNI [3,4] database

Yet there are some challenges to be addressed for classification of abnormalities in medical imagining like selection of appropriate model, describing the given data, finding the errors in the data, the adequacy of data used and confidence about the results. Therefore, there is no universal recognized method for medical image classification. So, it remains a challenging problem in computer vision and Machine learning. Fully automatic systems determine the tumor part without human intervention these systems generally include human intelligence and prior knowledge about the throughput. These algorithms which are mostly developed by using soft computing and model-based techniques prove to produce accurate results. The study of automatic brain tumor classification represents interesting research in Machine Learning and

* Corresponding author.
E-mail address: ashsshinde@gmail.com (A.S. Shinde).

https://doi.org/10.1016/j.advengsoft.2022.103221
Received 9 July 2022; Accepted 27 July 2022
Available online 10 August 2022
0965-9978/© 2022 Elsevier Ltd. All rights reserved.

www.mmiet.edu.in

Table 1
A Feature set of thirteen features.

Sr.No	Contrast	Correlation	Energy	Homogeneity	Mean	Standard Deviation	Entropy	RMS	Variance	Smoothness	Kurtosis	Skewness	IDM	Class
1	0.2088	0.1990	0.7621	0.9352	0.0031	0.0898	3.1735	0.0898	0.0080	0.9205	7.3282	0.4690	0.0577	Benign
2	0.2717	0.0931	0.7686	0.9338	0.0024	0.0898	3.2698	0.0898	0.0081	0.8974	7.9567	0.8862	0.4926	Benign
3	0.2414	0.1065	0.7440	0.9277	0.0030	0.0898	3.5550	0.0898	0.0080	0.9178	6.3661	0.6499	0.4729	Benign
4	0.2161	0.1382	0.7548	0.9325	0.0025	0.0898	3.3156	0.0898	0.0081	0.9032	6.2320	0.3121	0.5631	Benign
5	0.2250	0.0991	0.7691	0.9365	0.0021	0.0898	3.5182	0.0898	0.0080	0.8850	6.7672	0.4413	0.5462	Benign
6	0.2333	0.1284	0.7491	0.9308	0.0019	0.0898	2.6632	0.0898	0.0081	0.8778	7.2707	0.6117	0.0366	Benign
7	0.2033	0.1126	0.7554	0.9331	0.0019	0.0898	3.6549	0.0898	0.0080	0.8783	5.8117	0.3408	1.0010	Benign
8	0.2558	0.0895	0.7557	0.9314	0.0025	0.0898	3.0756	0.0898	0.0081	0.9040	7.7971	0.5774	0.2601	Benign
9	0.2341	0.1321	0.7530	0.9315	0.0035	0.0897	3.1562	0.0898	0.0080	0.9291	7.4848	0.5212	1.0392	Benign
10	0.2689	0.0977	0.7861	0.9410	0.0007	0.0898	2.7465	0.0898	0.0081	0.7186	10.9703	0.7365	0.1190	Benign
11	0.3059	0.1421	0.7862	0.9379	0.0063	0.0896	3.2051	0.0898	0.0080	0.9591	12.2408	1.1048	1.2156	Malignant
12	0.2255	0.1345	0.7466	0.9299	0.0043	0.0897	3.6004	0.0898	0.0081	0.9407	6.0137	0.5267	0.3801	Malignant
13	0.2433	0.0933	0.7613	0.9329	0.0037	0.0897	3.3710	0.0898	0.0081	0.9314	7.3506	0.6350	0.1378	Malignant
14	0.2439	0.1072	0.7310	0.9246	0.0046	0.0897	3.5484	0.0898	0.0081	0.9446	6.5235	0.6204	0.5030	Malignant
15	0.2280	0.0769	0.7577	0.9319	0.0030	0.0898	3.6700	0.0898	0.0080	0.9185	5.6210	0.4119	1.0350	Malignant
16	0.2314	0.1072	0.7418	0.9298	0.0042	0.0897	3.5516	0.0898	0.0080	0.9403	6.0614	0.5104	0.3130	Malignant
17	0.2517	0.0734	0.7402	0.9267	0.0035	0.0897	3.5239	0.0898	0.0080	0.9284	6.5220	0.4979	1.6524	Malignant
18	0.3073	0.1337	0.7598	0.9334	0.0060	0.0896	2.6626	0.0898	0.0080	0.9571	16.2926	1.6120	1.2859	Malignant
19	0.2155	0.0951	0.7378	0.9274	0.0028	0.0898	3.6283	0.0898	0.0080	0.9132	5.3238	0.3230	1.0419	Malignant
20	0.2870	0.0918	0.7590	0.9320	0.0055	0.0896	3.1117	0.0898	0.0080	0.9530	12.1609	1.1228	0.5619	Malignant

Table 2
Result of Naïve Bayes Classifier for 10 Cross Fold Validation.

n^{th} Cross Fold	Percent correct
1	83.33333
2	66.66667
3	66.66667
4	66.66667
5	83.33333
6	83.33333
7	83.33333
8	83.33333
9	83
	33,333
10	83.33333

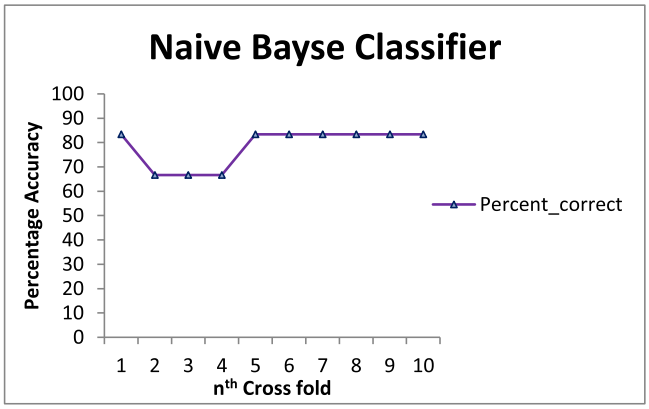

Fig. 1. Plot of Percentage Accuracy for Naïve Bayes Classifier.

Table 3
Mean Error for Naïve Bayes Classifier.

Mean absolute error	Root mean squared error
0.111185	0.259234
0.387215	0.585724
0.330763	0.566769
0.291527	0.506187
0.170592	0.407284
0.182931	0.409818
0.191837	0.391273
0.152055	0.366976
0.167413	0.408239
0.246425	0.416944

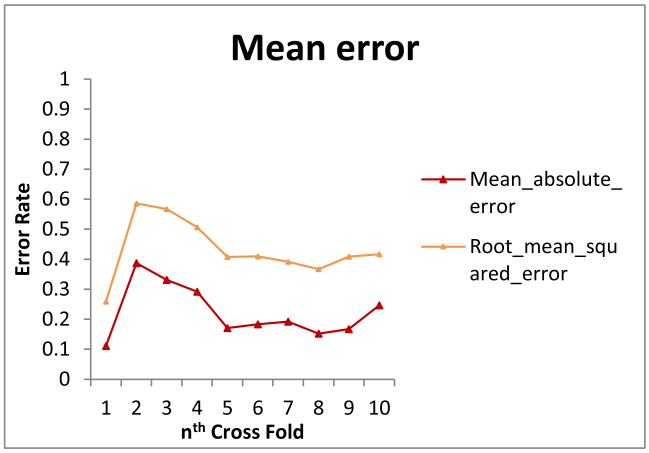

Fig. 2. Plot of mean error for Naïve Bayes Classifier.

www.nmiet.edu.in

Table 4
Detailed Accuracy Rate for Naïve Bayes Classifier.

True Positive Rate	0.900
False Positive Rate	0.300
Precision	0.75
Recall	0.900
Accuracy	80%

Artificial intelligence (AI)

The organization of this paper is as follows. In Section II, the existing scientific research in medical image classification is reviewed, along with the motivation for this research. Section III presents the materials and methods used in this work it describes the dataset implemented, it also shows the proposed work. Section IV, represents the experimental results obtained and finally the section V, elaborates the outcomes and conclusion.

2. Literature survey

The literature survey elaborates the details of research work studied in the domain to diagnose this life-threatening disease; it deals with the previous work carried out in the field of Tumor recognition and classification implementing computer vision and Machine learning. The initial papers describe the review of some of the best segmentation techniques using image processing followed by research based on automatic segmentation and classification techniques by building neural network and finally discussing about the recent techniques using Artificial Intelligence and Machine Learning.

Artificial Intelligence is an emerging trend not only in digital marketing but in almost every field, it has an extensive range of application in the area of brain tumor detection and classification. In the resent years most of the researchers made more of their inventions in the field of biomedical science through AI, this section deals with the review on some of the tumor detection and classification techniques using AI and ML.

Sergio Pereira, Adriano Pinto [5], in their paper mentioned that reliable and automatic techniques are required for tumor segmentation

Table 5
Classification Instances for Naïve Bayes Classifier.

Correctly Classified Instances	80
Incorrectly Classified Instances	20
Percentage Accuracy	80

Table 6
Confusion Matrix for Naïve Bayes Classifier.

True positive = 45	False Positive = 5
False Negative = 15	True Negative = 35

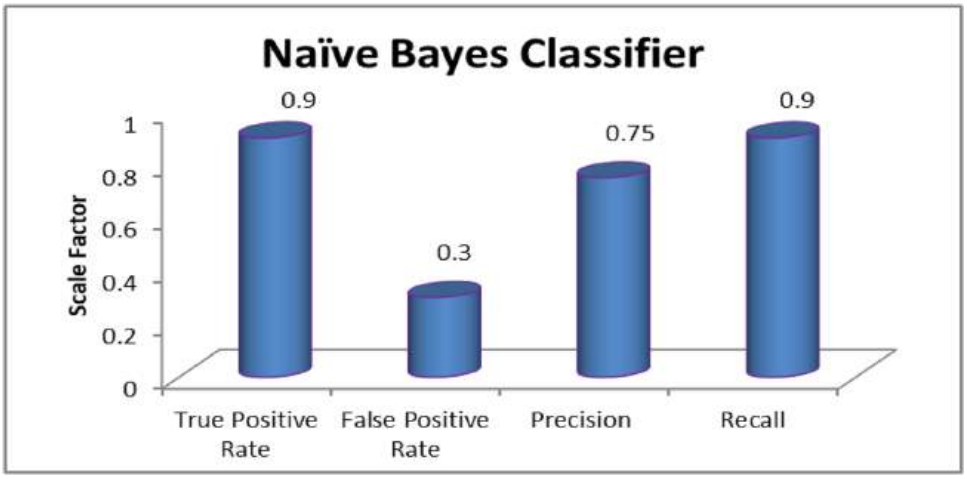

Fig. 3. Plot of Detailed Accuracy Rate for Naïve Bayes Classifier.

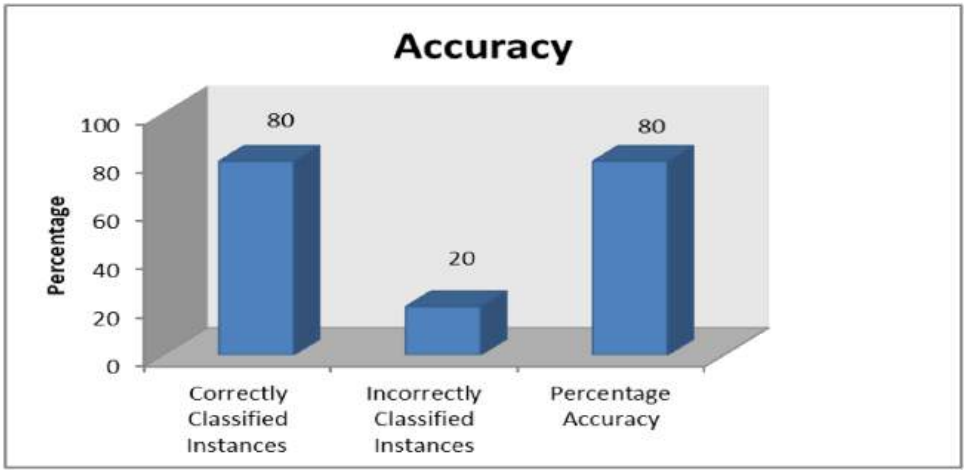

Fig. 4. Plot of Classification Instances for Naïve Bayes Classification.

www.nmiet.edu.in

Table 7
Result of Logistic Classifier for 10fold cross Validation.

n^{th} Cross Fold	Percent correct
1	75
2	50
3	100
4	75
5	75
6	100
7	100
8	100
9	100
10	100

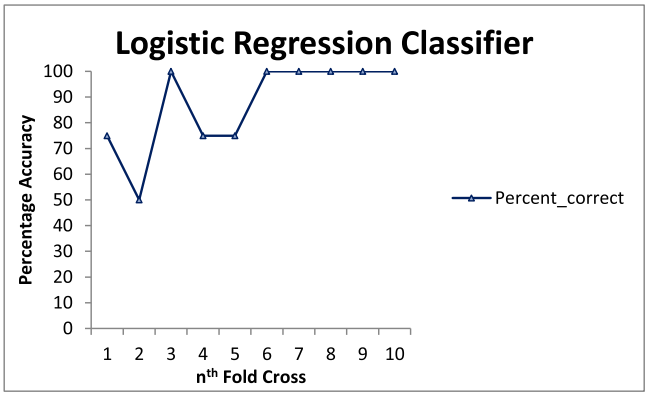

Fig. 5. Plot of Percentage Accuracy for Logistic.

Table 8
Mean Error for Logistic Classifier.

Mean absolute error	Root mean squared error
0.230653	0.458894
0.5	0.707107
0.000357	0.000646
0.249999	0.499997
0.175671	0.351273
9.43E-10	1.83E-09
1.32E-09	2.65E-09
0.048946	0.097892
7.5E-05	0.00015
5.2E-13	1.04E-12

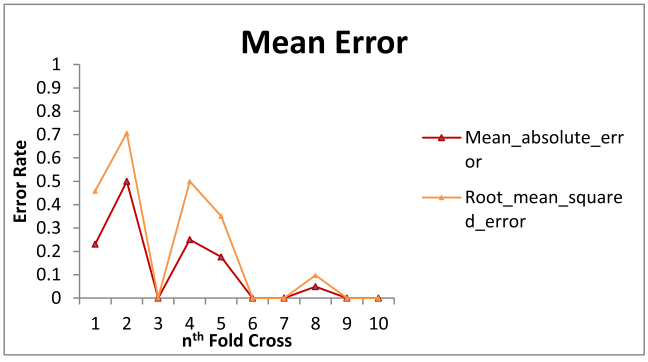

Fig. 6. Plot of mean error for Logistic Classifier.

and classification. The Convolution Neural Network (CNN), was proposed by the authors with 3 × 3 kernel that allows designing a deeper architecture, and gets an optimistic effect against over fitting by providing a smaller number of weights in the network. Though intensity

Table 9
Detailed Accuracy Rate for Logistic Classifier.

True Positive Rate	0.900
False Positive Rate	0.900
Precision	0.900
Recall	0.900
Accuracy	90%

normalization is not a pre-processing step in CNN the results of segmentation after normalization were very effective. Their algorithm was structured as follows 1. Initialization, important to achieve convergence 2. The activation function is applied which is responsible for non-linear transformation of the data. Rectifier linear unity (ReLU) gives better results than the classical sigmoid functions and also speeds up training [6]. 3. Pooling forms a feature map by combining spatially nearby features.4. Regularization to reduce over fitting. 5. Data Augmentation used to increase the number of training set. 6. Loss function it is a function to be minimized during training. Mohammad Havaei, Axel Davy et al. [7] presented a fully automatic segmentation method. This method is based on Deep Neural Network (DNN) the network is designed to classify low- and high-grade tumors. They explored an architecture based on CNN i.e. DNN adapted to image data, it exploits local as well as global features concurrently. Here the final layer i.e. the convolutional layer allows 40 fold speed up and their two phase training allows to handle the unevenness of tumor labels. Lastly, they explore the cascaded architecture here the additional source of information is provided by the CNN. High accuracy and with low computational time is the main feature of this algorithm. Heba Mohsen, El- Sayed A et al. [8] emphasized on machine learning as a powerful tool for complex problems. They developed Deep learning architecture for classification of the tumors into four classes they combined the classifier with discrete wavelet transform and principal component analyser. The flow of their system was tumor segmentation using Fuzzy C- Means, feature extraction applying DWT and feature selection by PCA and finally classification implementing the DNN. For classification 7-fold cross validation technique was built to train the data with a 7 hidden layer structure. Ali ARL and Davut Hanbay [9] proposed a three-stage method. Initially the pre-processing, secondly the Extreme Learning machine local respective fields (ELM-LRF) based on classification and finally segmenting the tumor. Initially the noise is removed by nonlocal means and local smoothening techniques, then it is classified by applying ELM-LRF and finally the tumor is segmented, they obtained the classification precession up to 97%. Elisee Illunga Mbuyamba, Juan Gabriel Avina [10]. The authors worked on the incorrect delineation of MRI where the distance between the foreground and the background is high. It was found that the region based active contour models are more sensitive to high mean intensity hence to solve the problem of high mean intensity they developed a model known as localized active counter model. This model with background intensity compensation balances the mean intensity that aims to diminish the attraction consequence of active contour to the unsolicited border lines. This approach increases the accuracy and reduces the computational time. They applied this model on the multimodal MRI data which was helpful to detect the foreground and could segment the abnormal region that can be further used for classification. A.Sankari and S.Vigneshwari [11], The authors suggested an automatic segmentation approach applying Convolutional Neural Network (CNN) with a 3 × 3 filter size. Here because of this small size the operation on the small portion permits to extract more deep design rather than having a constructive outcome with a smaller number of weights in the system. To enhance the image spatial domain methods are implemented. The CNN is trained using a class of labels that extracts features like edges lines corners etc. The system is a layer of unit here every unit in one layer is associated with the past layer i.e. every neuron is associated with the previous layer. The construction of the CNN is first is the convolution layer the second is the fully connected layer and the third is the pooling

www.mmiet.edu.in

Fig. 7. Plot of Detailed Accuracy Rate for Logistic Classifier.

Table 10
Classification Instances for Logistic Classifier.

Correctly Classified Instances	90
Incorrectly Classified Instances	10
Percentage Accuracy	90

layer. The MRI is the input where the convolution layer has learnable filters that performs a dot product among the small regions. They are also connected to the weights. Next is the fully connected layer where all the neurons are linked to the previous layer. The output layer computes the class score of the image to show the size and the location of the tumor. Muhammad Sajjad, Salman Khan et al. [12], worked on multi-grade tumor classification. They proposed a CNN based system for the classification of the tumors, the steps involved deep learning technique for segmentation of the tumor region, next data augmentation is applied to hike the training dataset. The employed augmentation techniques for the geometric transformation are flipping, rotation, skewness and shearing and the next are sharpening, Gaussian blur, emboss and edge detection used for noise invariance. Finally, CNN is implemented for multi-grade classification, it has 3 × 3 kernels for the convolution layer with 1 stride in the initial layer. Due to this it will be able to learn multiple grades of the tumor. The CNN architecture comprises of 19 weighted layers out of which 16 are convolutional and 3 are fully connected layers. The max pooling is led by the first convolutional layers. and the same is repeated for the next two layers. Next three last layers are fully connected resulting in almost 4096,4096,1000 features this form the feature vector which is fed as input for the soft max classifier to make the final decision of the grade of the tumor.

2.1. Motivation for the research

The outcome of the literature survey helped us to find the challenges

Table 11
Confusion Matrix of Logistic Classifier.

True positive = 45	False Positive = 5
False Negative = 5	True Negative = 45

Table 12
Result of Multi-Layer Perceptron Classifier for 10-fold cross Validation.

n^{th} Cross Fold	Percent correct
1	50
2	50
3	75
4	75
5	100
6	100
7	100
8	75
9	100
10	100

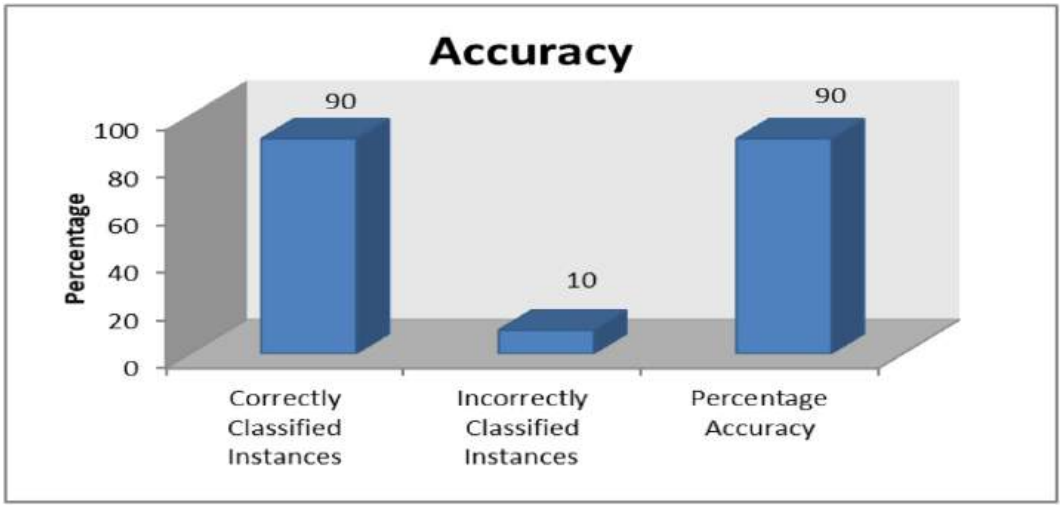

Fig. 8. Plot of Classification Instances for Logistic Classification.

www.nmiet.edu.in

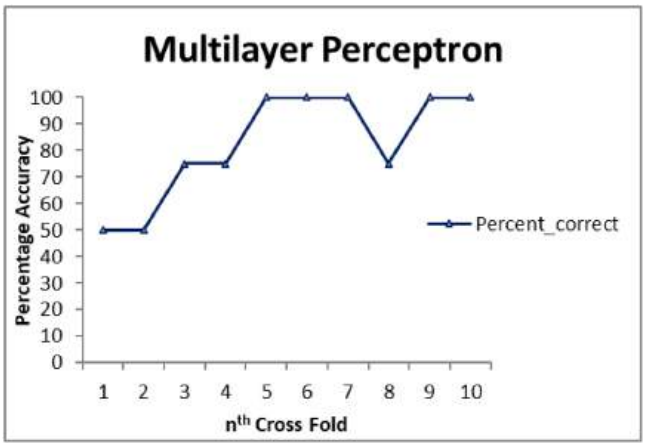

Fig. 9. Plot of Percentage Accuracy for MLP.

Table 13
Mean Error for MLP Classifier.

Mean absolute error	Root mean squared error
0.304202	0.435902
0.482741	0.679709
0.332008	0.393292
0.232097	0.429697
0.013611	0.016777
0.003172	0.003461
0.020229	0.039278
0.228384	0.452503
0.017527	0.033476
0.002333	0.002905

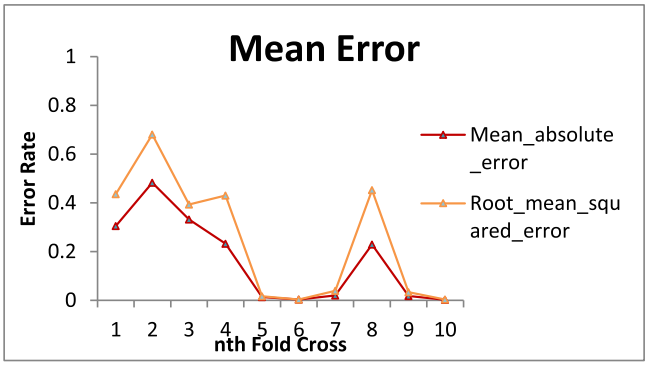

Fig. 10. Plot of mean error for MLP Classifier.

Table 14
Detailed Accuracy Rate for MLP Classifier.

True Positive Rate	0.900
False Positive Rate	0.1
Precision	0.900
Recall	0.900
Accuracy	90%

faced by researchers and to identify the gaps, it was noted through the literature survey that there exists a need to develop a Machine Learning approach that overcomes these limitations and produce better results it was found that most of the research carried out was for the classification of the image into normal and abnormal images the work can be further applied for the classification of the Brain tumors. Most of the methodologies learnt during the literature survey were implemented for data base that are available as benchmark data set which are pre-processed by the experts. The method of hybridization for multiclass classification which makes use of intensity, shape and texture features can be applied to increase accuracy. Due to the intra- and inter-intensity variability between the training data and test data, segmentation and classification is still challenging. This can be improvised by applying Machine Learning. Since MRI scans are multimodal sequences the best slice of image must be identified to get the correct class which is again done manually by the experts this can be eliminated by implementing the Machine learning techniques. The ML approach reduces the time complexity by eliminating the time required for selection of the MR sequence for segmentation which also effects the accuracy performance. Therefore, the prime objective of this research is to find an Optimal Classifier to Classify the Brain Tumor using Machine Learning Algorithm. Identifying the challenges inherent for Machine learning and applying appropriate AI technique. Comparison of different Machine Learning techniques to estimate the best classifier.

2.2. Objectives of the research work

Machine learning is evolving one of the most powerful tools in every field due to its optimal features. In the arena of medical science early diagnosis of the abnormality can save life. Brain tumor is amongst most aggressive diseases but if detected at an early stage and treated by proper plain life can be saved, with this view the prime objective of this research is to work on an Optimal Classifier to Classify the Brain Tumor using Machine Learning Algorithm so that it provides the radiologist with a second opinion for proper treatment plan for the patient.

3. Methodology followed

3.1. Pre-processing

In image analysis Pre-processing plays an important role it enhances the image to identifying the region of interest. Prior to the processing of the image for the desired task, preprocessing is an important phase where the undesired data is suppressed and the image is made ready for further analysis. The MR images are degraded by distortion during the image digitization and transmission process. The bias field distortion alters the image which causes variations in intensity when captured at different time intervals so to make the intensity and contrast range more analogous intensity normalization methods were proposed [13]. The most common noise removal technique is by applying filters. Various filters remove the different types of noise present in the image. Median filter is commonly used to eliminate the salt and pepper noise present. Gaussian filter eliminates the input MR image noise by suppressing the high frequency components that are more prone to noise resulting in a smooth image hence it is a low pass filter. The presence of extra-cranial tissue like the skin, bones, fat, skull etc. in the MRI of the brain has to be eliminated converting the heterogeneous image into homogeneous image. Anisotropic diffusion filters are well suited for preprocessing the MRI so that the undesired data is suppressed by preventing the fine details of the image for further analysis.

3.2. Feature extraction

Feature extraction techniques explore the images and the objects in the images to excerpt the maximum projecting features that represent the classes of the objects. It provides the classifier with a feature vector that characterizes the input data. Tumors are heterogeneous tissues therefore only the mean value is not sufficient to characterize the heterogeneity of various types of tumors. Discussing about the imaging features enables to understand the various modalities of the DICOM image that help in diagnostic task and the artifacts associated with the images. Three categories of features are extracted that designate the intensity, shape and texture of the image for examples

www.nmiet.edu.in

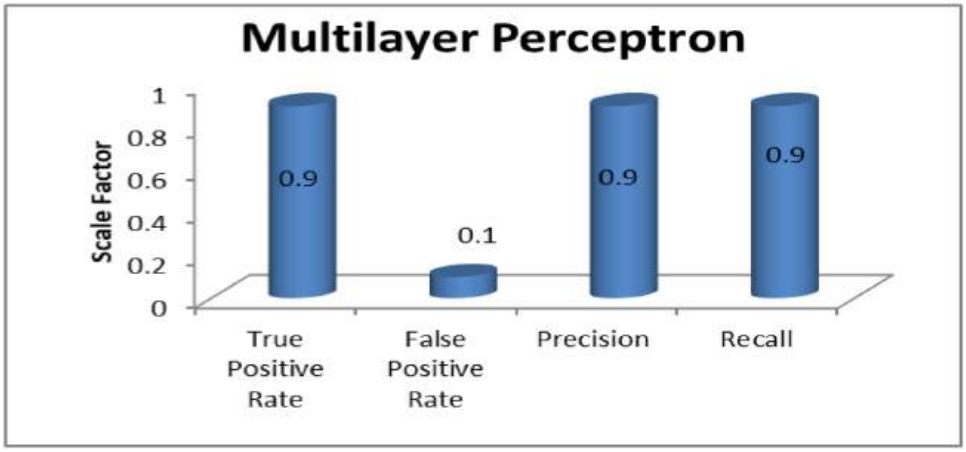

Fig. 11. Plot of Detailed Accuracy Rate for MLP Classifier.

Table 15
Classification Instances for MLP Classifier.

Correctly Classified Instances	90
Incorrectly Classified Instances	10
Percentage Accuracy	90

3.2.1. Intensity feature

It describes the Mean, Median intensity, Variance, Standard Variance, Skewness, Kurtosis etc.

3.2.2. Shape feature

Shape index, Area, Circularity, Perimeter, Irregularity etc.

3.2.3. Texture features

Covers a varied series of procedures built on first and second order image texture parameter such as the Correlation, Sum of square variance, Contrast, Entropy, Homogeneity, Energy, Cluster shade etc.

These feature vectors are plotted in the feature space each feature consisting of one dimension therefore the feature space is n-dimension for n feature vectors. Objects from the same class will cluster in one feature space and thus used for classification. As the feature space increases number of parameters for classification also increase.

The GLCM Features: The discrimination of the abnormal MRI from the normal MRI can be obtained through the gray level co-occurrence matrix (GLCM) [14], the selection of Haralick features that prove the applicability to analyze the irregular object outlines.

The GLCM is the measure of times a pair of pixel k_1,$k_2$with distance d and orientation θ will occur in a given matrix represented by $G_{\theta,d}(k_1, k_2)$.The dimensions of $\boldsymbol{\theta}$ are horizontal, vertical, diagonal and anti-

Table 16
Confusion Matrix of MLP Classifier.

True positive = 45	False Positive = 5
False Negative = 5	True Negative = 45

Table 17
Result of Support Vector Machine Classifier for 10 fold cross Validation.

Key Run	Percent correct
1	75
2	50
3	50
4	75
5	75
6	75
7	100
8	75
9	100
10	100

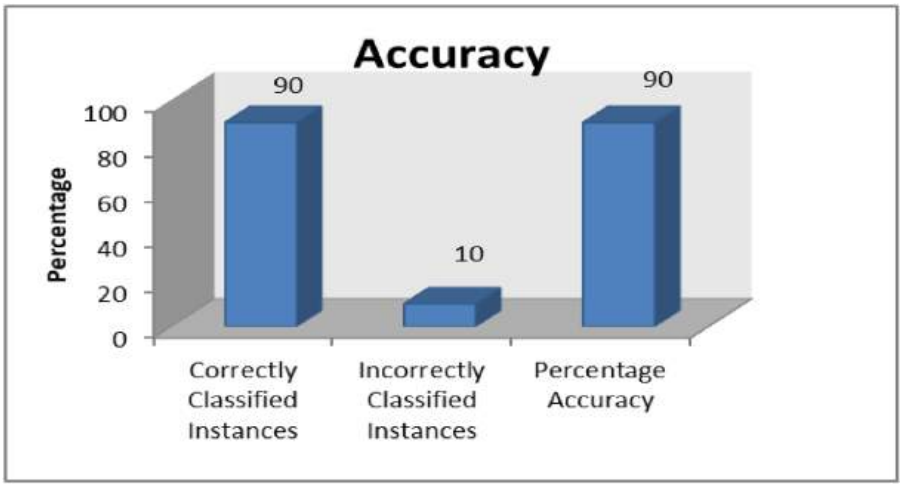

Fig. 12. Plot of Classification Instances for MLP Classification.

www.mmiet.edu.in

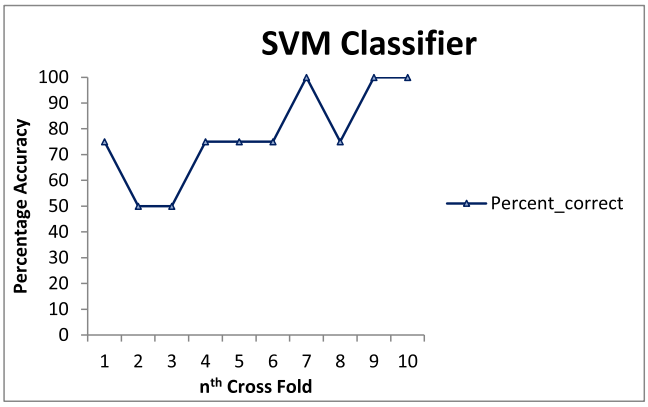

Fig. 13. Plot of Percentage Accuracy for SVM.

Table 18
Mean Error for SVM Classifier.

Mean absolute error	Root mean squared error
0.25	0.5
0.5	0.707107
0.5	0.707107
0.25	0.5
0.25	0.5
0.25	0.5
0	0
0.25	0.5
0	0
0	0

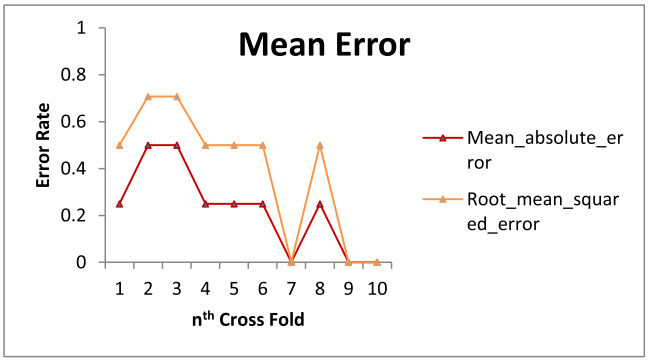

Fig. 14. Plot of mean error for SVM Classifier.

Table 19
Detailed Accuracy Rate for SVM Classifier.

True Positive Rate	1.00
False Positive Rate	0.300
Precision	0.769
Recall	1.00
Accuracy	85%

diagonal i.e.0^0,45^0,90^0,135^0.

3.3. Wavelet transform

A wavelet is a fast-decreasing wave line oscillation that has zero mean and they exist for a finite duration [15]. This enables to study every single component separately; wavelets are created from the basic wavelet Ψ(t). The two important wavelets transform concept are scaling and shifting defined by

$$\Psi_{s,\tau} = \frac{1}{\sqrt{S}}\Psi\left(\frac{t-\tau}{S}\right) \quad (1)$$

Where scaling refers to stretching and shrinking given by $\Psi(t/s)s > 0$ 'S' is a scaling factor the positive value resembles to the extent of the amount of a signal that is scaled in time, where S is inversely proportional to time and the constant of proportionality is the center frequency 'cf' wavelets have band pass characteristics in frequency domain $F_{eq} = cf/S\delta t$where $\delta_t$is the sampling interval. Stretching helps in finding slow varying changes while compressing helps in capturing abrupt changes. Shifting is the delaying or the advancing the concept of wavelength along the signal.

3.4. Discrete Wavelet Transform (DWT)

DWT is based on scaling and shifting of wavelets and are used in the application of de-noising and compression of the signal as it helps in representing many signals that occur naturally with a smaller number of coefficients known as sparkle representation. The DWT base scale is set to 2 and we can obtain different scales with $2^j wherej = 1, 2, 3, \ldots\ldots$. Translation occurs as an integer multiple represented as $2^j * mwherem = 1, 2, 3, \ldots\ldots\ldots$.This procedure is known as dyadic scaling and changing these results by reducing the redundancy.

The signal is filtered using high pass and low pass filters also known as Detailed (D) sub band and Approximation (A) sub band respectively, this typically filters the length of coefficient for each band which is equal to half the number of coefficients to the previous scale. The filters result in good computational performance as they have a small no of coefficients and with this method the signal of interest can be capture with some larger magnitude DWT coefficients while distortion in the signal consequences the smaller DWT coefficients. Hence the analysis of signal is done using the DWT at progressively narrow sub bands at different resolutions it likewise benefits in de-noising and compressing the signal. Table 1 gives an example of sample result of thirteen features that are extracted from the two classes of MRI scans.

3.4.1. Classification techniques

Classifying helps to understand the type of tumor depending on which the physician can plan the treatment. It is the region of interest to work upon for a given purpose therefore it is an important task in medical analysis for diagnosis of the tumor. Brain Tumors are broadly classified into Benign and Malignant. Classification categorizes each attribute to a predefined set of group or a class. This assigns the attributes to the target class; this predicts the class. Classification is performed with more discriminative features initially on the synthetic database then on the clinically database. Through the performance analysis it was analyzed that the accuracy of the synthetic images is greater than the clinical dataset hence to obtain good accuracy.

3.4.2. Naive Bayes classifier

Bayes theorem is the backbone of this classifier [16], here the event belonging to a particular class is calculated on the conditional probability for a given data given by the equation $P(C_k x) = P(C_k) + \frac{P(x|C_k)}{P(x)}$. The data $x \in$ class k and the best class is selected with the greatest probability this reduces the classification error therefore $P(C_k|x)$ is statistically independent given by $P(xC_k) = \sum_{i=0}^{n} P(x|C_k)$. Where x is a n dimensional vector of the data $= (x_1, x_2, \ldots\ldots, x_n)$. The probability of classification is determined during the training procedure where the calculation of the density function is also done. The Naïve Bayes is also called as the Maximum A Posterior (MAP) decision rule. The class is defined as given in Eq. (2)

$$Class(x) = argmax\ k \frac{1}{N}\sum_{j=1}^{N}\left(P\left(C_{i,j}\right)\prod_{i}^{n} P\left(x_i|C_{j,k}\right)\right) \quad (2)$$

www.mmiet.edu.in

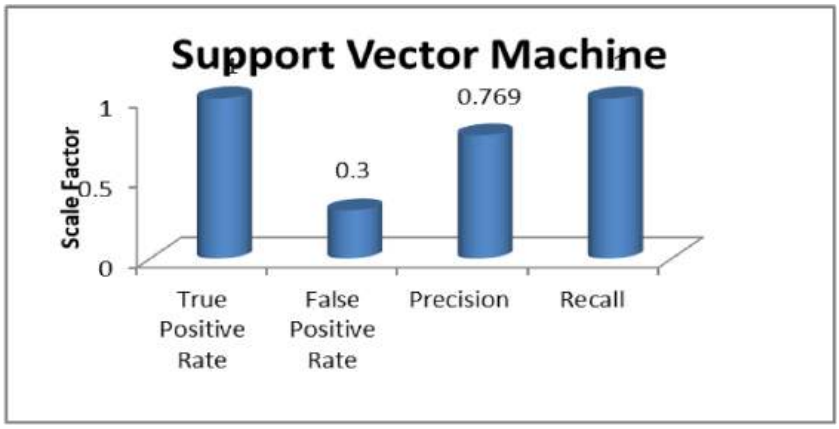

Fig. 15. Plot of Detailed Accuracy Rate for SVM Classifier.

Table 20
Classification Instances for the SVM Classifier.

Correctly Classified Instances	85
Incorrectly Classified Instances	15
Percentage Accuracy	85

Table 21
Confusion Matrix of SVM Classifier.

True positive = 50	False Positive = 0
False Negative = 15	True Negative = 35

3.4.3. Logistic regression as a linear classifier

A linear classifier gives an assured estimate of either 1 or 0 i.e. by passing the output of a linear function through the threshold function yet thresholding creates some problems the hypothesis hw(x) is a discontinuous function of input and is not differentiable [17]. These issues can be solved by softening the threshold function to a continuous differentiable function i.e. the integral of normal distribution and the logistic function, there are appropriate properties of the logistic functions given by

$$Logistic(Z) = \frac{1}{1+e^{-z}} \tag{3}$$

A soft boundary is formed by the hypothesis at the center and approaches to the extremes as it moves away from the boundary. This is known as fitting the weights that is used to minimize the loss; this is called as logistic regression it is the hyper plane separating the two classes. With this function the class label can be predicted but there are limitations for the MRI data as accurate predictions becomes limited since the numbers of features are greater than the observations. Therefore, by applying regularization this limitation can be overcome i.e. by adjusting the weights to higher value for features that are sensitive to

Table 22
Result of Decision Tree Classifier for 10-fold cross Validation.

Key Run	Percent correct
1	50
2	75
3	50
4	75
5	100
6	75
7	75
8	75
9	75
10	75

class labels and zero otherwise [18]. Gaussian prior is applied to weights leading to regularization and the maximized function is given as

$$L_g(\theta) = \sum_{i=1}^{N} \log\left(y^i | x^i, \theta\right) - \gamma^{\theta t}\theta \tag{4}$$

Where γ Controls the degree of regularization. Hence the weights of the irrelevant features are reduced.

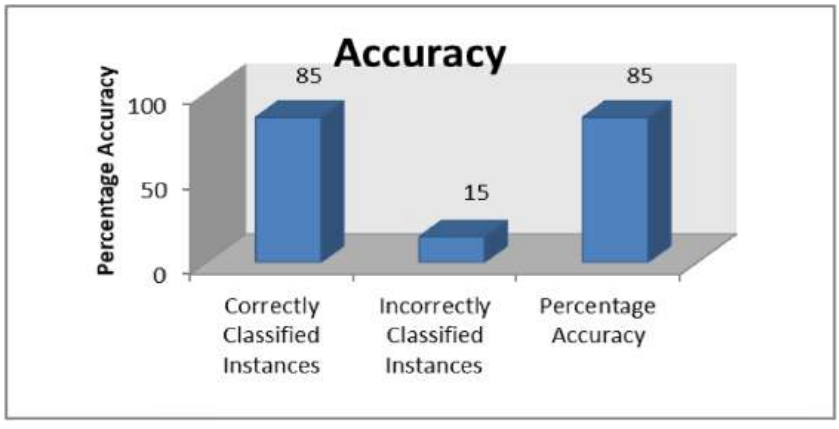

Fig. 16. Plot of Classification Instances for SVM Classifiers.

www.nmiet.edu.in

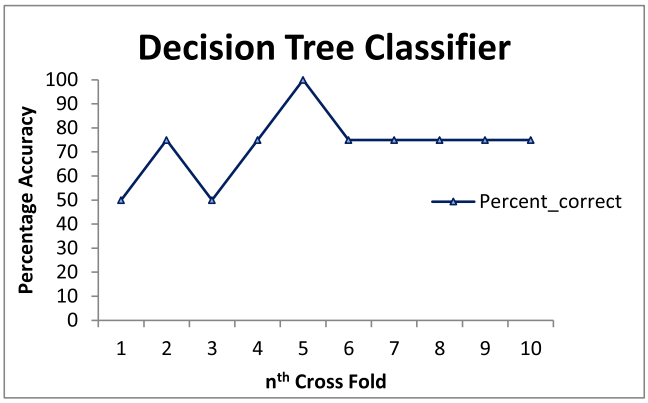

Fig. 17. Plot of Percentage Accuracy for Decision Tree.

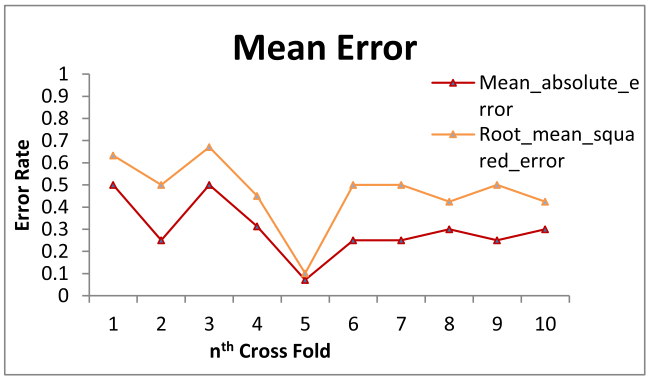

Fig. 18. Plot of mean error for Decision Tree Classifier.

Table 23
Mean Error for Decision Tree Classifier.

Mean absolute error	Root mean squared error
0.5	0.633431
0.25	0.5
0.5	0.67128
0.3125	0.450694
0.071429	0.101015
0.25	0.5
0.25	0.5
0.3	0.424264
0.25	0.5
0.3	0.424264

3.4.4. *Multilayer perceptron*

Multilayer neural network was explored during the 1980s [19] the multilayers of feature detectors were learnt from the training data. The Multilayer's are built on the back propagation algorithm [20] to compute the classification performance of the entire network that is dependent on the weight on every connection.

Multilayer is based on a unit called the Perceptron, is a single unit of a perceptron the input to a perceptron is a vector of real value x_0,x_1,x_2, …….$x_n$that computes the linear combination of these inputs. The output is unity if it is larger than the predefined threshold else the output is −1. Many of the Boolean functions like the AND, OR, NAND are represented by a single perceptron. The learning of a perceptron begins with a random weight that iteratively applies to each training samples modifying the weights until convergence to a hypothesis that classifies the data completely. According to the perceptron training rules the weights are modified at each step given by

$$w_i \leftarrow w_i + \Delta w_i \tag{5}$$

Where $\Delta w_i = \eta(t - o)x_i$ here η is the learning rate that moderates the degree to the changed weights,t is the target output and o is the output generated by the perceptron. This learning procedure converges within a finite no of iterations provided the samples are linearly separable and η

Table 24
Detailed Accuracy Rate for Decision Tree Classifier.

True Positive Rate	0.800
False Positive Rate	0.300
Precision	0.727
Recall	0.800
Accuracy	75%

Table 25
Classification Instances for the Decision Tree Classifier.

Correctly Classified Instances	75
Incorrectly Classified Instances	25
Percentage Accuracy	75

Fig. 19. Plot of Detailed Accuracy Rate for Decision Tree Classifier.

www.mmiet.edu.in

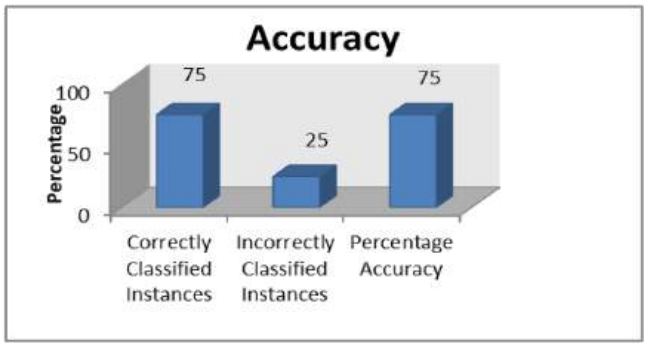

Fig. 20. Plot of Classification Instances for Decision tree Classifiers.

Table 26
Confusion Matrix of Decision Tree Classifier.

True positive = 40	False Positive = 10
False Negative = 15	True Negative = 35

Table 27
Comparison of results for different Machine Learning Techniques.

Classifiers	OASIS and ADNI Data set
Naïve Bayes	80%
Logistic Regression	90%
Multilayer Perceptron	90%
Support Vector Machine	85%
Decision Tree	75%

being sufficiently small. Convergence is not confident if the data is not linearly separable.

3.4.5. The support vector machine

SVM is a machine learning method coined from statistical theory applied for classification of images, broadly used in pattern recognition it has a good generalization performance and computational efficiently. It takes labeled data as the input from the two classes and the output is a labeled class of the two classes [21]. Training implicates feeding the known data along with prior decision values creating finite training set. Initiation of learning of the SVM classifier can be described as follows, if a vector $x \in R^n$ designate a pattern to be classified and y designate its training labels i.e. $y = \pm 1$ and if $\{(x_i y_i), i = 1, 2, \ldots\ldots\ldots l\}$ denote the training samples then the classifier can be constructed with the function $f(x)$.

Linear classifier is the simplest case where the input patterns are linearly separable and the linear function is of the form

$$f(x) = W^T x + b \tag{6}$$

hence for each training sample x_i the function produces

$$\begin{cases} f(x_i) \geq 0 \; for \; y_i = +1 \\ f(x_i) < 0 for \; y_i = -1 \end{cases} \tag{7}$$

Hence forming the various classes that are detached by the hyper plane$f(x) = W^T x + b = 0$.

There exist numerous hyper planes for a given set however the SVM classifier considers the hyper plane that maximizes the separating margin among the two classes [22].

Nonlinear SVM classifier is the extension of the linear classifier that uses a nonlinear operator $\phi(\cdot)$ that maps input pattern x into greater dimensional space which is defined by

$$f(x) = W^T \phi(x) + b \tag{8}$$

Eq. (8) is linear in terms transformed data $f(x)$ but nonlinear for original data $x \in R^n$ the parameters of the decision function $f(x)$ is resolute by minimization criteria given by

$$Min \; J(W, \xi) = \frac{1}{2} W^2 + C \sum \xi_i \quad i = 0, 1, 2, \ldots\ldots\ldots, l \tag{9}$$

Subjected to

$$y_i \left(W^T \phi(x_i) + b \right) \geq 1 - \xi_i, \; \xi_i \geq 0; \quad i = 1, 2, \ldots\ldots, l \tag{10}$$

The kernel function plays a vital part of mapping the input vector into a greater dimensional feature space it defines the relaxation of the margin to admit some of the points to occupy the opposite margin. It is essential to check whether the kernel is connected with the inner product of some nonlinear mapping. The kernel function must satisfy the Mercer's theorem [23] defines that for every square integral function $g(\cdot)$ the kernel should satisfy the following condition.

$$\iint K(x, y) g(x) g(y) d_x d_y \geq 0 \tag{11}$$

The frequently used kernel function includes polynomials and radial basis function (RBF), the polynomial kernel is defined as follows

$$K(x, y) = \left(x^T + 1 \right)^p \quad where \; p > 0 \tag{12}$$

And finally, the decision function is defined as

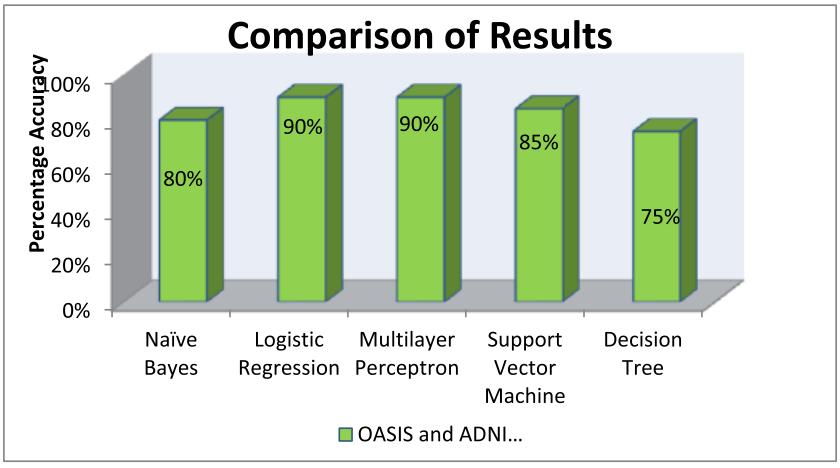

Fig. 21. Plot showing the comparison of results for different data set.

www.mmiet.edu.in

$$f(x) = \pm\left(\sum y_i \alpha_i \; k(x_i, x) - b\right) \tag{13}$$

Where x_i is a support vector, α_i Lagrange multiplier, $k(x_i,x)$ the convolutional of the inner product to get the feature space and the support vector that is equal to the decision function in the higher dimensional space.

3.4.6. Decision tree

A hierarchical data structure implementing the divide and rule method is the decision tree. It is an effectual nonparametric process applied for classification as well as regression that can be transformed to a set of rules that are easily understood [24]. Here the input space is divided into local regions that are defined by local model calculated from the training data. It is composed of internal decision nodes and terminated by leaves. Starting from the root for every input node a test is applied and one of the branches is selected depending on the outcome this process is repeated recursively till a leaf node is hit; i.e. a class is obtained at the leaf node.

Decision tree approximates the discrete value functions with noisy data and is capable of learning disjunctive expressions. It classifies the instances by categorizing them down the tree from the root to the leaf node [25] where the leaf node provides the classification of the instances. Node represents the test of some attribute of the instance and every branch downward from the node resembles to one of the possible values of this attribute. The top-down, greedy search are the core algorithms of the decision tree illustrated by ID3 (Quinlan 1986) succeeded by C4.5 (Quinlan 1993).

Selecting the best attribute at every step of the tree for achieving accurate classification is done by the ID3 algorithm that is defined by the statistical property called the information gain; which is the measure of how well an attribute separates the training samples with respect to the target classification.

The information gain is defined by

$$Gain(S,A) \equiv Entropy(S) - \sum_{v \in values(A)} \frac{|S_v|}{|S|} Entropy(S_v) \tag{14}$$

Where *values*(*A*)the values of attribute A, and S are is a subset for which A has the value $vS_v = \{S \in S | A(S) = v\}$. ID3 is characterized as searching a space of hypothesis which is set of possible decision trees. It executes a simple to complex hill climbing search through the hypothesis space starting with the empty tree.

4. Results of various implemented machine learning algorithms

4.1. Result of Naïve Bayes classifier

The results of Naïve Bayes classifier with respect to 10-fold cross validation on a set of 100 MRI scans is given in Table 2 and the same is plotted in Fig. 1. The mean absolute error and the root mean square error are tabulated in Table 3 and plotted in Fig. 2. The details of accuracy rate are tabulated in Table 4 and plotted in Fig. 3 these indicates the true positive rate, false positive, precision and recall, Table 5 gives the classification instances and the same are illustrates in Fig. 4, the confusion matrix is given in Table 6.

4.2. The result for the logistic classifier

With respect to percentage accuracy is tabulated in Table 7 and the same is plotted in Fig. 5, the mean error rates with respect to mean absolute error and root mean square error are tabulated in Table 8 and plotted in Fig. 6. The details of accuracy are given in Table 9 and illustrated in Fig. 7; Table 10 gives the classification instances applied to the logistic regression which are plotted in Fig. 8 and the confusion matrix is given in Table 11.

4.3. Result of the MLP

The results of percentage correct classification applied for multilayer Perceptron is given in Table 12 and plotted in Fig. 9, the mean error is given in Table 13 and exemplified in Fig. 10, the details of classification accuracy is tabulated in Table 14 which is illustrated in Fig. 11, the Table 15 gives the classification instances and plotted in Fig. 12 and the confusion matrix is given in Table 16.

4.4. Result of the SVM

The result of the SVM classifier with respect to accuracy in terms of percentage correct classification is particularized in Table 17 and plotted in Fig. 13 and the mean error are tabulated in Table 18 and the same is plotted in Fig. 14, the Table 19 gives the details of accuracy classification and the same is plotted in Fig. 15 and Table 20 gives the classification instances which is plotted in Fig. 16 the confusion matrix with respect to the SVM classifier is given in Table 21.

4.5. Result of the decision tree

The result of the decision tree with respect to correctly classified instances is given in Table 22 which is also illustrated in Fig. 17 the error with respect to mean absolute error and RMS error is tabulated in Table 23 which is again elaborated in Fig. 18, the detailed accuracy rate is given in Table 24 and the values are plotted in Fig. 19 the classification instances with respect to correct classification and accuracy is given in Table 25 and plotted in Fig. 20 and finally the confusion matrix is given in Table 26. Table 27 gives the comparison of results for different Machine Learning Techniques, the graph of the same is Plotted in Fig. 21.

5. Conclusion of the research

This research shows the state-of-art methods for classification of the tumor as cancerous and non-cancerous (Benign and Malignant). The advantage here is that it does not need any prior information about the probability distribution of different classes. Logistic and MLP are the branches of Machine learning that learns, and performing parallel computations. The most advantageous part in applying ML model is that the result of the system does not depends on the dataset and the structure of the network. Hence the Logistic and MLP may support the radiologist for classification of the tumors and for treatment planning which is the main objective of this research. Machine Learning for tumor classification without much human interference gives promising results, the Performance of the Logistic and MLP gives more accurate and promising results of about 90% on. Compared to the other traditional machine learning technique MLP has more powerful learning and expressing abilities that make remarkable achievements in classification task in the field of computer vision.

Declaration of Competing Interest

The authors declare that we have no conflict of interest.

References

[1] Devos A, Lukas L, Simonetti AW, Suykens JAK, Vanhamme L, van der Graaf M, Buydens LMC, Heerschap A, Van Huffel S. Does the combination of magnetic resonance imaging and spectroscopic imaging improve the classification of brain tumours?. In: The 26th Annual International Conference of the IEEE Engineering in Medicine and Biology Society. IEEE; 2004. p. 407–10. Vol. 1.
[2] Liu L, Zheng G, Bastian JD, Keel MJB, Nolte LP, Siebenrock KA, Ecker TM. Periacetabular osteotomy through the pararectus approach: technical feasibility and control of fragment mobility by a validated surgical navigation system in a cadaver experiment. Int Orthop 2016;40(7):1389–96.
[3] Open access series of imaging studies Available on http://www.oasis-brains.org/.
[4] http://adni.loni.usc.edu/data-samples/data-types/.

www.mmiet.edu.in

[5] Pereira S, Pinto A, Alves V, Silva CA. Brain tumor segmentation using convolutional neural networks in MRI images. IEEE Trans Med Imag 2016;35(5):1240–51.
[6] Krizhevsky A, Sutskever I, Hinton GE. Imagenet classification with deep convolutional neural networks. Adv Neural Inf Process Syst 2012:1097–105.
[7] Havaei M, Davy A, Warde-Farley D, Biard A, Courville A, Bengio Y, Pal C, Jodoin PM, Larochelle H. Brain tumor segmentation with deep neural networks. Med Image Anal 2017;35:18–31.
[8] Mohsen H, El-Dahshan ESA, El-Horbaty ESM, Salem ABM. Classification using deep learning neural networks for brain tumors. Future Comput Inf J 2018;3(1):68–71.
[9] Ari A, Hanbay D. Deep learning based brain tumor classification and detection system. Turkish J Electric Eng Comput Sci 2018;26(5):2275–86.
[10] Ilunga-Mbuyamba E, Avina–Cervantes JG, Garcia–Perez A, de Jesus Romero–Troncoso R, Aguirre–Ramos H, Cruz–Aceves I, Chalopin C. Localized active contour model with background intensity compensation applied on automatic MR brain tumor segmentation. Neurocomputing 2017;220:84–97.
[11] Sankari A, Vigneshwari S. Automatic tumor segmentation using convolutional neural networks. In: 2017 Third International Conference on Science Technology Engineering & Management (ICONSTEM). IEEE; 2017. p. 268–72.
[12] Sajjad M, Khan S, Muhammad K, Wu W, Ullah A, Baik SW. Multi-grade brain tumor classification using deep CNN with extensive data augmentation. J Comput Sci 2019;30:174–82.
[13] http://www.madehow.com/Volume-3/Magnetic-Resonance-Imaging-MRI.html.
[14] Alpaydin E. Introduction to machine learning. MIT press; 2014.
[15] Selvaraj H, Selvi ST, Selvathi D, Gewali L. Brain MRI slices classification using least squares support vector machine. Inte Intell Comput Med Sci Image Process 2007;1(1):21–33.
[16] Jang M, Park D. Stochastic classifier integration model. Int J Appl. Eng Res 2016;11(2):809–14.
[17] Russell SJ, Norvig P. Artificial intelligence: a modern approach. Malaysia: Pearson Education Limited; 2016.
[18] Ryali S, Supekar K, Abrams DA, Menon V. Sparse logistic regression for whole-brain classification of fMRI data. Neuroimage 2010;51(2):752–64.
[19] Krizhevsky A, Sutskever I, Hinton GE. Imagenet classification with deep convolutional neural networks. Adv Neural Inf Process Syst 2012:1097–105.
[20] Rumelhart DE, Hinton GE, Williams RJ. Learning internal representations by error propagation (No. ICS-8506). California Univ San Diego La Jolla Inst for Cognitive Science; 1985.
[21] Chaplot S, Patnaik LM, Jagannathan NR. Classification of magnetic resonance brain images using wavelets as input to support vector machine and neural network. Biomed Signal Process Control 2006;1(1):86–92.
[22] Burges CJ. A tutorial on support vector machines for pattern recognition. Data Min Knowl Discov 1998;2(2):121–67.
[23] Burges CJ, Scholkopf B, Smola AJ, editors. Advances in kernel methods: support vector learning. Cambridge, MA, USA: MIT press; 1999. p. 89–116.
[24] Lemort M, Canizares-Perez AC, Van der Stappen A, Kampouridis S. Progress in magnetic resonance imaging of brain tumours. Curr Opin Oncol 2007;19(6):616–22.
[25] Egmont-Petersen M, de Ridder D, Handels H. Image processing with neural networks—a review. Pattern Recognit 2002;35(10):2279–301.

www.nmiet.edu.in

Engineering Research Express

PAPER

Determining optimal parameters using Taguchi's design of experiments (DOE) for improving the quality of biogas generation process

RECEIVED
9 February 2022

REVISED
30 April 2022

ACCEPTED FOR PUBLICATION
11 May 2022

PUBLISHED
19 May 2022

Prakash Babu Kanakavalli[1] **and Satish R More**[1,2]

[1] Department of Mechanical Engineering, Velagapudi Ramakrishna Siddhartha Engineering College, Kanuru, Vijayawada, Andhra Pradesh, 520007, India

[2] Department of Mechanical Engineering, Nutan Maharashtra Institute of Engineering and Technology (NMIET), Talegaon, Pune, Maharashtra - 410507, India

E-mail: prakashmim06@gmail.com **and** moresatish11@yahoo.co.in

Keywords: biogas generation process, agricultural waste, design of experiments, methane percentage

Abstract

The use of an anaerobic process of biogas production depends on various parameters. Increasing the methane (CH_4) production percentage is a critical task in an anaerobic process. In the present investigation, the role of the four most common process parameters are temperature, pH value, solid concentration, and C/N ratio optimized for two responses i.e. biogas production and higher methane percentage. A Taguchi Design of Experiment (DOE) methodology was used to investigate and analyze the effects of different parameters using an L9 orthogonal array. The investigation results for both responses showed that solid concentration had a higher contribution of 65.37% and 73.37% for biogas production and methane percentage respectively. The second rank responsible parameter for both the responses is pH having the same contribution of 18%. the initial pH and rotation speed of the process was the most effective parameters for comparison with others. While the other factors' temperature and C/N ratio contribution are 15.54% and 0.13% for biogas production and 3.48% and 4.25% for methane percentage. Biogas production and methane percentage model found with correlation percentage (r^2) 0.98 and 0.92 respectively which is agreeable. The confirmation test results with Taguchi's model show errors of 7.46% and 2.43% for biogas and methane production percentages respectively.

1. Introduction

Renewable energy sources are important in today's modern society. Day by day energy demand increases and completion of energy demand is possible because of renewable energy sources and it is also helpful to control the global warming effect. In reality number of different renewable energy sources are available and that helps society to complete the energy demand [1, 2]. Such energy sources like solar, wind, and biomass are available in major unlimited sources. Biogas is an important source of renewable energy i.e. easily available in any place. Out of that, the biogas is produced with the breakdown process of organic matter. Biogas is mainly a combination of methane and carbon dioxide the production process happens in absence of oxygen. It can be produced with different types of materials like sewage, plant material, food or green waste, municipal and agricultural waste [3, 4]. The working of biogas production is depending on fermentation and an anaerobic digestion process that decomposes the waste by microorganisms for the generation of natural biogas. Practically any organic waste can be considered in the process, though factors such as temperature affect and pH the gas production [3, 5].

According to microorganism activity the production of biogas generation is controllable by considering or controlling various dependent factors like temperature, C/N ratio, pH, pressure, etc [6]. The optimisation of controlling factors are possible with various techniques Response Surface Methodology (RSM) and Design of Experiment (DOE). The experimental and methamatical model for biogas generation is developed using various

© 2022 IOP Publishing Ltd

www.nmiet.edu.in

(a)

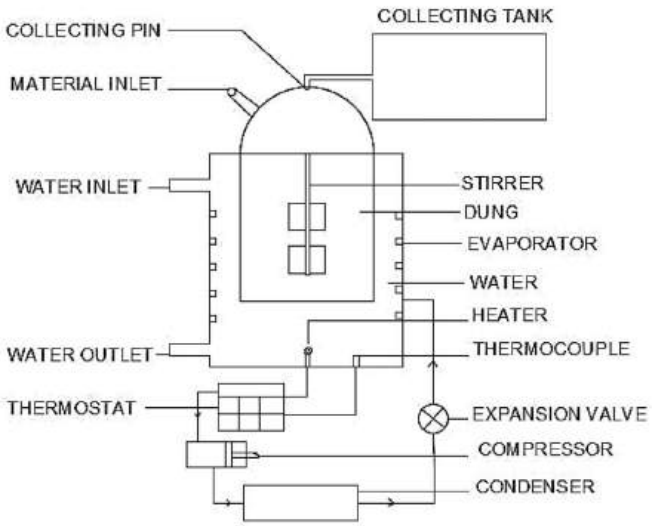

(b)

Figure 1. Biogas production experimental set-up.

optimisation techniques. Pre-treatment and anaerobic digestion method produce higher volume of biogas. In experimentation the optimum parametric condition like 37.3 °C temps, 2 min 42 s beating time produce 12.65% higher biogas using grass silage for maximum biogas yield i.e. 3410 cc [7]. The methane production from four lignocellulosic biomass feedstocks with yard waste, wheat straw, corn stover, and leaves is possible via solid-state anaerobic digestion. The maximum methane yield was achieved for 81.2 l kg^{-1} (VS) volatile solids corn stover, followed by (66.9 l kg^{-1} VS) wheat straw, (55.4 l kg^{-1} VS) leaves, and (40.8 l kg^{-1} VS) yard waste at a (S/I) ratio i.e. substrate to inoculum ratio of 2 [8].

The significant process parameters for pre-treatment and biogas production found using Grey Relational Analysis (GRA) and DOE methods. 7.5% TS of solid concentration, 7 of pH, 50 °C of temperature, 20.19 of C/N ratio, and ultrasonication pre-treatment are the best level for anaerobic digestion of food waste [9]. The multi-objective technique of GRA found 42.41% contribution of solid concentration, 23.08% pH, 16.19% C/N ratio and 5.59% temperature for anaerobic digestion of poultry litter [10]. Ahmed *et al* [11] investigated the effects of mesophilic anaerobic co-digestion of OFMSW i.e. Organic Fraction of Sewage Sludge and Municipal Solid Waste and on the improvement of volume biogas production. The experimentation is based on various types of sludge combinations i.e. Waste Activated Sludge (WAS), Primary Sludge (PS) and Mixed Sludge (MS), and variation in solid concentration of sludge. They found that MS was the best co-substrate (with the organic fraction of municipal solid waste) amongst the different sludge types studied and the highest biogas yield was produced at an organic fraction of municipal solid waste to mixed sludge ratio of 80:20. Beevi *et al* [12] investigated the optimal conditions for use of an Organic Fraction of Municipal Solid Waste (OFMSW) and

www.nmiet.edu.in

Figure 2. Details of biogas production experimental set-up.

biogas production using the RSM method. They found optimized condition for the maximum generation of biogas is 53.8 l $Kg^{-1}VS^{-1}$, which is in correlation with the predicted value 53.4 l $Kg^{-1}VS^{-1}$. The generation of good quality biogas is possible from restaurant solid waste, raw vegetable waste, and wastewater [13–16]. The Taguchi method was applied for optimizing various process parameters and improving the biogas production rate. Digestion time varies with raw waste materials, 26 days for wastewater, 10 to 18 weeks for waste vegetables, and restaurant solid waste. By using properly optimized process parameters 153% methane production will be increased with suitable digesters [13–15,17].

The researchers are tried to find the extraction method for biogas from different types of waste, and sludge available in society and agricultural areas. Generally, the common process parameters for biogas generation are temperature, pH value, solid concentration, and C/N ratio. The biogas production parameters (factors) are the most significant factors affecting the quantity and quality and cost of production. This work presents the influence of most effecting optimal parameters like Temperature, pH, Solid concentration, and Carbon nitrogen ratio on gas production. The experimental data was obtained using the DOE Taguchi technique. Signal to Noise (S/N) ratio, Analysis of Variance(ANOVA), and Taguchi analysis are used to investigate the biogas generation process parameters. A model was developed on which experiments will be carried out based on the Taguchi Design of experiments. The comparison between predicted and experimental results was carried out by conducting the conformations tests.

2. Experimental details

2.1. Biogas generation test rig

The digester used to carry out the experiments with a fixed dome type digester. The reactor was made of stainless steel with a volume of 25 liters as shown in figure 1. Figure 2 shows the details of the biogas generation test setup. The digestion was carried out at a mesophilic condition of 25 °C–27 °C temperature and pH were maintained at a neutral 7 pH. The digester is used for decomposing the organic matter for the generation of biogas. A 1000-watt capacity heater is used for heating the water. The compressor is used to increase the pressure of a gas i.e. at inlet low-pressure gas and outlet high-pressure gas will get. A condenser transfers heat from the refrigerant to

www.nmiet.edu.in

Table 1. Experimental testing parameters and their level for biogas experiments.

		Level		
Biogas parameters	Units/Symbols	1	2	3
Temperature	°C	25	26	27
Solid concentration	Kg/10 litres	9.5	13.5	17.5
pH	—	6.8	7.2	7.6
C/N Ratio	—	22:1	23:1	24:1

Table 2. S/N ratios for mass and methane content—biogas.

					Output response of biogas			
Sr No	Solid concentration (kg l^{-1})	Temperature (°C)	pH value	C/N ratio	Mass in kg	CH_4 (%)	S/N ratio for Mass	S/N ratio for CH_4
1	9.5	25	7.2	22.1	1.15	53.75	1.21	34.60
2	9.5	26	7.4	22.2	1.16	53.97	1.30	34.64
3	9.5	27	7.6	22.3	1.14	53.41	1.15	34.55
4	13.5	25	7.4	22.3	1.21	54.12	1.68	34.66
5	13.5	26	7.6	22.1	1.18	54.01	1.44	34.64
6	13.5	27	7.2	22.2	1.33	54.54	2.49	34.73
7	17.5	25	7.6	22.2	1.23	54.33	1.84	34.70
8	17.5	26	7.2	22.3	1.35	54.67	2.64	34.75
9	17.5	27	7.4	22.1	1.39	54.81	2.87	34.77

either air or water. The by-product is a gas refrigerant that condenses to a liquid. Throttling valve: The liquid boils and evaporates by suddenly reducing the expansion valve's pressure [6, 9]. This final step takes place in the evaporator to complete the cycle. The refrigerant then goes back to the compressor to repeat the process. Evaporator: When the liquid refrigerant enters the evaporator, heat is absorbed as it evaporates and produces cooling. The refrigerant is diverted to a tank where the pressure rises until it meets the pressure in the evaporator. Once pressure is equalized, the temperature in the tank and evaporator rises to ambient. Thermostat: It is used to adjust the temperature. Thermocouple: It is a sensor that is used for measuring temperature.

2.2. Experimental procedure

Before starting the experimental work, pre-experimental treatment is necessary. In pre-experimental treatment, the cow dung and pig dung which are used as the input in the digester should be dry and free from urine. Inoculum is the micro-organism rich mixture added into a digester to provide the microorganisms to drive the anaerobic digestion process. Providing the culture of the necessary bacteria for the fermentation is often called 'seeding' the digester.

In the experimental procedure, the fixed dome type digester is fixed at the proper position with the required electronic equipment for maintaining the temperature. The outer chamber is filled with water to create an artificial atmosphere for the digester. It contains a heater and refrigeration unit to maintain a constant temperature. Input materials cow dung and pig dung are mixed according to testing parameters table 1. The raw material is mixed with the water according to the required solid concentration. The pH of the material is varied with the help of acetic acid and sodium hydroxide. After giving the input to the digester, it wasclosed tightly with the dome by preventing air leakages. The power supply is given to the heater, refrigeration, and electrical equipment unit to create an artificial atmosphere for the digester. The stirring of the digester was done every 6 h for uniform fermentation. The selected hydraulic retention time for the generation of biogas is 15 days [3, 10, 13].The above process is repeated for the nine experiments as given in table 2. The generated biogas was collected in a collecting tank, then the mass and percentage of methane was measured.

2.3. Experimental Taguchi design

The DOE Taguchi's approach is used for analysis and finding the responsible effective control factors or parameters. The model is developed for production performance based on responses. This method is good for investigating the effect of single parameters on output. In the biogas production process, the output methane percentage and biogas quantity depend on the different input parameters. This method was chosen because it is more versatile than other analytical techniques in determining the impact of each input parameter on the

www.nmiet.edu.in

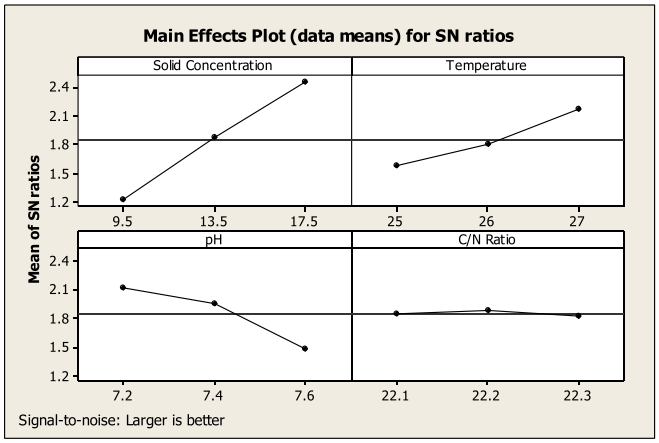

Figure 3. Main effects plot for S/N ratios (Biogas in kg).

Table 3. Response table for signal to noise ratio for biogas mass in kg.

Level	Solid concentration (kg/10 l)	Temperature (°C)	pH	Carbon nitrogen ratio
1	1.225	1.580	2.116	1.845
2	1.872	1.798	1.953	1.881
3	2.454	2.173	1.482	1.826
Delta	1.229	0.592	0.634	0.055
Rank	1	3	2	4

Table 4. Response table for signal to noise ratio for biogas methane (CH_4) percentage.

Level	Solid concentration (kg/10 l)	Temperature (°C)	pH	Carbon nitrogen ratio
1	34.60	34.66	34.70	34.68
2	34.68	34.68	34.70	34.69
3	34.74	34.69	34.63	34.66
Delta	0.14	0.03	0.06	0.03
Rank	1	4	2	3

percentage of methane produced. The L9 Taguchi design of the experimental approach was considered because it decreases the cost and duration of the experiment [18–21].

In this study, four parameters namely temperature, pH value, solid concentration, and C/N ratio were considered in order to study biogas generation and methane percentage. Table 1 shows the testing settings and levels used in all of the trials. Table 2 shows the operating conditions for each test. The results of the experiment were converted into a signal-to-noise (S/N) ratio. In general, There are different S/N ratios based on the sort of three characteristics; smaller the better, nominal the best, and larger the better [19–21]. For studying the maximal biogas generation with a higher percentage of methane gas, the larger the better characteristic of the S/N ratio was considered, as shown in equation (1).

The lager the better characteristic:

$$\frac{S}{N} = -10\log\frac{1}{n}\left(\sum\frac{1}{Y_i^2}\right) \tag{1}$$

Where n is the number of observations and y is the observed data i.e., biogas and methane percentage [19–21].

3. Results and analysis

3.1. Biogas and methane generation analysis using Taguchi experimental design

The analysis of the present experimental results was performed on MINITAB 14 software. The L_9 orthogonal array design along with the S/N ratio for the analysis of biogas and methane generation. Table 2 shows experimental results with the S/N ratio for both the responses. For finding the optimal possible parameters the

www.nmiet.edu.in

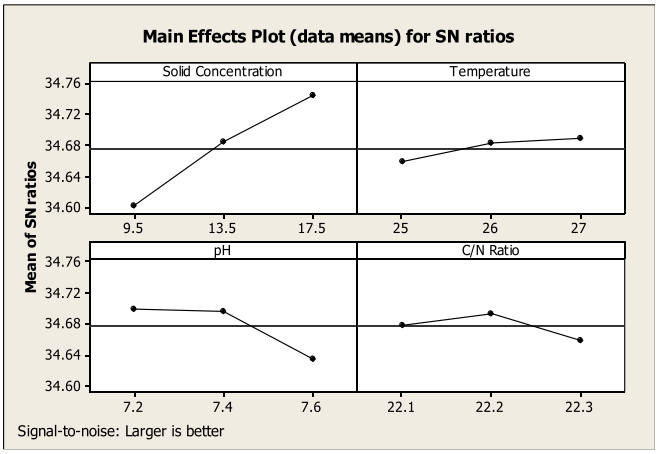

Figure 4. Main effects plot for S/N ratios (Biogas Methane (CH_4) Percentage).

Table 5. ANOVA for Biogas Mass (kg).

Source	Degree of freedom	Sum of square	Mean of square	% Contribution
Solid Concentration	2	2.269 31	1.134 66	65.53
Temperature	2	0.538 39	0.269 20	15.54
pH	2	0.650 57	0.325 28	18.78
C/N Ratio	2	0.004 64	0.002 32	0.13
Total	8	3.462 92		100

Table 6. ANOVA for biogas methane (CH_4%) Percentage.

Source	Degree of freedom	Sum of square	Mean of square	% Contribution
Solid Concentration	2	0.031 044	0.015 522	73.37
Temperature	2	0.001 475	0.000 737	3.48
pH	2	0.007 986	0.003 993	18.87
C/N Ratio	2	0.001 801	0.000 901	4.25
Total	8	0.042 306		100

larger the better-quality characteristic was selected for both the responses i.e. generation of biogas and methane percentage.

Tables 3 and 4 show the response tables for both responses and the S/N ratio obtained. Tables 3 and 4 indicate that temperature was the most affecting control element (parameter) among all four factors for the production of good quality biogas. The remaining three variables, solid concentration, pH value, and carbon-nitrogen ratio, are ranked second, third, and fourth in ways that influence the generation of high biogas with a higher methane percentage, respectively.

The graphical results of the main effect plot for the S/N rations were represented in figures 3 and 4. The maximum generation of biogas and methane CH_4 percentage was found at 27-degree Celsius temperature, 7.2 pH, 17.5 solid concentration 22.2 C N^{-1} ratio respectively from figures 3 and 4. Balaji [10] found the optimum level values of process parameters obtained for anaerobic digestion of pre-treated poultry litter are the solid concentration of 13.5% TS, pH of 7.4, temperature of 26 °C, and C/N 15.3 these results are closer to results found in the present investigation. Some other researchers found similar kind of results according to their process parameters, for example, Thirugnanasambandham [13] found the optimized conditions for maximum biogas yield (9 ml l^{-1}) were pH of 5, digestion time of 26 days, the volume of 1 l sample, and the rotation speed of 120 rpm, and temperature of 55 °C for generation of biogas from wastewater. Mukhopadhyay [15] The optimized parameters for biogas generation from raw vegetables are plastic content (15%), height to diameter (h/D) ratio (30), water content (125 ml), and digestion period (18 weeks).

www.nmiet.edu.in

Table 7. Confirmation experimental results for mass of Biogas (kg).

Solid concentration (kg/10l)	Temperature (°C)	pH value	C/N Ratio	Biogas (kg) in test	Biogas (kg) by model	% Error
17.5	27	7.2	22.2	1.5358	1.4212	7.46

Table 8. Confirmation experimental results for quality of biogas methane CH_4 %.

Solid concentration (kg/10l)	Temperature (°C)	pH value	C/N ratio	CH_4(%) in Test	CH_4(%g) by model	% Error
17.5	27	7.2	22.2	56.27	54.90	2.43

3.2. ANOVA for biogas mass (kg) and quality methane (CH_4) percentage

The ANOVA for biogas production and quality of methane percentage is shown in tables 5 and 6. Both tables 5 and 6 show the Analysis of Variance for S/N ratios, from the tables it is clear that the rank of significant parameters is correct. The solid concentration shows a higher percentage of contribution for biogas and methane production i.e. 65.53% and 73.37% respectively. While pH has a contribution of 18.78% and 18.87%. The temperature has a 15.54% contribution in biogas production and 3.48% in methane percentage. C/N ratio has less contribution i.e. 4.25% in methane percentage and less than 1% in biogas generation. Balaji [10] found Solid Concentration is the most influential factor due to its higher percentage contribution (42.41%) among the process parameters, which is followed by pH 23.08%, C/N 16.19% and temperature by 5.59% these factor contribution and sequence is approximately similar with our present results. Thirugnanasambandham [13] found pH and rotation speed of the process was the comparison of the most effective parameters with digestion time and temperature.

3.3. Predictive equation

The biogas generation and methane percentage were predicted using the nonlinear regressive predictive equation. It is used for finding the association between the responsible parameters (Factors) and response. The regression was found by using Minitab 14 software. The following form of the regression equation was obtained. Equation (2) for the prediction of biogas generation and equation (3) is used for the prediction of the percentage of methane gas.

The regression equations are:

$$\text{Gas Generation} = 1.95 + 0.0221\ \text{Solid Concentration} + 0.0443\ \text{Temperature} - 0.231\ \text{pH} - 0.0202\ \text{C/N Ratio} \quad (2)$$

$$CH_4\% = 71.4 + 0.112\ \text{Solid Concentration} + 0.0933\ \text{Temperature} - 1.01\ \text{pH} - 0.617\ \text{C/N Ratio} \quad (3)$$

The values of all constants were calculated by using the Minitab 14 software.

The accuracy of calculated constants was confirmed because a high correlation coefficient (r2) of 0.98 and 0.92 was obtained from equations (2) and (3) respectively.

3.4. Confirmation test

The optimal test parameters were selected and used to perform the confirmation test. The parameters are solid concentration, temperature, pH value, and C/N ratio for levels 3, 3, 1, 2 respectively at which the generation of biogas and methane (CH_4%) percentage is maximum. Tables 7 and 8 represents the result of the confirmation experimental test and the result obtained by the regression equation for biogas generation and percentage of methane gas respectively. By comparison of the regression and experimental results, a deviation of about 2.43% and 7.46% were found which are agreeable. Thus, it is found that the obtained regression (nonlinear) equation designates the biogas generation and percentage of methane gas with several control factors with a reasonable degree of approximation.

4. Conclusions

Here Taguchi method is used to investigate the effect of process parameters on biogas production and quality. Total nine experiments were performed with four parameters (factors) and a three-level combination using an L9 orthogonal array. The results are brief as follows.

www.nmiet.edu.in

- From the analysis of variance, it is clear that the four factors solid concentration, pH, temperature, and C/N ratio have a significant effect on biogas production and availability percentage of methane gas.
- The analysis of variance proves that the most influencing parameters in optimizing the biogas generation are solid concentration and pH with a contribution of 65.53% and 18.78%. While the other factors temperature and C/N ratio contribution are 15.54% and 0.13% respectively.
- Similarly, for the methane contained in biogas, the most influencing parameters are solid concentration and pH with a contribution of 73.37% and 18.87%, temperature having 3.48%, and C/N ratio having 4.25% contribution.
- Biogas production and methane percentage model find with correlation percentage (r^2) 0.98 and 0.92 respectively which is agreeable.
- The confirmation test conducted for both the response result shows errors in between experimental and predictive models are in the acceptable range.
- The maximum generation of biogas and methane percentage was found in the 27 °C temperature, 7.2 pH, 17.5 solid concentration 22.2 C N^{-1} ratio as per mean effect plot for SN ratio.
- The present study has limitations related to the experimental setup because it is self-developed and in-house manufactured. Also, time constrain for experimentation for each experiment more time is required to produce biogas therefor L9 set of experiments is considered.
- In future work to overcome this limitation standard test rig and measuring instrument will be preferred. Also, try to conduct minimum L16 experiments.

Data availability statement

The data that support the findings of this study are available upon reasonable request from the authors.

ORCID iDs

Prakash Babu Kanakavalli https://orcid.org/0000-0002-1134-9262

References

[1] Sorathia H S, Rathod P P and Sorathiya A S 2012 Bio-gas generation and factors affecting the bio-gas generation—a review study *International Journal of Advanced Engineering Technology* **3** 72–8
[2] Venkateswara Rao P, Saroj S B, Dey R and Mutnuri S 2010 Biogas generation potential by anaerobic digestion for sustainable energy development in India *Renew. Sustain. Energy Rev.* **14** 2086–94
[3] Santosh Y, Sreekrishnan T R, Kohli S and Rana V 2004 Enhancement of biogas production from solid substrates using different techniques—a review *Bioresour. Technol.* **95** 1–10
[4] Nsair A, Cinar S O, Alassali A, Abu Qdais H and Kuchta K 2020 Operational parameters of biogas plants: a review and evaluation study *Energies* **13** 3761
[5] Chena L, Rong-Gang C, Shua B and Zhi-Fu M 2017 A sustainable biogas model in China: the case study of Beijing Deqingyuan biogas project *Renew. Sustain. Energy Rev.* **78** 773–9
[6] Singh G, Jain V K and Singh A 2017 Effect of temperature and other factors on anaerobic digestion process, responsible for bio gas production *International Journal of Theoretical and Applied Mechanics* **12** 637–57
[7] Alfarjani F A 2012 Design and optimization of process parameters in bio-gas production systems *Thesis Master of Engineering (MEng)* School of Mechanical and Manufacturing Engineering Dublin City University
[8] Lo Niee L, Jian S and Yebo L 2012 Methane production from solid-state anaerobic digestion of lignocellulosic biomass *Biomass Bioenergy* **46** 125–32
[9] Deepanraj B, Sivasubramanian V and Jayaraj S 2017 Multi-response optimization of process parameters in biogas production from food waste using Taguchi—Grey relational analysis *Energy Convers. Manage.* **141** 429–38
[10] Balaji S, Sakthivel M, Pasupathy S A, Karthick Kumar K and Sukanya G 2018 Multi objective optimization of anaerobic digestion of poultry litter using taguchi grey relational analysis *International Journal of Applied Engineering Research* **13** 5216–22
[11] Ahmed B, Tyagi V K, Priyanka, Khan A A and Kazmi A A 2020 Optimization of process parameters for enhanced biogas yield from anaerobic co-digestion of OFMSW and bio-solids *Biomass Conversion and Biorefinery* **12** 607–18
[12] Sajeena Beevi B, Jose P P and Madhu G 2014 Optimization of process parameters affecting biogas production from organic fraction of municipal solid waste via anaerobic digestion *World Academy of Science, Engineering and Technology International Journal of Bioengineering and Life Sciences* **8** 43–8
[13] Thirugnanasambandham K 2017 Enhancement of biogas production from wastewater using a batch anaerobic process *Energy Sources Part A* **39** 1484–90
[14] Mansur A, Janari D and Setiawan Dan A 2016 The development of mini portable digester designs for domestic and restaurant solid waste processing to be clean biogas as energy's alternative to replace LPG *IOP Conf. Series: Materials Science and Engineering* **114** 012044

www.nmiet.edu.in

[15] Mukhopadhyay D, Sarkar J P and Dutta S 2013 Optimization of process factors for the efficient generation of biogas from raw vegetable wastes under the direct influence of plastic materials using Taguchi methodology *Desalin. Water Treat.* **51** 13–5
[16] Ellacuriaga M, García-Cascallana J and Gómez X 2021 Biogas production from organic wastes: integrating concepts of circular economy *Fuels* **2** 144–67
[17] Nicholas A-G, Sreenivas Rao R and Phil J H 2012 Optimizing anaerobic digestion by selection of the immobilizing surface for enhanced methane production *Bioresour. Technol.* **120** 248–55
[18] Senthilkumar N, Deepanraj B, Vasantharaj K and Sivasubramanian V 2016 Optimization and performance analysis of process parameters during anaerobic digestion of food waste using hybrid GRA-PCA technique *J. Renewable Sustainable Energy* **8** 063107
[19] More S R, Bhatt D V and Menghani J V 2017 Study of the parametric performance of solid particle erosion wear under the slurry pot test rig *Tribology in Industry* **39** 471–81
[20] Patnaik A 2008 Implementation of Taguchi design for erosion of fiber-reinforced polyester composite systems with SiC filler *J. Reinf. Plast. Compos.* **27** 1–19
[21] Patnaik A, Satapathy A, Mahapatra S S and Dash R R 2008 A modeling approach for prediction of erosion behavior of glass fiber–polyester composites *J. Polym. Res.* **15** 147–60

www.nmiet.edu.in

Parameter Dependencies and Optimization of True Random Number Generator (TRNG) using Genetic Algorithm (GA)

Publisher: IEEE

Cite This PDF

Vilas Deotare ; Dinesh Padole ; Lalitkumar Wadhwa **All Authors**

1 Cites in Paper

176 Full Text Views

Alerts

Manage Content Alerts

Add to Citation Alerts

Abstract

Document Sections

I. Introduction to Hardware - Software Co-design in Digital System Design

II The Basic Principal of Jitter Generation and Extraction:

III Fitness Parameters

IV Genetic Algorithms and Fitness Function:

V Simulation Results

Show Full Outline

Authors

Figures

References

Citations

Keywords

Downl PDF

Abstract:
In the hostile environment, use of pseudo-random numbers in encryption algorithm has become difficult due to increased computing power of attackers. To overcome from the ... **View more**

Metadata

Abstract:
In the hostile environment, use of pseudo-random numbers in encryption algorithm has become difficult due to increased computing power of attackers. To overcome from the hackers true random number generator solving by giving unique random sequence. Authors recommend based on experiment to add parameters dependencies of analog Phase-Locked Loop (PLL) based on TRNG, and it also tries to optimize few parameters using Genetic Algorithm (GA). The proposed approach selects optimum values for different parameters and increases flexibility, resource utilization, throughput. Digital architecture for optimized TRNG is obtained using Altera platform. Implementation the optimized TRNG on ALTERA QUARTUS-II DE0 board gives enhancement R and S parameters by 42.18% and 38.67% respectively.

Published in: 2021 8th International Conference on Smart Computing and Communications (ICSCC)

Date of Conference: 01-03 July 2021

DOI: 10.1109/ICSCC51209.2021.9528264

Date Added to IEEE *Xplore*: 06 September 2021

Publisher: IEEE

Conference Location: Kochi, Kerala, India

www.nmiet.edu.in

Metrics

More Like This

ISBN Information:

Contents

I. Introduction to Hardware -Software Co-design in Digital System Design

Arbitrary numbers are urgent in various cryptographic applications, for example, measurement, cryptography, and even workmanship. Irregular numbers utilized must satisfy rigid security prerequisites with reasonable measurable boundaries and adequate degree of eccentrics. With expanding registering intensity of assailants, it is getting hard to utilize pseudoirregular numbers, as there can be odds of determining next arbitrary number succession. The arrangement is to utilize genuine irregular numbers however much as could reasonably be expected. There have been endeavors to produce arbitrary numbers with various techniques, for example, discrete-time disorder, metastable inspecting, direct intensification, and so on, and each sort of approach is having its specific application region [1]. The irregular numbers ought to be produced at fast to keep the assailant from anticipating next arbitrary number arrangement. Simultaneously, arbitrary numbers created must have adequate degree of security for example yield TRNG ought not to be one-sided with contribution anytime. However, because of conditions of speed and security on various boundaries, accomplishing fast and security simultaneously is not really conceivable. Additionally, to that, any little combination in these boundaries affects the system. This lead to a progress of a numerical appear as information abdicate relations in arrange to achieve cautious boundaries setting as contradicted to going for preparatory tries. Be that as it may, this can be accomplished by utilizing progressed advancement procedures as apparatuses for acquiring the ideal boundaries setting for the TRNG [2]. Continue Reading electronic oscillators [3] [4] are utilized, and their recurrence precariousness is utilized to deliver TRNG. On the comparative ground, another plan is presented [5] where a yield of a straight input move register (LFSR) and a cell robot are haphazardly examined. The plan proposed in [6] utilizes enhancement and testing of background noise delivering TRNG. It comprises of basic and progressed parts. It brings around higher constrain utilize by escalated organize to bring commotion level to the degree of progressed basis level. The comparative thought utilized by Intel Organization [4] in which warm clamor is escalates and utilized to drive voltage controlled oscillator (VCO) which is at that point surveyed by another oscillator. The creative organize subordinate on metastable circuits is proposed in [7]. In proposed work; endeavors are done to illustrate the centrality of cutting edge headway method within the field of boundaries change of TRNG so the creators can accomplish their destinations alongside fulfilling different limitations and cut-off points of the model. In [1] and [8] examining of nerves in stage bolted circle (PLL) as a simple part is utilized to deliver TRNG. In this paper, the age of TRNG with following oddities: (a) Fitness work is proposed as far as R, S, BW and ND; (b) Constraints as far as nonlinear balances, ordinary equities, and limits are indicated to augment wellness work with ideal determination of wellness boundaries; (c) optimum estimations of boundaries, for example, KM, KD and FREF are chosen expanding R, S and ND with proficient equipment use utilizing hereditary calculation.

Authors

Figures

References

Citations

Keywords

Metrics

www.nmiet.edu.in

More Like This

A Low-Cost Very Large Scale Integration Architecture for Multistandard Inverse Transform
IEEE Transactions on Circuits and Systems II: Express Briefs
Published: 2010

Low-Cost Implementation of Independent Component Analysis for Biomedical Signal Separation Using Very-Large-Scale Integration
IEEE Transactions on Circuits and Systems II: Express Briefs
Published: 2020

Show More

IEEE Personal Account

CHANGE USERNAME/PASSWORD

Purchase Details

PAYMENT OPTIONS

VIEW PURCHASED DOCUMENTS

Profile Information

COMMUNICATIONS PREFERENCES

PROFESSION AND EDUCATION

TECHNICAL INTERESTS

Need Help?

US & CANADA: +1 800 678 4333

WORLDWIDE: +1 732 981 0060

CONTACT & SUPPORT

Follow

www.nmiet.edu.in

About IEEE *Xplore* | Contact Us | Help | Accessibility | Terms of Use | Nondiscrimination Policy | IEEE Ethics Reporting | Sitemap | IEEE Privacy Policy

A not-for-profit organization, IEEE is the world's largest technical professional organization dedicated to advancing technology for the benefit of humanity.

© Copyright 2024 IEEE - All rights reserved, including rights for text and data mining and training of artificial intelligence and similar technologies.

IEEE Account

» Change Username/Password

» Update Address

Purchase Details

» Payment Options

» Order History

» View Purchased Documents

Profile Information

» Communications Preferences

» Profession and Education

» Technical Interests

Need Help?

» **US & Canada:** +1 800 678 4333

» **Worldwide:** +1 732 981 0060

» Contact & Support

About IEEE *Xplore* | Contact Us | Help | Accessibility | Terms of Use | Nondiscrimination Policy | Sitemap | Privacy & Opting Out of Cookies

A not-for-profit organization, IEEE is the world's largest technical professional organization dedicated to advancing technology for the benefit of humanity.

© Copyright 2024 IEEE - All rights reserved. Use of this web site signifies your agreement to the terms and conditions.

www.nmiet.edu.in

Received April 5, 2020, accepted May 1, 2020, date of publication May 19, 2020, date of current version June 3, 2020.

Digital Object Identifier 10.1109/ACCESS.2020.2995788

Deep Learning Based Person Authentication Using Hand Radiographs: A Forensic Approach

SAGAR V. JOSHI[1] **AND RAJENDRA D. KANPHADE**[2]**, (Member, IEEE)**

[1]Department of Electronics and Telecommunication Engineering, Dr. D. Y. Patil Institute of Technology, Pune 411018, India

[2]Jayawantrao Sawant College of Engineering, Pune 411028, India

Corresponding author: Sagar V. Joshi (sagarvjoshi@gmail.com)

ABSTRACT Biometric radiographs have gained importance in recent times owing to the rise in crime and disaster incidents. In recent times, authentication and identification of a person has become an essential part of most of the computer vision automation systems. Conventional fingerprint, iris, face, palm prints fail to recognize the human when the external biometric parts have been damaged due to rashes, wounds, and severe burning. Security, robustness, privacy, and non-forgery are the critical aspects of any person authentication system. In such situations, identification based on radiographs of the skull, hand, and teeth are effective replacement methods. In this paper, a novel forensic hand radiograph based human authentication is proposed using a deep neural network. Three-layered convolutional deep neural network architecture is used for the feature extraction of hand radiographs and for recognition; KNN and SVM classifiers are used. As a part of the experimentation, a total of 750 hand radiographs acquired from 150 subjects of different age groups, professions, and gender are considered. The performance of the algorithm is evaluated based on cross-validation accuracy by varying striding pixels, polling window size, kernel size, and the number of filters. Our experiment reveals that hand radiographs contain biometric information that can be used to identify humans in disaster victim identification. The experimental study also indicates that the proposed approach is significantly effective than conventional methods for the person authentication using hand radiographs.

INDEX TERMS Biometrics, identification of persons, image forensics, neural networks, pattern recognition, radiography.

I. INTRODUCTION

Authentication is the process of automatically recognizing the correct person using computational algorithms based on features stored in computer systems. Presently, the biometric identification systems are based on static features like face [1], iris [2], palm print [3], voice [4] and fingerprint impression [5] of the user, which mostly remains unchanged over time. Whereas, dynamic biometric system features of the user may change over a period of time, such as an electrocardiogram-based system [6], keystroke, and touch dynamics [7]. With few techniques available to make any of these identifiers work for recognizable proof, the procedure and results are the same. For any procedure to work, what we need is a record of an individual's trademark kept in a database. After that, when the recognizable proof is required, a recent or on-hand record is compared and contrasted with the record of the database. The performance of a biometric identification system is measured based on accuracy, efficiency, security, and privacy. Biometric systems can be unimodal or multimodal. The unimodal biometric system is less reliable, less secure, and has limited usability, whereas multimodal biometric systems are a combination of multiple sensors, multiple algorithms, and numerous instances, making it more accurate, reliable, secure, and robust [8]. These systems are subjected to impersonation and spoofing attacks, which can be easily replicated, further degrading the quality and reliability of the person recognition system [9]. Many times, the catastrophes like tsunami, earthquake and fatal accidents damage the biometric parts and make it challenging to identify the person. Addressing this problem, forensic radiography plays a very vital role. Forensic radiography is a part of forensic medicine, which is concerned with identifying people using the post-mortem radiological images of different parts of the body including skeleton, skull and teeth [10]. Radiographs acquired before and after death are termed as antemortem (AM) and post-mortem (PM), respectively. Generally, in radiograph based

The associate editor coordinating the review of this manuscript and approving it for publication was Zhan-Li Sun.

This work is licensed under a Creative Commons Attribution 4.0 License. For more information, see https://creativecommons.org/licenses/by/4.0/

www.nmiet.edu.in

human recognition, the PM radiographs are compared with the AM radiographs stored in the database [10]. Dental records have been extensively used in disaster victim identification, such as 9/11 bombing and Asian tsunami [11], [12]. Many authors [13]–[17] successfully demonstrated the uses of dental radiographs for human identification. There are still a number of challenges to overcome like poor image quality, changes in the dentition over time, such as tooth eruption and loss, the emergence, abrasion, falling and replacement of dental restorations [13]–[17]. In such cases, hand radiographs can be considered for authentication purposes as bones cannot be easily damaged due to burning, rashes, and wounding. Human hand anatomy consists of proximal phalanges, middle phalanges, distal phalanges, metacarpals, and carpal bones. The different views for capturing hand radiographic images are the posteroanterior (PA) view, lateral view, oblique view, and anterior-posterior view [18]. This paper presents a novel method for the person authentication based on hand radiographs using a deep learning. Three-layered convolutional deep-learning architecture is used for the feature extraction of radiographs, and the k-nearest neighbor (KNN) and support vector machine (SVM) classifiers are used for the retrieval of subjects for different striding pixel, filter size, polling window and kernel size.

Deep learning has become popular in recent years because of its ability to extract the hidden features of the images. Deep learning algorithms have been successfully applied for detection, recognition, classification, segmentation, and retrieval of image data. Learning is an important step, which is used to get the optimum value of weights of the convolution filter. There are different learning algorithms for deep learning, such as Gradient Descent, Stochastic Gradient Descent, Momentum learning, Levenberg–Marquardt algorithm, and Back-propagation through a time learning algorithm [19]. The problem of variable feature length of the fully connected layer is reduced in R-CNN by using a selective search algorithm. R-CNN takes more substantial time for training, and it is challenging to train the fixed selective search algorithm [20], [21]. Alhussein *et al.* have implemented the transfer learning using two types of the convolutional neural network, namely Deep learning and Shallow learning. The fusion of these two algorithms resulted in 87.96 % accuracy for EEG pathology classification [22]. Zhou *et al.* used faster R-CNN for object detection, which has been used for ImageNet, PascalVoc, and COCO dataset. Faster R-CNN is quicker than R-CNN, as convolution is done only once rather than giving a broader region with convolution per region [23]. Zhao *et al.* [24] used the capsule convolutional neural network for robust and efficient iris recognition. Wang *et al.* [25] presented the rail surface area detection using cascade sampling and dilated convolution. Dilated convolution is used for multi-scale feature learning of rail surfaces with CNN architecture. Cascade sampling is a combination of average pooling, maximum pooling, and convolution to down sample the image. Hassan and Mahmood [26] successfully applied convolutional recurrent deep neural network architecture for the sentence classification. They have used CNN to train word embedding at the initial level and RNN tuning the parameters. A recurrent layer has been used instead of pooling a layer to avoid loss in image information.

In recent years, many researchers [27]–[34] have focused on bone age assessment, rheumatoid arthritis detection, bone segmentation, human identification and osteoporosis detection based on hand radiographs using advanced algorithms like convolutional neural network and deep neural network. El Soufi *et al.* [27] have proposed the system for human identification using hand x-ray images, which consist of segmentation of phalanges, complex Fourier transforms, and KNN classifier for classification. Kauffman *et al.* [28] extracted the 64 shape features per bones from the proximal phalanges, middle phalanges, and metacarpals using an active appearance model (AAM). A principal component analysis method with a likelihood ratio classifier is used for data classification. In our previous approach [29], dual cross pattern (DCP) features along with KNN (N=3 and N=5) and Classification Tree classifier have been successfully applied for human authentication based on hand radiographs. Harmsen *et al.* [30] presented the novel method for bone age assessment employing a support vector machine combined with a cross-correlation prototype. For feature extraction, cross-correlation function features have been extracted for the 14 epiphyseal regions of the hand finger bone images. It resulted in 96.16 % accuracy for the bone age assessment for the age group 1 to 19. Huo *et al.* [31] have proposed the joint space width quantification in radiographic finger bone image for the automatic early detection of rheumatoid arthritis. Bone regions have been segmented using a second-order derivative filter and Hausdorff distance is used for the joint space width measurement. Areeckal *et al* [32] presented the method for diagnosis of osteoporosis with geometric features of the third metacarpal using the watershed segmentation technique for metacarpal segmentation. For the detection of Rheumatoid arthritis (RA) using hand radiographic images, Mihail *et al.* [33] have offered an estimation of the hand skeletal shape using a deep CNN and conditional random fields. Wang *et al.* [34] offered skeletal maturity recognition based on the hand radiographs using a deep neural network for a dataset of 1101 hand and wrist radiographs. It resulted in a recognition accuracy of 92% and 90% for the radius and ulna, respectively. Sánchez *et al.* [35] developed a new human recognition method using benchmark ear and face database. For optimization of modular granular neural networks, a firefly algorithm, grey wolf [36] is suggested. Gupta and Gupta [37] proposed a multi-biometric authentication system using fusion of palm slap fingerprints, palm dorsal vein and hand geometry. This proposed fusion technique resulted into improved results. Afifi [38] proposed gender recognition and biometric identification technique using dorsal and palmar side of 11K human hand images. The experimental results concluded that, dorsal side also consist of effective distinctive feature similar to, if not better than, those available in palmar side. Only few researchers [28], [29], [34]

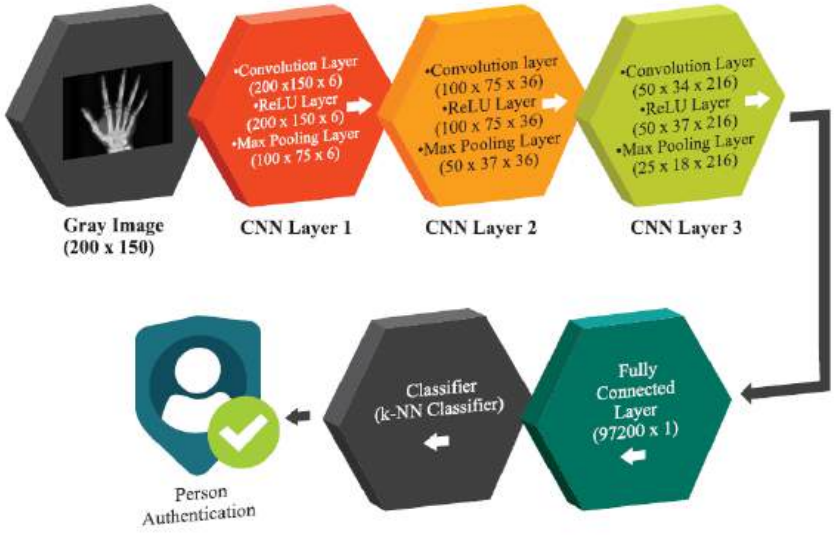

FIGURE 1. The logical module of the proposed method using KNN classifier. It consists of training and testing stage. In training stage, CNN is applied which includes mainly convolution layer, ReLU layer and Max pooling layer.

have focused on person authentication based on the hand radiographs, which can be primarily used in post-mortem identification or recognition of the person [39].

II. MATERIALS AND METHODS

Many authors [32]–[34], [40]–[45] used a dataset of children under the age of 18 for the bone age assessment (BAA) because the segmentation of carpals and phalanges is easy as, after the age of 18, bones are fully grown, and fusion is complete. Hence, it becomes a time-consuming and challenging task to select a particular algorithm or combination of different algorithms. The primary advantage of the proposed study is to win over the segmentation problem experienced by state of the art authors for BAA and identification of victims where traditional biometric techniques cannot be utilized. The deep neural network gives the internal connectivity map of images that retain the spatial and temporal information of the image and is sufficient to discriminate one image from another. The features are extracted by convolving the input images with the filter kernel, providing the interconnectivity between the content of the image, and can be considered as the best features for the image object. The word ''deep'' refers to the number of convolution layers used for the implementation. The flow diagram of the proposed system with three convolution layers is shown in Fig. 1.

A. CONVOLUTION NEURAL NETWORK (CNN)

CNN is inspired by the biological phenomenon of the animal visual cortex, which shows the connectivity pattern between different neurons. While using CNN, slight preprocessing is vital, like enhancement or filtering of an image, which is also essential in traditional handmade feature extraction techniques. CNN has a wide range of applications such as image processing, video processing, speech processing, and natural language processing. CNN consists of four significant steps, such as convolution layer, rectified linear unit (ReLU), maximum pooling layer, and fully connected layer. The architecture of the CNN single layer is shown in Fig. 2.

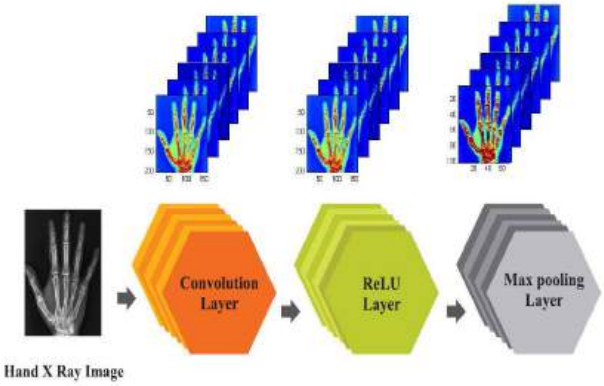

FIGURE 2. Architecture of CNN single layer and output images for selected kernel 3 × 3 × 6 at the first layer.

B. CONVOLUTION LAYER

Convolution layer is used for sharing the parameters and maintaining the sparsity of connections of the different image region. Equation (1) refers to the convolution process which gives the relationship between the input image (I_m) and filter kernel (W). Here, bo indicates bias used to adjust the output according to weighted sum of input neurons.

$$I_{CONV} = I_m * W + bo \tag{1}$$

www.nmiet.edu.in

An original image is first converted into the gray scale image and then convolution is applied. The weights of filter kernels are updated using the back-propagation learning algorithm. The original image is padded with zero to all sides to fit the convolution filter over the image. The size of the original grayscale image is 200 × 150 and filter kernel size is selected as 3 × 3 × 6. After an application of the convolution layer, it generates the output of 200 × 150 × 6. The output of the convolution layer is fed to ReLU layer.

C. ReLU LAYER

In the convolution layer, an image is multiplied by filter kernel, which may have some negative values. These negative values bring the non-linearity in the image. The non-linearity is then removed by using the rectified linear unit layer by converting all the negative values to zero using (2).

$$I_{ReLU} = f(x) = \begin{Bmatrix} I_{conv}(x, y), I_{conv}(x, y) > 0 \\ 0, I_{conv}(x, y) < 0 \end{Bmatrix} \quad (2)$$

where, I_{ReLU} is the ReLU layer image and I_{conv} is the convolutional layer image. The ReLU layer output size is 200 × 150 × 6, which is equal to the size of the convolution layer output. The output of the ReLU layer is given to max pooling layer.

D. MAX POOLING LAYER

Pooling is used for the minimization of the computing cost by reducing the dimension of the ReLU layer output. Pooling is also used to retain the position and rotational invariant features of an image. There are two types of pooling methods: Maximum and Average pooling. In maximum pooling, the maximum value of the given window is selected, while in average pooling, the average value of the window is selected (See Fig. 3). Unlike average pooling, maximum pooling suppresses the noise in the image along with feature reduction. Pooling is also used to maintain the localization of the shape of the local object in the image. The window size of 2 × 2 is selected for maximum pooling, which reduced the size to exactly half of the ReLU layer (100 × 75 × 6). The larger window size for the maximum pooling may result in the fine local information of the image.

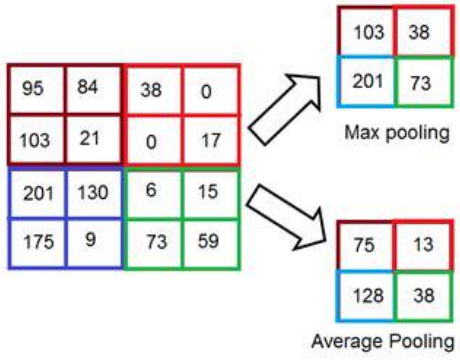

FIGURE 3. Process of maximum and average pooling.

E. FULLY CONNECTED LAYER

In the fully connected layer, the output matrix of a max-pooling layer is converted to a one-dimensional column vector. Most of the classifiers need the input data in one dimension vector. A fully connected layer connects each neuron in one layer to another layer, similar to a multi-layer perceptron.

F. LEARNING

The weights of the filter are adjusted by back propagation learning.

To adjust the weight, mean squared error based loss function is used (3).

$$E = \frac{1}{2} \sum (t\arg et - output)^2 \quad (3)$$

where, *target* is class label and *output* refers to weighted sum of fully connected layer. The main aim of the learning is to minimize the loss function. Equation (4) and (5) are used to update the weights and bias of network.

$$\omega_{ij}(\ell) = \omega_i(\ell) - \eta \frac{\partial \varepsilon}{\partial \omega_{ij}(\ell)} \quad (4)$$

$$\beta_i(\ell) = \beta_i(\ell) - \eta \frac{\partial \varepsilon}{\partial \beta_i(\ell)} \quad (5)$$

Here $\omega_i(\ell)$ and $\beta_i(\ell)$ are initial weight and bias of the network and η is learning rate. The gradients in (4) and (5) are calculated by (6) and (7).

$$\frac{\partial \varepsilon}{\partial \omega_{ij}(\ell)} = a_j(\ell - 1)\Delta_i(\ell) \quad (6)$$

$$\frac{\partial \varepsilon}{\partial \beta_i(\ell)} = \Delta_i(\ell) \quad (7)$$

where,

$$\Delta_i(\ell) = \mathrm{H}'(z_i(\ell)) \sum \omega_{ij}(\ell + 1)\, \Delta_i(\ell + 1) \quad (8)$$

Here $a_j(\ell)$ is activation map of ℓ^{th} neuron and $\mathrm{H}'(z_i(\ell))$ is output map of the hidden layer and $\Delta_i(\ell)$ is error delta.

G. CLASSIFIERS

As the Deep Neural Network (DNN) feature map has enough discriminative power, KNN and one versus all SVM classifiers with linear kernel are used for classification purpose. In general, the classifier is used to find the patterns and classify data mining. KNN is easy to implement and less time-consuming. The value of k is selected as an odd number, as even value of k may cause ambiguity in recognition. KNN is known as a lazy learner, because the training time for this algorithm is zero. During training, features are stored only, and at the time of testing, the nearest point is selected based on feature distance. The standard Euclidean distance (9) is used to calculate the similarity distance.

$$\delta_i = \sqrt{\sum_{i=1}^{n} (test - train)^2} \quad (9)$$

where; δ_i is Euclidean distance, test is a testing feature, train is training samples, and n is the total number of training samples. The larger value of k resulted in crowded neighbors and may give false decision if the number of samples is more. In this study, after experimentation, we preferred the value of k as 3. SVM is widely used for pattern regression and recognition. SVM along with the radial basis function, the kernel can be employed as one classifier. γ and C parameters, which employ a five-fold cross-validation process, are selected. One versus all SVM is used to classify multiple subjects as each subject represents a new class because it has different characteristics. In proposed CNN, fully connected layer converts the multidimensional feature map into one dimensional feature map. Instead of the conventional softmax classifier in CNN we have used SVM classifier with linear kernel which reduces the classification time. The linear kernel is used for the class separating hyper-plane creation. SVM is trained for one against other class features.

H. DATASET COLLECTION

The dataset used in the proposed work consists of a total of 750 right-hand radiographs recorded at different positions for 150 different subjects (5 radiographs per subject) belonging to different age groups, professions, and gender (See Table 1).

TABLE 1. Details of subjects used in dataset collection.

Sr. No.	Age group (years)	No. of Male Subjects	No. of Female Subjects
1	0 to 12 years	15	15
2	13 to 25 years	15	15
3	26 to 40 years	15	15
4	41 to 60 years	15	15
5	60 above	15	15

Although it is challenging to collect a large number of PM radiographs for validation of the proposed system, to evaluate the system on a larger dataset, AM hand radiographs captured from the same subjects at different time and position have been used. Some sample hand radiographs from the dataset are shown in Fig. 4.

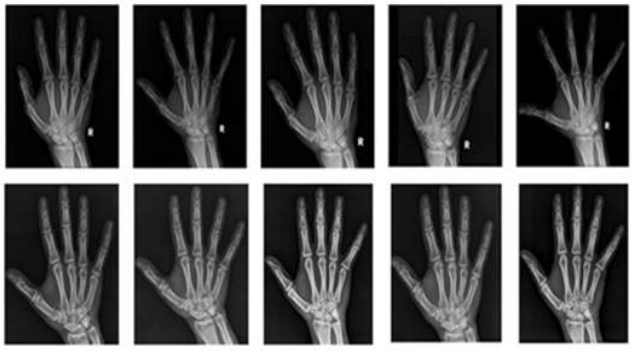

FIGURE 4. Sample images of hand radiographs from the dataset for two different subjects (row-wise).

Keeping the hand position fixed ensures a higher level of accuracy for experimentation purposes but not on a real-time basis. All the radiographs captured from the same subjects have different finger postures and distance between the fingers. Hence, by doing this, an attempt has been made to improve the accuracy level when matching is done on a real-time basis rather than to serve the experiment purpose solely. All radiographs are acquired from Siemens and Vision-C x-ray machine with all the necessary safety precautions and controlled radiation exposure. "All procedures performed in studies involving human participants were in accordance with the ethical standards of the institutional research committee and with the 1964 Helsinki declaration and its later amendments or comparable ethical standards" [46]. Radiographs from different x-ray machines have different dimensions; hence, they have been resized before feature extraction.

III. RESULT & DISCUSSION

The system is implemented using computer vision and image processing toolbox of MATLAB on Windows environment. The performance of the system is evaluated based on percentage cross validation accuracy which is calculated using (10).

$$\%\ \text{Cross Validation Accuracy} = \frac{\text{Correctly Recognized Samples} * 100}{\text{Total Number of samples}} \tag{10}$$

Increasing the number of layers of CNN in the deep learning architecture increases the discrimination power of the feature map, but a large number of layers increase the computation cost. In this study, three layers of CNN are selected, and the feature map size for different layers of deep learning architecture is as shown in Table 2.

TABLE 2. Feature map dimensions of different layers in deep leaning.

Deep Learning Layer	Sub-layer	Feature map size
CNN Layer –I	Convolution Layer	200 × 150
	ReLU Layer	200 × 150×6
	Max Pooling layer	100 × 75 × 6
CNN Layer-II	Convolution Layer	100×75 × 36
	ReLU Layer	100 × 75 × 6
	Max Pooling layer	50 × 37 ×36
CNN Layer-III	Convolution Layer	50 ×37 × 216
	ReLU Layer	50 × 37 × 216
	Max Pooling layer	25 × 18 × 216
Fully Connected Layer		97200 × 1

The output of the first convolution layer after the convolution of the original image of size 200 × 150 (See Fig. 5) with the 3 × 3 × 6 filer kernel resulted in six different feature maps. The output of the ReLU layer of the first CNN has the same dimension as that of a convolution layer output, but the ReLU layer output map has only positive values. All the negative neurons are neglected to remove the non-linearity. The output of the maximum pooling layer is sampled down to exactly half of the original image size, which reduces the dimensions of the feature map.

www.nmiet.edu.in

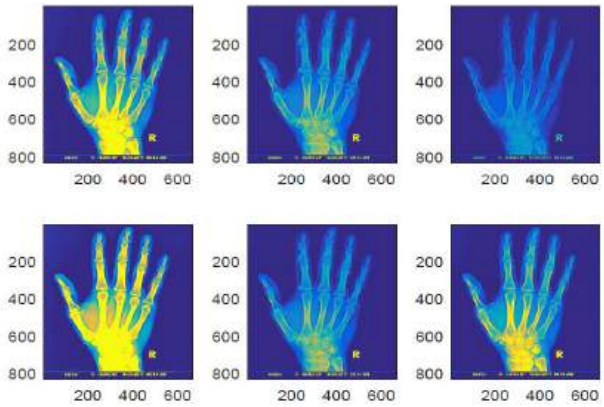

FIGURE 5. Visualization of CNN layer 1.

The output of the first CNN layer is again convolved with the filter kernel of size $3 \times 3 \times 6$, which is given to the ReLU layer for rectification. After the max-pooling of the second layer of CNN, the feature map has the $50 \times 37 \times 36$ dimension. The second layer of CNN generates 36 interconnected maps of the image. Output of CNN layer 2 is given to CNN layer 3, which is further convolved with the learned filter kernel of size $3 \times 3 \times 6$. After rectification, the feature map is given to the max-pooling layer, which further halves subsample for the image maps. The feature map size of the CNN layer three is $25 \times 18 \times 216$. The third layer of CNN generates the 216 interconnected maps of the image (See Fig. 6). As the number of filters increases, the connectivity showing discrimination between the different parts of the image increases. Table 3, 4, 5 and 6, 7, 8 shows cross validation accuracy for KNN and SVM for different striding pixel and different filter size.

It is observed that the six filter kernel gives better accuracy (97.60% for KNN and 99.20% for SVM) better than two (95.60% KNN and 97.60% for SVM) and four (94.40% KNN and 98.80% for SVM) filter size. KNN requires almost zero time for the training but at the classification level the time required is more, also KNN classifier gives poor performance for noisy data. As the time required for multi-layered CNN is more, SVM classifier is applied to minimize the classification time. In SVM, the testing data is compared with the support vectors which minimizes the classification time and gives better performance than KNN classifier.

The large number of the filters increases the size of the convolution layer output, which further results in higher computation cost. Therefore higher values of the number of the filters are neglected. The 3×3 filter window for a convolution gives better spatial and temporal connectivity information of the image and performs better than 2×2 and 5×5. The lower order window and higher-order windows lose the coarse and fine edge information, respectively. Filter window strides over the original image during the convolution process. If the window is stridden by one pixel, then it is the time-consuming task, and for the larger pixel striding, filtering may lose the connectivity between the different regions of an image. Therefore, two-pixel striding is used, which gives better connectivity between the subtle gradients of the image region. For the $N \times N$ pooling region, the image is scaled down by (1/N) times of the original hand radiograph features. For larger scaling, maximum pooling feature maps are losing the internal connectivity of the image. Therefore, the 2×2 pooling region scales the original image features to half of its original size. Also, max-pooling acts as a noise suppressor, unlike an average pooling, which makes it robust for noisy data. Increasing the number of

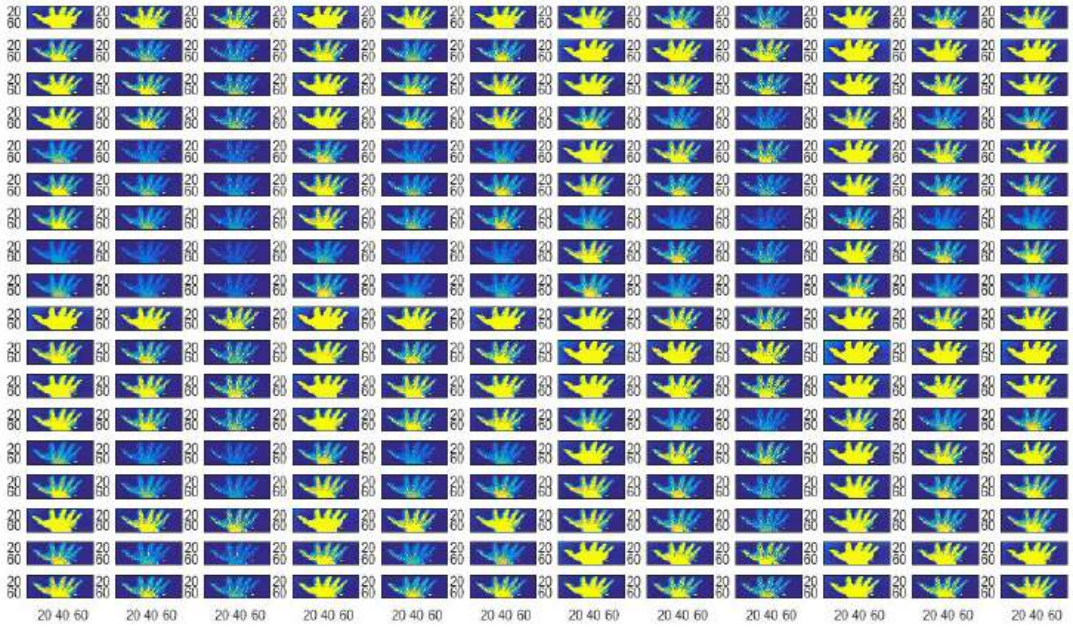

FIGURE 6. 216 interconnected maps for the input hand radiograph image generated by third layer of the CNN.

TABLE 3. Cross validation accuracy for KNN in percentage for striding pixel 1, 2 and 3 at filter size 2.

CNN Layer	Kernel Size 3×3			Kernel Size 4×4			Kernel Size 5×5		
	Pooling Window Size								
	2×2	3×3	5×5	2×2	3×3	5×5	2×2	3×3	5×5
Cross Validation Accuracy for Striding Pixel=1 and Number of Filters=2									
CNN-1	88	86	80	90.80	87.60	82.40	91.60	88.80	82.80
CNN-2	90	88.20	82	92	90	83.20	92.40	90.40	83.40
CNN-3	92.40	89.60	81.60	93.60	92	83.60	94.40	91.60	83.60
CNN-4	84	80	74	84.80	81.60	76	86.40	82.40	76.40
Cross Validation Accuracy for Striding Pixel=2 and Number of Filters=2									
CNN-1	90.80	88.40	82	92	89.60	83.60	93.20	90	84
CNN-2	91.20	89.20	84	93.60	92	84.40	94.40	92.80	85.60
CNN-3	94.40	**95.60**	83.60	91.60	93.20	85.60	94.40	94	86
CNN-4	85.60	82	76	86.80	83.60	77.20	87.20	84	78.40
Cross Validation Accuracy for Striding Pixel=3 and Number of Filters =2									
CNN-1	87.60	85.60	79.60	92.40	87.20	81.20	90.40	87.60	81.60
CNN-2	89.60	88	80.40	91.20	89.20	82	92	90	82
CNN-3	91.60	89	81.20	93.60	90	82.80	93.60	91.20	84
CNN-4	82.40	79.60	73.60	84.40	81.60	75.20	84.40	81.60	75.20

TABLE 4. Cross validation accuracy for KNN in percentage for striding pixel 1, 2 and 3 at filter size 4.

CNN Layer	Kernel Size 3×3			Kernel Size 4×4			Kernel Size 5×5		
	Pooling Window Size								
	2×2	3×3	5×5	2×2	3×3	5×5	2×2	3×3	5×5
Cross Validation Accuracy for Striding Pixel=1 and Number of Filters=4									
CNN-1	88.20	86.80	80.80	91	88	82.80	92	88	82
CNN-2	90	89.6	71.20	92	90	83.20	92.40	90	84
CNN-3	92	**94.40**	82	94	91.60	83.20	90	91..20	84
CNN-4	83.60	80.80	74.80	85.60	82	76	85.20	82	76.40
Cross Validation Accuracy for Striding Pixel=2 and Number of Filters=4									
CNN-1	88	86	80	90	87.60	81.60	92	88.40	84
CNN-2	90	88.20	80.80	91.60	90	82.40	92.80	92	84
CNN-3	92	**94.40**	81.60	93.60	91.20	83.60	89.60	92.80	85.60
CNN-4	83	80	74	84.40	81.60	75.60	85.60	82	76.80
Cross Validation Accuracy for Striding Pixel=3 and Number of Filters =4									
CNN-1	87.60	85.20	78.80	89.60	86.40	80.40	90	87.20	81.60
CNN-2	89.20	87.60	80	90	88.80	81.60	91.20	89.60	82
CNN-3	91.60	88.20	80.40	92	90	82	93.20	90.40	82
CNN-4	82	79.20	72.80	83.20	80.80	74.40	84	81.20	75.20

TABLE 5. Cross validation accuracy for KNN in percentage for striding pixel 1, 2 and 3 at filter size 6.

CNN Layer	Kernel Size 3×3			Kernel Size 4×4			Kernel Size 5×5		
	Pooling Window Size								
	2×2	3×3	5×5	2×2	3×3	5×5	2×2	3×3	5×5
Cross Validation Accuracy for Striding Pixel=1 and Number of Filters=6									
CNN-1	90	88	82	92	89.60	83.20	93.20	90	84
CNN-2	90	88.20	82.40	93.20	90	83.60	93.60	90.80	84
CNN-3	94	91.20	83.60	95.60	92.80	85.20	**96.20**	93.20	85.60
CNN-4	85.20	82	76	86.80	83.60	77.60	87.20	84	78.8
Cross Validation Accuracy for Striding Pixel=2 and Number of Filters=6									
CNN-1	90.80	88	82	93.20	90	84	94	91.20	85.60
CNN-2	91.20	89.20	84	94.00	90.60	84.40	94.4	91.60	85.60
CNN-3	94.80	**97.60**	84	92.40	93.60	85.80	94.40	96.20	86.80
CNN-4	85.60	82	76.80	87.60	84	78.40	88	85	79.60
Cross Validation Accuracy for Striding Pixel=3 and Number of Filters=6									
CNN-1	89	87.20	81.20	91.20	88.20	82.5	92.25	89.20	84
CNN-2	89.60	87.60	81.60	92	89.60	83.20	92.80	89.60	84
CNN-3	93.20	90	82..80	94.80	92	84.40	95.60	92.80	84.40
CNN-4	84	81.60	75.60	85.60	82.80	76.80	86.40	84	77.60

convolution layers in deep learning architecture increases the connectivity of neurons in the architecture and makes it more discriminative.

The experimental result reveals that the proposed technique can be used for the identification of victims where the traditional biometric approach cannot be utilized. Hand

www.nmiet.edu.in

TABLE 6. Cross validation accuracy for SVM in percentage for striding pixel 1, 2 and 3 at filter size 2.

CNN Layer	Kernel Size 3×3			Kernel Size 4×4			Kernel Size 5×5		
	Pooling Window Size								
	2×2	3×3	5×5	2×2	3×3	5×5	2×2	3×3	5×5
Cross Validation Accuracy for Striding Pixel=1 and Number of Filters=2									
CNN-1	89.6	87.6	81.6	92.0	89.2	84.0	93..20	90.40	84.20
CNN-2	91.6	89.60	85.2	93.6	92.4	84.80	93.60	91.60	84.40
CNN-3	94.40	91.20	83.60	94.40	92.80	85.20	95.60	93.20	85.20
CNN-4	85.20	81.6	76.4	86.40	82.40	77.6	87.20	82.80	77.60
Cross Validation Accuracy for Striding Pixel=2 and Number of Filters=2									
CNN-1	93.60	91.20	83.60	93.60	91.60	85.20	94.80	91.6	85.6
CNN-2	94.40	90.40	85.6	94.80	93.6	86.40	95.60	94.40	86.80
CNN-3	96.40	**97.60**	85.20	96.80	95.60	87.20	96.40	95.6	87.6
CNN-4	87.20	83.6	78	89.60	84.80	79.20	89.60	85.6	80
Cross Validation Accuracy for Striding Pixel=3 and Number of Filters=2									
CNN-1	89.20	87.20	82.40	94.40	89.20	83.20	92.80	89.60	83.60
CNN-2	91.60	89.60	83.20	93.20	92.40	83.2	93.60	92.40	86.40
CNN-3	93.20	91.20	84.40	94.40	91.60	84.80	95.60	93.20	86
CNN-4	84.40	81.60	76.80	85.60	83.20	77.20	86.40	83.60	77.20

TABLE 7. Cross validation accuracy for SVM in percentage for striding pixel 1, 2 and 3 at filter size 4.

CNN Layer	Kernel Size 3×3			Kernel Size 4×4			Kernel Size 5×5		
	Pooling Window Size								
	2×2	3×3	5×5	2×2	3×3	5×5	2×2	3×3	5×5
Cross Validation Accuracy for Striding Pixel=1 and Number of Filters=4									
CNN-1	90.40	88.40	82.80	93.20	89.20	83.20	93.20	90.80	84.40
CNN-2	91.60	90.4	73.20	94.40	92.40	85.20	93.60	92	86.40
CNN-3	93.60	96..40	83.20	95.20	93.60	85.20	91.60	93.20	87.60
CNN-4	85.20	83.20	78.0	88.40	83.60	78	88.40	84	78.40
Cross Validation Accuracy for Striding Pixel=2 and Number of Filters=4									
CNN-1	91.60	88	83.60	92.40	89.60	83.60	94	90.40	86
CNN-2	92.80	91.20	84.40	93.60	92.40	84.40	94.40	93.20	86.80
CNN-3	97.20	**98.80**	85.60	94.80	93.60	85.60	92.40	93.60	87.60
CNN-4	84.80	81.6	75.6	87.20	83.60	77.60	87.20	84.4	77.20
Cross Validation Accuracy for Striding Pixel=3 and Number of Filters=4									
CNN-1	89.20	87.20	80.80	91.20	88.80	82.40	92.40	89.60	83.60
CNN-2	91.20	89.20	83.60	92.80	90.40	83.20	93.20	91.60	84.40
CNN-3	93.60	90.40	84.40	94.40	91.20	83.60	94.80	92.40	83.60
CNN-4	83.60	81.20	74.80	85.20	81.60	78.40	85.60	83..60	78.40

TABLE 8. Cross validation accuracy for SVM in percentage for striding pixel 1, 2 and 3 at filter size 6.

CNN Layer	Kernel Size 3×3			Kernel Size 4×4			Kernel Size 5×5		
	Pooling Window Size								
	2×2	3×3	5×5	2×2	3×3	5×5	2×2	3×3	5×5
Cross Validation Accuracy for Striding Pixel=1 and Number of Filters=6									
CNN-1	91.60	89.6	84	93.6	92	85.20	94.80	93.2	86
CNN-2	92.80	90.80	84.80	95.20	92.80	86.80	95.60	92.80	87.60
CNN-3	96.40	93.20	85.60	97.20	94.40	87.20	98.00	95.20	88.80
CNN-4	86.40	84.80	78.40	89.20	85.60	79.60	89.20	86.40	81.60
Cross Validation Accuracy for Striding Pixel=2 and Number of Filters=6									
CNN-1	92.40	89.60	83.60	95.20	92.40	86.80	95.20	93.20	87.60
CNN-2	94.40	91.20	86.80	96..00	92.80	87.60	95.60	93.20	88..00
CNN-3	98.40	**99.20**	88.40	97..60	94.80	88.80	97..60	97.20	89.20
CNN-4	87..60	84.40	79.60	89.60	86.4	80.80	90.40	88.80	83.60
Cross Validation Accuracy for Striding Pixel=3 and Number of Filters=6									
CNN-1	91.60	90.40	83.20	94.40	90..80	84.80	94.40	91.20	86.40
CNN-2	92.40	89.60	84.80	95.20	91.20	85.20	95.20	92.00	87.20
CNN-3	95.20	92.40	86..80	96.40	93.60	87.60	97..20	94.80	88.40
CNN-4	86.	83.60	79.60	87.60	86.40	78.80	89.60	86.80	79.60

radiographs are non-replicable, and non-spoofing makes the proposed system more robust and reliable [9]. The accuracy of a deep learning system increases with the increase in the number of layers (from CNN-1 to CNN-3), and if computation time increases, the algorithm becomes slower and unreliable for real-time applications. It is observed that

after CNN-3 layer, a further increase in the number of the layer (CNN-4) decreases the retrieval accuracy.

There is no public hand radiograph dataset for the comparison of the proposed human identification system, so it is difficult to make a rational comparison. The main aim of the state of art papers is to predict the bone age in the range of 0–18 years [28], [32], [40]–[45] because the bones are entirely matured, and fusion is complete after the age of 18 years. In most of the state of art papers, assessment is done successfully; however, these methods are not suitable for the identification of adult victims. Kauffman *et al.* [28] presented an automated radiographic assessment of hand in Rheumatoid Arthritis (RA). The method is tested on 100 plain left and right hand radiographs of 40 different patients for joint space width segmentation using Active Appearance Model (AAM). In our previous work [29], we have performed human identification based on dual cross pattern (DCP) of hand radiographs. The dataset consists of 100 right hand radiographs of adults with age group of 18 year to 42 year. The average classification accuracy of 89.1% was achieved. The method of [32] is tested on 157 left hand x-ray images collected from Image Processing and Informatics Lab, University of Southern California with age group 17-18 years for automatic segmentation of third metacarpal bone for diagnosis of osteoporosis. The accuracy achieved is 94.9%. Wang *et al.* [34] proposed CNN based technique for Radius and Ulna bone classification. The classification accuracy of 92% and 90% for 400 radius images and 600 ulna images is achieved. The method of [40] is tested on for 120 images of children's below 18 years. The accuracy of 90% with the discrepancy of 2-year error rate between PROI & CROI was achieved. Pietka *et al.* [41] proposed bone age assessment method based on Epiphyseal/Metaphyseal region of interest (ROI) extraction. The feature extraction accuracy achieved is of 91%, 83%, and 75% for distal, middle and proximal ROI respectively from 200 left-hand images below the age of 14. Simu *et al.* [42] proposed method for the segmentation of radius and ulna bones from hand radiographs is tested on 19 images (1 for each age group from 0 to 18 year) collected from Children's Hospital Los Angeles, USA. The method proposed by Yuh *et al.* [43] for later stage bone age assessment using Wavelet transform, Singular Value Decomposition (SVD) and SVM is evaluated on 21 hand radiographs from 7 years old to 12 years old with average the accuracy of 92.41%. Niemeijer *et al.* [44] developed a technique for skeletal maturity estimation of children using Tanner Whitehouse method with error rate not more than one stage for 71 cases. Pathak *et al.* [45] presented an automatic skeletal maturity identification technique using hierarchical three stages of syntactic recognition for the structural development of 128 × 145 dimension radiographs of 10-12 year boy.

To compare our method, we implemented human identification system based on established networks. Table 9 shows a comparison of the average accuracy of the proposed method with the traditional deep learning architectures such as AlexNet, ResNet, VGGNet and InceptionNet. Because of minimization of non-linearity and increased number of filter maps, proposed method outperforms the existing architectures for the captured hand radiograph database.

TABLE 9. Comparison of average accuracy obtained by proposed method and established networks.

Deep Learning Architecture	Cross Validation Accuracy
AlexNet	91.60%
ResNet	92.80%
VGG Net	93.20%
Inception Net	94.00%
Proposed Method (Using KNN)	97.60%
Proposed Method (Using SVM)	99.20%

Proposed method includes many steps (Fig. 1) and the running time depend upon number of parameters like number of layers, kernel size, window size, samples size, striding pixel. Hence it is not trivial to give running time to every step. In this paper, instead of conventional soft-max classifier in CNN, we have used SVM classifier with linear kernel which minimizes the classification time.

Table 10 shows that increasing the number of training samples increases number of support vectors for SVM classifier, thus increases the cross validation accuracy. During complete experimentation, testing images were not the part of training images.

TABLE 10. Maximum (%) Cross validation accuracy achieved by KNN and SVM for the different training samples.

Training Data	Testing Data	Cross Validation Accuracy	
		KNN	SVM
30 % (225 Samples)	70 % (525 Samples)	89.60	91.60
40 % (300 Samples)	60 % (450 Samples)	91.20	93.60
50 % (375 Samples)	50 % (375 Samples)	93.60	94.40
60 % (450 Samples)	40 % (300 Samples)	95.20	97.20
66 % (500 Samples)	**34 % (250 Samples)**	**97.60**	**99.20**

IV. CONCLUSION

A novel human identification method using a deep neural network for matching hand radiographs is presented in this paper. The initial results on a primary dataset indicated that hand radiographs are an appropriate approach for human identification. Three layers of the convolutional neural network are used to get deeper connectivity of the image and to construct deep learning architecture. For classification, the KNN and SVM classifier are used. Extensive experiments are performed on 750 right hand radiographs acquired from 150 subjects. The performance of the algorithm is deliberated based on percentage cross-validation accuracy shows that the DNN with 3 layers, 3 × 3 filter kernels and 3 × 3 polling window resulted in 97.60% and 99.20% cross-validation accuracy for KNN and SVM respectively. Experimental results show that proposed method outperforms the existing architectures for the captured hand radiograph database. The experimental results also show that the proposed technique can be used as a substitute for a

www.nmiet.edu.in

dental-radiograph-based identification system in disaster victim identification. As compared to the conventional biometric identification, hand radiograph-based recognition is challenging as hand bones change over time, due to fracture and hard work. Several hurdles were faced during the retrieval of hand images from the database, such as pose, lighting, and variations related to the profession. It is observed that hard-working people have more variations in their bone texture. Experimental results also reveal that, the variability in hand positioning and image capturing setup can create nonconformity in the overall performance of the system, due to finger postures and the distance between the fingers while capturing radiographs. It is recommended to develop a method to standardize the way in which hand is positioned during radiographic acquisition. In future, a unified system based on hand radiographs can be designed to improve pose correction by combining quality-based frame selection and mark-based matching techniques. Different digital x-ray machines have different resolution but generally display a high contrast image due to various digital filtering techniques. How this affect the overall performance of the proposed system is not clear. In addition, the algorithm is sensitive to the number of training samples. To investigate this, it is important to acquire a larger set of new data over a period of several years from different x-ray machines with different age groups.

REFERENCES

[1] X. Qu, T. Wei, C. Peng, and P. Du, "A fast face recognition system based on deep learning," in *Proc. 11th Int. Symp. Comput. Intell. Design (ISCID)*, Hangzhou, China, Dec. 2018, pp. 289–292.
[2] J. Lin, J.-P. Li, H. Lin, and J. Ming, "Robust person identification with face and iris by modified PUM method," in *Proc. Int. Conf. Apperceiving Comput. Intell. Anal.*, Chengdu, China, Oct. 2009, pp. 321–324.
[3] I. Awate and B. A. Dixit, "Palm print based person identification," in *Proc. Int. Conf. Comput. Commun. Control Autom.*, Pune, India, Feb. 2015, pp. 781–785.
[4] R. G. M. M. Jayamaha, M. R. R. Senadheera, T. N. C. Gamage, K. D. P. B. Weerasekara, G. A. Dissanayaka, and G. N. Kodagoda, "VoizLock–human voice authentication system using hidden Markov model," in *Proc. 4th Int. Conf. Inf. Autom. Sustainability*, Colombo, Sri Lanka, Dec. 2008, pp. 330–335.
[5] X.-G. Huang, L. Shen, and Y.-H. Feng, "A user authentication scheme based on fingerprint and USIM card," in *Proc. Int. Conf. Intell. Inf. Hiding Multimedia Signal Process.*, Harbin, China, Aug. 2008, pp. 1261–1264.
[6] S. Keshishzadeh and S. Rashidi, "Single lead electrocardiogram feature extraction for the human verification," in *Proc. 5th Int. Conf. Comput. Knowl. Eng. (ICCKE)*, Mashhad, Iran, Oct. 2015, pp. 118–122.
[7] H. Saevanee and P. Bhattarakosol, "Authenticating user using keystroke dynamics and finger pressure," in *Proc. 6th IEEE Consum. Commun. Netw. Conf.*, Las Vegas, NV, USA, Jan. 2009, pp. 1–2.
[8] S. Shunmugam and R. K. Selvakumar, "Electronic transaction authentication—A survey on multimodal biometrics," in *Proc. IEEE Int. Conf. Comput. Intell. Comput. Res.*, Coimbatore, India, Dec. 2014, pp. 1–4.
[9] Z. Rui and Z. Yan, "A survey on biometric authentication: Toward secure and privacy-preserving identification," *IEEE Access*, vol. 7, pp. 5994–6009, 2019.
[10] Y. Kabbara, A. Shahin, A. Nait-Ali, and M. Khalil, "An automatic algorithm for human identification using hand X-ray images," in *Proc. 2nd Int. Conf. Adv. Biomed. Eng.*, Sep. 2013, pp. 167–170.
[11] P. O'Shaughnessy, "More than half of victims IDD," New York Daily News, New York, NY, USA, Sep. 2002. [Online]. Available: http://911research.wtc7.net/cache/planes/evidence/dailynews_halfvictimsidd.html
[12] P. Thepgumpanat. (Jan. 18, 2005). Thai Tsunami forensic centre produce first IDs. Reuters. [Online]. Available: http://www.alertnet.org/
[13] H. Chen and A. K. Jain, "Dental biometrics: Alignment and matching of dental radiographs," *IEEE Trans. Pattern Anal. Mach. Intell.*, vol. 27, no. 8, pp. 1319–1326, Aug. 2005.
[14] A. Heinrich, F. V. Güttler, S. Schenkl, R. Wagner, and U. K.-M. Teichgräber, "Automatic human identification based on dental X-ray radiographs using computer vision," *Sci. Rep.*, vol. 10, no. 1, Mar. 2020, Art. no. 3801.
[15] O. Nomir and M. Abdel-Mottaleb, "Fusion of matching algorithms for human identification using dental X-ray radiographs," *IEEE Trans. Inf. Forensics Security*, vol. 3, no. 2, pp. 223–233, Jun. 2008.
[16] A. B. Oktay, "Human identification with dental panoramic radiographic images," *IET Biometrics*, vol. 7, no. 4, pp. 349–355, Jul. 2018.
[17] G. Silva, L. Oliveira, and M. Pithon, "Automatic segmenting teeth in X-ray images: Trends, a novel data set, benchmarking and future perspectives," *Expert Syst. Appl.*, vol. 107, pp. 15–31, Oct. 2018.
[18] A. K. Bhat, B. Kumar, and A. Acharya, "Radiographic imaging of the wrist," *Indian J. Plastic Surg.*, vol. 44, no. 2 pp. 186–196, May 2011, doi: 10.4103/0970-0358.85339.
[19] A. Shrestha and A. Mahmood, "Review of deep learning algorithms and architectures," *IEEE Access*, vol. 7, pp. 53040–53065, Apr. 2019.
[20] J. Zhang, S. Yuasa, S. Fukuma, and S.-I. Mori, "A real-time GPU-based coupled fluid-structure simulation with haptic interaction," in *Proc. IEEE/ACIS 15th Int. Conf. Comput. Inf. Sci. (ICIS)*, Jun. 2016, pp. 1–6.
[21] C. Yin, Y. Zhu, J. Fei, and X. He, "A deep learning approach for intrusion detection using recurrent neural networks," *IEEE Access*, vol. 5, pp. 21954–21961, Oct. 2017.
[22] M. Alhussein, G. Muhammad, and M. S. Hossain, "EEG pathology detection based on deep learning," *IEEE Access*, vol. 7, pp. 27781–27788, Feb. 2019.
[23] X. Zhou, W. Gong, W. Fu, and F. Du, "Application of deep learning in object detection," in *Proc. IEEE/ACIS 16th Int. Conf. Comput. Inf. Sci. (ICIS)*, Wuhan, China, May 2017, pp. 631–634.
[24] T. Zhao, Y. Liu, G. Huo, and X. Zhu, "A deep learning iris recognition method based on capsule network architecture," *IEEE Access*, vol. 7, pp. 49691–49701, Apr. 2019.
[25] Z. Wang, X. Wu, G. Yu, and M. Li, "Efficient rail area detection using convolutional neural network," *IEEE Access*, vol. 6, pp. 77656–77664, Nov. 2018.
[26] A. Hassan and A. Mahmood, "Convolutional recurrent deep learning model for sentence classification," *IEEE Access*, vol. 6, pp. 13949–13957, Mar. 2018.
[27] K. El Soufi, Y. Kabbara, A. Shahin, M. Khalil, and A. Nait-Ali, "CIMOR: An automatic segmentation to extract bone tissue in hand X-ray images," in *Proc. 2nd Int. Conf. Adv. Biomed. Eng.*, Tripoli, Lebanon, Sep. 2013, pp. 171–174.
[28] J. A. Kauffman, C. H. Slump, and H. J. B. Moens, "Matching hand radiographs," in *Proc. Overview Workshops ProRISC-SAFE*, Veldhoven, The Netherlands, Nov. 2005, pp. 629–633.
[29] S. V. Joshi and R. D. Kanphade, "Forensic approach of human identification using dual cross pattern of hand radiographs," in *Proc. Int. Conf. Intell. Syst. Design Appl.*, Vellore, India, 2018, pp. 1075–1084.
[30] M. Harmsen, B. Fischer, H. Schramm, T. Seidl, and T. M. Deserno, "Support vector machine classification based on correlation prototypes applied to bone age assessment," *IEEE J. Biomed. Health Informat.*, vol. 17, no. 1, pp. 190–197, Jan. 2013.
[31] Y. Huo, K. L. Vincken, D. van der Heijde, M. J. H. De Hair, F. P. Lafeber, and M. A. Viergever, "Automatic quantification of radiographic finger joint space width of patients with early rheumatoid arthritis," *IEEE Trans. Biomed. Eng.*, vol. 63, no. 10, pp. 2177–2186, Oct. 2016.
[32] A. S. Areeckal, S. S. David, M. Kocher, N. Jayasheelan, and J. Kamath, "Fully automated radiogrammetric measurement of third metacarpal bone from hand radiograph," in *Proc. Int. Conf. Signal Process. Commun. (SPCOM)*, Bengaluru, India, Jun. 2016, pp. 1–5.
[33] R. P. Mihail, G. Liang, and N. Jacobs, "Automatic hand skeletal shape estimation from radiographs," *IEEE Trans. Nanobiosci.*, vol. 18, no. 3, pp. 296–305, Jul. 2019.
[34] S. Wang, Y. Shen, C. Shi, P. Yin, Z. Wang, P. W.-H. Cheung, J. P. Y. Cheung, K. D.-K. Luk, and Y. Hu, "Skeletal maturity recognition using a fully automated system with convolutional neural networks," *IEEE Access*, vol. 6, pp. 29979–29993, Jun. 2018.

www.nmiet.edu.in

[35] D. Sánchez, P. Melin, and O. Castillo, "Optimization of modular granular neural networks using a firefly algorithm for human recognition," *Eng. Appl. Artif. Intell.*, vol. 64, pp. 172–186, Sep. 2017.
[36] D. Sánchez, P. Melin, and O. Castillo, "A grey wolf optimizer for modular granular neural networks for human recognition," *Comput. Intell. Neurosci.*, vol. 2017, pp. 1–26, Aug. 2017.
[37] P. Gupta and P. Gupta, "Multibiometric authentication system using slap fingerprints, palm dorsal vein, and hand geometry," *IEEE Trans. Ind. Electron.*, vol. 65, no. 12, pp. 9777–9784, Dec. 2018.
[38] M. Afifi, "11K hands: Gender recognition and biometric identification using a large dataset of hand images," *Multimedia Tools Appl.*, vol. 78, no. 15, pp. 20835–20854, Mar. 2019.
[39] M. G. Koot, N. J. Sauer, and T. W. Fenton, "Radiographic human identification using bones of the hand: A validation study," *J. Forensic Sci.*, vol. 50, no. 2, pp. 1–6, 2005.
[40] E. Pietka, "Computer-assisted bone age assessment based on features automatically extracted from a hand radiograph," *Computerized Med. Imag. Graph.*, vol. 19, no. 3, pp. 251–259, May 1995.
[41] E. Pietka, A. Gertych, S. Pospiech, F. Cao, H. K. Huang, and V. Gilsanz, "Computer-assisted bone age assessment: Image preprocessing and epiphyseal/metaphyseal ROI extraction," *IEEE Trans. Med. Imag.*, vol. 20, no. 8, pp. 715–729, Aug. 2001.
[42] S. Simu, S. Lal, P. Nagarsekar, and A. Naik, "Fully automatic ROI extraction and edge-based segmentation of radius and ulna bones from hand radiographs," *Biocybernetics Biomed. Eng.*, vol. 37, no. 4, pp. 718–732, Jan. 2017.
[43] Y.-S. Yuh, C.-C. Liu, J.-D. Chang, and S.-S. Yu, "Later stage bone age assessment on hand radiographs," in *Proc. 7th IEEE Conf. Ind. Electron. Appl. (ICIEA)*, Singapore, Jul. 2012, pp. 1329–1332.
[44] M. Niemeijer, B. van Ginneken, C. A. Maas, F. J. Beek, and M. A. Viergever, "Assessing the skeletal age from a hand radiograph: Automating the Tanner-Whitehouse method," *Proc. SPIE*, vol. 5032, May 2003, pp. 1197–1205.
[45] A. Pathak, S. K. Pal, and R. A. King, "Syntactic recognition of skeletal maturity," *Pattern Recognit. Lett.*, vol. 2, no. 3, pp. 193–197, Mar. 1984.
[46] World Medical Association, "World medical association declaration of Helsinki: Ethical principles for medical research involving," *JAMA*, vol. 310, no. 20, pp. 2191–2194, Nov. 2013, doi: 10.1001/jama.2013.281053.

SAGAR V. JOSHI received the B.E. degree in electronics and telecommunication engineering and the M.E. degree in digital electronics from Sant Gadge Baba (SGB) Amravati University, Amravati, India, in 2008 and 2011, respectively. He is currently pursuing the Ph.D. degree with the Department of Electronics and Telecommunication Engineering, Dr. D. Y. Patil Institute of Technology, Pune, affiliated to Savitribai Phule Pune University, Pune, India.

He has published nine research articles in international and national journals and conferences. His research interests include digital image processing, biomedical engineering, artificial intelligence, and computer networks. He holds one copyright. He is the first University Topper of Summer 2011 Examination in M.E. (Digital Electronics) conducted by SGB Amravati University.

RAJENDRA D. KANPHADE (Member, IEEE) received the B.E. degree in electronics from Sant Gadge Baba (SGB) Amravati University, Amravati, India, in 1987, the M.E. degree in electronics from Dr. Babasaheb Ambedkar Marathwada University, Aurangabad, India, in 1993, and the Ph.D. degree electronics engineering from SGB Amravati University, Amravati, in 2008.

He has over 32 years of experience in the field of technical education. He is currently working as a Principal with the Jayawantrao Sawant College of Engineering, Pune, India. His areas of research are VLSI and embedded system design, analog and mixed signal design, and digital image processing. He has developed A Center of Excellence in the area "VLSI Design Technology" (a facility for Ph.D. / PG students) equipped with CADENCE design tools in association with Cadence, USA, and IIT Faculty, in 2004. He is on the panel of examiners for under graduate, post graduate, and Ph.D. examinations and also approved Ph.D. guide of Savitribai Phule Pune University, BAMU Aurangabad, NMIMS Deemed University Mumbai, SGB Amravati University, and RTM Nagpur University. Six Ph.D. students have completed and five students are completing their Ph.D. degree under his guidance. He has published 89 research articles in international and national journals and conferences.

Dr. Kanphade was the Chairman Board of Studies of E&TC, Industrial Electronics, Instrumentation and Applied Electronics Engineering of Sant Gadge Baba Amravati University, from 2002 to 2007.

www.nmiet.edu.in

Forensic Approach of Human Identification Using Dual Cross Pattern of Hand Radiographs

| Conference paper | First Online: 14 April 2019

| pp 1075–1084 | Cite this conference paper

Intelligent Systems Design and Applications

(ISDA 2018 2018)

Sagar V. Joshi & Rajendra D. Kanphade

Part of the book series: Advances in Intelligent Systems and Computing ((AISC,volume 941))

Included in the following conference series:
International Conference on Intelligent Systems Design and Applications

1121 Accesses

Abstract

www.nmiet.edu.in

The demand for personal identification systems has augmented in recent years, due to serious accidents and required for criminal investigation. Under natural calamity and human-made disasters sometimes it is impossible to use traditional biometric techniques based on fingerprints, iris, and face; in such cases, biometric radiographs like dental, hand and skull are the great alternatives for the victim's identification. The key objective of this study is to present a unique technique to deal with missing and unidentified person identification based on hand radiographs using Dual Cross Pattern (DCP). The proposed system has two main stages: feature vector extraction, and classification. In this paper, an attempt has been made to find out the most suitable classifier among k-nearest neighbor (k-NN) and Classification Tree based on the accuracy of retrieval of 10 subjects with 100 right-hand radiographs. The result achieved from experiments on a small primary database of radiographs reveals that matching hand radiographs based on DCP can be significantly used for human identification.

This is a preview of subscription content, log in via an institution to check access.

Access this chapter

Log in via an institution

Chapter

EUR 29.95
Price includes VAT (India)

Available as PDF
Read on any device
Instant download
Own it forever

Buy Chapter →

www.nmiet.edu.in

eBook EUR 160.49

Softcover Book EUR 199.99

Tax calculation will be finalised at checkout

Purchases are for personal use only

Institutional subscriptions →

Similar content being viewed by others

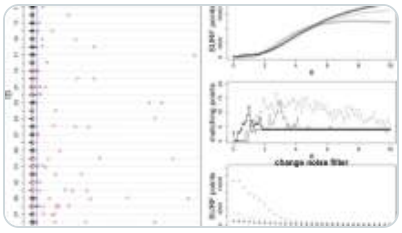

Automatic human identification based on dental X-ray radiographs using...

Article | Open access
02 March 2020

Use of Computed Tomography and Radiography Imaging in Person Identification

Chapter | © 2018

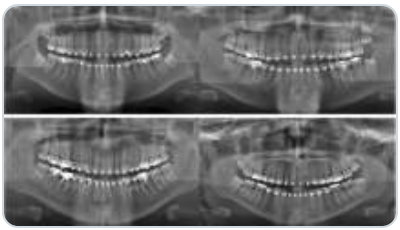

Statistical elimination based approach to jaw and tooth separation on panoramic radiograph...

Article | 02 March 2023

References

1. Manigandan, T., Sumathy, C., Elumalai, M., Sathasivasubramanian, S., Kannan, A.: Forensic radiology in dentistry. J. Pharm. Bioallied Sci. **7**(Suppl. 1), S260–S264 (2015)

Google Scholar

www.nmichen.edu

2. Chen, H., Jain, A.K.: Dental biometrics: alignment and matching of dental radiographs. IEEE Trans. Pattern Anal. Mach. Intell. **27**(8), 1319–1326 (2005)

Article Google Scholar

3. Forensic identification of 9/11 victims ends, New York, 23 February 2005

Google Scholar

4. Ross, A.A., Nandakumar, K., Jain, A.K.: Handbook of Biometrics. Springer, Heidelberg (2011)

Google Scholar

5. Nomir, O., Abdel-Mottaleb, M.: Hierarchical contour matching for dental X-ray radiographs. Pattern Recognit. **41**(1), 130–138 (2008)

Article Google Scholar

6. Abaza, A., Ross, A., Ammar, H.: Retrieving dental radiographs for post-mortem identification. In: 16th IEEE International Conference on Image Processing (ICIP), pp. 2537–2540 (2009)

Google Scholar

7. Senn, D.R., Stimson, P.G.: Forensic Dentistry, 2nd edn. Taylor & Francis, Boca Raton (2010)

Book Google Scholar

8. Jayaprakash, P.T., Srinivasan, G.J., Amravaneswaran, M.G.: Cranio-facial morph-analysis: a new method for enhancing reliability while identifying skulls by photo

www.nsnet.edu.in superimposition. Forensic Sci. Int. **117**(1–2), 121–143 (2001)

Article Google Scholar

9. Pushparani, C., Ravichandran, C.P., Sivakumari, K.: Radiography superimposition in personal identification - a case study involving surgical implants. J. Forensic Res. **3**, 140 (2012)

Article Google Scholar

10. Al-Amad, S., McCullough, M., Graham, J., Clement, J., Hill, A.: Craniofacial identification by computer-mediated superimposition. J. Forensic Odonto-Stomatol. **24**(2), 47–52 (2006)

Google Scholar

11. Nomir, O., Abdel-Mottaleb, M.: A system for human identification from X-ray dental radiographs. Pattern Recognit. **38**(8), 1295–1305 (2005)

Article Google Scholar

12. Pathak, A., Pal, S.K., King, R.A.: Syntactic recognition of skeletal maturity. Pattern Recognit. Lett. **2**(3), 193–197 (1984)

Article Google Scholar

13. Pathak, A., Pal, S.K.: Fuzzy grammars in syntactic recognition of skeletal maturity from X-rays. IEEE Trans. Syst. Man Cybern. **16**(5), 657–667 (1986)

Article Google Scholar

14. Pietka, E.: Computer-assisted bone age assessment based on features automatically extracted from a hand radiograph. Comput. Med. Imaging Graph. **19**(3), 251–259 (1995)

Article Google Scholar

15. Pietka, E., McNitt-Gray, M.F., Kuo, M.L., Huang, H.K.: Computer-assisted phalangeal analysis in skeletal age assessment. IEEE Trans. Med. Imaging **10**(4), 616–620 (1991)

Article Google Scholar

16. Pietka, E., Kaabi, L., Kuo, M.L., Huang, H.K.: Feature extraction in carpal-bone analysis. IEEE Trans. Med. Imaging **12**(1), 44–49 (1993)

Article Google Scholar

17. Kauffman, J.A., Slump, C.H., Moens, H.B.: Matching hand radiographs. In: Overview of the workshops ProRISC-SAFE, 17–18 November, Veldhoven, The Netherlands, pp. 629-633(2005)

Google Scholar

18. Lin, P., Zheng, C., Zhang, F., Yang, Y.: X-ray carpal-bone image boundary feature analysis using region statistical feature based level set method for skeletal age assessment application. Opt. Appl. **2**, 283–294 (2005)

Google Scholar

19. Martin-Fernandez, M.A., Martin-Fernandez, M., Alberola-Lopez, C.: Automatic bone age assessment: a registration approach. In: Proceedings on Medical Imaging, SPIE, vol. 5032, pp. 1765–76, San Diego, CA (2003)

www.nmiet.edu.in Google Scholar

20. Aja-Fernandez, S., de Luis-Garcıa, R., Martın-Fernandez, M.A., Alberola-Lopez, C.: A computational TW3 classifier for skeletal maturity assessment. A computing with words approach. J. Biomed. Inform. **37**(2), 99–107 (2004)

Article Google Scholar

21. Davis, L.M., Theobald, B.J., Lines, J., Toms, A., Bagnall, A.: On the segmentation and classification of hand radiographs. Int. J. Neural Syst. **22**, 1250020 (2012)

Article Google Scholar

22. Hue, T.T.M., Kim, J.Y., Fahriddin, M.: Hand bone radiograph image segmentation with ROI merging. Recent Researches in Mathematical Methods in Electrical Engineering and Computer Science, pp. 147–154 (2011)

Google Scholar

23. Mahmoodi, S., Sharif, B.S., Chester, E.G., Owen, J.P., Lee, R.: Skeletal growth estimation using radiographic image processing and analysis. IEEE Trans. Inf Technol. Biomed. **4**(4), 292–297 (2000)

Article Google Scholar

24. Hsieh, C.W., Jong, T.L., Tiu, C.M.: Bone age estimation based on phalanx information with fuzzy constrain of carpals. Med. Biol. Eng. Comput. **45**(3), 283–295 (2007)

Article Google Scholar

25. Mansourvar, M., Raj, R.G., Ismail, M.A., Kareem, S.A., Shanmugam, S., Wahid, S., et al.: Automated web based system for bone age assessment using histogram technique.

www.nmlabs.in. Malays. J. Comput. Sci. 25(3), 107–121 (2012)

Google Scholar

26. Guo, Z., Zhang, L., Zhang, D.: Rotation invariant texture classification using LBP variance (LBPV) with global matching. Pattern Recognit. 43(3), 706–719 (2010)

Article Google Scholar

27. Ahmadian, A., Mostafa, A.: An efficient texture classification algorithm using Gabor wavelet. In: 2003 Proceedings of the 25th Annual International Conference of the IEEE Engineering in Medicine and Biology Society, vol. 1, pp. 930–933 (2003)

Google Scholar

28. Ding, C., Choi, J., Tao, D., Davis, L.S.: Multi-directional multi-level dual-cross patterns for robust face recognition. IEEE Trans. Pattern Anal. Mach. Intell. 38(3), 518–531 (2016)

Article Google Scholar

Author information

Authors and Affiliations

Department of E&TC Engineering, Dr. D. Y. Patil Institute of Technology, Sant Tukaram Nagar, Pimpri, Pune, 411 018, Maharashtra, India

Sagar V. Joshi & Rajendra D. Kanphade

Corresponding author

Correspondence to Sagar V. Joshi .

Editor information

www.rmiet.edu.in

Editors and Affiliations

Machine Intelligence Research Labs, Auburn, WA, USA
Ajith Abraham

School of Information Technology and Engineering, Vellore Institute of Technology, Vellore, Tamil Nadu, India
Aswani Kumar Cherukuri

Tijuana Institute of Technology, Tijuana, Mexico
Patricia Melin

Machine Intelligence Research Labs, Auburn, WA, USA
Niketa Gandhi

Rights and permissions

Reprints and permissions

Copyright information

© 2020 Springer Nature Switzerland AG

About this paper

Cite this paper

Joshi, S.V., Kanphade, R.D. (2020). Forensic Approach of Human Identification Using Dual Cross Pattern of Hand Radiographs. In: Abraham, A., Cherukuri, A., Melin, P., Gandhi, N. (eds) Intelligent Systems Design and Applications. ISDA 2018 2018. Advances in Intelligent Systems and Computing, vol 941. Springer, Cham. https://doi.org/10.1007/978-3-030-16660-1_105

.RIS .ENW .BIB

DOI Published Publisher Name

https://doi.org/10.1007/978-3-030-16660-1_105

14 April 2019

Springer, Cham

Print ISBN
978-3-030-16659-5

Online ISBN
978-3-030-16660-1

eBook Packages
Intelligent Technologies and Robotics
Intelligent Technologies and Robotics (R0)

Publish with us

Policies and ethics

www.nmiet.edu.in
HELIX
The Scientific Explorer

https://doi.org/10.29042/2020-10-1-01-06

Helix (2020) 10 (1): 01-06

Forensic Human Identification using Dual Cross Patterns of Dental Panoramic Radiographs

*[1]Sagar V. Joshi, [2]Rajendra D. Kanphade, [3]Dinesh V. Bhalerao
[1,2]Department of E&TC Engineering, Dr. D. Y. Patil Institute of Technology, Sant Tukaram Nagar, Pimpri, Pune-411 018, Maharashtra, India
[3]Department of Technology, Savitribai Phule Pune University, Pune-411 007, Maharashtra, India
Email: sagarvjoshi@gmail.com, kanphaderd2015@gmail.com, bhalerao.dinesh3@gmail.com

Received: 13th August 2019, Accepted: 27th September 2019, Published: 29th February 2020

Abstract
Dental biometrics plays a very vital role in identifying the victims in natural and human-made disasters. The survivability and diversity of dental radiographs make them excellent alternatives over traditional biometric techniques using fingerprints, face, and iris. The main focus of this study is to deal with missing and unidentified person identification from a guide to automated based on dental panoramic radiographs using Dual Cross Pattern features that are complicated to be assessed only by visual examination. This paper seeks to identify an appropriate classifier amongst Feedforward Neural Network (FNN), Multiclass Support Vector Machine (m-SVM), k-Nearest Neighbor (k-NN) and Classification Tree (CT) based on retrieval accuracy of 10 adult subjects with 100 panoramic radiographs. The preliminary results on a small dataset are encouraging.

Keywords
Forensic Science, Dual Cross Pattern, Ante-Mortem (AM) Radiographs, Human Identification, Classification, Postmortem (PM) Radiographs.

Introduction

In forensic radiography, the unlabeled post-mortem (PM) radiographs of the body including the skeleton, skull, and teeth of the deceased are compared with the ante-mortem (AM) records of a missing person to determine the similarities between them [1,2,3]. The recent catastrophes have shown how important it is to rely on biometric radiographs to attract public awareness. For instance, the activist assault in the United States on September 11, 2001 [2], 20% of 973 victims were identified in the first year using dental protocols [2]. A large number of victims from the Asian tsunami in 2004 were also identified based on dental information. In Thailand, 75% of tsunami fatalities were recognized based on dental radiographs, 10% from fingerprint records, and only 0.5% by DNA profiles [3.4]. For the identification of other victims, a combination of different techniques was used [4, 5].Radiographs have played a significant role in solving severe cases in forensic science [6,7,8]. Figure 2(a-c) explores most commonly used radiographs; the periapical, bitewing, and panoramic respectively. WinID [9,10] is dental software which has been demonstrated useful in major disasters and the creation and maintenance of individual databases [9,10]. The OdontoSearch 3.2 computer program provides a way to assess the frequency of dental procedures but cannot be used to find the identity of the victims [1,11]. Mahoor and Mottaleb [12] proposed Bayesian classification for bitewing radiographs using Fourier descriptors of contours based on universal numbering system used in dentistry. Jain and Chen [13] again developed a shape registration technique based on contours of teeth and dental work. Subjects were retrieved by matching tooth contours using a method of shape registration and on the overlapping work areas. Hofer and Marana [14] designed a human identification method based on panoramic dental radiographs by extracting &matching dental work of 22 PM radiographs with the 46 AM radiographs of the database. Nomir and Mottaleb [15] introduced a dental x-ray matching technique depends on Hierarchical chamfer distance algorithm. Nomir and Mottaleb [16] again introduced a technique using the fusion of matching algorithms for AM and PM radiographs by using tooth contour, hierarchical chamfer distance and combine features extracted from force field energy function and Fourier descriptors. For dental bitewing radiographs, an efficient classification system was proposed by Lin and Lai [17]. Lin and Kuo [18] used spatial domain features and frequency domain metric for matching PM image with positive AM image based on dental work. Harandi and Pourghassem [19] proposed low-level image processing techniques for measuring the length of the root canal. Oktay [20] proposed a probabilistic graphical model-based automatic human identification using panoramic radiographs. Ajaz and Kathirvelu [21] suggested a human identification technique using dental work from panoramic radiographs. Figure 1 represents sample pre-dental and post-dental work panoramic radiographs from dataset

© 2020 The Author (s); Helix E-ISSN: 2319-5592; P-ISSN: 2277-3495

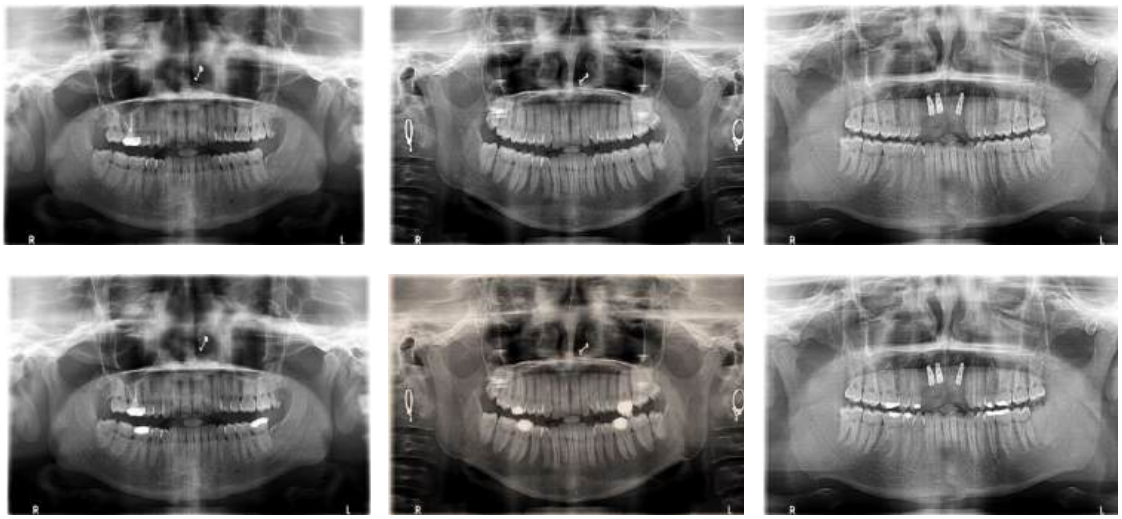

Fig. 1: Sample Panoramic Images from Dataset Captured at Different Time. Images in first row are the Pre- dental work and images in second row are Post-dental work images

Proposed System

The key advantage of the suggested method is to vanquish the segmentation concern encountered by state of art authors for teeth numbering system and identification of victims where traditional biometric techniques cannot be utilized. There are two stages involved in the human identification progression using dental panoramic radiographs (see Fig.2).When an image is entered into it, it can either be used to search for a neighboring record in the database or to build the database. In both cases, features are extracted from the image. After entries are made in the database, storing the extracted information is the last step of the process. At the time of retrieval, the final step is to compare all extracted data values from those records stored in the database. Pre-processing is generally helpful to remove blurring that is caused by both the machine as well as errors introduced by the individual while recording the panoramic image. It reduces the amount of speckle noise present in the image, which is a major problem encountered in radiographic images.

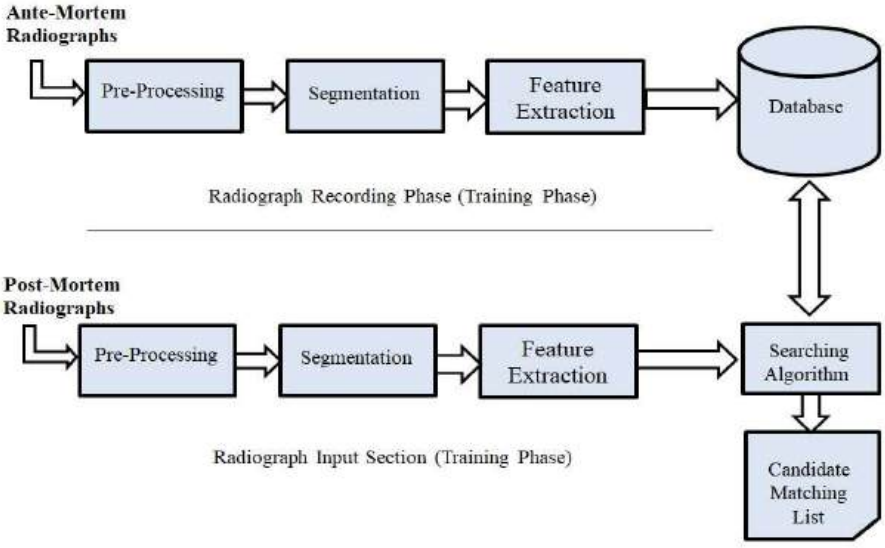

Fig. 2: General Architecture of Human Identification System Using Biometric Radiographs

1. Dual Cross Pattern (DCP) Feature Extraction

The three major steps in the development of the DCP image descriptor are image filtering, local sampling and pattern encoding. The key to DCP success is to execute pattern encoding and local sampling in the most descriptive direction

© 2020 The Author (s); Helix E-ISSN: 2319-5592; P-ISSN: 2277-3495

to encrypt second-order statistical information. In two stages the sampled points are encoded. Various Steps in DCP feature based image retrieval system is as follows:-

Step 1: Conversion of an input image into gray image

Step 2: Local Sampling: Carry out an eight-direction symmetrical sampling for each pixel of the image in the local neighborhood.

Step 3: Pattern Encoding: The textural data is quantized using pattern encoding in each sampling direction. For each image, two cross encoders generate the encoded images and derive the feature vector.

Step 4: Grouping: Combining feature vectors derived from two cross encoders.

Step 5: Comparison of query image feature vector with feature vector stored in database.

Step 6: The best matched images are recovered.

1.1 Local Sampling:

The center pixel $P_0$is computed by comparing its gray value with eight direction neighbors $(0,\frac{\pi}{4},\frac{\pi}{2},\frac{3\pi}{4},\pi,\frac{\pi}{4},\frac{5\pi}{4},\frac{3\pi}{2},\text{and}\frac{7\pi}{4})$ to get necessary amount of texture information. Two pixels are sampled from each direction and are represented as $\{P_{A1},P_{B1};P_{A2},P_{B2};P_{A3},P_{B3};P_{A4},P_{B4};P_{A5},P_{B5};P_{A6},P_{B6};P_{A7},P_{B7};P_{A8},P_{B8}\}$. $P_{A1};P_{A2}\dots P_{A8}$are uniformly distributed on the inner radius R_A (See fig.3), similarly $P_{B1};P_{B2}\dots P_{B8}$ are equally distributed on the inner radius R_B.

1.2 Pattern Encoding:

First, the texture details are encoded along each of the eight directions, which are followed by combining the pattern obtained for creating DCP code. A distinctive decimal number (See equation 1 and 2) is given in each sampling direction to quantize the textural information [22,23]. For the reduction of computational complexity, an exclusive grouping strategy is used in DCP. According to joint Shannon entropy, the total distinct levels in code will be too large for implementation, hence by grouping into two; each is called encoder, the total number of levels reduce to = 512 [22,23].

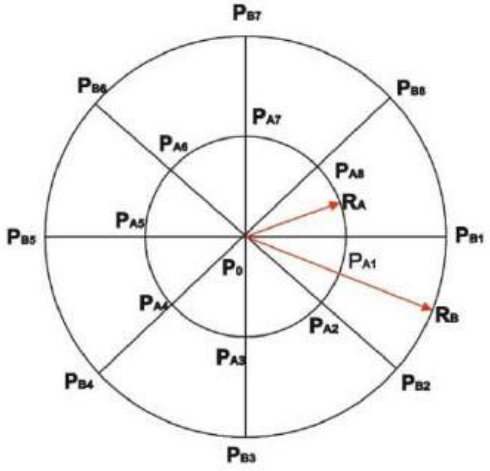

Fig.3: Local pixel sampling in DCP

$$\text{DCPp} = \text{D}\left(P_{A_i} - P_0\right) \times 2 + \text{D}\left(P_{B_i} - P_{A_i}\right) \qquad 0 \le i \le 7 \tag{1}$$

$$\text{Where },D(x) = \begin{cases} 1, & x \ge 0 \\ 0, & x < 0 \end{cases} \tag{2}$$

1.3 DCP Grouping:

Applying grouping technique on eight directions a total of 35 combinations are produced. A joint Shannon entropy criterion is used [23] for an optimum grouping of eight directions to preserve information required for image recovery.

$$H\left(DCP_0, DCP_1, DCP_2, DCP_3\right) = -\sum_{\text{dcp0}} \dots \sum_{\text{dcp3}} \text{P}\ (\text{dcp}_0\ \dots \text{dcp}_3) \log_2 \text{P}\ (\text{dcp}_0 \dots \text{dcp}_3) \tag{3}$$

© 2020 The Author (s); Helix E-ISSN: 2319-5592; P-ISSN: 2277-3495

Where, $(dcp_0 dcp_1, dcp_2, dcp_3)$ are particular values of $(DCP_0, DCP_1, DCP_2, DCP_3)$ respectively and $P(dcp_0 \ldots . dcp_3)$ is the Probability of $(DCP_0, DCP_1, DCP_2, DCP_3)$ values.The image is more independent of each other as the pixel are more scattered. Sample point separation with maximum distance result into maximum joint Shannon entropy in each subgroup [22][23].

$$DCP - 1 = \sum_{k=0}^{3} DCP_{2k} + 4^k \quad (4)$$

$$DCP - 2 = \sum_{k=0}^{3} DCP_{2k+1} + 4^k \quad (5)$$

The Final DCP descriptor of the image is formed by combination of DCP-1 and DCP-2 for every pixel

$$\mathrm{DCP} = \left\{ \sum_{k=0}^{3} \mathrm{DCP}_{2k} + 4^k, \sum_{k=0}^{3} \mathrm{DCP}_{2k+1} + 4^k \right\} \quad (6)$$

1.4 Panoramic Image Database & Influence of Block Numbers

In this paper, a total of 300 panoramic radiographs are collected from 30 adults including pre-dental work and post-dental work images at different head positions from Nidaan Diagnostics, Chinchwad, Pune, India. Keeping the head position fixed ensures a higher level of accuracy for experimentation purposes but not on a real-time basis. An attempt has been made to improve the accuracy level when matching is done on a real-time basis rather than to serve the experiment purpose solely. Out of the 30 adults, 10 adults are used for retrieval purpose (See table 1). The proposed system is implemented in MATLAB and executed on a computer with 3Gb RAM, Intel (R) Core 2 Duo processor, and WINDOWS 7 professional OS. Here, rather than selecting a single block per radiograph, the radiograph is divided into N blocks. The best descriptor of an image is achieved by selecting multiple blocks for local regions of the image. DCP feature vectors are calculated for block sizes 1x1, 2x2, 4x4, and 8x8, respectively, to study the influence of block size on retrieval accuracy and recognition time.

Table 1: Percentage Cross Validation Accuracy of DCP for Block Size N=1, N=2, N=3 and N=4. Red Value represents Incorrect Retrieval of Subject

Block Size (Feature Vector Length)	Name of Classifier	Cross Validation Accuracy in Percentage										Avg. Accuracy in percentage
		Subject										
		1	2	3	4	5	6	7	8	9	10	
N=1 (512)	k-NN (N=3)	90	50	70	80	50	70	80	50	60	40	64
	k-NN (N=5)	70	70	70	80	50	50	60	50	50	50	60
	CT	40	10	10	0	0	60	80	80	90	40	41
	m-SVM	100	20	50	40	40	100	10	40	100	90	59
	FNN	60	50	30	30	40	60	90	50	60	20	49
N=2 (2048)	k-NN (N=3)	90	90	80	90	80	80	90	90	80	80	85
	k-NN (N=5)	80	70	50	80	70	60	80	70	80	70	71
	CT	40	40	40	10	40	70	60	60	40	60	46
	m-SVM	100	90	100	40	30	0	0	40	90	100	59
	FNN	60	40	80	40	80	30	50	80	70	60	59
N=4 (8192)	k-NN (N=3)	90	80	80	90	90	90	90	90	90	90	88
	k-NN (N=5)	70	90	70	60	90	80	50	80	80	80	75
	CT	50	80	20	0	50	80	70	50	0	0	40
	m-SVM	100	90	100	100	100	60	80	50	90	90	86
	FNN	60	70	70	60	30	70	70	90	20	60	60
N=8 (32,768)	k-NN (N=3)	90	80	80	90	80	90	90	80	80	80	84
	k-NN (N=5)	80	90	80	80	80	70	70	70	70	70	76
	CT	20	50	40	20	30	40	10	10	20	70	31
	m-SVM	90	100	20	90	20	20	10	100	0	0	45

© 2020 The Author (s); Helix E-ISSN: 2319-5592; P-ISSN: 2277-3495

Experiment Results

The descriptor of DCP feature is extracted by merging DCP-1 and DCP-2 and used for the classification of 10 subjects (See table 1) using classifiers such as Multiclass Support Vector Machine (m-SVM), k-NN (N=3 and N=5), Classification Tree(CT) Classifier and, Feedforward neural network (FNN). By applying this, SVM along with the radial basis function, the kernel can be employed as one classifier. γ and C parameters, which employ a five-fold cross-validation process, are selected. One versus all SVM is used for multiclass classification as each potential subject denotes a new class since each subject holds unique features. The linear kernel is used for the class separating hyper-plane creation. SVM is trained for one against other class features. k-NN is the simplest classifier as it takes no time for training. Only the testing time is more as it finds the nearest neighbor using squared Euclidean distance. The FNN classifier used in this paper consists of 20 hidden layers. The scaled conjugate gradient method is used for training of the proposed neural network. The maximum number of training epoch used is 1000. The classifiers except m-SVM used in this study are reproducible from MATLAB inbuilt functions. The experimental results based on DCP feature vector of panoramic radiographs provide maximum retrieval accuracy level of 88% for a block size N=4 (feature vector length=8192) with k-NN (N=3), and 85% for a block size N=2 block size (feature vector length=2048) along with k-NN (N=3). The retrieval accuracy of DCP is minimized to 31% for N=8 block size (feature vector length=32768) with CT classifier.

Conclusion

The proposed technique is found to be suitable for the dataset of adults. Using DCP as a texture categorization method, human identification has been presented in this paper based on panoramic radiographs. The initial results on a minimum dataset indicated that dental panoramic radiographs are an appropriate approach for human identification. It is effortless and effective. Practically, it is indicated that by picking the suitable feature vector of an appropriate block size with acceptable classifiers can offer better texture categorization outcome. CT, m-SVM, FNN, and k-NN (N=3 and N=5) are the classifiers employed in DCP for human identification comparative study. Even though the proposed concept is easy, the experimental outcomes are favorable. It is evident that the result of this dental identification system is excellent. However, there is scope for future improvements. Future work will involve database extension of panoramic radiographs that servers various age groups and influences the complete performance of the proposed system. In future, to improve the pose correction, quality-based frame selection, and mark-based matching techniques can be combined to build a unified system based on panoramic radiographs.

Conflicts of Interest: None

References

[1] Manigandan, T., Sumathy, C., Elumalai, M., Sathasivasubramanian, S., & Kannan, A. (2015). Forensic radiology in dentistry. Journal of pharmacy & bioallied sciences, 7 (Suppl 1), S260.
[2] Forensic identification of 9/11 victims ends, New York, February 23, 2005.
[3] Jain AK, Flynn P, Ross AA, editors. Handbook of biometrics, Springer Science & Business Media, 2007 Oct 23.
[4] Hooper, R. (2005). Dental records beat DNA in tsunami IDs. New Scientist, 187(2516), 12-13.
[5] Abaza A, Ross A, Ammar H. "Retrieving dental radiographs for post-mortem identification," In 2009 16th IEEE International Conference on Image Processing (ICIP), IEEE, 2009.
[6] Dayal PK. Textbook of forensic odontology. paras medical publisher; 1998.
[7] Kahana, T., & Hiss, J. (1999). Forensic radiology. The British Journal of Radiology, 72(854), 129-133.
[8] Clark DH. Practical forensic odontology. Butterworth-Heinemann, 1992.
[9] McGarvey, J. WinID: Dental identification system, 2005.
[10] Pretty, I. A., & Sweet, D. (2001). forensic dentistry: A look at forensic dentistry–Part 1: The role of teeth in the determination of human identity. British dental journal, 190(7), 359.
[11] Kenney, J., Standish, S., Souviron, R., Vale, G., Mcgivney, J., & Jones, G. (1994). Body identification guidelines. Journal of the American dental association, 125(9), 1244.
[12] Mahoor MH, Abdel-Mottaleb M, "Automatic classification of teeth in bitewing dental images." in 2004 International Conference on Image Processing, 2004.
[13] Chen, H., & Jain, A. K. (2005). Dental biometrics: Alignment and matching of dental radiographs. IEEE transactions on pattern analysis and machine intelligence, 27(8), 1319-1326.
[14] Hofer, M., & Marana, A. N., "Dental biometrics: human identification based on dental work information," in XX Brazilian Symposium on Computer Graphics and Image Processing (SIBGRAPI 2007), pp. 281-286. IEEE, 2007.

 © 2020 The Author (s); Helix E-ISSN: 2319-5592; P-ISSN: 2277-3495

[15] Nomir, O., & Abdel-Mottaleb, M. (2008). Hierarchical contour matching for dental X-ray radiographs. Pattern Recognition, 41(1), 130-138.
[16] Nomir, O., & Abdel-Mottaleb, M. (2008). Fusion of matching algorithms for human identification using dental X-ray radiographs. IEEE Transactions on Information Forensics and Security, 3(2), 223-233.
[17] Lin PL, Lai YH, "An effective classification system for dental bitewing radiographs using entire tooth," in 2009 WRI Global Congress on Intelligent Systems, vol. 4, pp. 369-373. IEEE, 2009.
[18] Kuo CH, Lin PL, "An Effective Dental work extraction and matching method for Bitewing Radiographs," in 2010International Computer Symposium (ICS2010), pp. 495-499. IEEE, 2010.
[19] Harandi AA, Pourghassem H,"A semi automatic algorithm based on morphology features for measuring of root canal length," in 2011 IEEE 3rd International Conference on Communication Software and Networks, pp. 260-264. IEEE, 2011.
[20] Oktay, A. B. (2017). Human identification with dental panoramic radiographic images. IET Biometrics, 7(4), 349-355.
[21] Ajaz A, Kathirvelu D, "Dental biometrics: Computer aided human identification system using the dental panoramic radiographs," in 2013 International Conference on Communication and Signal Processing, pp. 717-721. IEEE, 2013.
[22] Joshi SV, Kanphade RD, "Forensic Approach of Human Identification Using Dual Cross Pattern of Hand Radiographs," in International Conference on Intelligent Systems Design and Applications, pp. 1075-1084. Springer, Cham, 2018.
[23] Ding, C., Choi, J., Tao, D., & Davis, L. S. (2015). Multi-directional multi-level dual-cross patterns for robust face recognition. IEEE transactions on pattern analysis and machine intelligence, 38(3), 518-531.

 © 2020 The Author (s); Helix E-ISSN: 2319-5592; P-ISSN: 2277-3495